THE UNIVERSITY OF
WARWICK

AUTHOR: **Andrea Fernanda Lopez-Clavijo** DEGREE: **Ph.D.**

TITLE: **Tandem Mass Spectrometry of non-enzymatically glycated peptides and proteins**

DATE OF DEPOSIT: .....

I agree that this thesis shall be available in accordance with the regulations governing the University of Warwick theses.

I agree that the summary of this thesis may be submitted for publication.

I **agree** that the thesis may be photocopied (single copies for study purposes only).

Theses with no restriction on photocopying will also be made available to the British Library for microfilming. The British Library may supply copies to individuals or libraries. subject to a statement from them that the copy is supplied for non-publishing purposes. All copies supplied by the British Library will carry the following statement:

> "Attention is drawn to the fact that the copyright of this thesis rests with its author. This copy of the thesis has been supplied on the condition that anyone who consults it is understood to recognise that its copyright rests with its author and that no quotation from the thesis and no information derived from it may be published without the author's written consent."

AUTHOR'S SIGNATURE: .....

USER'S DECLARATION

1. I undertake not to quote or make use of any information from this thesis without making acknowledgement to the author.
2. I further undertake to allow no-one else to use this thesis while it is in my care.

DATE SIGNATURE ADDRESS

.....

.....

.....

.....

.....

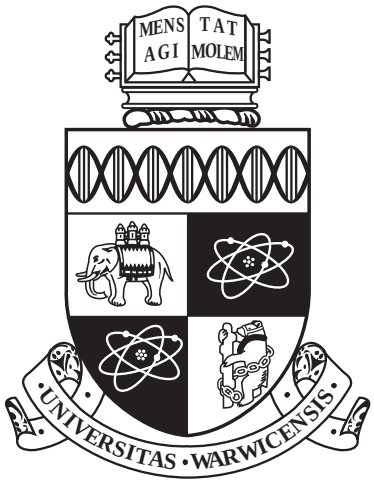

Tandem Mass Spectrometry of non-enzymatically glycated peptides and proteins

by

Andrea Fernanda Lopez-Clavijo

Thesis

A thesis submitted in partial fulfilment

of the requirements for the degree of

Doctor of Philosophy in Chemistry

Department of Chemistry

October 2013

THE UNIVERSITY OF
WARWICK

Contents

List of Tables

List of Figures

List of Schemes

Acknowledgments

I would like to dedicate this thesis to my mother. The tough decisions she had to make and her outstanding example made me the woman I am today. Thank you Mum, everything that I am today is because of your love, your perseverance, dedication and sacrifices. I am glad she had lived long enough, so I could make her proud. Another special dedication is to my husband: darling I will never regret following you to this country and believe me that I feel now, what you were feeling a year ago finishing your PhD. Nobody can deny that we love so much and we make a very good team. Last but no least, to my son, "my little one", who came to this country as a child and will be leaving as a teenager. Thank you for being so understanding, for putting a smile in my face and making me laugh, as well as for all your help, especially during the writing up process. I know I was overwhelming with chores, but, I hope, I also gave you a good example. Love you both, lots.

I would like to thank my supervisor Pete. He believed in me and my potential, "the will" to complete the PhD. Thank you Pete for the opportunity, for the chance to work with you and your team, for all your support and your encouraging words; I had learn a lot from you. Thanks to Chris Clarke, Christine Crout, Gillian Shipp and Barbara Barrat, and their Cannon Park Christian group. Without them I would have never learnt English. To my colleagues Becky, Pilar, and Isolda because their friendship made this journey very pleasant. To Dr. Nicholas Barker for the chance to have fun at the school's outreach. I am very grateful to Dr. Mark Barrow for his friendship, helpfulness and his disposition to share his knowledge at literally any time (very useful Friday

nights at the lab).

I would also like to thank the Department of Chemistry for the scholarship and all the staff and friends I made during my PhD: Jason from IT, Steve, Phil and Dave from chemistry stores, Marcus and Lee from the workshop, Olvi, Shukhbinder, and Samantha from finance office, Rob Jenkins, Ken Westwood and David Josey. Special thanks to all the members of Pete's research group. Thanks to Julia Smith from Bruker for her friendship and to my sister back home who has been looking after my mother all this time, thank you Sys. Finally, I would like to thank my examiners Dr. Helen Cooper and Professor Dr. Vasilios G. Stavros for their valuable time.

This journey is not complete until I acknowledge Professor Peter Carpenter in the Engineering department. He gave my husband the scholarship that unleashed all the marvellous experiences we have shared in this country. I only regret that we could never say personally thank you to him and not even got to known him. God bless him.

Thanks to God.

This research thesis was supported by the Warwick Centre for Analytical Science (ESPRC funded Grant EP/F03421/1).

This thesis was typeset with LaTeX 2$_\varepsilon$[1]

[1] LaTeX 2$_\varepsilon$ is an extension of LaTeX. LaTeX is a collection of macros for TeX. TeX is a trademark of the American Mathematical Society. The style package *warwickthesis* was used by the author.

Declarations

This thesis is submitted to the University of Warwick in support of my application for the degree of Doctor of Philosophy in Chemistry. It has been composed by myself and has not been submitted in any previous application for any degree.

The work presented (including data generated and data analysis) was carried out by the author.

Parts of this thesis have been published by the author:

Chapter 3: Determination of types and binding sites of advanced glycation end products for Substance P. Anal. Chem. 2012 (84), 10568-10575. Included in appendix E.

Abstract

The thesis presents the study of the reaction of glyoxal (ethanedial) with polypeptides. This reaction is important in the food industry as well as during ageing and diabetes mellitus. To study this reaction a Fourier transform ion cyclotron resonance mass spectrometer coupled with electron capture dissociation and collisionally activated dissociation was used. Initially this reaction was carried out in the neuropeptide Substance P to set up the reaction conditions, sample preparation, as well as the instrumental parameters in the mass spectrometer.

The results in Substance P revealed two compounds, with mass additions assigned as C_2O and $C_2H_2O_2$ from glyoxal, were formed. MS/MS results showed that the modification site for both species could be located at either the arginine residue or at the $N-$terminus. Thus, in order to distinguish $N-$terminus from arginine modification the position of the arginine was varied in four model peptides. The results indicated that both mass additions C_2O, $C_2H_2O_2$ were located at the arginine residue. Interestingly, two of those model peptides showed an unusual mass addition of 21.9843 Da, which was assigned as a new type of glyoxal modification at the arginine residue showing the addition of two carbon atoms from glyoxal and the loss of two hydrogen atoms from the peptide (C_2-H_2), herein referred to as 2-imino-imidazole.

In order to assess the involvement of other residues in the reaction with glyoxal a new set of experiments in acetylated and non-acetylated undecapeptides were carried out. Unexpectedly, these experiments revealed that two species with the same mass (16.01092 Da) were being formed in the non-acetylated peptide. One of the species corresponded to diglycation, where the results suggest that the glyoxal binding at the lysine residue is crosslinked with the $N-$terminus. The second species showing the addition of 116.01092 Da was formed at the arginine residue forming a species, here called a glyoxal dimer, at the arginine residue. The formation of the glyoxal dimer species was also observed in the acetylated peptide. Although is clear that crosslinking between the lysine residue and the N-terminus is not possible in the acetylated peptide, the results seem to indicate that crosslinking between the amino group of the lysine and the amide group of glutamine could occur. However, a systematic study varying the position of the lysine relative to the glutamine residue and also relative to the N-terminus needs to be addressed in the future in order to determine the extent of the involvement of the $N-$terminus and amide group in the glyoxal glycation reaction.

1 Introduction and Background

1.1 Motivation

The structure and function of proteins is altered during patho-physiological processes like uremia and diabetes mellitus. Advanced stages of diabetes often result in kidney disease,[1] referred to as end stage renal disease (ESRD) or diabetic nephropathy. Diabetic nephropathy has become a major health problem in the UK, U.S.A, and Australia.[2,3] For instance, a study conducted in 2009 estimated that about 9.2 billion will be spent over the next 30 years only in Australia to treat ESRD.[3] Part of this cost is associated with the long term dialysis or kidney transplant required by the patients. However, the major complication of individuals with ESRD is the high risk of cardiovascular death.[2] It is clear, then, that diabetes and its complications cause a serious detriment in the quality of life of the person who suffers it, as well as being a matter of serious concern in the finances of national health systems.

The development of diabetic nephropathy is often correlated to changes in the structure of the proteins, which implies that protein function and stability also changes. Alterations to protein structure can be related to the presence or the loss of post-translational modifications (PTMs). In the case of diabetes mellitus and its complications, the proteins are

mainly modified by reacting non-enzymatically[4] (in series or in parallel) with glucose and glucose auto-oxidation products (glyoxal, methylglyoxal and 3-deoxyglucosone).[5] This reaction forms a complex set of compounds termed as advanced glycation end-products (AGEs).[6] In this thesis, the PTM known as glycation, and in particular, glycation by glyoxal was studied in peptides in order to establish the experimental conditions, which will be later extended to proteins.

A widespread method to characterize PTMs is using mass spectrometry, which coupled with collisionally activated dissociation (CAD) and electron capture dissociation (ECD), allow identification of the PTMs binding sites.[7–10] Thus, in this work, fragmentation techniques like ECD and CAD are used to localise glyoxal-derived advanced glycation end-products (AGEs). This chapter describes the mass spectrometer used in this work, including an explanation about the CAD fragmentation technique. The principles of ECD are reviewed in chapter 2. Chapter 3 to chapter 6 present, in detail, the experiments used to assign glyoxal-derived AGEs in peptides. A summary of the results is presented in chapter 7 along with an ongoing project about glycation of proteins. The thesis conclusions are finally presented in chapter 8.

1.2 Mass spectrometry

Mass spectrometry is an analytical technique used to measure the mass to charge (m/z) ratio of charged molecules. The initial step in mass spectrometry is to generate the charged molecules, which is done in the ion source.

1.3 Ionization sources

Charged molecules are produced using ionization sources, where the neutral molecule is converted into an ion. There are many different types of ionization sources, but they all work by adding or removing a charged particle to/from the molecule of interest.[11] The molecular ion can be generated by electron removal, electron capture, protonation, cationization, or deprotonation. Common ionization sources are electron ionization (EI), inductively coupled plasma (ICP), matrix assisted laser desorption (MALDI) and electrospray ionization (ESI).

1.3.1 Electron ionization (EI)

Electron ionization (EI) utilises high energy electrons usually $70\,eV$ that interact with a vaporised molecule causing electron removal from the molecule of interest and subsequently generating ions according to the reaction equation (1.1).[12] This method only operates in gas phase molecules, in vacuum, so the molecule has to be small, volatile and thermally stable.[11] Usually, gas chromatography is used to introduce the sample in the gas form, which also provides analyte separation prior to mass spectrometry (MS) detection.

$$\mathrm{M} + \mathrm{e}^-_{70\,\mathrm{eV}} \longrightarrow \mathrm{M}^{+\bullet} + 2\,\mathrm{e}^- \tag{1.1}$$

EI produces extensive fragmentation so the precursor ion is not always observed.[13] Moreover, EI decreases effectiveness for molecules above $350 - 400\,MW$.[14] Thus, the extensive fragmentation together with the low volatility of large biomolecules limit EI application to polypeptides. However, further developments in ionization sources

brought the development of electrospray ionization (ESI),[15] which made possible the analysis of protein and peptides by mass spectrometry.

1.3.2 Inductively coupled plasma (ICP)

In a ICP ion source, the analyte solution is converted into a fine aerosol droplet using a nebulizer, making it easy to ionise in the plasma discharge. This type of source is useful to detect metals in the analyte solution in parts per billion concentration. The analyte is introduced into the ICP source as a fine aerosol formed by the high-speed flow of the nebulizer gas (usually argon), which is later transported to the plasma torch. The plasma torch consists of three concentric quartz tubes, delivering argon gas and analyte droplets to the the plasma discharge, where the analyte is ionized. The end of the tubes are centrally positioned in a radio frequency (RF) coil, typically held at 40 MHz, which creates an electromagnetic field that confines the plasma discharge.

The plasma discharge is initiated with a high-voltage spark applied to the argon gas outside of the plasma torch.[16] This causes losses of electrons from the argon atoms. Consequently, this electrons are accelerated in the magnetic field and collide with more neutral argon atoms, causing more electron losses. The collisions induce ionization of the argon atoms, which continues as a chain reaction until a mixture of argon atoms, argon ions and electrons is obtained forming the inductive coupled plasma. The analyte aerosol is then introduced into the plasma through the middle tube called the sample injector. The temperature at the centre of the plasma discharge is around $10,000\,K$ causing the aerosol sample to decompose into individual atoms, which are ionized by the plasma.

1.3.3 Matrix assisted laser desorption ionization (MALDI)

MALDI is an ionization technique often used in the analysis of polypeptides,[17,18] where the analyte sample (dissolved in MeOH:ACN:formic acid) is mixed with excess ($\sim 10^6$) of weak organic acid. This mixing can be performed in solution or during the crystallisation process on a metal plate. The crystal is, then, irradiated with a Nd:YAG laser beam (in the Bruker instrument used in this work), which creates a plasma plume. The composition of this plasma plume (figure 1.1) can be explained by considering two different models, the gas protonation model and the lucky survivor model. The gas protonation model considers that there are in the plasma plume neutral molecules of the analyte, which are ionized via proton transfer from the protonated matrix ions. In contrast, the lucky survivor model considers that the analyte has preserve its charge in the solid phase before desorption.[19] The lucky survivor model is the most accepted model to date.

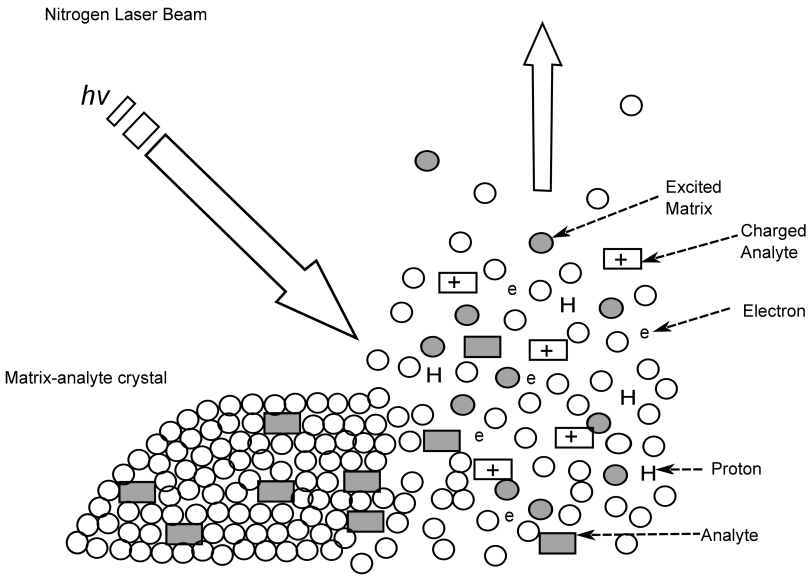

Figure 1.1: Illustration of MALDI plume. Figure reprinted with permission from El-Aneed, A and Cohen, A and Banoub, J[11]

The matrix is an small aromatic compound, which absorbs most of the photons minimis-

ing sample decomposition and increasing the efficiency of the energy transfer from the laser to the analyte. Additionally, there is not necessary to adjust the laser wavelength to match the absorption frequency of each analyte because the matrix absorbs most of the photons.[13] Thus, MALDI allows desorption and ionization of analyte of high molecular weight. Once the ions are produced, typically singly charged species ($[M + H]^{1+}$), they are transferred to the mass analyzer.

1.3.4 Electrospray ionization (ESI)

The use of electrospray requires that the protein/peptides are dissolved in solution. The solution is chosen to allow dissolution of the sample as well as evaporation. Typically, a mixture of water/acetonitrile or water/methanol, but many others are used, for example (50:10:39:1) mixture of methanol, isopropanol, water and acetic acid, employed in this work. The protein/peptide is then protonated, cationized, or deprotonated at atmospheric pressure.

Commonly, the protein/peptide solution is loaded into a syringe, which is automatically controlled, to pump at constant flow ($\sim$ 200 μL/min) into a needle. The needle is grounded (0 Volts) for the Bruker (Bruker Daltonics, Bremen, Germany) ESI sources and the spray shield is held at -4.0 kV (for positive ion generation) or +4.0 kV (for negative ion generation), the potential difference causes the charge to accumulate on the surface of the liquid forming a Taylor cone[20] as shown in figure 1.2. Once the charge repulsion is bigger than the surface tension, the droplets leave the cone in a fine mist of droplets.[21] During the migration of the charged molecules towards the spray shield, evaporation occurs. The decrease of the droplet radius causes an increase in the surface charge density until the droplet reaches the critical radius, or Rayleigh stability limit, where the Coulombic repulsion equals the surface tension.[22,23]

Three of the most accepted models are discussed below to explain the ion formation from the evaporating droplets (droplet shrinkage, figure 1.2). First, the "charge residue model (CRM)" described by Dole *et al.*[24] where a single analyte molecule is separated from the solvent or other molecules in the droplet by a series of fissions. During this separation the analyte molecule takes a part of charge excess and is desorbed in the gas phase. This leaves the analyte with a higher charge/mass ratio than the droplet as a whole. Consequently, a reduction in the Coulombic repulsion of the droplets is observed. This model is considered valid for high molecular weight molecules.

The second model was proposed by Thomson and Iribarne,[25] and is called the "ion evaporation model (IEM)", where a direct emission of the ions from the droplet occurs after the critical radius has been reached. In other words, when the solvent evaporates, the macromolecule is left as an ion. This model applies to molecules with a radii < 1 nm. The difference between these two models lies in the role played by the macromolecule: in the first one the molecule plays an active role whereas in the second model takes a passive behaviour.

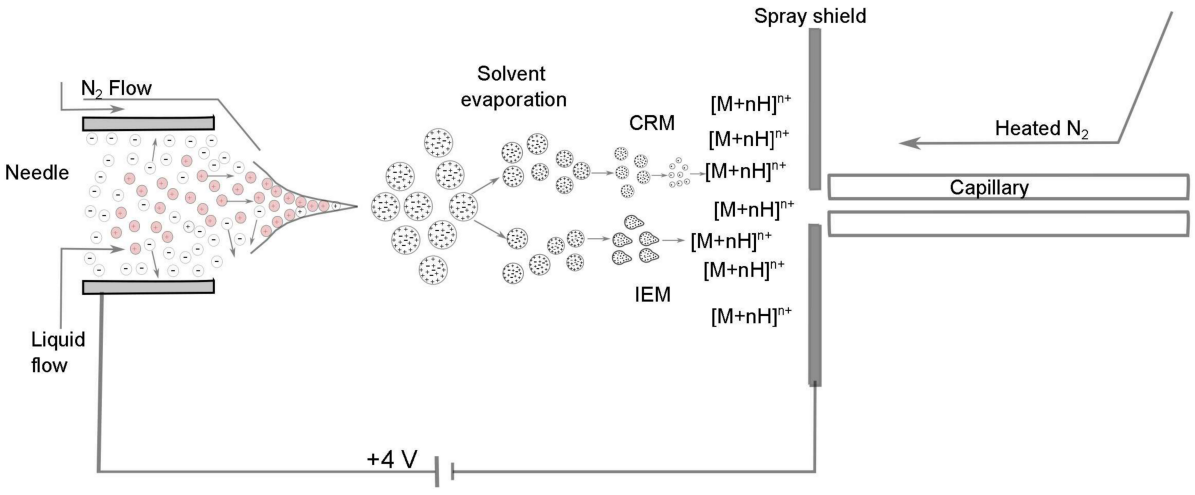

Figure 1.2: Schematic of ESI models: CRM (charge residue model) and IEM (ion evaporation model) with the needle grounded.

These two models are considered valid where no electrical field is present, particularly when zero voltage is applied to the capillary tip. Interestingly, a third model proposed that axial charge separation occurs inside the droplet in the presence of strong electrical fields. This model is called "field-induced droplet ionization (FIDI)", where the inhomogeneous distribution of the charge causes prolate ellipsoid droplets with terminating protrusions.[26] Thus, once Coulombic repulsion is bigger than surface tension, enriched ions are produced from the protrusions.

In the Warwick FT-ICR-MS lab, a variation of ESI is used in which a glass capillary is employed to deliver the sample at nL/min flow and is called nanoESI (nESI). [1] This technique requires lower spray shield voltages, is preferred when the amount of the sample available is limited, and is more stable than ESI to changes in the composition of the spray solution. For instance, it is possible to spray directly out of water in nESI whereas in ESI the spray is not stable.

1.4 Mass analyzers

There are a variety of mass analyzers that differ in their principles of operation as well as their performance characteristics, like the mass range limit, the dynamic range, the mass accuracy, the resolving power, the detection sensitivity and the fragmentation capabilities (MS/MS). The definitions of these concepts are presented below and throughout this section.

- The mass range is the lowest and highest m/z that can be measured in the mass analyzer.
- The dynamic range is the ratio of the intensity of the highest signal in the spectrum

[1] A Triversa NanoMate (Advion Ithaca, NY, U.S.A.) equipment can also deliver a flow at nL/min.[27]

to the smallest.

- The mass accuracy is given by the measure of the error of the experimental mass compared to the theoretical value.

- The resolving power (RP) is measured by the value of a single mass divided by the full width at half maximum (FWHM). It measures the ability to separate two ions of a defined mass difference.

$$RP = \frac{M}{\Delta M_{(FWHM)}} \tag{1.2}$$

where,

$$\Delta M = ((m/z)_1 - (m/z)_2) \tag{1.3}$$

- Sensitivity is the degree of response of the mass spectrometer to changes in the concentration. This response is measured by the ratio of the change of the peak intensity in the mass spectrum to the change in the concentration. The sensitivity depends on the ionization, transmission and detection efficiency of the mass spectrometer, which is defined as the ratio of the number of ions detected to the number of molecules in the sample. [13]

1.4.1 Quadrupole

The quadrupole consist of four parallel metallic rods of the same length and diameter. RF potential is applied to the parallel rods, so two opposite rods have one phase (labeled $+$, figure 1.3), whereas the other opposite pair have the opposite phase (labeled $-$, figure 1.3). This arrangement generates an oscillating electric field, which provides a pseudopotential. This pseudopotential confines the ions to travel along the the z axis. [28]

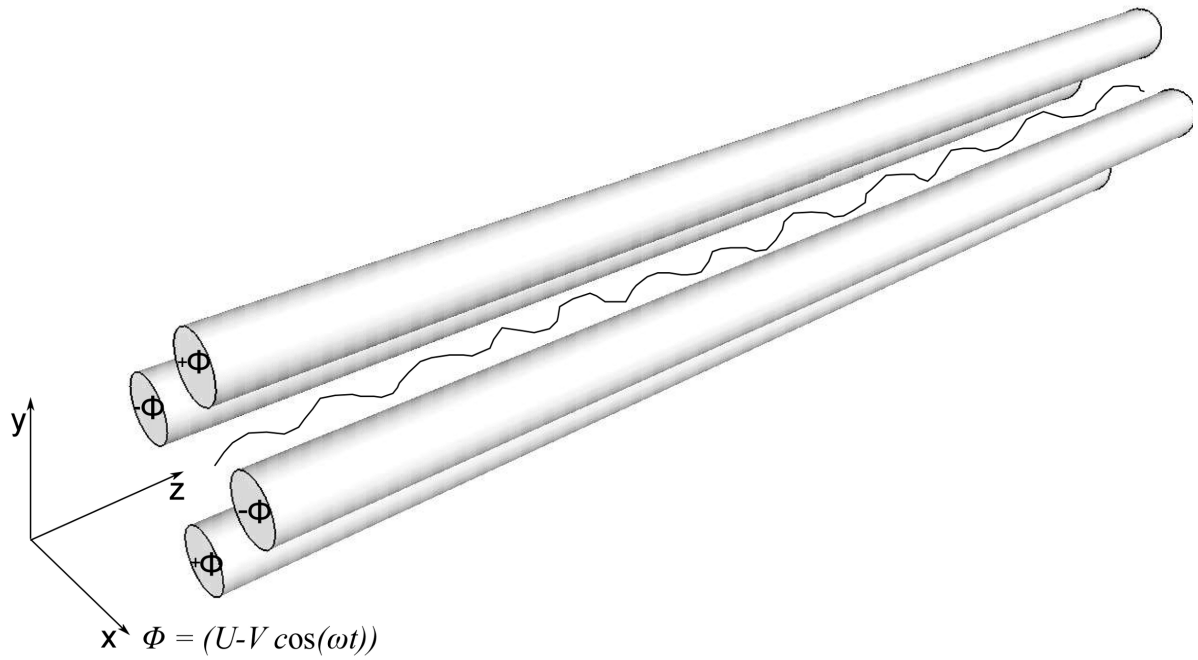

Figure 1.3: Quadrupole.

For instance, a positive ion entering the space between the rods is attracted by the negative rod, but before it reaches the rod the RF potential changes sign and the ion is then repelled. The movement of the ions can be predicted by the use of the Mathieu equations equations (1.4) and (1.5)

$$a_u = \frac{8zeU}{m\omega r_0^2} \tag{1.4}$$

$$q_u = \frac{4zeV}{m\omega^2 r_0^2} \tag{1.5}$$

Varying the values of U (DC potential) and V (RF amplitude), while keeping ω (RF drive frequency) and r_0 (distance of the rods divided by 2) constant, the position of a particular ion in the xy plane can be determined as a function of U and V. Moreover, as long as the position in x and the position in y do not exceed the r_0 the ion can pass

through the quadrupole without touching the rods. So, stability areas can be represented in a a_u, q_u diagram.[13] Depending on the position in the stability diagram, quadrupoles can thus, be used either as ion confinement "pipes" or as mass analyzers or mass filters.

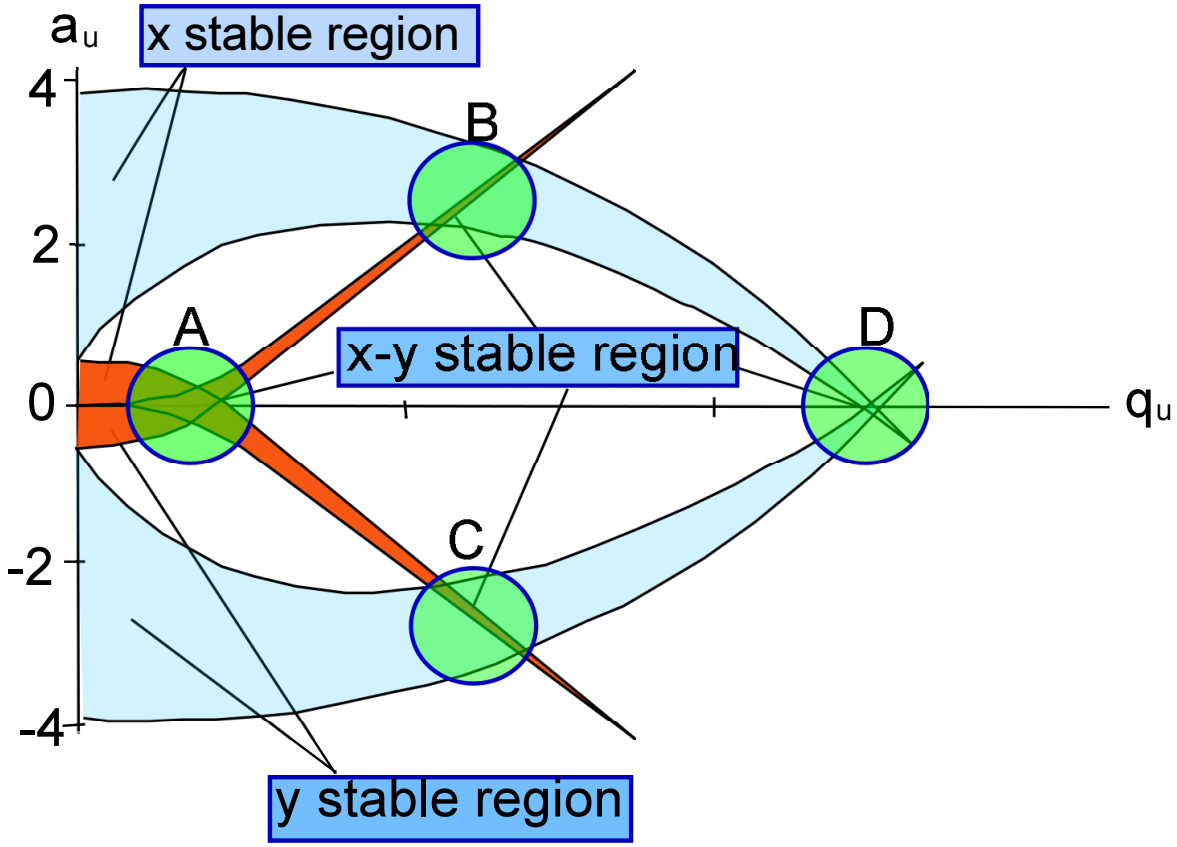

Figure 1.4: Stability areas for and ion along x and y. The four stability areas are labelled A to D. Figure adapted with permission from De Hoffman and Stroobant.[13]

The quadrupoles, when used as mass analyzers, have a typical mass range up to $4000\ Da$, a resolving power around 3000, and a mass accuracy of 100 ppm.[13] In the instrument used in this work an FT-ICR-MS, the quadrupole is not employed as mass analyzer. Instead, the quadrupole serves as either a mass filter (to perform isolation of the precursor ion before fragmentation) or to transport the ions from the ion source to the ICR cell (mass analyzer).

1.4.2 Time of flight (TOF)

This mass analyzer separates the ions based on their different velocities after acceleration through a potential V. The velocity, v, is mass dependent and is represented by the equation 1.6

$$v = \sqrt{\frac{2zeV}{m}} \tag{1.6}$$

where, z is charge of the molecule; V is the acceleration voltage applied; and m is the mass of the molecule. The separation of the ions occurs in a field-free region of determined length L, also referred to as a drift region, were the ions have a constant velocity. Thus, the m/z of the ions can be determined by measuring how long they take to reach the detector equation (1.7)

$$\frac{m}{z} = \left(\frac{2eV}{L^2}\right) t^2 \tag{1.7}$$

Ions with high m/z ions have less velocity than small ions and will be detected at different time intervals. Differentiating equation (1.7), it is clear that the resolving power in a TOF instrument can be expressed as,

$$R = \frac{m}{\Delta\, m} = \frac{t}{2\Delta\, t} \approx \frac{L}{2\Delta\, x} \tag{1.8}$$

where $\Delta\, x$ is the thickness of an ion packet. It is clear from equation (1.8) that in order to increase the resolving power, then, the drift path can be increased. However, a path too long causes ion loss, so an optimal length is between 1 to 2 m, although this configuration only reaches about 5000 resolving power and $200\, ppm$ of mass accuracy.

Another way to improve resolution is by both the use of a delayed extraction and an electrostatic mirror, also known as a reflectron. The reflectron deflects the ions and send them back through the drift tube increasing the resolving power to $20,000$ and the mass accuracy ($10\,ppm$).[13]

1.4.3 Orbitrap

An orbitrap is an electrostatic trap with the external shape of a barrel of $20\,mm$ of diameter, but separated in the middle to allow radial introduction of the ions.[13] The orbitrap has also a central electrode in an spindle shape with a maximum radius of $8\,mm$.[29] A later development in the external trap allow the introduction of the ions tangentially to the central electrode. The ions enter the orbitrap at high velocity and are forced to orbit the centre spindle, which is held a kV potential in the central electrode while keeping the external electrode at ground potential. The ions then will move in the radial direction around the centre electrode and oscillate in the axial direction see figure 1.5.

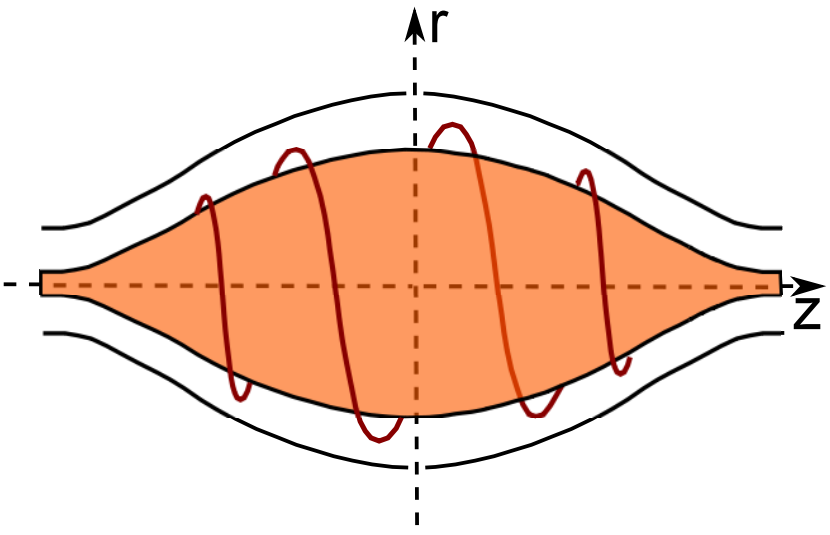

Figure 1.5: Orbitrap.

The axial frequency of the ions oscillating around the spindle is obtained by the equation (1.9)

$$\omega_z = \sqrt{\frac{q}{m}k} \tag{1.9}$$

where, k is the field curvature. This mass analyzer is also the detector and can achieve a resolving power of $100,000$ and mass accuracy below $5\,ppm$.[13]

1.4.4 Ion mobility

The physical principles underlying the operation of an ion mobility mass analyzer are based on exposing the ions to an electric field suspended in a gas medium. The application of the external force, from a low electric field, to the ions force them to move along the direction of the electric field with a drift velocity, controlled by the ions mobility, referred to as K in $cm^2/(Vs)$. In an uniform, low, electric field the ion cloud would travel with constant terminal velocity (equation (1.10)), parallel to the electric field direction, slowed by collisions with background gas. Hence, there is a reduced mass after the ions collide with the gas, μ, equation (1.11).

$$v = KE \tag{1.10}$$

$$\mu = \frac{m_i m_g}{m_i + m_g} \tag{1.11}$$

Additionally, the Mason-Schamp equation establish the dependance of the mobility and the cross section of an ion[30] in a low electric field is given by equation (1.12)

$$K = \frac{3q}{16}\left(\frac{2\pi k_B T}{\mu}\right)^{1/2}\frac{1}{N\Omega} \tag{1.12}$$

where, k_B is the Boltzmann constant; T is the gas temperature; N is the gas number density $(molecules/volume)$; and Ω is the rotationally averaged collision integral or collision cross section, which depends on the structures of the gas and the diffusing ion. Thus, in an ion mobility mass analyzer it is possible to separate the ion cloud according to their cross-section. The separation of the ions by their cross section is performed in the drift tube. An usual drift tube consisted of guard rings separated by insulating ceramic spacers connected by a resistor cascade, which provided a homogeneous electric field gradient throughout the drift tube.

Traveling-wave ion mobility

A popular technology used in the drift tube is the application of a traveling-wave (TW), which consists in the use of RF-potentials applied to the guard rings as shown in figure 1.6. These RF-potentials trap the ions radially, with superimposed voltage waves traveling from lens to lens. The ions ride on the waves back and forth until they fall behind catching the next wave. Ions with larger cross sections fall behind more often than ions with lower cross section because they experience more collisions and friction with the gas. Separation of the ions is then achieved and the time of arrival of the ions to the detector is measured as the drift time, as shown in figure 1.6 and figure 6.9 in chapter 6.

The mobility of the ions, in a TW is a function of the maximum velocity, c, which corresponds to the velocity at the steepest wave slope. The maximum velocity is also inversely proportional to the wave velocity, s. At $c \ll 1$ and fixed E (ignoring thermal

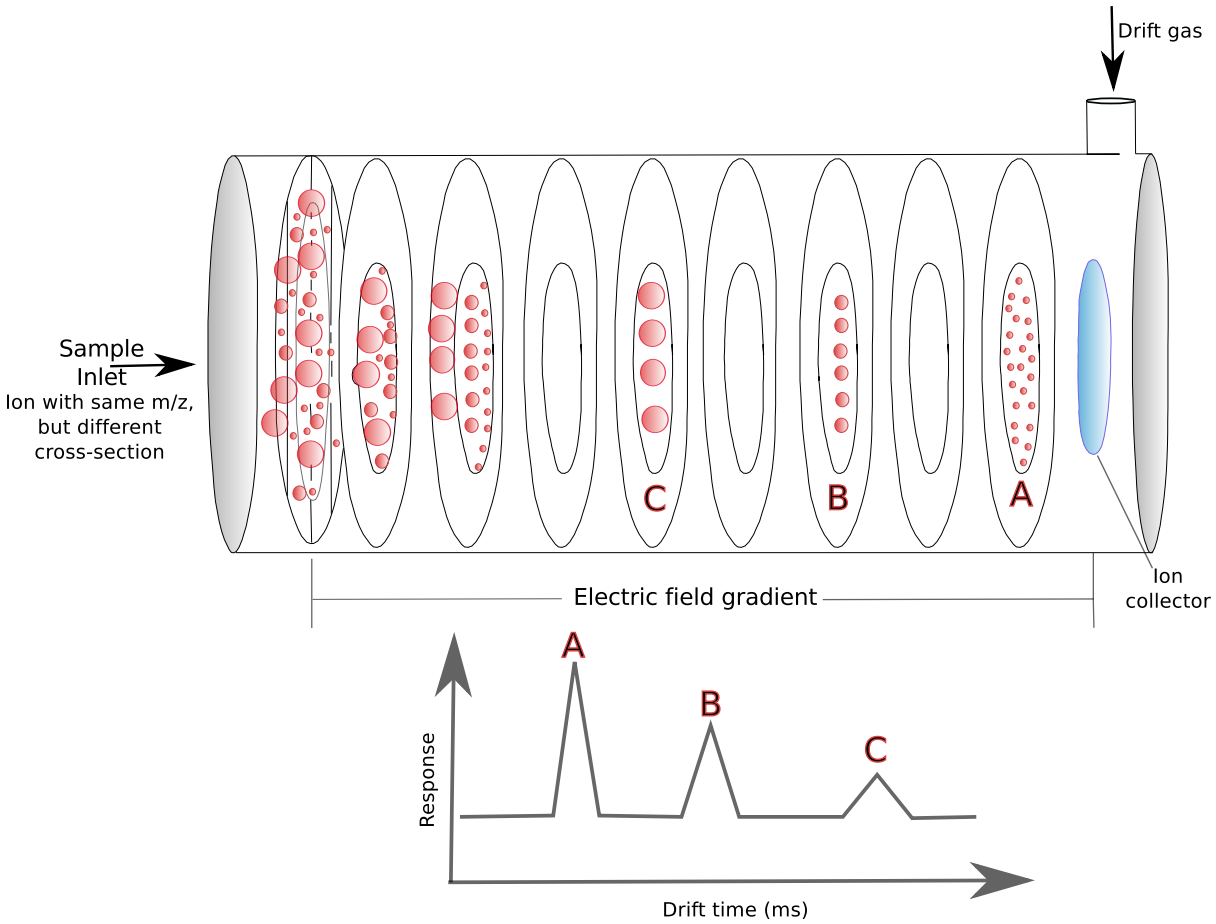

Figure 1.6: Schematic of the ion mobility drift channel and ion mobility spectra. A. B, and C are ions not isotopically resolved.

ion diffusion), c scales quadratically with the product of the mobility and the electric field, as shown in equation (1.13).[30] In the situation where $c \approx 1$, the ions travel with a mean velocity, $c \approx s$, where ion separation is dependant on the drift velocity while diffusion determines the ion packet width. In any case c cannot be higher than s and the limiting factor in equation (1.13) is s/E_{max}, where E_{max} is the electric field at the steepest wave slope.

$$c = \frac{(KE)^2}{s} \tag{1.13}$$

Another situation to be considered, is c at variable E,[30] where E varies with the axial

coordinate, x, as shown in equation (1.14)

$$c = \frac{K^2}{s}\left[\frac{\int_0^b \frac{E^2(x)dx}{s^2 - K^2E^2(x)}}{\int_0^b \frac{dx}{s^2 - K^2E^2(x)}}\right] \tag{1.14}$$

where s is the wave velocity; b is the wavelength in space of the traveling-wave.

Additionally, the TW ion mobility drift tube can be coupled to a TOF or quadrupole mass analyzers, such as the instrument used in this study a Synapt G2 (Waters, Manchester, U.K.), which was coupled with a TOF mass analyzer. Operated at pressure of $0.5\,mbar$ for the drift gas, (N_2), a RF amplitude of $40\,V$ and a IMS travelling wave velocities of $500\,m/s$.

1.4.5 Fourier transform ion cyclotron resonance cell (FTICR)

The mass analyzer in an FT-ICR-MS is a cyclotron resonance cell, which performs also as the detector. This mass analyzer is maintained at ultrahigh vacuum ($\sim 9\,X\,10^{-10}\,bar$) in a constant magnetic field. In particular, the magnet used in the present work used a $12\,T$ magnetic field. An example of an ICR cell is a cylindrical cell with trapping, excitation and detection plates as in shown in figure 1.7.

The ions entering the cell are trapped by an electrostatic potential applied between the trapping plates. This trapping potentials cause an axial motion of the ions inside the cell with a frequency ω_z defined by equation (1.15),[31] The trapping plate voltages used in this work were maintained below $1\,V$, with typical values of 0.6 to $0.65\,V$.

$$\omega_z = \sqrt{\frac{2Vq\alpha}{ma^2}} \tag{1.15}$$

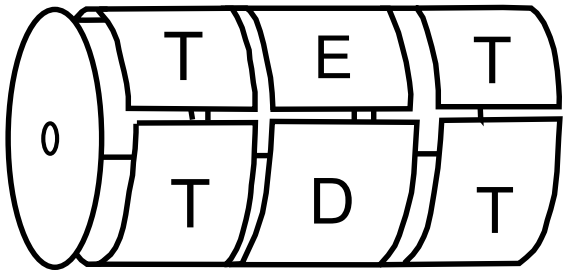

Figure 1.7: Ion cyclotron resonance cell. **T** indicates trapping plates; **E** indicates excitation plates; and, **D** indicates detection plates.

where, V is the trapping plate voltage; q is the charge of the ions and is equal to z multiplied by the electron charge or $1.6\,X\,10^{-19}\,C$); α is a geometry factor; m is the mass of the analyte of interest; and a is the distance in between the front and the back trapping plates.

The ions in a magnetic field oscillate with a theoretical "unperturbed" cyclotron frequency,[31] which is inversely proportional to the m/z of the ions equation (1.16).[32] In reality, the cyclotron frequency is reduced (ω_+) by the force caused by the trapping potentials and is then dependent of the axial frequency as in shown in equation (1.17).

$$\omega_C = \frac{qB}{m} \tag{1.16}$$

where, B is the magnetic field.

$$\omega_\pm = \frac{\omega_c}{2} \pm \sqrt{\left(\frac{\omega_c}{2}\right)^2 - \frac{\omega_z^2}{2}} \tag{1.17}$$

ω_- is the reduced magnetron frequency. The magnetron motion is responsible for the reduction of the cyclotron frequency due to causes diffusion of the ions.[31] The balance of the forces present in the ICR cell and a rearrangement results in a calibration equation of

$$\frac{m}{z} = \frac{C_2}{\omega_+^2} + \frac{C_1}{\omega_+} + C_0 \tag{1.18}$$

Where, C_2, C_1, and C_0 are calibration constants.[33]

The ions, then, are moving inside the cell following their respective cyclotron, magnetron and axial trajectories (figure 1.8). When the ion is initially injected into the cell low-amplitude axial motion allow to cool the ions in the cell. At the same time low-amplitude cyclotron and magnetron motion are present. Thus, for detection, the ions must be exited into a high-amplitude (typically $\sim 5\,cm$ diameter) cyclotron orbit. This is usually done using a frequency sweep or "chirp" through the frequencies of interest, which contains the band of frequencies corresponding to the desired m/z range.[31] During this process each ion respond to the RF pulse in accord to its corresponding cyclotron frequency. Thus, each ion packet is resonantly accelerated increasing its cyclotron radius to a higher orbit. This radius is independent of the m/z, as indicated in equation (1.19) Moreover, other excitation pulses can be employed, such as impulse excitation or stored waveform inverse Fourier transform (SWIFT).[34]

$$r = \frac{E_0 T_{\text{excitation}}}{2B} \tag{1.19}$$

where, E_0 is generated by the voltage (V_0) applied to opposite excitation plates, separated a distance d

$$E_0 = \frac{2V_0}{d} \tag{1.20}$$

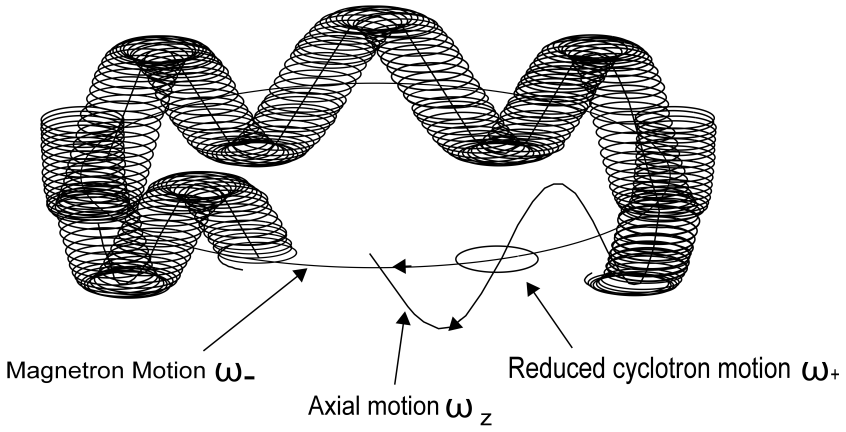

Figure 1.8: Ion motions in an ion cyclotron resonance cell.

The increase in the radius orbit of the ion cloud allows them to get in close proximity to the detection plates figure 1.9. The ions induce an accumulation of charges with the opposite sign to the detection plates and as the ions orbit the cell, close to the detection plates, image charge is induced, which alternates at each opposite plate generating an alternating voltage. This alternating voltage is amplified to generate a time domain signal (referred to as transient).[32] This time signal is then converted to represent the cyclotron frequency of the each individual ion using the mathematical function known as the Fourier transform (FT). The frequency domain spectrum is then converted by application of the equation (1.18) to obtain the mass spectrum.

The excited ion packet will eventually lose their energy and spiral back down to the centre of the cell causing a drop in the intensity of their detected signal, which in turn results in a fast decay of the transient. Sum up to this loss of energy, further collisions with background gas cause loss of coherence of the ion packet also affecting the duration of the transient. The duration of the transient T directly affects the resolving power as shown in equation (1.21)

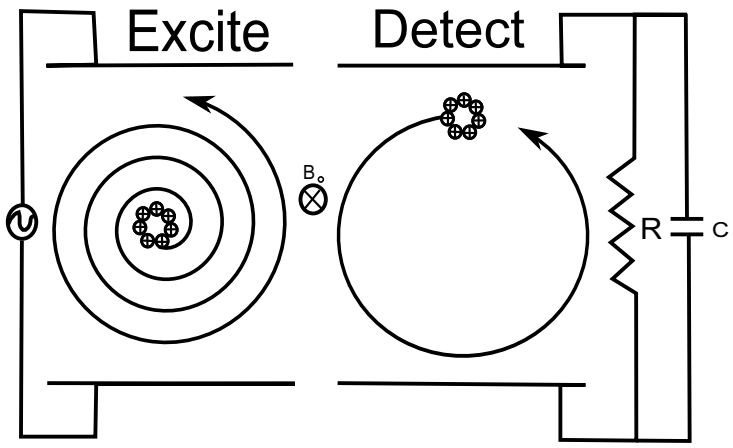

Figure 1.9: Excitation and detection of trapped ions in a cyclotron resonance cell.

$$RP = \frac{fT}{2} \tag{1.21}$$

where, f is the cyclotron frequency in Hz and is equal to equation (1.22)

$$f = \frac{\omega_c}{2\pi} \tag{1.22}$$

It seems clear that the resolving power is also dependent on the strength of the magnetic field. However, many other factors (operational or instrumental) contribute towards the decrease/increase of the resolving power. Instrumental parameters include the electric and magnetic field homogeneity, the cell geometry, ion transmission and electronics. In contrast, operational parameters like a high ion accumulation time of the ions before entering the cell decreases the resolving power. This, in particular, causes space charge effects where the collisions among the ions themselves originate almost immediate loss of coherence and a fast decay of the transient.[33,35] Another operational parameter that greatly affects resolution is the low-mass cutoff, which, anyway, can be changed as

desired. A typical low-mass cutoff for the fragmentation analysis of protein/peptides is m/z 150. In the present work the low-mass cutoff was set to m/z 150, too, although some minor variations were required for some specific tests. Additionally, this low-mass cut off is dictated by the sampling frequency, which must satisfy the Nyquist criteria. Therefore, the lowest m/z, that corresponds to the highest frequency of the ions in the cell, is set such that the sampling frequency is guaranteed to be at least twice the highest frequency of the ions. Equally, this sampling frequency is also limited by other instrumental parameters.

In the instrument employed in this work, at a typical mass of m/z 400, a resolving power of around $200,000$ is achieved. Moreover, a mass accuracy below 1 ppm is reached, when internal calibration is used, as shown in appendices A to D. Additionally, this instrument is coupled with fragmentation capabilities, such as collisionally activated dissociation (CAD),[9] electron capture dissociation (ECD),[8] and infrared multiphoton dissociation (IRMPD)-ECD.[36–39] which are described in section 1.5 and chapter 2.

1.5 Fragmentation techniques

Fragmentation of the ions occurs in three steps: first, isolation of the precursor ion followed by fragmentation (using CAD, ECD, IRMPD, among others), and finally, detection of the fragment ions. These three steps can occur in different mass analyzers localised in different places of the mass spectrometer, process which is referred to as tandem mass spectrometry (MS/MS) in space. On the contrary, fragmentation in the same mass analyzer is known as MS/MS in time. For instance, MS/MS in space is performed in triple quadrupole (QqQ), quadrupole combined with TOF mass analyzers and TOF/TOF. The instrument used in this work is capable of performing MS/MS in space and MS/MS in time, as desired. The typical configuration used is performing isolation of the parent

ion in the quadrupole and fragmentation in the collision cell for CAD or fragmentation by ECD in the cell.

Fragmentation capabilities in mass spectrometry allow characterisation and identification of protein/peptides PTMs, such as phosphorylation,[40] glycosylation,[41] carboxymethylation,[42] among others.[43–46] In order to elucidate protein/peptide sequence and localise PTMs a common nomenclature is adopted,[47,48] as shown in figure 1.10.

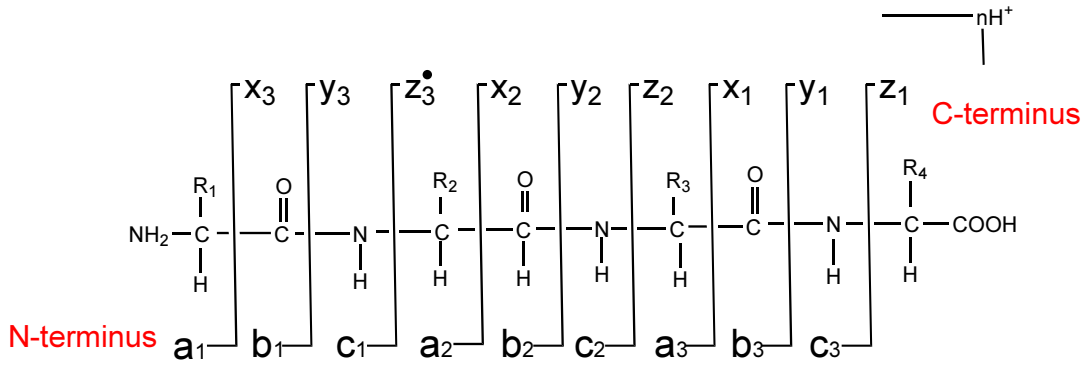

Figure 1.10: Example of Roepstorff and Biemann's nomenclature for proteins/peptides.

Once the fragmentation pattern is obtained the identity of the amino acid residue is then obtained from the mass difference of the same type of fragment ion series (c, b, and a fragment ions, from the $N-$terminus; or $z^{\bullet}$, y or x fragment ions, from the $C-$terminus), which must have the same charge. This approach allows one to determine the complete peptide/protein structure, which can be performed manually or by database searching. However, some types of modifications added to the protein are not included in the databases requiring a manual identification like the modifications studied in this work.

Interestingly, some isomeric amino acid residues like leucine and isoleucine are difficult to elucidate, unless either high energy collisionally activated dissociation (see section 1.5.1) or hot-electron capture dissociation (HECD, see section 2.4.1) are performed. Other amino acid residues are easily identifiable by low energy collisionally activated

dissociation, technique also labeled as CAD.[49] It is convenient to clarify that, regardless of the level of energy employed in the fragmentation, the technique is just known as CAD.[50] Even more important is to note that such a fragmentation technique is also, often, referred to as collision induced dissociation (CID).[9,51] Nevertheless, for simplicity, it has been deemed convenient to employ, in the this thesis, a single acronym to refer to such a technique, being CAD the label chosen for the present work. This collisionally activated dissociation technique, or CAD, is described in the following section 1.5.1.

1.5.1 Collisionally activated dissociation (CAD)/Collision induced dissociation (CID)

Collisionally Activated Dissociation is the most commonly employed fragmentation technique used for the analysis of a variety of samples. This technique is based in the collision of neutral gas molecules with a selected precursor ion.[9] Argon gas is used in the CAD experiments performed in this work, although other gases can also be employed. However, in order for the collisions to cause bond cleavage, the kinetic energy of the precursor ion needs to be raised to generate fragment ions. The kinetic energy of the precursor ion can vary from $1\,eV$ to $> 1000\,eV$. Thus, CAD can be distiguished as high-energy CAD and low-energy CAD.[13]

High-energy CAD is performed by a single collision of high kinetic energy ($> 1000\,eV$) precursor ions with neutral gas molecules. The high kinetic energy of the ions is induced by accelerating them in TOF-TOF and sector instruments. This type of fragmentation produces b/y, w, and d fragment ions in peptides and proteins (see figure 1.10). w and d fragment ions are useful to differentiate leucine and isoleucine amino acid residues, but also increase the complexity of the spectrum making difficult its interpretation.

Low energy-CAD, used in this study, is characterised by the low-energy used for fragmentation between (1 to $100\,eV$), where multiple collisions take place. A fraction of this translational energy is converted into internal energy and the ion reaches an excited state (activated ion).[52] The slow-heating mode ($\sim 10^{-2}s$) in which the energy is transferred into the ion induces fast energy redistribution (among the degrees of freedom of the molecule) and the precursor ion is then vibrationally excited.[53] This energy redistribution is fast compared with the dissociation time, and cleavage of the bond between the carbonyl carbon and the nitrogen atom is produced. The fragmentation pattern is characterised by b/y fragment ions and labile side chain losses from the precursor ion and from the fragment ions. The loss of these labile side chains make it difficult to directly identify the location of labile PTMs. Nonetheless, such a technique is widely used in protein/peptide analysis.[54–58]

The proposed reaction for collisionally activated dissociation at high and low energy can be represented as equation (1.23).

$$\mathrm{q} + [\mathrm{M} + \mathrm{nH}]^{\mathrm{n}+} + \mathrm{Ar} \longrightarrow \left([\mathrm{M} + \mathrm{nH}]^{\mathrm{n}+}\right)^{*} \longrightarrow \mathrm{fragments} + \mathrm{Q} \tag{1.23}$$

where, M represents the protein/peptide; q is the amount of translational energy converted into internal energy; and Q is the kinetic energy liberated in the fragmentation.[59] q is calculated from the conservation laws in a inelastic collision, where the motion of the system is described by the separation of the particles relative to the centre of mass (CM) of the system (equation (1.24)).[59,60]

$$q = \frac{1}{2}\left(\frac{Mm}{M+m}\right)v_i^2 - \frac{1}{2}\left(\frac{Mm}{M+m}\right)v_f^2 \tag{1.24}$$

Where, M is the mass of the parent ion; m is the mass of the target gas; v_i is the initial

relative velocity in the CM frame defined by the difference of the velocity of the parent ion, v_1, and the velocity of the target gas, v_2; v_f is the final relative velocity in the CM frame. It can be deduced from equation (1.24) that q has a maximum value when v_f is equal to zero (both particles travel together after a collision, which only happens in an adduction reaction).

Additionally,considering that the centre of mass collision energy, E_{CM} is given by equation (1.25)

$$E_{CM} = \left(\frac{m}{m+M}\right) \Delta E_{LAB} \tag{1.25}$$

where, E_{LAB} is the translational energy change of the ion in the laboratory frame of reference, and can be determined as is shown in equation (1.26)

$$E_{LAB} = q + \Delta E_m \tag{1.26}$$

where, ΔE_m is the kinetic energy change of the target gas. Assuming that $\Delta E_m = 0$ then, $E_{LAB} = q$ and that $v_f = 0$, the centre of mass collision energy, E_{CM} is dependant on the reduced mass and the initial kinetic energy of the ion and the gas target.

Mobile proton model and b fragments ions structure

A model has been proposed to explain the prevalent formation of b/y fragment ions in protonated protein/peptides during low-energy CAD.[61] This model is based on the mobility of the proton attached at the initial protonation site and then transferred to the amide backbone functionality. This mechanism is referred to as the mobile proton[62] and the proposed reaction mechanism is illustrated in figure 1.11 indicating protonation

at the amide N-terminus. However, protonation at the amide nitrogen atom is less probable than protonation at the carbonyl oxygen because of the low-gas phase basicity of this amide nitrogen atom. Nonetheless, the debate is still open whether the same fragmentation occurs from $O-$protonated and/or $N-$ protonated peptide/proteins.[62]

In figure 1.11 the protonation at the N-terminus causes an inductive cleavage[12] of the C−N bond, which subsequently generates an acylium ion. It has been argued that the acylium ion is not the structure of the b fragment ions, particularly b_2 fragment ions. Instead it is believed that the oxazolone ion is the structure of the b_2 fragment ions. One of the main arguments that support the theory about the formation of the oxazolone ion is the absence of the b_1 fragment ion in the CAD spectra of any protonated protein/peptide. If the b_2 fragment ions would have the acylium ion structure, then b_1 fragments ions will be present in the CAD spectra. The absence of the b_1 fragment ion is then explained by the oxazolone ion formation, which requires at least two amino acids to contribute towards its formation, as shown in figure 1.11.

Another proposed structure for the b_2 fragment ion, in peptides containing aliphatic or simple aromatic amino acid residues, is the structure known as diketopiperazine.[63] However, Bythell, B. J and Somogyi, A. and Paizs, B.[63] reported that the oxazolone has a low threshold energy compared to the diketopiperazine, further supporting the hypothesis about oxazolone ion formation in CAD of aliphatic or simple aromatic amino acid residues. Other experiments in histidine and lysine containing peptides reported that b_2 fragment ion structure can be both a diketopiperazine and an oxazolone ion, where the accessibility of an amino nitrogen is essential for diketopiperazine ion formation,[64] as shown in figure 1.12.

Interestingly, it has been suggested that b_5 fragment ion, under CAD conditions, undergoes a cyclization-reopening mechanism.[65] The cyclization structure contains a mobile

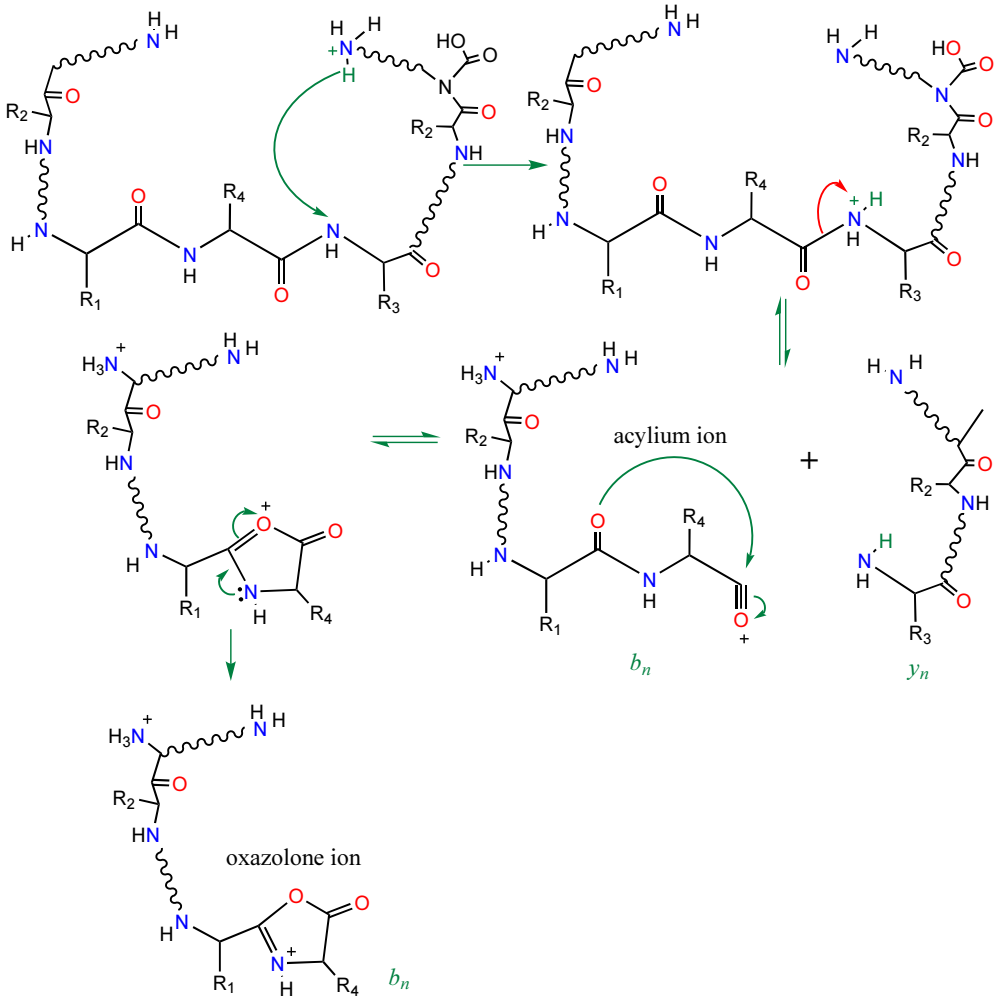

Figure 1.11: Proposed reaction mechanism for the mobile proton model. Figure adapted from Wysocki, V. H. and Tsaprailis, G. and Smith, L. L. and Breci, L. A.[62]

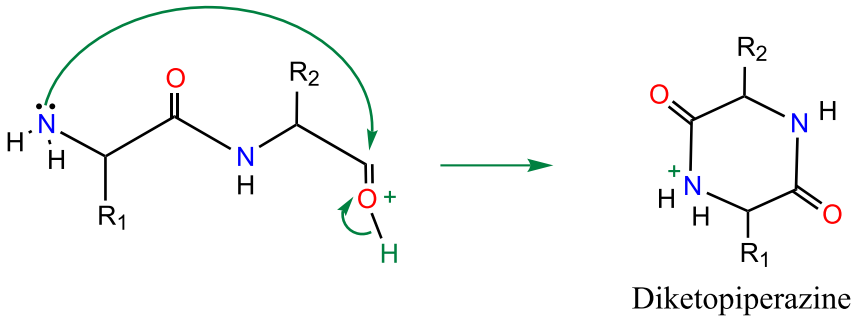

Figure 1.12: Proposed reaction mechanism for the formation of diketopiperazine ion in CAD.

proton allowing changes in the protonation site, which could cause reopening of the ring at different amide bonds. Consequently, the original sequence of the peptide gets

scrambled generating a "non-direct sequence" as shown in figure 1.13. The different fragmentation channels in low-energy CAD have been comprehensively reviewed by Paizs and Suhai.[66]

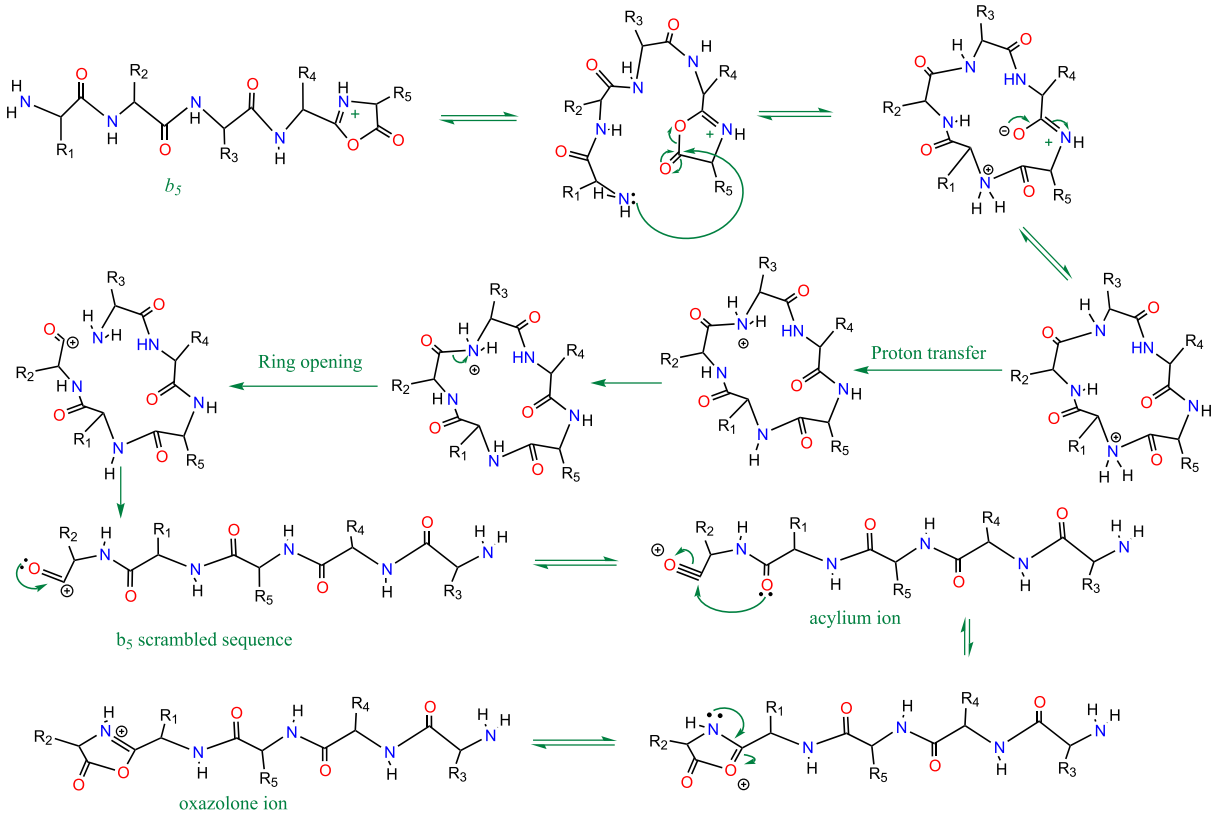

Figure 1.13: Proposed reaction mechanism for the cyclization-reopening mechanism in CAD. Figure adapted from Bleiholder et. al.[65]

1.5.2 Infrared multiphoton dissociation (IRMPD)

In this study, IRMPD was performed by using a low-power, continuous-wave CO_2 laser, which has a wavelength of $\sim$ $10.6\,\mu m$. Low energy IRMPD is dependant on laser intensity, which is the amount of power deposited area (cm^2).[53] This implies that the laser power and irradiance time needs to be adjusted in order to fragment the molecule. Multiple photon absorption (resonant or non-resonant) generates vibrational excitation of the protein/peptide. The vibrational excitation is reached when the vibrational energy

level matches the energy of the laser and incoherent absorption of multiple photos occurs. Thus, similarly to CAD, the energy is rapidly redistributed into the degrees of freedom of the protein/peptide.

IRMPD likewise to low-energy CAD generates b/y fragment ions, but IRMPD offer far greater control on the extent of the dissociation and the production of secondary fragment ions. The proposed reaction for IRMPD can be represented as equation (1.27).

$$[\mathrm{M}+\mathrm{nH}]^{\mathrm{n}+} + n(h\,\nu) \longrightarrow \left([\mathrm{M}+\mathrm{nH}]^{\mathrm{n}+}\right)^{*} \longrightarrow b/y \tag{1.27}$$

where, M represents the protein/peptide; h is Planck's constant; and ν is the frequency.

IRMPD has been successfully applied in the fragmentation of phosphorylated peptides due to the chromophore nature of the phosphate ion, at $10.6\,\mu m$.[67] The IRMPD spectra of phosphorylated peptides IRMPD was reported to exhibit abundant low m/z ions compared to CAD.[68] IRMPD has also been used in the analysis of sulfonated peptides[69] and in the study of glycosylation.[70,71] The use of IRMPD in derivatized species, particularly derivatized oligosaccharides with boronic acid, was reported to enhance photon absorption.[72] IRMPD has found a wide range of application as a tool to disrupt non-covalent interaction in protein/peptides,[73–76] enhancing ECD *cleavage* coverage (see sections 2.1.2, 2.4.1).

1.5.3 Electron capture dissociation (ECD)

ECD is another fragmentation technique employed in a variety of analyses, such as: localization of labile PTMs;[41–43,77–81] peptides sequencing;[82,83] structure elucidation of small molecules;[84,85] and, analysis of oligomers and cyclic peptides,[86,87] among

many others. ECD is based in the interaction of low energy electrons ($\sim 0.2\,eV$) with protonated species, causing charge neutralisation and generating $c/z^{\bullet}$ fragment ions, as is described, in detail, in chapter 2.

It is clear, then, that fragmentation (ECD and CAD) in mass spectrometry is useful to generate amino acid sequences of proteins/peptides. However, sometimes it is not possible to elucidate the protein sequence due to the absence of fragment ions during MS/MS experiments.[2] This is attributed to the secondary and tertiary conformation of the proteins. Thus, in order to surpass this limitation, a bottom-up protein approach can be used, which is discussed in the following section. The top-down analysis of proteins was also used in this work and is presented in chapter 7.

1.6 Top-down and bottom-up analysis of proteins in mass spectrometry

In this study two types of analysis (top-down and bottom-up) of proteins were employed to study the binding site of glyoxal to human serum albumin (HSA). The bottom-up analysis, used for HSA sequencing, is based on performing an enzymatic digestion of the protein prior to mass spectrometry analysis.[13] In contrast, sequencing of an intact protein by mass spectrometry applying MS/MS methods is referred to as the top-down approach.[88]

The bottom-up analysis of HSA required various steps:

- Determination of the molecular mass of the HSA was made using MALDI or ESI;[13] as is shown in chapter 7.

[2] It should be noted that, in any case, absence of fragment ions in proteins can be overcome by employing additional ion activation methods in conjunction with ECD (see section 2.4.1).

- Once the molecular mass is approximately known, it was necessary to denature the protein in order to break the non-covalent interactions, which made the secondary and tertiary structures of the protein and to expose the disulphide bonds within the protein. Denaturation was performed by:
  - by chemicals, in particular guanidine hydrochloride was used in this study.
  - by increasing the temperature until $60\,^{\circ}C$, which was the temperature where HSA was denaturated.
  - by precipitation with solvents, MeOH/chloroform was employed in this work.
- Reduction (with Dithiothreitol $15\,mM$, or DTT) and alkylation (with iodoacetamide $15\,mM$) of the disulphide bonds is performed after denaturation, to allow full access of the enzyme.
- Once the protein was purified from all the chemicals employed (DTT, it is ready to perform enzymatic digestion. The enzyme used in this work was trypsin, which cleaves on the $C-$terminal side of lysine (Lys or K) and arginine (Arg or R). Different ratios of $enzyme : protein$ were employed in this work, ranging from $1:20$ to $1:100$ (see chapter 7).
- Finally, the resulting peptides were analysed by MS/MS.

It is noteworthy that the bottom-up and the top-down approaches can be used as complementary techniques, particularly when identifying post-translational modifications like glycation.

1.6.1 Glycation

The Maillard reaction, also known as browning reaction,[89] has been widely studied in heated food because of its importance in the production of flavored and coloured compounds.[90?] In the human body this reaction is known as glycation,[91] which is important when a subject develops hyperglycaemia, a condition that favors the reaction of glucose with protein/peptides. One of such reactions, for example, is that of glucose with haemoglobin, whose product is the haemoglobin variant HbA_{1c}, known to be a marker in the development of diabetes.[92]

During diabetes, glucose autoxidation[93] and other metabolic process[91,94–96] generate reactive $\alpha-$dicarbonyl compounds ($\alpha-$oxoaldehydes), such as glyoxal, methylglyoxal and $3-$deoxyglucosone. Glucose and these glucose derivatives react non-enzymatically in a complex process of sequential and parallel reactions[97] with amino, guanidino, and thiol groups of proteins and peptides.[98–100] The variety of reaction pathways with protein/peptides, leads to a many different glycation products, which are generally referred to as advanced glycation end-products (AGEs). One of these AGEs is the compound known as Amadori product, formed from the reaction of glucose with amino groups of protein/peptides, as shown in scheme 1.1. The degradation of the Amadori product generates glyoxal, as is also illustrated in scheme 1.1.

The concentration of AGEs and their steady-state presence in the human body is linked to the development of diabetic complications like retinopathy, neuropathy, high risk of cardiovascular disease, and stroke.[101–105] For instance, among the variety of AGEs formed during hyperglycaemia, the glyoxal-derived AGE known as creatinine (see scheme 1.2f)[106] is considered a marker in the pathophysiology of uremia.[107] Given the apparently high relevance of these AGEs in a number of human pathologies, it is not surprising to find a substantial amount of research aiming to determine how the

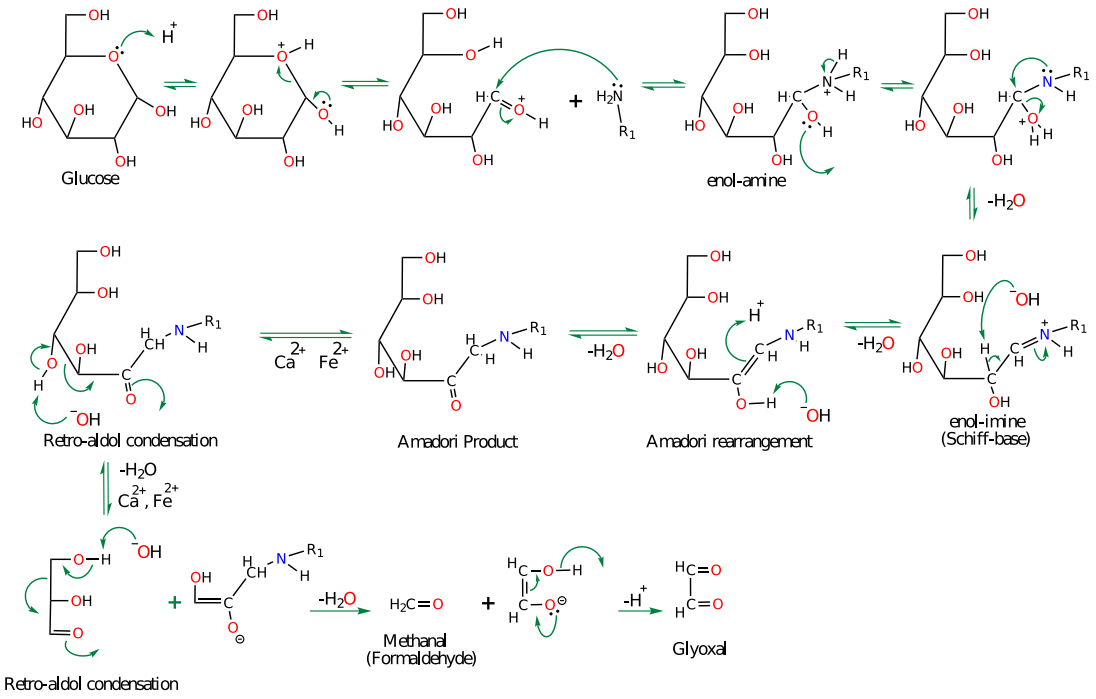

Scheme 1.1: Proposed reaction mechanism for the formation of glucose derived-AGEs (Amadori product) and proposed degradation of the Amadori product to form glyoxal.

precursors of AGEs modify protein and peptides. Such research has also contributed to determine types and structures of AGEs.[108–111] Nonetheless, multiple factors in sample preparation and detection methods make it difficult to compare the types of AGEs observed in protein/peptides.[112] For instance, as an example of the variety of types of AGEs reported in the literature, it is worth mentioning a few interesting cases:

- AGEs quantitatively formed from methylglyoxal and glyoxal at the arginine residue are:
  - The arginine residue derived hydroimidazolone (N^{δ}-(5-hydro-5-methyl- 4-imidazolon-2-yl)ornithine (MG-H1));[111,113]
  - $N^{\omega} - carboxymethyl - arginine$ (CMA);[111]
  - 4,5-dihydroxyimidazolidine;[114]

– 2-amino-3H-5-dihydro-imidazol-4-one (G-H3).[111,115]

Some of these compounds were also detected in this study and are presented in scheme 1.2.

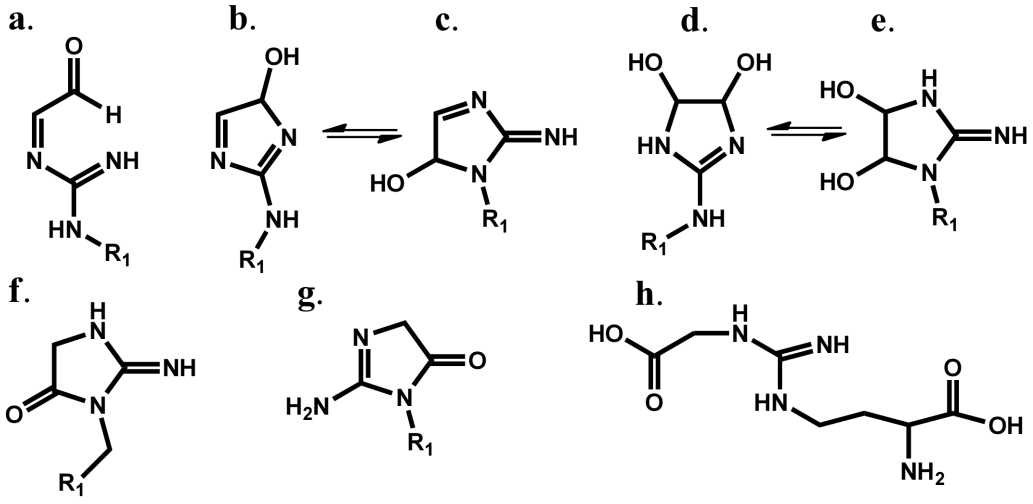

Scheme 1.2: Glyoxal-derived AGE strucutres. **a.** Schiff base at the guanidine group of arginine; **b.** 3-hydroxyimidazole (left). **c.** 2-imine-5-hydroxyimidazoline (right); **d.** 4,5-dihydroxyimidazoline (left); **e.** 2-imine-4,5-dihydroxyimidazolidine (right); **f.** 2-imine- imidazolidinone (creatinine side chain); **g.** 2-amino-3H-5-dihydro-imidazol-4-one (G-H3); **h.** N^{ω}-carboxymethyl-arginine (CMA).

- Lysine residues modified AGEs are:
  - N^{ϵ}-carboxymethyl-lysine (CML).[113,116–119] CML has been reported in both the reaction of methylglyoxal with proteins and in the oxidative degradation of $N-$fructosyl-lysine residues in proteins glycated by glucose;[92,115,118]
  - Lysine residues modified in proteins has been reported with glyoxal in human serum albumin (HSA), although most of the glyoxal glycation was reported at the arginine residues;[120]
  - Glyoxal-hemiaminal;[121]

  - Pyrazines[122] formed by the reaction of glyoxal with lysine residues.

- $N-$terminus modified AGE was reported as $N-$terminal pyrazinones.[123]

- AGE crosslinked species such as:

  - The glyoxal-lysine dimer, GOLD (6-{1-[(5S)-5-ammonio-6-oxido- 6-oxohexyl] imidazolium- 3-yl} -L-norleucinate),[124,125] formed by reaction of glyoxal with two lysine residues. However, GOLD is believed to be formed during strong acid and alkaline hydrolysis;[126]

  - GODIC (N_6-(2-{[(4S)-4-ammonio- 5-oxido-5-oxopentyl]amino}- 3,5-dihydro-4H-imidazol-4-yli-dene)-L-lysinate),[127,128] formed by the reaction of glyoxal with one lysine residue and one arginine residue;

  - DOGDIC (N^6-{2-{[(4S)-4-ammonio-5-oxido- 5-oxopentyl]amino}- 5-[(2S,3R)-2,3,4-trihydroxybutyl]- 3,5-dihydro-4H-imidazol-4-ylidene}-L-lysinate) is a crosslinking product derived from 3-deoxyglucosone;[128]

  - Pentosidine and glucosepan are crosslinked species formed between lysine, arginine and a reducing sugar.[129–131]

The crosslinking ability of the reducing sugars and its decomposition products (α-dicarbonyl compounds) cause damage to protein networks.[132] Other effects, for example in long-lived proteins like collagen, is the decrease in flexibility, whereas in short-lived proteins like HSA, causes insolubility.[133]

Given the variety of products that can be obtained during the glycation reaction, and the significant number of detection methods used to identify them, it is not difficult to realize that confusion about the types of AGEs observed $in-vivo$ and $in-vitro$ easily arises. Moreover, the lack of an standard method for assignment of glycation brings

about extensive literature of different types of AGEs.

In any case, one method for detection of dicarbonyl derived AGEs in proteins ($in-vivo$ and $in-vitro$) is stable isotope dilution analysis with tandem mass spectrometry. This method requires exhaustive enzymatic hydrolysis of peptide and protein substrates.[113] Mass spectrometry (MS) has also been used to characterize glycation products within proteins/peptides.[108,134–136] Moreover, MS coupled with fragmentation techniques such as collisionally activated dissociation (CAD), electron capture dissociation (ECD) and electron transfer dissociation (ETD),[137] has also been applied to assign the site of glycation modifications.[111,138–140]

1.7 Thesis outline and structure

In the present study, mass spectrometry (MS), coupled with CAD and ECD, has been used to characterize glycation products generated by the glyoxal with peptides/proteins. In particular, the main focus of this work was to assign the binding sites of glyoxal within polypeptides. A summary of the general structure and organization of this thesis is presented below,

Chapter 2 Principles of electron capture dissociation in proteins/peptides.

Chapter 3 Assignment of binding sites glyoxal-derived advanced glycation end-products for substance P.

Chapter 4 Tandem mass spectrometry for the study of glyoxal- derived advanced glycation end-products (AGEs) in peptides.

Chapter 5 Tandem mass spectrometry for the study of an unusual glyoxal- derived advanced glycation end-product.

Chapter 6 Study of an unexpected crosslinking and diglycation as advanced glycation end-products by tandem mass spectrometry.

Chapter 7 Summary of results and ongoing projects.

Chapter 8 Conclusions and future work. In this final chapter, general conclusions are presented, elicited from the different results in the thesis, and ideas about interesting future work are suggested.

2 Principles of electron capture dissociation in protein/peptides

2.1 Introduction

Electron capture dissociation (ECD) has been widely used, in conjunction with collisionally activated dissociation (CAD), to elucidate protein and peptide structure. The widespread use of ECD is based on the extensive $cleavage$ coverage giving complementary fragmentation to CAD and the retention of labile post-translational modifications (PTMs). This capability allows the location of labile PTM binding sites on proteins/peptides, which would be lost during other fragmentation techniques such as CAD and infrared multiphoton dissociation (IRMPD). ECD cleaves the $N - C\alpha$ backbone bond in the protein/peptide backbone chain. This chapter addresses some of the aspects of ECD that have been studied in the decade since its first development. Initially addressing the terminology employed; followed by some historical aspects about how ECD became particularly applied to labile PTMs binding site identification in proteomics. A discussion about common side chain losses usually observed in the ECD spectra along with the usual fragmentation pattern ($c/z^{\bullet}$) is covered. A summary about some related methods, such as electron impact excitation of ions from organics (EIEIO), hot electron

capture dissociation (HECD), electron induced dissociation (EID), Electron Excitation Dissociation (EED), electron detachment dissociation (EDD), activated ion electron capture dissociation (AI-ECD), electron capture induced dissociation (ECID), among others, are included to discuss the additional capabilities of electron reactions. The chapter includes a discussion about the ECD fragmentation mechanism on the $N - C\alpha$ bond, along with radical-directed dissociations, which have been matter of enthusiastic debate during the last decade. Finally, the chapter concludes with a discussion about ECD non-ergodic behaviour. This chapter does not intend to address the questions about how the electron is captured and the energy released upon electron capture. Moreover, ECD applications in DNA, RNA, oligomers, histones, metal-protein interactions, synthetic polymer cations, and the disulphide bond cleavage mechanism are outside the scope of the present chapter.

2.1.1 Terminology

ECD is considered the reaction of multiply-charged ions, $[M+nH]^{n+}$, with M representing the molecule), with low energy electrons ($\sim 0.2\,eV$).[8] This reaction leads to the cleavage of the protein/peptide backbone at the $N - C\alpha$ bond, thus generating low abundance c and $z^{\bullet}$ fragment ions. Fragments are labelled using the Roepstorff- Biemann nomenclature.[47,48] In addition to the cleaved polypeptide chain, high abundance of charge-reduced radical species, represented by $[M + nH]^{(n-1)1+\bullet}$ and hydrogen deficient, even electron charge-reduced species or $[M + (n-1)H]^{(n-1)1+}$ are also generated in ECD. The charge-reduced radical species has non-covalent bonds that hold the cleaved polypeptide main-chain fragments together temporarily,[36,141–143] as is illustrated in structure **I** on figure 2.1.

Figure 2.1 shows the proposed chemical structures of the charge-reduced species, the c

fragment ion, and $z^{\bullet}$ radical fragment ion. The hydrogen bonding on the charge-reduced species is depicted only with the purpose of illustration and is based on structures proposed by Turecek, F. and Syrstad, E. A. and Seymour, J. L. and Chen, X. and Yao, C.[144] Moreover, the c fragment ion can be represented as an enol-imine (Structure **IIb** in figure 2.1), although the amide moiety (Structure **IIa**) is thermodynamically more stable.[43] In contrast, $z^{\bullet}$ radical fragment ions are usually represented as $\alpha-$carbon radicals, which are stable in the gas phase.[145–147]

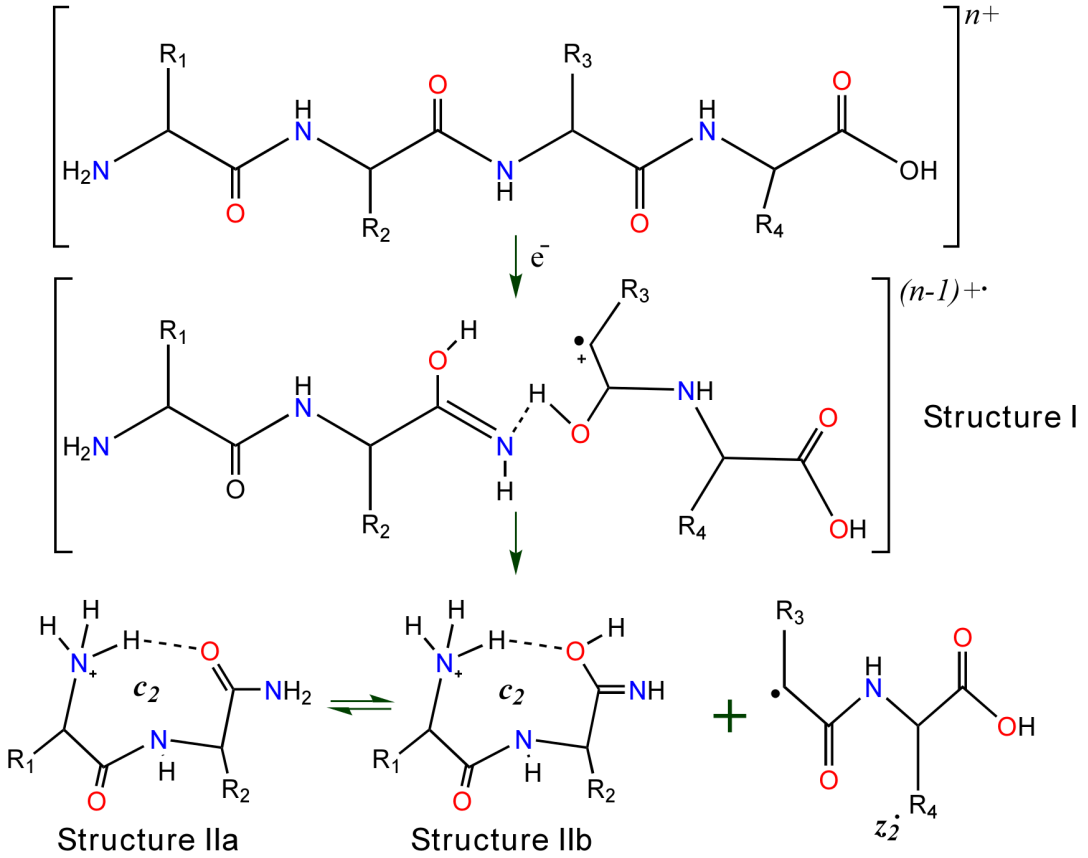

Figure 2.1: Schematic representation of ECD fragmentation at position 2 towards the $N-$terminus. The position of the hydrogen bonds can not be ascertained unless calculations of the dissociation and transition state energies of the radical cation and c_2 fragment ion are performed. Structure **IIa** = c_2 fragment enol-imine; Structure **IIb** = c_2 fragment amide. Note that the position of the charges is symbolically representing the point of largest charge density at the instant of electron capture. Illustration based on structures proposed by Turecek, F. and Syrstad, E. A. and Seymour, J. L. and Chen, X. and Yao, C.[144]

It should be noted that the presence of the $[M + (n-1)H]^{(n-1)1+}$ is caused by the loss of the radical $H^{\bullet}$, which is a predominant, non-informative channel during ECD. As from the charge-reduced species, the reaction can be represented by equation (2.1).[148]

$$[M + nH]^{n+} + e^{-} \_> \left([M + nH]^{(n-1)+\bullet}\right)^{*} \longrightarrow c_{(fragment\ ion)} + z^{\bullet}_{(radical\ fragment\ ion)} \quad (2.1)$$

Electron capture dissociation also produces $c^{\bullet}$ ($c^{\bullet} = c-H$, with $H = 1.007825\,Da$), and z fragment ions ($z = z^{\bullet} + H$) simultaneously with the $c/z^{\bullet}$ species.[149] Abundant z fragment ions are believed to be formed by hydrogen abstraction from their counterpart.[142] Another type of fragment ions produced in ECD are called non-standard ECD fragment ions,[150] such as b/y, $a/a^{\bullet}$ ($a^{\bullet} = a-H$), w, and u. For instance, the presence of b fragment ions is a function of the type of charge-carrying amino acid and the peptide structure.[151–153]

Cooper, H. J.[151] demonstrated that the b fragment ions observed in ECD are not produced by off-resonance excitation during the precursor ion isolation or black body infrared irradiation (BIRD) from the electron emitting-cathode. The author proved the absence of off-resonant excitation by performing isolation of the ions in a quadrupole instead of in the ICR cell. Additionally, by changing the grid potential to $-200\,V$ (instead of $+50\,V$ during the ECD experiment) the author prevented the electrons from entering the ICR cell and proved that b ions in ECD are not formed by BIRD from the cathode. Moreover, b ion generation was proposed to be independent of the peptide basicity, but dependant on the electron capture site and local structural features.[151,152] The formation of b fragment ions was not attributed to secondary fragmentation from the c fragment ions,[151] instead they probably follow a different fragmentation pathway (mobile proton model[62]) from the charge-reduced hydrogen

deficient species $[M + (n-1)H]^{(n-1)+}$.

In regard to the presence of $a/a^{\bullet}$ fragment ions in ECD, other authors attributed its presence to the loss of the CO group from the b fragment ions.[154] Moreover, the presence of $a^{\bullet}$ fragment ions could be derived via an unobserved $b^{\bullet}$ fragment ion.

Secondary fragments[150] like w and u fragment ions, are apparently derived from partial side chain losses of the $z^{\bullet}$ radical species. Other side chain losses observed in the ECD spectra, which can be used as diagnostic ions, are presented in section 2.3.

2.1.2 ECD efficiency vs. cleavage coverage

Reactions with low energy electrons in the ion cyclotron resonance cell leads to the production of low abundance fragment ions, which are then detected in the mass spectrometer. The low abundance of the fragment ions is attributed to low fragmentation efficiency. Efficiency is quantitatively determined by the ratio of output to input, or in other words, the ratio of the total abundance of all the fragment ions *after* fragmentation and the abundance of the precursor ion *before* fragmentation. This definition has been applied to measure the fragmentation efficiency of, for example, CAD.

Interestingly, the way that ECD efficiency has been calculated has varied in the literature through the last decade. In order to understand why there are different ways to calculate ECD efficiency it is necessary to recapitulate about the observed species in the ECD spectra and their provenance during ECD. First of all, the charge-reduced radical species ($[M + nH]^{(n-1)+\bullet}$) is produced by the capture of an electron on the precursor ion. Accordingly, the ratio of the intensity of the $[M+nH]^{(n-1)+\bullet}$ species to the intensity of the precursor ion before the experiment is a measure of the $capture$ efficiency. Second, the fragment ions (*e.g.* $c/z^{\bullet}$, $c^{\bullet}/z$, and a-type fragment ions) observed in the ECD spectra are

formed from the charge-reduced radical species. Therefore, the ratio of the sum of all the fragment ions to the intensity of the of $[\mathrm{M}+\mathrm{nH}]^{(\mathrm{n}-1)+\bullet}$ species before fragmentation is a measure of the fragmentation efficiency. Third, a predominant fragmentation channel is the non-informative loss of hydrogen radical forming the $[\mathrm{M}+(\mathrm{n}-1)\mathrm{H}]^{(\mathrm{n}-1)+}$, which can further fragment generating, for instance, b-type fragment ions. Therefore, the ratio of the sum of particular fragment ions, such as b-type fragment ions, to the intensity of the $[\mathrm{M}+(\mathrm{n}-1)\mathrm{H}]^{(\mathrm{n}-1)+}$ is defined as branching ratio. However, these definitions are not often used in the literature; instead, other definitions have been adopted, which are summarised below.

Initially, capture efficiency was performed summing the intensity of all isotopologues of the fragment ions and then dividing by the charge state of the ions,[43] giving efficiencies of around $80 \pm 15\%$. On the other hand, a different concept that has been introduced in order to calculate ECD efficiency is by calculating the proportion of how much of the precursor ion turns into fragment ions, and which has also been called *conversion* efficiency.[155] In particular, this type of efficiency is calculated as the ratio of the sum of the abundances of the observed fragment ions to the abundance of the precursor ion before fragmentation.[156,157]

The fragmentation efficiency in ECD has been defined as the sum of the intensities of the fragment ions (excluding the precursor ion and the charge-reduced species) divided by the total ion abundance in the ECD spectrum.[158] Additionally, Zubarev *et al.*[157] introduced the concept of *effective* efficiency of ECD per scan, which is calculated by summing the intensity of the product ions and the dividing such sum by the intensity of the precursor ion. Equation (2.2) shows another approach to calculate ECD efficiency by considering the charge state (n) of the precursor ion, with $n > 2$.[159]

$$E_{frag-ECD} = \left[\frac{\sum fragment\ ion\ abundances - abundance\ [\mathrm{M+nH}]^{n+}}{Precursor\ ion\ abundance}\right]\left(\frac{n}{n-1}\right) \tag{2.2}$$

These different methods of calculating ECD efficiency have made it difficult to compare published results, particularly when other concepts were also introduced. For instance, the concept of fragmentation efficiency has also been used as a measure of percentage of inter-residue backbone bond cleaved.[160,161] This concept is herein defined as *cleavage coverage*. It is noteworthy that the concept of *sequence* coverage, used throughout the protein mass spectrometry literature, can be misleading given that it is also used to define the fraction of peptides observed after enzymatic digestion.

Nevertheless, in spite of the variety of calculations for the ECD efficiency, a pattern emerges. In terms of *cleavage* coverage, ECD is more efficient than CAD, but in terms of *fragmentation* and *conversion* efficiency CAD can achieve higher values than ECD. However, the fragmentation efficiency of ECD can be improved by adjusting or modifying instrumental parameters. A discussion regarding such an improvement by adjustment of instrumental parameters can be found elsewhere.[156,159,162–164]

Finally, it is convenient to introduce the concept of the probability for dissociation in ECD, which is calculated by equation (2.3),[165] as well as the concept of probability for charged species to capture an electron during a defined time, which was introduced by Mormann et.al.[166] and it is shown in equation (2.4).

$$E_{pro-Disso} = \left[\frac{\sum (Intensity\ of\ ECD\ fragment\ ions)}{\sum (Intensity\ of\ ECD\ fragment\ ions) + Reduced\ intensity\ of\ the\ precursor\ ion}\right] \tag{2.3}$$

$$E_{eff} = \left[\frac{\sum (Intensity\ of\ ECD\ fragment\ ions) + Reduced\ intensity\ of\ the\ precursor\ ion}{\sum (Intensity\ of\ ECD\ fragment\ ions) + Reduced\ intensity\ of\ the\ precursor\ ion + Intensity\ of\ the\ precursor\ ion} \right] \tag{2.4}$$

In this work, where it is possible, clarity about all the different interpretations of ECD efficiency is made. Furthermore, in order to bring about some degree of contextualisation, a brief review about the historical aspects of ECD during its first year of existence is presented below.

2.2 Historical aspects

Fragmentation of small gaseous cations by electrons ($3 - 9\,eV$) in a Fourier transform ion cyclotron resonance mass spectrometer was developed in 1976.[167] Later on this technique was called electron impact excitation of ions from organics (EIEIO).[168] The dissociation produced a fragment cation and a neutral species, similar to those observed in CAD. This fragmentation pattern was attributed to either the relatively high energy of the electrons ($> 3\,eV$) or to the form in which this energy is redistributed in the molecule. EIEIO was later applied to bigger molecules like Gramicidin S in the ICR cell, using simultaneously laser and $70\,eV$ electron pulse to induce ionization of the peptide.[169] Almost twenty years later a modification of this technique was introduced using multiply charged protein ions interacting with low energy electrons ($\sim 0.2\,eV$), which it is referred to as electron capture dissociation (ECD).[8] This development was made possible by the use of ESI, as a sample introduction method for large biomolecules into the mass spectrometer.[22]

Zubarev *et al.*[8] attempted to reproduce previously reported c and z-type fragment ions

produced upon $193\,nm$ ($6.4\,eV$) dissociation. These ions were documented for masses between $2.8\,kDa$ and $8.6\,kDa$, although b/y fragment ions were observed for masses below $2.8\,kDa$.[170] Zubarev and co-workers[8] believed that electrons, and not photons, might be responsible for the observed c/z fragment ions. Therefore, they decided to employ a heated filament electron gun to produce electrons. Subsequently, they found that one or more charges, on a multiprotonated protein cation, were neutralised by electron capture and consequently fragmentation produced $c/z^{\bullet}$ species (figure 2.1). They proposed a mechanism for ECD, which was based on the high proton affinity of protonated Arg, Lys, and His that capture the electron ($H^{\bullet}$). This mechanism is discussed in section 2.5.1.

Following the introduction of ECD,[8] Axelsson et. al.[171] performed ECD in the neuropeptide Substance P. In that work the authors were trying to increase the kinetic energy of the electrons by varying the filament voltage ($-2\,V$ to $-15\,V$). This study suggested that the electron kinetic energy distribution during electron emission has a low energy tail, which may increase the probability of electron capture and thus cause fragmentation. In their work, $c/z^{\bullet}$, z, and b/y fragment ion series were observed. The presence of b/y fragment ions was attributed to the high capillary-skimmer voltage employed ($30\,V$ to $160\,V$). The authors observed the charge-reduced species, thus verifying that ECD involved charge neutralisation before dissociation. They also observed that $N-$terminal side of proline does not fragment under ECD conditions because this would require the cleavage of two bonds. This early experiment demonstrated that the interpretation of ECD spectra was simpler than CAD spectra.

Cleavage coverage was also used for comparison in the early days of ECD. Tested in model peptides, it was demonstrated that ECD could dissociate more backbone bonds than CAD.[161] Kruger et. al.[161] had also noticed that one key limitation of ECD was that the precursor ion must be at least a doubly-charged species in order to observe

dissociation of the peptide. Abundant $c/z^{\bullet}$ fragment ion together with low abundance $c^{\bullet}/z$, $a^{\bullet}$, and y fragment ions were reported. The presence of those low abundance species lead the authors think that ECD in peptides was not as specific as ECD in proteins. The main reason being that Zubarev et. al.[8] reported that ECD in proteins only produced abundant $c/z^{\bullet}$ fragment ions.

In particular, the $c^{\bullet}$ and z fragment ions are now thought to be characterised by H-atom abstraction from the $z^{\bullet}$, and from the c species, respectively. One likely explanation for the relatively lack of observation of $c^{\bullet}$ fragment ions in proteins is that the initially formed $z^{\bullet}$ species can abstract a H-atom from anywhere in the molecule, and not necessarily from "across" the initially cleavage point. If a $z^{\bullet}$ species merely scrambles the radical position and does not abstract an H-atom from the complementary c species, no mass change is observed. Since proteins are bigger than peptides, the probability of this occurring increases, which could explain the non-observation of $c^{\bullet}$ species in ECD of proteins.[8]

2.2.1 Influence of neighbouring amino acids in ECD

The influence of neighbouring amino acids during ECD experiments in proteins and peptides was addressed by Kruger et. al.[172] They observed that the $C-$terminal side of tryptophan yields nine times more abundant fragment ions, although this cleavage nearly eliminates $c/z^{\bullet}$ type fragment ions from forming at the next two $C-$terminal amino acid residues. Furthermore, cysteine caused a reduction in the abundance of fragment ions formed from cleavages of one and two residues away in either direction. Additionally, they found that proline completely blocks $c/z^{\bullet}$ cleavage on its $N-$terminal side, because to cleave at this position requires cleavage of two bonds. This has been referred to as the *proline effect*. Proline also exhibits the least cleavage abundance of all

amino acids on its $C-$terminal side.

Interestingly enough, in a study conducted in 2003 by Cooper[150] revealed $C-C$ bond cleavage in the proline side chain of glycine rich peptides containing sarcosine. Additionally, Fung[173] revealed $N-$terminal cleavage of proline, indicating that the proline effect is not that cleavage of proline is 100% prohibited, but that it is less common than other cleavages. Finally, Kruger et. al.[172] observed that CAD and IRMPD are more affected by the type of the neighbouring amino acid than ECD.

2.2.2 Determining the binding site of post-translational modifications

A protein can be naturally modified, enzymatically or non-enzymatically, by covalent attachment of one or more molecules, or by intra- or inter-molecular linkages. The binding site of some labile post-translational modifications (PTMs) was difficult to detect by certain tandem mass spectrometry techniques (*e.g.* CAD and IRMPD), because they cause the loss of the labile modification. However, ECD demonstrated its capabilities to identify the binding site of labile PTMs right from the beginning of its development.[8] Some of those labile modifications are included here as part of the history of ECD during the first year of introduction.

Carboxylation and sulfation

Carboxylation in synthetic peptides containing $\gamma-$carboxyglutamic acid (Gla) residues were analysed by ECD and compared with CAD and IRMPD.[42] CAD and IRMPD resulted in loss of CO_2 from the modification causing decarboxylation. On the contrary, ECD retained the modification identifying the binding site at the glutamic acid moiety. Losses

from the charge-reduced radical species were reported.[42] For instance, loss of the $^{\bullet}CO_2H$ moiety ($41.998\,Da$) may be caused by direct electron capture at the modification site.

S-cysteine sulfation (addition of SO_3H) was also considered by Kelleher *et al.*[42] They performed CAD on a modified peptide and observed partially modified b fragment ions, which made it difficult to identify the binding site. On the contrary, ECD showed that the fragment ions retained the modification and only losses of H_2O and H_2SO_3 from the precursor ion were reported.

O-glycosylation

O-glycosylation involves the addition of a sugar chain on the hydroxyl oxygen on the side chain of either serine, threonine, or, less frequently, tyrosine. ECD was successfully applied to $O-$glycosylated peptides where $c$fragment ions with addition of the modification were observed.[10] Even-electron z fragment ions and loss of the modification from $z^{\bullet}$ radical fragment ions were attributed to some radical-site-initiated reactions. The authors also noticed that if there was an amino acid residue glycosylated next to a proline, inhibition of the fragmentation occurs on both sides of proline due to a steric impediment for the radical hydrogen to be captured by the carbonyl on the protein backbone. Additionally, they found b fragment ions, which they associated with the vibrational activation during isolation of the precursor ion. In contrast, CAD caused loss of the modification, which was attributed to cleavage of the glycosidic bond by a proton transfer reaction with a low activation barrier.

Disulfide bonds

Cysteine engages in disulfide bonds ($S-S$) providing stability to the tertiary protein structure. ECD cleaves the disulfide bonds,[174] despite the fact that this was clearly contradicting the contemporary theory of the ECD mechanism, i.e. the electron should be captured by the higher proton affinity sites.[8] This contradiction lies in the fact that proton affinity at the $S-S$ bond is low compared with other protein functional groups, particularly the charged lysine and arginine residues. Zubarev, R. A. and Kruger, N. A. and Fridriksson, E. K. and Lewis, M. A. and Horn, D. M. and Carpenter, B. K. and McLafferty, F. W.[174] attempted to clarify the idea of electron capture at the site of higher proton affinity by performing $ab\,initio$ calculations for hydrogen radical atom affinity of disulfide bonds. They found, for example, that the $H^{\bullet}$ atom affinity for CH_3SSCH_3 is greater than hydrogen radical atom affinity for amide species ($CH_3CONHCH_3$), and $H^{\bullet}$ affinity for 3-methylindole is greater than for disulfide bonds.

Based on those results, Zubarev, R. A. and Kruger, N. A. and Fridriksson, E. K. and Lewis, M. A. and Horn, D. M. and Carpenter, B. K. and McLafferty, F. W.[174] proposed that the electron is captured at the protonated site and the $H^{\bullet}$ is transferred to the site with high hydrogen radical affinity, which is the disulfide bond. This $H^{\bullet}$ migration would yield a hypervalent intermediate that should spontaneously cleave (figure 2.2). Hence, they concluded that $H^{\bullet}$ attachment seems to be independent of the intramolecular distance between the $H^{\bullet}$ radical generated and the other protein functionalities. This model is called the "hot hydrogen" model for ECD and is discussed in section 2.5.1. However, the "hot hydrogen" model is also argued to be not applicable to ECD in disulfide bonds, as reported in other literature.[175–179]

Additionally, changes in the ECD fragmentation pattern of cyclic peptides with one, two, and four $S-S$ bonds and non-cyclic peptides were reported depending on the

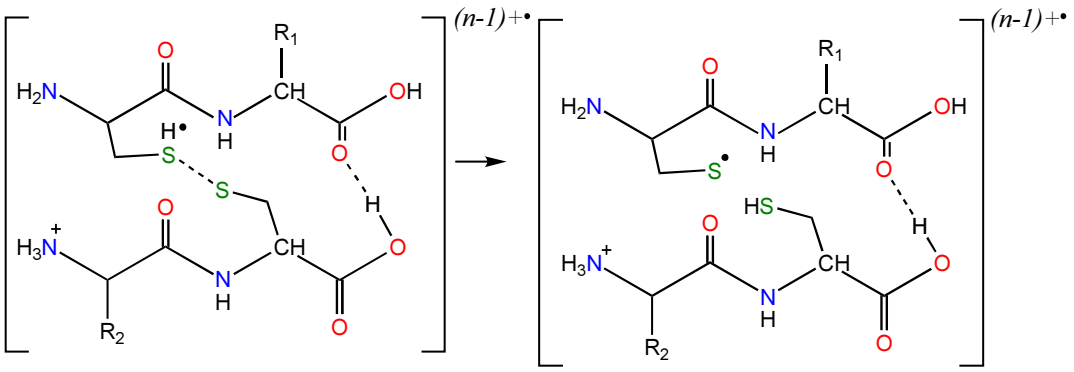

Figure 2.2: Schematic representation of the electron capture ($H^{\bullet}$) at disulfide bonds by the "hot hydrogen" model. Adapted from Zubarev, R. A. and Kruger, N. A. and Fridriksson, E. K. and Lewis, M. A. and Horn, D. M. and Carpenter, B. K. and McLafferty, F. W. [174]

number of $S-S$ bonds.[174] For cyclic peptides with one disulfide bond, Zubarev and co-workers observed that ECD cleaves at both the backbone $N-C\alpha$ position and $S-S$ bond, producing $c^{\bullet}$ and z (even electron species). However, for cyclic species with two $S-S$ bonds, ECD cleaves those two disulfide bonds, only transferring one hydrogen atom to the most highly charged species, as shown in figure 2.2. Further fragmentation (MS^3) of the observed products shows z fragment ions as well as $a^{\bullet}$, and y fragment ions. Interestingly, on Ribonuclease A, which contains four intrachain disulfide bonds, ECD did not show any fragment ions, only the charge-reduced radical species. Using gas phase deuterium exchange experiments, they were able to show that the charge-reduced species was a more "open" structure (more deuterium exchanged) than the equivalent precursor ion.[174]

Phosphorylation

Before ECD existed, phosphorylation was analysed by low-energy and high-energy CAD (see section 1.5.1).[180] Phosphorylation on tyrosine survives CAD fragmentation.

However, CAD of phosphorylated serine containing species with one or more phosphorylation sites becomes difficult due to poor *cleavage* coverage. ECD, favours backbone fragmentation without elimination of the modifying group and thus is particularly useful in successfully identifying phosphorylated sites in peptides.[181] Low intensity b and y fragment ions were also REPORTED.

Many more studies have been conducted to date using ECD with the aim to identify the site of post-translational modifications. As a result, many reviews about ECD in proteomics and the location of PTMs can be found in the literature.[7,79,182–184] This seems to prove that ECD is a powerful tool used to localise labile PTMs, mainly through observation of the major $c/z^{\bullet}$ fragment ion series. Additionally, other types of fragment ions and side chain losses have also been observed. Side chain losses in ECD could indicate the presence or absence of certain amino acids in the protein/peptide chain and thus can be used as structurally diagnostic peaks, which can ascertain the present of the associated amino acid.[185]

The following section is focused on summarising the side chain losses commonly observed in ECD spectra

2.3 Side chain losses

Kruger and co-workers[161] first reported additional small neutral losses from the charge-reduced radical species in ECD experiments. For example, losses of water, NH_3, and other side chain losses, which are presented in table 2.1. In some cases, side chain losses can constitute a major fragmentation pathway in ECD.[186] Studies of side chain losses in ECD spectra from ten peptides containing arginine, histidine, asparagine, glutamine, methionine and lysine were reported by Cooper et. al.[186] The authors found that some

particular side chain losses can indicate the presence of one particular amino acid in the peptide chain and thus it could be used as a structural diagnostic. Table 2.1 presents these side chain losses. Results from other different authors are also included.

Table 2.1: Side chain losses by ECD.

Amino acid in the peptide chain	**Losses**	**Mass (Da)**	**Comment**
Isoaspartic acid	$z_n - 57$, $c_{1-n}{}^{\bullet} + 57$		These losses in ECD could be used diagnostically.[c]
Serine / Threonine	$^{\bullet}CH_2OH$	31.018[a]	
	$^{\bullet}C_2H_4NO$	58.029[h]	Odd-electron neutral loss from $z^{\bullet}$ radical fragment ions.[h]
Methionine	C_3H_6S	74.019[b]	Even-electron neutral loss from charge-reduced species and from $z^{\bullet}$ radical fragment ions.[h]This loss was not observed in all peptides and thus can not be used as a diagnostic value.[d]
	$^{\bullet}C_2H_5S$	61.012[h]	Odd-electron neutral loss from $z^{\bullet}$ radical fragment ions and charge-reduced species.[h]
Lysine	$C_4H_{11}N$	73.089[b]	This loss was not observed in all peptides and thus can not be used as a diagnostic value.[d]

Table 2.1: (*continued*)

Amino acid in the peptide chain	**Losses**	**Mass (Da)**	**Comment**
	C_4H_9N	71.073^{h}	Even-electron neutral loss from charge-reduced species and from $z^{\bullet}$ radical fragment ions.[h]
	$^{\bullet}C_3H_8N$	58.066^{h}	Odd-electron neutral loss from $z^{\bullet}$ radical fragment ions.
Asparagine / Glutamine	CH_3NO	$45.022^{b,f}$	These losses in ECD could be used diagnostically.[d]
	C_2H_5NO	59.045^{f}	
	$^{\bullet}CONH_2$	44.014^{h}	Odd-electron neutral loss from $z^{\bullet}$ radical fragment ions.[h]
	$^{\bullet}C_2H_4NO$	58.029^{h}	
Arginine	CH_4N_2	$44.037^{a,b,h}$	Even-electron neutral loss from charge-reduced species.[h]These losses in ECD could be used diagnostically.[d]
	CH_5N_3	$59.048^{a,b,h}$	
	$C_4H_{11}N_3$	$101.095^{b,h}$	
	$^{\bullet}CH_3N_2$	43.029^{b}	
	$^{\bullet}C_3H_8N_3$	86.072^{b}	
	$C_4H_9N_3$	99.068^{b}	
	$C_3H_9N_3$	87.079^{h}	Even-electron neutral loss from charge-reduced species.[h]

Table 2.1: (*continued*)

Amino acid in the peptide chain	**Losses**	**Mass (Da)**	**Comment**
Glutamine	C_3H_5NO	71.037^{h}	Even-electron neutral loss from $z^{\bullet}$ radical fragment ions.[h]
Valine	$^{\bullet}CH_3$	15.024^{h}	Odd-electron neutral loss from $z^{\bullet}$ radical fragment ions.[h]
Tryptophan	C_9H_9N	$131.073^{e,h}$	Even-electron neutral loss from charge-reduced species.[i] This loss in ECD could be used diagnostically.[d]
	C_9H_7N	129.058^{h}	Even-electron neutral loss from charge-reduced species[h]
	$^{\bullet}C_8H_6N$	116.050^{h}	Odd-electron neutral loss from $z^{\bullet}$ radical fragment ions[h]
Tyrosine	C_7H_8O	108.058^{e}	
	C_7H_6O	106.042^{h}	Even-electron neutral loss from $z^{\bullet}$ radical fragment ions.[h]
Leucine/isoleucine	C_4H_8	$56.063^{f,h}$	Even-electron neutral loss from charge-reduced species.[h]
Leucine	$^{\bullet}C_3H_7$	43.055^{h}	Odd-electron neutral loss from $z^{\bullet}$ radical fragment ions.[h]
	$d_n - 43.0055^{i}$		Radical losses from d-type fragment ions under hot-ECD conditions.[i]

Table 2.1: (*continued*)

Amino acid in the peptide chain	**Losses**	**Mass (Da)**	**Comment**
Isoleucine	$^{\bullet}C_2H_5$	29.039[h]	Odd-electron neutral loss from $z^{\bullet}$ radical fragment ions.[h]
	$d_n - 29.039$[i]		Radical losses from d-type fragment ions under hot-ECD conditions.[i]
Histidine	$^{\bullet}C_4H_5N_2$	81.045[e]	
	$C_4H_6N_2$	82.053[b,e,h]	Even-electron neutral loss from charge-reduced species.[h]This loss in ECD could be used diagnostically.[d]
Glutamic acid	$^{\bullet}C_2H_3O_2$	59.013[h]	Odd-electron neutral loss from $z^{\bullet}$ radical fragment ions.[h]
	$C_3H_4O_2$	72.021[h]	Even-electron neutral loss from $z^{\bullet}$ radical fragment ions.[h]
Aspartic acid	CO_2	43.989[h]	Even-electron neutral loss from charge-reduced species.[h]
Cysteine	R−SH		Cysteine from disulfide bonds.[g]
	$^{\bullet}$S−R		
	$z_n - 91$		Alkylated cysteine from either carboxymetyl or carbamidomethyl groups.[g]

Table 2.1: (*continued*)

Amino acid in the peptide chain	Losses	Mass (Da)	Comment
	$^{\bullet}CH_2S$	45.988[h]	Even-electron neutral loss from $z^{\bullet}$ radical fragment ions.[h]

[a] N. A. Kruger et. al., 1999
[b] H. J. Cooper et. al., 2002
[c] Cournoyer, Lin, Bowman, & O'Connor, 2007
[d] H. J. Cooper et. al., 2003
[e] K. Haselmann, Budnik, Kjeldsen, Polfer, & Zubarev, 2002
[f] R. A. Zubarev et. al., 1999
[g] Chalkley, Brinkworth, & Burlingame, 2006
[h] Fung & Chan, 2005
[i] Kjeldsen, 2002

Losses on the arginine side chain ($C_3H_9N_3^{+\bullet}$ and $C_4H_{10}N_3^{+}$) were also observed by Turecek et. al.[187] Additionally, side chain loss CH_5N_3 ($59.048\,Da$) from arginine was attributed to an unpaired electron delocalised at the guanidine π^*-orbital, which is a good acceptor for an H-atom.[188] The subsequent losses of $^{\bullet}C_2H_5$, and/or C_3H_6 give total losses of $C_4H_{10}N_3$ and $C_3H_9N_3$, respectively, which are products of radical migration by a proton coupled-electron transfer mechanism,[189] where the charge and the electron migrate separately. Other arginine losses such as $C_3H_9N_3$ ($87.079\,Da$) and CH_4N_2 ($44.037\,Da$)[173] were reported in the charge-reduced species of 20 different nonapeptides (RGGGXGGGR, where X is one of the twenty amino acid residues). Side chain losses from the X amino acid residue, in the charge-reduced species, were observed after the arginine side chain was cleaved, with exception of X being tryptophan and histidine. Moreover, the $z^{\bullet}$ radical fragment ions of these nonapeptides did not exhibit losses of arginine and histidine.[173]

Histidine side chain loses from b^{2+} fragment ions were observed in peptides.[190] This histidine loss was explained, at the time, by the neutralisation of the nearby acylium ion due to the presence of the histidine close to the $C-$terminus. However, later ECD experiments and computational calculations in histidine containing pentapeptides (AAAHL and AAAHR/K) performed by Turecek, F. and Chung, T. W. and Moss, C. L. and Wyer, J. A. and Ehlerding, A. and Holm, A. I. S. and Zettergren, H. and Nielsen, S. B. and Hvelplund, P. and Chamot-Rooke, J. and Bythell, B. and Paizs, B.[187] explained the histidine side chain losses ($82.0526\,Da$, $110.0714\,Da$, $138.0664\,Da$ and $155.0929\,Da$), by the gradient on the dipole moment generated by the positive charge at the histidine ring, and the negative charge at the COOH group that favoured electron capture at the histidine ring in the π^*-orbital. Subsequently, exothermic proton migration from the COOH or $N-$terminal group to the imidazolium ring occurs. Thus, an imidazoline radical-cation and a carboxylate anion are formed (a zwitterion). Stabilisation of the imidazoline radical-cation leads to further cleavage on the C_α - C_β bond (loss of $C_4H_6N_2$, $82.0526\,Da$).

Leucine losses from the $z^\bullet$ radical fragment ions have been reported in leucine rich peptides.[150] Interestingly, this reported $z^\bullet$ radical fragment ions lost one and two leucine side chains, which implied cleavage of three covalent bonds under ECD conditions.[150] Additionally, w fragment ions from leucine residues were also reported in leucine rich peptides.[150] The w, u and $w^\bullet$ fragment ions are suggested to be derived from side chain losses from the $z^\bullet$ radical fragment ions in ECD.[191] The authors explain the presence of w and u by radical migration from the α-carbon to the β-carbon and along the side chain as proposed in 2003 by Leymarie, N. and Costello, C. E. and O'Connor, P. B.[192] see section 2.5.5.

Losses from the phenylalanine side chain, though possible in principle, are not observed in ECD spectra because cleavage at the bond on the phenylalanine side chain requires a

greater activation energy than cleavage at the $N - C\alpha$ backbone.[193] This implies that the loss of the benzyl group can occur, but $N - C\alpha$ backbone cleavage is faster and so side chain loss is not generally observed for phenylalanine.

ECD and computational studies in glutamic acid and asparagine rich peptides show fragmentation inhibition during ECD experiments.[165] This inhibition was attributed to a hydrogen bond formed between the carbonyl carbon of the glutamic acid moiety (or asparagine moiety) and the amide backbone hydrogen. This hydrogen bond provides extra-stability to the charge-reduced radical species (see figure 2.3). Increase in the inhibition of the fragmentation is observed if the number of glutamic acid residues in the peptide is increased, with $H^{\bullet}$ loss as the main fragmentation product.

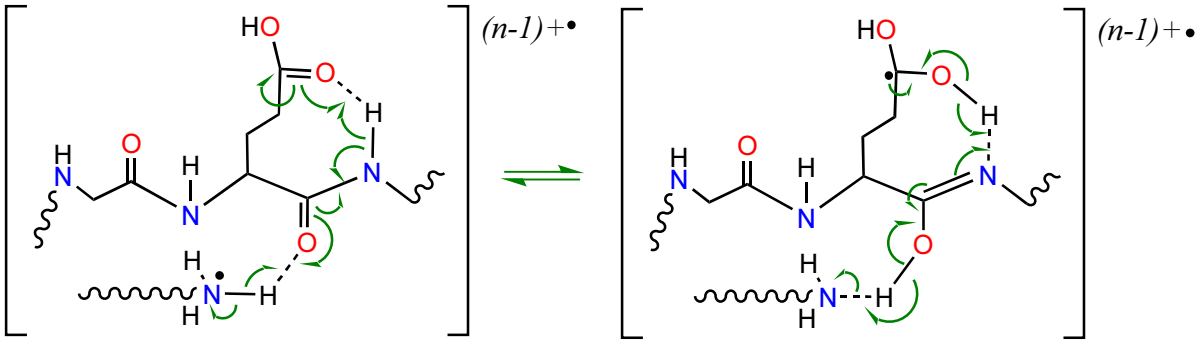

Figure 2.3: Schematic of the proposed ECD fragmentation inhibition observed in glutamic acid rich peptides. Adapted with permission from Chan and Chan.[165]

Furthermore, it has been argued that secondary fragmentation, which produces even-electron and/or odd-electron side chain moieties (as it is shown in table 2.1), can be driven by radical migration.[173,192] A discussion about radical-directed fragmentation is presented in section 2.5.5.

2.4 ECD related methods

Since the implementation of ECD other derived methods such as hot-ECD (HECD), electron induced dissociation (EID), and electron detachment dissociation (EDD), have been developed in FTICR mass spectrometer. EID and EDD were developed to overcome particular limitations of ECD, which are described below. Other techniques, such as activated ion-ECD (AI-ECD), and SORI-ECD have been used to improve ECD *cleavage coverage* and *conversion* efficiency (discussed in section 2.1.2). These techniques, to date, can be performed in a FTICR mass spectrometer and in modified quadrupole mass spectrometers,[194,195] although there are other electron based dissociations used in other instruments, for instance ECID used in accelerators[196] and electron transfer dissociation (ETD),[197] which can be used in both FTICR and other commercial mass spectrometers. Here a brief description of some electron based technique is presented with the intention of clarifying the key differences with ECD, and they are summarised in table 2.2.

2.4.1 ECD related methods in a FT-ICR mass spectrometer

Electron impact excitation of ions from organics (EIEIO)

The reaction of small ions (*e.g.* $C_6H_5CN^+$) with low energy electrons ($3 - 9\,eV$) was initially studied by Freiser and Beauchamp.[167] During this reaction the trapping efficiency, in the ICR cell, was affected by the electron emission current. The authors indicated that the electron excitation proceeds by a π to π^* transition and that the electron was efficiently captured at around $7\,eV$.[167] Later this technique was referred to as EIEIO,[168] where H-atom loss was the predominant product at low electron energies. Comparison of EIEIO with CAD and photodissociation, in small molecules, revealed that

similar products were obtained, although some differences were also observed. These differences in fragmentation products were attributed to both the amount of energy deposited by the electron and the form in which the energy is delivered (*e.g.* rotational, vibrational and electronic). Interestingly, this has been the motive of debate during ECD years.

All the small molecules used to interact with EIEIO[168] contained a benzene moiety, which after dissociation converts into a benzyne moiety $C_6H_4^+$. The benzyne moiety resonantly stabilises the radical and no further dissociation was reported.[168] Thus, the fragmentation was similar to CAD and photodissociation. Eleven years later, EIEIO was applied to Gramicidin S ionized by laser desorption and $70\,eV$ electron prior to EIEIO.[169] Wang, B. and McLafferty, F. W.[169] were able to observe additional ions to CAD and photodissociation, but the ionization technique used to produce the ions did not allow the authors to infer the additional capabilities of low electron fragmentation. For this reason, the early papers on EIEIO missed the discovery of ECD.

Hot electron capture dissociation (HECD)

HECD can be considered a variant of EIEIO where relatively high energy electrons ($3-13\,eV$) react with polypeptides.[198] The relative high energy of the electron generates electronic excitation prior to electron capture.[199] $c/z^\bullet$ fragment ions along with extensive b/y, a, and w fragment ions are normally observed in a HECD spectra. The secondary fragment ions are particularly abundant at lower m/z, and are not attributed to the excess of kinetic energy of the electrons prior to capture, but depend on the individual peptide structure.[150] Interestingly, w fragment ions and low abundance d fragment ions are useful to differentiate leucine from isoleucine moieties in the HECD spectra,[198,200] see table 2.1 in section 2.3. Low abundance d-type fragment ions are

derived from the $a^{\bullet}$ fragment ions.[198]

Electron induced dissociation (EID)

As previously discussed (section 2.1.1), ECD neutralises at least one charge; consequently the cation must have more than one charge in order to undergo fragmentation by ECD. This condition prevents application of ECD to singly-charged $[M+H]^{1+}$ species. Electron induced dissociation (EID) overcomes this limitation by irradiating the singly-charged ions with fast, high energy electrons ($15-25\,eV$), causing both ionization and electronic excitation to produce a hydrogen-deficient doubly-charged radical species. Subsequently, dissociation of the $[M+H]^{2+\bullet}$ ion produces $c/z^{\bullet}$ and a/x-type fragment ions.[201] This technique has been labeled differently throughout the years. For instance, it has also been reported as electron ionization dissociation,[202] and as electron excitation dissociation (EED).[58,203,204] In both cases, however, the authors reported that the interaction of singly-charged precursor ions with fast electrons generates a doubly-charged intermediate species.

In recent years EID has found application in the analysis of small, singly charged organic molecules of pharmaceutical interest,[84,85] in the analysis of zwitterionic clusters,[205] in the study of phosphate containing metabolites,[206] glycosaminoglycan tetrasaccharides,[207] polynuclear metal complexes,[208] and in the analysis of amino acids and small peptides.[199]

Electron detachment dissociation (EDD)

Another particular limitation of ECD, additional to those mentioned above, is that it cannot be used in negative precursor ions. Aiming to overcome this drawback, EDD

was conceived. For instance, the introduction of EDD allowed to perform fragmentation to deprotonated molecules $[M-nH]^{n-}$. During EDD experiments the negative precursor ions interact with electrons ($15-20\,eV$) to produce a radical anion $[M-nH]^{(n-1)-\bullet}$, along with a, $a^{\bullet}$, c, $c^{\bullet}$, $z^{\bullet}$, and z fragment ions.[209] EDD was also implemented in a quadrupole ion trap leading to dominant $a^{\bullet}$ and x fragments ions with increased frequency of fragmentation in the vicinity of acidic residues.[210] EDD has been successfully applied to the analysis of ganglioside,[211] glycosamiglycan tetrasaccharides,[212] sialylated oligosaccharides,[213] and to the study of DNA.[214,215]

Negative ion electron capture dissociation(niECD)

Negative ion electron capture dissociation has also been implemented to deprotonated molecules $[M-nH]^{n-}$. In a typical niECD experiment, the precursor ion is irradiated by low energy electrons ($\sim 4.5\,eV$) to yield a charge-increased radical species $[M-H]^{2-\bullet}$. As a result, c, and $z^{\bullet}$, fragment ions are produced.[216]

Sustained off-resonance irradiation-electron capture dissociation (SORI-ECD)

SORI-ECD is composed by two events separated in time, but sequential in a single analysis. In this technique, SORI is performed first, followed by a typical ECD experiment. During SORI, an off-resonant excitation frequency ($\sim 1-2\,kHz$ above the resonant frequency of the precursor ion) is applied to the precursor ion. This off-resonant excitation accelerates and decelerates the precursor ion confined in the ICR cell,[217,218] Gorshkov *et al.*[156] showed that the use of SORI with ECD can increase *capture efficiency* (see equation (2.4)) by increasing the effective overlap of the ion cloud with the electron beam.

In some cases, instead of performing SORI before the ECD experiments, a pre-excitation of the parent ion[166] can also be used to improve ECD *capture efficiency* (see equation (2.4)). This pre-excitation event consists of introducing a single frequency shot (*e.g.* $m/z\,100$) at the beginning of the ECD experiments to allow an even better overlap between the ion cloud and the electron beam. This technique has proven to be useful in the study of metal-protein complexes binding sites.[219]

Activated ion-electron capture dissociation (AI-ECD)

Horn and co-workers[220] showed that ECD of cytochrome c gave less *capture* efficiency (see section 2.1.2) due to the presence of multiple non covalent bonds in the protein tertiary structure. They proposed a method named activated ion electron capture dissociation to overcome this limitation. In such a method the activation of the precursor ion was obtained by using collisions with nitrogen gas, or infrared irradiation (IR), or black body IR. Activation by collision was the most successful, as reported at that time. In order to perform the activation by collisions, the gas was introduced into the ICR cell through a pulsed valve, while the ions and the electrons were admitted to the cell. This technique was then known as In-beam ECD and later referred to as *plasma*-ECD.[221]

Plasma-ECD performed varying the electron beam current from 0.1 to $0.33\,\mu A$, achieved $> 95\,\%$ removal of the precursor ion and making secondary electron capture more probable.[220] This technique generates a large number of similar abundance fragment ions compared with normal ECD or CAD ($c/z^{\bullet}$, b/y, and $a^{\bullet}$ fragment ions). The abundance of b and y fragment ions was linearly dependant on the pressure in the ICR cell. The increase in the cell pressure (7×10^{-7} to $3 \times 10^{-6}\,Torr$) was considered not critical for AI-ECD experiments, if the aim was purely to increase c and $z^{\bullet}$ fragment ions abundance. The use of *plasma*-ECD provided $> 50\,\%$ more inter-residue bond cleavages

(*cleavage* coverage) than CAD at the $N-$terminus of larger proteins.

One of the drawbacks of plasma-ECD was the long irradiation period required. Thus, attention was drawn to implement infrared irradiation as an activation method to couple with ECD,[37–39,222] today known as IRMPD-ECD. Activation performed with a CO_2 laser at $25\,W$ and $0.25\,s$ prior to ECD was enough to open up the protein folded conformation without inducing significant backbone dissociations.[223] Oh, H. and McLafferty, F. W.[223] performed IRMPD during the ECD event to prevent re-folding of the molecule when IRMPD was applied as a single event. They also varied the laser power to $25, 50$ or $100\,\%$ of full-power and observed an slight increase in *cleavage* coverage. However, at higher laser power, secondary fragmentation is observed along with b/y fragment ions. IRMPD-ECD has been used in the study of amphipatic peptides and proteins,[224] standard peptides,[73,74] and proteins.[67,75,76]

Blackbody infrared radiative dissociation (BIRD)[225] was also employed as an ion activation method during ECD. BIRD requires an increase in the temperature ranging from 25 to $175\,^{\circ}C$ in order to cleave the protein non-covalent bonds.[223,226] At $125\,^{\circ}C$ a high *cleavage* coverage (56/72) was achieved for bovine ubiquitin, as reported by. Oh, H. and McLafferty, F. W.[223] BIRD produced unique cleavages compared to IRMPD/CAD for larger proteins ($\sim 42\,kDa$), a phenomenon which was attributed by the authors to a higher dissociation of the protein tertiary structure, caused by the longer reaction time frame.[225] Additionally, BIRD-ECD favoured the loss of water from larger proteins (*e.g.* carbonic anhydrase, thiazole kinase, and thiaminaze I) at low temperatures.

Double resonance-electron capture dissociation (DR-ECD)

Double resonance is performed by resonant ejection of selected ion(s) in the ICR cell, while the precursor ion or ion of interest is kept within the cell. An excitation frequency

is applied, in resonance with the frequency of the selected ions to be ejected, so that they are removed from the cell during the ECD event.[227,228] For example, in the reaction equation (2.5), when A is ejected from the cell, changes in the intensity of C demonstrate the interrelationship between A and C.

$$\begin{aligned} A + B &\longrightarrow C + D \\ E + B &\longrightarrow C + G \end{aligned} \tag{2.5}$$

Thus, DR-ECD is performed by ejecting the selected ions during the ECD event. The ejection of a particular ion allows observation of the effect of this ejection in the abundance of another ion of a different frequency. For instance, DR-ECD has been applied when precursor ion decomposition is suspected during quadrupole isolation[73] and to study the lifetime of intermediate fragment ions.[229] Moreover, double resonance has also been applied in oligonucleotides during EDD and EID experiments,[214] and can be used in conjunction with other ion activation methods, such as IRMPD.[230]

Selective excitation of ions for consecutive activation (SEICA)

This fragmentation technique utilises the precursor ion that remains after ECD and subsequently a vibrational excitation is applied, for instance IRMPD.[157] This method requires implementation of three steps in the ICR cell. First, usual fragmentation under ECD conditions is performed. Second, the fragment ions are ejected from the cell while the precursor ion is kept at the centre of the cell. Finally, the precursor ion is fragmented by IRMPD. This method provided complementary information to ECD allowing an increase in *effective* efficiency of ECD per scan, as the authors argued.

2.4.2 Fragmentation methods in other instruments

Electron capture induced dissociation (ECID)

In an accelerator mass spectrometer, ions can be accelerated to $50\,keV$ to collide with a gas target under single-collision conditions.[231] The gas target is usually cesium[232] or sodium atoms,[233] although xenon[231] and C_{60}[234] have also been used. ECID, also referred to as fast collisional electron transfer, results in the formation of charge-reduced ions[187] by electron capture. In the study of peptides ECID produces c and $z^{\bullet}$ type fragment ions, z and neutral c fragments.[232] The neutral fragments are converted to anions due to secondary collisions with the neutral gas. Thus, neutral c fragments generate an unstable $c^{-\bullet}$, while stable z^{-} anions are produced by a second electron transfer from the $z^{\bullet}$ radical fragment ion. Other low abundance losses observed during ECID are b, y^{-} and x^{-} fragment anions. The y^{-} fragment ions are believed to be derived from electron capture of neutral y fragment ions generated by the CAD process during ECID, which correlates well with high abundance of b fragment ions.[232] Insights into the mechanism of ECID can be found elsewhere.[235]

kEv induced dissociation (KID)

This technique has been implemented in a double quadrupole-time of flight (TOF) mass spectrometer.[236] The protein ions produced by ESI collide with background gas in the quadrupole to cool the ions enough to be trapped. Bari et al.[236] performed extraction of the background gas before the trapped ions interact with $5\,keV$ atomic ions of H^{+}, He^{+}, and He^{2+}. The dissociation products are separated in the corresponding TOF section of the instrument in order to be finally detected. KID dissociation in peptides produced side chain losses and immonium ions detected at low m/z in the spectrum.

Series of fragment ions including a, b/y, c and z fragment ions are also formed in KID. A more detailed discussion on the KID mechanism can be found in Bari et al. [236]

Resonant electron capture (REC)

Resonant Electron Capture is based on the interaction of neutral peptides of low volatility with low energy electrons $(1-2\,eV)$. This results in the formation of negative ions. [237] In order to perform REC, Vasil'ev, Y. V. and Figard, B. J. and Morré, J. and Deinzer, M. L. [237] used a heated direct insertion probe to vaporise the peptides and to introduce them into the magnetic sector instrument. This resonant electron capture causes cleavage of the $N-C\alpha$ bond generating c and $z^{\bullet}$ fragment ions.

Electron transfer dissociation (ETD)

ETD involves radical-driven fragmentation of the precursor ion reacting with anions leading to the cleavage of the $N-C\alpha$ backbone bond of protein and peptides. Subsequently, charge-reduced radical species $[M+nH]^{(n-1)+\bullet}$, c and, $z^{\bullet}$ fragment ions are produced. [197] This technique can be implemented in many commercial mass spectrometers.

2.4.3 Fragmentation methods summary

For clarity purposes, a table summarizing some of the methods previously discussed is presented below

Table 2.2: Summary of fragmentation methods.

Technique	Proposed reaction	Brief description
ECD[a]	$[\mathrm{M}+\mathrm{nH}]^{\mathrm{n}+} + e^-_{<0.2eV} \longrightarrow \left([\mathrm{M}+\mathrm{nH}]^{(\mathrm{n}-1)+\bullet}\right)^* \longrightarrow c/z^\bullet$	Reaction of polypeptide cations with $\sim 0.2\,eV$ electrons.
EIEIO[b]	$[\mathrm{AB}]^+ + e^-_{3\,to\,9\,eV} \longrightarrow [\mathrm{AB}]^* \longrightarrow \mathrm{A}^+ + \mathrm{B}$	Reaction of positive small molecules with $3to9\,eV$ electrons.
HECD[c]	$[\mathrm{M}+\mathrm{nH}]^{\mathrm{n}+} + e^-_{13\,eV} \longrightarrow \left([\mathrm{M}+\mathrm{nH}]^{(\mathrm{n}-1)+\bullet}\right)^* \longrightarrow c/z^\bullet, b/y, w$	Reaction of polypeptide cations with $\sim 3to13\,eV$ electrons.
EID[d]	Step 1: $[\mathrm{M}+\mathrm{H}]^{1+} + e^-_{fast\leq 25eV} \longrightarrow [\mathrm{M}+\mathrm{H}]^{2+\bullet} + e^-_{fast} + e^-_{slow:0.2eV}$ Step 2: $[\mathrm{M}+\mathrm{H}]^{2+\bullet} + e^-_{slow} \longrightarrow ([\mathrm{M}+\mathrm{H}]^+)^* \longrightarrow c/z^\bullet, a/x$	Step 1: Reaction of singly-charged polypeptides with fast electrons to generate doubly-charged ions.
EDD[c]	$[\mathrm{M}-\mathrm{nH}]^{\mathrm{n}-} + e^-_{\sim 20eV} \longrightarrow \left([M-\mathrm{nH}]^{(\mathrm{n}-1)-\bullet}\right)^* + 2e^- \longrightarrow c/z^\bullet, c^\bullet/z, a, a^\bullet$	Reaction of negatively-charged polypeptides with fast electrons to generate doubly-charged anions.
niECD[c]	$[\mathrm{M}-\mathrm{H}]^{1-} + e^-_{\sim 4.5-6.5\,eV} -> \left([M-\mathrm{H}]^{(2-)-\bullet}\right)^* \longrightarrow c^\bullet/z, a^\bullet, b/y$	Reaction of negatively-charged polypeptides with electrons to generate doubly-charged anions.
ECID[f]	$[\mathrm{M}+\mathrm{nH}]^{\mathrm{n}+} + \mathrm{Cs} \longrightarrow \left([M+\mathrm{nH}]^{\mathrm{n}+}\right)^* \longrightarrow c/z^\bullet, b, y^-, x^-$	Single collision of accelerated ions with Cs atoms.
REC[g]	$\mathrm{M} + e^-_{<2eV} \longrightarrow (\mathrm{M})^* \longrightarrow c/z^\bullet$	Neutral molecules interact with free electrons.
ETD[h]	$[\mathrm{M}+\mathrm{nH}]^{\mathrm{n}+} + \mathrm{A}^{-\bullet} \longrightarrow \left([\mathrm{M}+\mathrm{nH}]^{(\mathrm{n}-1)+\bullet}\right)^* + \mathrm{A} \longrightarrow c/z^\bullet$	Multiple collisions of ions with anions.
CAD[i]	$[\mathrm{M}+\mathrm{nH}]^{\mathrm{n}+} + \mathrm{Ar} \longrightarrow \left([\mathrm{M}+\mathrm{nH}]^{\mathrm{n}+}\right)^* \longrightarrow b/y$	Multiple collisions of ions with Ar gas.

Table 2.2: (*continued*)

Technique	Proposed reaction	Brief description
IRMPD[j]	$[\mathrm{M}+\mathrm{nH}]^{\mathrm{n}+} + \mathrm{n}(h\,\nu) \longrightarrow \left([\mathrm{M}+\mathrm{nH}]^{\mathrm{n}+}\right)^{*} \longrightarrow b/y$	Reaction of polypeptides with multi-photons.
EI	$[\mathrm{AB}]^{+} + e^{-}_{70eV} \longrightarrow [\mathrm{AB}]^{*} \longrightarrow \mathrm{A}^{+} + \mathrm{B}^{\bullet} + 2e^{-}$	Reaction of small volatile molecules with $70\,eV$ electrons.

[a] Zubarev, R. A. and Kelleher, N L. and McLafferty, F W.[8]
[b] Cody, R. B. and Freiser, B. S.[168]
[c] Kjeldsen, F. and Haselmann, K. F. and Budnik, B. A. and Jense, F. and Zubarev, R. A.[198]
[d] Nielsen, M. L. and Budnik, B. A. and Haselmann, Kim F. and Olsen, Jesper V. and Zubarev, R. A.[203], Nielsen, M. L. and Budnik, B. A and Haselmann, K. F. and Zubarev, R. A.[204]
[e] Budnik, B. A. and Haselmann, K. F. and Zubarev, R. A.[209]
[f] Boltalina, O. and Hvelplund, P. and Jorgensen, T. and Larsen, M. and Larsson, M. and Sharoitchenko, D.[231]
[g] Vasil'ev, Y. V. and Figard, B. J. and Morré, J. and Deinzer, M. L.[237]
[h] Syka, J. E. P. and Coon, J. J. and Schroeder, M. J. and Shabanowitz, J. and Hunt, D. F.[197]
[i] Jennings, K R[9]
[j] Thorne, L. R. and Beauchamp, J. L. and in M.T. Bowers (Ed.)[238]

2.5 ECD Mechanism

2.5.1 "Hot Hydrogen" model or Cornell mechanism (McLafferty)

ECD is rooted in the gas phase structure of protonated proteins where energetically favoured protonation sites, particularly the side chains of arginine, lysine, and histidine, are stabilised by hydrogen bonds to backbone functionalities,[174] specifically the backbone carbonyl oxygen and nitrogen atoms.Zubarev, R. and Haselmann, K. and Budnik, B. and Kjeldsen, F. and Jensen, F.[239] proposed that during ECD the electron most probable landing site would be the site with the highest charge density. As the charge density decreases the probability for electron capture decreases. For example, the second most likely landing group is the backbone NH group and this would cause immediate

fragmentation. Other groups, away from the protonation site, could contribute towards charge density and the electron could be captured at a distance of at least a few amino acid residues away from the protonation site. After capture, the electron migrates to the protonation site due to intramolecular potential differences.

Capture of the electron at the protonated site would produce an hypervalent ammonium radical.[240] Subsequently, a hot hydrogen atom ($H^{\bullet}$) from the protonation site could be expelled and could be recaptured by a nearby carbonyl oxygen or a group with sufficient proton affinity (*e.g.* $S-S$ bonds, indole group of tryptophan side chain). The recapture at the carbonyl functionality forms a transient aminoketyl radical,[174] which dissociates exothermically by cleaving the $N-C\alpha$ bond.[241] Thus, with the original ECD experiments, it was thought that the mechanism involved dissociation of the $[M+nH]^{(n-1)+\bullet}$ species via an energetic or "hot H-atom" transfer to the backbone carbonyl see figure 2.4.

This mechanism did not take into account several factors; for instance, it did not consider the transition state energies of electron capture by protonated species.[240] The mechanism proposed did not consider that the positive charge must be close enough (*e.g.* within hydrogen bonding distance) to the $N-C\alpha$ bond, so the H-atom can be released by the hypervalent radical species and subsequently cause dissociation.[242] Additionally, as shown in figure 2.4, this mechanism generates only enol-imine c fragment ions, but not necessarily the amide moiety.[143] Finally, the "hot hydrogen model" cannot explain loss of the modifications from the $z^{\bullet}$ radical fragment ions and backbone dissociations at amide groups remote from the charged sites,[188] which are successfully explained by the radical reaction cascade model (see section 2.5.5).

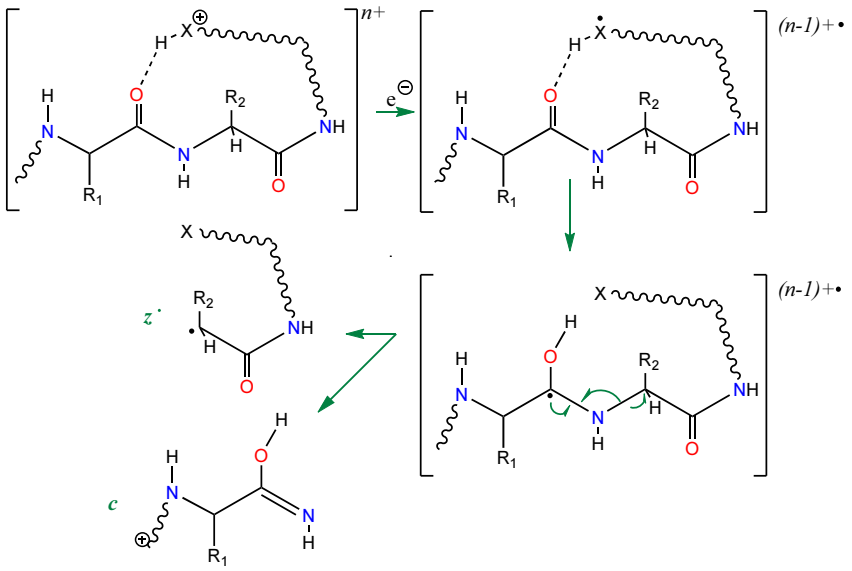

Figure 2.4: Schematic representation of the proposed reaction mechanism for electron capture dissociation based in the "hot hydrogen model" or Cornell mechanism. Figure adapted from Chen and Turecek.[188]

2.5.2 Utah mechanism (Simons)

ECD mechanisms can be arguably considered as a three step procedure: electron capture, H-atom dissociation from the protonated functionality (ammonium group), and H-atom transfer from the protonation site to the carbonyl oxygen. It should be noted that the last two steps are not necessarily sequential. For instance, the second and third steps are thought to proceed through a dissociation-recapture mechanism, where H-atom migration (transfer) generates an aminoketyl radical intermediate.[241] Additionally, two more steps are considered to develop in the ECD mechanism: the stabilisation of the aminoketyl radical complex and the cleavage of the $N - C\alpha$ backbone bond to produce c and $z^{\bullet}$ fragment ions. These two steps include the migration of a proton before (Washington mechanism) or after (Utah mechanism) $N - C\alpha$ backbone bond

cleavage. The Utah mechanism addresses in detail the first step of the ECD mechanism: the electron capture. Two theories have been developed regarding the Utah mechanism. A brief discussion of both is presented below.

Coulomb-stabilised direct attachment mechanism

This theory considers that the electron is captured directly into a Coulomb-stabilised OCN amide π^*orbital (see figure 2.5) at Rydberg orbitals having quantum numbers between 3- 6.[243] However, upon electron capture into a peptide/protein, the amide π^*orbital has a $\sim 2.5\,eV$ energetic barrier that the electron must overcome in order to be captured.[244] The electron energy is not enough to surmount this barrier, but instead Coulombic interactions of the π^*orbital with the positive charged sites and the dipole potentials within the molecule, will lower the barrier of the lowest unoccupied molecular orbital (LUMO) allowing the electron to be captured.[242,243,245,246] A crude depiction of the electron captured at a Coulomb-stabilised π^*orbital is shown in figure 2.6.

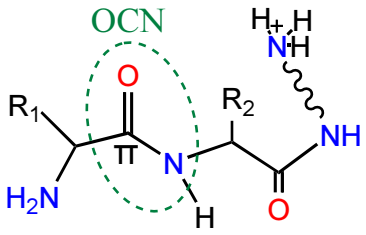

Figure 2.5: Schematic representation of the OCN amido π^*site.

The Coulomb stabilising potential at the OCN π^*amide group varies inversely with the distance (R_j) of every positive charge groups (Z_j) and can be estimated as is shown in equation (2.6). This estimation is based on the presence of a nearby positively charged group, such as $-NH_3^+$ or NH_2Na^+ interacting with a CH_3^- anion.[178,247]

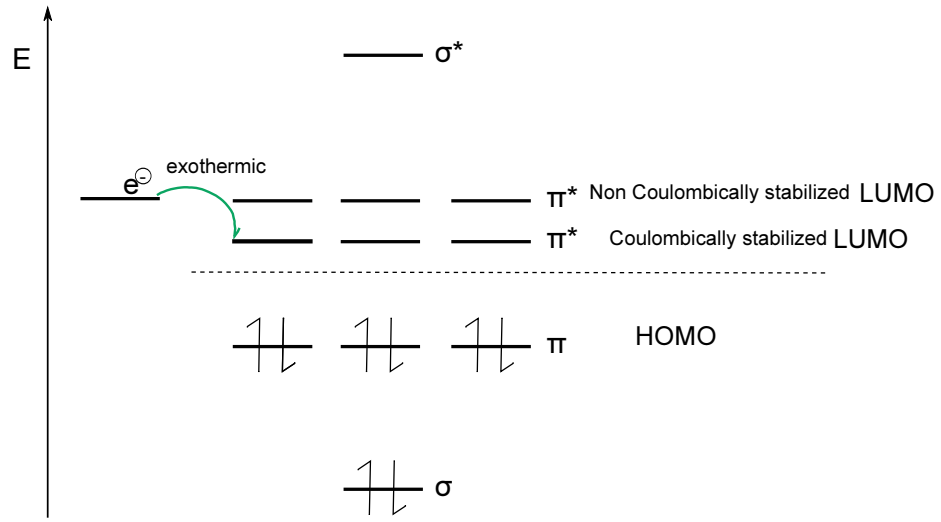

Figure 2.6: Qualitative crude depiction of the bonding and antibonding molecular orbitals to illustrate the electron captured at the Coulombically stabilised π^* LUMO available for *direct* electron capture.

$$c = 14.4(eV\text{Å}) \sum_{j=1}^{N} \frac{Z_j}{R_j(\text{Å})} \tag{2.6}$$

where, Z_j is the j^{th} charge; N is the number of charges; R_j is the distance between the j^{th} charge and the OCN amide group; and $14.4\,(eV\text{Å})$ is the value corresponding to the Coulomb constant times the square of the electron charge. This estimation does not include the effect of dipoles and its magnitude can fluctuate as the charged sites undergo dynamic motions.[242] For instance, to overcome a barrier of $2.5\,eV$, the charge site on a singly-charged peptide, should be at around $6\,$Å away from the OCN amide group. Hence, the electron can be directly captured in a Coulomb-stabilised OCN π^* amide group, see figure 2.7. The electron captured at the OCN π^* amide group causes elongation of the $N - C\alpha$ bond (*e.g.* through thermal vibrations) and once a small

energetic barrier is surmounted, the radical centre will move to the $N - C\alpha$ σ^* orbital causing dissociation.[242] This energetic barrier is small due to the presence of the radical and also the cleavage of the $N - C\alpha$[1] bond would form a new C=N π bond.[243]

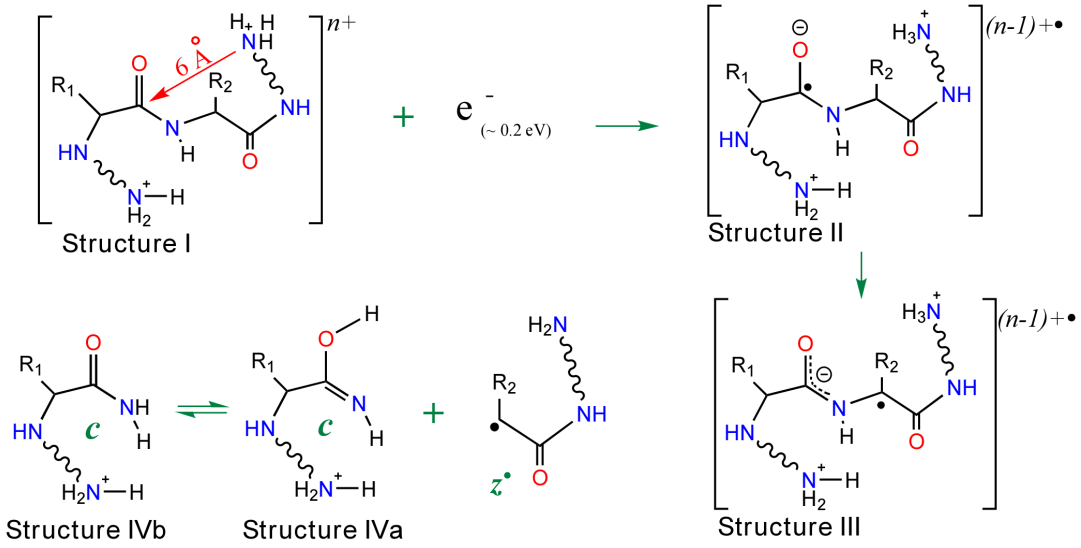

Figure 2.7: Schematic representation of the proposed direct electron capture by the Utah mechanism. Figure adapted with permission from Neff, D. and Sobczyk, M. and Simons, J.[242]

Intramolecular electron transfer mechanism - Through-bond or through-space electron migration

As discussed above, direct electron capture at the π^* orbital requires a Coulomb stabilised OCN amide group, where the identities of the charged sites are not expected to influence the degree of stabilisation.[248] However, the charged-sites sites play a more active role in the capture of an electron. Thus, Skurski, P. and Sobczyk, M. and Jakowski, J. and Simons, J.[143] proposed that it is possible that the electron can be captured at an excited Rydberg orbital centred on a positive charged site. This excited Rydberg orbital forms an excited-state hypervalent species also referred to as a Rydberg species.[143] The excited

[1] also known as α cleavage.[12]

Rydberg (hypervalent) are believed to undergo radiative or radiationless relaxation to the ground state and decay by N−H or $N - C\alpha$ cleavage.[246]

Once the electron is captured at the excited Rydberg orbital, but before the Rydberg orbital reaches the ground level,[178] the electron can migrate to a nearby Coulomb stabilised π^* orbital delocalised over an aromatic or amide group. This electron transfer or migration could occur in a through-space or through-bond manner.[242] Electron migration through-space is only possible if the Rydberg orbital that captured the electron comes into spatial overlap with the π^* orbital. Alternatively, for the electron to migrate through-space, it would need the right conditions such as a Coulomb stabilised π^* orbital where the positive charged-site is at approximately 6 Å away. Migration through-space can also occur from a Rydberg orbital centred at a positively charged-site to another Rydberg orbital centred at another positively charged-site.[249] Nonetheless, in order for the electron to migrate between those two Rydberg orbitals, the migrating Rydberg orbital must be in an excited Rydberg state. Moreover, the LUMO Rydberg orbital should have a low-energy (or equal energy) to the migrating Rydberg state.[178] These through-space electron migrations can occur between protonated and fixed charges, or two protonated charges only if the charged sites are at a distance of ~ 5 Å.[246]

In contrast, electron migration through-bond would occur if the Rydberg orbital, that captured the electron, overlaps with orbitals of other functional groups, which subsequently overlap with the OCN amide π^* orbital.[242] For instance, the electron captured at the Rydberg orbital centred at a positive site, forms an excited-state hypervalent species, which can then undergo a through-bond electron transfer to the π^* orbital of the OCN amide group. However, it is important to consider the radial size of the Rydberg orbital during electron migration, which depends on the quantum number of the orbital, n. If n is too small, the Rydberg orbital does not extend far enough to overlap with other orbitals, but if n is too large the highest unoccupied molecular orbital is too close to the

radial shell of the LUMO orbital and overlap is not favoured.[178]

Thus, so far the Utah mechanisms involves either Coulomb-stabilised direct attachment or intramolecular electron transfer mechanism during ECD. For both, it is believed that the Coulomb-stabilised direct attachment occurs in 1-10 % of the electron capture events, while the intramolecular electron transfer mechanism most likely takes place in the remainder of the cases of electron capture.[178] Another mechanism proposed by the research group at the University of Washington addresses in detail the questions about the structure of the intermediates formed after electron capture in ECD, which is discussed below.

2.5.3 Washington mechanism (Turecek)

In the study of the ECD mechanism in peptides/proteins it is necessary to establish the low energy conformers of the protonated peptides in the gas phase. The structures reported have shown to include solvation of one hydrogen atom, at the protonation site, to an amide carbonyl.[144,187,241] Thus, the next question to address is where the electron is captured.

Electron capture

A remote charge in the peptide causes an increase in the electron affinity of the amide group.[240] Thus, a charge-stabilised electronic state is delocalised over the amide group specifically at the carbonyl carbon, which captures the electron within the antibonding π orbital (π^*) of the C=O bond.[144]

N−H bond dissociation and O−H bond formation (Aminoketyl intermediate formation by hydrogen transfer)

After electron capture, a zwitterion is formed within the protonated peptide, where most of the negative charge density is delocalised at the carbonyl oxygen forming a "superbase". This superbase has sufficient proton affinity to weaken the hydrogen bonding at the protonated amino group, increasing the distance of the N−H bond, up to the saddle point for dissociation. As a result, an aminoketyl radical intermediate is formed as is shown in structure **II** of figure 2.8. This $H-$atom migration should occur in an excited state where charge-remote interactions in the peptide are negligible. However, if $H-$atom migration were to occur in the ground electronic state, there would be competition between both $H-$atom loss, from the protonated amino group, and $H-$migration (or $H-$atom transfer), from the protonated amino group to the carbonyl oxygen. Dissociation and transition state energies for N−H cleavage are exothermic ($28\,kJ/mol$) after overcoming a low energetic barrier ($12\,kJ/mol$) calculated for an amidated di-glycine peptide.[193] $H-$migration is also exothermic ($62\,kJ/mol$) for the amidated di-glycine peptide. Moreover, $H-$atom loss and $H-$atom migration are in competition with NH_3 loss. NH_3 loss is a product of a highly exothermic isomerisation ($115\,KJ/mol$ for the di-glycine peptide), and so is expected to rapidly dissociate. Nonetheless, the rate limiting process is the NH_3 dissociation and so that fragmentation pathway generally does not compete with $H-$atom loss and $H-$atom transfer.[193]

Aminoketyl intermediate stabilisation and $N-C\alpha$ bond dissociation

The unpaired electron on the aminoketyl carbon can be expected to destabilise the adjacent bonds.[193] For instance, the $N-C\alpha$ bond, $C_\alpha - H$ bond, and $C\alpha - C\beta$ bond. The cleavage of these bonds depends on their corresponding dissociation and activation

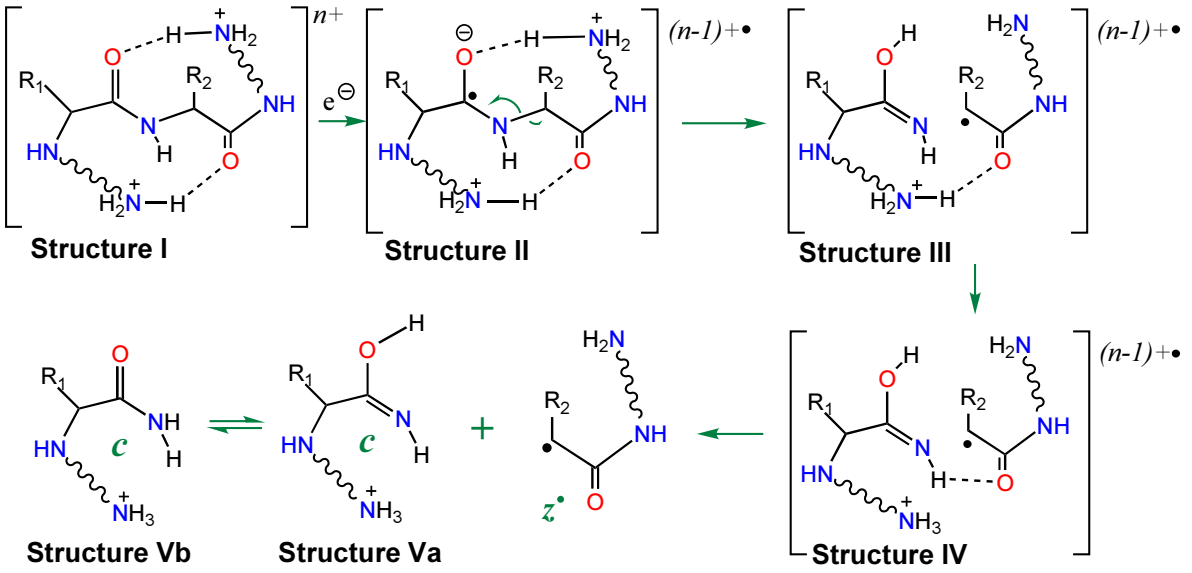

Figure 2.8: Schematic representation of the proposed reaction mechanism of the formation and stabilisation of the aminoketyl radical intermediate after electron capture. Utah mechanism. Figure adapted from structures proposed by Turecek, F. and Syrstad, E. A. and Seymour, J. L. and Chen, X. and Yao, C.[144] Note that the position of the charges is symbolically representing the point of largest charge density at the instant of electron capture. A more accurate picture would include molecular orbital diagrams.

energies. Moreover, $N - C\alpha$ cleavage does not produce the expected $c/z^{\bullet}$ fragment ions, because they are bound by a strong hydrogen bond.[193] This hydrogen bond is formed with a nearby carbonyl oxygen to stabilise the aminoketyl radical intermediate (structure **III** of figure 2.8).

This hydrogen bonding can decrease the electron density on the nearby carbonyl oxygen preventing formation of other hydrogen bonds, particularly from other protonation sites. The hydrogen bonding can also increase the charge density (increase the basicity) of the amide carbonyl group causing fast proton migration to the imine nitrogen, or

fast exothermic isomerisation[193] as shown in structure **IV**, figure 2.8. Finally, given sufficient internal energy the stablilised aminoketyl radical complex can dissociate forming $c/z^{\bullet}$ fragment ions. The $N-C\alpha$ bond cleavage could generate two structures for the c fragment ion, as shown in figure 2.8, the enol-imine (structure **Va**) or the amide moiety (structure **Vb**). Nonetheless, results have suggested that proton transfer takes place after $N-C\alpha$ bond dissociation generating the amide structure for the c fragment ion.[250]

2.5.4 Utah-Washington mechanism

The two mechanisms discussed above, Utah and Washington mechanisms, have been combined and are referred as the U-W mechanism. In the U-W mechanism the electron can be captured directly at the π^*orbital delocalised over the amide group or transferred from the capture site to the π^*orbital of the amide group. The direct electron attachment to an amide π^*-orbital is viable due to stabilisation by Coulomb interactions with positively charged groups.[178] The aminoketyl radical intermediate formed is in an electronic excited state, which is stabilised by Coulomb effects of charged groups that are effective over distances greater than 15 Å. The stabilised-aminoketyl radical complex formed is extremely basic (proton affinities $> 1200\,kJ/mol$).[188] This superbase amide can abstract a proton from a nearby proton donor group forming a fragile aminoketyl intermediate that dissociate into $c/z^{\bullet}$ fragment ions. However, in some cases this "superbase" does not abstract a proton and dissociate by cleavage of the $N-C\alpha$ backbone bond. The dissociation products are the $z^{\bullet}$ radical fragment ion and an enol-imidate anion, which is also a superbase (proton affinities $> 1400\,kJ/mol$). The enol-imidate superbase can also intramolecularly abstract a proton to form the c fragment ion. This mechanism is, to date, the most accepted ECD mechanism and it is independent of the chemical nature of the charge-carrying groups,[188] see figure 2.9.

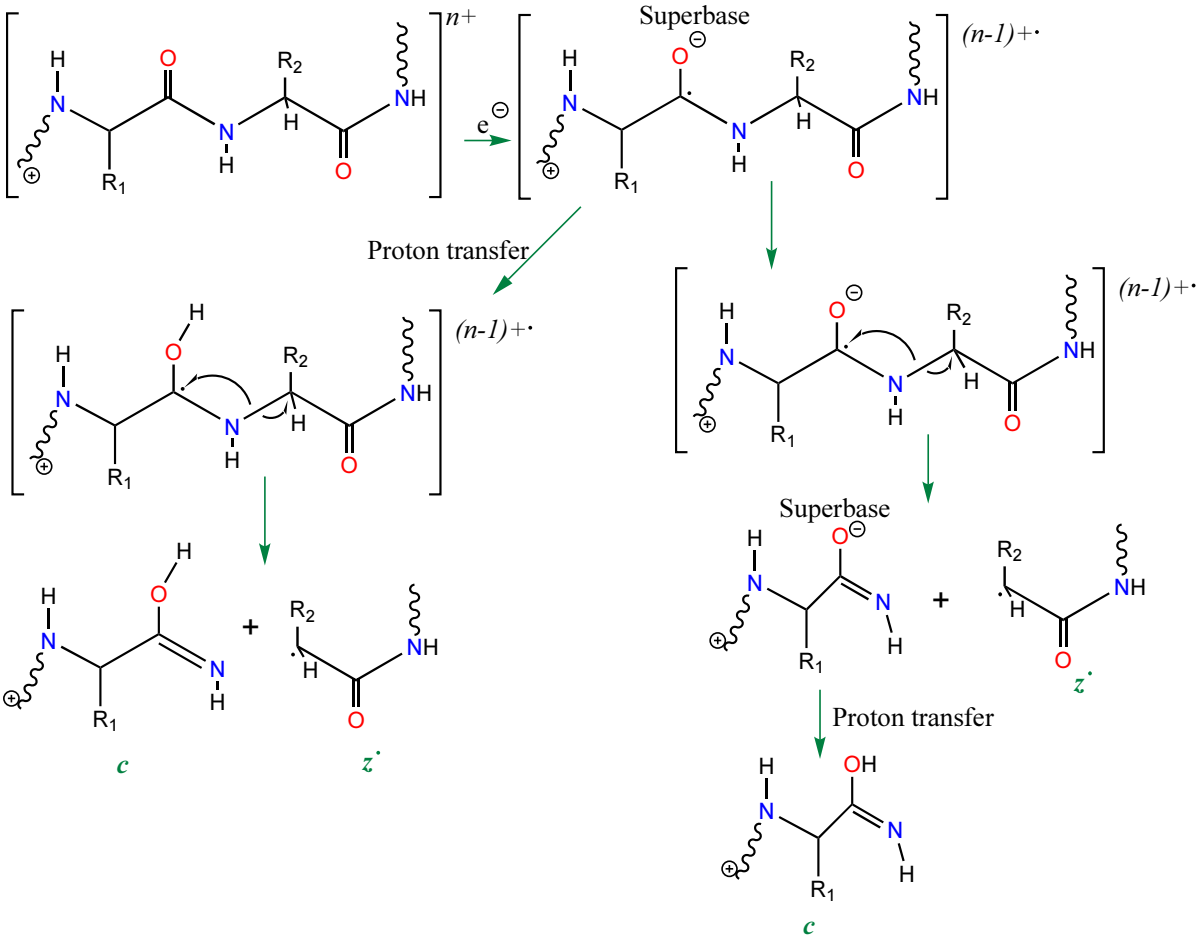

Figure 2.9: Schematic representation of the proposed ECD reaction mechanism by the Utah-Washington mechanism. Figure adapted from Chen and Turecek.[188]

2.5.5 Free radical reaction cascade model (radical mediated fragmentation)

The discussed U-W mechanism does seem to address the provenance of the side chain losses reported in linear peptides, which were reviewed above in section 2.3. Additionally, losses of small molecules (*e.g.* $H^{\bullet}$, H_2O, H_2O), amino acid, and side chain losses in cyclic peptides could not be explained by the mechanisms discussed above.[192] Moreover, these losses were inconsistent with the premise that if one electron is captured then one cleaved bond is obtained, because the fragments observed, in those cyclic peptides,

would require capture of two or more electrons. Thus, the losses observed in cyclic peptides made Leymarie, N. and Costello, C. E. and O'Connor, P. B.[192] propose the *free radical reaction cascade mechanism* to explain the fragmentation observed during ECD. In order to address this mechanism it is necessary to recapitulate two items. First, as stated before, the $z^{\bullet}$ radical fragment ion and the charge-reduced radical species $[\mathrm{M}+\mathrm{nH}]^{(\mathrm{n}-1)+\bullet}$ are the odd electron species in a typical ECD fragmentation of linear peptides.

In cyclic peptides, the $z^{\bullet}$ fragments are indistinguishable from the $[\mathrm{M}+\mathrm{nH}]^{(\mathrm{n}-1)+\bullet}$ charge-reduced radical cation, and the initial cleavage point cannot be determined. Therefore, in the corresponding ECD spectra, the peak representing this species ($[\mathrm{M}+\mathrm{nH}]^{(\mathrm{n}-1)+\bullet}$) likely contains cleaved species from all possible $N-C\alpha$ bonds around the cyclic peptide.

Accordingly with the U-W mechanism, after electron capture, the radical is located at the $\alpha-$carbon in both the $[\mathrm{M}+\mathrm{nH}]^{(\mathrm{n}-1)+\bullet}$ species and the $z^{\bullet}$ radical fragment ion. Thus, the *free radical reaction cascade mechanism* suggests that the radical at the $\alpha-$carbon could propagate along the peptide backbone,[192] inducing further fragmentation.

The radical at the $\alpha-$carbon can migrate along the cyclic peptide backbone by losing cyclic neutrals (figure 2.10a) and can also propagate by abstraction of an $\alpha H-$atom from another amino acid (figure 2.10b). This radical propagation by $\alpha H-$atom abstraction is an energetically favourable process due to the formation of one $H-C_{\alpha}$ bond by the cleavage of an additional $H-C_{\alpha}$ bond. Moreover, the energetic barriers can be minimised if the peptide is sufficiently flexible, which allows stabilisation of the radical.[192,251] Interestingly, the charge does not play a role in this radical fragmentation model and it has been assumed to be sequestered elsewhere, as shown in figures 2.10 to 2.12.[251] Therefore, fragmentation of both the charge reduced radical species and the radical fragment ions is primarily a radical-directed process rather than a charge-directed

process, although an exception is made for arginine containing peptides.[251]

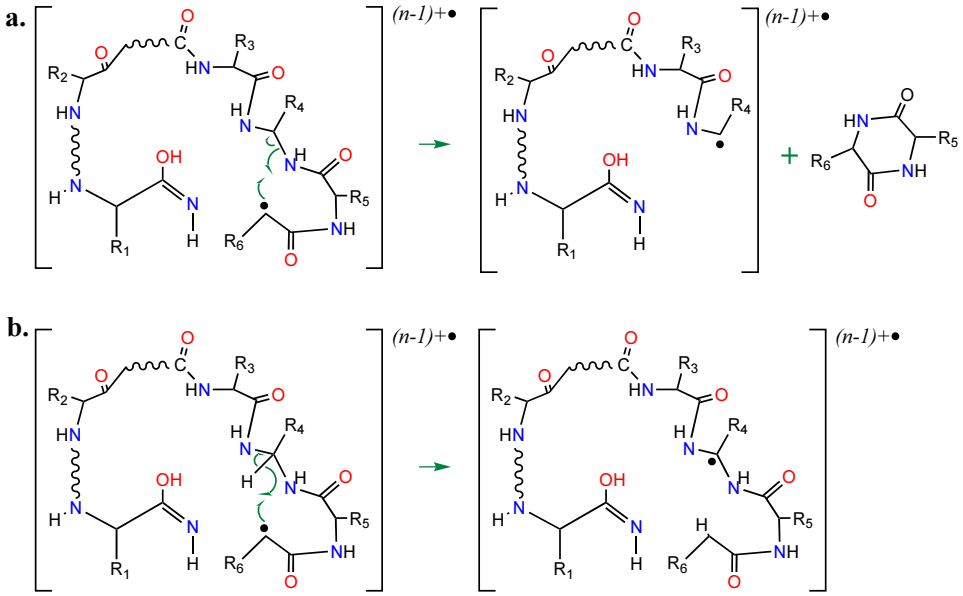

Figure 2.10: Schematic illustration of the radical mediated fragmentation pathway used to explain the losses observed in cyclic peptides, where the: **a.** radical is migrating along the peptide backbone bond to other $\alpha-$carbon causing loss of a small molecule; **b.** the radical is propagated by αH-atom abstraction from other amino acids. Figures adapted with permission from Leymarie, N. and Costello, C. E. and O'Connor, P. B.[192] copyright (2003) American Chemical Society

Neutral side chain losses of water and ammonium are also explained using the radical migration model,[192] which are shown in figure 2.11. Subsequent $H-$atom abstractions are possible, but would depend on energetic barriers, $H-$atom affinity, and the ability of the site to stabilise the radical.[142] Experiments on the deuterium exchange showed that the radical moves to the lowest energy site, which is the α-carbon of glycine.[142] The radical on the α-carbon of glycine is stabilised due to the planarity of the $C_\alpha - CO$ region, caused by the lack of side chain steric interactions.[146]

The free radical reaction cascade mechanism has also been motive of additional studies. For instance, other research groups explained that the radical at the α-carbon can also cause elimination of an odd-electron side chain species when the $\alpha H-$atom, from the α-carbon, is abstracted. The $\alpha H-$atom abstraction generates cleavage of the βcarbon-

γcarbon bond as shown in figure 2.12a.[202]

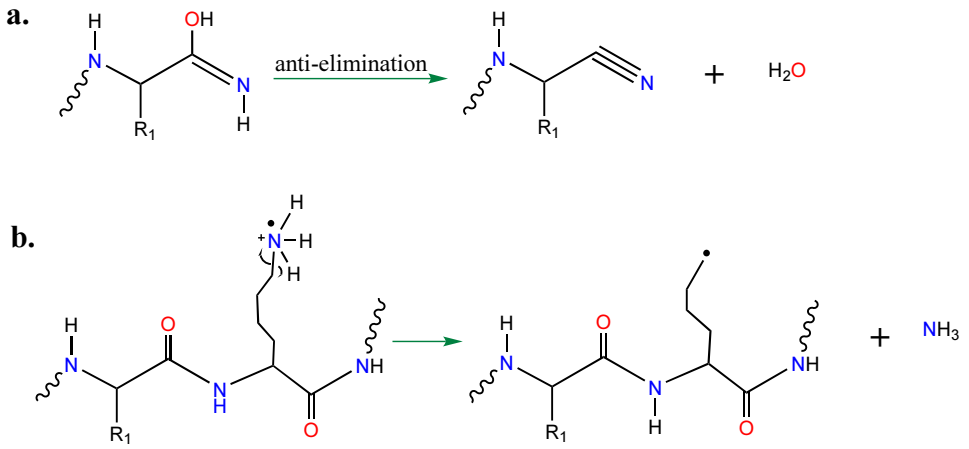

Figure 2.11: Schematic illustration of the radical mediated fragmentation pathway used to explain the neutral losses of: **a.** water and; **b.** ammonium. Figures adapted with permission from Leymarie, N. and Costello, C. E. and O'Connor, P. B.[192] copyright (2003) American Chemical Society.

Additionally, the radical can cause γ-hydrogen atom abstraction at amino acids with a γ-carbon in the side chain, γ-hydrogen abstraction can occur generating a stable radical at the α-carbon of the peptide backbone (figure 2.12b) and eliminating an even-electron side chain.[173,251] This γ-hydrogen atom abstraction is also observed in $z^{\bullet}$ radical fragment ions, which generates w-type fragment ions.[142]

The radical attached to the C_α can also migrate to other π^* orbitals, which has also been reported in the helix structures of proteins, but only by overcoming an energetic barrier.[143] However, the radical migration path in helical structures depends of the initial structure of the OCN group after electron capture (see figure 2.5). In other words, it depends on whether the oxygen attached to the α-carbon is forming an O$-$H bond or is a radical anion centre O^-, as shown in figure 2.13.

Some unusual side chain fragmentations, such as the one observed at the $N-$terminal side of proline are illustrated in figure 2.14a and are based on the $\alpha H-$atom abstraction from the α-carbon of proline.[173] $H-$atom abstractions from the β-carbon are observed

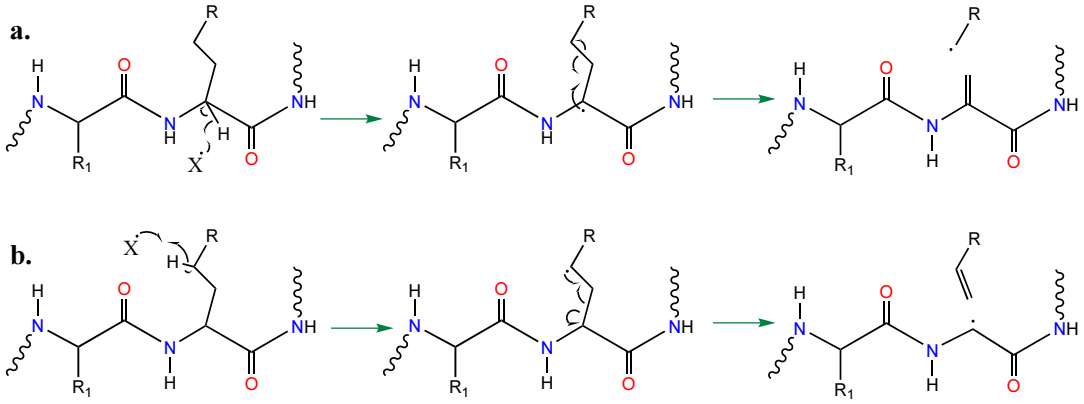

Figure 2.12: Schematic representation of the proposed reaction mechanism by the radical cascade model. **a.** Side chain losses by $\alpha-$hydrogen atom abstraction at the C_α causing loss of an odd-electron species.; **b.** Side chain losses by $\gamma-$hydrogen atom abstraction causing loss of an even-electron species. The charge is not shown in this radical migration process as it is not considered a charge-directed process; Figures adapted with permission from Sun, Q. and Nelson, H. and Ly, T. and Stoltz, B. M. and Julian, R. R.[251] copyright (2003) American Chemical Society.

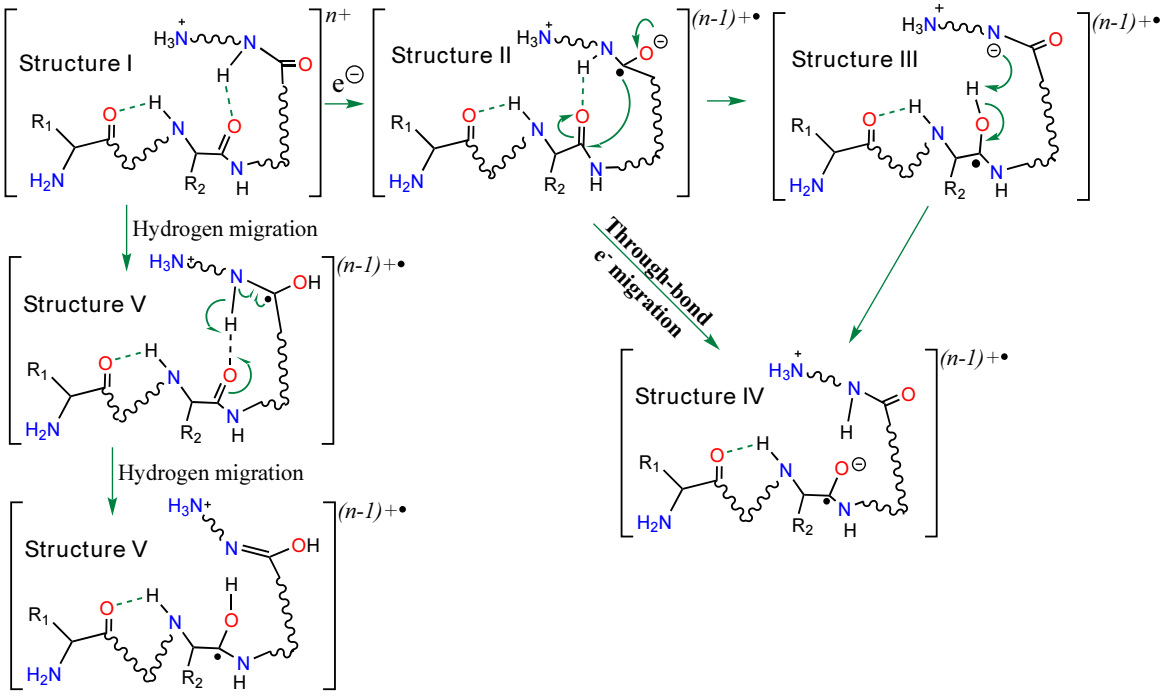

Figure 2.13: Schematic illustration of the radical mediated fragmentation pathway used to explain the radical migration in helical structures. Figure adapted with permission from Skurski, P. and Sobczyk, M. and Jakowski, J. and Simons, J.[143]

in serine and threonine containing peptides, where the radical located at the β-carbon can be resonantly stabilised by the hydroxyl group. This intermediate decomposes causing cleavage at the $N - C\alpha$ and generating a $c^{\bullet}$ and a non radical z fragment ion one hydrogen lighter. This is illustrated in figure 2.14b.

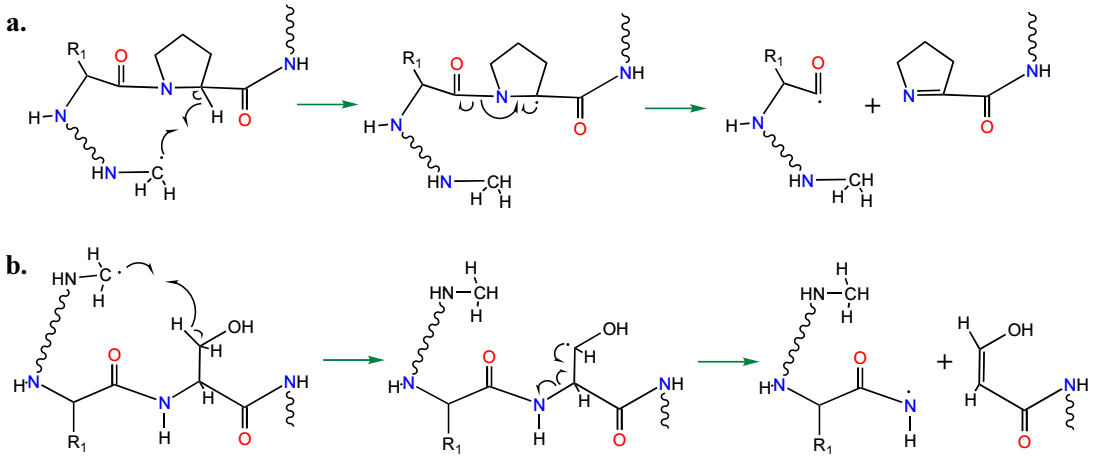

Figure 2.14: Schematic illustration of the radical mediated fragmentation pathway used to explain: **a.** Proline $N-$terminus cleavage by α-hydrogen atom abstraction; **b.** βH-atom abstractions at the β-carbon. Figures adapted with permission from Fung and Chan. [173]

Thus, after the initial electron capture and cleavage of the $N - C\alpha$ backbone bond, further dissociation of both the charge-reduced radical species and from the $z^{\bullet}$ radical fragment ion is dominated by radical chemistry. [251] In a radical-directed process the radical is an active and/or dominant participant in the chemistry. These radical directed processes generate additional fragmentation products, such as side chain losses, losses from the $z^{\bullet}$ radical fragment ions, H$^{\bullet}$-radical loss, and other types of fragments such as those observed in cyclic peptides and discussed above. [87,173,192] Moreover, radical-directed fragmentation would not occur indefinitely in the peptide/protein. The radical will move until one out of three possible conditions is satisfied: either the radical is stabilised at a low reactivity position (*e.g.* resonant stabilisation); [192] or, the radical moves too slow to be detected in the mass spectrometer; [2] or loss of H$^{\bullet}$-radical occurs.

[2] The time scale of the measurement in a mass spectrometer is usually of the order of seconds.

It is noteworthy that in the radical migration model H-atom abstraction competes with $H^{\bullet}$-radical loss.[192] So, if the $H^{\bullet}$-radical is lost, a radical-directed fragmentation would not occur. However, in arginine containing peptides the charge is sequestered at the guanidino moiety and becomes a fixed-charge. Fixed-charges in peptides increase the abundance of side chain losses and the number of backbone cleavages decreases as the number of fixed-charges increases.[252] In peptides with two arginine residues the *neutral* side chain loss of arginine occurs first from the charge-reduced radical species. Subsequently, other side chain losses can be observed.[173] Similar fragmentation behaviour is observed for tryptophan and histidine containing residues. This behaviour was explained by fast fragmentation at the recombination site.[3]

2.6 Non-Ergodicity

When ECD was introduces as an analysis technique in polypeptides, it was hypothesized that the fragmentation involved non-ergodic behaviour because the capture of one electron can only releases $\sim 6\,eV$ of energy, which is barely enough to break one $N-C\alpha$ bond.[8] A process is referred to as non-ergodic if the *fragmentation rate* is fast compared to the rate of the energy redistribution among the many vibrational degrees of freedom of the polypeptide.[253] This implies that the energy is not redistributed among the internal vibrational modes of the polypeptide and the excess energy would reside in the $N-C\alpha$ bond causing $N-C\alpha$ bond cleavage[254] A detailed discussion about ergodicity of gas-phase ions has been presented elsewhere.[255]

In order to address the discussion about non-ergodicity/ergodicity, it is necessary to consider ECD rate and energies associated with ECD fragmentation. As it was previously discussed in section 2.5.2, the Coulomb stabilisation at the π^* orbital is sufficient

[3]The recombination site is considered to be the protonation site and the electron capture site.

to decrease the energy of the orbital allowing exothermical capture of an electron ($\sim 4-6\,eV$ taken from the electron affinity of protonated nitrogen in an amine or amide moiety).[8,254] The polypeptide is then in an excited state where the non-fixed energy is free to move around the molecule, *e.g.* vibrational and rotational energy, (excluding the zero-point energy). This intramolecular energy transfer, also referred to as *recombination energy*, is suggested to occur in a time scale of 10^{-11} to $10^{-12}\,s$,[256] and is believed to induce fragmentation in the excited electronic state rather than inducing vibration in the electronic ground state.[53] However, the debate has been focused on finding out whether the energy is redistributed faster than 10^{-11} to $10^{-12}\,s$. Hence, the following discussion is focused on the electron migration rates using the Utah mechanism discussed in section 2.5.2.

The electron migration considered by the Utah mechanism can follow two pathways.[242,246] First, the electron is captured at an excited $n-$Rydberg orbital, with $n > 10$ and with the orbital centred at a positive site. Subsequently, electron migration towards a Coulomb stabilised π^* orbital could occur, but only before the Rydberg electron has time to completely relax to the ground Rydberg state. If the ground state is reached and the electron has not migrated, prompt ($\sim 10-9\,s$) H-atom and NH_3 loss is observed in the ECD spectrum.[254] So, low-energy Rydberg states ($n < 20$) are suggested to be involved in electron migration to other Coulomb stabilised π^* orbitals. Additionally, the Rydberg orbital relaxation, from the excited state to the ground state, occurs at a rate of approximately $10^6\,s^{-1}$ while electron migration occurs at a rate of $10^{10}\,s^{-1}$ per transition.[254] Therefore, electron migration to a Coulomb stabilised π^* orbital is faster than Rydberg orbital relaxation.

The second pathway of electron migration considers the electron captured at a Rydberg orbital centred at a positive site and that the electron could migrate to another positive site. Transfer to this new location from a lower or equal energy Rydberg orbital has been

considered to be possible.[254] The mathematical treatment of this case suggests that a faster rate is expected to be obtained from an electron migrating between Rydberg orbitals with the same quantum number. Moreover, the migration rates decrease as the quantum number grows.[254] However, conclusive experimental evidence to support this pathway of electron migration has not been found[254] Indirect experimental evidence, which supports this second pathway has been reported using electron traps, which have high electron affinity and can intercept the electron, causing inhibition of the backbone fragmentation.[257–259]

Additionally, the electron migration from an excited Rydberg orbital to a Coulomb stabilised π^* orbital proceeds via a vertical transition (Frank-Condon transition), where the electron binding energy is very similar to the vertical binding energy of the π^* attached state (figure 2.15).

Finally, high-level *ab initio* calculations of dissociation rates of the aminoketyl radical intermediate have shown an ergodic behaviour of peptides.[193,260] However, it is not possible to extrapolate these results to longer systems (proteins) due to the complexity of the multiple charged peptide/protein ions simulations and/or calculations.[193,254] It seems clear, then, that to date the debate about the non-ergodic character of ECD is still open.

2.7 Concluding remarks

ECD in a FT-ICR-MS has become a preferred ion activation technique for structural identification of protein/peptides. In this chapter the nomenclature and some of the concepts used in ECD experiments were presented. In particular, a discussion about ECD efficiency was addressed on the many different ways to calculate it, which makes

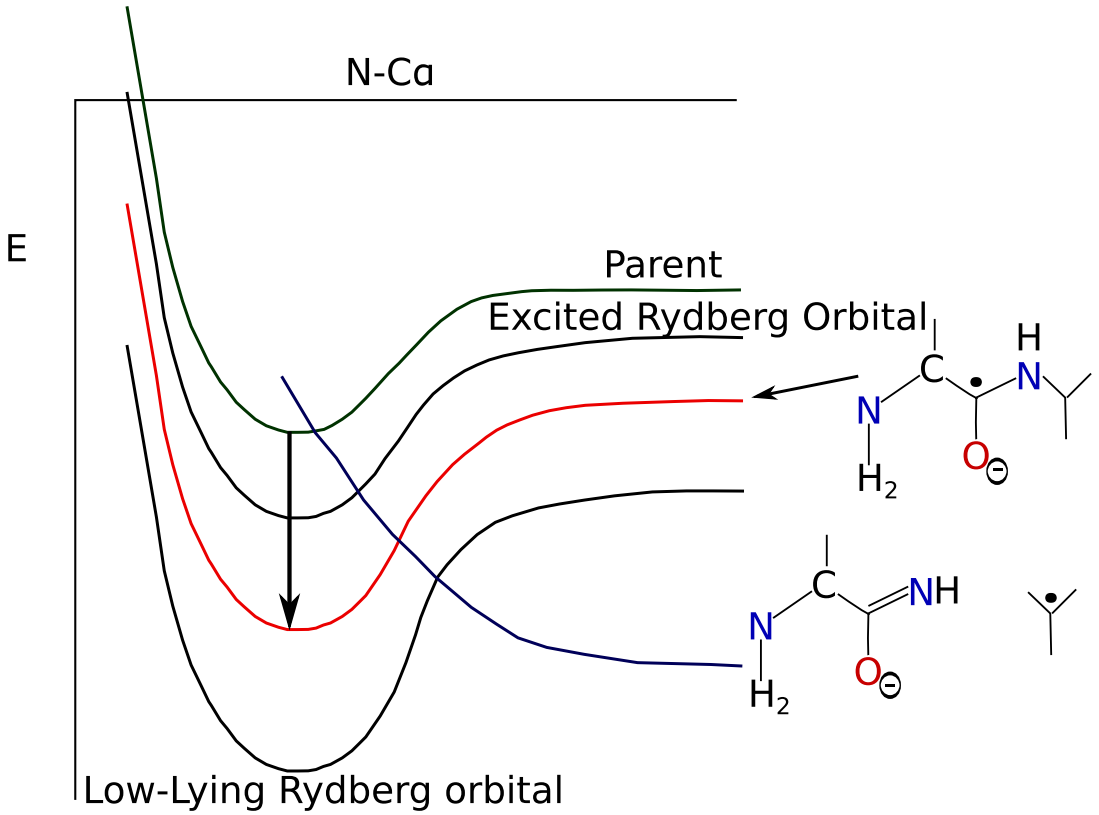

Figure 2.15: Qualitative depiction of the potential energy hypersurfaces of species containing $N - C\alpha$ bond subjected to electron capture at the Rydberg orbital centred at a positive site and vertical migration of the electron to the Coulomb stabilised π^* orbital. Figure adapted with permission from Neff, D. and Sobczyk, M. and Simons, J.[242]

comparisons in the literature difficult. Additionally, a summary of the side chain losses, from the charge-reduced radical species, as well as from the $z^\bullet$ radical fragment ion, as reported in ECD literature, was presented. Similarly, a brief summary of other ECD related methods was done in order to show how particular limitations of ECD have been circumvented. Moreover, based on the seemingly reached general consensus, the ECD mechanism for the dissociation of the $N - C\alpha$ backbone bond was explained. Another mechanism presented was the *free radical reaction cascade mechanism*, which occurs after $N - C\alpha$ backbone cleavage. Such a mechanism allows to explain additional side chain losses from the charge-reduced radical species and from the $z^\bullet$ radical fragment ion. Finally, a few comments about non-ergodicity were discussed, but the debate still continues.

3

Assignment of binding sites glyoxal-derived advanced glycation end-products for substance P

3.1 Introduction

In this study, the dicarbonyl glycation reaction is studied through glyoxal binding to the neuropeptide Substance P using Fourier transform ion cyclotron resonance mass spectrometry (FT-ICR-MS). Substance P has the amino acid sequence RPKPQQFFGLM, and normally contains an amidated $C-$terminus. Thus, the guanidino group of arginine, the amino group of lysine, the $N-$terminus and the amidated $C-$terminus are the potential glyoxal glycation sites for Substance P. The glyoxal-derived glycation products (AGE) were fragmented by ECD, double resonance-ECD and CAD and glyoxal binding site was assigned within 1 ppm error (accurate mass assignments are available in the Appendix A).

3.2 Materials and methods

Substance P and Substance P acetate salt, ammonium acetate ($\sim$ 99.6 %), triethylamine, ammonium phosphate monobasic, and acetic acid ($\geq$ 99 % pure) were purchased from Sigma-Aldrich (St. Louis, MO, U.S.A). Methanol (LC-MS grade), ethanol (HPLC grade), and isopropyl alcohol (IPA, GLC-pesticide grade) were purchased from Fisher-Scientific (Loughborough, Leicestershire, U.K.), and were used without further purification. All aqueous solutions were prepared using water from a Milli-Q water system (Millipore Inc., Durham, U.K.). Micro-dialysis cassettes (GeBa flex-tube, $1\,kDa$ cut-off), were obtained from Chembio Diagnostic Systems, Inc. (Hertfordshire, U.K.). Glyoxal solution ($\sim$ 39% in water) was purchased from TCI Europe (Zwijndrecht, Belgium). High purity glyoxal solution was difficult to obtain because higher concentration favours the formation of glyoxal dimers and trimers through dioxolane rings.[261] Nuclear magnetic resonance analysis of glyoxal solution showed hydrolysis and dimer species, as previously reported by Whipple, E. B.[262]

3.2.1 Substance P glycation

In-vitro glycation with glyoxal at a concentration of $800\,\mu mol/L$ was performed with Substance P ($1mg/mL$), or amidated Substance P ($1\,mg/mL$). The reaction was carried at 37 °C in MeOH:H_2O (50:50), 100 % water, and phosphate buffer [$30\,mM$ ammonium phosphate monobasic ($NH_4H_2PO_4$) and $30\,\mu$L triethylamine ($N(CH_2CH_3)_3$) pH 7.5], for 21 and 12 hours, respectively. The samples reacted in phosphate buffer were dialysed against water and $10\,mM$ CH_3COONH_4, over a period of 24 h, dried, and redissolved in MeOH/H_2O (50:50). Prior to injection in the FTICR-MS, samples were prepared to a concentration of $\sim$1 to $5\,pmol/\mu$L using electrospray solution (composed either of MeOH or EtOH/IPA/Acetic acid/H_2O; 50:10:1:39). Methanol was used as an inhibitor of

glyoxal polymerisation instead of acetonitrile, which promotes glyoxal dimerisation.[263]

3.2.2 Mass spectrometry

The experiments were performed in a 12 T solariX FTICR-MS (described in chapter 1). The sample was electrosprayed in positive ion mode with a capillary voltage of $4.5\,kV$. To perform ECD, the precursor ion was isolated in the quadrupole (Q1), and accumulated in the collision cell ($15\,s$). After being transferred and trapped in the infinity cell[264] the ions were irradiated with low-energy electrons ($\sim 1\,eV$) for 150 and 250 ms. Double resonance ECD (DR-ECD),[227,228] was performed in the cell varying the ejection pulse between 120 to 220 ms. The laser pulse for the infrared multiphoton dissociation (IRMPD),[39,265] experiment was kept at 90 ms followed by electron injection. CAD experiments were performed in the hexapole or collision cell prior to selection of the precursor ion in the quadrupole with collision energies around $10-30\,eV$. The data was processed with Data Analysis software 4.0 SP 3, and internally calibrated.

3.3 Results and discussion

Experiments were carried out in phosphate buffer, because of its biological relevance, and in MeOH/H_2O (50:50) in order to develop the method aiming to assign the types of glyoxal-derived glycation products (AGE) and its binding site for amidated Substance P. Figure 3.1a, shows doubly $[M+2\,H]^{2+}$ and triply charged $[M+3\,H]^{3+}$ ions from unmodified amidated Substance P. The spectrum also shows four more doubly charged ions, $[M+C_2O+2\,H]^{2+}$, $[M+C_2H_2O_2+2\,H]^{2+}$, and A and B species. The mass of the peptide was increased by both $39.9949\,Da$ in the case of C_2O addition and $58.0055\,Da$ assigned as $C_2H_2O_2$. Species A and B showed a mass difference of $14.0156\,Da$ (CH_2),

with respect to both modified ions, which were identified as ion/molecule reaction ions with methanol. These A and B ions were eliminated when the reaction was carried out in $100\,\%$ water, and ethanol was used in the electrospray solution, figure 3.1b.

The reaction in phosphate buffer, sprayed in methanol-containing solution, showed the same ions discussed above for figure 3.1a. The glyoxal-derived AGE observed ions $[\mathrm{M} + \mathrm{C_2O} + 2\,\mathrm{H}]^{2+}$ (m/z 694.3688), and $[\mathrm{M} + \mathrm{C_2H_2O_2} + 2\,\mathrm{H}]^{2+}$ (m/z 703.3741), are formed following the proposed reaction pathway showed in Scheme 3.1, for both reaction solutions ($\mathrm{MeOH/H_2O}$ and phosphate buffer). Scheme 3.1 shows the possible structures that may be formed by glyoxal; in particular structures 3.1e and scheme 3.1f were identified by De Haan, D. O. and Corrigan, A. L. and Smith, K. W. and Stroiik, D. R., D. R. and Turley, J. J. and Lee, F. E. and Tolbert, M. A. and and Cordova, K. E. and Ferrell, G. R.[266] to coexist in a 3:1 ratio. Thus, the glyoxal-derived AGEs formed by the net addition of $\mathrm{C_2O}$ and $\mathrm{C_2H_2O_2}$ were fragmented by ECD and CAD in order to identify the glyoxal binding site.

3.3.1 Substance P modified by $\mathrm{C_2O}$

Figure 3.2a shows the ECD spectra of the precursor ion $[\mathrm{M} + \mathrm{C_2O} + 2\,\mathrm{H}]^{2+}$ reacted in $\mathrm{MeOH/H_2O}$ (50:50), with two kind of c fragment ions: unmodified c_4 - c_{10}, and modified $c_4^\dagger$ - $c_{10}^\dagger$. A dagger symbol was added to the standard Roepstorff nomenclature[47] ($c/z^\bullet$), to differentiate the ions with the glyoxal modification. The radical $z_9{}^\bullet$ fragment ion, loss of water from the modified $c_n^\dagger$, y_9, and side chain losses from the charge-reduced species were also observed. The pair $c_1/z_{10}{}^\bullet$, $c_3/z_8{}^\bullet$, $c_1^\dagger/z_{10}{}^\bullet$, and $c_3^\dagger/z_8{}^\bullet$, together c_2 and $c_2^\dagger$ were absent in the spectrum. Figure 3.2a additionally shows the unmodified doubly charged $[\mathrm{M} + 2\,\mathrm{H}]^{2+}$ ion, which is unusual during ECD experiments, because the capture of low-energy electrons by the molecule generates the charge-reduced radical

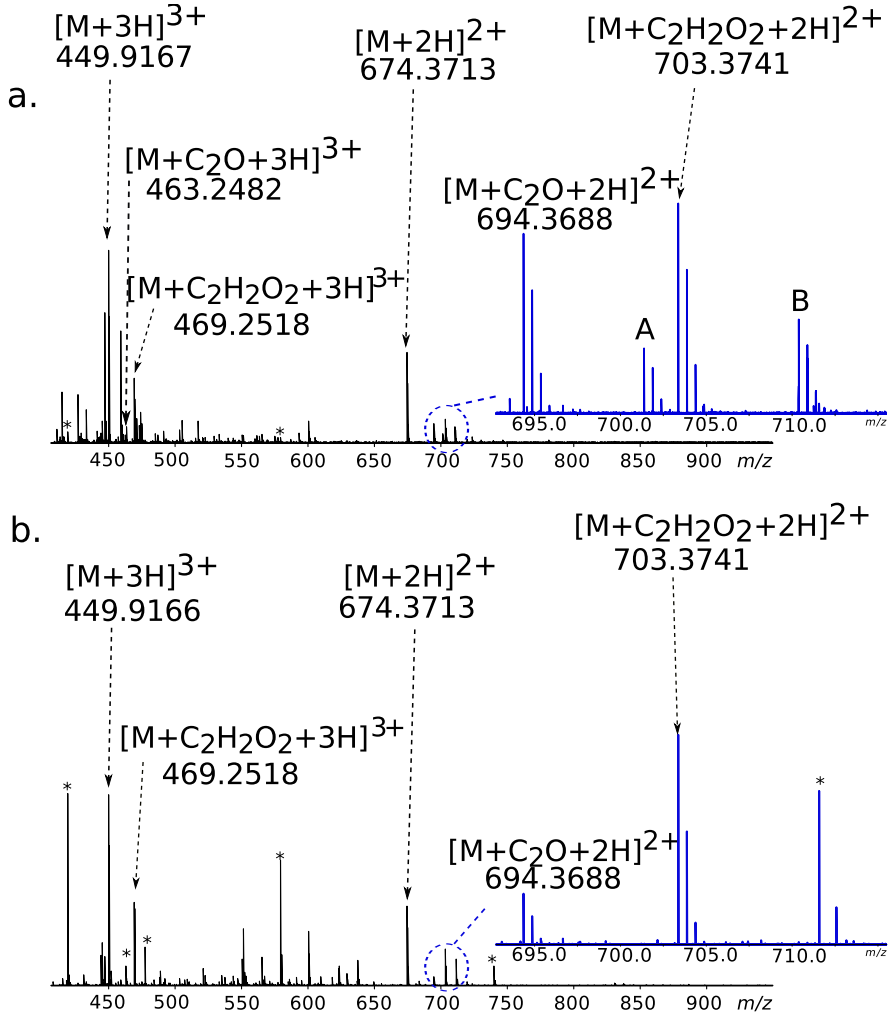

Figure 3.1: Direct infusion spectrum of: **a.** glyoxal-derived glycation products (AGEs) reacted in MeOH/H_2O (50:50) and ionized with a solution containing MeOH, IPA, H_2O, and acetic acid; **b.** glyoxal-derived glycation products (AGEs) reacted in 100 % H_2O and ionized with a solution containing EtOH, MeOH, IPA, H_2O, and acetic acid.

species ($[M + C_2O + 2H]^{2+} + e^-$ becomes $[M + C_2O + 2H]^{1+\bullet}$), and not the loss of the modification. Thus, isolation spectrum of the precursor ion $[M + C_2O + 2H]^{2+}$ was acquired in order to determine if the $[M + 2H]^{2+}$ ion originated during quadrupole isolation. The isolation spectrum of the precursor ion $[M + C_2O + 2H]^{2+}$ shows low abundance of the molecular ion $[M + 2H]^{2+}$ indicating that loss of C_2O is a low-energy, facile process. The presence of the $[M + 2H]^{2+}$ ion indicates that during isolation some small, unknown, amount of energy was given to the precursor ion $[M + C_2O + 2H]^{2+}$,

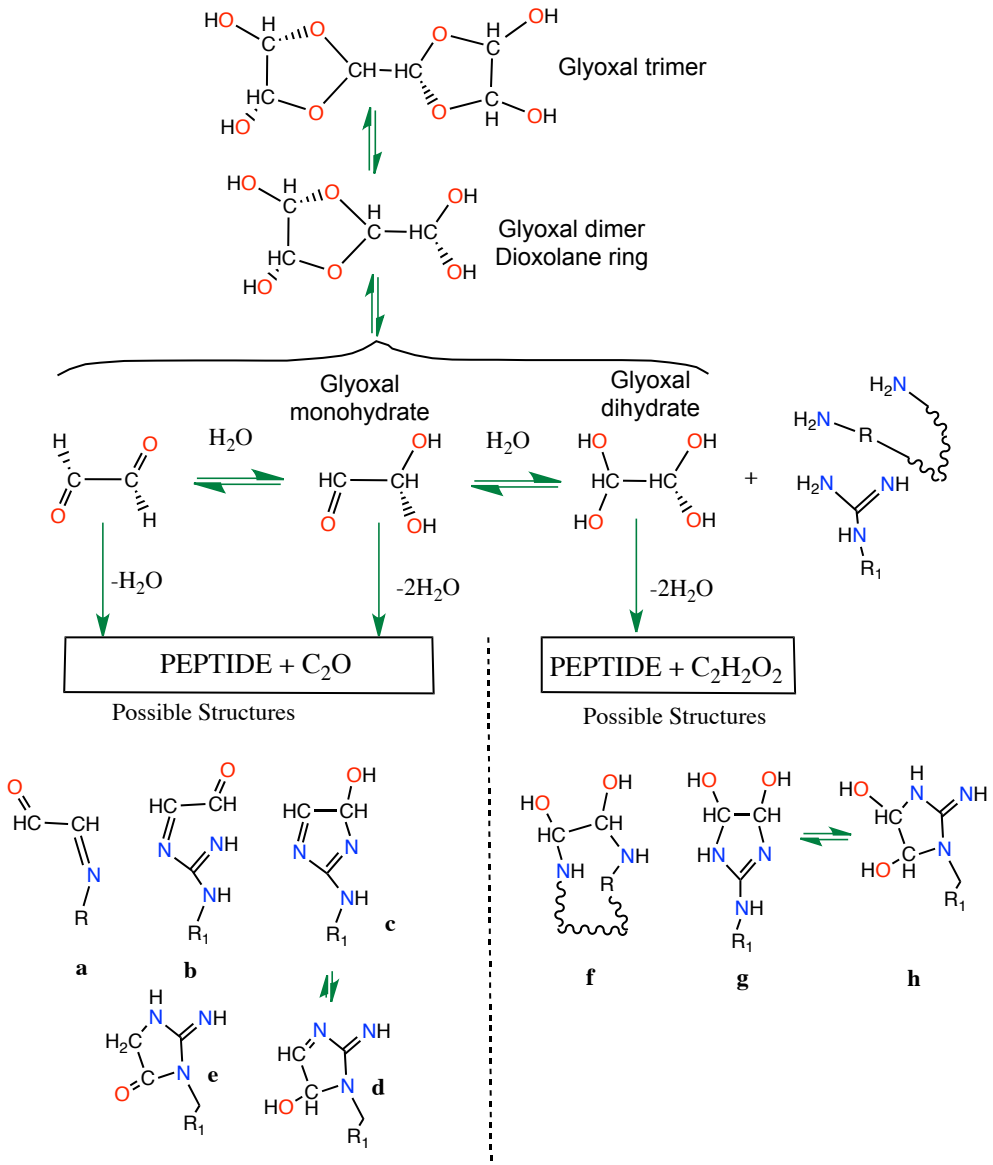

Scheme 3.1: Glyoxal-derived glycation products (AGEs) based in the presence of monohydrate and dihydrate species in glyoxal reagent ($\sim$ 39 %) in water. Structures: **a.** Schiff base at the $N-$terminus or amine group of lysine; **b.** Schiff base at the guanidine group of arginine; **c.** 3-hydroxyimidazole; **d.** 2-imino-5-hydroxyimidazoline; **e.** 2-imino-imidazolidinone (also known as a creatinine side chain); **f.** crosslinking between amino group of lysine with the $N-$terminus; **g.** 3,4-dihydroxyimidazoline; and **h.** 2-imino-imidazolidine.

which activates it causing loss of the modification and generating the $[\mathrm{M}+2\,\mathrm{H}]^{2+}$ ion. The $[\mathrm{M}+2\,\mathrm{H}]^{2+}$ ion may therefore be responsible for the secondary fragmentation (c_4 - c_{10}) observed during the ECD experiment.

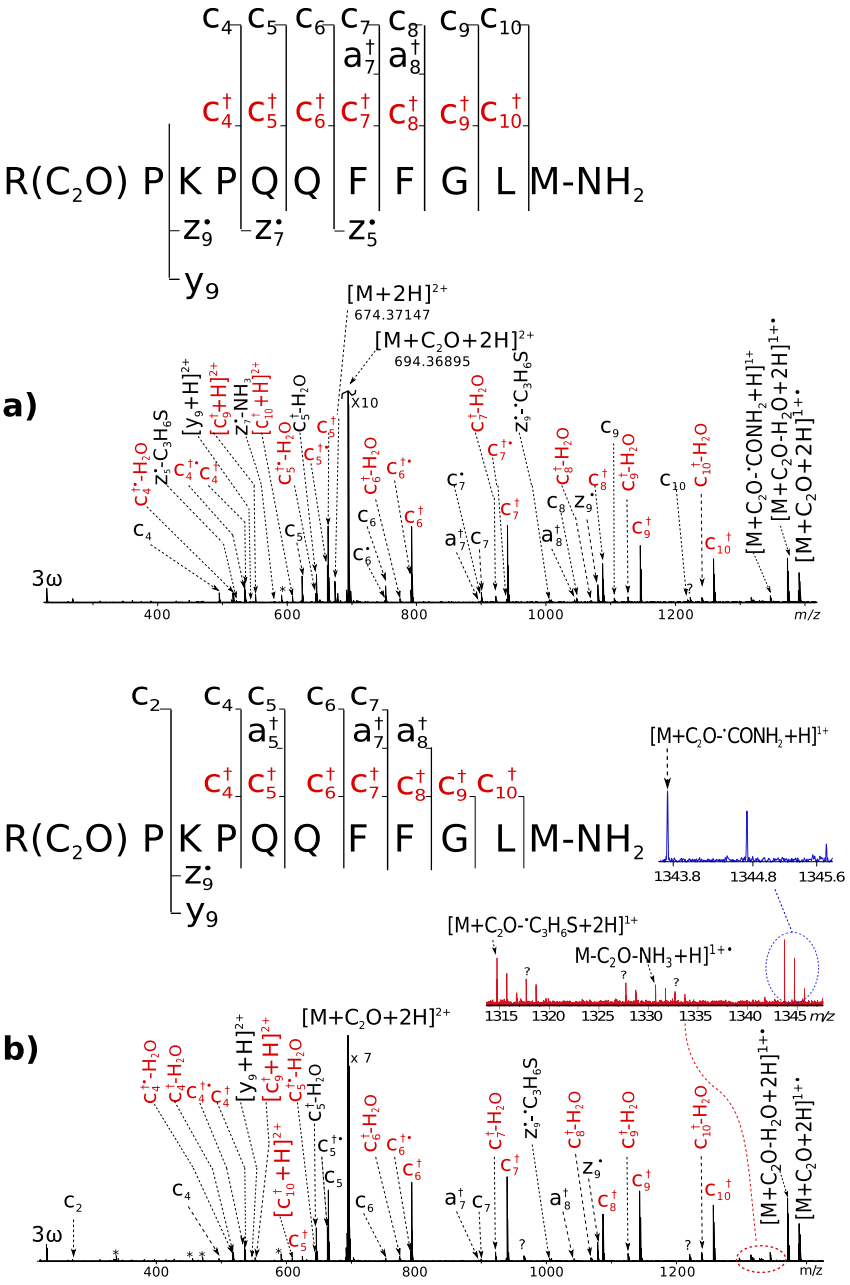

Figure 3.2: MS/MS spectra of the precursor ion $[M + C_2O + 2H]^{2+}$ of glycated amidated substance P reacted in MeOH/H_2O (50:50): **a.** ECD spectrum; **b.** DR(674.37)-ECD(694.37) spectrum with ejection of $[M + 2H]^{2+}$ species. The symbol ? indicates unassigned peaks by the current understanding of the fragmentation mechanism, and * indicates background peaks where no isotopologues were observed. Peak assignments are presented in Tables A-1 and A-2 Appendix A.

Additionally, because the $[M + 2H]^{2+}$ ion and the c_4 -c_{10} ions were formed during ECD, preisolation yielded no new information about their provenance. So, in order

to test if they were secondary fragments formed from the $[M + 2H]^{2+}$ ion, double resonance-ECD[229] was used to eject the ion $[M + 2H]^{2+}$ during the ECD experiment of the precursor ion $[M + C_2O + 2H]^{2+}$. The notation adopted for the double resonance experiments is represented as DR(X)-ECD(Y), where X is the m/z value of the ejected fragment and Y corresponded to the m/z value of the precursor ion. The DR(674.37)-ECD(694.36) spectrum of glycated, amidated Substance P for the precursor ion $[M + C_2O + 2H]^{2+}$ (Figure 3.2b), exhibited similar features as those described above for the ECD spectrum, but the difference lies in the absence of c_8, c_9, c_{10}, $z_7^{\bullet}$, and $z_5^{\bullet}$. The observed relative intensities of the c_n and $c_n^{\dagger}$ fragment ions (n = 2-10) were normalized to check their lineage. The normalized relative intensity (I_i) was calculated by application of the equation 3.1.

$$I_i = \frac{I_{(k_I)}}{\sum_{n=2}^{n=10} I_{(c_n)} + \sum_{n=2}^{n=10} I_{(c_n^{\dagger})}} \tag{3.1}$$

Where, I_i takes the values of the relative abundance of the ions of every individual c_n and $c_n^{\dagger}$ fragment ions. These values are plotted in Figure 3.3 where it is observed that I_i of the c fragment ions decreased and I_i of $c_n^{\dagger}$ and $z_9^{\bullet}$ fragment ions increased during the DR-ECD experiment. Thus, based on those results, it is inferred that all c fragment ions observed in the DR-ECD and ECD spectrum are secondary fragments of the unmodified $[M + 2H]^{2+}$ ion and are derived from a long-lived radical intermediate species (milliseconds to microsecond time frame).[229] Additionally, from Figure 3.3, the radical fragment $z_9^{\bullet}$ is considered a long-lived species[229] and is a fragment from the doubly-charged modified species.

The $c_n^{\dagger}$ fragment ions locate the C_2O modification within four residues of the $N-$terminus and the presence of $z_9^{\bullet}$ and y_9 in Figure 3.2b, indicate an unmodified lysine. Thus,

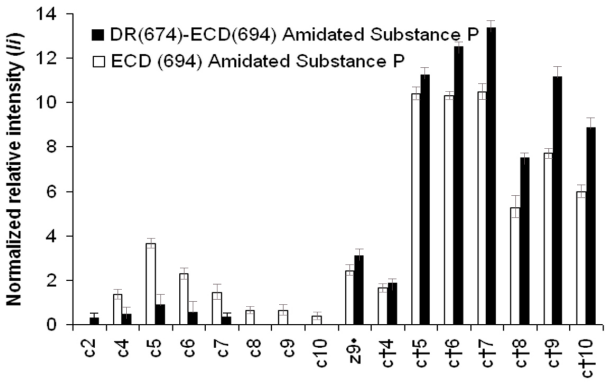

Figure 3.3: Comparison of the relative intensity of the c_n and $c_n^{\dagger}$ (n = 2-10) fragment ions of the precursor ion $[M+C_2O+2\,H]^{2+}$ observed in the ECD and DR(674.37)-ECD(694.36) spectra of glycated amidated Substance P (reacted in MeOH/H_2O (50:50)). The relative intensity of each c_n and $c_n^{\dagger}$ fragment ion was calculated by application of the equation 3.1 where I_i is the relative intensity of the ion.

the glyoxal-derived AGE for Substance P is located at the arginine residue and more specifically at the guanidine group. The guanidine group at the arginine residue reacts with glyoxal causing the loss of water and resulting in the net addition of C_2O (39.9949 Da), which can form structure **b** and/or structure **c** (hydroxyimidazole) shown in Scheme 3.1.

3.3.2 Substance P modified by $C_2H_2O_2$

Figure 3.4 shows the DR(674.37)-ECD(703.37) spectrum of the precursor ion $[M + C_2H_2O_2 + 2\,H]^{2+}$ with unmodified c_n, and modified $c_n^{\ddagger}$ (n = 4-10) fragment ions. The double dagger (‡) symbol is added to the standard Roepstorff nomenclature to identify the modified fragments. $z_9^{\bullet}$ radical fragment ion, side chain losses from the charge-reduced species, and up to two losses of water from the $c^{\ddagger}$ fragment ions are observed in Figure 3.4, with absence of c_2, $c_2^{\ddagger}$, $c_1^{\dagger}$ $z_{10}^{\bullet}$ and $c_3^{\dagger}$ $z_8^{\bullet}$ fragment ions. Thus, according with those results the modified $c_n^{\ddagger}$ (n = 4-10) fragment ions locate the modification $C_2H_2O_2$ toward the $N-$terminus and the presence of $z_9^{\bullet}$ indicate that the lysine residue

is unmodified. The $C_2H_2O_2$ moiety is located also at the arginine residue as shown in Scheme 3.1. The proposed structures **e** and **f** in Scheme 3.1, are formed at the guanidine group forming the proposed dihydroxyimidazoline group by the loss of two molecules of water.

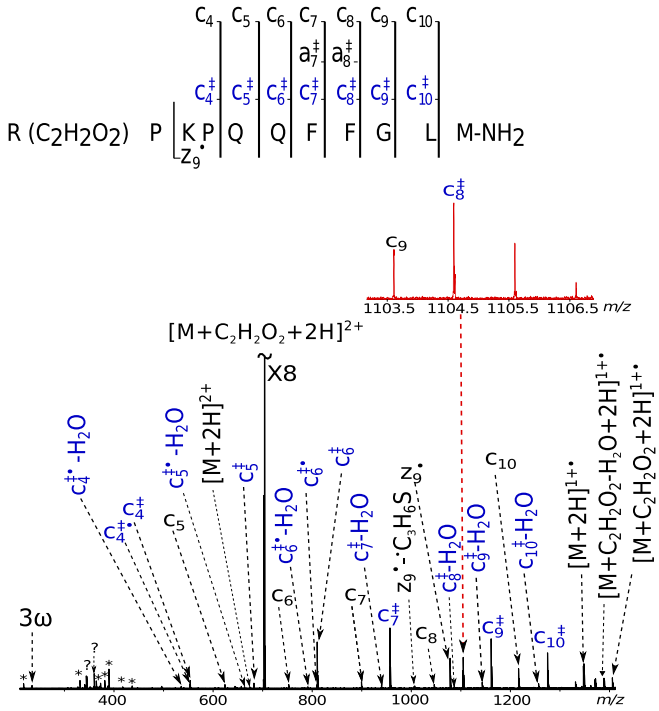

Figure 3.4: DR(674.37)-ECD(703.37) spectrum of the precursor ion $[M + C_2H_2O_2 + 2\,H]^{2+}$ with ejection of $[M + 2\,H]^{2+}$ species of the glycated amidated Substance P reacted in MeOH:H2O (50:50). The symbol ? indicates unassigned peaks by the current understanding of the fragmentation mechanism and * indicates background peaks where no isotopologues were observed. Peak assignments are presented in Table A-3 Appendix A.

All the results of the ECD and DR-ECD spectra for the precursor ions $[M + C_2O + 2\,H]^{2+}$ (Figure 3.2), and $[M + C_2H_2O_2 + 2\,H]^{2+}$ (Figure 3.4), shared three features. First, the absence of the complementary pair $c_1^{\dagger}$ / $z_{10}^{\bullet}$, $c_3^{\dagger}$ / $z_8^{\bullet}$, $c_1^{\ddagger}$ $z_{10}^{\bullet}$ and $c_3^{\ddagger}$ / $z_8^{\bullet}$ that is due to proline, which requires cleavage of two bonds in order to observe the fragments.[171] Second, c_2 was absent in the ECD spectrum (figure 3.2a), but appeared in the DR-ECD spectrum (figure 3.2b), whereas $c_2^{\dagger}$, and $c_2^{\ddagger}$ were completely absent. The c_2 fragment ion from unmodified Substance P is rarely observed in the ECD spectrum.[171,267] Third, the

loss of water from every $c^{\dagger}$ and $c^{\ddagger}$ fragment ion, is attributed to the glyoxal modification. So, it was hypothesized that hydrogen bond interactions may be involved for both glyoxal modifications, which may be broken during the ECD event causing the loss of water. Thus, IRMPD was applied to amidated Substance P, prior to the ECD experiment, in order to facilitate disruption of the non-covalent interactions (figure 3.5). The obtained relative intensity of the $c_n^{\dagger}$ and $c_n^{\dagger}$ - H_2O (n = 4-10) fragment ions was normalised using equation 3.1 and plotted in figure 3.6. It is observed that I_i of $c_n^{\dagger}$ - H_2O (n = 4-10) during the IRMPD-ECD experiment increased in all observed fragments. Thus, use of infrared heating to disrupt the hydrogen bonding network induced water loss from the glyoxal-derived AGEs.

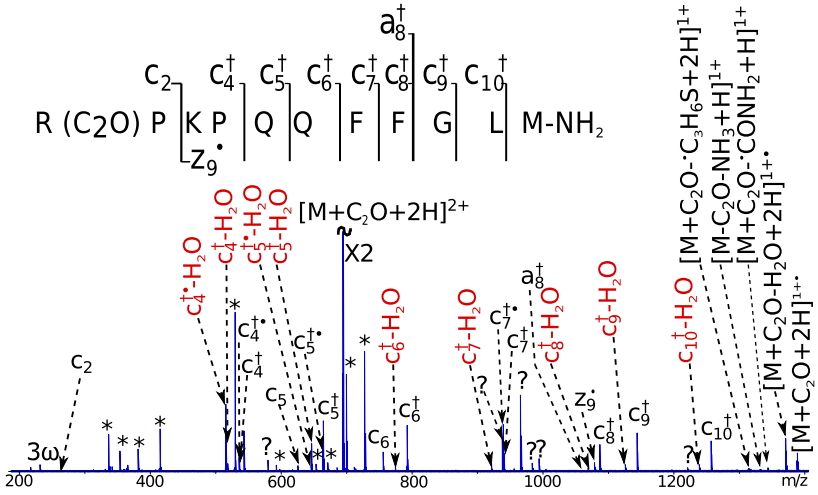

Figure 3.5: IRMPD-ECD spectrum of the precursor ion $[M + C_2O + 2H]^{2+}$ of the glyoxal-derived glycation product formed at amidated Substance P in MeOH:H_2O (50:50). The symbol ? indicates unassigned peaks by the current understanding of the fragmentation mechanism and * indicates background peaks where no isotopologues were observed. Peak assignments are presented in Table A-4 Appendix A.

On the basis of the previous results it is possible to propose an ECD mechanism for the loss of water of the glyoxal-derived AGEs for Substance P. Therefore, after the electron is captured in the peptide, it is suggested that the modified guanidine group at the arginine residue loses water forming the imidazole radical moiety, as shown in Scheme 3.2a. Moreover, for the dihydroxyimidazoline group, it is proposed that the capture of the

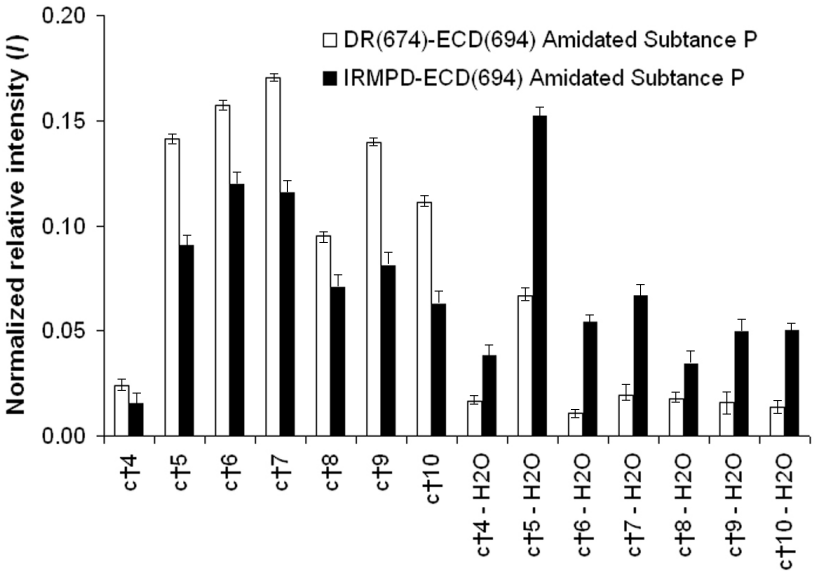

Figure 3.6: Comparison of relative intensity of the $c_n^\dagger$ and $c_n^\dagger$ - H_2O fragment ions for the DR(674.37)-ECD(694.37) and IRMPD-ECD spectra of glycated amidated Substance P reacted in MeOH/H_2O (50:50). The relative intensity was calculated using equation 3.1, only considering the relative intensity of the $c_n^\dagger$ and $c_n^\dagger$ - H_2O fragment ions.

electron initially generates the loss of one molecule of water forming an intermediate structure. The imidazole ring (structure II in Scheme 3.2b) is believed to be formed by an extra loss of water that is not driven by the radical, although the energy deposited during electron capture, as well as the additional stabilisation energy from conjugation of the π system with the radical, would promote this additional loss.

Fragmentation with CAD, for both glyoxal-derived AGEs (modifications with net addition of C_2O and $C_2H_2O_2$), for amidated Substance P agrees with the ECD and DR-ECD spectra are shown in the (figure 3.7). Moreover, similar results were obtained about the types (net addition of C_2O and $C_2H_2O_2$), and binding sites of glyoxal-derived AGEs formed at the free acid form of Substance P. (see Figure 3.8 for $[M + C_2O + 2\,H]^{2+}$ modification and Tables A-9 and A-10 in appendix A or the $[M + C_2H_2O_2 + 2\,H]^{2+}$ modification).

Additionally, as was mentioned before, similar glyoxal-derived AGEs formed for amidated Substance P were observed under biological conditions (modifications with net addition

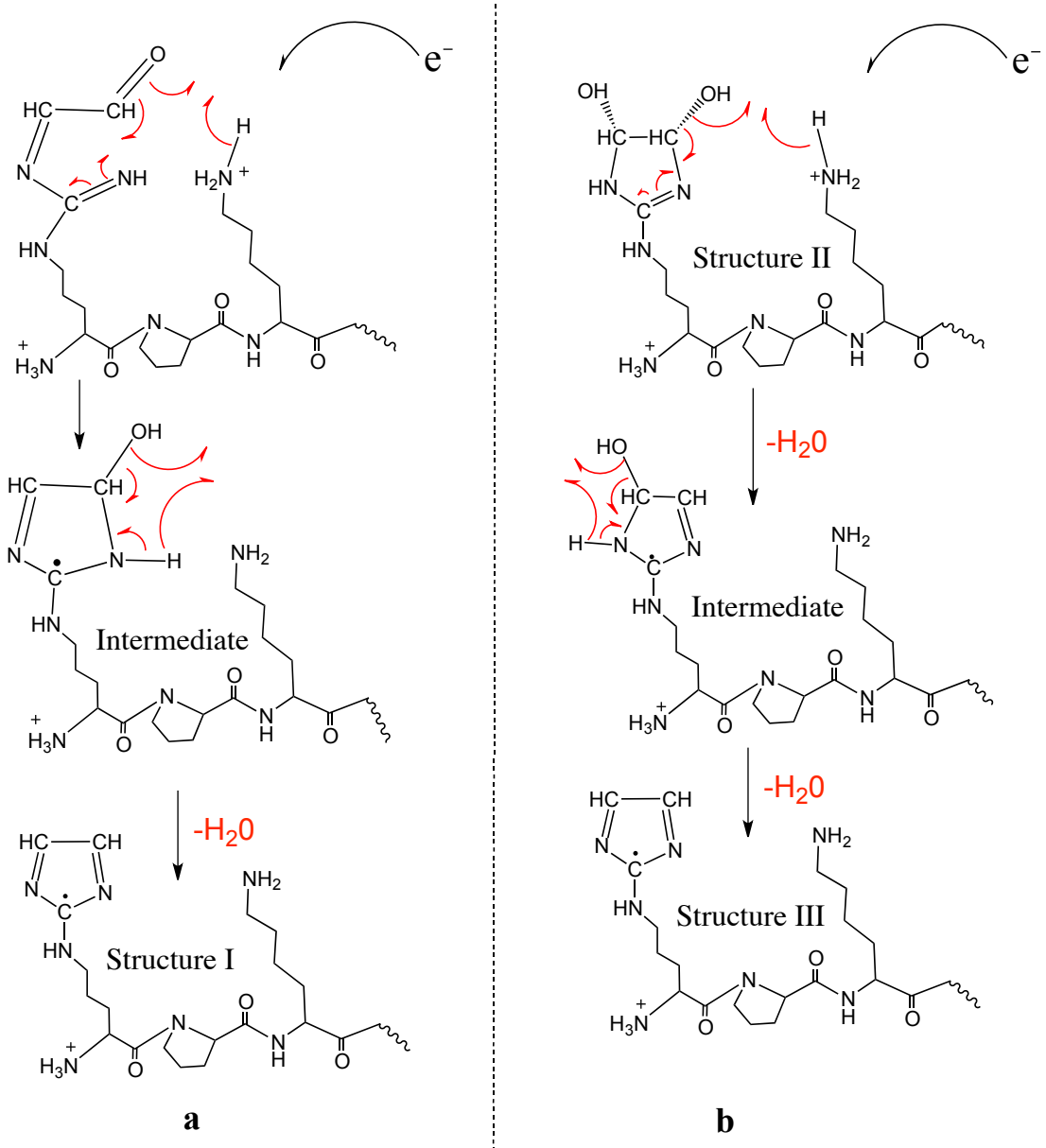

Scheme 3.2: Proposed reaction mechanism of the loss of water after electron capture dissociation from the glyoxal-derived glycation products (AGE) formed at the guanidine group. **a.** The AGE product formed at the guanidine group (open ring) loses one molecule of water after electron capture generating the radical imidazole moiety structure I; **b**The 3,4-dihydroxyimidazole (structure II) loses one molecule of water after electron capture generating the intermediate structure, but the extra loss of water that originates the radical imidazole moiety structure III is believed not to be driven by the capture of another electron.

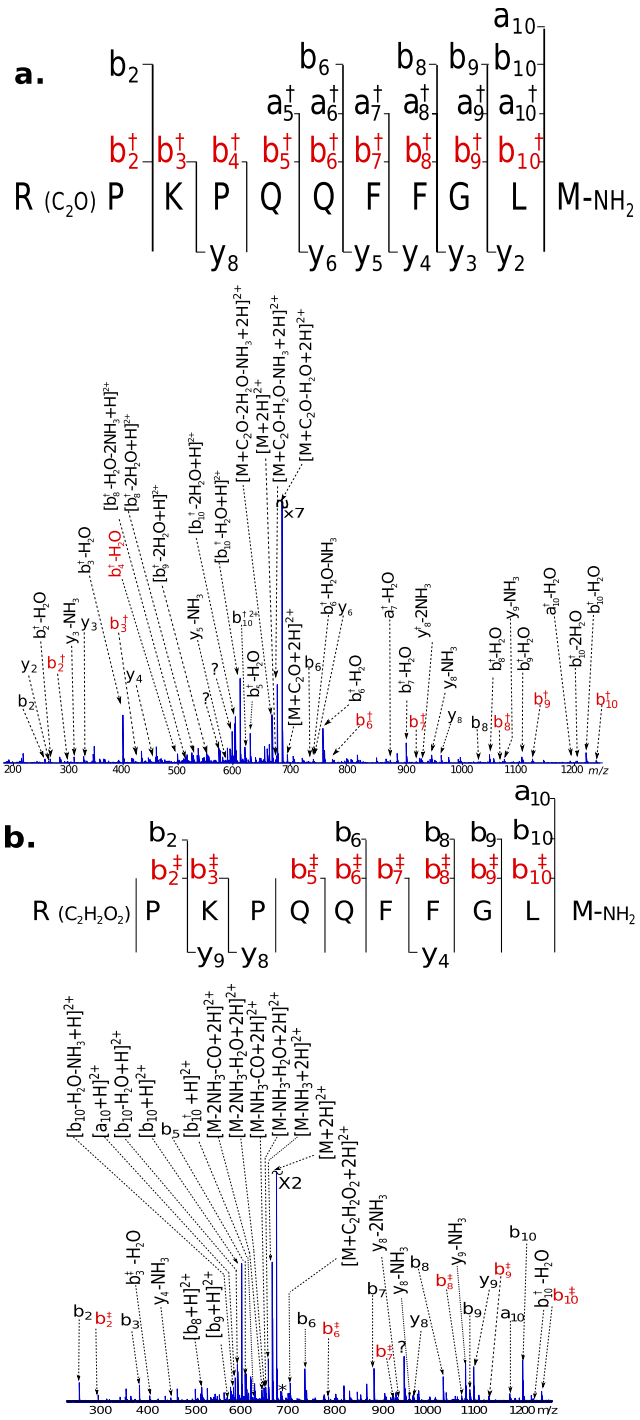

Figure 3.7: MS/MS spectra of the glyoxal-derived glycation product formed at amidated Substance P; **a.** CAD fragmentation pattern for the precursor ion $[M + C_2O + 2H]^{2+}$ of ; **b.** CAD fragmentation pattern for the precursor ion $[M + C_2H_2O_2^+2H]^{2+}$. The symbol ? indicates unassigned peaks by the current understanding of the fragmentation mechanism. Peak assignments are presented in appendix A, Tables A-5 and A-6. A.

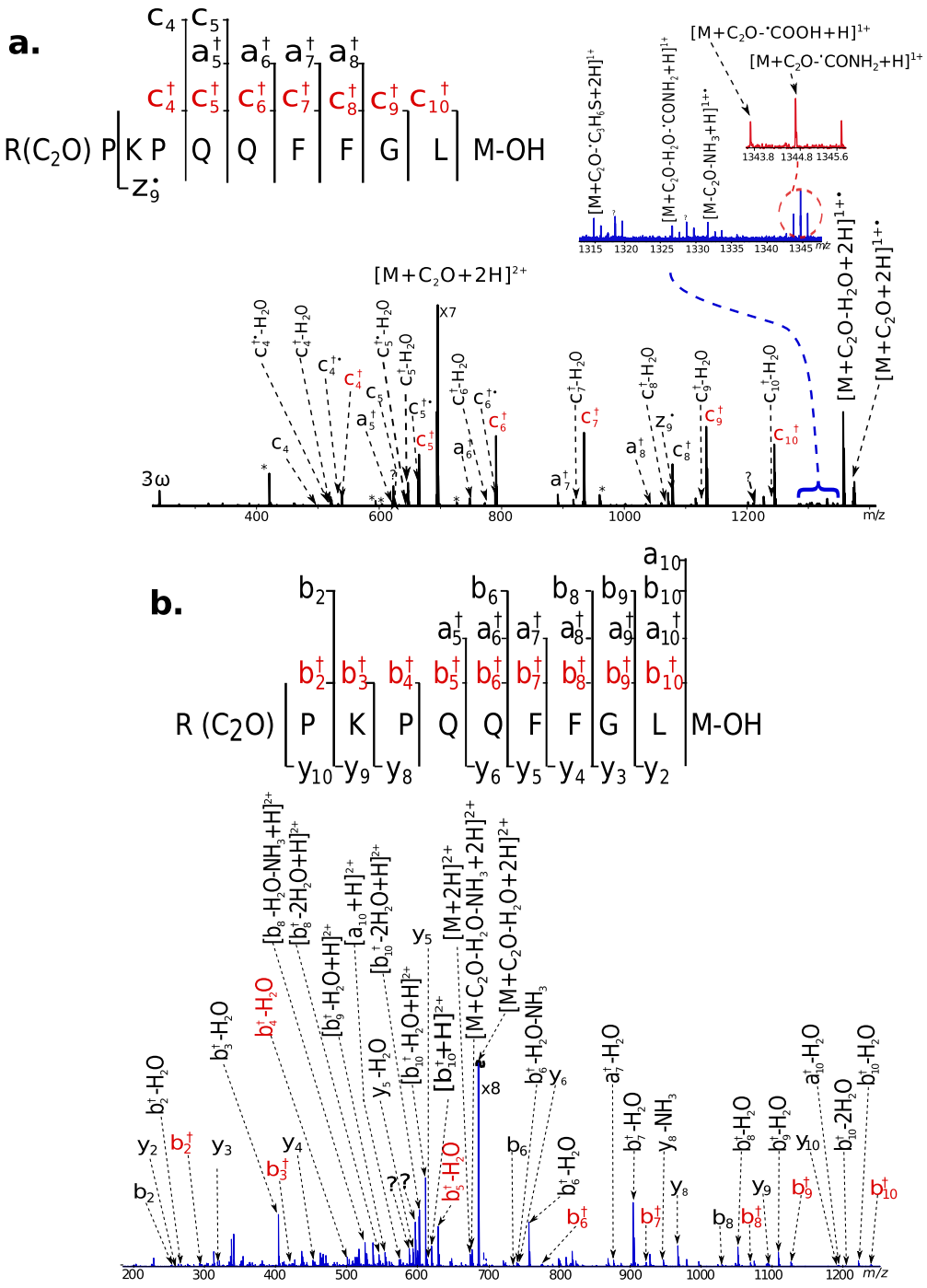

Figure 3.8: MS/MS spectra of the free acid form of Substance P reacted with glyoxal in MeOH:H_2O (50:50): **a.** DR(674.86)-ECD(694.86) spectrum of the precursor ion $[M + C_2O + 2H]^{2+}$; **b.** CAD spectrum of the precursor ion $[M + C_2O + 2H]^{2+}$. The symbol ? indicates unassigned peaks by the current understanding of the fragmentation mechanism and * indicates background peaks where no isotopologues were observed. Peak assignments are presented in Tables A-7 and A-8 Appendix A.

of C_2O and $C_2H_2O_2$. Thus, further analysis of the DR-ECD and CAD spectrum of both precursor ions $[M + C_2O + 2H]^{2+}$ and $[M + C_2H_2O_2 + 2H]^{2+}$ showed that glyoxal-derived AGES and dihydrated glyoxal-derived AGEs are modified at the guanidine group in the arginine moiety (refer to figure 3.9 and Tables A-11-14 appendix A). This preferred glycation site, that does not change at physiological conditions (pH 7.5), can be explained from the high pKa of arginine compared with lysine or the $N-$terminus amino group (pKa 12.48, 10.53 and 9.0 respectively).[267]

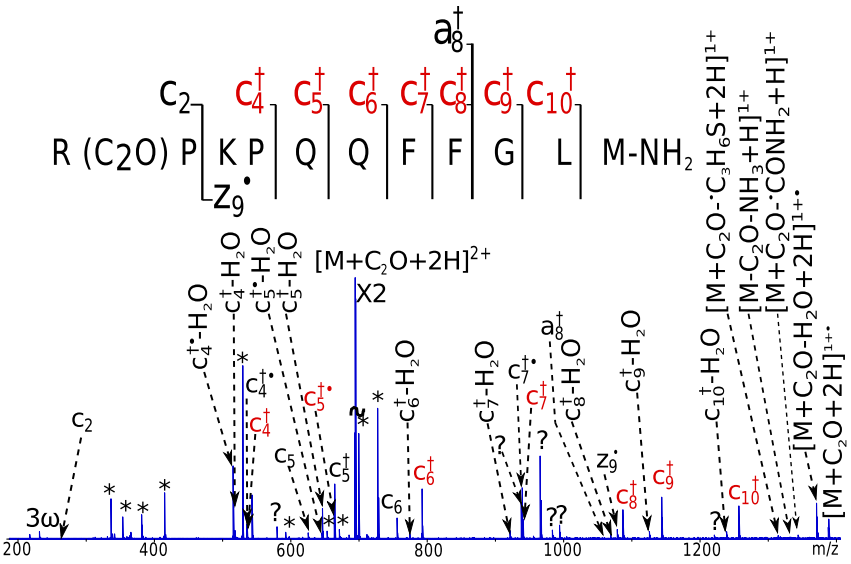

Figure 3.9: DR(674)-ECD(694) of the precursor ion $[M + C_2O + 2H]^{2+}$ amidated Substance P reacted with glyoxal at pseudo-physiological conditions (pH 7.5). Peak assignments are presented in Table A-11 appendix A.

Moreover, studies of glyoxal with only arginine found that protonation of one of the three nitrogen atoms at the side chain did not limit the reactivity of the guanidine group, and products at the $N-$terminus (α-amino group) rarely happen.[114] Glycation at the amide group of glutamine residues was not observed that can be attributed to the lowest nucleophilicity (low basicity) of the lone pair of the nitrogen atom. It can be concluded that different species may be present as a result of glycation by glyoxal, particularly the creatinine compound generated at the guanidine group of arginine, which is used as a bio-marker in renal failure. Although in this work no evidence was found for

intramolecular or intermolecular cross-linking, the formation of imidazolone (a common product found in methylglyoxal-derived glycation products) [268] or diglycation [121] at longer reaction times may show otherwise.

3.4 Conclusions

The glyoxal-derived glycation products (AGEs) obtained from the reaction of glyoxal with amidated and free acid form of Substance P, at pseudo-physiological conditions (pH 7.5) and MeOH:H_2O, were analysed by CAD, ECD, and double-resonance ECD experiments. Tandem mass spectrometry allowed assignment of the binding site to either the guanidine group at the side chain of the arginine residue of the $N-$terminus. Some structures were proposed at the guanidine moiety, such as the hydroxyimidazoline and dihydroxyimidazoline compounds formed with the guanidine group of the arginine residue. In the ECD, DR-ECD, and IRMPD-ECD experiments, a characteristic loss of water from every modified $c_n^{\dagger}$ and $c_n^{\ddagger}$ fragment ion was observed. Thus, it is proposed that the electron is captured at the modification site and subsequently a water loss is generated in addition to the typical fragmentation pattern of the peptide at the backbone N-Cα bond.

It seems, then, that a better understanding of the glycation reaction by the α-dicarbonyl compound glyoxal can be obtained from analysing the results in small peptides, as discussed above. However, it is clear that care must be taken when this reaction is executed in methanol, due to the appearance of ion molecule reactions. In any case, for the reaction times employed in the experiments outlined in this chapter (see section 3.2.1), it was not observed any involvement of amino groups from the lysine residues and the amidated $C-$terminus. Nevertheless, $N-$terminus involvement in the glycation reaction was considered to be a possibility due to the location of the arginine

residue in the peptide chain. In order to further shed light on the likelihood of such an involvement of the $N-$terminus, it was considered necessary to perform the reaction of glyoxal in other model peptides varying the position of the arginine residue. Further experimentation by MS aiming to address the potential glycation of the $N-$terminus is presented and discussed in chapter 4.

4 Tandem mass spectrometry for the study of glyoxal-derived advanced glycation end-products (AGEs) in peptides

4.1 Introduction

In the present chapter the experiments of model peptides reacted with glyoxal in MeOH/H_2O, intended to reproduce the conditions used for Substance P in chapter 3, are presented and discussed. Additionally, in order to assess the robustness of the glycation reaction by glyoxal to the reaction conditions, as well as to sample purification, two variations to the methodology adopted before were introduced: phosphate saline buffer (PBS) was used during the glycation reaction; and, the reaction was followed by precipitation with methanol/chloroform, as a clean up step, prior to direct infusion into the mass spectrometer.

The modified species were fragmented by collisionally activated dissociation (CAD) and electron capture dissociation (ECD) to determine glyoxal binding site in the peptides presented in table 4.1. All the ,peptides with some biological relevance, were chosen without an $N-$terminal arginine residue in order to distinguish side chain arginine

glycation from $N-$terminal glycation. Glyoxal-derived AGEs were ionized using an electrospray source (ESI) in positive mode and accumulated in the quadruple mass filter prior to CAD and ECD. Likewise for Substance P, ejection of unmodified ions was performed during the ECD experiments, by using double resonance ECD, which allowed determination of $(c/z^{\bullet})$ fragment ions lineage.[229] The glyoxal-derived AGEs were confidently assigned with a mass error < 1 ppm (peak assignment tables are presented in the Appendix B)

Table 4.1: Model peptides sequences and glyoxal modified ions reacted in MeOH/H_2O and phosphate buffered saline (PBS).

Peptide Sequence	**Unmodified ion** (m/z)	**Modified precursor ion fragmented**
KM-11 KPRPQQFFGLM$-NH_2$ $(1436.7387\ Da)$	$[M + 2\,H]^{2+}$ $(m/z = 674.37134)$	$[M + C_2O + 2\,H]^{2+}$ $(m/z = 694.33688)$
		$[M + C_2H_2O_2 + 2\,H]^{2+}$ $(m/z = 703.37408)$
AcKM-11 Ac$-$KPRPQQFFGLM$-NH_2$ $(1388.73869\ Da)$	$[M + 2\,H]^{2+}$ $(m/z = 695.37663)$	$[M + C_2O + 2\,H]^{2+}$ $(m/z = 715.37408)$
		$[M + C_2H_2O_2 + 2\,H]^{2+}$ $(m/z = 724.37937)$
EK-15 ERQIKKQTALVELVK $(1782.0727\ Da)$	$[M + 3\,H]^{3+}$ $(m/z = 595.0315)$	$[M + C_2O + 3\,H]^{3+}$ $(m/z = 608.36315)$
		$[M + C_2H_2O_2 + 3\,H]^{3+}$ $(m/z = 614.36667)$
FR-25 FQNALLVRYTKKVPQV STPLVEVSR $(2871.6334\ Da)$	$[M + 4\,H]^{4+}$ $(m/z = 718.91566)$	$[M + C_2O + 4\,H]^{4+}$ $(m/z = 728.9144)$
		$[M + C_2H_2O_2 + 4\,H]^{4+}$ $(m/z = 733.341700)$

4.2 Materials and methods

4.2.1 Materials

The model peptides were custom synthesized by GeneCust Europe (Dudelange, Luxemburg). Acetic acid ($\geq 99\,\%$ pure), sodium phosphate monobasic (Na_2HPO_4), sodium chloride (NaCl), and potassium phosphate dibasic KH_2PO_4 were purchased from Sigma-Aldrich (St. Louis, Missouri, U.S.A). All aqueous solutions were prepared using water from a Milli-Q water system (Millipore Inc., Durham, U.K.). A P-97 Flaming/Brown micropipette puller tip manufactured from Sutter Instrument Company (Novato, C.A. U.S.A.) was used to obtain glass capillaries employed for nano-ESI. Methanol (LC-MS grade), isopropanol (GLC-pesticide grade), and chloroform (HPLC grade) were obtained from Fisher-Scientific (Loughborough, Leicestershire, U.K.). Glyoxal solution ($\sim 39\%$ in water) was purchased from TCI Europe (Zwijndrecht, Belgium).[261]

4.2.2 Model peptide purification

$1\,mg$ of model peptides was dissolved with $1\,mL$ of MeOH/H_2O (50:50). A precipitation was performed with MeOH/chloroform and left at $-20\,℃$ for 20 minutes. Centrifugation at $5000\,rpm$ in a Technico-MAXI centrifuge (Fisher Scientific, Leicestershire, U.K.), was performed during 6 min to deposit the protein pellet at the bottom of the Eppendorf tube. The supernatant was then carefully extracted with pipette tips allowing metal salts and polar compounds to dissolve into the MeOH upper layer and thus being removed. The pellet was then dried in a SpeedVac system (Savant SPD121P, Thermo Fisher Scientific Inc. Waltham, MA, U.S.A.) at $35\,℃$ and stored at $-80\,℃$.

4.2.3 Glycation of model peptides in MeOH/H_2O

The dried, purified peptides were re-dissolved in MeOH:H_2O (50:50). Three aliquots were taken from the purified peptides and reacted with glyoxal ($800\,\mu mol/L$). The reaction was carried out at $37\,℃$ for 21 hours at a starting pH of 7.5. The three reacted peptides were diluted with ionization solution, which contains methanol, water, isopropanol, and acetic acid (50:39:10:1), to a final concentration of $\sim 0.1 \mu M$. Methanol was employed to reproduce the conditions reported in chapter 3.[73]

4.2.4 Glycation of model peptides in PBS

In order to simulate pseudo-physiological conditions, the purified peptides were re-dissolved in phosphate buffered saline (PBS) solution, prepared using $144\,mg$ of sodium phosphate monobasic (Na_2HPO_4), $818\,mg$ sodium chloride (NaCl), $24\,mg$ potassium phosphate dibasic KH_2PO_4 in $100\,mL$ of water to obtain a pH 7.2 ± 0.2. Three aliquots of the dissolved peptide were taken to react with glyoxal ($400\,nM$) over 6 hours. After reaction, the three aliquots of each glycated peptides were cleaned from the buffer solution by the same purification procedure described above. The dried pellet was re-dissolved in $100\,\%$ water and then diluted with ionization solution (ethanol, water, isopropanol, and acetic acid (50:39:10:1)), to a final concentration of $\sim 0.1\,\mu M$ prior to direct injection into the mass spectrometer.

4.2.5 Mass spectrometry

The 12 Tesla FTICR mass spectrometer was employed only in positive mode. The positive ions were generated using ESI and nESI. The capillary voltages were held at $4.5\,kV$ and

$0.8\,kV$ for ESI and nESI, respectively. In the MS/MS experiments the ions were isolated in the quadrupole (Q1) and accumulated for $1-30\,s$, as required by the precursor ion. Equally, CAD experiments were also performed with argon gas at collision voltages ranging between 15 to $20\,V$. The fragment ions were then transported to the ICR cell[264] for excitation and detection. As in the previous tests, a dispenser cathode[163] was used to perform the ECD experiments at $1.3\,V$ and $1.5\,A$. During this set of tests using ECD, the pulse length was varied between 120 and $200\,ms$ as necessary. Double resonance ECD experiments (DR-ECD)[228] were performed varying the ejection pulse between 100 and $220\,ms$. The results, as in the section 3.2.2, were analysed using the DataAnalysis 4.0 SP 3 software, from Bruker Daltonics, with internal calibration. The masses employed to perform the internal calibration are summarised in tables presented in Appendix B, and indicated with a * symbol.

4.3 Results and discussion

In figure 4.1a is shown the direct infusion spectrum of the reacted KM-11 peptide in MeOH/H_2O. In this spectrum is possible to identify: singly, doubly, and triply-charged unmodified ions; glyoxal modified ions; and the species labeled as A and B, which correspond to an ion/molecule reaction product generated with methanol (§ 3.3). The glyoxal modified species showed a net increase of $39.9949\,Da$ (C_2O) and a net increase of $58.0055\,Da$ ($C_2H_2O_2$) to the mass of the peptide. These modified species, $[M + C_2O + 2\,H]^{2+}$ and $[M + C_2H_2O_2 + 2\,H]^{2+}$, are also observed in PBS as well as in the direct infusion spectrum of the acetylated KM-11 peptide reacted in both MeOH/H_2O and PBS as is shown in figure 4.1b, (see appendix B table B-2 to B-4).

The direct infusion spectrum of the reacted peptides in PBS showed more species, at a lower signal to noise ratio, than the direct infusion spectrum of the reacted peptide

in MeOH/H_2O, which was attributed to the chemical interferences added by the PBS solution. This chapter is focused on the doubly-charged modified ions $[M+C_2O+2H]^{2+}$ and $[M+C_2H_2O_2+2H]^{2+}$, which were isolated and fragmented using DR-ECD and CAD. The notation adopted for the DR-ECD experiment is DR(X)-ECD(Y), where X is the m/z of the ejected ion and Y is the m/z of the precursor ion as mentioned in (section 3.3).

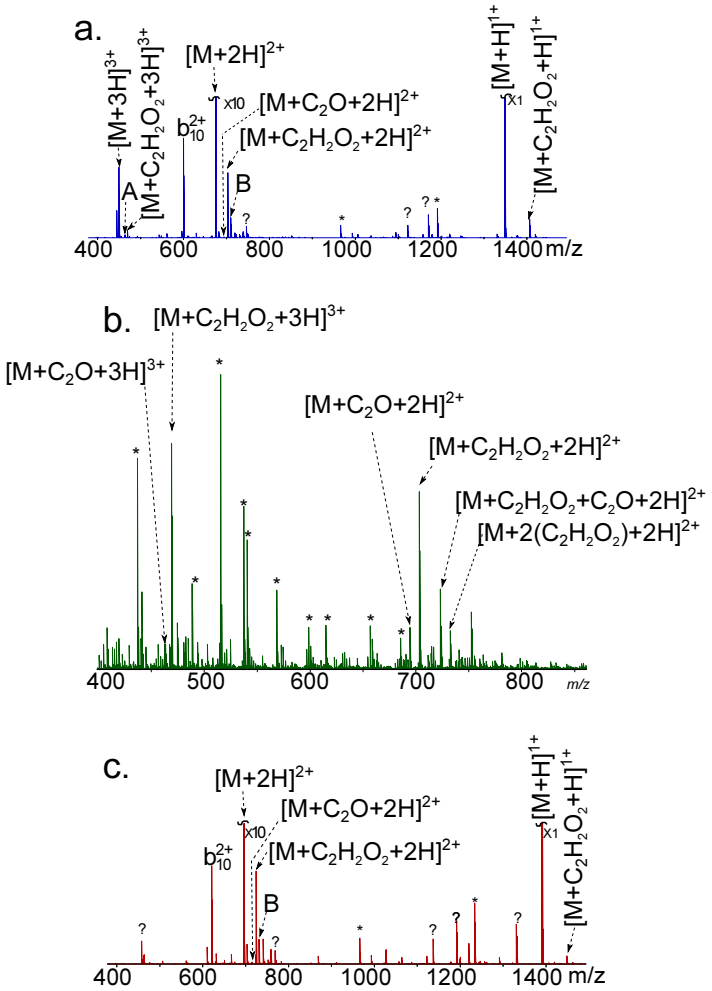

Figure 4.1: **a.** Direct infusion spectrum of glyoxal-derived glycation AGE for the KM-11 peptide in MeOH/H_2O (50:50), ($A = [M + C_2O + 3H]^{3+}$); **b.** Direct infusion spectrum of glyoxal-derived glycation AGE for the KM-11 peptide in PBS; **c.** Direct infusion spectrum of glyoxal-derived glycation AGE for the AcKM-11 peptide in MeOH:H_2O (50:50), ($B = [M + C_2H_2O_2 + CH_2 + 2H]^{2+}$). Detailed peak assignments are available in Table B-1 and B-2 of the appendix B.

4.3.1 Undecapeptides KM-11 and Ac-KM-11

Peptides modified by net increase of $39.9949\,Da$ (C_2O)

In figure 4.2a is presented the DR(674)-ECD(703) spectrum of the precursor ion $[M + C_2O + 2H]^{2+}$ for the KM-11 peptide in MeOH/H_2O. As it can be observed in such a spectrum, two types of c fragment ions were identified: unmodified and modified. The modification corresponds to the addition of $39.9949\,Da$ to the mass of every observed fragment. These modified species have been identified by the addition of the dagger symbol (†) to the Roepstorff and Biemman's nomenclature ($c/z^{\bullet}$).[47,48] In particular, analysing the figure 4.2a it is possible to see the modified $c_4^{\dagger}$ to $c_{10}^{\dagger}$ fragment ions and the modified $z_9^{\dagger\bullet}$ radical fragment.

Unmodified c, y fragment ions, the $z_9^{\bullet}$ radical fragment ion, side chain losses from the charge-reduced species and loss of water from every modified $c^{\dagger}$ fragment ion, were also observed in figure 4.2. Proline in position 4 inhibits cleavage in position 3 from the $N-$terminus and therefore formation of unmodified c_3 and/or modified $c_3^{\dagger}$ was not observed or expected.[171] Thus, the presence of modified $c_4^{\dagger}$ to $c_{10}^{\dagger}$ fragment ions indicate that the glyoxal-derived AGE formed by the net mass addition of C_2O is located towards the $N-$terminus. In particular, the presence of the $z_9^{\dagger\bullet}$ radical fragment ion locates the glyoxal modification at the arginine residue in position 3.

The CAD data of the precursor ion $[M + C_2O + 2H]^{2+}$ in MeOH/H_2O, is presented in figure 4.2b and Table B-6 of the appendix B. The spectrum shows modified $b_3^{\dagger}$, $b_5^{\dagger}$ to $b_{10}^{\dagger}$, $a_{10}^{\dagger}$, $y_9^{\dagger}$, $y_{10}^{\dagger}$ fragment ions, unmodified b, y fragment ions, and water loss from every modified fragment ion. CAD result agrees with the DR-ECD results in MeOH/H_2O for the precursor ion $[M + C_2O + 2H]^{2+}$, locating the glyoxal-derived AGE at the side chain of the arginine residue. Similar results for the KM-11 peptide in PBS are obtained from

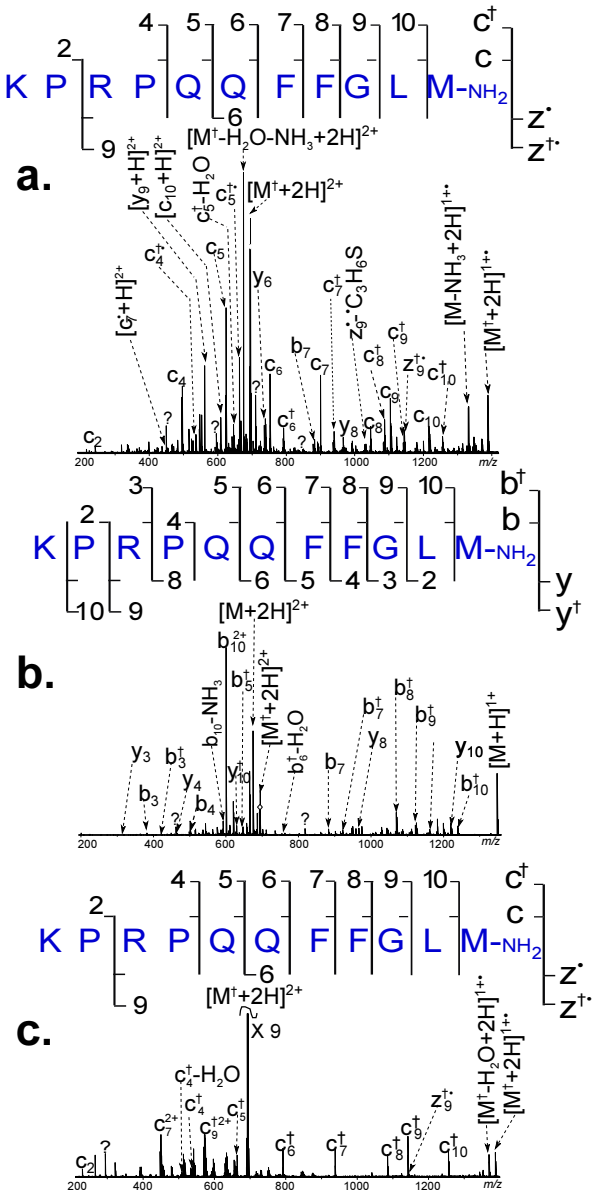

Figure 4.2: MS/MS spectrum of the glyoxal modified KM-11 peptide **a.** DR(674)-ECD(694) spectrum of the precursor ion $[M + C_2O + 2\,H]^{2+}$ with ejection of $[M + 2\,H]^{2+}$ (peptide reacted in MeOH/H_2O); **b.** CAD spectrum of the precursor ion $[M^+C_2O^+2H]^{2+}$ (peptide reacted in MeOH/H_2O); **c.** DR(674)-ECD(694) spectrum of the precursor ion $[M + C_2O + 2\,H]^{2+}$ with ejection of $[M + 2\,H]^{2+}$ (peptide reacted in PBS) . The symbol ? indicates unassigned peaks by the current understanding of the fragmentation mechanism. Highlighted modified ions in the spectrum and detailed peak assignments are available in Tables B-5 to B-7 of the Appendix B.

the DR(674)-ECD(694) spectrum of the $[M + C_2O + 2\,H]^{2+}$ species, which is shown in figure 4.2c.

As mentioned before the direct infusion spectrum of the reaction with glyoxal of the $N-$terminal acetylated KM-11 peptide in MeOH/H_2O (figure 4.1c) also showed the modified $[M^+C_2O + 2\,H]^{2+}$ species discussed above, which were further fragmented by DR-ECD and CAD. The DR(695)-ECD(715) spectrum of the precursor ion $[M + C_2O + 2\,H]^{2+}$ in MeOH/H_2O is shown in figure 4.3a. Modified $c_4^\dagger$ to $c_{10}^\dagger$ fragment ions, and the modified $z_9^{\dagger\bullet}$ radical fragment ion are present in the spectrum. In addition, modified $b_3^\dagger$, $b_5^\dagger$ to $b_{10}^\dagger$, and $y_{10}^\dagger$ fragment ions were observed in the CAD spectrum of the precursor ion $[M + C_2O + 2\,H]^{2+}$ in MeOH/H_2O, as shown in figure 4.3b. Equally, $a_3^\dagger$, $b_5^\dagger$ to $b_{10}^\dagger$, $y_9^\dagger$ and $y_{10}^\dagger$ fragment ions are present the CAD spectrum of the precursor ion $[M + C_2O + 2\,H]^{2+}$ in PBS (figure 4.3c). These results indicate that the addition of C_2O occurs at the arginine residue in position 3 in MeOH/H_2O and in PBS.

Scheme 4.1 shows the proposed reaction for the formation of the glyoxal-derived AGE at the guanidine group of arginine, where protonation at the carbonyl oxygen generates an appreciable polarisation of the carbonyl carbon, which made it susceptible to attack by nucleophiles. The nitrogen atom, of the amino and/or guanidino groups in protein/peptides, acts as a nucleophile forming a carbon-nitrogen bond. The intermediate steps of the reaction and the possible glyoxal-derived AGE structures are described in scheme 3.1 and Lopez-Clavijo, A. F. and Barrow, M. P. and Rabbani, N. and Thornalley, P. J. and O'Connor, P. B.[73]

Peptides modified by net increase of $58.0055\,Da$ ($C_2H_2O_2$)

Fragmentation of the precursor ion $[M + C_2H_2O_2 + 2\,H]^{2+}$ in MeOH/H_2O and in PBS solution also shows unmodified and modified $c/z^\bullet$ fragment ions. The modified products

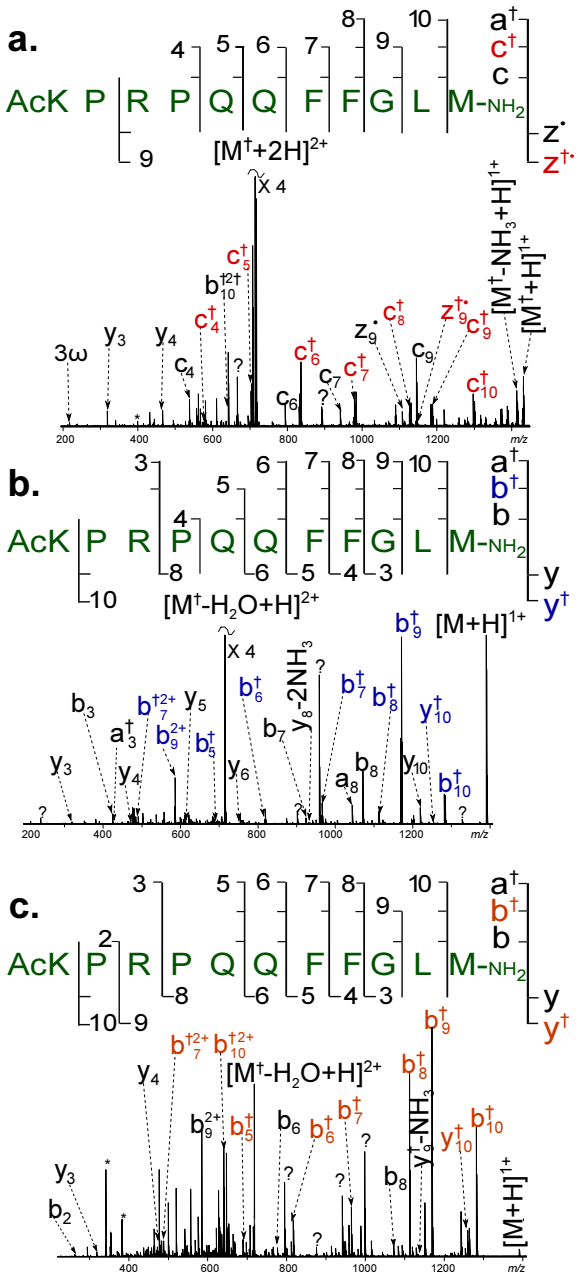

Figure 4.3: MS/MS spectra of the AcKM-11 peptide: **a.** DR(695)-ECD(715) spectrum of the precursor ion $[\mathrm{M} + \mathrm{C_2O} + 2\,\mathrm{H}]^{2+}$ with ejection of $[\mathrm{M} + 2\,\mathrm{H}]^{2+}$ (peptide reacted MeOH/H_2O); **b.** CAD spectrum of the precursor ion $[\mathrm{M} + \mathrm{C_2O} + 2\,\mathrm{H}]^{2+}$ (peptide reacted MeOH/H_2O); **c.** CAD spectrum of the precursor ion $[\mathrm{M}+\mathrm{C_2O}+2\,\mathrm{H}]^{2+}$ (peptide reacted in PBS). Detailed peak assignments are presented in Tables B-8 to B-10 of the Appendix B.

showed a net addition of $58.0055\,Da$ to every fragment ion $c/z^{\bullet}$ observed. Modified $c/z^{\bullet}$ fragment ions are distinguished from the unmodified ones by addition of the double

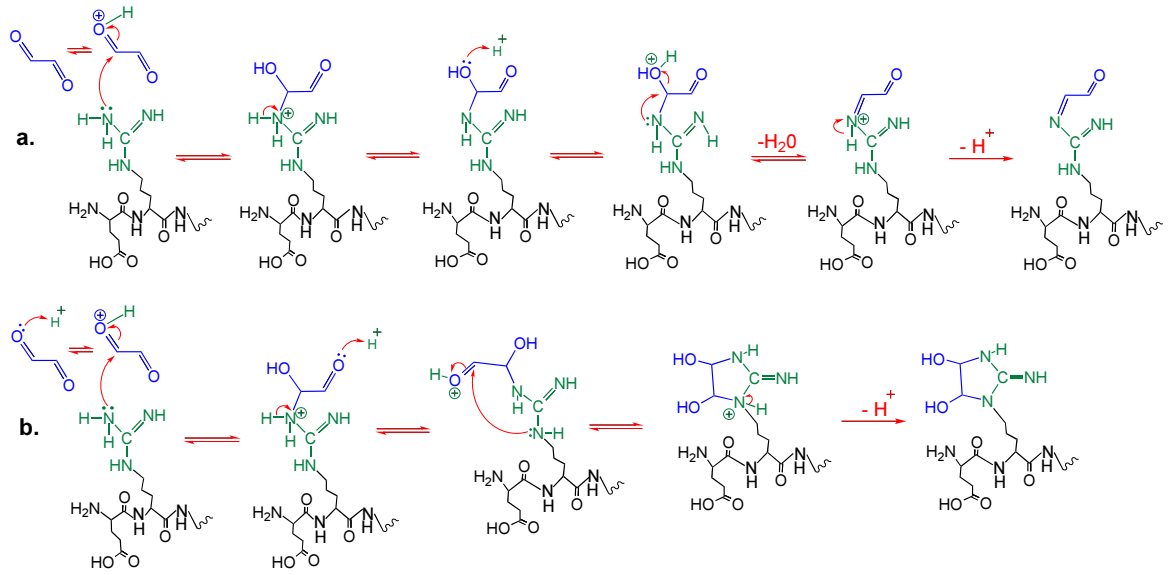

Scheme 4.1: **a.** Proposed reaction for the net addition of $39.9949\,Da$ forming the proposed Schiff base structure at the guanidino group of arginine **b.** Proposed reaction for the net addition of $58.0055\,Da$ forming the proposed structure dihydroimidzolidine. One possible structure of the reaction products is presented here, although other possible structures may be present scheme 3.1.

dagger symbol (‡) to the Roepstorff and Biemman's nomenclature.

The DR(674)-ECD(703) spectrum of the precursor ion $[\mathrm{M} + \mathrm{C_2H_2O_2} + 2\,\mathrm{H}]^{2+}$ for the KM-11 peptide in MeOH/$\mathrm{H_2O}$ is shown in figure 4.4a. Modified $c_n^{\ddagger}$ $(n = 4 \ldots 10)$, the modified $z_9^{\ddagger\bullet}$ radical fragment ion, unmodified c_4 to c_{10} fragment ions, loss of water from every modified $c^{\ddagger}$ fragment ion, and side chain losses from the charge-reduced species were observed. Thus, the presence of the modified $z_9^{\ddagger\bullet}$ radical fragment ion assigns the net addition of $\mathrm{C_2H_2O_2}$ as taking place at the arginine residue. The CAD data for the KM-11 peptide of the precursor ion $[\mathrm{M} + \mathrm{C_2H_2O_2} + 2\,\mathrm{H}]^{2+}$, presented in figure 4.4b and figure 4.4c in MeOH/$\mathrm{H_2O}$ and in PBS, respectively, agrees with the result obtained by DR(674)-ECD(703). Moreover, the results obtained for the $N-$terminus acetylated KM-11 peptide (figure 4.5) also locate the glyoxal-derived AGE as being formed at the guanidino group of the arginine residue in both reaction solutions (MeOH/$\mathrm{H_2O}$ and PBS Appendix B). The proposed reaction for the formation of the glyoxal-derived AGE is

shown in scheme 4.1b.

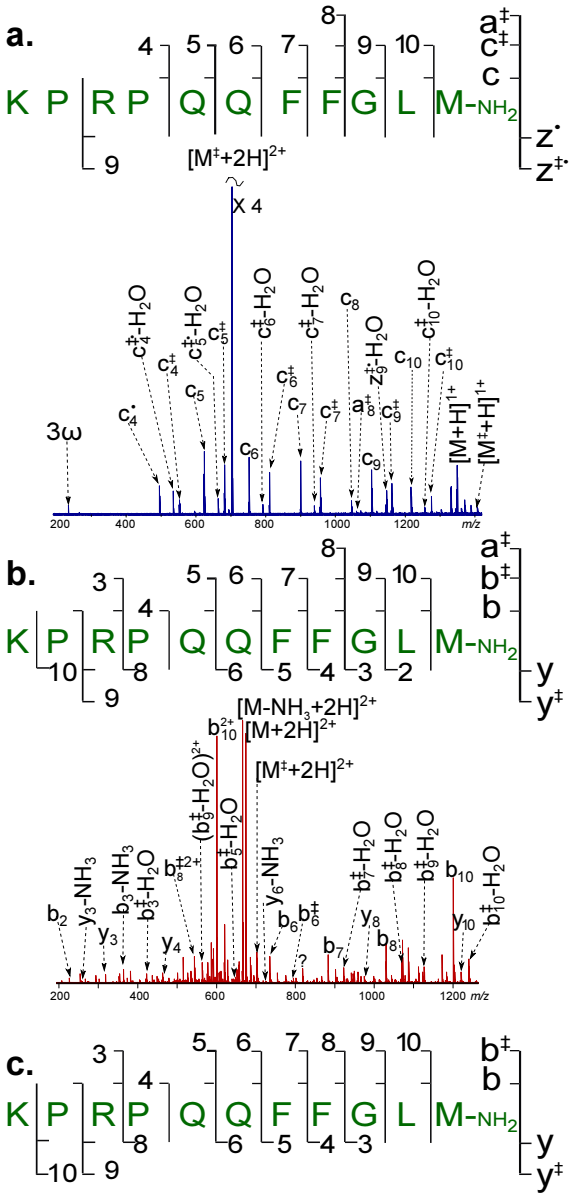

Figure 4.4: MS/MS spectrum of the KM-11 peptide: **a.** DR(674)-ECD(703) spectrum of the precursor ion $[M + C_2H_2O + 2H]^{2+}$ with ejection of $[M + 2H]^{2+}$ (peptide reacted in MeOH/H_2O); **b.** CAD spectrum of the precursor ion $[M + C_2H_2O + 2H]^{2+}$ (peptide reacted in MeOH/H_2O); **c.** Peptide map of the CAD spectrum of the precursor ion $[M + C_2H_2O + 2H]^{2+}$ (peptide reacted in PBS). The symbol ? indicates unassigned peaks by the current understanding of the fragmentation mechanism and * indicates background peaks where no isotopologues were observed. Peak assignments are presented in Table B-11 to B-13 of Appendix B.

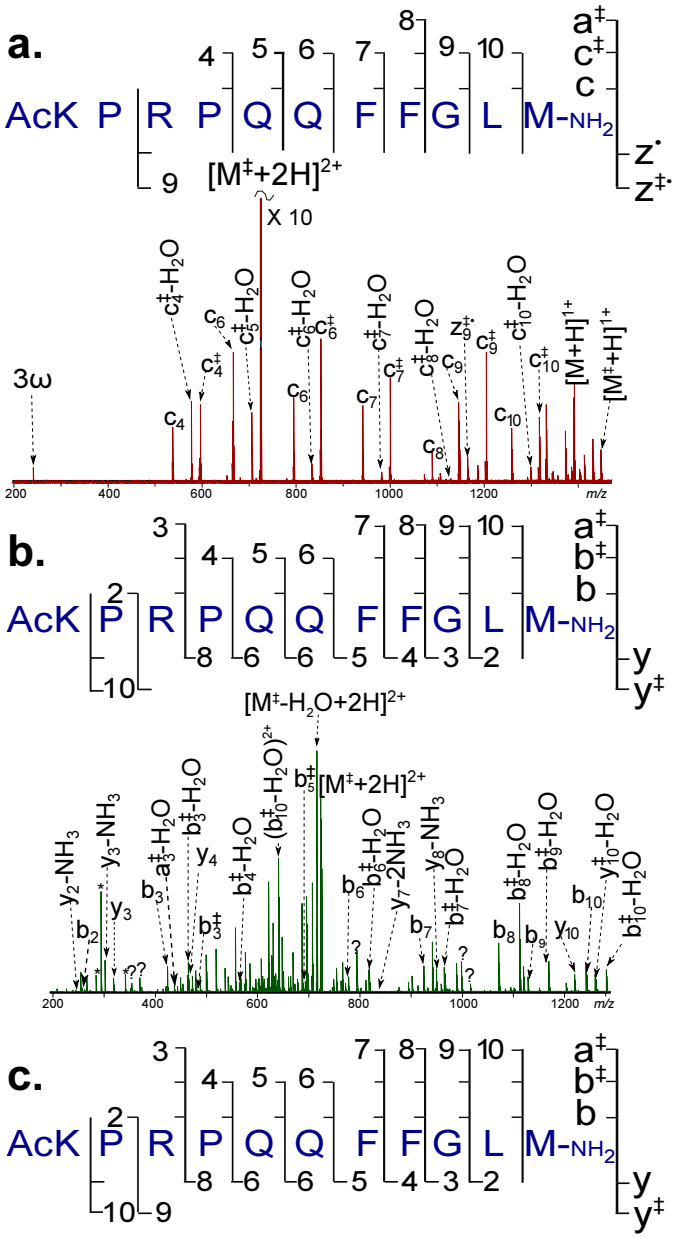

Figure 4.5: MS/MS spectra of the AcKM-11 peptide **a.** DR(695)-ECD(724) spectrum for the precursor ion $[M + C_2H_2O_2 + 2H]^{2+}$ with ejection of $[M + 2H]^{2+}$ (peptide reacted in MeOH/H_2O); **b.** CAD spectrum of the precursor ion $[M + C_2H_2O_2 + 2H]^{2+}$ (peptide reacted in MeOH:H_2O); **c.** Peptide map of the CAD spectrum of the precursor ion $[M + C_2H_2O_2 + 2H]^{2+}$ (peptide reacted in PBS). The symbol ? indicates unassigned peaks by the current understanding of the fragmentation mechanism. Detailed peak assignments are available in Table B-14 to B-16 of Appendix B.

All DR-ECD spectra, the loss of water from every modified $c^{\dagger}$ and $c^{\ddagger}$ fragment ion and from the $z_9^{\ddagger\bullet}$ radical fragment ion is observed. This water loss further supports the hypothesis proposed in chapter 3 that the capture of the electron triggers water loss at the modified guanidine moiety forming an stable imidazole radical species (see scheme 3.2). Thus, losses of one or two molecules of water loss from every modified c, $z^{\bullet}$, b, and y fragment ions are generated in addition to the typical backbone fragmentation pattern of the peptide and could help to indicate the presence of glyoxal-derived AGEs.

In addition, in all CAD spectra shown so far, it is clear that the presence of unmodified y fragments ions in positions 2-8 indicates that neither the $C-$terminus nor other amino acid residues were modified by addition of $C_2H_2O_2$ or C_2O.

4.3.2 EK-15 and FR-25 peptides

The type of mass addition of C_2O and $C_2H_2O_2$ moieties was also observed in direct infusion spectra of the peptides EK-15 and FR-25 . Further fragmentation, of both modified precursor ions and for both peptides, by DR-ECD and CAD revealed again binding site at the arginine moiety. The modified species were located at the arginine in position 2 from the $N-$terminus for the EK-15 peptide. Whereas, in the FR-25 peptide these modified species were formed at the arginine residue in position 8 from the $N-terminus$. (See figures 4.6 and 4.7 and tables B-17 to B-23 in the Appendix B).

It is noteworthy that a couple of unusual mass to charge ratios ($m/z = 602.35963$ and $m/z = 724.4117$), were observed in the direct infusion spectra of these two peptides (EK-15 and FR-25), when reacted in both MeOH/H_2O and PBS. These particular values of m/z were assigned to the presence of a new modified glyoxal-derived AGE and labeled in this work as $[M + (C_2{-}H_2) + nH]^{n\mathrm{H}}$, with $n = 3, 4$; this modified AGE features a mass addition of $m = 21.9843\, Da$. Interestingly enough, such as an observation had been not

obtained in any of the results previously discussed in this work, neither in the literature. Although this mass addition could also correspond to a sodium adduct, such a possibility was discarded thanks to the ultra-high resolution offered by the FT-ICR-MS employed in this work, which enabled us to assign in a confident manner this $[M + (C_2 - H_2) + nH]^{nH}$ species as a new modified glyoxal-derived AGE. This is further discussed in more detail in chapter 5.

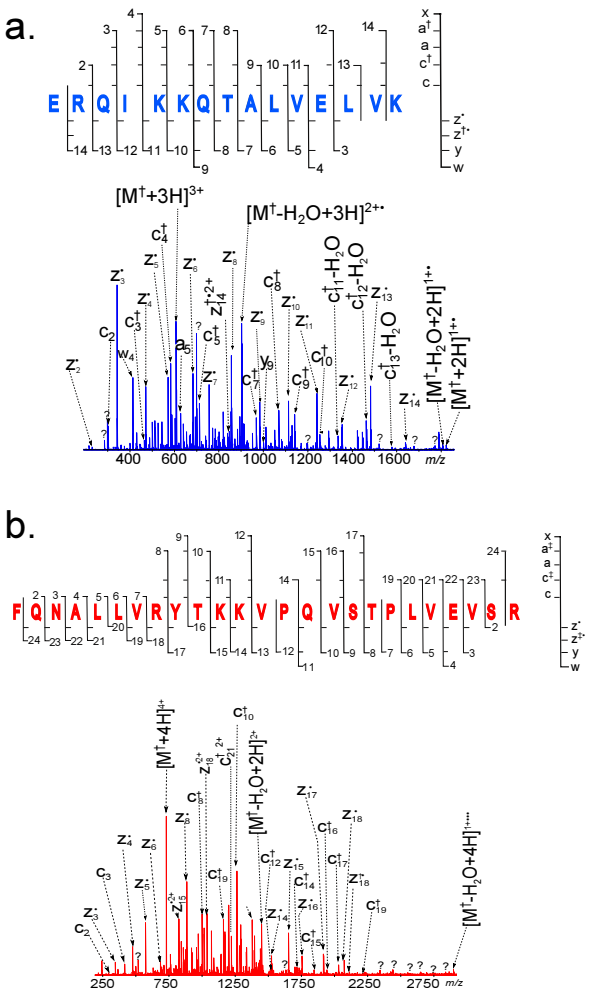

Figure 4.6: **a.** DR(595.03)-ECD(608.37) spectrum of the precursor ion $[M+C_2O+3\,H]^{3+}$ with ejection of $[M+3\,H]^{3+}$ for the peptide EK-15 reacted in MeOH:H_2O; **b.** DR(718.92)-ECD(728.91) spectrum of the precursor ion $[M + C_2O + 4\,H]^{4+}$ with ejection of $[M + 4\,H]^{4+}$ for the peptide FR-25 reacted in MeOH:H_2O. The symbol ? indicates unassigned peaks by the current understanding of the fragmentation mechanism. Detailed peak assignments are available in Table B-14 to B-16 of Appendix B.

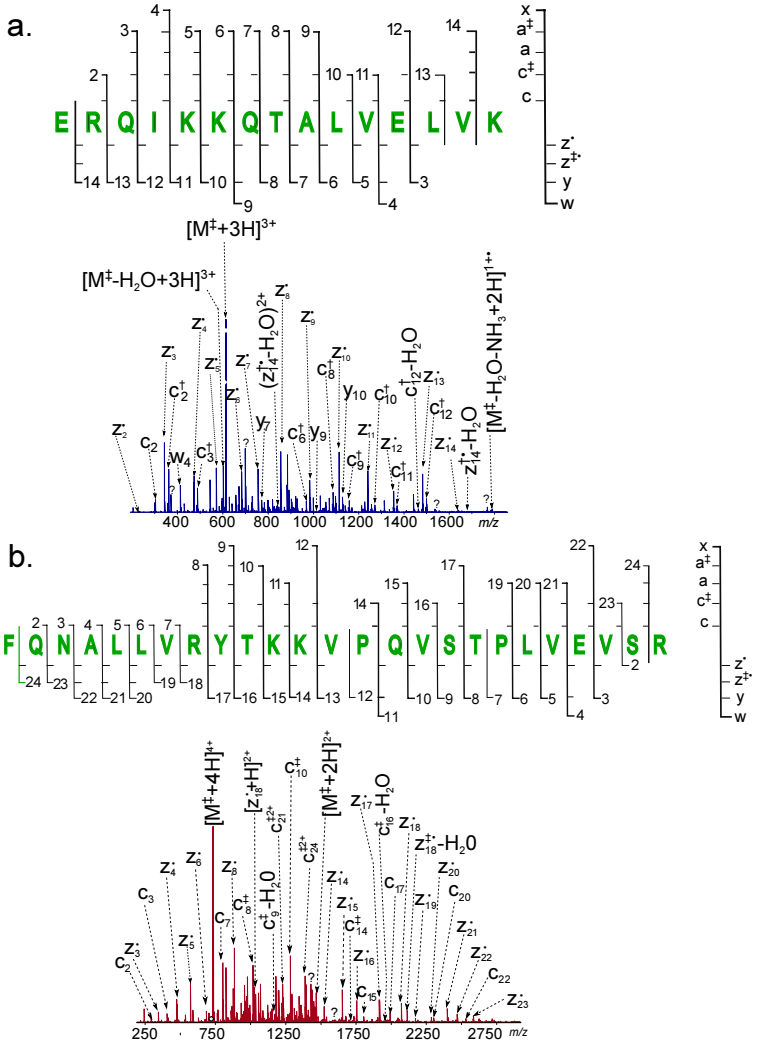

Figure 4.7: **a.** DR(595.03)-ECD(614.36) spectrum of the precursor ion $[M + C_2H_2O + 3H]^{3+}$ with ejection of $[M + 3H]^{3+}$ of the EK-15 peptide reacted in MeOH:H_2O; **b.** DR(718.91)-ECD(733.42) spectrum of the precursor ion $[M + C_2H_2O + 4H]^{4+}$ with ejection of $[M + 4H]^{4+}$ of the FR-25 peptide reacted in MeOH:H_2O. The symbol ? indicates unassigned peaks by the current understanding of the fragmentation mechanism. Detailed peak assignments are available in Table B-20 and B-22 of Appendix B.

4.4 Conclusions

$C-$terminus amidated and $N-$terminus acetylated undecapeptides (KM-11) were reacted with glyoxal under pseudo-physiological and non-physiological conditions, i.e. pH ~ 7.4 and $4 >$pH> 7.5, respectively. Two net mass additions were assigned as C_2O and $C_2H_2O_2$ by using an FT-ICR mass spectrometer. These two glyoxal-derived AGEs survive ECD and CAD fragmentation showing a typical backbone fragmentation pattern.

DR-ECD results allowed to clearly identify the binding site of C_2O and $C_2H_2O_2$ modifications, by exhibiting modified $c/z^{\bullet}$ fragment ion series in the fragmentation pattern. Accordingly, the fragmentation pattern obtained by using CAD showed modified b/y fragment ion for both modifications.

Using the results of the fragmentation pattern both mass additions of C_2O and $C_2H_2O_2$ were located at the arginine side chain. Interestingly, this location site for both modifications remained unaffected regardless of the reaction solution or purification procedures employed. For instance, whereas in the tests defined in chapter 3 dialysis was used as purification method, in the tests target of the present chapter the purification was performed by precipitation with MeOH/chloroform. This factor did not affect the final outcome, in terms of binding site assignment, indicating that the presence and location of the modifications were not sensible to this particular change.

It is important to highlight that the water loss from the modified $c^{\dagger}$ and $c^{\ddagger}$ fragment ions was a permanent characteristic in all DR-ECD spectra. In fact, such a result turned out to be fully consistent with the hypothesis proposed in § 3.3.2, and illustrated in the proposed reaction mechanism of the scheme 3.2.

The experiments outlined and discussed in the present chapter were performed using KM-11, AcKM-11, EK-15 and FR-25. All of these peptides are characterised by the absence of

an arginine residue at the first position, taken from the $N-$terminus to the $C-$terminus, within the peptide chain. The use of such peptides lacking of the arginine residue proved to be an adequate selection in order to differentiate $N-$terminus glycation from arginine glycation. In fact, the fragmentation patterns obtained by DR-ECD and CAD, for all the target peptides, showed that there was not involvement of the $N-$terminus in the glycation reaction by glyoxal.

It seems clear, again, that for the reaction times employed in the experiments outlined in this chapter, there was no involvement of amino groups from the lysine residues and the amidated $C-$terminus. Based on these results, and in order to establish lysine involvement, it was deemed necessary to perform the reaction of glyoxal at longer reaction times. This is precisely addressed and discussed in chapter 6. Equally, the observation of an unusual m/z ratio, which was assigned to the presence of [M + (C_2-H_2) + nH]$^{n\mathrm{H}}$ species, was noteworthy. Given the novelty of such an observation, a further and more detailed exploration was performed, and those results are presented and discussed in chapter 5. The experiments regarding this new-identified species were carried out using the same conditions outlined in the present chapter.

It is worth mention that the [M + (C_2-H_2) + nH]$^{n\mathrm{H}}$ species were not observed for both undecapeptides (KM-11 and AcKM-11), at the conditions of the experiment used in this work. It can be hypothesized that the presence of this modification is dependant on the size of the peptide and the number of basic residues. This would require changing systematically the number of basic amino acids and the length of the peptide chain, which is outside of the scope of the present work.

5

Tandem mass spectrometry for the study of an unusual glyoxal- derived advanced glycation end-product

5.1 Introduction

In chapter 3 and chapter 4 the detection by mass spectrometry of two species of glyoxal-derived AGEs was discussed and their binding site was identified at the arginine residue. Additionally, as mentioned in chapter 4, model peptides EK-15 and FR-25 (table 4.1), were reacted with glyoxal using the conditions described in section 4.2 (phosphate buffer saline and MeOH/H_2O solution). The direct infusion spectra of both peptides (EK-15 and FR-25) showed an unusual m/z peak. The direct infusion spectra revealed a mass addition of $21.9843\,Da$ to the mass of the peptide. Thus, it seems necessary to establish whether this mass addition ($21.9843\,Da$) corresponded to a new type of glyoxal-derived AGE. Therefore, similar reaction, mass spectrometry, and CAD and DR-ECD [228,229] conditions were used as is indicated in section 4.2

Interestingly enough, the EK-15 and FR-25 peptides are tryptic digest fragments of human serum albumin (HSA), with positions within the protein equal to 520-534 and 403-421, respectively.[269] The EK-15(520-534) peptide has one arginine residue in

position 521 and two lysine residues in positions 524 and 525, which are the possible reaction sites for glycation by glyoxal. In contrast, FR-25(403-421) peptide have amino acid residues in positions R410, K413, and K414, which in turn could also be modified by glyoxal. R410 is one previously reported hotspot for methylglyoxal glycation in human serum albumin.[108] So, ultra-high mass resolution mass spectrometry of both EK-15 and FR-25 peptides reacted with glyoxal revealed an unusual glyoxal-derived AGE formed at the arginine side chain (R521 and R410). This species were confidently assigned with a mass error $\leq 1\,ppm$. (Peak assignment tables C-1 to C-19 are presented in appendix C).

5.2 Materials and methods

As mentioned before, the materials employed in the experiments outlined in this chapter are similar to those used in the tests described in chapter 4 (see section 4.2). Therefore, only new materials and methods used in this work are briefly described below.

5.2.1 Mass spectrometry

An inductively coupled plasma (ICP)-MS 7400cx (Agilent Technologies, Berkshire, U.K.) was employed to analyse the sodium content of glyoxal and model peptides prior to reaction with glyoxal. The model peptides were also subjected to the purification step described in section 4.2 prior to sodium analysis. Plasma gas was introduced at a flow of $15\,L/min$, whereas the plasma power was held at 1550 W. The auxiliary gas was constantly held at a flow of $0.8\,mL/min$. Single element standard calibration from QMX (Essex, U.K.) was performed to quantify the sodium content in both glyoxal and the purified peptides.

5.3 Results and discussion

5.3.1 Peptides reacted with glyoxal in MeOH/H_2O

The direct infusion spectrum for the peptide EK-15 reacted with glyoxal in MeOH/H_2O shows the presence of modified and unmodified double, triply and quadruply- charged species figure 5.1. Two modified species denoted by the mass addition of C_2O and $C_2H_2O_2$ were described in chapter 4 (see table 4.1). In this chapter the discussion focuses on the results regarding the presence of the reaction product assigned as $[M + C_2{-}H_2 + 3\,H]^{3+}$.

This previously unreported modification, appeared as a triply-charged ion in figure 5.1e the $[M + C_2{-}H_2 + 3\,H]^{3+}$ species. The species shows a mass corresponding to the net addition of $21.98436\,Da$ to the mass of the unmodified peptide. This modification was also observed for the FR-25 peptide. However, three possible mass additions for $21.98436\,Da$ can be hypothesised, the mass addition of a Mg adduct $[M + Mg + H]^{3+}$, the mass addition of a Na adduct $[M + Na + 2\,H]^{3+}$, or the net mass addition of two carbon atoms from glyoxal minus the loss of H_2 from the peptide, as summarised in table 5.1.

The presence of the magnesium adduct is rejected due to the high mass error. The sodiated hypothesis was also discounted for four reasons: first, the calculated mass error for this assignment, in both peptides (table 5.1), is high compared to the mass errors for all other assigned species in the spectra (appendix C table C- 1, C-2). Thus, the error values for the sodiated species are well outside the 95 % confidence interval. Second, ICP-MS analysis of the purified and unglycated EK-15 and FR-25 peptides did not show any significant content of sodium, and the sodium concentration of the glyoxal reagent prior to dilution was $< 100\,ppb$. Additionally, the direct infusion FTICR spectra of the

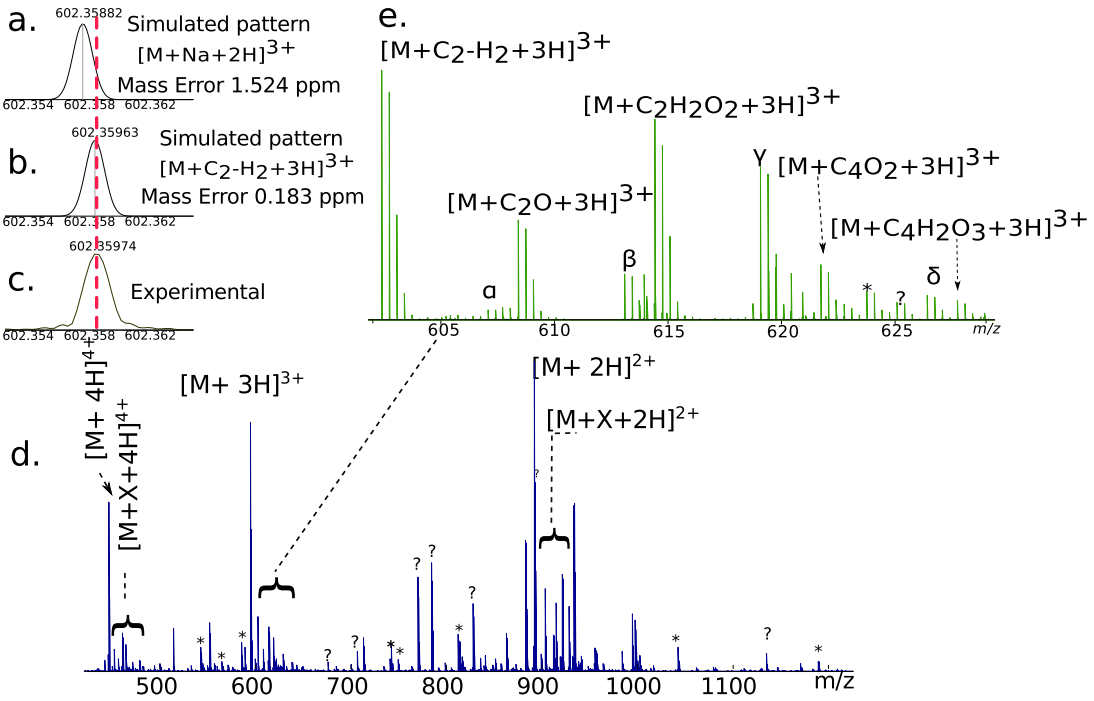

Figure 5.1: Direct infusion spectrum of the EK-15 peptide showing the monoisotopic ion with the net addition of $21.98436\,Da$. **a.** Simulated pattern of the sodium adduct; **b.** Simulated pattern with the addition of $C_2{-}H_2$; **c.** The monoisotopic ion from the experimental data; **d.** Direct infusion spectrum of the EK-15 peptide; **e.** Enhance of the direct infusion spectrum showing the triply-charged modified ions. X= glyoxal modifications and α, β, γ, and δ are peaks showing the ion/molecule reaction with MeOH. The symbol ? indicates unassigned peaks and * indicates background noise peaks where no isotopologues were present. A detailed peak assignment is available as table C-1 in the appendix C.

Table 5.1: Comparison of the masses of possible magnesium or sodium adducts and glyoxal-derived AGEs for the EK-15 and FR-25 peptides reacted in MeOH/H_2O.

Peptide	**Modified ion**	**Theoretical** (m/z)	**Experimental value** (m/z)	**Error** (ppm)	**Error Std. Dev. (ppm)**
EK-15	$[M + Mg + H]^{3+}$	602.35503	602.35974	7.8193	0.275[a]
	$[M + Na + 2\,H]^{3+}$	602.35882		1.524	
	$[M + C_2{-}H_2 + 3\,H]^{3+}$	602.35963		0.183	
FR-25	$[M + Mg + 2\,H]^{4+}$	724.40827	724.41171	4.749	0.342[a]
	$[M + Na + 3\,H]^{4+}$	724.41111		0.819	
	$[M + C_2{-}H_2 + 4\,H]^{4+}$	724.41172		−0.026	

[a] Standard Deviation (Std. Dev.) of the error for the internally calibrated direct infusion spectra of the EK-15 and FR-25 peptide. Details can be found in appendix C, table C-1 and table C-2.

non-reacted peptides (EK-15 and FR-25) did not show evidence of sodiated species, which suggest that precipitation with MeOH/chloroform, employed to desalt the model peptides, was sufficient to eliminate significant sodium interference. Third, sodiated fragment ions are absent in the MS/MS spectra as is shown below (section 5.3.1 and 5.3.1).

Fourth, no evidence was found of other sodiated ions such as $[M + 2\,Na + H]^{3+}$ or $[M + 3\,Na]^{3+}$ species in the glycated and unglycated spectrum of EK-15 peptide, or $[M + 2\,Na + 2\,H]^{4+}$, $[M + 3\,Na + H]^{4+}$, or $[M + 4\,Na]^{4+}$ species in the glycated and unglycated spectrum of FR-25 peptide. Furthermore, both peptides (EK-15 and FR-25) were analysed by nESI from solutions contained $3.4\,\mu mol$ of sodium chloride, in order to induce the formation of sodiated ions and no glyoxal was used to this set of samples (see figure 5.2). The theoretical value of the sodiated ions were compared to the experimental value in table 5.2. The mass to charge of the observed ions and mass error of the sodiated ions peaks, in the resultant mass spectra, provided additional confidence to the assignments of the original glycated peptide ion as described above.

Table 5.2: Comparison of the sodiated species induced by addition of sodium chloride to the EK-15 and FR-25 peptides.

Peptide	**Modified ion**	**Theoretical** (m/z)	**Experimental value** (m/z)	**Error (ppm)**	**Error Std. Dev. (ppm)**
EK-15	$[M + Na + 2\,H]^{3+}$	602.35882	602.35910	0.158	0.127[a]
	$[M + 2\,Na + H]^{3+}$	609.68614	609.68649	−0.019	
	$[M + 3\,Na]^{3+}$	617.01345	617.01381	−0.305	
FR-25	$[M + Na + 3\,H]^{4+}$	724.41111	724.41145	0.461	0.399[a]
	$[M + 2\,Na + 2\,H]^{4+}$	729.90660	729.90655	−0.070	
	$[M + 3\,Na + H]^{4+}$	735.40209	735.40209	0.005	
	$[M + 4\,Na]^{4+}$	740.89757	740.89770	0.173	

[a] Standard Deviation (Std. Dev.) of the error for the internally calibrated direct infusion spectra of the EK-15 and FR-25 peptide infused with sodium chloride. Details can be found in appendix C, table C-3 and table C-4.

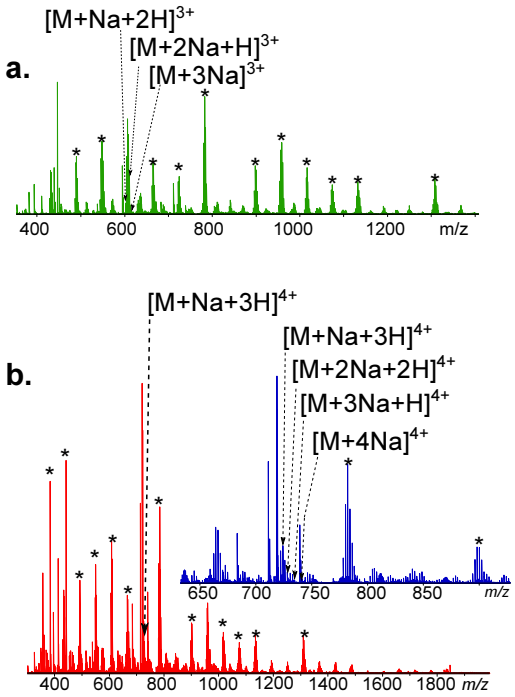

Figure 5.2: Direct infusion spectra of the sodiated **a.** EK-15 and **b.** FR-25 peptide. Sodiation was induced by addition of $3.4\,\mu mol/L$ of sodium chloride to the model peptides and no glyoxal was added. The symbol * indicates sodium adduct peaks. Highlighted sodiated species of particular interest, for detailed peak assignments see the appendix C, table C-4 and C-5.

The addition of $21.98436\,Da$, thus, likely corresponds to a type of glyoxal-derived AGE (net mass addition of C_2 from glyoxal minus the mass of H_2 from the peptide, $C_2{-}H_2$, are shown in scheme 5.1. The $[M + C_2{-}H_2 + 3\,H]^{3+}$ species was fragmented using DR-ECD and CAD of the triply and quadruply-charged precursor ion of modified EK-15 and FR-25 peptides, respectively. Again, as shown in chapter 3 and chapter 4, during quadrupole isolation of the modified species (table 4.1) a low abundance ion is observed. This low abundance ion corresponds to the unmodified species $[M + 3\,H]^{3+}$ and $[M + 4\,H]^{4+}$, respectively for the EK-15 and FR-25 peptides (see table 4.1). The unmodified ion is then ejected in the ICR cell, during ECD, using a DR-ECD experiment. [228,229]

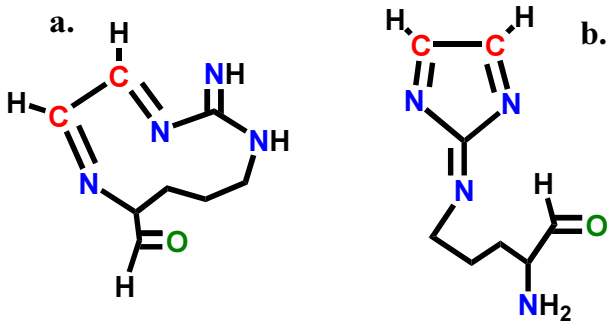

Scheme 5.1: Proposed possible structures for the glyoxal-derived AGE with addition of $21.98436\,Da$ ($C_2{-}H_2$). **a.** crosslinking between amino group of lysine with the N-terminus; **a.** 2-imine imidazole species formed at the guanidine group of arginine. These structures are proposed only with the purpose of illustration where no structural isomers are considered.

In this work the fragment ions generated by DR-ECD and CAD dissociation techniques are identified by the addition of the star symbol (*) to the Roepstorff and Biemman's nomenclature ($c/z^{\bullet}$). The unmodified fragment ions do not have any superscript added to the c/z nomenclature,[47,48] equally, as considered in previous chapters (chapter 3 and chapter 4).

EK-15 peptide

Figure 5.3 shows the DR(595.03)-ECD(602.36) spectrum for the EK-15 peptide. Modified c^* ($n = 2 - 12, 14$) fragment ions show addition of $21.98436\,Da$. Unmodified $z^{\bullet}$ radical fragment ions as well as unmodified c, y, a, and w fragment ions were also observed. Loss of water from the charge-reduced species is also present in the spectrum. The modified c^* fragment ions locate the modification at the arginine in position 2. To further support the rejection of the sodiated hypothesis, as an example, a comparison of the experimental mass obtained for the c_3^* fragment ion ($453.22041\,Da$), with the theoretical mass value of the glyoxal modification and with a possible sodium adduct is made in table 5.3 and figure 5.4. The mass difference between the theoretical mass of the putative sodium adduct $[c_3 + \mathrm{Na}]^+$ and the measured mass, is 5.2 ppm, while the

same mass difference for the glyoxal modification, is only -0.09 ppm. Since the standard deviations of the error in the calibration is 0.362 ppm, 5.2 ppm is approximately 14 standard deviations away. For the FR-25 peptide the corresponding $[c_8 + \mathrm{Na}]^+$ ion is ~ 4 standard deviations away, and at 4 standard deviations, assuming normally distributed errors, there is less than $0.01\,\%$ probability that fragments with sodiated species are a correct assignment.

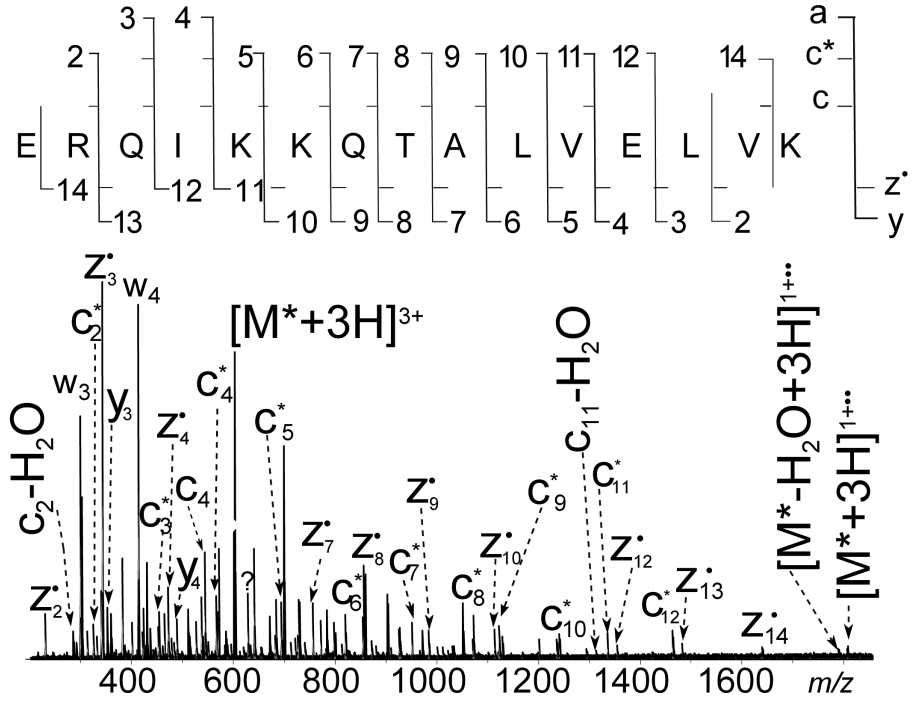

Figure 5.3: DR(595.03)-ECD(602.36) spectrum of the precursor ion $[\mathrm{M} + \mathrm{C_2{-}H_2} + 3\,\mathrm{H}]^{3+}$ with ejection of $[\mathrm{M} + 3\,\mathrm{H}]^{3+}$ of the EK-15 peptide in $\mathrm{MeOH/H_2O}$ solution. The symbol ? indicates unassigned peaks by the current understanding of the fragmentation mechanism. Highlighted modified c^* in the spectrum, for detailed peak assignments see the table C-5 of the supporting information appendix C.

The CAD spectrum (figure 5.5) shows modified b_n^* $(n = 2 - 14)$ and a modified y_{14}^* fragment ions. Unmodified y, b, a fragment ions, losses of $\mathrm{NH_3}$ from the glutamine, and $\mathrm{H_2O}$ from the glutamic acid are present at some b, b^*, and y fragment ions (see table C-10 appendix C). The modified b^* and y^* fragment ions locate the modification at the arginine in position 2. A CAD spectrum of sodiated species with mobile protons should present

Table 5.3: Comparison of the c^* and b^* fragment ion masses of sodium adducts and glyoxal- derived AGEs.

Peptide	**Modified ion**	**Theoretical (m/z)**	**Experimental value (m/z)**	**Error (ppm)**	**Error Std. Dev. (ppm)**
EK-15 MeOH/H_2O	$[c_3 + Na]^+$	453.21804	453.22041	5.229	0.362
	c_3^*	453.22045		−0.088	
EK-15 PBS	$[b_3 + Na]^+$	436.19150	436.19391	5.523	0.428
	b_3^*	436.19390		−0.002	
FR25 MeOH/H_2O	$[c_8 + Na]^+$	981.56099	981.56298	2.027	0.279
	b_3^*	981.56284		0.143	
FR25 PBS	$[b_8 + Na]^+$	964.53389	964.53606	2.249	0.594
	b_8^*	964.536295		0.347	

$[b + Na]^+$, $[a + Na]^+$ and $[y + Na]^+$ fragment ion species.[270,271] However, the sodium, if present, is more likely to bind at the C-terminus, so abundant $[y + Na]^+$ should also be present in the spectrum.[271] However, $[b + Na]^+$, $[a + Na]^+$ and $[y + Na]^+$ fragment ions are absent in the CAD spectrum of the EK-15 peptide reacted in MeOH/H_2O and shown in figure 5.5. Thus, the absence of the sodiated fragment ions, together with the modified c^* fragment ion series, indicate that the addition of $21.9844\ Da$ is far more likely to correspond to the glyoxal modification (C_2−H_2) than to sodiation.

FR-25 peptide

The DR(718.91)-ECD(724.41) spectrum of the FR-25 peptide (figure 5.6, table C-11 appendix C) shows modified c^* fragment ions in positions 8 to 25. Modified $z^*_{18}{}^\bullet$, $z^*_{23}{}^\bullet$ and unmodified $z_n{}^\bullet$ radical, fragment ions, a^* , x_9 , unmodified y fragment ions, losses of water, and NH_3 are present in the spectrum. Thus, the presence of c^* fragment ions and $z^{*\bullet}$ indicate that the modification is located at the arginine residue in position 8. Moreover, the results showed so far, for both peptides, indicate that the glyoxal-derived

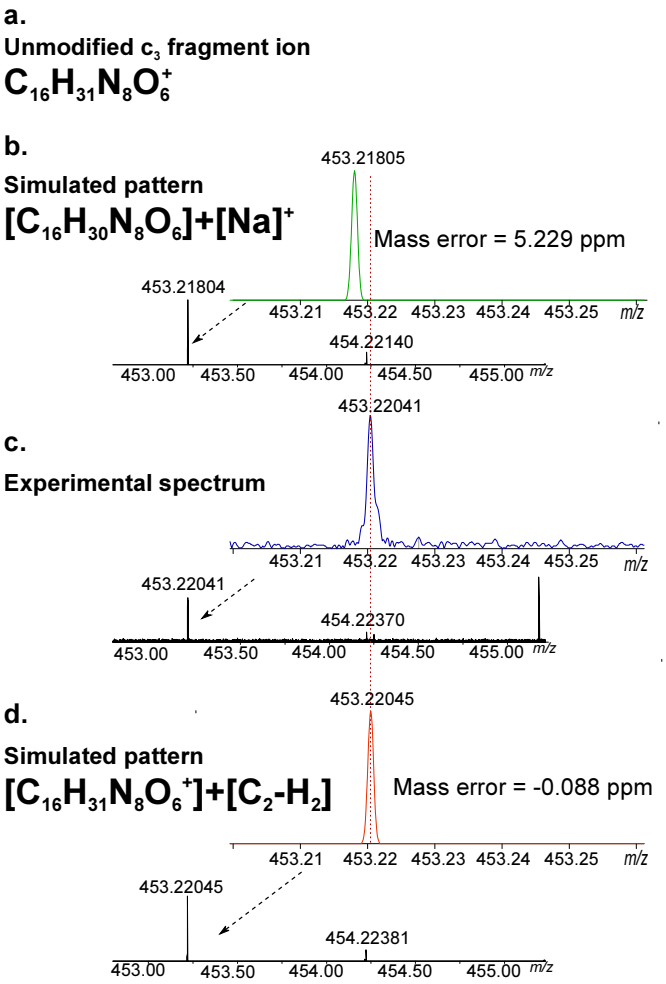

Figure 5.4: Comparison of the c_3 fragment ion for the EK-15 peptide in MeOH/H_2O solution: **a.** elemental composition of the unmodified c_3 fragment ion; **b.** simulated pattern of the c_3 fragment ion modified with possible addition of a sodium adduct; **c.** experimental spectrum highlighting the c_3^* fragment ion; **d.** simulated pattern of the c_3^* fragment ion modified with the addition of C_2 minus H_2. Spectrum internally calibrated with unmodified ions (see table C-6) appendix C.

AGE compound is formed with the guanidine group at the arginine residue (proposed possible structure **b**, scheme 5.1, although other structural isomers may be present).

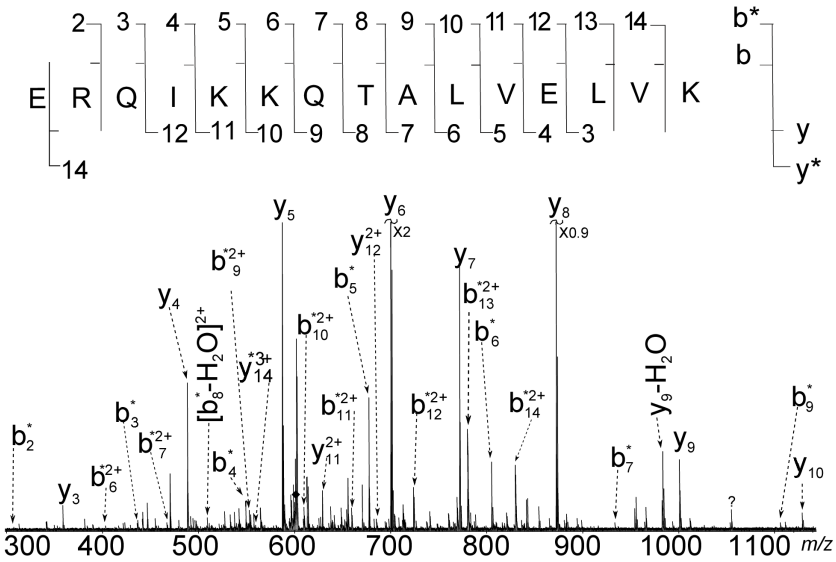

Figure 5.5: CAD spectrum of the precursor ion $[M + C_2{-}H_2 + 3\,H]^{3+}$ of the EK-15 peptide in MeOH/H_2O solution. The symbol ? indicates unassigned peaks by the current understanding of the fragmentation mechanism. Detailed peak assignments are available in the Tables C-10 of the appendix C.

5.3.2 Peptides reacted with glyoxal in PBS

In order to test under pseudo-physiological conditions, the peptides were reacted with glyoxal at $pH\ 7.2 \pm 0.2$ maintained by a phosphate buffer saline solution. This experiment was also repeated three times. The direct infusion spectra of desalted EK-15 and FR-25, reacted with glyoxal, showed similar modified species as C_2O ($39.9943\,Da$), $C_2H_2O_2$ ($58.0055\,Da$), discussed in chapter 4 and the unusual modification $C_2{-}H_2$ ($21.98436\,Da$)).

EK-15 peptide

The DR(595.03)-ECD(602.36) data for the EK-15 peptide with the addition of $21.98436\,Da$ shows the complementary pairs $c_n^*/z_n^{*\bullet}$, (with $n = 3 - 12$), $c_2^*/z_{13}{}^{\bullet}$, and fragment ions c_{13}^*, c_{14}^* , and the radical fragment ion $z_{14}^{*\bullet}$ (table C-16). No evidence of fragment ions

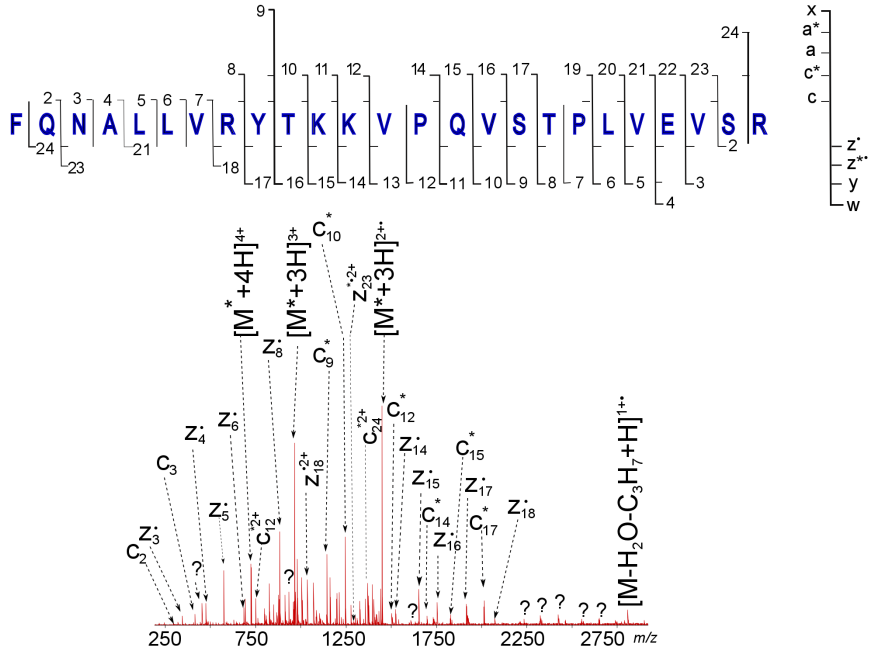

Figure 5.6: DR(718.91)-ECD(724.41) spectrum of the precursor ion $[M+C_2-H_2+4\,H]^{4+}$ with ejection of $[M+4\,H]^{4+}$ of the FR-25 peptide in MeOH/H_2O. The symbol ? indicates unassigned peaks by the current understanding of the fragmentation mechanism. Detailed peak assignments are available in the tables C-17 of the appendix C.

with the addition of sodium were observed in the spectrum (*e.g.* $[c+\mathrm{Na}]^+$). Additionally, the CAD spectrum shows modified b^* fragment ions, unmodified y, b, a fragment ions, side chain losses of H_2O, and NH_3 (figure 5.7, table C-16). Losses of Na, $[b+\mathrm{Na}]^+$, and $[a+\mathrm{Na}]^+$ fragment ions are absent in the spectra, but low abundance $[y+\mathrm{Na}]^+$ fragment ions in positions 3, and 6 to 9 were observed.

The presence of the $[y+\mathrm{Na}]^+$ fragment ions agrees with previous findings that the sodium binds to the C- terminal carboxylic acid.[270] However, for instance, the m/z of the b^* fragment ions (table 5.3), with the glyoxal modification C_2-H_2 has a low error compared with a potential $[b_n+\mathrm{Na}]^+$ fragment ion series. Thus, the presence of highly abundant modified c^*, b^* , z^*_{14} and y^*_{14} fragment ions, together with a low abundance of $[y+\mathrm{Na}]^+$ species, indicates the presence of two ion species with the same

mass in the samples reacted in PBS. The highly abundant one, that corresponds to the glyoxal modification ($C_2{-}H_2$) and the low abundant, second one, that corresponds to the formation of $[M + Na + 2\,H]^{3+}$. The low abundance of the $[M + Na + 2\,H]^{3+}$ species and consequently of the $[y + Na]^+$ fragment ions are attributed to the residual presence of NaCl from the PBS buffer after the desalting procedure described above. CAD and DR-ECD results localize the glyoxal modification ($C_2{-}H_2$) site to the arginine residue in position 2, for the EK-15 peptide.

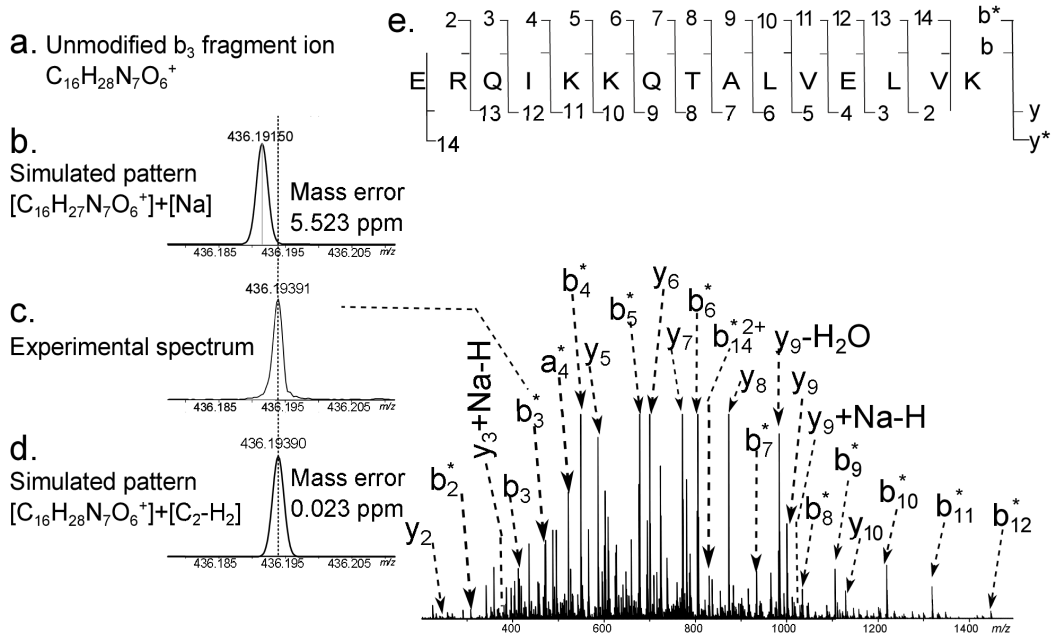

Figure 5.7: CAD spectrum of the precursor ion $[M + C_2{-}H_2 + 3\,H]^{3+}$ of the EK-15 peptide in PBS buffer with enhance of the b_3 fragment ion: **a.** elemental composition of the unmodified b_3 fragment ion **b.** simulated pattern of the b_3 fragment ion with addition of the sodium adduct; **c.** experimental spectrum highlighting the b_3^* fragment ion; **d.** simulated pattern of the b_3 fragment ion with the addition of C_2 minus H_2; **e.** peptide map of the CAD spectrum. Spectrum internally calibrated with unmodified ions (see table C-7) to compare the monoisotopic modified b_3 fragment ions. Detailed peak assignments of the spectrum are available in the Tables C-19 appendix C.

Addition of $21.98436\,Da$ was also observed for the FR-25 peptide under pseudo-physiological conditions. Further analysis of the CAD spectrum showed that a glyoxal-derived species is formed at the guanidine group in the arginine moiety in position 8 (refer to table

C-20, appendix C).

Additionally, sodium chloride, up to a concentration of $3.4\,\mu M$, was directly added to the glycated EK-15 peptide diluted in the electrospray solution. The sodiated-glycated peptides were then ionized by nano-ESI and fragmented by CAD. The CAD spectrum revealed an increase in the abundance of the $[y + \mathrm{Na}]^+$ fragment ions observed in the pseudo-physiological conditions. The glycated EK-15 peptide, in MeOH/H_2O, was also fragmented by CAD. The data (table C-21) showed the presence of $[y + \mathrm{Na}]^+$ fragment ions in positions 3, 6, 7, 9, and $[a_{10} + \mathrm{Na}]^+$ fragment ions. The main difference with the CAD data presented in figure 5.5 and table C-8 (appendix C) is precisely, the presence of the sodiated fragment ions. These results further support the presence of two ion species with the same mass, $[\mathrm{M} + \mathrm{Na} + 2\,\mathrm{H}]^{3+}$ and $[\mathrm{M} + (\mathrm{C_2} - \mathrm{H_2}) + 3\,\mathrm{H}]^{3+}$, due to residual NaCl in the glycated peptides using PBS solution.

The results presented here suggest that the addition of $21.98436\,Da$ to the peptide mass, at both pseudo-physiological and non-physiological conditions, corresponds to an unusual type of glyoxal-derived AGE. This compound is formed at the guanidino moiety at the arginine residue and the proposed reaction in shown in scheme 5.2. The addition of $21.98436\,Da$ to the peptide mass could also be formed by dehydration during the electrospray process. However, as this modification disappeared after 21 hours of reaction in MeOH/H_2O and after 12 hours of reaction in PBS buffer, it is most likely that they are formed in solution. A reasonably likely interpretation of these results is that this unusual modification with glyoxal is a kinetic product (a rapidly formed intermediate product, which is not the final most stable product), due to the formation of a five member ring moiety. Moreover, this modification disappears over time to allow the formation the formation of the thermodynamic product (a dihydrated five member ring), which shows the addition of $C_2H_2O_2$ at the guanidino group of arginine and it was proposed to be the 4,5 dihydroxyimidazoline.[73] Nonetheless, thermodynamics

and kinetic studies as well as further research for the formation of this compound in biological systems needs to be addressed before any biological conclusions can be drawn from these results.

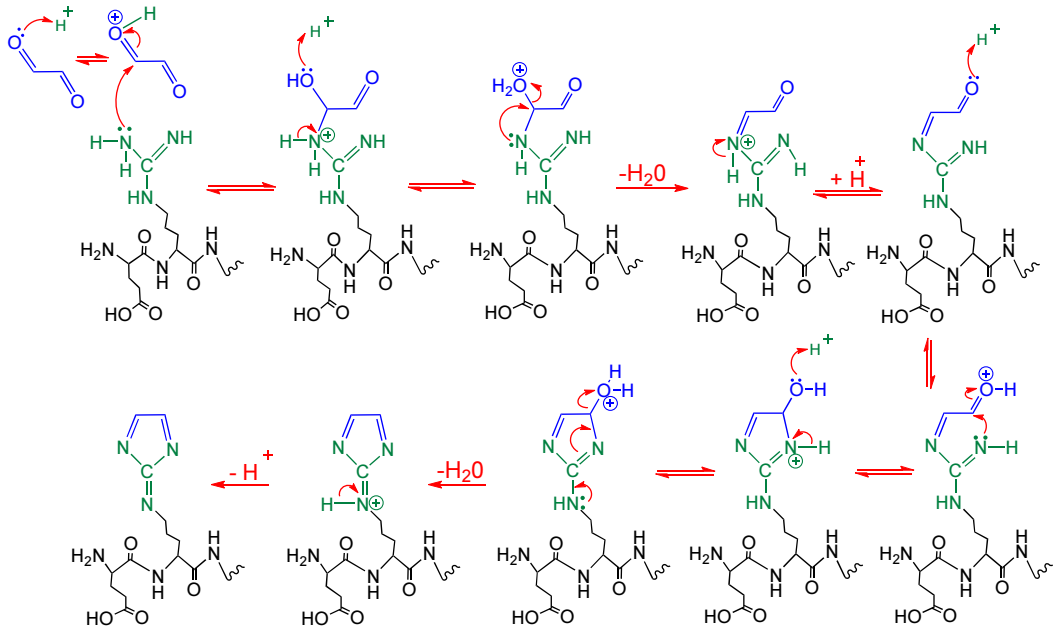

Scheme 5.2: Schematic of the proposed reaction for the mass addition of $21.98436\,Da$ forming the glyoxal-derived AGE. Although, the reaction is depicted forming a possible chemical structure, other structural isomers may be present. The hypothesized reaction is illustrated with glyoxal dehydrate, however, unhydrated and monohydrated species also coexist in the glyoxal reagent (39%).[262]

5.4 Conclusions

Glyoxal was reacted, under non-physiological and pseudo-physiological conditions, with model peptides EK-15 and FR-25, both fragments of human serum albumin. The reaction products were analysed using ECD and CAD in a Fourier transform ion cyclotron resonance mass spectrometer (FT-ICR-MS). The glyoxal bound to the guanidino group of the arginine residue forming an unusual glyoxal-derived AGE in both peptides used in this study. This glyoxal modification increased the mass of the peptide by $21.98436\,Da$ and was assigned as $C_2{-}H_2$. A general structure was proposed as the 2-imino-imidazole. It is noteworthy that although a structure is being proposed, no structural conformation has been considered. It is clear then that a further study on the possible isomers is required, in order to asses the validity of the proposed structure.

Examining the results for the FR-25 peptide it is important to note that, surprisingly, the arginine in position 25, i.e. 25Arg from the $N-$terminus, was not found to be susceptible to glycation by glyoxal, neither under MeOH/H_2O or PBS reaction solutions. Nevertheless, as it could be expected for this case, the arginine in position 8, i.e. 8Arg, was modified by the glyoxal reagent, forming the unusual compound previously indicated (scheme 5.2). Considering this finding, it is herein argued that the conformation of the peptide in the reaction solutions used in this work, might be allowing the exposure of the arginine in position 8, and at the same time be protecting the arginine in position 25. In summary, we argue that the absence of the modification in 25Arg could be explained by the inaccessibility of the arginine at the $C-$terminus in the peptide chain. However, the validity of this argument shall be assessed by additional experimentation, varying systematically the position of the arginine in any polypeptide chain. Thus, although additional experimentation is deemed necessary to prove this hypothesis, such additional experimentation was considered beyond the scope of the present work. More research

activity is then required, but we hope that the arguments outlined above can be a potential motivation for such an extended research.

The results also showed that two compounds with the same mass were formed when sodium was present during the glycation reaction with glyoxal. In the experiments carried out in this work the source of sodium was provided by the PBS reaction solution. Thanks to the use of the ultrahigh resolution of the FT-ICR-MS, an accurate detection of such species was possible, with mass assignments exhibiting errors $\leq 1ppm$ in every case. It is worth to mention that the detection of mass differences below $2.4\,mDa$ is either not possible or extremely difficult to achieve with low resolution mass spectrometers. This may explain why this type of modification (2-imino-imidazole) has not been reported before.

Finally, given the reaction times employed in the experiments outlined in the present chapter, and as equally mentioned in § 4.4, it was deemed necessary to glycate the peptides at longer reaction times in order to assess the involvement of the lysine and/or other basic residues within the peptide. This is addressed in the following chapter.

6

Study of an unexpected crosslinking and diglycation as advanced glycation end-products by tandem mass spectrometry

6.1 Introduction

The experimental evidence presented and discussed in chapters 3 to 5 showed that glyoxal is an arginine glycating agent that reacts at 21 hours in MeOH/H_2O, and at 6 hours when used with PBS. In the analyses discussed previously three modifications to the peptides were detected at the guanidino group of the arginine residue. These modifications were assigned as: a C_2O addition ($39.99\,Da$); a $C_2H_2O_2$ addition ($58.055\,Da$); and, finally, a modification including a two-atom addition of carbon, i.e. C_2 (provided by the glyoxal), and a two-atom loss of hydrogen, i.e. H_2 (lost by each peptide), which accounts for a net mass increase of $21.9843\,Da$ to the peptide mass after the reaction with glyoxal, and represented as $C_2{-}H_2$. It is appropriate to clarify that although the C_2O and $C_2H_2O_2$ modifications were detected for all tested peptides employed in this study, the $C_2{-}H_2$ modification was only detected in the FR-25 and EK-15 peptides, as mentioned before (see chapter 5).

In spite of the satisfactory results obtained so far regarding the determination of a number of modifications by glyoxal at the arginine residue, there still remains to clarify the possibility of involvement, if any, of the lysine residue and/or other basic sites within any of the peptides selected for this work.

Arguably, it could be hypothesized that the lack of evidence regarding the involvement of the lysine residue, or of any other basic site, is due to the extension of the range of reaction times selected for the performed tests. Therefore, in order to explore this hypothesis, a set of experiments at longer reaction times was carried out using model peptides KM-11 and AcKM-11. In keeping with the previous experiments, MeOH/H_2O and PBS are used too as reaction solutions for the experiments discussed in this chapter.

6.2 Materials and methods

Acetylated and non-acetylated undecapeptides, with one arginine and one lysine residue available for glycation, were used to react with glyoxal for up to 29 days with analysis by MS/MS at 4, 7, 11, and 29 days in MeOH/H_2O, and for 12 hours in PBS. Mass spectrometry results from a Fourier transform ion cyclotron resonance mass spectrometer are used to show the presence of glycated compounds. A more detailed description of the methods and materials is presented below.

6.2.1 Materials

The peptides used for the experiments target of this section are the acetylated and non-acetylated undecapeptides, as described and summarised in table 6.1. Additionally, due to the similar nature of the target experiments of this part of the present work, the

materials employed here were consistent with those described in chapter 4 (see section 4.2).

Table 6.1: Common modified ions for the model peptides reacted with glyoxal in MeOH/H_2O and PBS.

Peptide Sequence	**Unmodified ion (m/z)**	**Observed modified ions in MeOH/H_2O**[a]	**Observed modified ions in PBS**[a]
KM-11 KPRPQQFFGLM$-NH_2$ (1346.72813 Da)	$[M+2H]^{2+}$ (674.37134)	$[M+2(C_2H_2O_2)+2H]^{2+}$ (m/z 732.37680) Error -0.027 ppm	$[M+2(C_2H_2O_2)+2H]^{2+}$ (m/z 732.37654) Error 0.384 ppm
AcKM-11 AcKPRPQQFFGLM$-NH_2$ (1388.73869 Da)	$[M+2H]^{2+}$ (695.37663)	$[M+2(C_2H_2O_2)+2H]^{2+}$ (m/z 753.38140) Error 0.149 ppm	$[M+2(C_2H_2O_2)+2H]^{2+}$ (m/z 753.38140) Error -0.942 ppm

[a] Detailed peak assignment is showed in Table D-1 to D-4 appendix D, respectively.

6.2.2 Glycation of model peptides in MeOH/H_2O

The peptides were purified using the procedure described in section 4.2. Subsequently, the peptides were re-dissolved in MeOH/H_2O (50:50). Three aliquots from this peptide-containing solution were put to react with glyoxal ($800\,\mu mol/L$). The reaction was carried out at $37\,℃$ for up to 29 days at a starting pH of 7.5, monitoring by MS/MS analysis at 4, 7, 11, and 29 days. The reacted peptides were diluted with an ionization solution containing methanol, water, isopropanol, and acetic acid (50:39:10:1), up to a final concentration of $\sim 0.1\,\mu M$.

6.2.3 Glycation of model peptides in PBS

For the reaction in PBS, peptides were purified in exactly same manner as described above. However, for this case, the purified peptides were dissolved in PBS (pH $= 7.2 \pm 0.2$) and three aliquots were taken to react with glyoxal ($400\,nM$) over a 10-hour incubation. After the reaction the three glycated peptides were cleaned from the buffer solution

using a purification procedure alike to that described in section 4.2. Interestingly, the reaction in PBS at longer reaction times and higher concentration caused insolubility of the pellet after desalting. Consequently different glyoxal concentrations and reaction times were employed until solubility of the sample was achieved.

The dried pellet was re-dissolved in 100% water and then diluted with ionization solution to a final concentration of $\sim 0.1\,\mu M$ prior to injection into the mass spectrometer.

6.2.4 Mass spectrometry

Similar set of conditions as those used in section 4.2 for mass spectrometry were used for the analysis of the reacted peptides. In this case nano electrospray (n-ESI) was used to ionise the reacted peptides. Double resonance ECD experiments[228] were performed by varying the ejection pulse between 70 and $120\,ms$. Internal calibration was performed with DataAnalysis software 4.0 SP 3 (Bruker Daltonics). The masses used for calibration are indicated with a symbol * in the tables contained within the appendix D.

Ion mobility spectra were acquired with a Synapt G2 (Waters, Manchester, U.K.) traveling wave mass spectrometer (TWIMS). The sample, diluted with ionization solution (as above), was loaded into a grounded metallic coated glass capillary. To generate the ions the spray shield voltage was kept at $1.3\,kV$, the cone voltage was $20\,-\,180\,V$, and the ion source temperature was maintained at 90 $^{\circ}C$. The ion of interest was isolated in the quadrupole prior to ion mobility separation. The T-wave velocity and peak height voltages were $500\,m/s$ and $40\,V$, respectively. The T-wave mobility cell was operated at a pressure of 0.55 mbar and nitrogen was employed as separation gas. External calibration was performed using sodium iodide standard ($1\,mg/mL$) from (Waters Corporation, Manchester, UK). Data processing was carried out by use of the Waters Driftscope 2.1 software and MassLynx 4.1 (Waters Corporation, Manchester, UK).

6.3 Results and discussion

The direct infusion spectra of the glycated peptide KM-11 (KPRPQQFFGLM$-NH_2$), reacted in MeOH/H_2O and in PBS solutions, are shown in figure 6.1. Similar reaction products were obtained when this peptide was reacted with glyoxal in MeOH/H_2O (as shown in figure 6.1a) and in PBS (as shown in figure 6.1b), and common ions included a $[M + 2\,(C_2H_2O_2) + 2\,H]^{2+}$ ($m/z\,732.3768$) species. Equally, as mentioned above, the acetylated version of the KM-11 peptide was reacted with glyoxal in MeOH/H_2O and in PBS. Similar species to those observed in the reaction of the non-acetylated peptide were obtained, also including the $[M + 2\,(C_2H_2O_2) + 2\,H]^{2+}$ ion (a summary of these findings is presented in Tables D-3 and D-4 of the appendix D).

In table 6.1 the mass error of the $[M + 2\,(C_2H_2O_2) + 2\,H]^{2+}$ species, for both peptides (KM-11 and AcKM-11), is presented for both reaction solutions (MeOH/H_2O and PBS) with standard deviations of the errors between 0.315 and $0.519\,ppm$ (see tables D-1 to D-4 in appendix D). Thus, it is hypothesized that the net addition of two molecules of $C_2H_2O_2$ to the peptide corresponds to diglycation at the arginine and at the lysine residues, respectively, as shown in scheme 6.1. In order to test this hypothesis, ECD and CAD fragmentation techniques were employed to accurately assign glyoxal binding sites using a FT-ICR-MS.

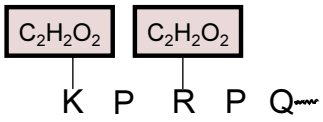

Scheme 6.1: Illustration of diglycation at the lysine and at the arginine residue by the addition of one molecule of $C_2H_2O_2$ from glyoxal. These diglycation is represented by the formation of $[M + 2\,(C_2H_2O_2) + 2\,H]^{2+}$ species.

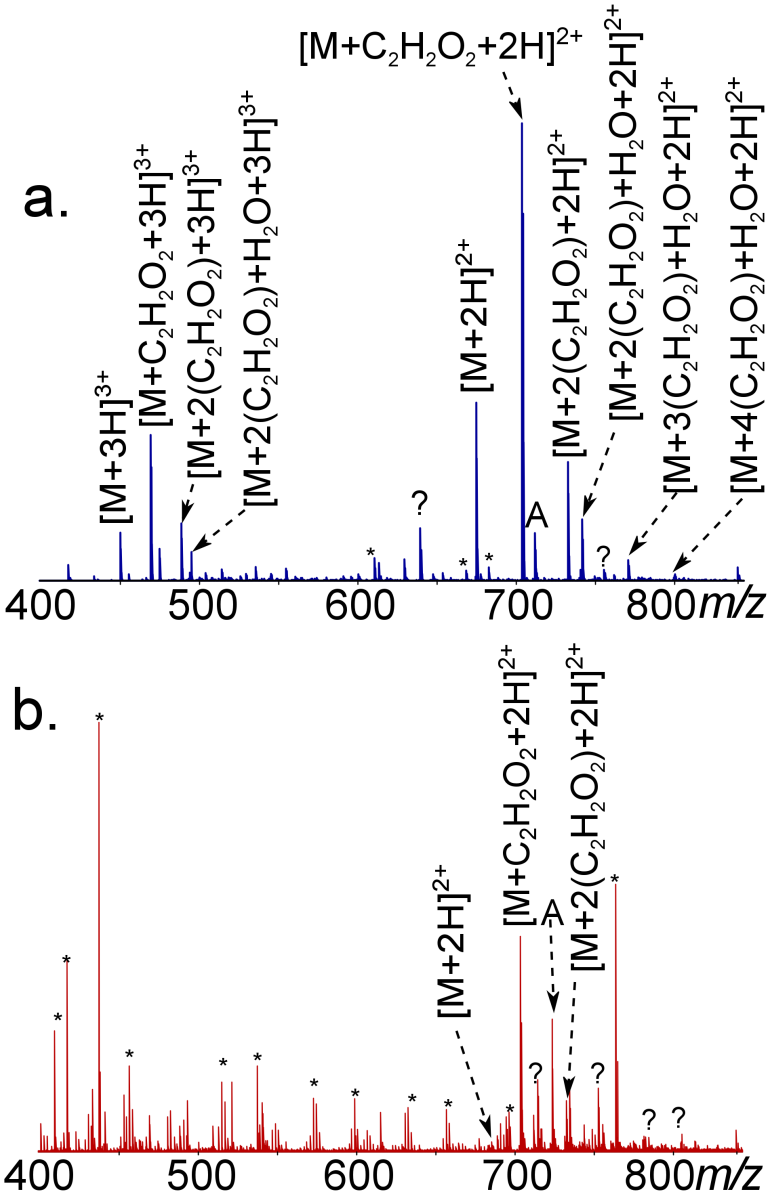

Figure 6.1: Direct infusion spectrum of the KM-11 reacted with glyoxal: **a.** in MeOH/H_2O; **b.** in PBS. A=$[M + C_4H_2O_3 + 2H]^{2+}$]. The symbol ? indicates unassigned peaks and an * indicates chemical noise, probably from the PBS buffer. Labeled peaks are assigned in the detailed peak assignment tables D-1 and D-2 of the appendix D.

6.3.1 Fragmentation of KM-11 peptide

The spectrum of the quadrupole isolation of the diglycated $[M + 2\,(C_2H_2O_2) + 2\,H]^{2+}$ ($m/z\,732.37680$) species, revealed low abundance of a monoglycated $[M + C_2H_2O_2 +$

$2\,H]^{2+}$ ($m/z\,703.37391$) ion. The presence of the monoglycated $[M + C_2H_2O_2 + 2\,H]^{2+}$ ion is attributed to activation of the diglycated precursor ion $[M + 2\,(C_2H_2O_2) + 2\,H]^{2+}$ during quadrupole isolation, which causes loss of one molecule of $C_2H_2O_2$. Consequently, the quadrupole isolated precursor ion ($[M + 2\,(C_2H_2O_2) + 2\,H]^{2+}$) was further separated from the monoglycated species in the ICR cell by application of the double resonance (DR) experiment during ECD. This experiment allows ejection of the monoglycated $[M + C_2H_2O_2 + 2\,H]^{2+}$ species while performing ECD.

The DR-ECD spectrum of the diglycated species showed three types of fragment ions ($c/z^{\bullet}$): unmodified, with single modification (addition of one molecule of $C_2H_2O_2$, and with double modification (addition of two molecules of $C_2H_2O_2$. In the present chapter these fragment ions are distinguished using a prescribed nomenclature, as follows. Singly-modified fragment ions are identified by adding a double dagger symbol (‡) to the Roepstorff and Biemann's nomenclature ($c/z^{\bullet}$),[47,48] this single modification was associated with the addition of one molecule of $C_2H_2O_2$ (i.e., a net addition of $58.00546\,Da$ to the fragment ion mass). Doubly-modified fragment ions are identified by adding the hash symbol (#) to the normalized ($c/z^{\bullet}$) nomenclature; this modification was linked to the addition of two molecules of $C_2H_2O_2$ (i.e., a net addition of $116.01092\,Da$ to the fragment ion mass). Finally, for clarity, the unmodified fragment ions are indicated by using the standard $c/z^{\bullet}$ nomenclature, with no superscript added.[47,48]

The DR(703)-ECD(732) spectrum of the diglycated modified ion $[M + 2\,(C_2H_2O_2) + 2\,H]^{2+}$, in MeOH/$H_2O$ solution is shown in figure 6.2. $c_n^{\#}$ modified fragment ions in position 4 to 10 are observed in the spectrum. The monoglycated modified c fragment ion in position 2 shows addition of one molecule of $C_2H_2O_2$ and is represented as $c_2^{\ddagger}$ in figure 6.2. Diglycated $z_9^{\#\bullet}$ radical fragment ion, unmodified c, y, fragment ions, and $z^{\bullet}$ radical fragment ions are also present in the spectrum. The modified c fragment ion in position 3 were not detected due to the presence of proline.[171,272]

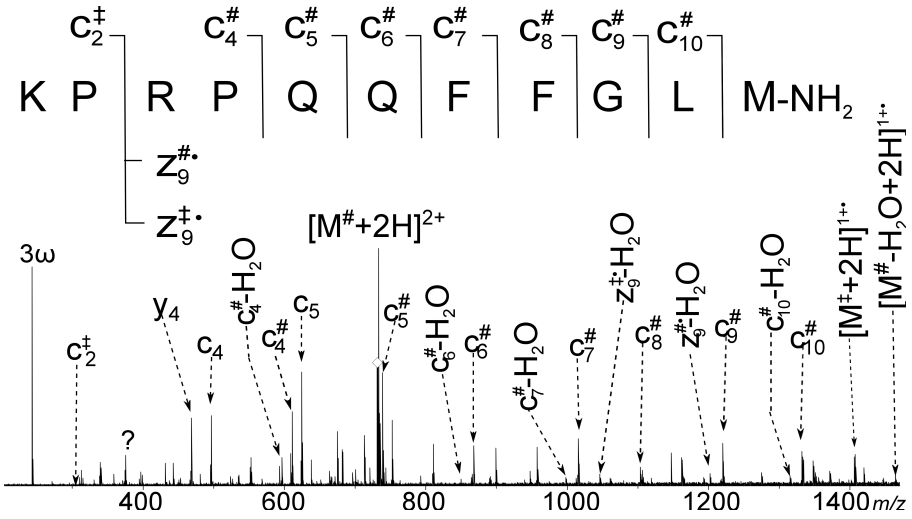

Figure 6.2: DR(703)-ECD(732) spectrum of the KM-11 peptide of the precursor ion $[\mathrm{M} + 2\,(\mathrm{C_2H_2O_2}) + 2\,\mathrm{H}]^{2+}$ with ejection of $[\mathrm{M} + \mathrm{C_2H_2O_2} + 2\,\mathrm{H}]^{2+}$ in $\mathrm{MeOH/H_2O}$ solution. The symbol ? indicates unassigned peak by the current understanding of the fragmentation mechanism. Highlighted modified $c^{\#}$, $c_2^{\ddagger}$, and $z_9^{\#\bullet}$ fragment ions in the spectrum and unlabelled peaks are assigned in the detailed peak assignment Table D-5 of the appendix D.

The presence of the monoglycated modified $c_2^{\ddagger}$ fragment ion could be attributed to fragmentation of the monoglycated species, which although ejected by the double resonance experiment, could also be formed during ECD. In order to test the provenance of monoglycated modify $c_2^{\ddagger}$, $c_4^{\ddagger}$ to $c_{10}^{\ddagger}$ fragment ions, $z_9^{\ddagger\bullet}$ radical fragment ions, along with the diglycated $z_9^{\#\bullet}$ radical fragment ion their relative intensities were normalized (see equation (3.1)) and plotted in figure 6.3. Furthermore, ECD experiments were performed without double resonance, and the intensities of the $c_n^{\ddagger}$ fragment ions ($n = 2, 4, \ldots, 10$), were also normalized and plotted in figure 6.3. Comparison of the normalized relative intensity of the modified $c_n^{\ddagger}$ fragment ion, $z_9^{\#\bullet}$ and $z_9^{\ddagger\bullet}$ radical fragment ions, from the ECD(703) and DR(703)-ECD(732) spectra, revealed that the intensity of the monoglycated $c_2^{\ddagger}$, $z_9^{\ddagger\bullet}$ radical fragment ion, and diglycated $z_9^{\#\bullet}$ radical fragment ion did not decrease during the DR-ECD experiment. Normally, in a DR-ECD experiment, the decrease in the normalized relative intensity of a particular fragment ion indicates the parentage of the ejected ion.[228] Thus, as the intensity of the monoglycated $c_2^{\ddagger}$ fragment

ion and $z_9^{\ddagger\bullet}$ radical fragment ion did not decrease, it is though that these species are likely to be derived from the diglycated species ($[M + 2\,(C_2H_2O_2) + 2\,H]^{2+}$), and not from the ejected monoglycated species.

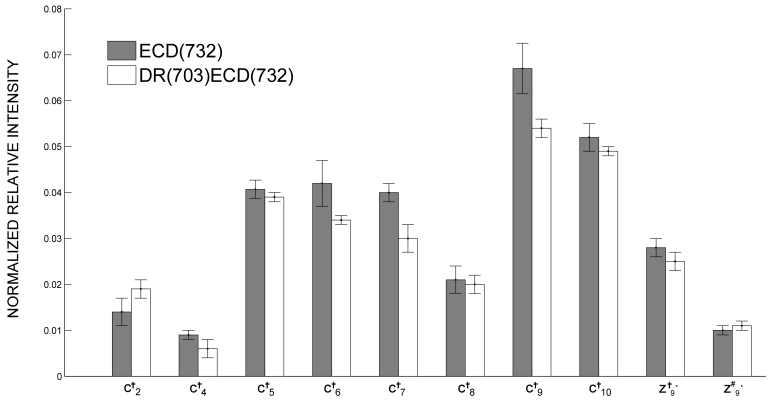

Figure 6.3: Comparison of the relative intensity of the $c_n^{\ddagger}$ fragment ions and $z_9^{\#\bullet}$, and $z_9^{\ddagger}$ radical fragment ions for the ECD(732) and DR(703)-ECD(732) spectra for the KM-11 peptide.

The CAD spectrum presented in figure 6.4, for the diglycated ion ($[M + 2\,(C_2H_2O_2) + 2\,H]^{2+}$) in MeOH/$H_2O$, shows modified $b_n^{\#}$ ($n = 3-10$) with addition of two molecules of $C_2H_2O_2$, and $b_2^{\ddagger}$ fragment ions with the addition of one molecule of $C_2H_2O_2$. Unmodified y, b, a fragment ions, losses of NH_3, loss of the modification, and up to three losses of H_2O from the charge reduced-species were also observed in the spectrum. The results showed so far indicate that both the lysine, in position 1, and the arginine, in position 3 are modified by glyoxal in the MeOH/H_2O solution, with $c_2^{\ddagger}$ and $b_2^{\ddagger}$ fragment ions likely associated to the diglycated species $[M + 2\,(C_2H_2O_2)^{+}2\,H]^{2+}$.

The KM-11 peptide was also reacted with glyoxal in PBS and the modified diglycated ion $[M + 2\,(C_2H_2O_2) + 2\,H]^{2+}$ species was also present. The DR(703)-ECD(732) spectrum of the $[M + 2\,(C_2H_2O_2) + 2\,H]^{2+}$ species, showed in figure 6.5, agrees with the previous results. In summary, addition of two molecules of $C_2H_2O_2$ is observed in $c_4^{\#}$ to $c_{10}^{\#}$, $b_3^{\#}$ to $b_{10}^{\#}$, $z_9^{\#\bullet}$, $y_9^{\#}$, $y_{10}^{\#}$ fragment ions, and addition of one molecule of $C_2H_2O_2$ is shown in

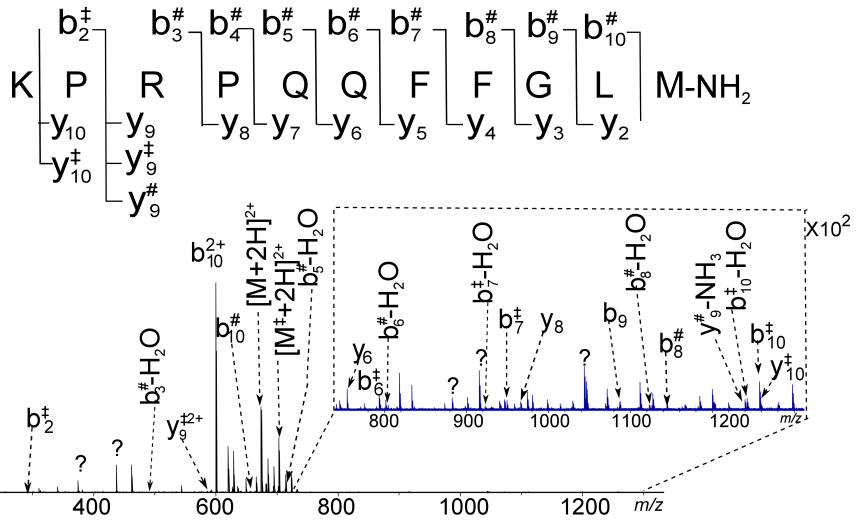

Figure 6.4: CAD spectrum of the precursor ion $[\mathrm{M} + 2\,(\mathrm{C_2H_2O_2}) + 2\,\mathrm{H}]^{2+}$ for the KM-11 peptide in MeOH/H_2O solution. The symbol ? indicates unassigned peaks by the current understanding of the fragmentation mechanism. Highlighted modified $b^{\#}$ fragment ions in the spectrum and unlabelled peaks are assigned in the detailed peak assignment table D-7 of the appendix D.

$c_2^{\ddagger}$, $b_2^{\ddagger}$, and $y_9^{\ddagger}$ fragment ions. It seems clear then that the lysine residue (position 1) is modified by one molecule of $C_2H_2O_2$ and the arginine residue (position 3) is modified either by one or two molecules of $C_2H_2O_2$.

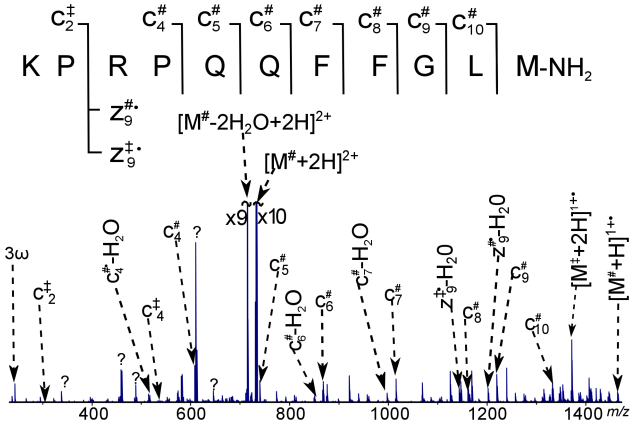

Figure 6.5: DR(703)-ECD(732) spectrum of the precursor ion $[\mathrm{M} + 2\,(\mathrm{C_2H_2O_2}) + 2\,\mathrm{H}]^{2+}$ with ejection of $[\mathrm{M} + \mathrm{C_2H_2O_2} + 2\,\mathrm{H}]^{2+}$ of the KM-11 peptide in PBS solution. The symbol ? indicates unassigned peaks by the current understanding of the fragmentation mechanism. Highlighted modified $c^{\#}$, $c_2^{\ddagger}$, and $x_9^{\#\bullet}$ fragment ions and unlabelled peaks are assigned in the detailed peak assignment Table D-8 of the supplementary information.

Based on these findings, two possible compounds with the same mass could be formed in the KM-11 peptide in both MeOH/H_2O and PBS solution. The first compound that represents diglycation was shown in scheme 6.1, which has an elemental composition of $C_{67}H_{103}N_{18}O_{17}S$ and is represented as $[M + 2\,(C_2H_2O_2) + 2\,H]^{2+}$ with a theoretical m/z of 732.37683. This compound correlates well with the observed $c_2^{\ddagger}$, $b_2^{\ddagger}$ fragment ions, and $z_9^{\ddagger\bullet}$ radical fragment ion. These fragments as discussed above, are likely to be derived from the diglycated $[M + 2\,(C_2H_2O_2) + 2\,H]^{2+}$ species.

A second compound shows the addition of two molecules of $C_2H_2O_2$ at the arginine residue, as in illustrated in scheme 6.2. Interestingly, this compound has similar elemental composition and theoretical m/z as described above (see scheme 6.2) and herein is represented by $[M + C_4H_4O_4 + 2\,H]^{2+}$. This second compound accounts for the presence of $z_9^{\#\bullet}$ radical fragment ion, $y_9^{\#}$, and $y_{10}^{\#}$ fragment ions. Thus, due to the mixed presence of the $c_2^{\ddagger}$, $b_2^{\ddagger}$, and $z_9^{\ddagger\bullet}$ along with the presence of $z_9^{\#\bullet}$, $y_9^{\#}$, and $y_{10}^{\#}$ fragment ions is likely that glyoxal is forming with the KM-11 peptide two isomeric compounds with the same mass, which are detected in the mass spectrometer as m/z 732.37682.

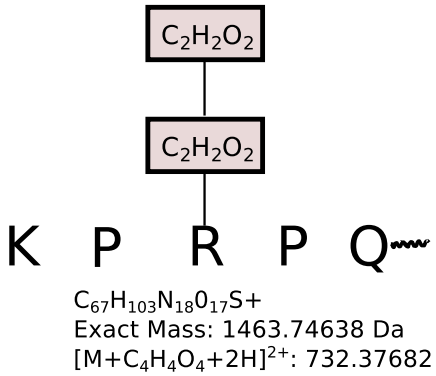

Scheme 6.2: Illustration of the addition of two molecules of $C_2H_2O_2$ at the arginine residue. These diglycation is represented by the formation of $[M + C_4H_4O_4) + 2\,H]^{2+}$ species.

The $[M + C_4H_4O_4) + 2\,H]^{2+}$ species could have the chemical structures proposed in scheme 6.3. The structure proposed in scheme 6.3a represents the formation of N^{δ}-[2-

(dihydroxymethyl)-2H,3aH,4H,6aH-[1,3]dioxolo[5,6-d]imidazolin-5-yl]-L-ornithine, herein referred to as glyoxal dimer at the arginine residue. A second structure could be the formation of Schiff base at the arginine residue, as is illustrated in scheme 6.3. It is noteworthy that the proposed formation of the glyoxal dimer (scheme 6.3a) is energetically favored over the Schiff base species (scheme 6.3), because of the formation of the stable dioxolane ring. [261]

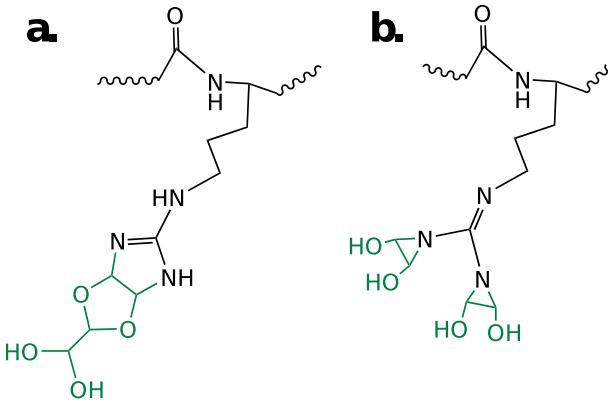

Scheme 6.3: Representation of the proposed species for the KM-11 peptide reacted with glyoxal in MeOH/H_2O and in PBS solutions showing addtion of $C_4H_4O_4$ at the arginine residue: **a.** proposed glyoxal dimer structure formed at the arginine residue (N^{δ}-[2-(dihydroxymethyl)-2H,3aH,4H,6aH-[1,3]dioxolo[5,6-d]imidazolin-5-yl]-L-ornithine); **b.** proposed Schiff base structure.

In contrast the diglycated $[M + 2\,(C_2H_2O_2) + 2\,H]^{2+}$species (scheme 6.1) could have the lysine residue modified by glyoxal crosslinking with the N-terminus as shown scheme 6.4a, but also other chemical structures are possible as proposed in scheme 6.4b and scheme 6.4c. It seems clear then that acetylation at the N-terminus could block the formation of the possible glyoxal crosslinked species. Moreover, if the species proposed in scheme 6.1b and scheme 6.4c are formed, acetylation at the N-terminus should not affect the fragmentation pattern and in particular $c_2^{\ddagger}$, and $b_2^{\ddagger}$ fragment ions should be present in the MS/MS experiments. Thus, further experiments were carried out in order to differentiate the proposed intramolecular crosslinking (scheme 6.4a) from the Schiff base formation (scheme 6.4b) or formation of other species (scheme 6.4c) at the lysine

residue, using an acetylated version of the KM-11 peptide (AcKM-11).

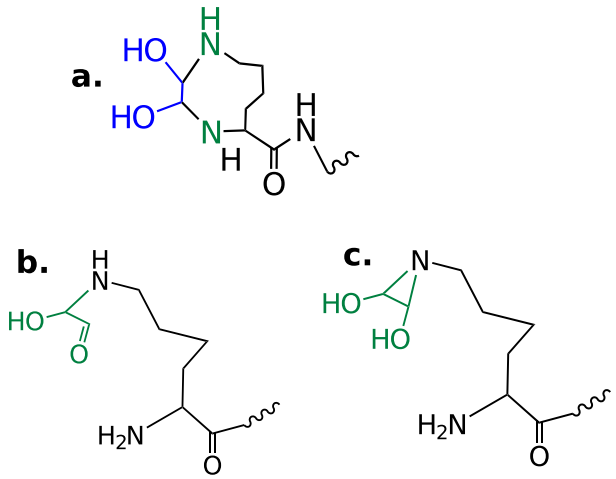

Scheme 6.4: Illustration of the possible structures formed at the lysine residue for the KM-11 peptide reacted with glyoxal in MeOH/H_2O and in PBS solutions **a.** Lysine residue crosslinked with glyoxal and the $N-$terminus ; **b.** Schiff base formed at the lysine residue; **b.** heterocyclic amine.

6.3.2 Fragmentation of AcKM-11 peptide.

The direct infusion spectrum of the AcKM-11 peptide showed the addition of two molecules of $C_2H_2O_2$ (m/z 753.38211) , which were formed in MeOH/H_2O and in PBS solution (figure 6.6). Isolation of the $[M + 2\,(C_2H_2O_2) + 2\,H]^{2+}$ species again revealed monoglycated ions, which were ejected during the DR-ECD experiment.

Figure 6.7a shows the DR(724)-ECD(753) spectrum of the precursor ion $[M+2\,(C_2H_2O_2)+2\,H]^{2+}$ in MeOH/H_2O solution. Modified $c_n^{\#}$ and $c_n^{\ddagger}$ fragment ions in position 4 to 10, modified $z_9^{\#\bullet}$, $z_9^{\ddagger\bullet}$ radical fragment ions and unmodified c, and y, fragment ions are also observed in such a spectrum. No evidence was found of the modified c fragment ion in position 2 in the DR(724)-ECD(753) spectrum at 4, 7, 11, and 29 days. Equally, comparison of the normalized relative intensity of the modified $c_n^{\ddagger}$, $c_n^{\#}$ fragment ions, $z_9^{\#\bullet}$, and $z_9^{\ddagger\bullet}$ radical fragment ions obtained by ECD(753) and DR(724)-ECD(753) suggest

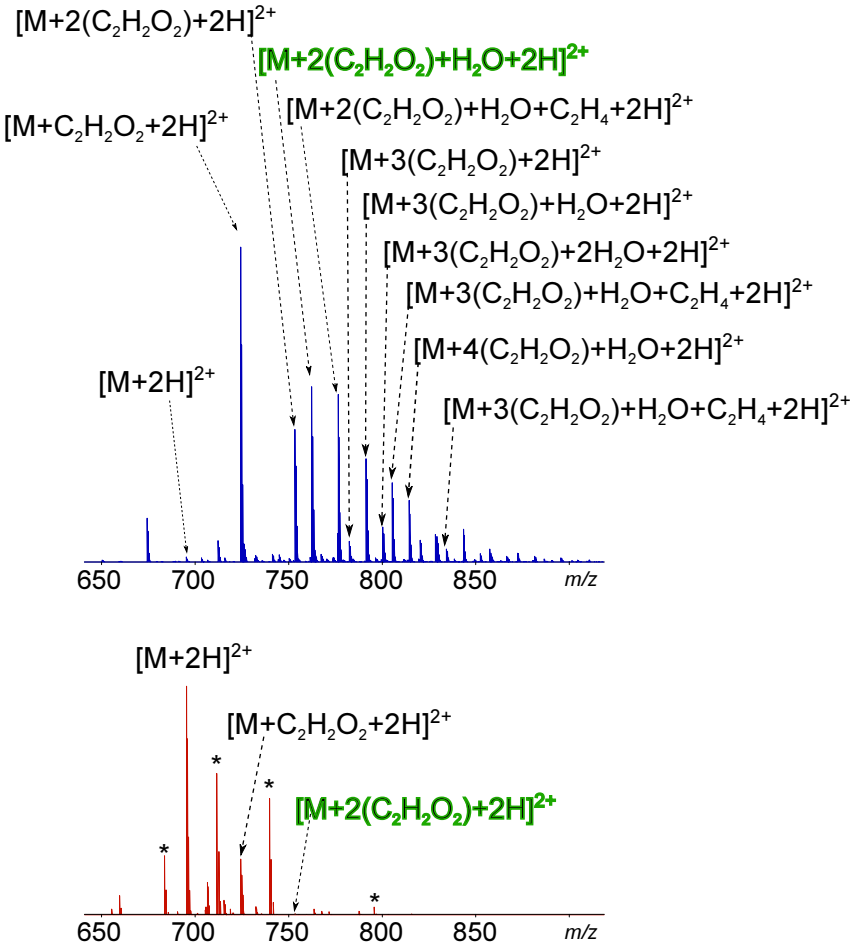

Figure 6.6: Direct infusion spectra of the AcKM-11peptide: **a.** reacted in MeOH/H_2O; **b.** reacted in PBS solution.

that the $c_4^{\ddagger}$, $c_6^{\ddagger}$, $c_7^{\ddagger}$, $c_9^{\ddagger}$, $c_{10}^{\ddagger}$, and $z_9^{\ddagger\bullet}$ species are formed from the precursor ion diglycated $[\mathrm{M} + 2\,(\mathrm{C_2H_2O_2}) + 2\,\mathrm{H}]^{2+}$ species (see figure 6.8).

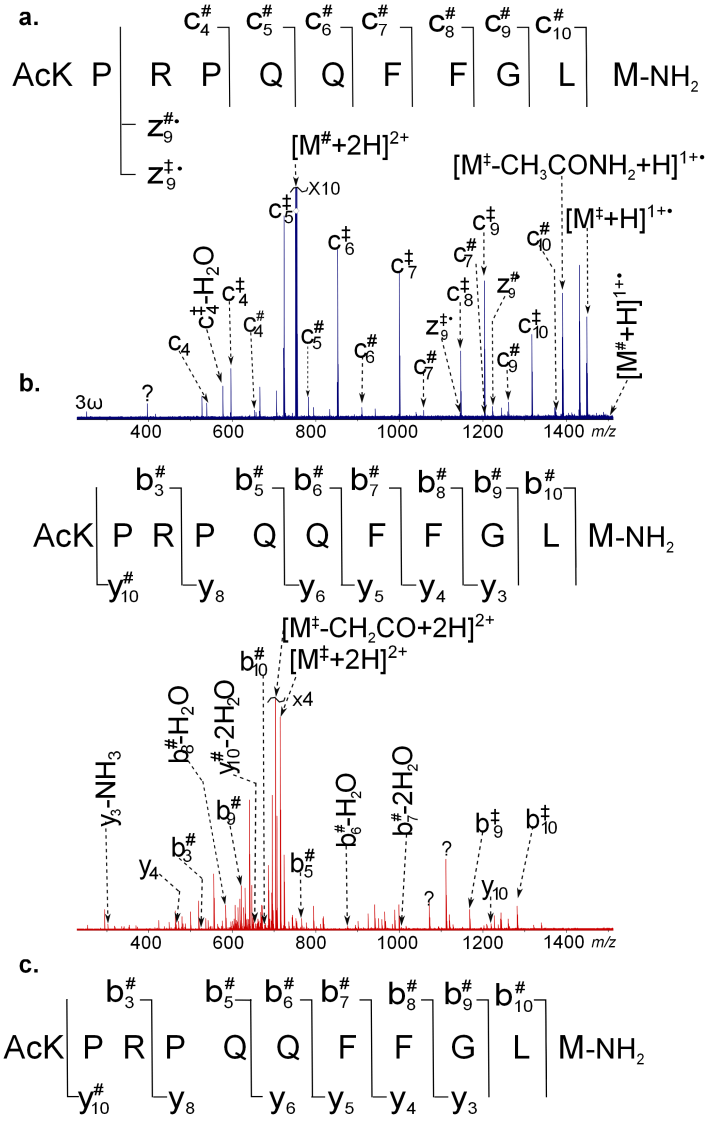

Figure 6.7: Spectra of the Ac-KM-11 peptide: a. DR(724)-ECD(753) spectrum of the precursor ion $[M+2\,(C_2H_2O_2)+2\,H]^{2+}$ with ejection of $[M+C_2H_2O_2+2\,H]^{2+}$ in MeOH/H_2O; b. CAD spectrum of the precursor ion $[M+2\,(C_2H_2O_2)+2\,H]^{2+}$ in MeOH/H_2O solution; c. CAD fragmentation pattern of the precursor ion $[M+2\,(C_2H_2O_2)+2\,H]^{2+}$ in PBS solution. The symbol ? indicates unassigned peaks by the current understanding of the fragmentation mechanism. Highlighted modified $c^{\#}$, $b^{\#}$, $y^{\#}_{10}$, and $z^{\#\bullet}_{9}$ fragment ions in the spectrum and unlabelled peaks are assigned in the detailed peak assignment Tables D-9, D-10 and D-11 presented in appendix D.

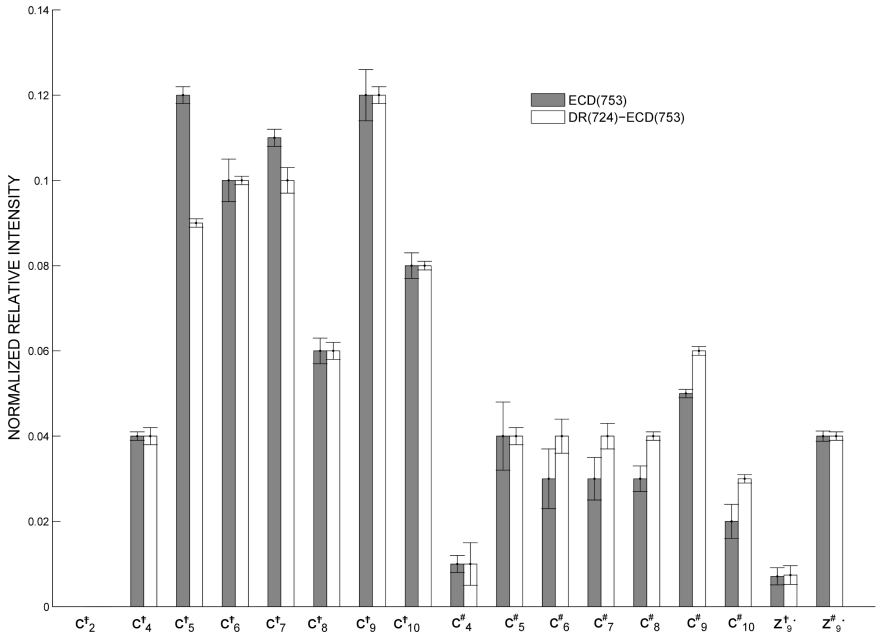

Figure 6.8: Comparison of the relative intensity of the $c^{\ddagger}$ and $c^{\#}$ fragment ions for the ECD(753) and DR(724)-ECD(753) spectra of the AcKM-11 peptide.

Inhibition of the fragmentation towards the $N-$terminus is also observed in the CAD spectrum of the precursor ion $[\mathrm{M} + 2\,(\mathrm{C_2H_2O_2}) + 2\,\mathrm{H}]^{2+}$ in MeOH/$\mathrm{H_2O}$ solution (figure 6.7b), where the modified $b_2^{\ddagger}$ fragment ion and its complementary pair $y_9^{\ddagger}$ are absent, together with $y_9^{\#}$. Similar results are also observed in the fragmentation pattern obtained from the CAD spectrum of the precursor ion $[\mathrm{M} + 2\,(\mathrm{C_2H_2O_2}) + 2\,\mathrm{H}]^{2+}$ in PBS solution (figure 6.7c). Therefore, the presence of modified $c_4^{\#}$ to $c_{10}^{\#}$, $b_3^{\#}$, $b_5^{\#}$ to $b_{10}^{\#}$, $y_{10}^{\#}$ fragment ions, and the modified $z_9^{\#\bullet}$ radical fragment ion indicate that the arginine residue in position 3 is modified by the addition of two molecules of $\mathrm{C_2H_2O_2}$ in MeOH/$\mathrm{H_2O}$ and in PBS solution, which could have the previously proposed structures shown in scheme 6.3. Comparing the fragmentation pattern of the KM-11 and AcKM-11 peptides obtained by CAD and DR-ECD experiments is noticeable the change of the peptide map of the acetylated peptide. Moreover, the absence of $b_2^{\ddagger}$ / $y_9^{\ddagger}$, and $y_9^{\#}$ fragment ions suggest that Schiff base formation (scheme 6.4b) and/or heterocyclic amines (scheme 6.4c) could not be formed at the amino group of the lysine residue in neither the acetylated nor the

non-acetylated KM-11 peptide. These data strongly suggest that the lysine residue in the non-acetylated KM-11 peptide is crosslinked by glyoxal with the N-terminus, and the reaction mechanism is shown in scheme 6.5. However, a systematic study varying the position of the lysine residue relative to the N-terminus is required in order to assess the extent of the glyoxal crosslinking ability between the lysine and the N-terminus.

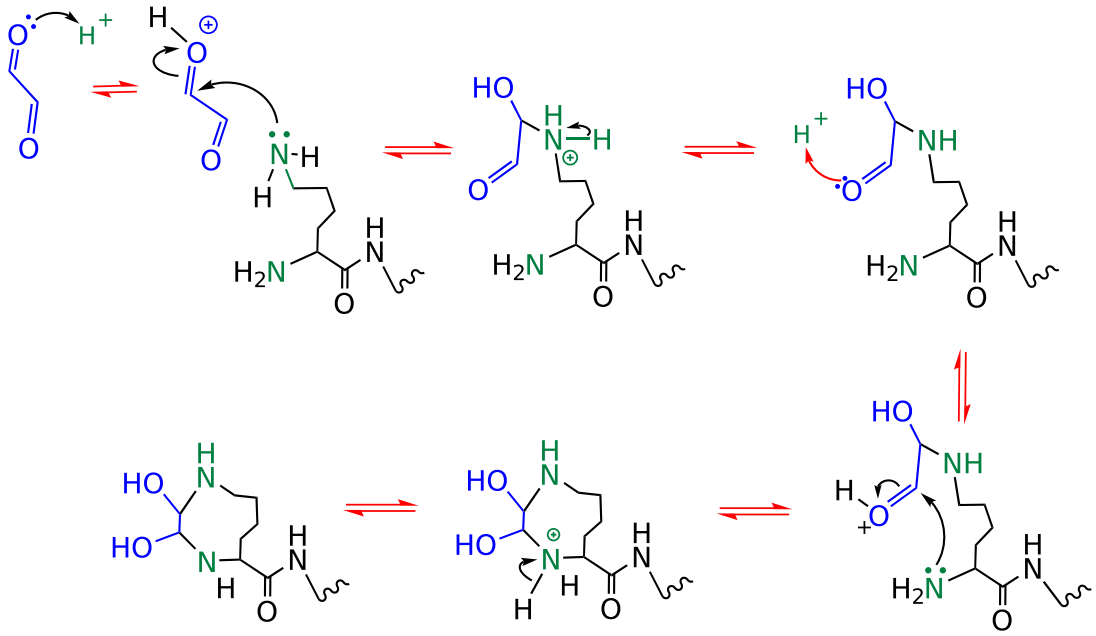

Scheme 6.5: Proposed reaction mechanism for the formation crosslinked species formed with glyoxal at the lysine residue and the $N-$terminus.

Additionally, in the acetylated peptide is difficult difficult to establish whether the lysine residue is involved in the glycation. Nonetheless, the consistent presence of the modified $b_5^{\#}$ to $b_{10}^{\#}$ and $c_5^{\#}$ to $c_{10}^{\#}$ fragment ions, together with inhibition of the fragmentation in position 2 from the $N-$terminus and 9 from the $C-$terminus ($b_2^{\ddagger}$ / $y_9^{\ddagger}$, and $y_9^{\#}$) suggest that intramolecular cyclization between the lysine amino group and the side chain of glutamine in position 4 could occur. The presence of different isomers in the AcKM-11 peptide was checked with ion mobility mass spectrometry. The DriftScope displays of selected ion mobility spectra are presented in figure 6.9. Quadrupole isolation, prior to separation by their drift time, shows isomeric species, which correlate with the observed

spectra in figure 6.7. However, further research varying the relative position between lysine and glutamine is necessary before any definitive conclusion can be drawn about glutamine side chain involvement during the glycation reaction.

Finally, what is important to note is that the results indicate the presence of two products formed during the reaction of glyoxal with the non-acetylated KM-11 peptide in MeOH/H_2O and in PBS solution. These two species have the same net mass addition of $116.01092\,Da$ forming the diglycated ion $[M + 2\,(C_2H_2O_2) + 2\,H]^{2+}$. Fragmentation of the diglycated ion suggest the formation of the glyoxal dimer (N^5-[2-(dihydroxymethyl)-2H,3aH,4H,6aH-[1,3]dioxolo[5,6-d]imidazolin-5-yl]-L-ornithine). The proposed structure does not show any stereochemistry, and other structural compounds at the arginine residue that can potentially be formed. Intramolecular crosslinking of the lysine residue and the $N-$terminus is also consistent with the results. However, a deep understanding of the formation of these compounds in biological systems is needed in order to address the extent of the glycation reaction. Equally, it is clear that the determination of the crosslinked glutamine-glyoxal-lysine residues requires conformational calculations. In any case, given the scope of the current project, those calculations were omitted in the present study.

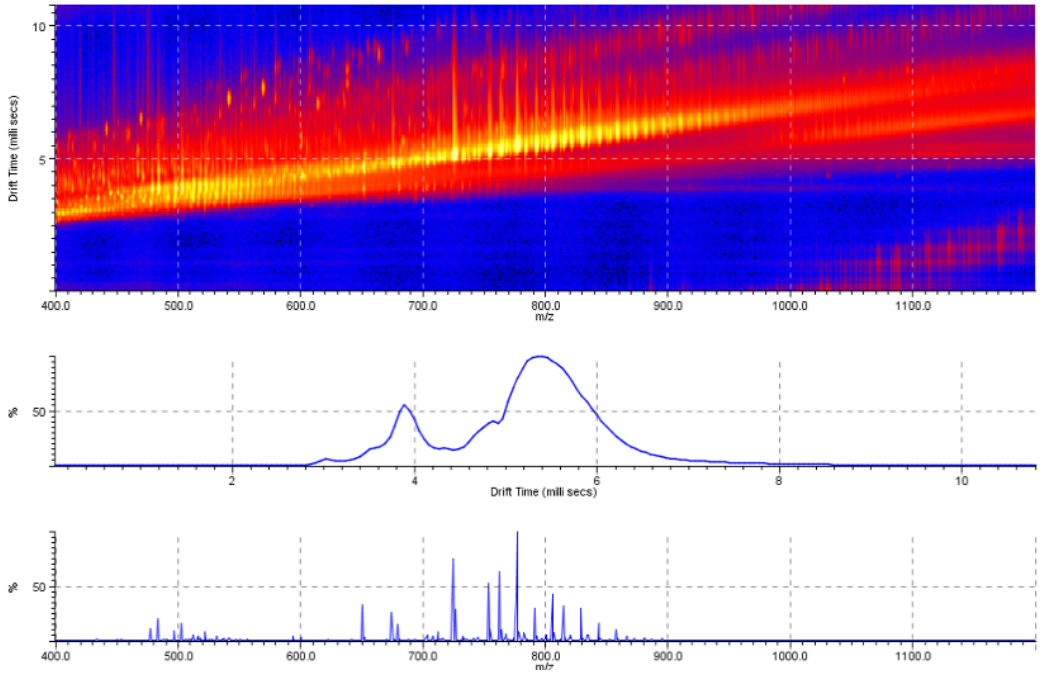

(a) DriftScope display of the ion mobility spectra obtained for acetylated peptide KM-11

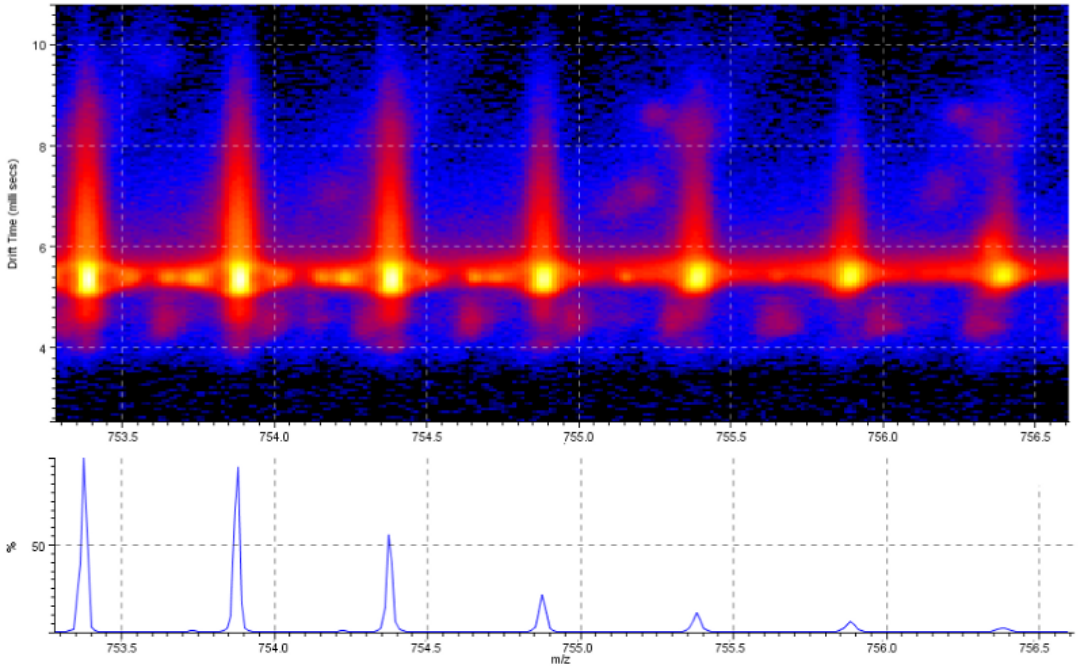

(b) DriftScope display of the ion mobility spectra obtained for the AcKM-11 peptide

Figure 6.9: Results of ion mobility mass spectrometry of the AcKM-11 peptide in MeOH/H_2O. a DriftScope display of the ion mobility spectra for acetylated peptide KM-11; b DriftScope display of the ion mobility spectra obtained for the isolated ion $[M + 2\,(C_2H_2O_2) + 2\,H]^{2+}$ $(m/z\,753.381)$ in MeOH/H2O of the AcKM-11 peptide.

6.4 Conclusions

Glyoxal was reacted with acetylated and non-acetylated undecapeptides in MeOH/H_2O (50:50) and PBS solution (four representative cases in total), and studied using an FTICR-MS. Reaction products for both peptides, showing the addition of two molecules of $C_2H_2O_2$, were subjected to DR-ECD and CAD fragmentation.

Unexpectedly, the fragmentation pattern obtained for the acetylated peptide showed the presence of two compounds with the same mass addition of $116.01092\,Da$, $i.e.$ $(C_2H_2O_2)_2$. The results strongly indicated that one compound was formed by crosslink of one molecule of glyoxal, the $N-$terminus and the lysine side chain. Additionally, the second compound was assigned as N^5-[2-(dihydroxymethyl)-2H, 3aH,4H,6aH-[1,3]dioxolo[5,6-d] imidazolin-5-yl]-L-ornithine formed at the guanidine group of arginine.

For the acetylated peptide it is clear that crosslinking with the $N-$terminus is not possible. However, the results suggest that crosslinked species might be formed between the lysine side chain, the glyoxal reagent and the glutamine residue. Nevertheless, a systematic study is required in order to determine with greater confidence the participation of the glutamine residue in the formation of crosslinked species with glyoxal, although this was deemed to be beyond the scope of the present work.

The N^5-[2-(dihydroxymethyl)-2H,3aH,4H,6aH-[1,3]dioxolo[5,6-d] imidazolin-5-yl]-L-ornithine was also formed at the guanidine group of arginine in the acetylated peptide. It seems necessary to clarify that although a structure is being proposed, no structural conformation of the compounds has been considered. Therefore, further studies are required in order to assess the validity of the proposed structure. In any case, these findings were true for the experiments using both type of reaction solutions, regardless of the peptide employed

It is hypothesised that the compound assigned as N^5-[2-(dihydroxymethyl) -2H,3aH,4H,6aH-[1,3]dioxolo[5,6-d] imidazolin-5-yl]-L-ornithine, formed at longer reaction times, might be the first, product of one molecule of glyoxal dimer reacted with the model peptide. On the other hand, it could be obtained by the reaction of one molecule of glyoxal with the modified peptide that contains the dihydroxyimidazoline moiety at the arginine residue. It is suggested that the second pathway is more likely to occur due to the fact that the aforementioned compound was not observed at early stages of the glycation reaction. However, further studies are needed to prove the validity of such a hypothesis.

7 Summary of results and ongoing projects

7.1 Summary of results

The glycation reaction of glyoxal with model peptides was studied in this work using a Fourier transform ion cyclotron resonance mass spectrometer. The model peptides were reacted with glyoxal under pseudo-physiological (phosphate buffer) and non-physiological ($MeOH/H_2O$) conditions at two different reaction times as is shown in table 7.1. The reacted peptides were analysed by mass spectrometry using an FT-ICR-MS. Interestingly, a variety of products were found in the reaction of glyoxal with the model peptides. These reaction products were characterised by measuring how much the mass of the peptide changed compared to its initial mass before reaction with glyoxal. The increase in mass was, then, assigned as different types of reaction products $39.9949\,Da$ (C_2O), $58.0055\,Da$ ($C_2H_2O_2$), $21.9843\,Da$ (C_2-H_2), $116.01092\,Da$ ($(C_2H_2O_2)_2$, and crosslinked species (see table 7.1).

Table 7.1: Summary of the assigned species found in model Peptides reacted with glyoxal in MeOH/H_2O and phosphate buffer.

Peptides	**Reaction Times**		**Aminoacid residues**			**Type of mass change**				
	MeOH	**Phosphate buffer**	$N-$ **terminus**	**K**	**R**	C_2O	$C_2H_2O_2$	C_2-H_2	$(C_2H_2O_2)_2$	**Cross-linking**
Substance P	21 h	6 h	**X**	**X**	✓	✓	✓	**X**	**X**	**X**
KM-11	21 h	6 h	**X**	**X**	✓	✓	✓	**X**	**X**	**X**
AcKM-11	21 h	6 h	**X**	**X**	✓	✓	✓	**X**	**X**	**X**
EK-15	21 h	6 h	**X**	**X**	✓	✓	✓	✓	**X**	**X**
FR-25	21 h	6 h	**X**	**X**	✓	✓	✓	✓	**X**	**X**
KM-11	29 $days$	12 h	✓	✓	✓	**X**	✓	**X**	✓	✓
AcKM-11	29 $days$	12 h	**X**	✓	✓	**X**	✓	**X**	✓	✓

7.2 Ongoing projects

The glycation reaction with glyoxal was performed in human serum albumin (HSA) aiming to extend the results found in model peptides. The reaction was carried out in PBS using the reaction conditions and dialysis, as the purification step, prior to mass spectrometry analysis. These set of conditions were described in section 3.2.1. However, the purification procedure caused loss of the glycated HSA. It was thought that this loss could be caused due to glycated HSA bound to the dialysis membrane. Therefore, purification by precipitation was also employed as described in section § 4.2.2, but this caused insolubility of the glycated HSA. Many variations to the glyoxal concentration and reaction times were employed until it was obtained the direct infusion, top-down, spectra of glyoxal glycated HSA at a glyoxal concentration of $100\,nM$ using precipitation by MeOH/chloroform prior to MS analysis. The reaction was monitored at 1 hour (figure 7.1) and ionized with $10\,mM$ of ammonium acetate in order to minimise the complexity of the spectra caused by interference with methanol. [1]

It is observed from the spectra at 5 hours of reaction that additional low abundance

[1] ion/molecule reactions with methanol were reported in section 3.3.

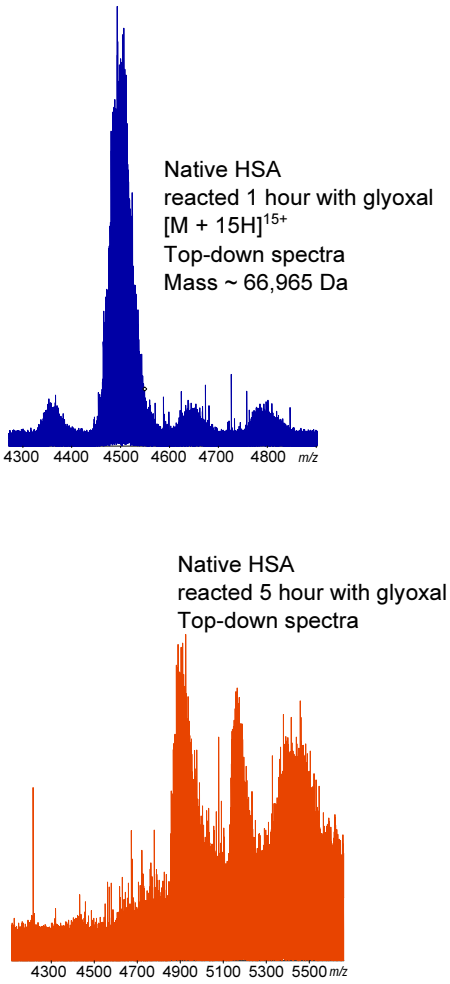

Figure 7.1: Top-down direct infusion spectrum of glyoxal glycated HSA.

glycated products are formed (see figure 7.1). It is noteworthy that the complexity of the spectra of the glycated HSA at longer reaction times likely depends on the number of lysine and arginine residues available for glycation and the number of possible modifications that can be formed with glyoxal. In a simplistic assumption and only considering that the location of the elements does matter and that any combination can be possible, even allowing repetition, the total number of possible permutations can be

calculated as in equation (7.1),

$$T = \sum_{k=1}^{k_{\max}} n^k \tag{7.1}$$

where n is the number of possible modifications observed with glyoxal, k is the number of residues to glycate, and $k_{\max}$ is the maximum number of residues to glycate. For instance, assuming that the maximum number of possible residues to glycate in a protein is four, and that the total number of possible modifications is five, then the total number of possible permutations is

$$T = \sum_{k=1}^{4} (5)^k = 780 \tag{7.2}$$

The application of fragmentation by ECD and CAD did not yield any useful structural information. Thus, it was decided to use the bottom-up approach presented in § 1.6, but, so far, it was not possible to identify any glycated peptide in the spectrum because of the probable low abundance of the glycated species in the direct infusion spectrum. Other approaches prior mass spectrometry analysis were considered, such as fraction collection using a high performance liquid chromatography (HPLC).

8 Conclusions and future work

8.1 Conclusions

An ultra-high performance Fourier transform ion cyclotron resonance mass spectrometer was used to characterize glyoxal modifications on model peptides. High confidence in the assignments was obtained due to the high resolution and mass accuracy achieved with the mass spectrometer. The experimental methods were established in chapter 3 using substance P as a model.

Reproducibility of the results was tested with other model peptides and was shown in chapter 4, and the appearance of a new type of modification was analysed and discussed in chapter 5. Finally, a variation on the experimental method was introduced by changing the reaction time and the results were discussed in chapter 6. Chapter 7 summarised the results and addresses the challenges of glyoxal modifications in proteins.

The glyoxal reaction products that showed a mass change of $39.9949\,Da$ (C_2O), $58.0055\,Da$ ($C_2H_2O_2$), $21.9843\,Da$ ($C_2{-}H_2$), and $116.01092\,Da$ ($(C_2H_2O_2)_2$) were subjected to DR-ECD and CAD fragmentation in order to identify the location of the modification. As is observed in table 7.1 only arginine residues were modified at 21 hours of reaction in

MeOH/H_2O and 6 hours of reaction in PBS. At longer reaction times other basic residues are modified by glyoxal, producing crosslinked species.

Some chemical structures were proposed, such as the hydroxyimidazoline, dihydroxyimidazoline were previously reported in the literature. However, a new glyoxal-derived species referred here to as 2-imino-imidazole was formed at the guanidine group of the arginine residue. Interestingly, the compound N^5-[2-(dihydroxymethyl) -2H,3aH,4H,6aH -[1,3]dioxolo[5,6-d] imidazolin-5-yl]-L-ornithine is also formed at the guanidino group of arginine at longer reaction times. It is noteworthy that although a structure is being proposed, no structural conformation has been considered. It is clear, then, that a further study on the possible isomers is required, in order to asses the validity of the proposed structures.

A characteristic loss of water from every modified $c_n^{\dagger}$ $c_n^{\ddagger}$, and c_n^{*} fragment ion was observed. Thus, it is proposed that the electron is captured at the modification site and subsequently a water loss is generated in addition to the typical fragmentation pattern of the peptide at the backbone N-Cα bond. It is important to highlight that the water loss from the modified fragment ions was a permanent characteristic in all DR-ECD spectra. In fact, such a result turned out to be fully consistent with the hypothesis proposed in § 3.3.2, and illustrated in the proposed reaction mechanism of the scheme 3.2.

From the results presented in chapter 3 it is clear that care must be taken when this reaction is executed in methanol, due to the appearance of ion molecule reactions with the solvent. Also, care must be taken when sodium is present in the reaction solution due to the formation of two species with the same that can overshadow the presence of the glyoxal modification ($C_2{-}H_2$) if the mass spectrometer used for detection can not achieve the resolution to separate mass differences below $2.4\,mDa$.

The location and type of mass additions, such as C_2O, $C_2H_2O_2$, ($C_2{-}H_2$), and $(C_2H_2O_2)_2$

remained unaffected regardless of the reaction solution employed (MeOH/H_2O or PBS). Equally, the type of mass addition and the modification site was not altered C_2O, $C_2H_2O_2$ by changes in the purification procedures. For instance, whereas in the tests defined in chapter 3 dialysis was used as purification method, in the tests target of the chapter 4 the purification was performed by precipitation with MeOH/Chloroform. This factor did not affect the final outcome, in terms of binding site assignment and types of mass additions, indicating that the presence and location of the modifications were not sensitive to this particular change.

It seems clear from the results of the $C-$terminus amidated model peptides presented in chapters 3 to 5 that there was no involvement of the C-terminus amide group in the reaction with glyoxal at any reaction condition employed in this work.

The results presented in chapter 6 strongly suggest that the N-terminus and the lysine residue form a crosslinked species with glyoxal. This species is formed at longer reaction times where arginine glycation was also observed. Blockage of the $N-$terminus strongly indicate that lysine residue is crosslinked with other amino acid residues (glutamine) within the peptide. However, studies varying systematically the relative position of the lysine and the glutamine need to be carried out in the future in order to extent these results to another samples.

The current research has defined some of the fundamental chemistry involved in glyoxal binding to peptides. Nevertheless, it seems, then, that a better understanding of the glycation reaction by the α-dicarbonyl compound glyoxal can be obtained from analysing the results in small peptides, as discussed in previous chapters. This study represents a step in understanding the different glyoxal-derived AGEs formed at different reaction conditions and sample preparation procedures. In order to extend this research into analysis of clinical samples, additional understanding of competitive binding between

the amino acid residues and between peptides in complex biological samples will be needed. Moreover, understanding the implication of changes in sample purification of complex biological samples in the glycation results is also needed, thus protein glycation in the medical sphere can be fully understood.

8.2 Future work

An interesting observation from chapter 3 was the presence of the species with the mass addition of C_2-H_2 $(21.98436\,Da)$. This species was present in peptides containing 15 and 25 amino acids and at least four amino acid residues available for glycation. However, this mass addition (C_2-H_2), was absent in the undecapeptides substance P, KM-11 and AcKM-11, which contained two residues available for glyoxal glycation. It is suggested here that the presence of this modification might be dependant on both the size of the peptide and the number of basic residues present in the peptide. In order to further prove this hypothesis, studies where the size and the number of lysine and arginine residues are systematically varied within the peptide are necessary.

It would be interesting to check the binding site of the modified species observed in figure 5.1 and figure 6.1, such as the C_4O_2, $C_4H_2O_3$, (figure 5.1) and $C_4H_2O_3$, 2 ($C_2H_2O_2$) + H_2O, 3 ($C_2H_2O_2$) + H_2O, and 4 ($C_2H_2O_2$) + H_2O (figure 6.1).

The compound assigned as N^5-[2-(dihydroxymethyl) -2H,3aH,4H,6aH -[1,3]dioxolo[5,6-d] imidazolin-5-yl] -L-ornithine chapter 6, observed at longer reaction times, might be formed by either the direct reaction of one molecule of glyoxal dimer or by the reaction of one molecule of glyoxal with the modified peptide that contains the dihydroxyimidazoline moiety at the arginine residue. It is believed that the compound N^5-[2-(dihydroxymethyl)-2H,3aH,4H,6aH -[1,3]dioxolo[5,6-d] imidazolin-5-yl]-L-ornithine

is not derived from the direct addition of the glyoxal dimer species. This hypothesis is based in the fact that direct addition of glyoxal was not observed at early stages of the glycation reaction. However, further studies are needed to prove the validity of such a hypothesis.

Appendices

A

Mass Error tables with assignments used to interpret the data of Chapter 3

LIST OF TABLES

Table A-1. ECD mass error analysis for the parent ion $[M+C_2O+2H]^{2+}$ of the glyoxal-derived glycation product formed at amidated Substance P in MeOH:H_2O (50:50). * indicates mass to charge used for calibration.

THEORICAL (m/z)	EXPERIMENTAL (m/z)	ASSIGNMENTS	ERROR (ppm)
496.33541	* 496.33516	c_4	-0.494
517.31194	517.31171	$c^{\dagger}_4{}^{\bullet}$-$H_2O$	-0.435
523.27891	523.27876	$z_5{}^{\bullet}$-C_3H_6S	-0.285
535.32250	535.32235	$c^{\dagger}_4{}^{\bullet}$	-0.280
536.33033	536.33021	$c^{\dagger}_4$	-0.214
547.79441	547.79402	y_9^{2+}	-0.703
552.30906	* 552.30894	c_9^{2+}	-0.222
580.27139	580.27142	$z_7{}^{\bullet}$-NH_3	0.060
	592.30739	?	
608.85110	608.85170	$[c_{10}+H]^{2+}$	0.994
624.39399	* 624.39398	c_5	-0.008
645.37051	645.37048	$c^{\dagger}_5{}^{\bullet}$-$H_2O$	-0.046
646.37834	646.37840	$c^{\dagger}_5$ - H_2O	0.101
663.38108	663.38113	$c^{\dagger}_5{}^{\bullet}$	0.083
664.38890	664.38899	$c^{\dagger}_5$	0.135
666.36225	666.36208	$[c_{11}$ -$NH_3]^{2+}$	-0.255
674.37134	674.37147	$[M+2H]^{2+}$	0.200
694.36879	694.36895	$[M^{\dagger}+2H]^{2+}$	0.227
751.44529	751.44476	$c_6{}^{\bullet}$	-0.699
752.45257	* 752.45277	c_6	0.272
774.43692	774.43710	$c^{\dagger}_6$ - H_2O	0.239
791.43966	791.43980	$c^{\dagger}_6{}^{\bullet}$	0.183
792.44748	792.44768	$c^{\dagger}_6$	0.252
895.50172	895.50140	$a^{\dagger}_7$	-0.352
898.51315	898.51426	$c_7{}^{\bullet}$	1.235
899.52098	899.52122	c_7	0.272
921.50533	921.50541	$c^{\dagger}_7$-H_2O	0.092
938.50807	938.50794	$c^{\dagger}_7{}^{\bullet}$	-0.133
939.51589	939.51609	$c^{\dagger}_7$	0.213
1004.54379	1004.54407	$z_9{}^{\bullet}$ - C_3H_6S	0.279
1042.57013	1042.57076	$a^{\dagger}_8$	0.609
1046.58939	* 1046.58938	c_8	-0.005
1068.57374	1068.57364	$c^{\dagger}_8$- H_2O	-0.089
1078.56281	1078.56266	$z_9{}^{\bullet}$	-0.139
1086.58430	1086.58434	$c^{\dagger}_8$	0.037

THEORICAL (m/z)	EXPERIMENTAL (m/z)	ASSIGNMENTS	ERROR (ppm)
1103.61085	1103.61070	c_9	-0.131
1125.59520	1125.59490	$c^{\dagger}_9 - H_2O$	-0.262
1143.60576	1143.60568	$c^{\dagger}_9$	-0.070
1216.69491	* 1216.69447	c_{10}	-0.358
	1220.63633	?	
1238.67926	1238.67898	$c^{\dagger}_{10} - H_2O$	-0.222
1256.68982	1256.68935	$c^{\dagger}_{10}$	-0.374
1314.71856	1314.71841	$[M^{\dagger}-C_3H_6S + 2H]^{1+\cdot}$	-0.117
	1317.66500	?	
	1330.70640	?	
1343.71723	1343.71585	$[M^{\dagger} - {}^{\bullet}CONH_2+H]^{1+}$	-1.023
1370.72757	* 1370.72705	$[M^{\dagger} -H_2O+2H]^{1+\bullet}$	-0.095
1387.73031	* 1387.72973	$[M^{\dagger} +H]^{1+}$	-0.418
		mean	-0.159
		St. Dv.	0.376

TableA-2. DR(674)-ECD(694) mass error analysis for the parent ion $[M+C_2O+2H]^{2+}$of the glyoxal-derived glycation product formed at amidated Substance P in MeOH:H_2O (50:50). * indicates mass to charge used for calibration.

THEORICAL (m/z)	EXPERIMENTAL (m/z)	ASSIGNMENTS	ERROR (ppm)
271.18769	* 271.18766	c_2	-0.092
	415.21121	?	
	437.19323	?	
496.33541	* 496.33524	c_4	-0.332
517.31194	517.31186	$c^{\dagger}_4{}^{\bullet}-H_2O$	-0.145
518.31976	518.31966	$c^{\dagger}_4-H_2O$	-0.193
535.32250	535.32242	$c^{\dagger}_4{}^{\bullet}$	-0.149
536.33033	* 536.33025	$c^{\dagger}_4$	-0.140
547.79441	547.79428	y_9^{2+}	-0.228
552.30906	552.30904	c_9^{2+}	-0.041
	581.31180	?	
	592.30762	?	
608.85110	608.85114	$[c_{10}+H]^{2+}$	0.074
620.37473	620.37519	$a^{\dagger}_5$	0.750
624.39399	* 624.39408	c_5	0.152
645.37051	645.37047	$c^{\dagger}_5{}^{\bullet}-H_2O$	-0.062

THEORICAL (m/z)	EXPERIMENTAL (m/z)	ASSIGNMENTS	ERROR (ppm)
646.37834	646.37827	$c^{\dagger}_{5} - H_2O$	-0.101
663.38108	663.38102	$c^{\dagger}_{5}{}^{\bullet}$	-0.083
664.38890	664.38883	$c^{\dagger}_{5}$	-0.105
666.36225	666.36202	$[c_{11} - NH_3]^{2+}$	-0.345
694.36879	694.36868	$[M^{\dagger}+2H]^{2+}$	-0.162
752.45257	* 752.45297	c_6	0.538
773.42909	773.42938	$c^{\dagger}_{6}{}^{\bullet} - H_2O$	0.375
774.43692	774.43706	$c^{\dagger}_{6} - H_2O$	0.187
791.43966	791.43992	$c^{\dagger}_{6}{}^{\bullet}$	0.335
792.44748	792.44779	$c^{\dagger}_{6}$	0.391
895.50172	895.50257	$a^{\dagger}_{7}$	0.955
	899.52125	?	
921.50533	921.50548	$c^{\dagger}_{7} - H_2O$	0.168
	937.73782	?	
938.50807	938.50838	$c^{\dagger}_{7}{}^{\bullet}$	0.336
939.51589	939.51617	$c^{\dagger}_{7}$	0.298
	965.76939	?	
1004.54379	1004.54393	$z_9{}^{\bullet} - C_3H_6S$	0.139
	1007.52553	?	
1042.57013	1042.57037	$a^{\dagger}_{8}$	0.235
1068.57374	1068.57383	$c^{\dagger}_{8} - H_2O$	0.089
1078.56281	* 1078.56286	$z_9{}^{\bullet}$	0.046
1086.58430	1086.58443	$c^{\dagger}_{8}$	0.120
1125.59520	1125.59538	$c^{\dagger}_{9} - H_2O$	0.164
1143.60576	1143.60570	$c^{\dagger}_{9}$	-0.052
	1220.63681	?	
1238.67926	1238.67902	$c^{\dagger}_{10} - H_2O$	-0.190
1256.68982	1256.68941	$c^{\dagger}_{10}$	-0.326
1296.70855	1296.70848	$[M^{\dagger} - C_3H_6S - H_2O + 2H]^{1+\bullet}$	-0.053
1314.71856	1314.71881	$[M^{\dagger} - C_3H_6S + 2H]^{1+\bullet}$	0.187
	1317.66460	?	
1330.70885	1330.70905	$[M - NH_3 + H]^{1+}$	0.150
1343.71723	1343.71645	$[M^{\dagger} - {}^{\bullet}CONH_2 + H]^{1+}$	0.577
1353.70158	1353.70171	$[M^{\dagger} - H_2O - NH_3 + 2H]^{1+\bullet}$	0.100
1370.72702	* 1370.72689	$[M^{\dagger} - H_2O + 2H]^{1+\bullet}$	-0.095
1387.73031	* 1387.72956	$[M^{\dagger} + H]^{1+}$	-0.540
		mean	-0.101

THEORICAL (m/z)	EXPERIMENTAL (m/z)	ASSIGNMENTS	ERROR (ppm)
		St. Dv.	0.291

Table A-3. DR(674)-ECD(703) mass error analysis for the parent ion $[M+C_2H_2O_2+2H]^{2+}$of the glyoxal-derived glycation product formed at amidated Substance P MeOH:H_2O (50:50). * indicates mass to charge used for calibration.

THEORICAL (m/z)	EXPERIMENTAL (m/z)	ASSIGNMENTS	ERROR (ppm)
	332.11950	*	
	341.30578	*	
	344.13180	?	
	345.11579	*	
	360.15078	?	
	365.10062	*	
	373.11070	*	
	381.29765	*	
	390.12496	*	
496.33541	* 496.33537	c_4	-0.071
517.31193	517.31201	$c^{\ddagger}_4{}^{\bullet}-2H_2O$	0.155
518.31976	518.31967	$c^{\ddagger}_4$-2H_2O	-0.164
535.32250	535.32250	$c^{\ddagger}_4{}^{\bullet}$–$H_2O$	0.000
553.33306	553.33309	$c^{\ddagger}_4{}^{\bullet}$	0.054
554.34089	554.34071	$c^{\ddagger}_4$	-0.316
624.39399	* 624.39413	c_5	0.232
646.37834	646.37814	$c^{\ddagger}_5$-2H_2O	-0.302
663.38108	663.38135	$c^{\ddagger}_5{}^{\bullet}$–$H_2O$	0.415
681.39164	681.39129	$c^{\ddagger}_5{}^{\bullet}$	-0.514
682.39947	682.39946	$c^{\ddagger}_5$	-0.007
703.37408	703.37370	$[M^{\ddagger}+2H]^{2+}$	-0.540
752.45257	752.45272	c_6	0.206
774.43692	774.43684	$c^{\ddagger}_6$-2H_2O	-0.097
791.43966	791.43965	$c^{\ddagger}_6{}^{\bullet}$–$H_2O$	-0.006
792.44748	792.44775	$c^{\ddagger}_6$–H_2O	0.341
809.45022	809.45032	$c^{\ddagger}_6{}^{\bullet}$	0.124
810.45805	810.45794	$c^{\ddagger}_6$	-0.130
899.52098	* 899.52069	c_7	-0.317
913.51228	913.51332	$a^{\ddagger}_7$	1.138
921.50533	921.50509	$c^{\ddagger}_7$-2H_2O	-0.255
939.51589	939.51554	$c^{\ddagger}_7$–H_2O	-0.373

THEORICAL (m/z)	EXPERIMENTAL (m/z)	ASSIGNMENTS	ERROR (ppm)
957.52646	957.52654	$c^{\ddagger}_{7}$	0.089
1004.54379	1004.54366	$z_9^{\bullet}$ - C_3H_6S	-0.129
	1007.52567	?	
1046.58939	* 1046.58936	c_8	-0.024
1060.58069	1060.58078	$a^{\ddagger}_{8}$	0.085
1078.56281	1078.56252	$z_9^{\bullet}$	-0.269
1086.58430	1086.58425	$c^{\ddagger}_{8}$–H_2O	-0.046
1104.59487	1104.59477	$c^{\ddagger}_{8}$	-0.086
1103.61085	* 1103.61052	c_9	-0.294
1125.59519	1125.59518	$c^{\ddagger}_{9}$-$2H_2O$	-0.013
1143.60576	1143.60539	$c^{\ddagger}_{9}$ - H_2O	-0.324
1161.61633	1161.61603	$c^{\ddagger}_{9}$	-0.254
1216.69491	* 1216.69447	c_{10}	-0.358
1238.67926	1238.68000	$c^{\ddagger}_{10}$ - $2H_2O$	0.601
1256.68982	1256.68903	$c^{\ddagger}_{10}$ - H_2O	-0.629
1274.70039	1274.70014	$c^{\ddagger}_{10}$	-0.192
1331.71668	1331.71657	$[M\text{-}NH_3\text{+}2H]^{1+\bullet}$	-0.079
1343.71668	1343.71707	$[M^{\ddagger}$ -$^{\bullet}CONH_2$-H_2O+H$]^{1+}$	0.294
1347.73540	1347.73507	$[M+H]^{1+}$	-0.241
1348.74377	1348.74359	$[M+2H]^{1+\bullet}$	-0.133
1361.72724	1361.72718	$[M^{\ddagger}$ -$^{\bullet}CONH_2$+H$]^{1+}$	-0.044
1370.72757	1370.72699	$[M^{\ddagger}$ -$2H_2O$+2H$]^{1+\bullet}$	-0.423
1371.71214	1371.71144	$[M^{\ddagger}$ -H_2O-NH_3+2H$]^{1+\bullet}$	-0.510
1388.73814	* 1388.73808	$[M^{\ddagger}$ -H_2O+2H$]^{1+\bullet}$	-0.997
1405.74088	* 1405.74033	$[M^{\ddagger}$ +H$]^{1+}$	-0.388
		Mean	-0.342
		St.Dv.	0.044

Table A-4. IRMPD-ECD mass error analysis for the parent ion $[M+C_2O+2H]^{2+}$ of the glyoxal-derived glycation product formed at amidated Substance P in MeOH:H_2O (50:50). * indicates mass to charge used for calibration.

THEORICAL (m/z)	EXPERIMENTAL (m/z)	ASSIGNMENTS	ERROR (ppm)
496.33541	* 496.33519	c_4	0.433
517.31194	517.31171	$c^{\dagger}_{4}{}^{\bullet}$-$H_2O$	0.435
518.31976	518.31955	$c^{\dagger}_{4}$-H_2O	0.405
535.32250	535.32234	$c^{\dagger}_{4}{}^{\bullet}$	0.299
536.33033	536.33019	$c^{\dagger}_{4}$	0.252

THEORICAL (m/z)	EXPERIMENTAL (m/z)	ASSIGNMENTS	ERROR (ppm)
547.79441	547.79422	y_9^{2+}	0.338
552.30906	552.30895	$[c_9+H]^{2+}$	0.204
	581.31180	*	
	592.30762	*	
	593.31090	*	
600.33809	600.33767	$[b_{10}+H]^{2+}$	-0.704
608.85110	608.85110	$[c_{10}+H]^{2+}$	-0.008
624.39399	* 624.39402	c_5	-0.056
645.37051	645.37048	$c^{\dagger}_5{}^{\bullet}$-$H_2O$	0.046
646.37834	646.37835	$c^{\dagger}_5$ - H_2O	-0.023
663.38108	663.38114	$c^{\dagger}_5{}^{\bullet}$	-0.098
664.38890	664.38898	$c^{\dagger}_5$	-0.120
674.37134	* 674.37140	$[M + 2H]^{2+}$	-0.096
694.36879	694.36886	$[M^{\dagger} + 2H]^{2+}$	-0.097
752.45257	* 752.45297	c_6	-0.538
773.42909	773.42938	$c^{\dagger}_6{}^{\bullet}$-$H_2O$	-0.375
774.43692	774.43706	$c^{\dagger}_6$ - H_2O	-0.187
791.43966	791.43992	$c^{\dagger}_6{}^{\bullet}$	-0.335
792.44748	792.44779	$c^{\dagger}_6$	-0.391
895.50172	895.50257	$a^{\dagger}_7$	-0.955
	899.52125	?	
921.50533	921.50548	$c^{\dagger}_7$-H_2O	-0.168
	937.73782	?	
938.50807	938.50838	$c^{\dagger}_7{}^{\bullet}$	-0.336
939.51589	939.51617	$c^{\dagger}_7$	-0.298
	965.76939	?	
1004.54379	1004.54393	$z_9{}^{\bullet}$ - C_3H_6S	-0.139
	1007.52553	?	
1042.57013	1042.57037	$a^{\dagger}_8$	-0.235
1068.57374	1068.57383	$c^{\dagger}_8$- H_2O	-0.089
1078.56281	1078.56286	$z_9{}^{\bullet}$	-0.046
1086.58430	1086.58443	$c^{\dagger}_8$	-0.120
1103.61085	* 1103.61126	c_9	-0.376
1125.59520	1125.59538	$c^{\dagger}_9$ - H_2O	-0.164
1143.60576	1143.60570	$c^{\dagger}_9$	0.052
	1220.63681	?	
1238.67926	1238.67902	$c^{\dagger}_{10}$ - H_2O	0.190
1256.68982	1256.68941	$c^{\dagger}_{10}$	0.326

THEORICAL (m/z)	EXPERIMENTAL (m/z)	ASSIGNMENTS	ERROR (ppm)
1296.70800	1296.70758	$[M^{\dagger} - C_3H_6S - H_2O + 2H]^{1+\bullet}$	0.323
	1309.71461	?	
	1312.69702	?	
1314.71911	1314.71916	$[M^{\dagger} - C_3H_6S + 2H]^{1+\bullet}$	-0.035
	1317.66527	?	
1330.70885	1330.70824	$[M-C_2O-NH_3 + H]^{1+}$	-0.458
1343.71668	1343.71599	$[M^{\dagger} - {}^{\bullet}CONH_2+H]^{1+}$	-0.510
1353.70103	1353.70029	$[M^{\dagger} - H_2O - NH_3 + 2H]^{1+\bullet}$	-0.543
1369.71975	* 1369.71826	$[M^{\dagger} - H_2O + H]^{1+}$	-1.084
1370.72702	1370.72679	$[M^{\dagger} - H_2O + 2H]^{1+\bullet}$	-0.569
1387.73031	* 1387.72936	$[M^{\dagger} + H]^{1+}$	0.685
		mean	-0.063
		St. Dv.	0.318

Table A-5. CAD mass error analysis for the parent ion $[M+C_2O+2H]^{2+}$ of the glyoxal-derived glycation product formed at amidated Substance P in MeOH:H_2O (50:50). * indicates mass to charge used for calibration.

THEORICAL (m/z)	EXPERIMENTAL (m/z)	ASSIGNMENTS	ERROR (ppm)
254.16114	* 254.16114	b_2	0.000
262.15837	262.15836	y_2	0.038
	267.14918	*	
276.14549	276.14549	$b^{\dagger}_2 - H_2O$	0.000
294.15606	294.15606	$b^{\dagger}_2$	-0.017
	295.14410	*	
302.15329	302.15328	y_3-NH_3	0.083
	307.14409	*	
	313.27371	*	
	318.18122	*	
319.17983	* 319.17984	y_3	-0.031
	335.09487	*	
	350.25776	?	
	352.16557	?	
	354.17720	*	
	363.08979	*	
	364.27341	?	
379.20883	379.20883	$[b^{\dagger}_6-H_2O+H]^{2+}$	-0.013
404.24045	404.24048	$b^{\dagger}_3 - H_2O$	-0.074
	420.22819	?	
422.25102	422.25108	$b^{\dagger}_3$	-0.154

THEORICAL (m/z)	EXPERIMENTAL (m/z)	ASSIGNMENTS	ERROR (ppm)
449.22170	449.22171	y_4-NH_3	-0.033
452.74303	452.74306	$[b^{\dagger}_7$-H_2O+H$]^{2+}$	-0.066
	457.75353	?	
	463.19762	?	
	464.26161	?	
466.24824	* 466.24828	y_4	-0.086
	471.75089	?	
	478.76038	?	
	486.77435	?	
	490.26110	*	
	495.99993	*	
501.29321	501.29329	$b^{\dagger}_4$ -H_2O	-0.160
503.76651	503.76657	$[a^{\dagger}_8$-H_2O-NH_3+H$]^{2+}$	-0.129
509.25096	509.25076	$[b^{\dagger}_8$-H_2O-2NH_3+H$]^{2+}$	0.398
512.28005	512.27980	$[a^{\dagger}_8$-H_2O+H$]^{2+}$	0.488
515.28533	* 515.28511	$[b_8$+H$]^{2+}$	0.432
517.27223	517.27200	$[b^{\dagger}_8$-2H_2O+H$]^{2+}$	0.435
526.27751	526.27728	$[b_9$-H_2O-NH_3+H$]^{2+}$	0.432
528.79078	528.79054	$[a_9$+H$]^{2+}$	0.454
	532.27741	?	
540.79078	540.79066	$[a^{\dagger}_9$-H_2O+H$]^{2+}$	-0.222
543.79606	* 543.79585	$[b_9$+H$]^{2+}$	0.391
545.78296	545.78272	$[b^{\dagger}_9$-2H_2O+H$]^{2+}$	0.431
	548.28678	?	
	552.29463	*	
554.78824	554.78802	$[b^{\dagger}_9$-H_2O+H$]^{2+}$	0.392
563.79325	563.79323	$[b^{\dagger}_9$+H$]^{2+}$	0.031
	565.28260	?	
	573.79584	?	
	574.29751	?	
	576.28170	?	
	581.80894	?	
582.81954	582.81937	$[b_{10}$-H_2O-NH_3+H$]^{2+}$	0.287
586.34064	586.34061	$[a_{10}$+H$]^{2+}$	0.043
	591.79757	?	
593.31970	593.31944	$[b^{\dagger}_{10}$-3H_2O+H$]^{2+}$	0.442
596.29011	596.29016	y_5-NH_3	-0.092
	597.33260	?	
600.33809	600.33789	$[b_{10}$+H$]^{2+}$	0.337
601.35688	601.35697	$a^{\dagger}_5$ -H_2O	
602.32499	602.32477	$[b^{\dagger}_{10}$-2H_2O+H$]^{2+}$	0.357
613.31665	* 613.31669	y_5	-0.065

THEORICAL (m/z)	EXPERIMENTAL (m/z)	ASSIGNMENTS	ERROR (ppm)
611.33000	611.33004	$[b^{\dagger}_{10}-H_2O+H]^{2+}$	-0.074
620.33528	620.33530	$[b^{\dagger}_{10}+H]^{2+}$	-0.036
629.35179	629.35185	$b^{\dagger}_{5}-H_2O$	-0.095
	638.85116	?	
645.33423	645.33428	$[M^{\dagger}-2H_2O-2NH_3-CO+2H]^{2+}$	-0.085
	647.37838	?	
647.36236	647.36246	$b^{\dagger}_{5}$	-0.162
	650.81852	?	
	652.84863	?	
659.33168	659.33175	$[M^{\dagger}-2H_2O-2NH_3+2H]^{2+}$	-0.102
662.85278	662.85286	$[M^{\dagger}-H_2O-NH_3-CO+2H]^{2+}$	-0.121
667.84496	667.84502	$[M^{\dagger}-2H_2O-NH_3+2H]^{2+}$	-0.097
674.37134	* 674.37141	$[M+2H]^{2+}$	-0.111
676.85024	676.85028	$[M^{\dagger}-H_2O-NH_3+2H]^{2+}$	-0.063
685.36351	685.36352	$[M^{\dagger}-H_2O+2H]^{2+}$	-0.015
694.36879	694.36879	$[M^{\dagger}+2H]^{2+}$	0.004
724.34869	724.34877	y_6-NH_3	-0.117
729.41546	729.41542	$a^{\dagger}_{6}-H_2O$	
735.42602	735.42606	b_6	-0.054
740.38383	740.38385	$b^{\dagger}_{6}-H_2O-NH_3$	-0.034
741.37523	* 741.37526	y_6	-0.040
757.41037	757.41042	$b^{\dagger}_{6}-H_2O$	-0.066
775.42094	775.42103	$b^{\dagger}_{6}$	-0.123
	783.38257	?	
	790.42468	?	
	809.40945	?	
	816.48387	?	
	823.46141	?	
	852.45496	?	
876.48387	876.48394	$a^{\dagger}_{7}-H_2O$	-0.080
904.47878	904.47886	$b^{\dagger}_{7}-H_2O$	-0.088
922.48935	922.48932	$b^{\dagger}_{7}$	0.027
932.43348	932.43352	y_8-2NH_3	-0.043
	946.52577	?	
949.46003	949.46007	y_8-NH_3	-0.047
	956.51364	?	
966.48657	966.48662	y_8	-0.052
	979.51495	?	
	1023.55283	?	
	1024.56011	$a^{\dagger}_{8}-H_2O$	

THEORICAL (m/z)	EXPERIMENTAL (m/z)	ASSIGNMENTS	ERROR (ppm)
1029.56284	* 1029.56300	b_8	-0.155
	1048.57284	?	
1051.54719	1051.54727	$b^{\dagger}_8$ -H_2O	-0.076
	1058.55631	?	
1069.55776	1069.55816	$b^{\dagger}_8$	-0.379
	1091.54236	?	
1108.56865	1108.56874	$b^{\dagger}_9$ -H_2O	-0.081
	1110.55330	?	
1126.57922	1126.57954	$b^{\dagger}_9$	-0.288
	1146.58441	?	
	1160.60403	?	
	1179.61365	?	
1193.65780	1193.65816	$a^{\dagger}_{10}$ -H_2O	0.306
1203.64215	* 1203.64255	$b^{\dagger}_{10}$ -$2H_2O$	-0.336
	1205.62483	?	
1221.65271	1221.65276	$b^{\dagger}_{10}$ -H_2O	-0.041
1239.66328	* 1239.66335	$b^{\dagger}_{10}$	-0.061
		Mean	0.016
		St.Dv.	0.0263

Table A-6. CAD mass error analysis for the parent ion $[M+C_2H_2O_2+2H]^{2+}$ of the glyoxal-derived glycation product formed at amidated Substance P in MeOH:H_2O (50:50). * indicates mass to charge used for calibration.

THEORICAL (m/z)	EXPERIMENTAL (m/z)	ASSIGNMENTS	ERROR (ppm)
	200.77000	*	
	203.77743	*	
	226.11859	*	
	228.45627	*	
254.16114	* 254.16115	b_2	0.039
294.15606	294.15607	$b^{\ddagger}_2$	0.051
	341.30505	*	
	350.25776	?	
	352.16557	*	
	354.17720	*	
	363.08979	*	
	364.27341	?	
	371.20376	*	
	373.22342	*	
379.20883	379.20883	$[b^{\ddagger}_6$-H_2O+H$]^{2+}$	0.013
382.25610	* 382.25610	b_3	0.000
404.24045	404.24035	$b^{\ddagger}_3$ -H_2O	-0.247
449.22170	449.22167	y_4-NH_3	-0.056
	501.24555	*	

THEORICAL (m/z)	EXPERIMENTAL (m/z)	ASSIGNMENTS	ERROR (ppm)
515.28533	515.28503	$[b_8+H]^{2+}$	-0.587
543.79606	543.79585	$[b_9+H]^{2+}$	-0.391
563.79325	563.79322	$[b^{\ddagger}_9+H]^{2+}$	-0.049
582.81954	582.81937	$[b_{10}-H_2O-NH_3+H]^{2+}$	-0.287
586.34037	586.34035	$[a_{10}+H]^{2+}$	-0.026
591.33281	591.33251	$[b_{10}-H_2O+2H]^{2+}$	-0.507
600.33809	* 600.33780	$[b_{10}+H]^{2+}$	-0.487
607.36744	607.36742	b_5	-0.033
	609.31598	*	
611.33000	611.32990	$[b^{\ddagger}_{10}-H_2O+H]^{2+}$	-0.155
	614.83660	*	
	619.34566	*	
620.33528	620.33525	$[b^{\ddagger}_{10}+H]^{2+}$	-0.044
	627.85892	*	
647.36236	647.36242	$b^{\ddagger}_5$	0.100
643.34733	643.34726	$[M-2NH_3-CO+2H]^{2+}$	-0.113
648.33951	648.33946	$[M-2NH_3-H_2O+2H]^{2+}$	-0.073
651.86061	651.86060	$[M-NH_3-CO+2H]^{2+}$	-0.008
656.85278	656.85278	$[M-NH_3-H_2O+2H]^{2+}$	0.000
665.85806	* 665.85805	$[M-NH_3+2H]^{2+}$	-0.019
674.37134	674.37141	$[M+2H]^{2+}$	0.111
735.42602	735.42599	b_6	-0.041
775.42094	775.42108	$b^{\ddagger}_6$	-0.187
882.49443	* 882.49440	b_7	0.034
922.48935	922.48882	$b^{\ddagger}_7$	-0.567
932.43348	932.43406	y_8-2NH_3	0.622
	946.51477	?	
949.46003	949.46007	y_8-NH_3	0.047
966.48657	966.48633	y_8	-0.248
1029.56284	1029.56298	b_8	0.136
	1036.57201	?	
1051.54719	1051.54727	$b^{\ddagger}_8 -H_2O$	0.076
	1058.55631	*	
1069.55776	1069.55794	$b^{\ddagger}_8$	0.173
1077.55499	1077.55504	y_9-NH_3	-0.051
1086.58430	* 1086.58440	b_9	-0.092
1094.58153	1094.58162	y_9	0.082
	1103.58215	?	
	1105.59774	?	
1126.57922	1126.57896	$b^{\ddagger}_9$	-0.226
1171.67345	1171.67346	a_{10}	-0.013

THEORICAL (m/z)	EXPERIMENTAL (m/z)	ASSIGNMENTS	ERROR (ppm)
1191.63429	1191.63551	y_{10}	-1.024
1199.66836	1199.66854	b_{10}	-0.150
	1205.62483	?	
1221.65271	* 1221.65332	$b^{\ddagger}_{10}$ -H_2O	0.499
1239.66328	* 1239.66351	$b^{\ddagger}_{10}$	0.190
		Mean	-0.086
		St.Dv.	0.036

Table A-7. DR(674.86)-ECD(694.86) mass error analysis of the parent ion $[M + C_2O + 2H]^{2+}$ of glyoxal-derived glycation product formed at free acid form of Substance P in MeOH:H_2O (50:50). * indicates mass to charge used for calibration.

THEORICAL (m/z)	EXPERIMENTAL (m/z)	ASSIGNMENTS	ERROR (pppm)
496.33541	* 496.33536	c_4	-0.091
517.31194	517.31208	$c^{\dagger}_4{}^{\bullet}$-$H_2O$	0.280
518.31976	518.31990	$c^{\dagger}_4$-H_2O	0.270
535.32250	535.32242	$c^{\dagger}_4{}^{\bullet}$	-0.149
536.33033	536.33025	$c^{\dagger}_4$	-0.140
	592.30759	*	
	593.31113	*	
	602.64730	*	
	603.37268	*	
624.39399	* 624.39408	c_5	0.152
645.37051	645.37047	$c^{\dagger}_5{}^{\bullet}$-$H_2O$	-0.062
646.37834	646.37827	$c^{\dagger}_5$ - H_2O	-0.101
663.38108	663.38102	$c^{\dagger}_5{}^{\bullet}$	-0.083
664.38890	664.38883	$c^{\dagger}_5$	-0.105
	682.39944	?	
694.86081	694.86069	$[M^{\dagger} + 2H]^{2+}$	-0.169
	727.53949	?	
748.43385	748.43363	$a^{\dagger}_6$	-0.294
773.42909	773.42901	$c^{\dagger}_6{}^{\bullet}$-$H_2O$	-0.103
774.43692	774.43684	$c^{\dagger}_6$ - H_2O	-0.097
791.43966	791.43945	$c^{\dagger}_6{}^{\bullet}$	-0.259
792.44748	792.44733	$c^{\dagger}_6$	-0.189
895.50226	895.50203	$a^{\dagger}_7$	-0.257
921.50533	921.50519	$c^{\dagger}_7$-H_2O	-0.146
	937.73767	?	
938.50807	938.50808	$c^{\dagger}_7{}^{\bullet}$	0.016

THEORICAL (m/z)	EXPERIMENTAL (m/z)	ASSIGNMENTS	ERROR (pppm)
939.51589	939.51570	$c^{\dagger}_{7}$	-0.202
	965.76895	?	
	1008.50933	?	
1042.57013	1042.57077	$a^{\dagger}_{8}$	0.619
1068.57374	1068.57369	$c^{\dagger}_{8}$- H_2O	-0.042
1079.54683	* 1079.54661	$z_9^{\bullet}$	-0.204
1086.58430	1086.58419	$c^{\dagger}_{8}$	-0.101
	1117.49388	?	
1125.59520	1125.59525	$c^{\dagger}_{9}$ - H_2O	0.049
1143.60577	1143.60564	$c^{\dagger}_{9}$	-0.109
	1212.67607	?	
	1221.62094	?	
1238.67926	1238.67917	$c^{\dagger}_{10}$ - H_2O	-0.073
1256.68983	1256.68985	$c^{\dagger}_{10}$	0.020
1297.69257	1297.69335	$[M^{\dagger} - C_3H_6S - H_2O + 2H]^{1+\bullet}$	0.602
	1300.67469	?	
1315.70313	1315.70315	$[M^{\dagger} - C_3H_6S + 2H]^{1+\bullet}$	0.012
	1318.64933	?	
1326.69013	1326.68999	$[M^{\dagger} - H_2O - {}^{\bullet}CONH_2 + H]^{1+}$	-0.106
1331.69342	1331.69369	$[M - C_2O - NH_3 + H]^{1+}$	0.203
1343.71613	1343.71648	$[M^{\dagger} - {}^{\bullet}COOH + H]^{1+}$	0.264
1344.70125	1344.70070	$[M^{\dagger} - {}^{\bullet}CONH_2 + 2H]^{1+}$	0.405
1354.68505	1354.68501	$[M^{\dagger} - H_2O - NH_3 + 2H]^{1+\bullet}$	-0.026
1361.72724	1361.72774	$[M^{\dagger} - CO + 2H]^{1+\bullet}$	0.367
1371.71159	* 1371.71173	$[M^{\dagger} - H_2O + 2H]^{1+\bullet}$	0.102
	1387.67436	?	
1388.71488	* 1388.71470	$[M^{\dagger} + H]^{1+}$	-0.130
1389.72161	1389.72151	$[M^{\dagger} + 2H]^{1+\bullet}$	-0.068
		mean	-0.048
		St. Dv.	0.260

Table A-8 DR(674)-ECD(703) mass error analysis of amidated, glycated Substance P MeOH:H_2O (50:50), for the parent ion $[M + C_2H_2O_2 + 2H]^{2+}$. * indicates mass to charge used for calibration.

THEORICAL (m/z)	EXPERIMENTAL (m/z)	ASSIGNMENTS	ERROR (ppm)
	332.11950	*	
	341.30578	*	
	344.13180	?	

THEORICAL (m/z)	EXPERIMENTAL (m/z)	ASSIGNMENTS	ERROR (ppm)
	345.11579	*	
	360.15078	?	
	365.10062	*	
	373.11070	*	
	381.29765	*	
	390.12496	*	
496.33541	* 496.33537	c_4	-0.071
517.31193	517.31201	$c^{\ddagger}_{4}{}^{\bullet}-2H_2O$	0.155
518.31976	518.31967	$c^{\ddagger}_{4}$-2H_2O	-0.164
535.32250	535.32250	$c^{\ddagger}_{4}{}^{\bullet}$–$H_2O$	0.000
553.33306	553.33309	$c^{\ddagger}_{4}{}^{\bullet}$	0.054
554.34089	554.34071	$c^{\ddagger}_{4}$	-0.316
624.39399	* 624.39413	c_5	0.232
646.37834	646.37814	$c^{\ddagger}_{5}$-2H_2O	-0.302
663.38108	663.38135	$c^{\ddagger}_{5}{}^{\bullet}$–$H_2O$	0.415
681.39164	681.39129	$c^{\ddagger}_{5}{}^{\bullet}$	-0.514
682.39947	682.39946	$c^{\ddagger}_{5}$	-0.007
703.37408	703.37370	$[M^{\ddagger} + 2H]^{2+}$	-0.540
752.45257	* 752.45272	c_6	0.206
774.43692	774.43684	$c^{\ddagger}_{6}$-2H_2O	-0.097
791.43966	791.43965	$c^{\ddagger}_{6}{}^{\cdot}$–$H_2O$	-0.006
792.44748	792.44775	$c^{\ddagger}_{6}$–H_2O	0.341
809.45022	809.45032	$c^{\ddagger}_{6}{}^{\cdot}$	0.124
810.45805	* 810.45794	$c^{\ddagger}_{6}$	-0.130
899.52098	* 899.52069	c_7	-0.317
913.51228	913.51332	$a^{\ddagger}_{7}$	1.138
921.50533	921.50509	$c^{\ddagger}_{7}$-2H_2O	-0.255
939.51589	939.51554	$c^{\ddagger}_{7}$–H_2O	-0.373
957.52646	957.52654	$c^{\ddagger}_{7}$	0.089
1004.54379	1004.54366	$z_9{}^{\bullet}$ - C_3H_6S	-0.129
	1007.52567	?	
1046.58939	1046.58936	c_8	-0.024
1060.58069	1060.58078	$a^{\ddagger}_{8}$	0.085
1078.56281	1078.56252	$z_9{}^{\bullet}$	-0.269
1086.58430	1086.58425	$c^{\ddagger}_{8}$–H_2O	-0.046
1104.59487	1104.59477	$c^{\ddagger}_{8}$	-0.086
1103.61085	* 1103.61052	c_9	-0.294

THEORICAL (m/z)	EXPERIMENTAL (m/z)	ASSIGNMENTS	ERROR (ppm)
1125.59519	1125.59518	$c^{\ddagger}_{9}$-2H_2O	-0.013
1143.60576	1143.60539	$c^{\ddagger}_{9}$ - H_2O	-0.324
1161.61633	1161.61603	$c^{\ddagger}_{9}$	-0.254
1216.69491	* 1216.69447	c_{10}	-0.358
1238.67926	1238.68000	$c^{\ddagger}_{10}$ - 2H_2O	0.601
1256.68982	1256.68903	$c^{\ddagger}_{10}$ - H_2O	-0.629
1274.70039	1274.70014	$c^{\ddagger}_{10}$	-0.192
1331.71668	1331.71657	$[M\text{-}NH_3+2H]^{1+\bullet}$	-0.079
1343.71668	1343.71707	$[M^{\ddagger}\text{-}^{\bullet}CONH_2\text{-}H_2O+H]^{1+}$	0.294
1347.73540	1347.73507	$[M+H]^{1+}$	-0.241
1348.74377	1348.74359	$[M+2H]^{1+\bullet}$	-0.133
1361.72724	1361.72718	$[M^{\ddagger}\text{-}^{\bullet}CONH_2+H]^{1+}$	-0.044
1370.72757	1370.72699	$[M^{\ddagger}\text{-}2H_2O+2H]^{1+\bullet}$	-0.423
1371.71214	1371.71144	$[M^{\ddagger}\text{-}H_2O\text{-}NH_3+2H]^{1+\bullet}$	-0.510
1388.73814	* 1388.73808	$[M^{\ddagger}\text{-}H_2O+2H]^{1+\bullet}$	-0.997
1405.74088	* 1405.74033	$[M^{\ddagger}+H]^{1+}$	-0.388
		Mean	-0.342
		St.Dv.	0.044

Table A-9. CAD mass error analysis for the parent ion $[M+C_2O+2H]^{2+}$of glyoxal-derived glycation product formed at free acid form of Substance P in MeOH:H_2O (50:50). * indicates mass to charge used for calibration.

THEORICAL (m/z)	EXPERIMENTAL (m/z)	ASSIGNMENTS	ERROR (ppm)
254.16114	* 254.16112	b_2	-0.079
276.14549	* 276.14548	$b^{\dagger}_{2}$ -H_2O	-0.036
294.15606	* 294.15605	$b^{\dagger}_{2}$	-0.017
	307.14409	*	
	313.27372	*	
	318.18121	*	
320.1644	* 320.16387	y_3	-1.655
	338.34175	*	
	341.30505	*	
	354.17722	?	
	363.08981	?	
379.20883	379.20887	$[b_6\text{-}H_2O+H]^{2+}$	0.119
404.24045	404.24051	$b^{\dagger}_{3}$ -H_2O	0.148
422.25102	422.25109	$b^{\dagger}_{3}$	0.178
452.74303	452.74311	$[b^{\dagger}_{6}\text{-}H_2O+H]^{2+}$	0.177
	463.19768	?	

THEORICAL (m/z)	EXPERIMENTAL (m/z)	ASSIGNMENTS	ERROR (ppm)
467.23281	* 467.23235	y_4	-0.985
	486.77435	?	
	490.26117	?	
	495.99993	?	
501.29321	501.29333	$b^{\dagger}_4$ -H_2O	0.239
503.76651	503.76660	$[a^{\dagger}_8$-H_2O-NH_3+H$]^{2+}$	0.189
	506.77184	?	
509.25096	509.25077	$[b^{\dagger}_8$-H_2O-2NH_3+H$]^{2+}$	-0.378
512.28005	512.27987	$[a^{\dagger}_8$-H_2O+H$]^{2+}$	-0.351
515.28533	515.28511	$[b_8$+H$]^{2+}$	-0.432
517.27223	* 517.27205	$[b^{\dagger}_8$-2H_2O+H$]^{2+}$	-0.338
	524.79013	?	
526.27751	526.27734	$[b_9$-H_2O-NH_3+H$]^{2+}$	-0.318
	533.30332	?	
535.28252	535.28280	$[b^{\dagger}_8$+H$]^{2+}$	0.528
	537.79591	?	
540.79078	540.79059	$[a^{\dagger}_9$-H_2O+H$]^{2+}$	-0.351
543.79606	543.79588	$[b_9$+H$]^{2+}$	-0.336
545.78296	545.78281	$[b^{\dagger}_9$-2H_2O+H$]^{2+}$	-0.266
548.28669	* 548.28686	$[y_8$+H$]^{2+}$	0.310
	548.28678	?	
554.78824	554.78809	$[b^{\dagger}_9$-H_2O+H$]^{2+}$	-0.266
	560.30865	?	
563.79325	563.79336	$[b^{\dagger}_9$+H$]^{2+}$	0.200
	574.34614	?	
577.82736	577.82699	$[a_{10}$-NH_3+H$]^{2+}$	-0.645
582.81954	582.81936	$[b_{10}$-H_2O-NH_3+H$]^{2+}$	-0.305
586.34064	586.34045	$[a_{10}$+H$]^{2+}$	-0.316
593.31970	593.31946	$[b^{\dagger}_{10}$-3H_2O+H$]^{2+}$	-0.409
596.29066	596.29011	y_5-H_2O	-0.914
	597.33267	?	
600.33809	* 600.33796	$[b_{10}$+H$]^{2+}$	-0.221
601.35688	601.35706	$a^{\dagger}_5$ -H_2O	0.308
602.32499	602.32484	$[b^{\dagger}_{10}$-2H_2O+H$]^{2+}$	-0.241
611.33000	611.33014	$[b^{\dagger}_{10}$-H_2O+H$]^{2+}$	0.232
614.30122	614.30081	y_5	-0.667
620.33528	620.33541	$[b^{\dagger}_{10}$+H$]^{2+}$	0.214
629.35179	629.35193	$b^{\dagger}_5$ -H_2O	0.222
647.36236	647.36255	$b^{\dagger}_5$	0.301
663.34480	663.34436	$[M^{\dagger}$ -H_2O-NH_3-CO+2H$]^{2+}$	-0.656
668.33697	668.33697	$[M^{\dagger}$ -2H_2O-NH_3+2H$]^{2+}$	0.000

THEORICAL (m/z)	EXPERIMENTAL (m/z)	ASSIGNMENTS	ERROR (ppm)
674.86390	* 674.86348	$[M+2H]^{2+}$	-0.615
677.34225	677.34239	$[M^{\dagger}-H_2O-NH_3+2H]^{2+}$	0.203
685.85553	* 685.85566	$[M^{\dagger}-H_2O+2H]^{2+}$	0.197
694.86081	694.86095	$[M^{\dagger}+2H]^{2+}$	0.205
724.34869	724.34881	y_6-NH_3	0.173
729.41546	729.41551	$a^{\dagger}_6-H_2O$	0.075
735.42602	* 735.42633	b_6	
740.38383	740.38399	$b^{\dagger}_6-H_2O-NH_3$	0.223
742.35980	742.35944	y_6	-0.485
757.41037	757.41051	$b^{\dagger}_6-H_2O$	0.185
775.42094	775.42105	$b^{\dagger}_6$	0.148
	783.38247	?	
	790.42472	?	
	809.40948	?	
	816.48404	?	
	823.46141	?	
	868.48295	?	
904.47878	904.47890	$b^{\dagger}_7-H_2O$	0.133
922.48935	922.48944	$b^{\dagger}_7$	0.103
950.44460	950.44411	y_8-NH_3	-0.510
967.47114	* 967.47068	y_8	-0.475
	974.52133	?	
	996.54142	?	
	1023.55220	?	
1029.56284	1029.56303	b_8	0.185
1051.547	1051.54722	$b^{\dagger}_8-H_2O$	0.029
	1057.55829	?	
1069.55776	1069.55771	$b^{\dagger}_8$	-0.042
	1074.58437	?	
1095.5661	* 1095.56542	y_9	-0.621
1108.56865	1108.56861	$b^{\dagger}_9-H_2O$	-0.036
1126.57922	1126.57927	$b^{\dagger}_9$	0.049
1192.61886	1192.61781	y_{10}	-0.880
1193.65780	1193.65749	$a^{\dagger}_{10}-H_2O$	-0.256
1203.64215	1203.64163	$b^{\dagger}_{10}-2H_2O$	-0.430
1221.65271	* 1221.65287	$b^{\dagger}_{10}-H_2O$	0.133
1239.66328	* 1239.66319	$b^{\dagger}_{10}$	-0.068
		Mean	-0.122
		St.Dv.	0.049

Table A-10. CAD mass error analysis for the parent ion $[M+C_2H_2O_2+2H]^{2+}$ of glyoxal-derived glycation product formed at free acid form of Substance P in MeOH:H_2O (50:50). * indicates mass to charge used for calibration.

THEORICAL (m/z)	EXPERIMENTAL (m/z)	ASSIGNMENTS	ERROR (ppm)
254.16114	* 254.16112	b_2	-0.079
263.14294	263.14236	y_2	
276.14549	276.14548	$b^{\ddagger}_2$ -H_2O	-0.036
294.15606	294.15605	$b^{\ddagger}_2$	-0.017
	295.14410	?	
	307.14409	*	
	313.27372	*	
	318.18121	?	
	335.09488	?	
	338.34175	*	
	341.30505	*	
	350.25780	?	
	352.16559		
	354.17722	*	
	363.08981	*	
	364.27342	?	
	371.20376	*	
	373.22351	*	
	378.28910	?	
379.20883	379.20887	$[b_6$-H_2O+H$]^{2+}$	0.119
404.24045	404.24051	$b^{\ddagger}_3$ -H_2O	0.148
	406.17955	?	
	420.22821	*	
422.25102	422.25109	$b^{\ddagger}_3$	0.178
452.74303	452.74311	$[b^{\ddagger}_6$-H_2O+H$]^{2+}$	0.177
	463.19768	?	
	464.26161	*	
467.23281	* 467.23235	y_4	-0.985
	486.77435	*	
	490.26117	*	
	495.99993	*	
	501.24570	*	
501.29321	501.29333	$b^{\ddagger}_4$ -H_2O	0.239
503.76651	503.76660	$[a^{\ddagger}_8$-H_2O-NH_3+H$]^{2+}$	0.189
509.25096	509.25077	$[b^{\ddagger}_8$-H_2O-2NH_3+H$]^{2+}$	-0.378
512.28005	512.27987	$[a^{\ddagger}_8$-H_2O+H$]^{2+}$	-0.351
515.28533	515.28511	$[b_8$+H$]^{2+}$	-0.432
517.27223	517.27205	$[b^{\ddagger}_8$-2H_2O+H$]^{2+}$	-0.338
	517.76406	?	
	518.26575	*	
	524.79013	?	

THEORICAL (m/z)	EXPERIMENTAL (m/z)	ASSIGNMENTS	ERROR (ppm)
526.27751	526.27734	$[b_9\text{-}H_2O\text{-}NH_3+H]^{2+}$	-0.318
	533.30332	?	
535.28252	535.28280	$[b^{\ddagger}_8+H]^{2+}$	0.528
	537.79591	?	
	538.79935	*	
540.79078	540.79059	$[a^{\ddagger}_9\text{-}H_2O+H]^{2+}$	-0.351
543.79606	543.79588	$[b_9+H]^{2+}$	-0.336
545.78296	545.78281	$[b^{\ddagger}_9\text{-}2H_2O+H]^{2+}$	-0.266
	546.27482	?	
	540.80250	*	
548.28669	* 548.28686	$[y_8+H]^{2+}$	0.310
554.78824	554.78809	$[b^{\ddagger}_9\text{-}H_2O+H]^{2+}$	-0.266
	555.81409	?	
	560.30865	*	
563.79325	563.79336	$[b^{\ddagger}_9+H]^{2+}$	0.200
	574.34614	?	
	576.28178	*	
577.82736	577.82699	$[b_{10}\text{-}CO\text{-}NH_3+H]^{2+}$	-0.645
	580.80581	?	
582.81954	582.81936	$[b_{10}\text{-}H_2O\text{-}NH_3+H]^{2+}$	-0.305
586.34064	586.34045	$[a_{10}+H]^{2+}$	-0.316
593.31970	593.31946	$[b^{\ddagger}_{10}\text{-}3H_2O+H]^{2+}$	-0.409
596.29066	596.29011	$y_5\text{-}H_2O$	-0.914
	597.33267	?	
600.33809	600.33796	$[b_{10}+H]^{2+}$	-0.221
601.35688	601.35706	$a^{\ddagger}_5\ \text{-}H_2O$	0.308
602.32499	602.32484	$[b^{\ddagger}_{10}\text{-}2H_2O+H]^{2+}$	-0.241
611.33000	611.33014	$[b^{\ddagger}_{10}\text{-}H_2O+H]^{2+}$	0.232
614.30122	* 614.30081	y_5	-0.667
620.33528	620.33541	$[b^{\ddagger}_{10}+H]^{2+}$	0.214
629.35179	629.35193	$b^{\ddagger}_5\ \text{-}H_2O$	0.222
647.36236	647.36255	$b^{\ddagger}_5$	0.301
663.34480	663.34436	$[M^{\ddagger}\text{-}H_2O\text{-}NH_3\text{-}CO+2H]^{2+}$	-0.656
668.33697	668.33697	$[M^{\ddagger}\text{-}2H_2O\text{-}NH_3+2H]^{2+}$	0.000
674.86390	674.86348	$[M+2H]^{2+}$	-0.615
677.34225	677.34239	$[M^{\ddagger}\text{-}H_2O\text{-}NH_3+2H]^{2+}$	0.203
685.85553	685.85566	$[M^{\ddagger}\text{-}H_2O+2H]^{2+}$	0.197
694.86081	694.86095	$[M^{\ddagger}+2H]^{2+}$	0.205
	721.41447	?	
724.34869	724.34881	$y_6\text{-}NH_3$	0.173
729.41546	729.41551	$a^{\ddagger}_6\text{-}H_2O$	0.075

THEORICAL (m/z)	EXPERIMENTAL (m/z)	ASSIGNMENTS	ERROR (ppm)
735.42602	735.42633	b_6	
740.38383	740.38399	$b^{\ddagger}_6$ -H_2O-NH_3	0.223
742.35980	* 742.35944	y_6	-0.485
	742.43601	?	
757.41037	757.41051	$b^{\ddagger}_6$ -H_2O	0.185
775.42094	775.42105	$b^{\ddagger}_6$	0.148
904.47878	904.47890	$b^{\ddagger}_7$ -H_2O	0.133
922.48935	922.48944	$b^{\dagger}_7$	0.103
950.44460	950.44411	y_8-NH_3	-0.510
967.47114	* 967.47068	y_8	-0.475
	974.52133	?	
	996.54142	*	
	1023.55220	?	
1029.56284	1029.56303	b_8	0.185
	1051.54722	$b^{\ddagger}_8$ -H_2O	
	1057.55829	?	
1069.55776	1069.55771	$b^{\dagger}_8$	-0.042
	1074.58437	?	
1091.534255	1091.54217	?	
	1093.59391	*	
1095.56610	* 1095.56542	y_9	-0.621
1108.56865	1108.56861	$b^{\ddagger}_9$ -H_2O	-0.036
1126.57922	1126.57927	$b^{\ddagger}_9$	0.049
1192.61886	* 1192.61781	y_{10}	-0.880
1193.65780	1193.65749	$a^{\ddagger}_{10}$ -H_2O	-0.256
1203.64215	1203.64163	$b^{\ddagger}_{10}$ -$2H_2O$	-0.430
1221.65271	1221.65287	$b^{\ddagger}_{10}$ -H_2O	0.133
1239.66328	* 1239.66319	$b^{\ddagger}_{10}$	-0.068
		mean	-0.138
		St. Dv.	0.049

Table A-11. DR(674)-ECD(694) mass error analysis for the parent ion $[M+C_2O+2H]^{2+}$ of glyoxal-derived glycation product formed at amidated Substance P at biological conditions (pH 7.5). * indicates mass to charge used for calibration.

THEORICAL (m/z)	EXPERIMENTAL (m/z)	ASSIGNMENTS	ERROR (ppm)
271.18769	* 271.18766	c_2	-0.092
	381.29684	*	
	415.21095	*	
	438.19362	*	

THEORICAL (m/z)	EXPERIMENTAL (m/z)	ASSIGNMENTS	ERROR (ppm)
496.33541	* 496.33517	c_4	-0.473
	515.39601	?	
517.31194	517.31174	$c^{\dagger}_4{}^{\bullet}$-$H_2O$	-0.377
518.31976	518.31953	$c^{\dagger}_4$-H_2O	-0.444
535.32250	535.32233	$c^{\dagger}_4{}^{\bullet}$	-0.318
536.33033	* 536.33014	$c^{\dagger}_4$	-0.345
	592.30749	?	
645.37051	645.37066	$c^{\dagger}_5{}^{\bullet}$-$H_2O$	0.232
646.37834	646.37842	$c^{\dagger}_5$ - H_2O	0.132
663.38108	663.38124	$c^{\dagger}_5{}^{\bullet}$	0.249
664.38890	* 664.38906	$c^{\dagger}_5$	0.241
	682.39944	?	
694.36879	694.36904	$[M^{\dagger}+2H]^{2+}$	0.356
774.43692	774.43706	$c^{\dagger}_6$ - H_2O	0.187
791.43966	791.43981	$c^{\dagger}_6{}^{\bullet}$	0.196
792.44748	792.44733	$c^{\dagger}_6$	-0.189
921.50533	921.50564	$c^{\dagger}_7$-H_2O	0.342
	937.73807	?	
938.50807	938.50760	$c^{\dagger}_7{}^{\bullet}$	-0.495
939.51589	939.51611	$c^{\dagger}_7$	0.234
	993.80067	?	
1004.54379	1004.54364	$z_9{}^{\bullet}$ - C_3H_6S	-0.149
1042.57013	1042.57063	$a^{\dagger}_8$	0.484
1068.57374	1068.57355	$c^{\dagger}_8$- H_2O	-0.173
1078.56281	* 1078.56280	$z_9{}^{\bullet}$	-0.009
1086.58430	1086.58428	$c^{\dagger}_8$	-0.018
1125.59520	1125.59526	$c^{\dagger}_9$ - H_2O	0.058
1143.60576	1143.60557	$c^{\dagger}_9$	-0.166
	1220.63744	?	
1238.67926	1238.67905	$c^{\dagger}_{10}$ - H_2O	-0.165
1256.68982	1256.68926	$c^{\dagger}_{10}$	-0.446
1314.71856	1314.71860	$[M^{\dagger}-C_3H_6S+2H]^{1+\bullet}$	0.027
1343.71668	1343.71621	$[M^{\dagger}-{}^{\bullet}CONH_2+H]^{1+}$	-0.346
1370.72757	* 1370.72658	$[M^{\dagger}-H_2O+2H]^{1+\bullet}$	-0.722
1387.73031	* 1387.72948	$[M^{\dagger}+H]^{1+}$	-0.598
		mean	-0.090
		St. Dv.	0.3123

Table A-12. DR(674)-ECD(703) mass error analysis for the parent ion $[M+C_2H_2O_2+2H]^{2+}$ of glyoxal-derived glycation product formed at amidated Substance P at biological conditions (pH 7.5). * indicates mass to charge used for calibration.

THEORICAL (m/z)	EXPERIMENTAL (m/z)	ASSIGNMENTS	ERROR (ppm)
	331.28460	*	
	341.30532	*	
	344.01439	*	
	345.01281	*	
	357.00860	?	
	359.31586	?	
	373.23520	*	
	381.29778	*	
	422.28790	*	
	437.19365	*	
496.335405	* 496.33553	c_4	0.252
517.311935	517.31193	$c^{\ddagger}_4{}^{\bullet}-2H_2O$	-0.010
	524.33451	?	
535.322500	535.32253	$c^{\ddagger}_4{}^{\bullet}$-$H_2O$	0.056
536.330325	536.33039	$c^{\ddagger}_4$-H_2O	0.121
553.333060	553.33313	$c^{\ddagger}_4{}^{\bullet}$	0.127
554.340885	554.34092	$c^{\ddagger}_4$	0.063
	610.31815	*	
623.38616	623.38618	$c_5{}^{\bullet}$	0.032
624.39399	* 624.39402	c_5	0.056
645.37051	645.37056	$c^{\ddagger}_5{}^{\bullet}-2H_2O$	0.077
646.37834	646.37840	$c^{\ddagger}_5$ - 2H_2O	0.101
663.38108	663.38106	$c^{\ddagger}_5{}^{\bullet}$-$H_2O$	-0.023
664.38890	664.38892	$c^{\ddagger}_5$ - H_2O	0.030
674.37134	674.37151	$[M+2H]^{2+}$	0.260
681.39164	681.39165	$c^{\ddagger}_5{}^{\bullet}$	0.015
682.39947	682.39947	$c^{\ddagger}_5$	0.007
703.37408	703.37403	$[M^{\ddagger}+2H]^{2+}$	-0.071
	715.31659	*	
	728.54292	*	
752.45257	* 752.45297	c_6	0.538
	755.57084	*	
791.43966	791.43965	$c^{\ddagger}_6{}^{\bullet}$- H_2O	-0.006
792.44748	792.44748	$c^{\ddagger}_6$ - H_2O	0.000

THEORICAL (m/z)	EXPERIMENTAL (m/z)	ASSIGNMENTS	ERROR (ppm)
809.45022	809.45006	$c^{\ddagger}_{6}{}^{\bullet}$	-0.198
810.45805	810.45800	$c^{\ddagger}_{6}$	-0.056
895.50172	895.50249	$a^{\ddagger}_{7}$ - H_2O	0.865
899.52098	* 899.52101	c_7	0.039
913.51228	913.51278	$a^{\ddagger}_{7}$	0.547
938.50807	938.50731	$c^{\ddagger}_{7}{}^{\bullet}$- H_2O	-0.804
939.51589	939.51598	$c^{\ddagger}_{7}$ - H_2O	0.096
	952.75699	?	
957.52646	957.52649	$c^{\ddagger}_{7}$	0.037
	966.77274	?	
	980.78841	?	
1004.54379	1004.54407	$z_9{}^{\bullet}$ - C_3H_6S	0.279
	1007.52572	?	
1042.57013	1042.57076	$a^{\ddagger}_{8}$- H_2O	0.609
1046.58939	1046.58958	c_8	0.186
1060.58069	1060.58045	$a^{\ddagger}_{8}$	-0.226
1078.56281	* 1078.56299	$z_9{}^{\bullet}$	0.167
1086.58430	1086.58425	$c^{\ddagger}_{8}$- H_2O	-0.046
1104.59487	1104.59457	$c^{\ddagger}_{8}$	-0.267
1103.61085	* 1103.61111	c_9	0.240
1143.60576	1143.60606	$c^{\ddagger}_{10}$ - H_2O	0.262
1161.61633	1161.61666	$c^{\ddagger}_{9}$	0.288
1216.69491	1216.69537	c_{10}	0.382
1256.68982	1256.69020	$c^{\ddagger}_{10}$ - H_2O	0.302
1274.70039	1274.70088	$c^{\ddagger}_{10}$	0.388
1331.71668	1331.71738	$[M^{\ddagger}$ -NH_3+2H$]^{1+\bullet}$	0.529
1343.71668	1343.71689	$[M^{\ddagger}$ -$^{\bullet}CONH_2$-H_2O+H$]^{1+}$	0.160
1347.73540	1347.73612	$[M+H]^{1+}$	0.538
1348.74377	1348.74325	$[M+2H]^{1+\bullet}$	-0.386
1361.72724	1361.72824	$[M^{\ddagger}$ -$^{\bullet}CONH_2$+H$]^{1+}$	0.734
1370.72757	1370.72843	$[M^{\ddagger}$ -2H_2O+2H$]^{1+\bullet}$	0.627
1371.71214	1371.71144	$[M^{\ddagger}$ -H_2O-NH_3+2H$]^{1+\bullet}$	-0.510
	1387.72764	?	
1388.73814	* 1388.73897	$[M^{\ddagger}$ -H_2O+2H$]^{1+\bullet}$	0.601
1405.74088	* 1405.74139	$[M^{\ddagger}$ +H$]^{1+}$	0.366
		Mean	0.151
		St. Dv.	0.065

Table A-13. CAD error analysis for the parent ion $[M+C_2O+2H]^{2+}$ of glyoxal-derived glycation product formed at amidated Substance P at biological conditions (pH 7.5). * indicates mass to charge used for calibration.

THEORICAL (m/z)	EXPERIMENTAL (m/z)	ASSIGNMENTS	ERROR (ppm)
254.16114	* 254.16115	b_2	0.039
294.15606	294.15607	$b^{\dagger}_2$	0.051
379.20883	378.28909	?	
382.25610	* 382.25610	b_3	0.000
404.24045	404.24035	$b^{\dagger}_3$ -H_2O	-0.247
449.22170	449.22167	y_4-NH_3	-0.056
515.28533	515.28503	$[b_8+H]^{2+}$	-0.587
543.79606	* 543.79585	$[b_9+H]^{2+}$	-0.391
545.78296		$[b^{\dagger}_9-2H_2O+H]^{2+}$	
563.79325	563.79322	$[b^{\dagger}_9+H]^{2+}$	-0.049
582.81954	582.81937	$[b_{10}-H_2O-NH_3+H]^{2+}$	-0.287
586.34037	586.34035	$[a_{10}+H]^{2+}$	-0.026
591.33281	591.33251	$[b_{10}-H_2O+2H]^{2+}$	-0.507
600.33809	* 600.33780	$[b_{10}+H]^{2+}$	-0.487
607.36744	607.36742	b_5	-0.033
611.33000	611.32990	$[b^{\dagger}_{10}-H_2O+H]^{2+}$	-0.155
	614.83660	*	
	619.34566	*	
620.33528	620.33525	$[b^{\dagger}_{10}+H]^{2+}$	-0.044
647.36236	647.36242	$b^{\dagger}_5$	0.100
643.347333	643.34726	$[M-2NH_3-CO+2H]^{2+}$	-0.113
648.339508	648.33946	$[M-2NH_3-H_2O+2H]^{2+}$	-0.073
651.860605	651.86060	$[M-NH_3-CO+2H]^{2+}$	-0.008
656.852780	656.85278	$[M-NH_3-H_2O+2H]^{2+}$	0.000
665.85806	665.85805	$[M-NH_3+2H]^{2+}$	-0.019
674.37134	674.37141	$[M+2H]^{2+}$	0.111
735.42602	735.42599	b_6	-0.041
775.42094	775.42108	$b^{\dagger}_6$	-0.187
882.49443	* 882.49440	b_7	0.034
922.48935	922.48882	$b^{\dagger}_7$	-0.567
932.43348	932.43406	y_8-$2NH_3$	0.622
949.46003	949.46007	y_8-NH_3	0.047
966.48657	966.48633	y_8	-0.248
1029.56284	1029.56298	b_8	0.136
1051.54719	1051.54727	$b^{\dagger}_8$ -H_2O	0.076
1069.55776	1069.55794	$b^{\dagger}_8$	0.173
1077.55499	1077.55504	y_9-NH_3	-0.051

THEORICAL (m/z)	EXPERIMENTAL (m/z)	ASSIGNMENTS	ERROR (ppm)
1086.58430	1086.58440	b_9	-0.092
1094.58153	1094.58162	y_9	0.082
1126.57922	1126.57896	$b^{\dagger}_9$	-0.226
1171.67345	1171.67346	a_{10}	-0.013
1191.63429	1191.63551	y_{10}	-1.024
1199.66836	* 1199.66854	b_{10}	-0.150
1221.65271	* 1221.65332	$b^{\dagger}_{10}$ -H_2O	0.499
1239.66328	* 1239.66351	$b^{\dagger}_{10}$	0.190
		Mean	-0.086
		St. Dv.	

Table A-14. CAD mass for the parent ion $[M+C_2H_2O_2+2H]^{2+}$of glyoxal-derived glycation product formed at amidated Substance P at biological conditions (pH 7.5). * indicates mass to charge used for calibration.

THEORICAL (m/z)	EXPERIMENTAL (m/z)	ASSIGNMENTS	ERROR (ppm)
254.16114	* 254.16115	b_2	0.039
294.15606	294.15607	$b^{\ddagger}_2$	0.051
	341.30505	?	
	350.25776	?	
	352.16557	*	
	354.17720	?	
	363.08979	?	
	371.20376	?	
	378.28909	?	
382.25610	* 382.25610	b_3	0.000
404.24045	404.24035	$b^{\ddagger}_3$ -H_2O	-0.247
449.22170	449.22167	y_4-NH_3	-0.056
466.24824	466.24944	y_4	
	501.24555	.	
515.28533	515.28503	$[b_8+H]^{2+}$	-0.587
543.79606	543.79585	$[b_9+H]^{2+}$	-0.391
563.79325	563.79322	$[b^{\ddagger}_9+H]^{2+}$	-0.049
582.81954	582.81937	$[b_{10}$-H_2O-$NH_3+H]^{2+}$	-0.287
586.34037	586.34035	$[a_{10}+H]^{2+}$	-0.026
591.33281	591.33251	$[b_{10}$-$H_2O+2H]^{2+}$	-0.507
600.33809	600.33780	$[b_{10}+H]^{2+}$	-0.487
607.36744	* 607.36742	b_5	-0.033
	609.31598	?	
611.33000	611.32990	$[b^{\ddagger}_{10}$-$H_2O+H]^{2+}$	-0.155
	614.83660	*	

THEORICAL (m/z)	EXPERIMENTAL (m/z)	ASSIGNMENTS	ERROR (ppm)
	619.34566	*	
620.33528	620.33525	$[b^{\ddagger}_{10}+H]^{2+}$	-0.044
	627.85892	?	
647.36236	647.36242	$b^{\ddagger}_{5}$	0.100
643.34733	643.34726	$[M-2NH_3-CO+2H]^{2+}$	-0.113
648.33951	648.33946	$[M-2NH_3-H_2O+2H]^{2+}$	-0.073
651.86061	651.86060	$[M-NH_3-CO+2H]^{2+}$	-0.008
656.85278	656.85278	$[M-NH_3-H_2O+2H]^{2+}$	0.000
665.85806	665.85805	$[M-NH_3+2H]^{2+}$	-0.019
674.37134	674.37141	$[M+2H]^{2+}$	0.111
735.42602	735.42599	b_6	-0.041
775.42094	775.42108	$b^{\ddagger}_{6}$	-0.187
882.49443	* 882.49440	b_7	0.034
922.48935	922.48882	$b^{\dagger}_{7}$	-0.567
	929.48822	?	
932.43348	932.43406	y_8-2NH_3	0.622
	946.51477	?	
949.46003	949.46007	y_8-NH_3	0.047
966.48657	966.48633	y_8	-0.248
	974.52046	?	
1029.56284	* 1029.56298	b_8	0.136
	1036.57201	?	
1051.54719	1051.54727	$b^{\ddagger}_{8}$ $-H_2O$	0.076
	1058.55631	?	
1069.55776	1069.55794	$b^{\ddagger}_{8}$	0.173
1077.55499	1077.55504	y_9-NH_3	-0.051
1086.58430	1086.58440	b_9	-0.092
1094.58153	1094.58162	y_9	0.082
	1103.58215	?	
	1105.59774	?	
1126.57922	1126.57896	$b^{\ddagger}_{9}$	-0.226
1171.67345	1171.67346	a_{10}	-0.013
1191.63429	1191.63551	y_{10}	-1.024
1199.66836	* 1199.66854	b_{10}	-0.150
	1205.62483	?	
1221.65271	1221.65332	$b^{\ddagger}_{10}$ $-H_2O$	0.499
1239.66328	* 1239.66351	$b^{\ddagger}_{10}$	0.190
		Mean	-0.086
		St. Dv.	0.043

B

Mass Error tables with assignments used to interpret the data of Chapter 4

TABLE OF CONTENTS.

Table B-1. Mass error analysis of the direct infusion spectrum of the KM-11 peptide reacted in MeOH/H_2O (50:50). * indicates the ions used for calibration.

THEORETICAL ***(m/z)***	**EXPERIMENTAL** ***(m/z)***	**ASSIGNMENT**	**ERROR (ppm)**
* 449.91665	449.91663	$[M+3H]^{3+}$	-0.043
463.24829	463.24831	$[M+C_2O+3H]^{3+}$	0.036
469.25182	469.25183	$[M+C_2H_2O_2+3H]^{3+}$	0.028
488.58698	488.58699	$[M+2(C_2H_2O_2)+3H]^{3+}$	0.021
600.33782	600.33819	b_{10}^{2+}	0.616
* 674.37134	674.37156	$[M+2H]^{2+}$	0.320
694.36880	694.36871	$[M+C_2O+2H]^{2+}$	-0.129
703.37408	703.37432	$[M+C_2H_2O_2+2H]^{2+}$	-0.251
710.38191	710.38207	$[M+C_2H_2O_2+CH_2+2H]^{2+}$	0.225
723.37154	723.37123	$[M+C_2H_2O_2+2H]^{2+}$	-0.433
* 732.37682	732.37674	$[M+2(C_2H_2O_2)+2H]^{2+}$	-0.116
* 1347.73542	1347.73545	$[M+H]^{1+}$	0.019
		Mean	0.024
		St. Dv.	0.272

Table B-2. Mass error of the direct infusion spectra of the KM-11 peptide reacted in PBS. * indicates the ions used for calibration.

THEORETICAL ***(m/z)***	**EXPERIMENTAL** ***(m/z)***	**ASSIGNMENT**	**ERROR (ppm)**
* 469.25182	469.25180	$[M+C_2H_2O_2+3H]^{3+}$	0.042
488.58698	488.58699	$[M+2(C_2H_2O_2)+3H]^{3+}$	-0.020
600.33782	600.33760	b_{10}^{2+}	0.366
* 674.37134	674.37202	$[M+2H]^{2+}$	0.997
* 685.36352	685.36366	$[M+(C_2-H_2)+2H]^{2+}$	0.204
694.36880	694.36872	$[M+C_2O+2H]^{2+}$	-0.115
703.37408	703.37359	$[M+C_2H_2O_2+2H]^{2+}$	-0.697
* 723.37154	723.37109	$[M+C_4H_2O_3+C_2O+2H]^{2+}$	-0.622
		Mean	0.019
		St. Dv.	0.542

Table B-3. Mass error of the direct infusion spectra of the AcKM-11 peptide reacted in MeOH/H_2O. * indicates the ions used for calibration.

THEORETICAL ***(m/z)***	**EXPERIMENTAL** ***(m/z)***	**ASSIGNMENT**	**ERROR (ppm)**
* 463.92018	463.92019	$[M+3H]^{3+}$	-0.194
483.25534	483.25543	$[M+C_2H_2O_2+3H]^{3+}$	0.186
* 621.34311	621.34298	b_{10}^{2+}	-0.209
695.37663	695.37620	$[M+2H]^{2+}$	-0.618
715.37408	715.37410	$[M+C_2O+2H]^{2+}$	0.028
724.37937	724.37934	$[M+C_2H_2O_2+2H]^{2+}$	-0.041
* 753.38211	753.38218	$[M+2(C_2H_2O_2)+2H]^{2+}$	0.092
* 1389.74597	1389.74494	$[M+H]^{1+}$	-0.742
		mean	-0.187
		St. Dv.	0.334

Table B-4. Mass error of the direct infusion spectra of the reacted AcKM-11 peptide reacted in PBS. * indicates the ions used for calibration.

THEORETICAL ***(m/z)***	**EXPERIMENTAL** ***(m/z)***	**ASSIGNMENT**	**ERROR (ppm)**
463.92018	463.92030	$[M+3H]^{3+}$	0.254
483.25534	483.25545	$[M+C_2H_2O_2+3H]^{3+}$	0.234
695.37663	695.37683	$[M+2H]^{2+}$	0.291
706.36880	706.36866	$[M+(C_2-H_2)+2H]^{2+}$	-0.198
715.37408	715.37370	$[M+C_2O+2H]^{2+}$	-0.536
724.88104	724.88119	$[M+C_2H_2O_2+C_2O+2H]^{2+}$	0.203
753.38211	753.38140	$[M+2(C_2H_2O_2)+2H]^{2+}$	-0.942
1389.74597	1389.74599	$[M+H]^{1+}$	0.017
		Mean	-0.085
		St. Dv.	0.448

Table B-5. DR(674)-ECD(694) error analysis of the KM-11 peptide reacted in MeOH/H_2O (50:50) for the precursor ion $[M+C_2O+2H]^{2+}$. * indicates the ions used for calibration.

THEORETICAL ***(m/z)***	**EXPERIMENTAL** ***(m/z)***	**ASSIGNMENTS**	**ERROR (ppm)**
* 243.18154	243.18154	c_2	0.205
319.17983	319.17976	y_3	-0.219
365.22956	365.22951	b_3-NH_3	-0.137
376.72992	376.73006	c_6^{2+}	0.358
382.25610	382.25614	b_3	0.092
449.76022	449.76019	$c_7^{\bullet 2+}$	-0.062
450.26413	450.26410	c_7^{2+}	-0.067
466.24824	466.24823	y_4	-0.021
479.30887	479.30894	b_4	0.156
483.74693	483.74655	y_8^{2+}	-0.786
495.32758	495.32756	$c_4^{\bullet}$	-0.050
496.33541	496.33540	c_4	-0.020
517.31193	517.31194	$c^{\dagger}_4{}^{\bullet}$-$H_2O$	0.010
523.29442	523.29442	$c_8^{\bullet 2+}$	-0.006
523.79833	523.79836	c_8^{2+}	0.048
535.32250	535.32249	$c^{\dagger}_4{}^{\bullet}$	-0.019
536.33033	536.33027	$c^{\dagger}_4$	-0.103
552.30907	552.30907	c_9^{2+}	0.009
561.79748	561.79748	y_9^{2+}	0.000
572.30652	572.30654	$c^{\dagger}_9{}^{2+}$	0.031
580.38036	580.38065	a_5	0.500
581.79494	581.79505	$y^{\dagger}_9{}^{2+}$	0.189
591.82455	591.82460	$(b_{10}$-$NH_3)^{2+}$	0.084

THEORETICAL *(m/z)*	EXPERIMENTAL *(m/z)*	ASSIGNMENTS	ERROR (ppm)
600.33782	600.33787	b_{10}^{2+}	0.078
607.36744	607.36747	b_5	0.041
608.85109	608.85109	c_{10}^{2+}	-0.008
610.32386	610.32391	y_{10}^{2+}	0.082
613.31665	613.31663	y_5	-0.033
623.38617	623.38615	$c_5^{\bullet}$	-0.024
624.39399	624.39398	c_5	-0.016
628.34464	628.34412	$c^{\dagger}_{10}{}^{\bullet 2+}$	-0.828
628.84855	628.84861	$c^{\dagger}_{10}{}^{2+}$	0.091
645.37051	645.37050	$c^{\dagger}_5{}^{\bullet}\text{-}H_2O$	-0.023
646.37834	646.37848	$c^{\dagger}_5\text{-}H_2O$	0.217
657.34479	657.34486	$[M\text{-}2NH_3\text{+}H]^{2+}$	0.099
663.38108	663.38099	$c^{\dagger}_5{}^{\bullet}$	-0.136
664.38891	664.38888	$c^{\dagger}_5$	-0.038
665.85807	665.85807	$[M\text{-}2NH_3\text{+}2H]^{2+}$	0.000
685.85553	685.85516	$[M\text{-}NH_3\text{+}2H]^{2+}$	-0.539
694.36880	694.36877	$[M^{\dagger}\text{+}2H]^{2+}$	-0.040
696.37020	696.37045	$a^{\dagger}_5\text{-}2NH_3\text{-}H_2O$	0.359
707.32214	707.32205	$y_6\text{-}2NH_3$	-0.127
724.34869	724.34858	$y_6\text{-}NH_3$	-0.152
735.42602	735.42599	b_6	-0.048
741.37523	741.37522	y_6	-0.013
751.44475	751.44469	$c_6^{\bullet}$	-0.073
752.45257	752.45256	c_6	-0.013
767.42256	767.42182	$a_7\text{-}2NH_3\text{-}2H_2O$	-0.971
773.42909	773.42969	$c^{\dagger}_6{}^{\bullet}\text{-}H_2O$	0.769
774.43692	774.43731	$c^{\dagger}_6\text{-}H_2O$	0.504
775.42094	775.42087	$b^{\dagger}_6$	-0.090
791.43966	791.43960	$c^{\dagger}_6{}^{\bullet}$	-0.076
792.44749	792.44746	$c^{\dagger}_6$	-0.032
852.40727	852.40702	$y_7\text{-}NH_3$	-0.293
882.49443	882.49442	b_7	-0.017
898.51315	898.51313	$c_7^{\bullet}$	-0.028
899.52098	899.52100	c_7	0.022
921.50533	921.50594	$c^{\dagger}_7{}^{\bullet}\text{-}H_2O$	0.662
922.48935	922.48885	$b^{\dagger}_7$	-0.542
938.50807	938.50829	$c^{\dagger}_7{}^{\bullet}$	0.234
939.51590	939.51598	$c^{\dagger}_7$	0.090
966.48657	966.48651	y_8	-0.062
1012.53630	1012.53626	$b_8\text{-}NH_3$	-0.040
1032.54994	1032.55002	$z_9^{\bullet}\text{-}C_3H_6S$	0.077
1042.57067	1042.57046	$a^{\dagger}_8$	-0.206
1045.58156	1045.58197	$c_8^{\bullet}$	0.387
1046.58939	1046.58951	c_8	0.115
1069.55776	1069.55731	$b^{\dagger}_8$	-0.421
1072.54485	1072.54472	$z^{\dagger}_9{}^{\bullet}\text{-}C_3H_6S$	-0.121
1086.58431	1086.58434	$c^{\dagger}_8$	0.032
1103.61085	1103.61089	c_9	0.036

THEORETICAL *(m/z)*	EXPERIMENTAL *(m/z)*	ASSIGNMENTS	ERROR (ppm)
1106.56896	1106.56903	$z_9^{\bullet}$	0.063
1122.58768	1122.58751	y_9	-0.151
1125.59520	1125.59409	$c^{\dagger}_9$-H_2O	-0.986
1143.60577	1143.60577	$c^{\dagger}_9$	0.004
1146.56388	1146.56377	$z^{\dagger}_9{}^{\bullet}$	-0.096
1162.58260	1162.58229	$y^{\dagger}_9$	-0.267
1216.69491	1216.69490	c_{10}	-0.008
1239.66328	1239.66366	$b^{\dagger}_{10}$	0.307
1256.68982	1256.68990	$c^{\dagger}_{10}$	0.060
1286.69631	1286.69550	$[M-{}^{\bullet}CONH_2-NH_3+H]^{1+}$	-0.630
1303.72177	1303.72221	$[M^{\dagger}-HCONH_2-H_2O+2H]^{1+\bullet}$	0.337
1314.71857	1314.71864	$[M^{\dagger}-C_3H_6S+2H]^{1+\bullet}$	-0.368
1330.70886	1330.70897	$[M-NH_3+H]^{1+}$	0.496
1331.71724	1331.71698	$[M-NH_3+2H]^{1+\bullet}$	-0.195
1335.66667	1335.66557	$[M-H_2O-2NH_3+H]^{1+}$	-0.816
1347.73540	1347.73532	$[M+H]^{1+}$	-0.067
1353.70104	1353.70082	$[M^{\dagger}-H_2O-NH_3+2H]^{1+\bullet}$	-0.159
1370.72785	1370.72783	$[M^{\dagger}-H_2O+2H]^{1+\bullet}$	-0.015
1388.73815	1388.73809	$[M^{\dagger}+2H]^{1+\bullet}$	-0.072
		Mean	-0.011
		St. Dv.	0.351

Table B-6. CAD(694) error analysis of the KM-11 peptide reacted in MeOH/H_2O (50:50) for the precursor ion $[M+C_2O+2H]^{2+}$. * indicates the ions used for calibration.

THEORETICAL *(m/z)*	EXPERIMENTAL *(m/z)*	ASSIGNMENTS	ERROR (ppm)
226.15500	226.15505	b_2	0.243
262.15837	262.15846	y_2	0.343
302.15329	302.15336	y_3-NH_3	0.232
319.17983	319.17993	y_3	0.313
364.24554	364.24562	b_3-H_2O	0.220
382.25610	382.25610	b_3	-0.013
404.24045	404.24059	$b^{\dagger}_3$-H_2O	0.334
422.25102	422.25101	$b^{\dagger}_3$	-0.024
441.75086	441.75075	b_7^{2+}	-0.244
449.22170	449.22182	y_4-NH_3	0.267
453.23504	453.23489	$(b^{\dagger}_7$-$NH_3)^{2+}$	-0.336
466.24824	466.24825	y_4	0.021
479.30887	479.30890	b_4	0.073
492.77461	492.77435	$(a_8$-$NH_3)^{2+}$	-0.517
501.28761	501.28765	a_8^{2+}	0.084
506.27978	506.27972	$(b_8$-$H_2O)^{2+}$	-0.119
506.77179	506.77189	$(b_8$-$NH_3)^{2+}$	0.197
515.28506	515.28510	b_8^{2+}	0.072
526.27724	526.27699	$(b^{\dagger}_8$-$H_2O)^{2+}$	-0.470

THEORETICAL *(m/z)*	EXPERIMENTAL *(m/z)*	ASSIGNMENTS	ERROR (ppm)
526.76925	526.76896	$(b^{\dagger}_{8}\text{-}NH_3)^{2+}$	-0.546
534.79051	534.79082	$(b_9\text{-}H_2O)^{2+}$	0.580
535.28252	535.28259	$b^{\dagger}_{8}{}^{2+}$	0.131
543.79579	543.79593	$b_9{}^{2+}$	0.252
549.79579	549.79523	$a^{\dagger}_{9}{}^{2+}$	-1.023
554.78797	554.78803	$(b^{\dagger}_{9}\text{-}H_2O)^{2+}$	0.113
555.27998	555.28007	$(b^{\dagger}_{9}\text{-}NH_3)^{2+}$	0.167
563.79325	563.79332	$b^{\dagger}_{9}{}^{2+}$	0.124
577.82736	577.82728	$(a_{10}\text{-}NH_3)^{2+}$	-0.147
582.81927	582.81930	$(b_{10}\text{-}H_2O\text{-}NH_3)^{2+}$	0.055
586.34037	586.34053	$(a_{10}+H]2+$	0.276
591.33254	591.33272	$(b_{10}\text{-}H_2O)^{2+}$	0.304
591.82455	591.82477	$(b_{10}\text{-}NH_3)^{2+}$	0.372
596.29011	596.29026	$y_5\text{-}NH_3$	0.252
597.33254	597.33273	$(a^{\dagger}_{10}\text{-}H_2O)^{2+}$	0.318
600.33782	600.33801	$b_{10}{}^{2+}$	0.311
602.81673	602.81698	$(b^{\dagger}_{10}\text{-}H_2O\text{-}NH_3)^{2+}$	0.423
606.33782	606.33792	$a^{\dagger}_{10}{}^{2+}$	0.157
607.36744	607.36764	b_5	0.321
610.32386	610.32389	$y_{10}{}^{2+}$	0.049
611.33000	611.33017	$(b^{\dagger}_{10}\text{-}H_2O)^{2+}$	0.282
611.82201	611.82209	$(b^{\dagger}_{10}\text{-}NH_3)^{2+}$	0.135
613.31665	613.31672	y_5	0.114
620.33528	620.33543	$b^{\dagger}_{10}{}^{2+}$	0.242
630.32132	630.32165	$y^{\dagger}_{10}{}^{2+}$	0.528
643.34761	643.34767	$[M\text{-}HCONH_2\text{-}NH_3+2H]^{2+}$	0.093
647.36236	647.36242	$b^{\dagger}_{5}$	0.093
654.33951	654.33943	$[M^{\dagger}\text{-}\ HCONH_2\text{-}H_2O\text{-}NH_3+2H]^{2+}$	-0.126
656.85279	656.85326	$[M\text{-}H_2O\text{-}NH_3+2H]^{2+}$	0.723
657.34479	657.34543	$[M\text{-}2NH_3+2H]^{2+}$	0.966
662.85279	662.85316	$[M^{\dagger}\text{-}\ HCONH_2\text{-}H_2O\ +2H]^{2+}$	0.566
665.36606	665.36644	$[M\text{-}H_2O+2H]^{2+}$	0.571
665.85807	665.85868	$[M\text{-}NH_3+2H]^{2+}$	0.919
671.85807	671.85866	$[M^{\dagger}\text{-}\ HCONH_2+2H]^{2+}$	0.878
674.37134	674.37188	$[M+2H]^{2+}$	0.801
676.85025	676.85008	$[M^{\dagger}\text{-}H_2O\text{-}NH_3+2H]^{2}$	-0.251
677.34226	677.34238	$[M^{\dagger}\text{-}2NH_3+2H]^{2+}$	0.177
685.36352	685.36310	$[M^{\dagger}\text{-}H_2O+2H]^{2+}$	-0.613
685.85553	685.85526	$[M^{\dagger}\text{-}NH_3+2H]^{2+}$	-0.394
694.36880	694.36841	$[M^{\dagger}+2H]^{2+}$	-0.562
696.37020	696.36980	$a^{\dagger}_{6}\text{-}2NH_3\text{-}H_2O$	-0.574
707.32214	707.32173	$y_6\text{-}2NH_3$	-0.580
735.42602	735.42591	b_6	-0.156
741.37523	741.37536	y_6	0.175
757.41038	757.40975	$b^{\dagger}_{6}\text{-}H_2O$	-0.825
854.49952	854.49885	a_7	-0.784
865.46789	865.46775	$b_7\text{-}NH_3$	-0.162
882.49443	882.49427	b_7	-0.187

THEORETICAL *(m/z)*	EXPERIMENTAL *(m/z)*	ASSIGNMENTS	ERROR (ppm)
905.46281	905.46212	$b^{\dagger}_{7}$-NH_3	-0.757
922.48935	922.48971	$b^{\dagger}_{7}$	0.390
932.43348	932.43378	y_8-$2NH_3$	0.322
949.46003	949.45980	y_8-NH_3	-0.242
966.48657	966.48643	y_8	-0.145
1001.56793	1001.56691	a_8	-1.018
1012.53630	1012.53625	b_8-NH_3	-0.049
1041.56284	1041.56240	$a^{\dagger}_{8}$	-0.427
1051.54720	1051.54691	$b^{\dagger}_{8}$-H_2O	-0.271
1052.53121	1052.53128	$b^{\dagger}_{8}$-NH_3	0.062
1105.56114	1105.56121	y_9-NH_3	0.063
1108.56866	1108.56807	$b^{\dagger}_{9}$-H_2O	-0.528
1109.55267	1109.55269	$b^{\dagger}_{9}$-NH_3	0.014
1122.58768	1122.58715	y_9	-0.472
1126.57922	1126.57849	$b^{\dagger}_{9}$	-0.648
1144.57203	1144.57243	$y^{\dagger}_{9}$-H_2O	0.349
1145.55605	1145.55610	$y^{\dagger}_{9}$-NH_3	0.044
1162.58260	1162.58303	$y^{\dagger}_{9}$	0.370
1171.67345	1171.67323	a_{10}	-0.188
1182.64182	1182.64203	$b^{\dagger}_{10}$-NH_3	0.173
1185.58735	1185.58679	y_{10}-$2NH_3$	-0.472
1199.66836	1199.66756	b_{10}	-0.671
1202.61390	1202.61360	y_{10}-NH_3	-0.249
1211.66836	1211.66782	$a^{\dagger}_{10}{}^{\dagger}_{10}$	-0.450
1219.64044	1219.64013	y_{10}	-0.254
1222.63674	1222.63630	$b^{\dagger}_{10}$-NH_3	-0.356
1239.66328	1239.66306	$b^{\dagger}_{10}$	-0.177
1347.73541	1347.73655	$[M+H]^{1+}$	0.849
		Mean	-0.024
		St. Dv.	0.428

Table B-7. DR(674)-ECD(694) error analysis of the KM-11 peptide reacted in PBS for the precursor ion $[M+C_2O+2H]^{2+}$. * indicates the ions used for calibration.

THEORETICAL *(m/z)*	EXPERIMENTAL *(m/z)*	ASSIGNMENTS	ERROR (ppm)
* 243.18154	243.18159	c_2	0.001
450.26413	450.26419	c_7^{2+}	0.133
517.31193	517.31189	$c^{\dagger}_{4}{}^{\bullet}$-$H_2O$	-0.087
535.32250	535.32251	$c^{\dagger}_{4}{}^{\bullet}$	0.001
536.33033	536.33033	$c^{\dagger}_{4}$	0.018
579.26356	579.26345	y_5-$2NH_3$	-0.190

THEORETICAL *(m/z)*	EXPERIMENTAL *(m/z)*	ASSIGNMENTS	ERROR (ppm)
620.33528	620.33498	$b^{\dagger}_{10}{}^{2+}$	-0.484
624.39399	624.39404	c_5	0.080
628.34464	628.34402	$c^{\dagger}_{10}{}^{2+\bullet}$	-0.986
645.37051	645.37052	$c^{\dagger}_{5}{}^{\bullet}$-$H_2O$	0.008
646.37834	646.37798	$c^{\dagger}_{5}$-H_2O	-0.557
663.38108	663.38107	$c^{\dagger}_{5}{}^{\bullet}$	-0.015
664.38891	664.38893	$c^{\dagger}_{5}$	0.038
685.36352	685.36330	$[M^{\dagger}$-H_2O+2H$]^{2+}$	-0.321
694.36880	694.36873	$[M^{\dagger}$+2H$]^{2+}$	-0.101
696.37020	696.36995	$a^{\dagger}_{5}$-2NH_3-H_2O	-0.359
707.32214	707.32266	y_6-2NH_3	0.735
752.45257	752.45253	c_6	-0.053
773.42909	773.42918	$c^{\dagger}_{6}{}^{\bullet}$-$H_2O$	0.110
774.43692	774.43692	$c^{\dagger}_{6}$-H_2O	0.000
791.43966	791.43970	$c^{\dagger}_{6}{}^{\bullet}$	0.051
792.44749	792.44749	$c^{\dagger}_{6}$	0.006
921.50533	921.50529	$c^{\dagger}_{7}$-H_2O	-0.043
938.50807	938.50756	$c^{\dagger}_{7}{}^{\bullet}$	-0.543
939.51590	939.51595	$c^{\dagger}_{7}$	0.059
1042.57067	1042.57050	$a^{\dagger}_{8}$	-0.168
1072.54485	1072.54482	$z^{\dagger}_{9}{}^{\bullet}$-$C_3H_6S$	-0.028
1086.58431	1086.58423	b_9	-0.069
1125.59520	1125.59540	$c^{\dagger}_{9}$-H_2O	0.178
1143.60577	1143.60586	$c^{\dagger}_{9}$	0.083
1146.56388	1146.56357	$z^{\dagger}_{9}{}^{\bullet}$	-0.270
1162.58260	1162.58262	$y^{\dagger}_{9}$	0.017
1238.67926	1238.67922	$c^{\dagger}_{10}$-H_2O	-0.032
1256.68982	1256.68990	$c^{\dagger}_{10}$	0.060
1296.70856	1296.70890	$[M^{\dagger}$-H_2O-C_3H_6S+2H$]^{1+\bullet}$	0.262
1325.70557	1325.70595	$[M^{\dagger}$-H_2O-$^{\bullet}CONH_2$+H$]^{1+}$	0.287
1325.70611	1325.70595	$[M^{\dagger}$-$^{\bullet}CONH_2$-H_2O+H$]^{1+}$	-0.124
1330.70886	1330.70957	$[M$-NH_3+H$]^{1+}$	0.537
1331.71668	1331.71829	$[M$-NH_3+2H$]^{1+\bullet}$	0.788
1343.71613	1343.71645	$[M^{\dagger}$-$^{\bullet}CONH_2$ +H$]^{1+}$	0.238
1370.72758	1370.72768	$[M^{\dagger}$-2H_2O-NH_3 +H$]^{1+}$	0.073
1387.73032	1387.73086	$[M^{\dagger}$ +H$]^{1+}$	0.389
1388.73870	1388.73846	$[M^{\dagger}$ +2H$]^{1+\bullet}$	-0.173
		mean	-0.003
		St. Dv.	0.458

Table B-8. DR(695)-ECD(715) error analysis of the AcKM-11 peptide reacted in MeOH/H_2O (50:50) for the precursor ion $[M+C_2O+2H]^{2+}$. * indicates the ions used for calibration.

THEORETICAL *(m/z)*	EXPERIMENTAL *(m/z)*	ASSIGNMENTS	ERROR (ppm)
285.19211	285.19211	c_2	0.018
319.17983	319.17982	y_3	-0.031
466.24824	466.24825	y_4	0.021
537.33815	537.33823	$c_4^{\bullet}$	0.149
538.34597	538.34599	c_4	0.028
544.80362	544.80371	c_8^{2+}	0.169
561.79748	561.79747	y_9^{2+}	-0.018
573.31435	573.31431	c_9^{2+}	-0.066
577.33307	577.33304	$c^{\dagger}_4{}^{\bullet}$	-0.043
578.34089	578.34084	$c^{\dagger}_4$	-0.086
613.31665	613.31661	y_5	-0.065
641.34056	641.34056	$b^{\dagger}_{10}{}^{2+}$	-0.004
665.39673	665.39670	$c_5^{\bullet}$	-0.045
665.85779	665.85812	$[M- CH_3CONH_2+2H]^{2+}$	0.491
666.40455	666.40456	c_5	0.008
686.86335	686.86391	$[M^{\dagger}- HCONH_2+2H]^{2+}$	0.815
695.37662	695.37665	$[M^{\dagger}+2H]^{2+}$	0.039
705.39165	705.39163	$c^{\dagger}_5{}^{\bullet}$	-0.021
706.39947	706.39946	$c^{\dagger}_5$	-0.014
706.86081	706.86082	$[M^{\dagger}-NH_3+2H]^{2+}$	0.014
715.37408	715.37404	$[M^{\dagger}+2H]^{2+}$	-0.056
716.39642	716.39576	a_6-2NH3	-0.914
777.43659	777.43718	b_6	0.759
793.45531	793.45574	$c_6^{\bullet}$	0.542
794.46313	794.46320	c_6	0.082
833.45023	833.45041	$c^{\dagger}_6{}^{\bullet}$	0.222
834.45805	834.45812	$c^{\dagger}_6$	0.084
941.53155	941.53150	c_7	-0.048
964.49991	964.49960	$b^{\dagger}_7$	-0.327
966.48657	966.48644	y_8	-0.135
981.52646	981.52648	$c^{\dagger}_7$	0.020
1032.54994	1032.54984	$z_9^{\bullet}$-C_3H_6S	-0.097
1084.58124	1084.58164	$a^{\dagger}_8$	0.369
1088.59995	1088.59999	c_8	0.032
1106.56896	1106.56890	$z_9^{\bullet}$	-0.054
1111.56832	1111.56769	$b^{\dagger}_8$	-0.571
1122.58768	1122.58714	y_9	-0.481
1128.59487	1128.59512	b_9	0.222
1145.62142	1145.62146	c_9	0.039
1146.56388	1146.56306	$z^{\dagger}_9{}^{\bullet}$	-0.715
1185.61633	1185.61615	$c^{\dagger}_9$	-0.152
1220.63367	1220.63375	$a^{\dagger}_{10}$-$2NH_3$	0.066
1241.67893	1241.67895	b_{10}	0.016
1254.68620	1254.68530	$c^{\dagger}_{10}$-$^{\bullet}CONH_2$	-0.721
1257.69765	1257.69746	$c_{10}^{\bullet}$	-0.151
1258.70547	1258.70583	c_{10}	0.282

THEORETICAL *(m/z)*	EXPERIMENTAL *(m/z)*	ASSIGNMENTS	ERROR (ppm)
1281.67385	1281.67344	$b^{\dagger}_{10}$	-0.316
1298.70039	1298.70020	$c^{\dagger}_{10}$	-0.146
1331.71668	1331.71769	$[M\text{-}CH_3CONH_2+2H]^{1+\bullet}$	0.758
1356.72969	1356.72862	$[M^{\dagger}\text{-}C_3H_6S+2H]^{1+\bullet}$	-0.789
1385.72719	1385.72746	$[M^{\dagger}\text{-}HCONH_2+2H]^{1+\bullet}$	0.195
1389.74597	1389.74559	$[M+H]^{1+}$	-0.273
	1402.75360	?	
1413.72272	1413.72194	$[M^{\dagger}\text{-}NH_3+2H]^{1+\bullet}$	-0.548
1430.749260	1430.74855	$[M^{\dagger}+2H]^{1+\bullet}$	-0.496
		mean	-0.038
		St. Dv.	0.369

Table B-9. CAD(715) error analysis of the AcKM-11 peptide reacted in MeOH/H_2O (50:50) for the precursor ion $[M+C_2O+2H]^{2+}$. * indicates the ions used for calibration.

THEORETICAL *(m/z)*	EXPERIMENTAL *(m/z)*	ASSIGNMENTS	ERROR (ppm)
302.15329	302.15323	$y_3\text{-}NH_3$	-0.199
319.17983	319.17980	y_3	-0.094
407.24012	407.24009	$b_3\text{-}NH_3$	-0.086
424.26667	424.26667	b_3	0.000
436.26667	436.26657	$a^{\dagger}_3$	-0.229
449.22170	449.22169	$y_4\text{-}NH_3$	-0.022
451.23759	451.23756	$(a^{\dagger}_7\text{-}H_2O\text{-}NH_3)^{2+}$	-0.055
454.24287	454.24291	$(b_7\text{-}NH_3)^{2+}$	0.092
462.75614	462.75604	b_7^{2+}	-0.216
464.26159	464.26165	$b^{\dagger}_3$	0.129
466.24824	466.24823	y_4	-0.021
468.75614	468.75633	$a^{\dagger}_7{}^{2+}$	0.400
482.75360	482.75359	$b^{\dagger}_7{}^{2+}$	-0.016
513.77989	513.77938	$(a_8\text{-}NH_3)^{2+}$	-0.989
521.31943	521.31942	b_4	-0.019
522.29289	522.29287	a_8^{2+}	-0.034
527.77707	527.77706	$(b_8\text{-}NH_3)^{2+}$	-0.025
536.29035	536.29039	b_8^{2+}	0.084
542.29035	542.29042	$a^{\dagger}_8{}^{2+}$	0.134
547.28252	547.28246	$(b^{\dagger}_8\text{-}H_2O)^{2+}$	-0.110
547.77453	547.77467	$(b^{\dagger}_8\text{-}NH_3)^{2+}$	0.256
556.28780	556.28787	$(b_9\text{-}NH_3)^{2+}$	0.120
561.79748	561.79781	y_9^{2+}	0.587
564.80107	564.80115	b_9^{2+}	0.133
570.80108	570.80109	$a^{\dagger}_9{}^{2+}$	0.022
575.79325	575.79334	$(b^{\dagger}_9\text{-}H_2O)^{2+}$	0.156
576.28526	576.28529	$(b^{\dagger}_9\text{-}NH_3)^{2+}$	0.052
584.79853	584.79854	$b^{\dagger}_9{}^{2+}$	0.013
596.29011	596.29017	$y_5\text{-}NH_3$	0.101

THEORETICAL *(m/z)*	EXPERIMENTAL *(m/z)*	ASSIGNMENTS	ERROR (ppm)
598.83265	598.83216	$(a_{10}\text{-}NH_3)^{2+}$	-0.815
601.81059	601.81062	$(y_{10}\text{-}NH_3)^{2+}$	0.050
603.82455	603.82464	$(b_{10}\text{-}H_2O\text{-}NH_3)^{2+}$	0.149
607.34565	607.34561	a_{10}^{2+}	-0.063
609.82455	609.82426	$(a^{\dagger}_{10}\text{-}H_2O\text{-}NH_3)^{2+}$	-0.476
610.32386	610.32397	y_{10}^{2+}	0.180
612.82983	612.82995	$(b_{10}\text{-}NH_3)^{2+}$	0.191
613.31665	613.31675	y_5	0.163
618.33782	618.33793	$(a^{\dagger}_{10}\text{-}H_2O)^{2+}$	0.174
621.34311	621.34309	b_{10}^{2+}	-0.024
627.34311	627.34324	$a^{\dagger}_{10}{}^{2+}$	0.211
630.32132	630.32139	$y^{\dagger}_{10}{}^{2+}$	0.115
632.33528	632.33525	$(b^{\dagger}_{10}\text{-}H_2O)^{2+}$	-0.047
632.82729	632.82740	$(b^{\dagger}_{10}\text{-}NH_3)^{2+}$	0.174
641.34056	641.34066	$b^{\dagger}_{10}{}^{2+}$	0.152
649.37801	649.37810	b_5	0.139
661.37801	661.37817	$a^{\dagger}_5$	0.242
664.35289	664.35265	$[M\text{-}HCONH_2\text{-}NH_3\text{+}2H]^{2+}$	-0.366
674.37134	674.37144	$[M\text{-}CH_2CO\text{+}2H]^{2+}$	0.148
678.35008	678.35013	$[M\text{-}2NH_3\text{+}2H]^{2+}$	0.077
683.85807	683.85827	$[M^{\dagger}\text{-}CH_3CONH_2\text{+}2H]^{2+}$	0.296
686.86335	686.86346	$[M^{\dagger}\text{-}HCONH_2\text{+}2H]^{2+}$	0.160
689.34225	689.34223	$[M^{\dagger}\text{-}H_2O\text{-}2NH_3\text{+}2H]^{2+}$	-0.033
689.37293	689.37300	$b^{\dagger}_5$	0.109
692.86335	692.86347	$[M^{\dagger}\text{-}HCONH_2\text{+}2H]^{2+}$	0.170
694.36880	694.36929	$[M^{\dagger}\text{-}CH_2CO\text{+}2H]^{2+}$	0.709
697.85553	697.85524	$[M^{\dagger}\text{-}H_2O\text{-}NH_3\text{+}2H]^{2+}$	-0.416
698.34754	698.34778	$[M^{\dagger}\text{-}2NH_3\text{+}2H]^{2+}$	0.344
699.36987	699.36982	$a_6\text{-}3NH_3$	-0.071
706.36880	706.36825	$[M^{\dagger}\text{-}H_2O\text{+}2H]^{2+}$	-0.779
706.86081	706.86072	$[M^{\dagger}\text{-}NH_3\text{+}2H]^{2+}$	-0.127
707.32214	707.32212	$y_6\text{-}2NH_3$	-0.028
724.34869	724.34862	y_6	-0.097
741.37523	741.37468	y_6	-0.742
771.42602	771.42573	$a^{\dagger}_6\text{-}H_2O$	-0.382
777.43659	777.43653	b_6	-0.077
789.43659	789.43634	$a^{\dagger}_6$	-0.317
799.42094	799.42087	$b^{\dagger}_6\text{-}H_2O$	-0.088
817.43151	817.43136	$b^{\dagger}_6$	-0.177
918.49443	918.49481	$a^{\dagger}_7\text{-}H_2O$	0.408
924.50500	924.50506	b_7	0.065
932.43348	932.43380	$y_8\text{-}2NH_3$	0.343
936.50500	936.50499	$a^{\dagger}_7$	-0.011
946.48935	946.48984	$b^{\dagger}_7\text{-}H_2O$	0.518
947.47337	947.47343	$b^{\dagger}_7\text{-}NH_3$	0.063
949.46003	949.46028	$y_8\text{-}NH_3$	0.263
964.49991	964.50001	$b^{\dagger}_7$	0.098
966.48657	966.48684	y_8	0.279

THEORETICAL *(m/z)*	EXPERIMENTAL *(m/z)*	ASSIGNMENTS	ERROR (ppm)
1043.57849	1043.57834	a_8	-0.149
1054.54687	1054.54668	b_8-NH_3	-0.175
1066.54687	1066.54724	a_9-$2NH_3$	0.352
1071.57341	1071.57316	b_8	-0.233
1083.57341	1083.57311	$a^{\dagger}_8$	-0.277
1093.55776	1093.55784	$b^{\dagger}_8$-H_2O	0.073
1094.54178	1094.54156	$b^{\dagger}_8$-NH_3	-0.201
1105.56114	1105.56091	y_9-NH_3	-0.208
1122.58768	1122.58769	y_9	0.009
1128.59487	1128.59508	b_9	0.186
1133.55267	1133.55287	$b^{\dagger}_9$-H_2O-NH_3	0.172
1140.59487	1140.59486	$a^{\dagger}_9$	-0.009
1150.57922	1150.57929	$b^{\dagger}_9$-H_2O	0.061
1151.56324	1151.56369	$b^{\dagger}_9$-NH_3	0.391
1168.58978	1168.59012	$b^{\dagger}_9$	0.287
1185.58735	1185.58728	y_{10}-$2NH_3$	-0.059
1219.64044	1219.64055	y_{10}	0.090
1224.65239	1224.65191	$b^{\dagger}_{10}$-NH_3	-0.388
1225.58227	1225.58163	$y^{\dagger}_{10}$-$2NH_3$	-0.518
1241.67893	1241.67909	b_{10}	0.129
1242.60881	1242.60847	$y^{\dagger}_{10}$-NH_3	-0.274
1253.67893	1253.67852	$a^{\dagger}_{10}$	-0.327
1259.63535	1259.63471	$y^{\dagger}_{10}$	-0.512
1263.66328	1263.66258	$b^{\dagger}_{10}$-H_2O	-0.554
1264.64730	1264.64779	$b^{\dagger}_{10}$-NH_3	0.387
1281.67385	1281.67343	$b^{\dagger}_{10}$	-0.324
1389.74597	1389.74584	$[M+H]^{1+}$	-0.094
		mean	-0.011
		St. Dv.	0.358

Table B-10. CAD(715) error analysis of the AcKM-11 peptide reacted in PBS for the precursor ion $[M+C_2O+2H]^{2+}$. * indicates the ions used for calibration.

THEORETICAL *(m/z)*	EXPERIMENTAL *(m/z)*	ASSIGNMENTS	ERROR (ppm)
268.16556	268.16556	b_2	0.000
319.17983	319.17951	y_3	-1.003
466.24824	466.24871	y_4	1.008
403.22141	403.22111	$a^{\dagger}_3$-$2NH_3$	-0.744
460.24977	460.24985	$(a^{\dagger}_7$-$H_2O)^{2+}$	0.168
482.75360	482.75312	b_9^{2+}	-0.994
607.34565	607.34554	a_{10}^{2+}	-0.178
612.82983	612.82941	$(b_{10}$-$NH_3)^{2+}$	-0.690
613.31665	613.31610	y_5	-0.897
618.33782	618.33717	$(a^{\dagger}_{10}$-$H_2O)^{2+}$	-1.055
621.34311	621.34287	b_{10}^{2+}	-0.378
621.80804	621.80737	$(y^{\dagger}_{10}$-$NH_3)^{2+}$	-1.086

THEORETICAL *(m/z)*	EXPERIMENTAL *(m/z)*	ASSIGNMENTS	ERROR (ppm)
623.82201	623.82134	$(b^{\dagger}_{10}\text{-}H_2O\text{-}NH_3)^{2+}$	-1.070
627.34311	627.34251	$a^{\dagger}_{10}{}^{2+}$	-0.948
630.32132	630.32074	$y^{\dagger}_{10}{}^{2+}$	-0.916
632.33528	632.33469	$(b^{\dagger}_{10}\text{-}H_2O)^{2+}$	-0.933
632.82729	632.82675	$(b^{\dagger}_{10}\text{-}NH_3)^{2+}$	-0.853
641.34056	641.34019	$b^{\dagger}_{10}{}^{2+}$	-0.581
649.37801	649.37814	b_5	0.200
661.37801	661.37779	$a^{\dagger}_5$	-0.333
664.35289	664.35230	$[M\text{-}2NH_3\text{+}2H]^{2+}$	-0.893
671.36236	671.36197	$b^{\dagger}_5\text{-}H_2O$	-0.581
683.85807	683.85773	$[M^{\dagger}\text{-}H_2O\text{-}NH_3\text{+}2H]^{2+}$	-0.494
686.86335	686.86345	$[M\text{-}NH_3\text{+}2H]^{2+}$	0.146
689.34225	689.34245	$[M^{\dagger}\text{-}H_2O\text{-}2NH_3\text{+}2H]^{2+}$	0.287
689.37293	689.37289	$b^{\dagger}_5$	-0.051
692.86335	692.86360	$[M^{\dagger}\text{-}\ NH_3\text{+}2H]^{2+}$	0.357
697.85552	697.85583	$[M^{\dagger}\text{-}\ NH3\text{-}H_2O\text{+}2H]^{2+}$	0.437
697.85553	697.85583	$[M^{\dagger\dagger}\text{-}H_2O\text{-}NH_3\text{+}2H]^{2+}$	0.430
698.34754	698.34745	$[M^{\dagger}\text{-}2NH_3\text{+}2H]^{2+}$	-0.129
706.36880	706.36900	$[M^{\dagger}\text{-}H_2O\text{+}2H]^{2+}$	0.283
706.86081	706.86102	$[M^{\dagger}\text{-}NH_3\text{+}2H]^{2+}$	0.297
707.32214	707.32226	$y_6\text{-}2NH_3$	0.170
724.34869	724.34861	$y_6\text{-}NH_3$	-0.110
741.37523	741.37539	y_6	0.216
771.42602	771.42677	$a^{\dagger}_6\text{-}H_2O$	0.966
777.43659	777.43675	b_6	0.206
800.40496	800.40526	$b^{\dagger}_6\text{-}NH_3$	0.375
817.43151	817.43210	$b^{\dagger}_6$	0.728
918.49443	918.49516	$a^{\dagger}_7\text{-}H_2O$	0.789
929.46281	929.46342	$b^{\dagger}_7\text{-}H_2O\text{-}NH_3$	0.662
964.49991	964.50080	$b^{\dagger}_7$	0.923
966.48657	966.48731	y_8	0.766
1066.57067	1066.57071	$a^{\dagger}_8\text{-}H_2O$	0.033
1094.54178	1094.54279	$b^{\dagger}_8\text{-}NH_3$	0.923
1111.56833	1111.56847	$b^{\dagger}_8$	0.126
1128.59487	1128.59486	b_9	-0.009
1145.55605	1145.55544	$y^{\dagger}_9\text{-}NH_3$	-0.532
1150.57922	1150.57997	$b^{\dagger}_9\text{-}H_2O$	0.652
1166.60198	1166.60296	$a^{\dagger}_{10}\text{-}2NH_3\text{-}2H_2O$	0.844
1168.58978	1168.59012	$b^{\dagger}_9$	0.291
1202.61390	1202.61385	$y_{10}\text{-}NH_3$	-0.042
1213.68402	1213.68319	a_{10}	-0.680
1219.64044	1219.64003	y_{10}	-0.336
1224.59824	1224.59791	$y^{\dagger}_{10}\text{-}H_2O\text{-}NH_3$	-0.274
1225.58227	1225.58215	$y^{\dagger}_{10}\text{-}2NH_3$	-0.094
1259.63535	1259.63567	$y^{\dagger}_{10}$	0.254
1281.67385	1281.67259	$b^{\dagger}_{10}$	-0.983
1389.745970	1389.74587	$[M+H]^{1+}$	-0.072

mean	-0.046
St. Dv.	0.586

Table B-11. DR(674)-ECD(703) error analysis of the KM-11 peptide reacted in MeOH/H_2O (50:50) for the precursor ion $[M+C_2H_2O_2+2H]^{2+}$. * indicates the ions used for calibration.

THEORETICAL *(m/z)*	EXPERIMENTAL *(m/z)*	ASSIGNMENTS	ERROR (ppm)
* 495.32758	495.32758	$c_4^{\bullet}$	-0.010
496.33541	496.33541	c_4	0.000
535.32250	535.32252	$c^{\ddagger}_4{}^{\bullet}$-$H_2O$	0.037
536.33033	536.33033	$c^{\ddagger}_4$-H_2O	0.009
553.33307	553.33305	$c^{\ddagger}_4{}^{\bullet}$	-0.027
554.34089	554.34092	$c^{\ddagger}_4$	0.054
561.79748	561.79759	y_9^{2+}	0.196
623.38617	623.38616	$c_5^{\bullet}$	-0.008
* 624.39399	624.39400	c_5	0.016
663.38108	663.38107	$c^{\ddagger}_5{}^{\bullet}$-$H_2O$	-0.015
664.38891	664.38893	$c^{\ddagger}_5$-H_2O	0.038
681.39165	681.39161	$c^{\ddagger}_5{}^{\bullet}$	-0.051
682.39947	682.39948	$c^{\ddagger}_5$	0.015
694.36880	694.36883	$[M^{\dagger}$-$H_2O+2H]^{2+}$	0.043
703.37408	703.37410	$[M^{\ddagger}+2H]^{2+}$	0.028
705.35410	705.35398	y_6-$2H_2O$	-0.170
751.44475	751.44479	$c_6^{\bullet}$	0.060
* 752.45257	752.45258	c_6	0.013
791.43966	791.43963	$c^{\ddagger}_6{}^{\bullet}$-$H_2O$	-0.038
792.44749	792.44760	$c^{\ddagger}_6$-H_2O	0.145
809.45023	809.45032	$c^{\ddagger}_6{}^{\bullet}$	0.117
810.45805	810.45808	$c^{\ddagger}_6$	0.037
898.51315	898.51267	$c_7^{\bullet}$	-0.540
* 899.52098	899.52103	c_7	0.056
939.51590	939.51581	$c^{\ddagger}_7$-H_2O	-0.090
956.51864	956.51863	$c^{\ddagger}_7{}^{\bullet}$	-0.005
957.52646	957.52649	$c^{\ddagger}_7$	0.031
*1046.58939	1046.58950	c_8	0.105
1060.58124	1060.58119	$a^{\ddagger}_8$-H_20	-0.047
1072.54485	1072.54467	$z^{\ddagger}_9{}^{\bullet}$-$C_3H_6S$	-0.168
1086.58431	1086.58412	b_9	-0.170
*1103.61085	1103.61091	c_9	0.054
1104.59487	1104.59496	$c^{\ddagger}_8$-	0.081
1106.56896	1106.56985	$z_9^{\bullet}$	0.804
1143.60577	1143.60598	$c^{\ddagger}_9$-H_2O	0.188
1146.56388	1146.56382	$z^{\ddagger}_9{}^{\bullet}$-$H_2O$	-0.048
1161.61633	1161.61633	$c^{\ddagger}_9$	0.000
1164.57444	1164.57449	$z^{\ddagger}_9{}^{\bullet}$	0.043
*1216.69491	1216.69483	c_{10}	-0.066
1256.68982	1256.68974	$c^{\ddagger}_{10}$-H_2O	-0.068

THEORETICAL *(m/z)*	EXPERIMENTAL *(m/z)*	ASSIGNMENTS	ERROR (ppm)
1274.70039	1274.70030	$c^{\ddagger}_{10}$	-0.071
1303.72177	1303.72055	$[M\text{-}HCONH_2+2H]^{1+\bullet}$	-0.510
1331.71668	1331.71673	$[M\text{-}NH_3+2H]^{1+\bullet}$	0.038
1343.71614	1343.71626	$[M^{\ddagger}\text{-}H_2O\text{-}^{\bullet}CONH_2+1H]^{1+}$	0.089
*1347.73540	1347.73557	$[M+H]^{1+}$	0.126
1370.72785	1370.72773	$[M^{\ddagger}\text{-}2H_2O+H]^{1+}$	0.088
1388.73815	1388.73812	$[M^{\ddagger}\text{-}H_2O+2H]^{1+\bullet}$	0.022
*1405.74089	1405.74103	$[M^{\ddagger}+H]^{1+}$	0.103
		mean	-0.011
		St. Dv.	0.265

Table B-12. CAD (703) error analysis of the KM-11 peptide reacted in MeOH/H_2O (50:50) for the precursor ion $[M+C_2H_2O_2+2H]^{2+}$. * indicates the ions used for calibration.

THEORETICAL *(m/z)*	EXPERIMENTAL *(m/z)*	ASSIGNMENTS	ERROR (ppm)
* 226.15500	226.15506	b_2	0.287
245.13183	245.13186	$y_2\text{-}NH_3$	0.122
262.15837	262.15841	y_2	0.153
302.15329	302.15333	$y_3\text{-}NH_3$	0.132
319.17983	319.17999	y_3	0.501
365.22956	365.22954	$b_3\text{-}NH_3$	-0.055
* 382.25610	382.25614	b_3	0.092
404.24045	404.24045	$b^{\ddagger}_3\text{-}2H_2O$	-0.012
422.25102	422.25102	$b^{\ddagger}_3\text{-}H_2O$	0.000
441.75086	441.75086	b_7^{2+}	0.005
449.22170	449.22174	$y_4\text{-}NH_3$	0.089
453.23504	453.23508	$(b^{\ddagger}_7\text{-}H_2O\text{-}NH_3)^{2+}$	0.083
461.74831	461.74834	$(b^{\ddagger}_7\text{-}H_2O)^{2+}$	0.054
* 466.24824	466.24833	y_4	0.193
479.30887	479.30876	b_4	-0.219
501.28761	501.28761	a_8^{2+}	0.004
506.27978	506.27968	$(b_8\text{-}H_2O)^{2+}$	-0.198
506.77179	506.77178	$(b_8\text{-}NH_3)^{2+}$	-0.020
512.77179	512.77174	$(a^{\ddagger}_8\text{-}H_2O\text{-}NH_3)^{2+}$	-0.098
515.28506	515.28513	b_8^{2+}	0.130
521.28506	521.28516	$(a^{\ddagger}_8\text{-}H_2O)^{2+}$	0.187
526.27724	526.27751	$(b_9\text{-}H_2O\text{-}NH_3)^{2++}$	0.517
534.79051	534.79052	$(b_9\text{-}H_2O)^{2+}$	0.019
535.28252	535.28266	$(b^{\ddagger}_8\text{-}H_2O)^{2+}$	0.262
543.79579	543.79582	b_9^{2+}	0.050
544.28780	544.28794	$b^{\ddagger}_8{}^{2+}$	0.253
554.78797	554.78786	$(b^{\ddagger}_9\text{-}2H_2O)^{2+}$	-0.194
555.27998	555.27996	$(b^{\ddagger}_9\text{-}H_2O\text{-}NH_3)^{2+}$	-0.032
556.28781	556.28765	$b_5\text{-}3NH_3$	-0.288
563.79325	563.79331	$(b^{\ddagger}_9\text{-}H_2O)^{2+}$	0.106

THEORETICAL *(m/z)*	EXPERIMENTAL *(m/z)*	ASSIGNMENTS	ERROR (ppm)
564.28526	564.28546	$(b^{\ddagger}_{9}\text{-}NH_3)^{2+}$	0.354
572.79853	572.79868	$b^{\ddagger}_{9}{}^{2+}$	0.258
573.81399	573.81414	$(b_{10}\text{-}2H_2O\text{-}NH_3)^{2+}$	0.270
577.33508	577.33522	$(a_{10}\text{-}H_2O)^{2+}$	0.237
577.82736	577.82725	$(a_{10}\text{-}NH_3)^{2+}$	-0.199
582.81927	582.81942	$(b_{10}\text{-}H_2O\text{-}NH_3)^{2+}$	0.261
586.34037	586.34054	$a_{10}{}^{2+}$	0.293
590.34090	590.34121	$b_5\text{-}NH_3$	0.525
591.33254	591.33272	$(b_{10}\text{-}H_2O)^{2+}$	0.304
591.82455	591.82472	$(b_{10}\text{-}NH_3)^{2+}$	0.287
* 596.29011	596.29028	$y_5\text{-}NH_3$	0.285
597.33254	597.33272	$(a^{\ddagger}_{10}\text{-}2H_2O)^{2+}$	0.301
597.82455	597.82467	$(a^{\ddagger}_{10}\text{-}H_2O\text{-}NH_3)^{2+}$	0.201
600.33782	600.33795	$b_{10}{}^{2+}$	0.212
602.81673	602.81697	$(b^{\ddagger}_{10}\text{-}2H_2O\text{-}NH_3)^{2+}$	0.406
606.33782	606.33792	$(a^{\ddagger}_{10}\text{-}H_2O)^{2+}$	0.161
607.36744	607.36750	b_5	0.091
610.32386	610.32389	$y_{10}{}^{2+}$	0.049
611.33000	611.33006	$(b^{\ddagger}_{10}\text{-}2H_2O)^{2+}$	0.102
611.82201	611.82214	$(b^{\ddagger}_{10}\text{-}H_2O\text{-}NH_3)^{2+}$	0.217
* 613.31665	613.31678	y_5	0.212
615.34311	615.34320	$a^{\ddagger}_{10}{}^{2+}$	0.150
620.33528	620.33534	$(b^{\ddagger}_{10}\text{-}H_2O)^{2+}$	0.097
629.34056	629.34060	$b^{\ddagger}_{10}{}^{2+}$	0.060
647.36236	647.36254	$b^{\ddagger}_{5}\text{-}H_2O$	0.278
648.33951	648.33967	$[M\text{-}H_2O\text{-}2NH_3\text{+}H]^{2+}$	0.242
656.85279	656.85295	$[M\text{-}H_2O\text{-}NH_3\text{+}2H]^{2+}$	0.251
657.34479	657.34492	$[M\text{-}2NH_3\text{+}2H]^{2+}$	0.190
665.85807	665.85824	$[M\text{-}NH_3\text{+}2H]^{2+}$	0.258
668.33697	668.33737	$[M^{\ddagger}\text{-}H_2O\text{-}2NH_3\text{+}2H]^{2+}$	0.599
671.85807	671.85838	$[M^{\ddagger}\text{-}H_2O\text{-}HCONH_2\text{+}2H]^{2+}$	0.465
674.37134	674.37134	$[M+H]^{2+}$	0.000
676.85025	676.85000	$[M^{\ddagger}\text{-}2H_2O\text{-}NH_3\text{+}2H]^{2+}$	-0.369
677.34225	677.34207	$[M^{\ddagger}\text{-}H_2O\text{-}2NH_3\text{+}H]^{2+}$	-0.269
685.36352	685.36319	$[M^{\ddagger}\text{-}2H_2O\text{+}H]^{2+}$	-0.474
685.85553	685.85529	$[M^{\ddagger}\text{-}H_2O\text{-}NH_3\text{+}2H]^{2+}$	-0.350
694.36880	694.36860	$[M^{\ddagger}\text{-}H_2O\text{+}2H]^{2+}$	-0.288
694.86081	694.86030	$[M^{\ddagger}\text{-}NH_3\text{+}2H]^{2+}$	-0.734
707.32214	707.32217	$y_6\text{-}2NH_3$	0.042
707.43111	707.43105	a_6	-0.085
718.39948	718.39939	$b_6\text{-}NH_3$	-0.125
* 724.34869	724.34863	$y_6\text{-}NH_3$	-0.083
735.42602	735.42599	b_6	-0.048
757.41038	757.41057	$b^{\ddagger}_{6}\text{-}2H_2O$	0.257
758.39440	758.39463	$b^{\ddagger}_{6}\text{-}H_2O\text{-}NH_3$	0.310
775.42094	775.42092	$b^{\ddagger}_{6}\text{-}H_2O$	-0.026
793.43151	793.43188	$b^{\ddagger}_{6}$	0.473
854.49952	854.49961	a_7	0.105

THEORETICAL *(m/z)*	EXPERIMENTAL *(m/z)*	ASSIGNMENTS	ERROR (ppm)
865.46789	865.46813	b_7-NH_3	0.277
* 882.49443	882.49466	b_7	0.255
894.49443	894.49450	$a^{\ddagger}_7$-H_2O	0.073
904.47879	904.47932	$b^{\ddagger}_7$-$2H_2O$	0.592
905.46281	905.46306	$b^{\ddagger}_7$-H_2O-NH_3	0.282
922.48935	922.48953	$b^{\ddagger}_7$-H_2O	0.195
932.43348	932.43378	y_8-$2NH_3$	0.322
940.49991	940.50006	$b^{\ddagger}_7$	0.154
* 966.48657	966.48688	y_8	0.321
1001.56793	1001.56833	a_8	0.399
1012.53630	1012.53680	b_8-NH_3	0.494
1051.54720	1051.54734	$b^{\ddagger}_8$-$2H_2O$	0.138
1052.53121	1052.53117	$b^{\ddagger}_8$-H_2O-NH_3	-0.043
1069.55776	1069.55781	$b^{\ddagger}_8$-H_2O	0.047
*1086.58431	1086.58458	b_9	0.253
1108.56866	1108.56877	$b^{\ddagger}_9$-$2H_2O$	0.104
1109.55267	1109.55367	$b^{\ddagger}_9$-H_2O-NH_3	0.897
1110.55669	1110.55591	$b^{\ddagger}_9$-$2NH_3$	-0.707
*1122.58768	1122.58805	y_9	0.330
1126.57922	1126.57958	$b^{\ddagger}_9$-H_2O	0.320
1144.58978	1144.58909	$b^{\ddagger}_9$	-0.607
1162.58260	1162.58313	$y^{\ddagger}_9$-H_2O	0.456
1171.67345	1171.67380	a_{10}	0.299
1182.64182	1182.64211	b_{10}-NH_3	0.245
1185.58735	1185.58624	y_{10}-$2NH_3$	-0.936
1199.66836	1199.66843	b_{10}	0.054
1202.61390	1202.61393	y_{10}-NH_3	0.025
1211.66836	1211.66747	$a^{\ddagger}_{10}$-H_2O	-0.739
*1219.64044	1219.63995	y_{10}	-0.402
1221.65271	1221.65253	$b^{\ddagger}_{10}$-$2H_2O$	-0.151
1222.63674	1222.63693	$b^{\ddagger}_{10}$-H_2O-NH_3	0.159
1239.66328	1239.66286	$b^{\ddagger}_{10}$-H_2O	-0.339
*1257.67385	1257.67300	$b^{\ddagger}_{10}$	-0.672
		mean	0.051
		St. Dv.	0.369

Table B-13. CAD (703) error analysis of the KM-11 peptide reacted in PBS for the precursor ion $[M+C_2H_2O_2+2H]^{2+}$. * indicates the ions used for calibration.

THEORETICAL *(m/z)*	EXPERIMENTAL *(m/z)*	ASSIGNMENTS	ERROR (ppm)
* 226.15500	226.15501	b_2	0.066
319.17983	319.17967	y_3	-0.501
365.22956	365.22923	b_3-NH_3	-0.904
382.25610	382.25591	b_3	-0.510
404.24045	404.24041	$b^{\ddagger}_3$-$2H_2O$	-0.111

THEORETICAL *(m/z)*	EXPERIMENTAL *(m/z)*	ASSIGNMENTS	ERROR (ppm)
405.22447	405.22414	$b^{\ddagger}_3$-H_2O-NH_3	-0.827
422.25102	422.25085	$b^{\ddagger}_3$-H_2O	-0.403
440.26159	440.26185	$b^{\ddagger}_3$	0.602
449.22170	449.22164	y_4-NH_3	-0.134
* 466.24824	466.24816	y_4	-0.172
501.28760	501.28733	a_8^{2+}	-0.549
515.28506	515.28507	b_8^{2+}	0.014
535.28252	535.28230	$(b^{\ddagger}_8$-$H_2O)^{2+}$	-0.411
543.79579	543.79587	b_9^{2+}	0.142
544.28780	544.28732	$b^{\ddagger}_8{}^{2+}$	-0.886
553.28421	553.28371	$(y_9$-$NH_3)^{2+}$	-0.904
554.78797	554.78761	$(b^{\ddagger}_9$-$2H_2O)^{2+}$	-0.644
555.27998	555.27998	$(b^{\ddagger}_9$-H_2O-$NH_3)^{2+}$	0.005
556.28781	556.28751	b_5-$3NH_3$	-0.539
563.79325	563.79328	$(b^{\ddagger}_9$-$H_2O)^{2+}$	0.053
572.79853	572.79864	$b^{\ddagger}_9{}^{2+}$	0.188
577.82736	577.82738	$(a_{10}$-$NH_3)^{2+}$	0.026
586.34037	586.34056	a_{10}^{2+}	0.327
* 590.34090	590.34076	b_5-NH_3	-0.237
591.82455	591.82477	$(b_{10}$-$NH_3)^{2+}$	0.372
596.29011	596.28993	y_5-NH_3	-0.302
597.33254	597.33248	$(a^{\ddagger}_{10}$-$2H_2O)^{2+}$	-0.100
597.82455	597.82430	$(a^{\ddagger}_{10}$-H_2O-$NH_3)^{2+}$	-0.418
600.33782	600.33793	b_{10}^{2+}	0.178
602.81673	602.81718	$(b^{\ddagger}_{10}$-$2H_2O$-$NH_3)^{2+}$	0.755
606.33782	606.33800	$(a^{\ddagger}_{10}$-$H_2O)^{2+}$	0.293
607.36744	607.36733	b_5	-0.189
610.32386	610.32415	y_{10}^{2+}	0.475
611.33000	611.33017	$(b^{\ddagger}_{10}$-$2H_2O)^{2+}$	0.282
611.82201	611.82210	$(b^{\ddagger}_{10}$-H_2O-$NH_3)^{2+}$	0.151
613.31665	613.31672	y_5	0.114
615.34311	615.34310	$a^{\ddagger}_{10}{}^{2+}$	-0.008
620.33528	620.33542	$(b^{\ddagger}_{10}$-$H_2O)^{2+}$	0.226
621.80804	621.80806	$(y^{\ddagger}_{10}$-$NH_3)^{2+}$	0.024
629.34056	629.34062	$b^{\ddagger}_{10}{}^{2+}$	0.091
630.32132	630.32168	$y^{\ddagger}_{10}{}^{2+}$	0.575
643.34761	643.34767	$[M$-CO-$2NH_3$+$2H]^{2+}$	0.093
647.36236	647.36242	$b^{\ddagger}_5$-H_2O	0.093
648.33951	648.33961	$[M$-H_2O-$2NH_3$+$^{2+}H]^{2+}$	0.150
656.85279	656.85312	$[M$-H_2O-NH_3+$2H]^{2+}$	0.510
657.34479	657.34511	$[M$-$2NH_3$+$2H]^{2+}$	0.479
665.85807	665.85839	$[M$-NH_3+$2H]^{2+}$	0.484
668.33697	668.33723	$[M^{\ddagger}$-$2H_2O$-$2NH_3$+$2H]^{2+}$	0.389
671.85807	671.85847	$[M^{\ddagger}$-H_2O-$HCONH_2$+$2H]^{2+}$	0.599
674.37134	674.37171	$[M$+$2H]^{2+}$	0.549
676.85025	676.84989	$[M^{\ddagger}$-$2H_2O$-NH_3+$2H]^{2+}$	-0.532
685.36352	685.36279	$[M^{\ddagger}$-$2H_2O$+$2H]^{2+}$	-1.058
685.85553	685.85596	$[M^{\ddagger}$-H_2O-NH_3+$2H]^{2+}$	0.627

THEORETICAL *(m/z)*	EXPERIMENTAL *(m/z)*	ASSIGNMENTS	ERROR (ppm)
694.36880	694.36868	$[M^{\ddagger}-H_2O+2H]^{2+}$	-0.173
694.86081	694.86073	$[M^{\ddagger}-NH_3+2H]^{2+}$	-0.115
707.43111	707.43161	a_6	0.707
* 735.42602	735.42655	b_6	0.714
741.37523	741.37457	y_6	-0.890
758.39440	758.39444	$b^{\ddagger}_6-H_2O-NH_3$	0.059
775.42094	775.42085	$b^{\ddagger}_6-H_2O$	-0.116
882.49443	882.49425	b_7	-0.210
922.48935	922.48912	$b^{\ddagger}_7-H_2O$	-0.249
940.49991	940.50021	$b^{\ddagger}_7$	0.314
949.46003	949.45983	y_8-NH_3	-0.211
966.48657	966.48587	y_8	-0.724
1029.56284	1029.56278	b_8	-0.063
1069.55776	1069.55822	$b^{\ddagger}_8-H_2O$	0.430
1086.58431	1086.58328	b_9	-0.943
1109.55267	1109.55262	$b^{\ddagger}_9-H_2O-NH_3$	-0.050
*1122.58768	1122.58837	y_9	0.615
1126.57922	1126.57876	$b^{\ddagger}_9-H_2O$	-0.408
1162.58260	1162.58237	$y^{\ddagger}_9-H_2O$	-0.194
1199.66836	1199.66835	b_{10}	-0.013
1219.64044	1219.64167	y_{10}	1.008
1221.65271	1221.65296	$b^{\ddagger}_{10}-2H_2O$	0.201
*1239.66328	1239.66427	$b^{\ddagger}_{10}-H_2O$	0.799
		mean	
		St. Dv.	

Table B-14. DR(695)-ECD(724) error analysis of the AcKM-11 peptide reacted in MeOH/H_2O (50:50) for the precursor ion $[M+C_2H_2O_2+2H]^{2+}$. * indicates the ions used for calibration.

THEORETICAL *(m/z)*	EXPERIMENTAL *(m/z)*	ASSIGNMENTS	ERROR (ppm)
* 466.24824	466.24821	y_4	-0.064
537.33815	537.33815	$c_4^{\bullet}$	0.000
538.34597	538.34597	c_4	-0.009
577.33307	577.33304	$c^{\ddagger}_4{}^{\bullet}-H_2O$	-0.043
578.34089	578.34093	$c^{\ddagger}_4-H_2O$	0.069
595.34363	595.34362	$c^{\ddagger}_4{}^{\bullet}$	-0.017
596.35145	596.35144	$c^{\ddagger}_4$	-0.025
665.39673	665.39673	$c_5^{\bullet}$	0.000
* 666.40455	666.40453	c_5	-0.038
705.39165	705.39163	$c^{\ddagger}_5{}^{\bullet}-H_2O$	-0.021
706.39947	706.39949	$c^{\ddagger}_5-H_2O$	0.028
707.32214	707.32211	y_6-2NH_3	-0.042
715.37408	715.37411	$[M^{\ddagger}-H_2O+2H]^{2+}$	0.042
723.40221	723.40218	$c^{\ddagger}_5{}^{\bullet}$	-0.041
724.34869	724.34872	$y-NH_3$	0.041

THEORETICAL *(m/z)*	EXPERIMENTAL *(m/z)*	ASSIGNMENTS	ERROR (ppm)
724.37937	724.37935	$[M^{‡}+2H]^{2+}$	-0.028
724.41003	724.40994	$c^{‡}_{5}$	-0.131
793.45531	793.45538	$c_{6}^{\bullet}$	0.088
* 794.46313	794.46313	c_{6}	-0.006
833.45023	833.45027	$c^{‡}_{6}{}^{\bullet}$-H_2O	0.054
834.45805	834.45808	$c^{‡}_{6}$-H_2O	0.036
851.46079	851.46077	$c^{‡}_{6}{}^{\bullet}$	-0.023
852.46861	852.46858	$c^{‡}_{6}$	-0.041
940.52372	940.52371	$c_{7}^{\bullet}$	-0.011
941.53155	941.53153	c_{7}	-0.016
980.51864	980.51854	$c^{‡}_{7}{}^{\bullet}$-H_2O	-0.097
981.52646	981.52653	$c^{‡}_{7}$-H_2O	0.071
998.52920	998.52932	$c^{‡}_{7}{}^{\bullet}$	0.120
999.53702	999.53706	$c^{‡}_{7}$	0.035
1072.54485	1072.54456	$z^{‡}_{9}{}^{\bullet}$-C_3H_6S-H_2O	-0.270
1088.59995	1088.60009	c_{8}	0.124
1090.55542	1090.55611	$z^{‡}_{9}{}^{\bullet}$-C_3H_6S	0.633
1102.59181	1102.59178	$a^{‡}_{8}$	-0.023
1106.56896	1106.56822	$z_{9}^{\bullet}$	-0.669
1128.59487	1128.59427	$c^{‡}_{8}$-H_2O	-0.532
* 1145.62142	1145.62136	c_{9}	-0.048
1146.56388	1146.56376	$z^{‡}_{9}{}^{\bullet}$-H_2O	-0.105
1146.60543	1146.60548	$c^{‡}_{9}$	0.039
1164.57444	1164.57441	$z^{‡}_{9}{}^{\bullet}$	-0.026
1185.61633	1185.61642	$c^{‡}_{9}$-H_2O	0.076
1203.62690	1203.62689	$c^{‡}_{9}$	-0.004
1257.69765	1257.69821	$c_{10}^{\bullet}$	0.445
1258.70547	1258.70562	c_{10}	0.115
1298.70039	1298.70020	$c^{‡}_{10}$-H_2O	-0.146
1315.70313	1315.70351	$c^{‡}_{10}{}^{\bullet}$	0.289
1316.71096	1316.71107	$c^{‡}_{10}$	0.087
1330.70879	1330.70871	$[M\text{-}CH_3CONH_2+H]^{1+}$	-0.465
1331.71662	1331.71689	$[M\text{-}CH_3CONH_2+2H]^{1+\bullet}$	0.613
1347.73541	1347.73557	$[M\text{-}CH_2CO+H]^{1+}$	-0.383
1348.74323	1348.74359	$[M\text{-}CH_2CO+2H]^{1+\bullet}$	-0.073
1356.72969	1356.72917	$[M^{‡}\text{-}H_2O\text{-}C_3H_6S+2H]^{1+\bullet}$	-0.386
	1371.71170	?	
1385.72719	1385.72715	$[M^{‡}\text{-}HCONH_2.\text{-}H_2O+2H]^{1+\bullet}$	-0.028
	1388.73815	?	
* 1405.74089	1405.74103	$[M^{‡}\text{-}CH_2CO+H]^{1+}$	0.099
		mean	
		St. Dv.	

Table B-15. CAD (724) error analysis of the Ac-KM-11 peptide reacted in MeOH/H_2O (50:50) for the precursor ion $[M+C_2H_2O_2+2H]^{2+}$. * indicates the ions used for calibration.

THEORETICAL *(m/z)*	EXPERIMENTAL *(m/z)*	ASSIGNMENTS	ERROR (ppm)
* 245.13183	245.13181	y_2-NH_3	-0.082
262.15837	262.15838	y_2	0.038
268.16556	268.16558	b_2	0.075
272.15553	272.15532	$(b^{\ddagger}_6$-$2H_2O)^{2+}$	-0.772
302.15329	302.15329	y_3-NH_3	0.000
319.17983	319.17983	y_3	0.000
424.26667	424.26666	b_3	-0.024
436.26667	436.26664	$a^{\ddagger}_3$-H_2O	0.183
446.25102	446.25111	$b^{\ddagger}_3$-$2H_2O$	0.202
447.23504	447.23525	$b^{\ddagger}_3$-H_2O-NH_3	0.470
449.22170	449.22169	y_4-NH_3	-0.022
451.23759	451.23746	$(a^{\ddagger}_7$-$2H_2O$-$NH_3)^{2+}$	-0.277
464.26159	464.26157	$b^{\ddagger}_3$-H_2O	-0.032
* 466.24824	466.24820	y_4	-0.086
468.75614	468.75606	$(a^{\ddagger}_7$-$H_2O)^{2+}$	-0.171
473.74831	473.74828	$(b^{\ddagger}_7$-$2H_2O)^{2+}$	-0.074
474.24032	474.24038	$(b^{\ddagger}_7$-H_2O-$NH_3)^{2+}$	0.116
482.27215	482.27209	$b^{\ddagger}_3$	-0.124
482.75360	482.75359	$(b^{\ddagger}_7$-$H_2O)^{2+}$	-0.016
491.75888	491.75882	$b^{\ddagger}_7{}^{2+}$	-0.122
522.29289	522.29271	$a_8{}^{2+}$	-0.341
527.77707	527.77682	$(b8$-$NH_3)^{2+}$	-0.479
533.28506	533.28496	$(a^{\ddagger}_8$-$2H_2O)^{2+}$	-0.192
533.77707	533.77689	$(a^{\ddagger}_8$-H_2O-$NH_3)^{2+}$	-0.342
536.29035	536.29012	$b_8{}^{2+}$	-0.420
538.76925	538.76878	$(b_9$-H_2O-$2NH_3)^{2+}$	-0.868
539.26126	539.26097	$(b^{\ddagger}_8$-H_2O-$2NH_3)^{2+}$	-0.533
542.29035	542.29012	$(a^{\ddagger}_8$-$H_2O)^{2+}$	-0.415
547.77453	547.77430	$(b^{\ddagger}_8$-H_2O-$NH_3)^{2+}$	-0.420
551.29563	551.29553	$a^{\ddagger}_8{}^{2+}$	-0.177
556.77981	556.77957	$(b^{\ddagger}_8$-$NH_3)^{2+}$	-0.436
561.31435	561.31392	$b^{\ddagger}_4$-H_2O	-0.757
562.28780	562.28731	$(a^{\ddagger}_9$-H_2O-$NH_3)^{2+}$	-0.876
564.80107	564.80077	$b_9{}^{2+}$	-0.540
565.29309	565.29284	$b^{\ddagger}_8{}^{2+}$	-0.433
567.27998	567.27981	$(b^{\ddagger}_9$-$2H_2O$-$NH_3)^{2+}$	-0.295
570.80107	570.80071	$(a^{\ddagger}_9$-$H_2O)^{2+}$	-0.639
575.79325	575.79292	$(b^{\ddagger}_9$-$2H_2O)^{2+}$	-0.573
576.28526	576.28506	$(b^{\ddagger}_9$-H_2O-$NH_3)^{2+}$	-0.347
584.79853	584.79822	$(b^{\ddagger}_9$-$H_2O)^{2+}$	-0.534
585.29054	585.29026	$(b^{\ddagger}_9$-$NH_3)^{2+}$	-0.483
593.80381	593.80351	$b^{\ddagger}_9{}^{2+}$	-0.514
* 596.29011	596.28977	y_5-NH_3	-0.570
601.81059	601.81023	$(y_{10}$-$NH_3)^{2+}$	-0.598
603.82455	603.82413	$(b_{10}$-H_2O-$NH_3)^{2+}$	-0.696

THEORETICAL *(m/z)*	EXPERIMENTAL *(m/z)*	ASSIGNMENTS	ERROR (ppm)
607.34565	607.34530	a_{10}^{2+}	-0.573
610.32386	610.32347	y_{10}^{2+}	-0.639
612.82983	612.82945	$(b_{10}\text{-}NH_3)^{2+}$	-0.625
613.31665	613.31630	y_5	-0.571
618.33782	618.33757	$(a^{\ddagger}_{10}\text{-}2H_2O)^{2+}$	-0.408
618.82983	618.82943	$(a^{\ddagger}_{10}\text{-}H_2O\text{-}NH_3)^{2+}$	0.650
621.31604	621.31564	$(y^{\ddagger}_{10}\text{-}2H_2O)^{2+}$	-0.636
621.34311	621.34273	b_{10}^{2+}+	-0.604
623.82201	623.82162	$(b^{\ddagger}_{10}\text{-}2H_2O\text{-}NH_3)^{2+}$	-0.621
624.31402	624.31359	$(b^{\ddagger}_{10}\text{-}H_2O\text{-}2NH_3)^{2+}$	-0.685
627.34311	627.34271	$(a^{\ddagger}_{10}\text{-}H_2O)^{2+}$	-0.630
630.32132	630.32091	$(y^{\ddagger}_{10}\text{-}H_2O)^{2+}$	-0.646
630.81333	630.81291	$(y^{\ddagger}_{10}\text{-}NH_3)^{2+}$	-0.662
632.33528	632.33489	$(b^{\ddagger}_{10}\text{-}2H_2O)^{2+}$	-0.617
632.82729	632.82689	$(b^{\ddagger}_{10}\text{-}H_2O\text{-}NH_3)^{2+}$	-0.632
636.34839	636.34793	$a^{\ddagger}_{10}{}^{2+}$+	-0.719
639.32660	639.32617	$y^{\ddagger}_{10}{}^{2+}$	-0.673
641.34056	641.34016	$(b^{\ddagger}_{10}\text{-}H_2O)^{2+}$	-0.628
641.83257	641.83201	$(b^{\ddagger}_{10}\text{-}NH_3)^{2+}$	-0.876
* 649.37801	649.37757	b_5	-0.678
650.34585	650.34538	$b^{\ddagger}_{10}{}^{2+}$	-0.715
669.34479	669.34421	$[M\text{-}H_2O\text{-}2NH_3\text{+}2H]^{2+}$	-0.874
672.86589	672.86549	$[M\text{-}HCONH_2\text{+}2H]^{2+}$	-0.599
678.35008	678.34956	$[M\text{-}2NH_3\text{+}2H]^{2+}$	-0.764
683.85807	683.85750	$[M^{\ddagger}\text{-}2H_2O\text{-}HCONH_2\text{+}2H]^{2+}$	-0.830
684.35008	684.34968	$[M^{\ddagger}\text{-}H_2O\text{-}HCONH_2\text{-}NH_3\text{+}2H]^{2+}$	-0.581
686.86335	686.86287	$[M\text{-}NH_3\text{+}2H]^{2+}$	-0.699
689.34225	689.34168	$[M^{\ddagger}\text{-}2H_2O\text{-}2NH_3\text{+}2H]^{2+}$	-0.831
689.37293	689.37242	$b^{\ddagger}_5\text{-}H_2O$	-0.733
692.86335	692.86291	$[M^{\ddagger}\text{-}H_2O\text{-}HCONH_2\text{+}2H]^{2+}$	-0.635
694.36880	694.36810	$[M^{\ddagger}\text{-}CH_2CO\text{-}H_2O\text{+}2H]^{2+}$	-1.005
697.85553	697.85501	$[M^{\ddagger}\text{-}2H_2O\text{-}NH_3\text{+}2H]^{2+}$	-0.745
698.34753	698.34702	$[M^{\ddagger}\text{-}H_2O\text{-}2NH_3\text{+}2H]^{2+}$	-0.737
701.86863	701.86791	$[M^{\ddagger}\text{-}HCONH_2\text{+}2H]^{2+}$	-1.029
706.86081	706.86031	$[M^{\ddagger}\text{-}H_2O\text{-}NH_3\text{+}2H]^{2+}$	-0.707
* 707.32214	707.32167	$y_6\text{-}2NH_3$	-0.664
715.37408	715.37355	$[M^{\ddagger}\text{-}H_2O\text{+}2H]^{2+}$	-0.741
715.38859	715.38807	$a_6\text{-}2NH_3$	-0.720
715.86609	715.86551	$[M\text{-}NH_3\text{+}2H]^{2+}$	-0.810
724.34869	724.34829	$y_6\text{-}NH_3$	-0.552
724.37937	724.37889	$[M^{\ddagger}\text{+}2H]^{2+}$	-0.663
741.37523	741.37467	y_6	-0.755
749.44168	749.44158	a_6	-0.127
754.39948	754.39897	$a^{\ddagger}_6\text{-}2H_2O\text{-}NH_3$	-0.676
771.42602	771.42544	$a^{\ddagger}_6\text{-}2H_2O$	-0.758
774.40189	774.40163	$a^{\ddagger}_6\text{-}2NH_3$	-0.342
777.43659	777.43607	b_6	-0.669
789.43659	789.43656	$a^{\ddagger}_6\text{-}H_2O$	-0.038

THEORETICAL *(m/z)*	EXPERIMENTAL *(m/z)*	ASSIGNMENTS	ERROR (ppm)
799.42094	799.42034	$b^{\ddagger}_{6}$-2H_2O	-0.751
800.40496	800.40416	$b^{\ddagger}_{6}$-H_2O-NH_3	-0.999
817.43151	817.43102	$b^{\ddagger}_{6}$-H_2O	-0.593
827.44370	827.44377	a_7-2NH_3-2H_2O	0.091
835.38072	835.38108	y_7-2NH_3	0.431
835.44207	835.44178	$b^{\ddagger}_{6}$	-0.347
896.51009	896.50945	a_7	-0.708
901.46789	901.46743	$a^{\ddagger}_{7}$-2H_2O-NH_3	-0.510
907.47846	907.47768	b_7-NH_3	-0.854
* 924.50500	924.50461	b_7	-0.422
932.43348	932.43305	y_8-2NH_3	-0.461
936.50500	936.50489	$a^{\ddagger}_{7}$-H_2O	-0.117
946.48935	946.48871	$b^{\ddagger}_{7}$-2H_2O	-0.676
947.47337	947.47309	$b^{\ddagger}_{7}$-H_2O-NH_3	-0.296
948.47739	948.47741	$b^{\ddagger}_{7}$-2NH_3	0.021
949.46003	949.45971	y_8-NH_3	-0.337
964.49991	964.49948	$b^{\ddagger}_{7}$-H_2O	-0.451
966.48657	966.48616	y_8	-0.424
982.51048	982.50948	$b^{\ddagger}_{7}$	-1.018
1043.57849	1043.57856	a_8	0.062
1054.54687	1054.54694	b_8-NH_3	0.071
1083.57341	1083.57345	$a^{\ddagger}_{8}$-H_2O	0.037
1093.55776	1093.55784	$b^{\ddagger}_{8}$-2H_2O	0.073
1094.54178	1094.54184	$b^{\ddagger}_{8}$-H_2O-NH_3	0.055
1095.54580	1095.54562	$b^{\ddagger}_{8}$-2NH_3	-0.164
1111.56832	1111.56860	$b^{\ddagger}_{8}$-H_2O	0.247
1128.59487	1128.59498	b_9	0.097
1145.55605	1145.55618	$y^{\ddagger}_{9}$-H_2O-NH_3	0.113
1150.57922	1150.57922	$b^{\ddagger}_{9}$-2H_2O	0.000
1151.56324	1151.56350	$b^{\ddagger}_{9}$-H_2O-NH_3	0.226
1152.56726	1152.56691	$b^{\ddagger}_{9}$-2NH_3	-0.304
1162.58260	1162.58358	$y^{\ddagger}_{9}$-H_2O	0.847
1168.58978	1168.59043	$b^{\ddagger}_{9}$-H_2O	0.552
1213.68402	1213.68430	a_{10}	0.235
*1219.64044	1219.64096	y_{10}	0.426
1241.62479	1241.62548	$y^{\ddagger}_{10}$-2H_2O	0.556
1241.67893	1241.67964	b_{10}	0.572
1242.60881	1242.60940	$y^{\ddagger}_{10}$-H_2O-NH_3	0.475
1253.67893	1253.67925	$a^{\ddagger}_{10}$-H_2O	0.255
1259.63536	1259.63548	$y^{\ddagger}_{10}$-H_2O	0.095
*1281.67385	1281.67448	$b^{\ddagger}_{10}$-H_2O	0.498
		mean	
		St. Dv.	

Table B-16. CAD (724) error analysis of the AcKM-11 peptide reacted in PBS for the precursor ion $[M+C_2H_2O_2+2H]^{2+}$. * indicates the ions used for calibration.

THEORETICAL *(m/z)*	EXPERIMENTAL *(m/z)*	ASSIGNMENTS	ERROR (ppm)
* 245.13183	245.13180	y_2-NH_3	-0.122
262.15837	262.15838	y_2	0.038
268.16556	268.16561	b_2	0.186
302.15329	302.15337	y_3-NH_3	0.265
319.17983	319.17993	y_3	0.313
409.21939	409.21948	$(b^{\ddagger}_6$-$H_2O)^{2+}$	0.214
418.22467	418.22465	$b^{\ddagger}_6{}^{2+}$	-0.060
424.26667	424.26667	b_3	0.000
436.26667	436.26637	$a^{\ddagger}_3$-H_2O	-0.688
446.25102	446.25125	$b^{\ddagger}_3$-$2H_2O$	0.515
448.75869	448.75877	$a_7{}^{2+}$	0.189
449.22170	449.22176	y_4-NH_3	0.134
460.24287	460.24315	$(a^{\ddagger}_7$-H_2O-$NH_3)^{2+}$	0.614
462.75614	462.75605	$b_7{}^{2+}$	-0.194
464.26159	464.26166	$b^{\ddagger}_3$-H_2O	0.162
* 466.24824	466.24820	y_4	-0.086
468.75614	468.75591	$(a^{\ddagger}_7$-$H_2O)^{2+}$	-0.491
473.74831	473.74851	$(b^{\ddagger}_7$-$2H_2O)^{2+}$	0.412
474.24032	474.24031	$(b^{\ddagger}_7$-H_2O-NH3$)^{2+}$	-0.032
482.27215	482.27207	$b^{\ddagger}_3$	-0.166
482.75360	482.75353	$(b^{\ddagger}_7$-$H_2O)^{2+}$	-0.140
491.75888	491.75901	$b^{\ddagger}_7{}^{2+}$	0.264
513.77989	513.77941	$(a_8$-$NH_3)^{2+}$	-0.930
521.31943	521.31948	b_4	0.096
522.29289	522.29279	$a_8{}^{2+}$	-0.188
527.28506	527.28507	$(b_8$-$H_2O)^{2+}$	0.013
527.77707	527.77702	$(b_8$-$NH_3)^{2+}$	-0.100
533.28506	533.28475	$(a^{\ddagger}_8$-$2H_2O)^{2+}$	-0.586
533.77707	533.77697	$(a^{\ddagger}_8$-H_2O-$NH_3)^{2+}$	-0.192
536.29035	536.29040	$b_8{}^{2+}$	0.103
538.76925	538.76963	$(b_9$-H_2O-$2NH_3)^{2+}$	0.709
539.26126	539.26151	$(b^{\ddagger}_8$-H_2O-$2NH_3)^{2+}$	0.468
542.29035	542.29044	$(a^{\ddagger}_8$-$H_2O)^{2+}$	0.175
547.77453	547.77455	$(b^{\ddagger}_8$-H2O-$NH_3)^{2+}$+	0.037
551.29563	551.29588	$a^{\ddagger}_8{}^{2+}$	0.453
556.28780	556.28785	$(b_9$-$NH_3)^{2+}$	0.084
561.31435	561.31494	$b^{\ddagger}_4$-H_2O	1.060
562.28780	562.28776	$(a^{\ddagger}_9$-H_2O-$NH_3)^{2+}$	-0.076
564.80107	564.80099	$b_9{}^{2+}$	-0.150
565.29309	565.29290	$b^{\ddagger}_8{}^{2+}$	-0.327
567.27998	567.27958	$(b^{\ddagger}_9$-$2H_2O$-$NH_3)^{2+}$	-0.701
570.80107	570.80103	$(a^{\ddagger}_9$-$H_2O)^{2+}$	-0.079
575.79325	575.79316	$(b^{\ddagger}_9$-$2H_2O)^{2+}$+	-0.156
576.28526	576.28587	$(b^{\ddagger}_9$-H_2O-$NH_3)^{2+}$	1.059
584.79853	584.79850	$(b^{\ddagger}_9$-$H_2O)^{2+}$	-0.056

THEORETICAL *(m/z)*	EXPERIMENTAL *(m/z)*	ASSIGNMENTS	ERROR (ppm)
585.29054	585.29047	$(b^{\ddagger}_{9}\text{-}NH_3)^{2+}$	-0.124
593.80381	593.80390	b^{2+}+	0.143
* 596.29011	596.29017	$y_5\text{-}NH_3$	0.101
601.81059	601.81067	$(y_{10}\text{-}NH_3)^{2+}$	0.133
607.34565	607.34569	a_{10}^{2+}	0.066
610.32386	610.32392	y_{10}^{2+}	0.098
612.82983	612.82982	$(b_{10}\text{-}NH_3)^{2+}$	-0.021
613.31665	613.31679	y_5	0.228
618.82983	618.82974	$(a^{\ddagger}_{10}\text{-}H_2O\text{-}NH_3)^{2+}$	-0.149
621.31604	621.31604	$(y^{\ddagger}_{10}\text{-}2H_2O)^{2+}$	0.008
621.34311	621.34326	b_{10}^{2+}	0.249
623.82201	623.82229	$(b^{\ddagger}_{10}\text{-}2H_2O\text{-}NH_3)^{2+}$	0.453
624.31402	624.31429	$(b^{\ddagger}_{10}\text{-}H_2O\text{-}2NH_3)^{2+}$	0.436
627.34311	627.34320	$(a^{\ddagger}_{10}\text{-}H_2O)^{2+}$	0.151
630.32132	630.32138	$(y^{\ddagger}_{10}\text{-}H_2O)^{2+}$	0.099
630.81333	630.81319	$(y^{\ddagger}_{10}\text{-}NH_3)^{2+}$	-0.218
632.33528	632.33522	$(b^{\ddagger}_{10}\text{-}2H_2O)^{2+}$	-0.095
632.82729	632.82729	$(b^{\ddagger}_{10}\text{-}H_2O\text{-}NH_3)^{2+}$	0.000
636.34839	636.34836	$a^{\ddagger}_{10}{}^{2+}$	-0.043
639.32660	639.32663	$y^{\ddagger}_{10}{}^{2+}$	0.047
641.34056	641.34066	$(b^{\ddagger}_{10}\text{-}H_2O)^{2+}$	0.152
* 649.37801	649.37814	b_5	0.200
650.34585	650.34602	$b^{\ddagger}_{10}{}^{2+}$	0.269
663.86061	663.86012	$[M\text{-}H_2O\text{-}HCONH_2\text{+}2H]^{2+}$	-0.738
664.35289	664.35265	$[M\text{-}NH_3\text{-}HCONH_2\text{+}2H]^{2+}$	-0.366
669.34479	669.34444	$[M\text{-}H_2O\text{-}2NH_3\text{+}2H]^{2+}$+	-0.530
671.36236	671.36214	$b^{\ddagger}_{5}\text{-}2H_2O$	-0.328
672.86589	672.86578	$[M\text{-}HCONH_2\text{+}2H]^{2+}$	-0.168
674.37134	674.37147	$[M\text{-}CH_2CO\text{+}2H]^{2+}$	0.193
677.85807	677.85810	$[M\text{-}H_2O\text{-}NH_3\text{+}2H]^{2+}$+	0.047
678.35008	678.35000	$[M\text{-}2NH_3\text{+}2H]^{2+}$	-0.115
683.85807	683.85799	$[M^{\ddagger}\text{-}2H_2O\text{-}\ HCONH_2\text{+}2H]^{2+}$	-0.113
684.35008	684.35011	$[M^{\ddagger}\text{-}H_2O\text{-}2NH_3\text{+}2H]^{2+}$	0.047
686.37134	686.37133	$[M\text{-}H_2O\text{+}2H]^{2+}$	-0.015
686.86335	686.86348	$[M\text{-}NH_3\text{+}2H]^{2+}$	0.189
689.34225	689.34227	$[M^{\ddagger}\text{-}2H_2O\text{-}2NH_3\text{+}2H]^{2+}$	0.025
689.37293	689.37303	$b^{\ddagger}_{5}\text{-}H_2O$	0.152
689.83426	689.83429	$[M^{\ddagger}\text{-}H_2O\text{-}3NH_3\text{+}2H]^{2+}$	0.040
692.86335	692.86348	$[M^{\ddagger}\text{-}H_2O\text{-}HCONH_2\text{+}2H]^{2+}$	0.188
694.36880	694.36823	$[M\text{-}H_2O\text{-}CH_2CO\text{+}2]^{2+}$	-0.817
695.37663	695.37662	$[M\text{+}2H]^{2+}]$	-0.014
697.85553	697.85577	$[M\text{-}2H_2O\text{-}NH_3\text{+}2H]^{2+}$	0.344
698.34753	698.34777	$[M^{\ddagger}\text{-}H_2O\text{-}2NH_3\text{+}2H]^{2+}$	0.337
701.86864	701.86896	$[M^{\ddagger}\text{-}HCONH_2\text{+}2H]^{2+}$	0.463
706.36880	706.36810	$[M^{\ddagger}\text{-}2H_2O\text{+}2H]^{2+}$	-0.991
706.86081	706.86150	$[M^{\ddagger}\text{-}H_2O\text{-}NH_3\text{+}2H]^{2+}$	0.976
707.32214	707.32282	$y_6\text{-}2NH_3$	0.961
799.42094	799.42094	$b^{\ddagger}_{6}\text{-}2H_2O$	0.000

THEORETICAL *(m/z)*	EXPERIMENTAL *(m/z)*	ASSIGNMENTS	ERROR (ppm)
817.43151	817.43091	$b^{\ddagger}_6$-H_2O	-0.728
835.38072	835.38096	y_7-$2NH_3$	0.287
835.44207	835.44123	$b^{\ddagger}_6$	-1.005
901.46789	901.46825	$a^{\ddagger}_7$-$2H_2O$-NH_3	0.399
* 924.50500	924.50467	b_7	-0.357
932.43348	932.43340	y_8-$2NH_3$	-0.086
936.50500	936.50470	$a^{\ddagger}_7$-H_2O	-0.320
946.48935	946.48905	$b^{\ddagger}_7$-$2H_2O$	-0.317
947.47337	947.47368	$b^{\ddagger}_7$-H_2O-NH_3	0.327
948.47739	948.47777	$b^{\ddagger}_7$-$2NH_3$	0.401
964.49991	964.49949	$b^{\ddagger}_7$-H_2O	-0.441
966.48657	966.48593	y_8	-0.662
982.51048	982.50975	$b^{\ddagger}_7$	-0.743
990.53082	990.53175	a_8-$2H_2O$-NH_3	0.939
1043.57849	1043.57809	a_8	-0.388
1054.54687	1054.54710	b_8-NH_3	0.223
1066.54687	1066.54678	a_9 -$2NH_3$	-0.080
1071.52848	1071.52932	$a^{\ddagger}_9$-$2NH_3$-$2H_2O$	0.784
1083.57341	1083.57337	$a^{\ddagger}_8$-H_2O	-0.037
1093.55776	1093.55717	$b^{\ddagger}_8$-$2H_2O$	-0.540
1094.54178	1094.54151	$b^{\ddagger}_8$-H_2O-NH_3	-0.247
1095.54580	1095.54509	$b^{\ddagger}_8$-$2NH_3$	-0.648
1111.56832	1111.56911	$b^{\ddagger}_8$-H_2O	0.706
1150.57922	1150.57844	$b^{\ddagger}_9$-$2H_2O$	-0.678
1162.58260	1162.58155	$y^{\ddagger}_9$-H_2O	-0.903
1168.58978	1168.58999	$b^{\ddagger}_9$-H_2O	0.175
1185.58735	1185.58818	y_{10}-$2NH_3$	0.700
1202.61389	1202.61311	y_{10}-NH_3	-0.653
1213.68402	1213.68290	a_{10}	-0.919
*1219.64044	1219.64002	y_{10}	-0.344
1236.67620	1236.67614	$a^{\ddagger}_{10}$-$2H_2O$	-0.044
1241.62479	1241.62375	$y^{\ddagger}_{10}$-$2H_2O$	-0.838
1241.67893	1241.67869	b_{10}	-0.193
*1242.60881	1242.60803	$y^{\ddagger}_{10}$-H_2O-NH_3	-0.628
		mean	
		St. Dv.	

Table B-17. DR(595.03)-ECD(608.36) mass error analysis of the EK-15 peptide reacted in MeOH/H_2O solution for the precursor ion $[M+C_2O+3H]^{3+}$. * indicates the masses used for calibration.

THEORETICAL (m/z)	EXPERIMENTAL (m/z)	ASSIGNMENTS	ERROR (ppm)
* 303.17752	303.17752	c_2	0.000
325.16187	325.16189	$c^{\dagger}_2$ - H_2O	0.062
	334.17210	?	
343.17244	343.17243	$c^{\dagger}_2$	-0.015

	THEORETICAL (m/z)	EXPERIMENTAL (m/z)	ASSIGNMENTS	ERROR (ppm)
*	343.24655	343.24655	$z_3^{\bullet}$	0.000
	344.25438	344.25437	z_3	-0.015
		348.15138	?	
	359.26527	359.26529	y_3	0.056
	387.22247	387.22247	a_3	0.000
	400.75868	400.75866	c_6^{2+}	-0.050
		411.75076	?	
	413.22554	413.22552	$c_3 - H_2O$	-0.036
	413.27584	413.27584	w_4	0.012
	427.21739	427.21738	$a^{\dagger}_3$	-0.012
	431.23610	431.23610	c_3	0.000
	453.22045	453.22046	$c^{\dagger}_3 - H_2O$	0.022
	464.78797	464.78796	c_7^{2+}	-0.022
*	471.23102	471.23101	$c^{\dagger}_3$	-0.011
	472.28914	472.28914	$z_4^{\bullet}$	0.000
	473.29697	473.29699	z_4	0.053
		473.31942	?	
	488.30786	488.30785	y_4	-0.020
	500.30653	500.30653	a_4	0.000
	500.80549	500.80544	y_9^{2+}	-0.100
	515.31181	515.31180	c_8^{2+}	-0.019
	526.30959	526.30959	$c_4 - H_2O$	-0.010
	540.30145	540.30145	$a^{\dagger}_4$	0.009
	544.32016	544.32016	c_4	0.000
	550.83037	550.83031	c_9^{2+}	-0.100
	556.84361	556.84363	$z_{10}^{\bullet\,2+}$	0.036
	561.82254	561.82231	$(c^{\dagger}_9 - H2O)^{2+}$	-0.409
	566.30451	566.30450	$c^{\dagger}_4 - H_2O$	-0.018
	571.35755	571.35755	$z_5^{\bullet}$	0.000
		582.29941	?	
*	584.31508	584.31507	$c^{\dagger}_4$	-0.009
	587.37627	587.37628	y_5	0.017
	589.02799	589.02801	$[M - H_2O + 3H]^{3+}$	0.040
	602.35963	602.35964	$[M^{\dagger} - H_2O + 3H]^{3+}$	0.025
	608.36315	608.36310	$[M^{\dagger} + 3H]^{3+}$	-0.077
	620.89109	620.89103	$z_{11}^{\bullet\,2+}$	-0.096
	628.40149	628.40142	a_5	-0.111
	641.38629	641.38683	$z_6^{\bullet} - C_3H_7$	0.850
	650.38584	650.38576	$a^{\dagger}_5 - H_2O$	-0.123
	654.40456	654.40453	$c_5 - H_2O$	-0.038
	656.90660	656.90656	c_{11}^{2+}	-0.061

	THEORETICAL (m/z)	EXPERIMENTAL (m/z)	ASSIGNMENTS	ERROR (ppm)
	668.39641	668.39632	$a^{\dagger}_5$	-0.127
	672.41512	672.41512	c_5	0.000
	677.43312	677.43316	$z_{12}^{\bullet\ 2+}$	0.059
	684.44161	684.44160	$z_6^{\bullet}$	-0.015
*	694.39947	694.39946	$c^{\dagger}_5$- H_2O	-0.014
		699.41610	?	
	700.46033	700.46030	y_6	-0.043
		705.93754	?	
	712.41004	712.40999	$c^{\dagger}_5$	-0.063
	721.42790	721.42790	$c_{12}^{\ 2+}$	0.007
		726.42567	?	
*	732.42007	732.42008	$(c^{\dagger}_{12}\text{-}H_2O)^{\ 2+}$	0.014
		738.42032	?	
	741.42535	741.42532	$c^{\dagger}_{12}{}^{\ 2+}$	-0.044
	741.46241	741.46246	$z_{13}^{\bullet\ 2+}$	0.067
	749.47177	749.47175	$y_{13}^{\ 2+}$	-0.027
	755.47872	755.47873	$z_7^{\bullet}$	0.013
	768.96464	768.96479	$(c_{13}\text{-}H_2O)^{2+}$	0.192
	771.49744	771.49740	y_7	-0.052
	777.96993	777.97015	$c_{13}^{\ 2+}$	0.289
	782.49952	782.49953	c_6- H_2O	0.019
	788.96210	788.96207	$(c^{\dagger}_{13}\text{-}2\ H_2O)^{2+}$	-0.038
	796.49136	796.49194	$a^{\dagger}_6$	0.728
	799.50226	799.50229	$c_6^{\bullet}$	0.044
		800.46373	?	
	800.51008	800.51009	c_6	0.012
		804.48386	?	
	818.49885	818.49881	$(c_{14}\text{-}\ H_2O)^{2+}$	-0.046
	819.51297	819.51289	$z_{14}^{\bullet\ 2+}$	-0.092
	822.49443	822.49445	$c^{\dagger}_6$- H_2O	0.024
	825.49477	825.49469	$a^{\dagger}_{14}{}^{\ 2+}$	-0.100
	827.50413	827.50447	$c_{14}^{\ 2+}$	0.411
	827.52233	827.52283	$y_{14}^{\ 2+}$	0.610
	829.49102	829.49088	$(c^{\dagger}_{14}\text{-}2\ H_2O)^{\ 2+}$	-0.172
		833.51004	?	
	838.49631	838.49628	$(c^{\dagger}_{14}\text{-H2O})^{\ 2+}$	-0.030
	839.51042	839.51077	$z^{\dagger}_{14}{}^{\bullet\ 2+}$	0.414
*	840.50500	840.50494	$c^{\dagger}_6$	-0.065
	847.50159	847.50157	$c^{\dagger}_{14}{}^{\ 2+}$	-0.021
		854.51065	?	

	THEORETICAL (m/z)	EXPERIMENTAL (m/z)	ASSIGNMENTS	ERROR (ppm)
	856.52640	856.52662	$z_8^{\bullet}$	0.257
	872.54512	872.54516	y_8	0.046
	883.03834	883.03825	$[M - H_2O + 2H]^{2+}$	-0.102
	894.03052	894.03059	$[M^{\dagger} - 2H_2O + 2H]^{2+}$	0.084
	903.03580	903.03580	$[M^{\dagger} - H_2O + 2H]^{2+}$	0.003
	910.55810	910.55835	$c_6 - H_2O$	0.280
	912.04108	912.04102	$[M^{\dagger} + 2H]^{2+}$	-0.066
	912.54499	912.54417	$[M^{\dagger} + 3H]^{2+\bullet}$	-0.899
	924.54995	924.54975	$a^{\dagger}_7$	-0.211
		928.52210	?	
	928.56866	928.56895	c_7	0.312
		932.54245	?	
	950.55301	950.55296	$c^{\dagger}_7 - H_2O$	-0.053
	966.57442	966.57427	$z_9^{\bullet} - H_2O$	-0.150
*	968.56358	968.56340	$c^{\dagger}_7$	-0.181
	984.58498	984.58488	$z_9^{\bullet}$	-0.102
	1000.60370	1000.60347	y_9	-0.230
	1007.58706	1007.58704	$a^{\dagger}_8 - H_2O$	-0.020
	1011.60578	1011.60570	$c_8 - H_2O$	-0.074
		1022.53180	?	
	1025.59763	1025.59729	$a^{\dagger}_8$	-0.327
		1028.58453	*	
	1029.61634	1029.61606	c_8	-0.272
		1033.59009	?	
		1040.65889	?	
	1051.60069	1051.60055	$c^{\dagger}_8 - H_2O$	-0.133
		1056.61728	?	
	1065.61634	1065.61635	$b_9 - H_2O$	0.009
*	1069.61126	1069.61105	$c^{\dagger}_8$	-0.192
	1082.64289	1082.64277	$c_9 - H_2O$	-0.106
		1084.66117	?	
	1094.64557	1094.64572	$y_{10} - 2NH_3$	0.137
	1096.63474	1096.63406	$a^{\dagger}_9$	-0.616
	1100.65345	1100.65300	c_9	-0.409
	1112.67994	1112.67976	$z_{10}^{\bullet}$	
	1122.63780	1122.63766	$c^{\dagger}_9 - H_2O$	-0.125
	1128.69866	1128.69841	y_{10}	-0.221
*	1140.64837	1140.64811	$c^{\dagger}_9$	-0.224
	1166.64613	1166.64559	QIKKQTALVEL-H_2O-$4NH_3$	-0.463

	THEORETICAL (m/z)	EXPERIMENTAL (m/z)	ASSIGNMENTS	ERROR (ppm)
	1195.72695	1195.72664	c_{10}- H_2O	-0.255
	1213.73751	1213.73871	c_{10}	0.989
	1222.74053	1222.74035	y_{11} - $2NH_3$	-0.147
		1225.76381	?	
	1235.72186	1235.72148	$c^{\dagger}_{10}$ - H_2O	-0.308
	1240.77490	1240.77461	$z_{11}^{\bullet}$	-0.234
*	1253.73243	1253.73217	$c^{\dagger}_{10}$	-0.203
	1256.79362	1256.79336	y_{11}	-0.207
	1294.79536	1294.79511	c_{11} - H_2O	-0.189
	1312.80592	1312.80505	c_{11}	-0.663
		1316.78006	?	
	1334.79027	1334.78997	$c^{\dagger}_{11}$ - H_2O	-0.225
	1349.74501	1349.74452	$a^{\dagger}_{12}$ -$3H_2O$-$2NH_3$	-0.363
	1352.80084	1352.80044	$c^{\dagger}_{11}$	-0.292
	1353.85896	1353.85871	$z_{12}^{\bullet}$	-0.185
	1369.87768	1369.87658	y_{12}	-0.803
	1423.837945	1423.83769	c_{12}- H_2O	-0.179
		1445.82216	?	
*	1463.83286	1463.83252	$c^{\dagger}_{12}$- H_2O	-0.232
	1481.84343	1481.84315	$c^{\dagger}_{12}$	-0.186
	1481.91754	1481.91714	$z_{13}^{\bullet}$	-0.270
		1495.93347	?	
	1497.93626	1497.93669	y_{13}	0.287
	1536.92201	1536.92143	c_{13}- H_2O	-0.374
*	1576.91692	1576.91833	$c^{\dagger}_{13}$- H_2O	0.894
	1635.99042	1635.99012	c_{14}- H_2O	-0.180
*	1639.02648	1639.02559	z_{14}	-0.540
	1806.07214	1806.07273	$[M^{\dagger}-H_2O+2H]^{1+\bullet}$	0.329
*	1824.08270	1824.08089	$[M^{\dagger}+2H]^{1+\bullet}$	-0.992
			Mean	-0.342
			St.Dv.	0.044

Table B-18. CAD mass error analysis of the EK-15 peptide reacted in MeOH/H_2O solution for the precursor ion $[M+C_2O+3H]^{3+}$. * indicates the masses used for calibration.

	THEORETICAL (m/z)	EXPERIMENTAL (m/z)	ASSIGNMENTS	ERROR (ppm)
*	246.18121	246.18123	y_2	0.081
	268.14041	268.14041	b_2 -H_2O	0.000
	308.13533	308.13533	$b^{\dagger}_2$ -H_2O	0.016
*	326.14589	326.14593	$b^{\dagger}_2$	0.123
	359.26527	359.26526	y_3	-0.028

	THEORETICAL (m/z)	EXPERIMENTAL (m/z)	ASSIGNMENTS	ERROR (ppm)
	367.23398	367.23396	TALV-H_2O	-0.041
	374.23484	374.23484	$(b_6\text{-}2H_2O)^{2+}$	-0.007
	374.72685	374.72672	$(b_6\text{-}H_2O\text{-}NH_3)^{2+}$	-0.354
	379.17245	379.17241	$b_3\text{ -}H_2O\text{-}NH_3$	-0.092
	379.19760	379.19759	QTAL-H_2O-NH_3	-0.026
	383.24013	383.24009	b_6^{2+}	-0.091
	385.24454	385.24451	TALV	-0.078
	394.23230	394.23224	$(b^{\dagger}_6\text{-}2H_2O)^{2+}$	-0.152
	395.22889	395.22885	ALVE-H_2O	-0.089
	396.19899	396.19895	$b_3\text{ -}H_2O$	-0.101
	397.20817	397.20813	QTAL-NH_3	-0.088
	403.23758	403.23757	$(b^{\dagger}_6\text{-}H_2O)^{2+}$	-0.031
	411.23505	411.23498	KQTA-H_2O	-0.158
*	412.24287	412.24283	$b^{\dagger}_6{}^{2+}$	-0.085
	413.23945	413.23946	ALVE	0.024
	413.27584	413.27579	VELV-CO	-0.109
	427.29149	427.29143	LVEL-CO	-0.129
	429.24561	429.24555	KQTA	-0.140
	429.75086	429.75075	$(b_7\text{-}2H_2O\text{-}NH_3)^{2+}$	-0.256
	436.19391	436.19390	$b^{\dagger}_3\text{ -}H_2O$	-0.011
	437.27584	437.27568	LVEL-CO	-0.354
	438.26413	438.26408	$(b_7\text{-}2H_2O)^{2+}$	-0.120
	438.75614	438.75612	$(b_7\text{-}H_2O\text{-}NH_3)^{2+}$	-0.051
	441.27075	441.27073	VELV-CO	-0.045
	447.26942	447.26939	$(b_7\text{-}H_2O)^{2+}$	-0.056
		447.77104	?	
*	454.20447	454.20441	$b^{\dagger}_3$	-0.132
	455.28640	455.28634	LVEL	-0.132
	458.26159	458.26158	$(b^{\dagger}_7\text{-}2H_2O)^{2+}$	-0.022
		464.26162	?	
	467.26687	467.26684	$(b^{\dagger}_7\text{-}H_2O)^{2+}$	-0.070
		468.28163	?	
	470.29730	470.29727	$y_4\text{-}H_2O$	-0.053
	476.27216	476.27214	$b^{\dagger}_7{}^{2+}$	-0.031
		477.28186	?	
		477.79585	?	
	481.28814	481.28812	$a_4\text{ -}H_2O$	-0.031
	482.79493	482.79482	$(y_9\text{-}2H_2O)^{2+}$	-0.217
	486.30346	486.30346	KKQT	0.000
	488.30786	488.30783	y_4	-0.061
	491.80021	491.80022	$(y_9\text{-}H_2O)^{2+}$	0.025
	495.29256	495.29254	QTALV-H_2O	-0.030
	496.27657	496.27653	TALVE-H_2O	-0.071

	THEORETICAL (m/z)	EXPERIMENTAL (m/z)	ASSIGNMENTS	ERROR (ppm)
	497.79326	497.79324	$(b_8\text{-}H_2O)^{2+}$	-0.030
		498.32849	?	
	508.31295	508.31299	ALVEL-H_2O	0.089
	508.78543	508.78547	$(b^{\dagger}_8\text{-}2H_2O)^{2+}$	0.079
	509.28305	509.28300	b_4 -H_2O	-0.098
	510.26707	510.26710	b_4 -NH_3	0.059
	514.28713	514.28711	TALVE-H_2O	-0.041
	515.79326	515.79317	$(b_9\text{-}2H_2O\text{-}NH_3)^{2+}$	-0.165
*	517.79071	517.79065	$(b^{\dagger}_8\text{-}H_2O)^{2+}$	-0.121
	521.28305	521.28300	$a^{\dagger}_4$ -H_2O	-0.096
	522.30346	522.30356	KKQTA-H_2O-NH_3	0.191
	524.30653	524.30632	$(b_9\text{-}2H_2O)^{2+}$	-0.396
	524.31911	524.31906	KQTAL-H_2O	-0.086
	524.79854	524.79843	$(b_9\text{-}H_2O\text{-}NH_3)^{2+}$	-0.205
	526.32351	526.32352	ALVEL	0.019
	526.34599	526.34596	RQIK	-0.057
	527.29362	527.29358	b_4	-0.066
	531.26740	531.26726	$b^{\dagger}_4$ -$2H_2O$	-0.264
	533.31181	533.31179	$(b_9\text{-}H_2O)^{2+}$	-0.038
		536.99418	?	
	539.29362	539.29351	$a^{\dagger}_4$	-0.195
	539.33001	539.32996	KKQTA-H_2O	-0.083
	542.31709	542.31716	b_9^{2+}	0.124
	542.32967	542.32970	KQTAL	0.055
	549.27797	549.27791	$b^{\dagger}_4$ -H_2O	-0.100
		550.30670	?	
	552.01731	552.01714	y_{14}^{3+}	-0.308
	553.30927	553.30923	$(b^{\dagger}_9\text{-}H_2O)^{2+}$	-0.068
	554.35481	554.35476	LVELV	-0.090
	555.84769	555.84772	$(y_{10}\text{-}H_2O)^{2+}$	0.058
	556.33970	556.33973	$(y_{10}\text{-}NH_3)^{2+}$	0.058
	557.34057	557.34053	KKQTA	-0.072
	562.31455	562.31459	$b^{\dagger}_9{}^{2+}$	0.071
		563.29352	?	
	564.85297	564.85288	y_{10}^{2+}	-0.159
*	567.28853	567.28850	$b^{\dagger}_4$	-0.053
	569.36571	569.36558	y_5-H_2O	-0.220
		577.34884	?	
	580.84856	580.84854	$(b_{10}\text{-}2H_2O)^{2+}$	-0.030
	587.37627	587.37626	y_5	-0.017
	589.02799	589.02797	$[M\text{-}C_2O\text{-}H_2O+3H]^{3+}$	-0.028
	589.85384	589.85383	$(b_{10}\text{-}H_2O)^{2+}$	-0.017

	THEORETICAL (m/z)	EXPERIMENTAL (m/z)	ASSIGNMENTS	ERROR (ppm)
	595.03151	595.03153	$[M+C_2O+3H]^{3+}$	0.036
	596.35610	596.35603	$[M+C_2O-2H_2O+3H]^{3+}$	-0.123
	597.39701	597.39720	ALVELV-CO	0.326
	598.85912	598.85901	b_{10}^{2+}	-0.188
	600.84602	600.84602	$(b^{\dagger}_{10}-2H_2O)^{2+}$	0.008
	602.35963	602.35960	$[M+C_2O-H_2O+3H]^{3+}$	-0.042
	606.32458	606.32468	$QTALVE-2H_2O$	0.165
		607.03155	?	
	608.36315	608.36308	$[M+C_2O+3H]^{3+}$	-0.110
	609.36063	609.36062	$TALVEL-H_2O$	-0.008
	609.85157	609.85126	$(b^{\dagger}_{10}-H_2O)^{2+}$	-0.508
*	618.85658	618.85651	$b^{\dagger}_{10}{}^{2+}$	-0.113
	620.35147	620.35164	$b_5 -H_2O-NH_3$	0.282
	623.38752	623.38758	$KQTALV-H_2O$	0.104
	624.33515	624.33527	$QTALVE-H_2O$	0.200
		625.31912	?	
	628.90045	628.90041	y_{11}^{2+}	-0.064
	637.37801	637.37801	$b_5 -H_2O$	0.000
	648.39333	648.39315	b_{11}^{2+}	-0.274
	655.38858	655.38862	b_5	0.069
	659.38550	659.38542	$(b^{\dagger}_{11}-H_2O)^{2+}$	-0.125
	668.39079	668.39086	$b^{\dagger}_{11}{}^{2+}$	0.112
	677.37293	677.37293	$b^{\dagger}_5 -H_2O$	0.007
	682.44977	682.44980	y_6-H_2O	0.051
	685.44248	685.44229	y_{12}^{2+}	-0.277
	694.90406	694.90426	$(b_{12}-2H_2O)^{2+}$	0.291
*	695.38349	695.38352	$b^{\dagger}_5$	0.043
	700.46033	700.46037	y_6	0.057
	703.90934	703.90937	$(b_{12}-H_2O)^{2+}$	0.043
	712.91462	712.91471	b_{12}^{2+}	0.123
	732.91208	732.91210	$b^{\dagger}_{12}{}^{2+}$	0.027
	760.45137	760.45141	$(b_{13}-H_2O)^{2+}$	0.053
	765.47297	765.47310	$b_6 -H_2O$	0.170
	771.49744	771.49750	y_7	0.078
	783.48354	783.48373	b_6	0.249
	787.47485	787.47504	$(a_{13}-H_2O-NH_3)^{2+}$	0.248
		618.30909	?	
	795.98812	795.98858	$(a_9-H_2O)^{2+}$	0.581
	800.98029	800.98043	$(b_{14}-2H_2O)^{2+}$	0.172
	805.46789	805.46796	$b^{\dagger}_6 -H_2O$	-0.093
	809.98558	809.98559	$(b_{14}-H_2O)^{2+}$	-0.019

	THEORETICAL (m/z)	EXPERIMENTAL (m/z)	ASSIGNMENTS	ERROR (ppm)
	818.99086	818.99089	$(b_{14}\text{-}H_2O)^{2+}$	-0.040
*	823.47845	823.47863	$b^{\dagger}_{6}$	-0.219
		829.98302	?	
	838.98832	838.98853	$[b^{\dagger}_{14}\text{-}H_2O+H]^{2+}$	-0.256
	854.53456	854.53462	$y_8\text{-}H_2O$	-0.076
	872.54512	872.54528	y_8	0.183
	880.52507	880.52506	$[M+C_2O\text{-}H_2O\text{-}NH_3\text{-}CO+2H]^{2+}$	-0.009
	893.53155	893.53191	$b_7\text{-}H_2O$	0.403
*	915.51590	915.51607	$b^{\ddagger}_{7}\text{-}2H_2O$	0.186
	964.58257	964.58252	$y_9 - 2H_2O$	-0.052
	965.56659	965.56693	$y_9 - H_2O\text{-}NH_3$	0.352
	982.59314	982.59341	$y_9 - H_2O$	0.280
	983.57716	983.57746	$y_9\text{-}NH_3$	0.310
	994.57923	994.579040	$b_8\text{-}H_2O$	-0.191
*	1000.60370	1000.60408	y_9	0.380
	1034.57415	1034.57424	$b^{\dagger}_{8}\text{-}H_2O$	0.092
	1092.67753	1092.67747	$y_{10} - H_2O$	-0.055
	1105.61126	1105.61214	$b^{\dagger}_{9}\text{-}H_2O$	0.800
*	1123.62182	1123.62251	$b^{\dagger}_{9}$	0.614
	1128.69866	1128.69907	y_{10}	0.363
	1178.70040	1178.70085	$b_{10}\text{-}H_2O$	0.382
	1218.69532	1218.69568	$b^{\dagger}_{10}\text{-}H_2O$	0.300
*	1277.76881	1277.76989	$b_{11}\text{-}H_2O$	0.845
			Mean	-0.342
			St.Dv.	0.044

Table B-19. DR(718.91)-ECD(728.91) mass error analysis of the FR-25 peptide reacted in MeOH/H_2O solution for the precursor ion $[M+C_2O+4H]^{4+}$. * indicates the masses used for calibration.

	THEORETICAL (m/z)	EXPERIMENTAL (m/z)	ASSIGNMENTS	ERROR (ppm)
*	246.13226	246.13233	$z_2^{\bullet}$	0.284
	247.14009	247.14019	z_2	0.405
	293.16081	293.16099	c_2	0.614
	345.20067	345.20079	$z_3^{\bullet}$	0.348
	346.20850	346.20864	z_3	0.404
		403.20623	?	
*	407.20374	407.20390	c_3	0.393
	415.22996	415.23012	w_4	0.385
	473.23598	473.23565	$z_4\text{–}H^{\bullet}$	-0.697
	474.24326	474.24342	$z_4^{\bullet}$	0.337
	475.25109	475.25126	z_4	0.368

	THEORETICAL (m/z)	EXPERIMENTAL (m/z)	ASSIGNMENTS	ERROR (ppm)
	478.24085	478.24100	c_4	0.314
*	490.26198	490.26213	y_4	0.306
		499.21758	?	
	514.29837	514.29860	$z_5^{\bullet}$-CH_3COOH	0.457
	572.30385	572.30422	y_5 - NH_3	0.655
	573.31167	573.31187	$z_5^{\bullet}$	0.349
*	574.31950	574.31992	z_5	0.731
		582.29941	?	
	589.33039	589.33049	y_5	0.170
	591.32491	591.32506	c_5	0.254
	686.39573	686.39596	$z_6^{\bullet}$	0.335
*	687.40356	687.40413	z_6	0.829
	696.39333	696.39359	$c^{\dagger}_{11}{}^{2+}$	0.377
		697.24148	?	
	698.39573	698.39631	$z_{13}{}^{2+}$	0.830
		698.16238	?	
	702.41445	702.41485	y_6	0.569
*	704.40897	704.40945	c_6	0.681
		711.44696	?	
	728.91436	728.91479	$[M^{\dagger}+4H]^{4+}$	0.590
	738.43399	738.43392	$a^{\dagger}_{12}{}^{2+}$	-0.095
	740.44335	740.44353	$c_{12}{}^{2+}$	0.243
		743.39626	?	
	760.44080	751.43622	$(c^{\dagger}_{12}$-$H_2O)^{2+}$	0.918
	753.43793	753.43839	$(z_{14}$-$H_2O)^{2+}$	0.611
*	751.43553	760.44105	$c^{\dagger}_{12}{}^{2+}$	0.319
	761.93930	761.93955	$z_{14}{}^{\bullet 2+}$	0.328
	769.94866	769.94923	$y_{14}{}^{2+}$	0.740
	799.46721	799.46747	y_7	0.325
	802.46956	802.46966	$c_7{}^{\bullet}$	0.125
*	803.47738	803.47771	c_7	0.411
	825.48259	825.48338	$(z^{\bullet}_{15}-H^{\bullet})^{2+}$	0.954
	833.99614	833.99609	$y_{15}{}^{2+}$	-0.060
	849.49611	849.49677	$(c^{\dagger}_{14}$-$H_2O)^{2+}$	0.777
*	858.50139	858.50166	$c^{\dagger}_{14}{}^{2+}$	0.312
	861.16984	861.17025	$z_{23}{}^{\bullet 3+}$	0.472
	865.47778	865.47808	y_8 -H_2O-NH_3	0.347
	867.49343	867.49392	$z_8^{\bullet}$- H_2O	0.565
		869.47294	?	
	876.00698	876.00679	$(z^{\bullet}_{16}-H^{\bullet})^{2+}$	0.408
	876.51062	876.51093	$z_{16}{}^{\bullet 2+}$	0.354

	THEORETICAL (m/z)	EXPERIMENTAL (m/z)	ASSIGNMENTS	ERROR (ppm)
	883.48780	883.48822	$z^{\bullet}_{8}-H^{\bullet}$	0.481
	884.49617	884.49697	$z_{8}^{\bullet}$	0.904
		885.02191	?	
*	900.51489	900.51483	y_{8}	-0.067
	900.52387	900.52446	a_{15}^{2+}	0.655
	903.85604	903.85664	$z_{24}^{\bullet\ 3+}$	0.668
	913.52540	913.52517	$(c^{\dagger}_{15}-H_2O)^{2+}$	-0.252
		916.54914	?	
	922.53068	922.53097	$c^{\dagger}_{15}{}^{2+}$	0.312
	950.05807	950.05834	$a^{\dagger}_{16}{}^{2+}$	0.284
	952.06743	952.06724	c_{16}^{2+}	-0.200
		955.51004	?	
	955.55978	955.56037	$a^{\dagger}_{8}$	0.623
	958.04229	958.04256	$z_{17}^{\bullet\ 2+}$	0.287
	959.57849	959.57906	c_{8}	0.594
	965.54653	965.54565	$[M^{\dagger}-H_2O+3H]^{3+}$	-0.913
	965.88247	965.88276	$[M^{\dagger}-H_2O+4H]^{3+\bullet}$	0.300
	966.05165	966.05209	y_{17}^{2+}	0.455
	971.52820	971.52871	$z_{9}^{\bullet}$	0.525
	971.55005	971.55051	$[M^{\dagger}+3H]^{3+}$	0.470
	972.06489	972.06526	$c^{\dagger}_{16}{}^{2+}$	0.383
	980.55502	980.55546	$c^{\dagger}_{8}{}^{\bullet}$ - H_2O	0.454
*	981.56284	981.56383	$c^{\dagger}_{8}$- H_2O	1.009
	987.54692	987.54703	y_{9}	0.111
	993.57409	993.57393	$a^{\dagger}_{17}{}^{2+}$	-0.159
	998.56558	998.56604	$c^{\dagger}_{8}{}^{\bullet}$	0.461
	999.57341	999.57392	$c^{\dagger}_{8}$	0.515
	1006.57562	1006.57541	$(c^{\dagger}_{17}- H_2O)^{2+}$	-0.209
	1015.07699	1015.58124	$c^{\dagger}_{17}{}^{\bullet\ 2+}$	-0.158
	1015.58090	1015.07683	$c^{\dagger}_{17}{}^{2+}$	0.332
	1027.08756	1027.08735	$(z_{18}^{\bullet}-H_2O)^{2+}$	-0.202
	1035.58920	1035.58923	$(z_{18}^{\bullet}-H^{\bullet})^{2+}$	0.029
	1036.09284	1036.09311	$z_{18}^{\bullet\ 2+}$	0.261
*	1036.59675	1036.59683	z_{18}^{2+}	0.077
	1047.58893	1047.58963	$(z^{\dagger}_{18}-H_2O)^{2+}$	0.668
	1052.58605	1052.58621	z_{10}.- H_2O	0.152
	1056.09030	1056.09050	$z^{\dagger}_{18}{}^{\bullet\ 2+}$	0.189
	1069.58933	1069.58911	$z_{10}-H^{\bullet}$	-0.206
	1070.59661	1070.59707	$z_{10}^{\bullet}$	0.430

THEORETICAL (m/z)	EXPERIMENTAL (m/z)	ASSIGNMENTS	ERROR (ppm)
1085.62705	1085.62736	$z_{19}^{\bullet\,2+}$	0.286
1086.13096	1086.13117	$z_{19}^{\,2+}$	0.193
1086.61533	1086.61555	y_{10}	0.202
1106.12842	1106.12742	$z^{\dagger}_{19}{}^{\bullet\,2+}$	-0.904
1114.63112	1114.63132	$c^{\dagger}_{19}{}^{\,2+}$	0.179
1118.62311	1118.62316	$a^{\dagger}_{9}$	0.045
1122.64182	1122.64228	c_9	0.410
1142.16908	1142.16978	$z_{20}^{\bullet 2+}$	0.613
1142.67299	1142.67326	$z_{20}^{\,2+}$	0.236
* 1143.61835	1143.61932	$c^{\dagger}_{9}{}^{\bullet}$ - H_2O	0.848
1161.62891	1161.62928	$c^{\dagger}_{9}{}^{\bullet}$	0.319
1162.16787	1162.16860	$(c^{\dagger}_{20}$ - $H_2O)^{2+}$	0.628
1162.63674	1162.63723	$c^{\dagger}_{9}$	0.421
1171.17315	1171.17341	$c^{\dagger}_{20}{}^{\,2+}$	0.222
1189.70582	1189.70592	$(z_{21}^{\bullet}$ - $H_2O)^{\,2+}$	0.084
1197.64791	1197.64777	z_{11}-$H^{\bullet}$	-0.117
1198.65519	1198.65556	$z_{11}^{\bullet}$	0.309
1199.21502	1199.21542	$z_{21}^{\,2+}$	0.334
1210.20719	1210.20834	$(z^{\dagger}_{21}$ - $H_2O)^{\,2+}$	0.950
1211.70208	1211.70199	$(c^{\dagger}_{21}$ - $H_2O)^{\,2+}$	-0.074
1214.67391	1214.67420	y_{11}	0.239
1218.70856	1218.70903	$z^{\dagger}_{21}{}^{\bullet\,2+}$	0.386
1219.21248	1219.21319	$z^{\dagger}_{21}{}^{\,2+}$	0.582
1219.67079	1219.67096	$a^{\dagger}_{10}$	0.139
1220.70736	1220.70768	$c^{\dagger}_{21}{}^{\,2+}$	0.262
1223.68950	1223.68905	c_{10}	-0.368
1226.22030	1226.22014	$(z_{22}^{\bullet}$-NH3$)^{\,2+}$	-0.130
1234.22966	1234.23035	$z_{22}^{\bullet\,2+}$	0.559
1234.73357	1234.73396	$z_{22}^{\,2+}$	0.316
1245.67385	1245.67352	$c^{\dagger}_{10}$ - H_2O	-0.265
1245.72575	1245.72621	$(z^{\dagger}_{22}$ - $H_2O)^{\,2+}$	0.369
1254.73103	1254.73138	$z_{22}^{\,2+}$	0.279
* 1262.67659	1262.67660	$c^{\dagger}_{10}{}^{\bullet}$	0.008
1263.68442	1263.68486	$c^{\dagger}_{10}$	0.348
1264.72728	1264.72763	$c_{22}^{\bullet\,2+}$	0.277
1276.22337	1276.22232	$(c^{\dagger}_{22}$ - $H_2O)^{\,2+}$	-0.823
1282.74976	1282.75038	$(z_{23}$ - $H_2O)^{\,2+}$	0.483
1285.22865	1285.22898	$c^{\dagger}_{22}{}^{\,2+}$	0.257
1291.25113	1291.25135	$z_{23}^{\bullet\,2+}$	0.170
* 1291.75504	1291.75538	$z_{23}^{\,2+}$	0.263
1302.74721	1302.74713	$(z^{\dagger}_{23}$ - $H_2O)^{\,2+}$	-0.061
1311.72667	1311.72686	y_{12}	0.145
1325.75758	1325.75856	$(c^{\dagger}_{23}$ - $H_2O)^{\,2+}$	0.739
1334.76286	1334.76329	$c^{\dagger}_{23}{}^{\,2+}$	0.322
1351.78446	1351.78560	c_{11}	0.843

THEORETICAL (m/z)	EXPERIMENTAL (m/z)	ASSIGNMENTS	ERROR (ppm)
1355.78433	1355.78471	z_{24}^{2+}	0.280
1356.27206	1356.27142	$a^{\dagger}_{24}{}^{2+}$	-0.472
1369.27359	1369.27427	$(c^{\dagger}_{24}- H_2O)^{2+}$	0.497
1372.76099	1372.76043	$c^{\dagger}_{11}{}^{\bullet}- H_2O$	-0.408
1375.27787	1375.27774	$z^{\dagger}_{24}{}^{\bullet 2+}$	-0.095
1378.27887	1378.27930	$c^{\dagger}_{24}{}^{2+}$	0.312
* 1390.77155	1390.77158	$c^{\dagger}_{11}{}^{\bullet}$	0.022
1391.77938	1391.77976	$c^{\dagger}_{11}{}^{\bullet}$	0.273
1394.77636	1394.77643	$z_{13}^{\bullet}$	0.050
1410.79508	1410.79546	y_{13}	0.269
1430.81342	1430.81335	$[M^{\dagger}- 3H_2O +4H]^{2+\bullet\bullet}$	-0.051
1447.81616	1447.81732	$[M^{\dagger}- H_2O +2H]^{2+}$	0.801
1448.82398	1448.82444	$[M^{\dagger}- H_2O +4H]^{2+\bullet\bullet}$	0.317
1456.82144	1456.82002	$[M^{\dagger}+2H]^{2+}$	-0.975
1457.82927	1457.82947	$[M^{\dagger}+4H]^{2+\bullet\bullet}$	0.137
1501.86377	1501.86420	$c^{\dagger}_{12}- H_2O$	0.286
1504.83695	1504.83657	$y_{14}-2NH_3$	-0.253
* 1519.87434	1519.87450	$c^{\dagger}_{12}$	0.105
1521.86404	1521.86302	$z_{14}-H^{\bullet}$	-0.670
1522.87132	1522.87115	$z_{14}^{\bullet}$	-0.112
1523.87915	1523.87809	z_{14}	-0.696
1538.89004	1538.89053	y_{14}	0.318
1632.93191	1632.93194	$y_{15}-2NH_3$	0.018
1633.96354	1633.96475	$z_{15}^{\bullet}- H_2O$	0.741
1649.95900	1649.95911	$z_{15}-H^{\bullet}$	0.067
1650.96628	1650.96564	$z_{15}^{\bullet}$	-0.388
1651.97411	1651.97480	z_{15}	0.418
1666.98500	1666.98621	y_{15}	0.726
1697.98494	1697.98415	$c^{\dagger}_{14}- H_2O$	-0.465
* 1714.98768	1714.98731	$c^{\dagger}_{14}{}^{\bullet}$	-0.216
1715.99551	1715.99542	$c^{\dagger}_{14}$	-0.052
1732.99557	1732.99579	$y_{16}- H_2O -NH_3$	0.127
1735.01122	1735.00942	$z_{16}- H_2O$	-1.037
1751.00668	1751.00702	$z_{16}-H^{\bullet}$	0.194
1752.01396	1752.01251	$z_{16}^{\bullet}$	-0.828
1753.02179	1753.02249	z_{16}	0.399
1826.04352	1826.04452	$c^{\dagger}_{15}- H_2O$	0.548
* 1844.05409	1844.05461	$c^{\dagger}_{15}$	0.282
1898.07455	1898.07366	$z_{17}^{\bullet} - H_2O$	-0.469
1914.07001	1914.06918	$z_{17}-H^{\bullet}$	-0.434
1915.07729	1915.07534	$z_{17}^{\bullet}$	-1.018
1916.08512	1916.08426	z_{17}	-0.449
1925.11193	1925.11073	$c^{\dagger}_{16}- H_2O$	-0.623
1931.09601	1931.09494	y_{17}	-0.554
* 1942.11467	1942.11520	$c^{\dagger}_{16}{}^{\bullet}$	0.273

1943.12250	1943.12255	$c^{\dagger}_{16}$	0.026
2012.14396	2012.14189	$c^{\dagger}_{17} - H_2O$	-1.029
2029.14670	2029.14798	$c^{\dagger}_{17}{}^{\bullet}$	0.631
* 2030.15453	2030.15394	$c^{\dagger}_{17}$	-0.291
2054.17566	2054.17653	$z^{\dagger}_{18}{}^{\bullet} - H_2O$	0.424
2072.18623	2072.18745	z_{18}	0.589
* 2111.17332	2111.17144	$z^{\dagger}_{18}{}^{\bullet}$	-0.891
2112.18382	2112.18329	$c^{\dagger}_{18} - H_2O$	-0.251
* 2228.25497	2228.25719	$c^{\dagger}_{19}$	0.996
* 2897.64853	2897.64915	$[M^{\dagger} - H_2O + 4H]^{1+\bullet\bullet\bullet}$	0.216
		Mean	-0.133
		St.Dv.	0.537

Table B-20 DR(595.03)-ECD(614 37) mass error analysis for the precursor ion $[M+C_2H_2O_2+3H]^{3+}$ of the glyoxal-derived glycation product formed at EK-15 peptide in MeOH/H_2O solution. * indicates the masses used for calibration.

THEORETICAL (m/z)	**EXPERIMENTAL (m/z)**	**ASSIGNMENTS**	**ERROR (ppm)**
* 303.17752	303.17751	c_2	-0.033
325.16187	325.16184	$c^{\ddagger}_2 - 2H_2O$	-0.092
343.17244	343.17243	$c^{\ddagger}_2 - H_2O$	-0.015
343.24655	343.24655	$z_3^{\bullet}$	0.000
344.25438	344.25436	z_3	-0.044
* 361.18300	361.18300	$c^{\ddagger}_2$	0.000
359.26527	359.26529	y_3	0.056
	372.27175	?	
387.22247	387.22241	a_3	-0.155
400.75868	400.75863	$c_6{}^{2+}$	-0.125
413.27584	413.27584	w_4	0.012
431.23610	431.23609	c_3	-0.023
445.22795	445.22796	$a^{\ddagger}_3$	0.034
453.22045	453.22046	$c^{\ddagger}_3 - 2H_2O$	0.022
464.78797	464.78792	$c_7{}^{2+}$	-0.108
471.23102	471.23102	$c^{\ddagger}_3 - H_2O$	0.011
* 472.28914	472.28914	$z_4^{\bullet}$	0.000
489.24158	489.24158	$c^{\ddagger}_3$	0.000
488.30786	488.30787	y_4	0.020
500.30653	500.30646	a_4	-0.140
500.80549	500.80544	$y_9{}^{2+}$	-0.100
* 515.31181	515.31174	$c_8{}^{2+}$	-0.136
522.29088	522.29069	$a^{\ddagger}_4 - 2H_2O$	-0.354
526.30959	526.30959	$c_4 - H_2O$	-0.010
	528.36161	?	

	THEORETICAL (m/z)	EXPERIMENTAL (m/z)	ASSIGNMENTS	ERROR (ppm)
	540.30145	540.30144	$a^{\ddagger}_4$ - H_2O	-0.009
	544.32016	544.32016	c_4	0.000
	550.83037	550.83023	c_9^{2+}	-0.245
		554.31710	?	
	556.84361	556.84328	$z_{10}^{\bullet 2+}$	-0.593
	558.31201	558.31200	$a^{\ddagger}_4$	-0.009
	566.30451	566.30453	$c^{\ddagger}_4$ - $2H_2O$	0.035
	571.35755	571.35755	$z_5^{\bullet}$	0.000
	584.31508	584.31508	$c^{\ddagger}_4$ - H_2O	0.009
	587.37627	587.37631	y_5	0.068
	596.35610	596.35612	$[M^{\ddagger}-3H_2O+3H]^{3+}$	0.028
	602.32564	602.32568	$c^{\ddagger}_4$	0.066
	608.36315	608.36313	$[M^{\ddagger}-H_2O+3H]^{3+}$	-0.027
	614.36667	614.36669	$[M^{\ddagger}+3H]^{3+}$	0.035
	620.89109	620.89100	$z_{11}^{\bullet +}$	-0.145
	628.40149	628.40145	a_5	-0.064
	641.38629	641.38685	$z_6^{\bullet}$-C_3H_7	0.881
	650.38584	650.38601	$a^{\ddagger}_5$ -$2H_2O$	0.269
	654.40456	654.40469	c_5- H_2O	0.206
*	656.90660	656.90696	c_{11}^{2+}	0.548
	668.39641	668.39641	$a^{\ddagger}_5$ - H_2O	0.007
	672.41512	672.41511	c_5	-0.015
	677.43312	677.43300	$z_{12}^{\bullet 2+}$	-0.177
	684.44161	684.44162	$z_6^{\bullet}$	0.015
	686.40697	686.40703	$a^{\ddagger}_5$	0.095
	694.39947	694.39948	$c^{\ddagger}_5$ - $2H_2O$	0.014
		699.41613	?	
	700.46033	700.46035	y_6	0.029
	712.41004	712.41005	$c^{\ddagger}_5$-H_2O	0.021
		712.49533	?	
	721.42790	721.42794	c_{12}^{2+}	0.062
*	730.42060	730.42062	$c^{\ddagger}_5$	0.027
	741.46241	741.46253	$z_{13}^{\bullet 2+}$	0.162
	749.47177	749.47151	y_{13}^{2+}	-0.347
	755.47872	755.47873	$z_7^{\bullet}$	0.013
	771.49744	771.49747	y_7	0.039
	777.96993	777.96998	c_{13}^{2+}	0.071
	788.96210	788.96242	$(c^{\ddagger}_{13}$-$3H_2O)^{2+}$	0.406
	796.49136	796.49193	$a^{\ddagger}_6$-H_2O	0.716
	800.51008	800.51008	c_6	0.000

	THEORETICAL (m/z)	EXPERIMENTAL (m/z)	ASSIGNMENTS	ERROR (ppm)
	805.49732	805.49732	a_{14}^{2+}	0.006
	819.51297	819.51297	$z_{14}^{\bullet\,2+}$	0.006
	822.49443	822.49442	$c^{\ddagger}_{6} - 2H_2O$	-0.012
	825.49477	825.49472	$(a^{\ddagger}_{14}-H_2O)^{2+}$	-0.064
	827.50413	827.50415	c_{14}^{2+}	0.024
	827.52233	827.52243	y_{14}^{2+}	0.127
	829.49102	829.49094	$(c^{\ddagger}_{14}-3H_2O)^{2+}$	-0.099
	830.50514	830.50520	$(z^{\ddagger\bullet}_{14}-2H_2O)^{2+}$	0.072
	834.50005	834.50015	$a^{\ddagger}_{14}{}^{2+}$	0.117
*	838.49631	838.49641	$(c^{\ddagger}_{14}-2H_2O)^{2+}$	0.125
	839.51042	839.51036	$(z^{\ddagger\bullet}_{14}-H_2O)^{2+}$	-0.074
	840.50500	840.50500	$c^{\ddagger}_{6} - H_2O$	0.006
		845.50408	?	
	847.50159	847.50165	$(c^{\ddagger}_{14}-H2O)^{2+}$	0.074
	856.52640	856.52669	$z_8^{\bullet}$	0.339
	858.51556	858.51544	$c^{\ddagger}_{6}$	-0.140
	872.54512	872.54516	y_8	0.046
	883.03834	883.03835	$[M -H_2O+2H]^{2+}$	0.011
	884.03399	884.03424	$[M-NH_3+3H]^{2+}$	0.283
	892.04362	892.04373	$[M +2H]^{2+}$	0.121
	894.03052	894.03047	$[M^{\ddagger}-3H_2O+2H]^{2+}$	-0.050
	898.54726	898.54741	$[M^{\ddagger}-H_2O-CO+2H]^{2+}$	0.164
	903.03580	903.03574	$[M^{\ddagger}-2H_2O+2H]^{2+}$	-0.064
	912.04108	912.04131	$[M^{\ddagger}-H_2O+2H]^{2+}$	0.252
	913.03700	913.03708	$[M^{\ddagger}-NH_3+3H]^{2+\bullet}$	0.383
	921.04636	921.04649	$[M^{\ddagger}+2H]^{2+}$	0.138
	924.54995	924.54969	$a^{\ddagger}_{7}-H_2O$	-0.276
	928.56866	928.56860	c_7	-0.065
	942.56051	942.56007	$a^{\ddagger}_{7}$	-0.462
	950.55301	950.55309	$c^{\ddagger}_{7}- 2H_2O$	0.084
	966.57442	966.57443	$z_9^{\bullet}-H_2O$	0.016
*	968.56358	968.56340	$c^{\ddagger}_{7} - H_2O$	-0.181
	984.58498	984.58495	$z_9^{\bullet}$	-0.030
	986.57414	986.57398	$c^{\ddagger}_{7}$	-0.162
		998.63578	?	
	1000.60370	1000.60367	y_9	-0.030
	1007.58706	1007.58692	$a^{\dagger}_{8} - H_2O$	-0.139
	1011.60578	1011.60591	$c_8- H_2O$	0.133

	THEORETICAL (m/z)	EXPERIMENTAL (m/z)	ASSIGNMENTS	ERROR (ppm)
	1025.59763	1025.59716	$a^{\dagger}_{8}$	-0.453
	1029.61634	1029.61624	c_{8}	-0.097
	1043.60819	1043.60725	$a^{\ddagger}_{8}$	-0.896
	1051.60069	1051.60072	$c^{\ddagger}_{8}$- 2H_2O	0.029
	1065.61634	1065.61625	b_{9}-H_2O	-0.084
*	1069.61126	1069.61116	$c^{\ddagger}_{8}$ - H_2O	-0.089
	1083.62691	1083.62677	b_{9}	-0.125
	1085.60617	1085.60593	$a^{\ddagger}_{9}{}^{\bullet}$-$C_2H_4$	-0.221
	1087.62182	1087.62166	$c^{\ddagger}_{8}$	-0.147
	1094.64557	1094.64549	y_{10}-2NH_3	-0.073
	1096.63473	1096.63457	$a^{\ddagger}_{9}$-H2O	-0.150
	1100.65345	1100.65338	c_{9}	-0.064
	1112.67994	1112.67992	$z_{10}^{\bullet}$	-0.018
	1114.64529	1114.64514	$a^{\ddagger}_{9}$	-0.139
*	1122.63780	1122.63786	$c^{\ddagger}_{9}$- 2H_2O	0.053
	1128.69866	1128.69852	y_{10}	-0.124
	1140.64837	1140.64819	$c^{\ddagger}_{9}$ - H_2O	-0.153
	1158.65893	1158.65878	$c^{\ddagger}_{9}$	-0.129
	1213.73751	1213.73738	c_{10}	-0.107
	1222.74053	1222.74033	y_{11} - 2NH_3	-0.164
	1235.72186	1235.72203	$c^{\ddagger}_{10}$- 2H_2O	0.138
	1240.77490	1240.77475	$z_{11}^{\bullet}$	-0.121
*	1253.73243	1253.73207	$c^{\ddagger}_{10}$- H_2O	-0.283
	1256.79362	1256.79351	y_{11}	-0.088
	1267.74808	1267.74790	b_{11} - C_2H_4	-0.138
	1271.74299	1271.74302	$c^{\ddagger}_{10}$	0.024
	1312.80592	1312.80595	c_{11}	0.023
	1334.79027	1334.79009	$c^{\ddagger}_{10}$- 2H_2O	-0.135
*	1352.80084	1352.80075	$c^{\ddagger}_{10}$- H_2O	-0.063
	1353.85896	1353.85878	$z_{12}^{\bullet}$	-0.133
	1368.79575	1368.79562	$a^{\ddagger}_{12}{}^{\bullet}$-$C_2H_4$	-0.095
	1369.87768	1369.87740	y_{12}	-0.204
	1370.81140	1370.81173	$c^{\ddagger}_{11}$	0.241
	1423.83795	1423.83752	c_{12}- H_2O	-0.298
	1441.84851	1441.84843	c_{12}	-0.055
*	1463.83286	1463.83280	$c^{\ddagger}_{12}$- 2H_2O	-0.041
	1481.84343	1481.84338	$c^{\ddagger}_{12}$- H_2O	-0.030
	1481.91754	1481.91749	$z_{13}^{\bullet}$	-0.034
*	1499.85399	1499.85436	$c^{\ddagger}_{12}$	0.247

	THEORETICAL (m/z)	EXPERIMENTAL (m/z)	ASSIGNMENTS	ERROR (ppm)
	1554.93257	1554.93273	c_{13}	0.103
	1639.02648	1639.02537	z_{14}	-0.674
*	1654.00098	1654.00020	c_{14}	-0.472
	1678.01357	1678.01448	$z^{\ddagger}_{14}{}^{\bullet}$ - H_2O	0.545
	1679.02139	1679.02147	$z^{\ddagger}_{14}$ - H_2O	0.048
*	1750.05851	1750.05785	$[M -NH_3 -H_2O+3H]^{1+\bullet\bullet}$	-0.377
	1766.05342	1766.05178	$[M -NH_3 +H]^{1+}$	-0.926
	1783.07997	1783.08025	$[M +H]^{1+}$	0.160
		1789.06987	?	
*	1806.07214	1806.07088	$[M^{\ddagger}-2H_2O+2H]^{1+\bullet}$	-0.695
			Mean	-0.342
			St.Dv.	0.044

Table B-21. CAD mass error analysis of the EK-15 peptide reacted in MeOH/H_2O solution for the precursor ion $[M+C_2H_2O_2+3H]^{3+}$. * indicates the masses used for calibration.

	THEORICAL (m/z)	EXPERIMENTAL (m/z)	ASSIGNMENTS	ERROR (ppm)
*	246.18121	246.18119	y_2	-0.081
	268.14041	268.14041	b_2 -H_2O	0.000
	286.15098	286.15099	b_2	0.052
	308.13533	308.13533	$b^{\ddagger}_2$ -$2H_2O$	0.016
*	326.14589	326.14580	$b^{\ddagger}_2$ -H_2O	-0.276
	351.20269	351.20266	KKQ	-0.085
	358.20850	358.20848	KQT	-0.056
	359.26527	359.26528	y_3	0.028
	362.14590	362.14590	b_3 -H_2O-$2NH_3$	0.000
	365.72157	365.72165	$(b_6$-$2H_2O$-$NH_3)^{2+}$	0.219
	367.23398	367.23396	TALV-H_2O	-0.041
	370.25612	370.25611	RQI-CO	-0.014
	374.23484	374.23483	$(b_6$-$2H_2O)^{2+}$	-0.033
	374.72685	374.72687	$(b_6$-H_2O-$NH_3)^{2+}$	0.047
	379.17245	379.17244	b_3 -H_2O-NH_3	-0.013
	379.19760	379.19760	QTAL-H_2O-NH_3	0.000
	380.15647	380.15646	b_3 -$2NH_3$	-0.013
	383.24013	383.24015	$b_6{}^{2+}$	0.065
	385.24454	385.24454	TALV	0.000
	386.21464	386.21463	a_3	-0.026
	392.24541	392.24541	$b_6{}^{2+}$	0.006
	394.20850	394.20846	KQTA-H_2O-NH_3	-0.101
	394.23230	394.23229	$(b^{\ddagger}_6$-$3H_2O)^{2+}$	-0.025
	395.22889	395.22885	ALVE-H_2O	-0.089
	396.19895	396.19899	b_3 -H_2O	0.101

	THEORICAL (m/z)	EXPERIMENTAL (m/z)	ASSIGNMENTS	ERROR (ppm)
	397.18301	397.18296	b_3 -NH_3	-0.126
	397.20817	397.20815	QTAL-NH_3	-0.038
	398.25103	398.25101	RQI	-0.050
*	403.23758	403.23757	$(b^{\dagger}_6$-$2H_2O)^{2+}$	-0.031
	411.23505	411.23502	KQTA-H_2O	-0.061
	413.23945	413.23947	ALVE	0.048
	413.27584	413.27583	VELV-CO	-0.012
	414.20950	414.20955	b_3	-0.121
	424.75869	424.75868	$(a_7$-H_2O-$NH_3)^{2+}$	0.012
	426.20956	426.20955	$a^{\ddagger}_3$ -H_2O	0.012
	427.29149	427.29153	LVEL-CO	0.105
	429.24561	429.24565	KQTA	0.093
	429.75086	429.75085	$(b_7$-$2H_2O$-$NH_3)^{2+}$	-0.023
	430.24287	430.24292	$(b_7$-H_2O-$2NH_3)^{2+}$	0.116
		434.76618	?	
	436.19390	436.19390	$b^{\ddagger}_3$ -$2H_2O$	0.000
	437.27584	437.27590	LVEL-CO	0.149
	438.26413	438.26414	$(b_7$-$2H_2O)^{2+}$	0.017
	438.75614	438.75612	$(b_7$-H_2O-$NH_3)^{2+}$	-0.051
	441.27075	441.27076	VELV-CO	0.023
	447.26942	447.26942	$(b_7$-$H_2O)^{2+}$	0.011
	447.76143	447.76145	$(b_7$-$NH_3)^{2+}$	0.056
	454.20447	454.20457	$b^{\ddagger}_3$-H_2O	0.220
	455.28640	455.28641	LVEL	0.022
	486.26410	486.26419	b_7^{2+}	0.185
	458.26159	458.26164	$(b^{\ddagger}_7$ -$3H_2O)^{2+}$	0.109
		464.26160	?	
	467.26687	467.26690	$(b^{\ddagger}_7$ -$2H_2O)^{2+}$	0.059
		468.28167	?	
	470.29730	470.29730	y_4-H_2O	0.011
	476.27216	476.27217	$b^{\ddagger}_7{}^{2+}$	0.021
	481.28814	481.28813	a_4 -H_2O	-0.010
	482.27216	482.27216	a_4 -NH_3	0.010
	482.79493	482.79494	$(y_9$-$2H_2O)^{2+}$	0.031
	486.30346	486.30346	KKQT	0.000
	488.30786	488.30788	y_4	0.041
	491.80021	491.80022	$(y_9$-$H_2O)^{2+}$	0.025
	495.29256	495.29253	QTALV-H_2O	-0.050
	496.27657	496.27658	TALVE-H_2O	0.030
	497.79326	497.79325	$(b_8$-$H_2O)^{2+}$	-0.010
	499.29870	499.29871	a_4	0.020
	503.27249	503.27243	$a^{\ddagger}_4$-$3H_2O$	-0.109
	506.79854	506.79852	b_8^{2+}	-0.035

	THEORICAL (m/z)	EXPERIMENTAL (m/z)	ASSIGNMENTS	ERROR (ppm)
	508.31295	508.31295	ALVEL-H_2O	0.010
	508.78543	508.78545	$(b^{\ddagger}_8\text{-}3H_2O)^{2+}$	0.039
	509.28305	509.28304	$b_4\text{-}H_2O$	-0.020
	510.26707	510.26708	$b_4\text{-}NH_3$	0.020
	513.30312	513.30311	QTALV	-0.019
	514.28713	514.28712	TALVE-H_2O	-0.019
	515.79326	515.79327	$(b_9\text{-}2H_2O\text{-}NH_3)^{2+}$	0.029
	517.79071	517.79084	$(b^{\ddagger}_8\text{-}2H_2O)^{2+}$	0.246
	521.28305	521.28305	$a^{\ddagger}_4\text{-}2H_2O$	0.000
	522.30346	522.30343	KKQTA-H_2O-NH_3	-0.057
	523.28748	523.28747	KKQTA-$2NH_3$	-0.019
	524.30653	524.30633	$(b_9\text{-}2H_2O)^{2+}$	-0.377
	524.31911	524.31914	KQTAL-H_2O	0.067
	524.79854	524.79851	$(b_9\text{-}H_2O\text{-}NH_3)^{2+}$	-0.052
	526.32351	526.32354	ALVEL	0.057
	526.34599	526.34598	RQIK	-0.019
	527.29362	527.29358	b_4	-0.066
	531.26740	531.26726	$b^{\ddagger}_4\text{-}3H_2O$	-0.264
	533.31181	533.31180	$(b_9\text{-}H_2O)^{2+}$	-0.019
		534.33778	?	
	535.29870	535.29866	$(b^{\ddagger}_9\text{-}4H_2O)^{2+}$	-0.079
	539.29362	539.29363	$a^{\ddagger}_4\text{-}H_2O$	0.028
	539.33001	539.32997	KKQTA-H_2O	-0.065
*	542.31709	542.31709	b_9^{2+}	-0.005
	542.32967	542.32968	KQTAL	0.018
	544.30399	544.30410	$(b^{\ddagger}_9\text{-}3H_2O)^{2+}$	0.211
		544.32018	?	
	549.27797	549.27794	$b^{\ddagger}_4\text{-}2H_2O$	-0.046
	550.29838	550.29835	R($C_2H_2O_2$)QIK-$2NH_3$	-0.055
	552.01731	552.01731	y_{14}^{3+}	0.000
	553.30927	553.30927	$(b^{\ddagger}_9\text{-}2H_2O)^{2+}$	0.005
	554.35481	554.35483	LVELV	0.036
	555.84769	555.84762	$(y_{10}\text{-}H_2O)^{2+}$	-0.121
	556.33970	556.33964	$(y_{10}\text{-}NH_3)^{2+}$	-0.103
	557.34057	557.34052	KKQTA	-0.090
	562.31455	562.31462	$(b^{\ddagger}_9\text{-}H_2O)^{2+}$	0.124
	564.85297	564.85288	y_{10}^{2+}	-0.159
	567.28853	567.28844	$b^{\ddagger}_4\text{-}H_2O$	-0.159
		568.83732	?	
	569.36571	569.36557	$y_5\text{-}H_2O$	-0.237
	572.33529	572.33542	$(b_{10}\text{-}2H_2O\text{-}NH_3)^{2+}$	0.236
	575.85638	575.85640	$(a_{10}\text{-}H_2O)^{2+}$	0.030

	THEORICAL (m/z)	EXPERIMENTAL (m/z)	ASSIGNMENTS	ERROR (ppm)
		577.34886	?	
	580.84856	580.84853	$(b_{10}\text{-}2H_2O)^{2+}$	-0.047
		581.30417	?	
	581.34057	581.34054	$(b_{10}\text{-}H_2O\text{-}NH_3)^{2+}$	-0.047
	584.86167	584.86163	a_{10}^{2+}	-0.060
	587.37627	587.37629	y_5	0.034
	589.02799	589.02798	$[M\text{-}C_2H_2O_2\text{-}H_2O+3H]^{3+}$	-0.011
	589.85384	589.85386	b_{10}^{2+}	0.034
	590.34585	590.34592	$(b_{10}\text{-}NH_3)^{2+}$	0.119
	595.03151	595.03150	$[M+C_2O+3H]^{3+}$	-0.014
	595.85384	595.85383	$(a^{\dagger}_{10}\text{-}H_2O)^{2+}$	-0.017
	596.35610	596.35603	$[M+C_2H_2O_2\text{-}3H_2O+3H]^{3+}$	-0.123
	597.39701	597.39710	ALVELV-CO	0.159
	598.85912	598.85911	b_{10}^{2+}	-0.021
	600.84602	600.84602	$[b^{\ddagger}_{10}\text{-}3H_2O+H]^{2+}$	0.008
	602.35963	602.35957	$[M+C_2H_2O_2\text{-}2H_2O+3H]^{3+}$	-0.091
	604.85912	604.85919	$(a^{\ddagger}_{10}\text{-}H_2O)^{2+}$	0.112
	606.32458	606.32459	QTALVE-$2H_2O$	0.013
	606.36097	606.36092	KQTALV-H_2O-NH_3	-0.082
	607.30860	607.30861	QTALVE-H_2O-NH_3	0.016
	608.36315	608.36308	$[M+C_2H_2O_2\text{-}H_2O+3H]^{3+}$	-0.110
*	609.85157	609.85123	$(b^{\ddagger}_{10}\text{-}2H_2O)^{2+}$	-0.558
	609.38310	609.38300	a_5	-0.156
	616.87732	616.87719	$(a_{11}\text{-}H_2O\text{-}NH_3)^{2+}$	-0.203
	618.85658	618.85630	$(b^{\ddagger}_{10}\text{-}H_2O)^{2+}$	-0.452
	620.35147	620.35145	b_5 -H_2O-NH_3	-0.024
	624.33515	624.33517	QTALVE-H_2O	0.040
	628.90045	628.90057	y_{11}^{2+}	0.191
	637.37801	637.37803	b_5 -H_2O	0.031
	648.39333	648.39331	b_{11}^{2+}	-0.027
	655.38858	655.38858	b_5	0.008
	659.38550	659.38541	$(b^{\ddagger}_{11}\text{-}2H_2O)^{2+}$	-0.140
	667.38858	667.38857	$a^{\ddagger}_5\text{-}H_2O$	-0.007
	677.37293	677.37290	$b^{\ddagger}_5\text{-}2H_2O$	-0.037
	682.44977	682.44949	$y_6\text{-}H_2O$	-0.403
	685.44248	685.44249	y_{12}^{2+}	0.015
	694.90406	694.90401	$(b_{12}\text{-}2H_2O)^{2+}$	-0.068
	695.38349	695.38361	$b^{\ddagger}_5\text{-}H_2O$	0.173
*	700.46033	700.46036	y_6	0.043
	703.90936	703.90937	$(b_{12}\text{-}H_2O)^{2+}$	0.014
	712.91462	712.91465	b_{12}^{2+}	0.039

	THEORICAL (m/z)	EXPERIMENTAL (m/z)	ASSIGNMENTS	ERROR (ppm)
	749.47177	749.47195	$(y_{13})^{2+}$	0.240
	760.45137	760.45143	$(b_{13}\text{-}H_2O)^{2+}$	0.079
	765.47297	765.47300	$b_6\text{-}H_2O$	0.039
	769.45665	769.45668	b_{13}^{2+}	0.036
	771.49744	771.49750	y_7	0.078
	777.47297	777.47309	$a^{\ddagger}_6\text{-}2H_2O$	0.154
		778.40941	?	
	783.48354	783.48358	b_6	0.057
	787.47485	787.47478	$(a_{13}\text{-}H_2O\text{-}NH_3)^{2+}$	-0.083
	788.44134	788.44180	$b^{\ddagger}_6\text{-}2H_2O\text{-}NH_3$	0.583
	789.45411	789.45425	$(b^{\ddagger}_{13}\text{-}H_2O)^{2+}$	0.177
	795.48354	795.48355	$a^{\ddagger}_6\text{-}H_2O$	0.019
	795.98812	795.98839	$(a_9\text{-}H_2O)^{2+}$	0.342
	800.98029	800.98043	$(b_{14}\text{-}2H_2O)^{2+}$	0.172
	805.46789	805.46786	$b^{\ddagger}_6\text{-}2H_2O$	-0.031
	809.98558	809.98559	$(b_{14}\text{-}H_2O)^{2+}$	-0.019
	818.99086	818.99083	$(b_{14}\text{-}H_2O)^{2+}$	0.034
	820.97775	820.97776	$(b^{\dagger}_{14}\text{-}3H_2O)^{2+}$	-0.012
	823.47845	823.47863	$b^{\ddagger}_6\text{-}H_2O$	-0.219
*	841.48902	841.48888	$b^{\ddagger}_6$	0.160
	854.53456	854.53463	$y_8\text{-}H_2O$	-0.088
		868.52514	?	
	872.54512	872.54528	y_8	-0.183
		891.49348	?	
	893.53155	893.53156	$b_7\text{-}H_2O$	0.011
	911.54212	911.54213	b_7	0.016
	915.51590	915.51607	$b^{\ddagger}_7\text{-}3H_2O$	0.186
	923.54212	923.54258	$a^{\ddagger}_7\text{-}H_2O$	0.503
	933.52647	933.52676	$b^{\ddagger}_7\text{-}2H_2O$	0.316
*	951.53703	951.53688	$b^{\ddagger}_7\text{-}H_2O$	-0.158
	964.58252	964.58264	$y_9 - 2H_2O$	0.124
	965.56693	965.56672	$y_9 - H_2O\text{-}NH_3$	-0.217
	982.59314	982.59323	$y_9 - H_2O$	0.097
	983.57715	983.57725	$y_9\text{-}NH_3$	0.097
	994.57923	994.57928	$b_8\text{-}H_2O$	0.050
	1000.60370	1000.60383	y_9	0.130
	1012.58980	1012.58977	b_8	-0.025
*	1034.57415	1034.57371	$b^{\ddagger}_8\text{-}2H_2O$	-0.420
	1065.61634	1065.61663	$b_9\text{-}H_2O$	0.272
	1092.67753	1092.67768	$y_{10} - H_2O$	0.137
	1083.62691	1083.62701	b_9	0.097

	THEORICAL (m/z)	EXPERIMENTAL (m/z)	ASSIGNMENTS	ERROR (ppm)
	1105.61126	1105.61142	$b^{\ddagger}_9$-2H_2O	0.149
*	1123.62182	1123.62139	$b^{\ddagger}_9$-H_2O	-0.383
	1128.69866	1128.69877	y_{10}	0.097
	1141.63239	1141.63284	$b^{\ddagger}_9$	0.399
	1161.67386	1161.67314	b_{10} -H_2O-NH_3	-0.615
	1178.70040	1178.70042	b_{10} -H_2O	0.017
	1196.71097	1196.71062	b_{10}	-0.288
*	1218.69532	1218.69505	$b^{\ddagger}_{10}$-2H_2O	-0.217
	1277.76881	1277.76931	b_{11} -H_2O	0.391
	1295.77938	1295.77954	b_{11}	0.127
	1317.76373	1317.76372	$b^{\ddagger}_{11}$-2H_2O	-0.004
*	1335.77429	1335.77403	$b^{\ddagger}_{11}$-H_2O	-0.195
	1406.81140	1406.81080	b_{12} -H_2O	-0.426
*	1424.82197	1424.82238	b_{12}	0.291
			Mean	-0.122
			St.Dv.	0.049

Table B-22. DR(718.91)-ECD(733.42) mass error analysis of the FR-25 peptide reacted in MeOH/H_2O solution for the precursor ion $[M + C_2H_2O_2 + 4H]^{4+}$. * indicates the masses used for calibration.

	THEORETICAL (m/z)	EXPERIMENTAL (m/z)	ASSIGNMENTS	ERROR (ppm)
*	246.13226	246.13228	$z_2^{\bullet}$	0.081
	247.14009	247.14015	z_2	0.243
	293.16081	293.16081	c_2	0.000
*	345.20067	345.20066	$z_3^{\bullet}$	-0.029
	346.20850	346.20846	z_3	-0.116
	361.21939	361.21934	y_3	-0.138
	407.20374	407.20372	c_3	-0.049
	415.22996	415.22995	w_4	-0.012
*	474.24326	474.24322	$z_4^{\bullet}$	-0.084
	475.25109	475.25109	z_4	0.011
	478.24085	478.24083	c_4	-0.042
	490.26198	490.26197	y_4	-0.020
	572.30385	572.30389	y_5 - NH_3	0.079
*	573.31167	573.31165	$z_5^{\bullet}$	-0.035
	574.31950	57431980	z_5	0.522
	589.33039	589.33058	y_5	0.322
	591.32491	591.32489	c_5	-0.034
	676.39587	676.39591	c_{11}^{2+}	0.059
	685.38791	685.38781	y_6 - NH_3	-0.139
	685.38736	685.38781	$z^{\bullet}_6$–$H^{\bullet}$	0.664
*	686.39573	686.39570	$z_6^{\bullet}$	-0.044

	THEORETICAL (m/z)	EXPERIMENTAL (m/z)	ASSIGNMENTS	ERROR (ppm)
	702.41445	702.41465	y_6	0.285
	704.40897	704.40891	c_6	-0.085
	733.41700	733.41724	$[M^{\ddagger}+4H]^{4+}$	0.326
	761.93930	761.93955	$z_{14}^{\bullet\ 2+}$	0.328
*	769.44609	769.44609	$c^{\dagger}_{12}{}^{\ 2+}$	0.000
	769.94866	769.94801	$y_{14}^{\ 2+}$	-0.844
	799.46721	799.46727	y_7	0.075
	803.47738	803.47739	c_7	0.012
	825.48259	825.48312	$(z^{\bullet}_{15}-H^{\bullet})^{2+}$	0.639
	833.99614	833.99609	$y_{15}^{\ 2+}$	-0.060
	858.50139	858.50148	$(c^{\ddagger}_{14}\text{-}H_2O)^{2+}$	0.102
	861.16984	861.16973	$z_{23}^{\bullet\ 3+}$	-0.132
	865.47778	865.47792	$y_8\text{-}H_2O\text{-}NH_3$	0.162
	867.50668	867.50677	$c^{\ddagger}_{14}{}^{\ 2+}$	0.110
	876.00643	876.00651	$(z^{\bullet}_{16}-H^{\bullet})^{2+}$	0.088
	876.51062	876.51067	$z_{16}^{\bullet\ 2+}$	0.057
*	880.50500	880.50480	$z^{\ddagger}_{23}{}^{\bullet\ 3+}$	-0.231
	883.48780	883.48856	$z^{\bullet}_{8}-H^{\bullet}$	0.866
	884.49617	884.49657	$z_8^{\bullet}$	0.452
	900.51489	900.51525	y_8	0.400
	902.53323	902.53322	$c_{15}^{\ 2+}$	-0.006
	903.85604	903.85601	$z_{24}^{\bullet\ 3+}$	-0.030
	915.56486	915.56515	a_8	0.317
	922.53068	922.53110	$(c^{\ddagger}_{15}\text{-}H_2O)^{\ 2+}$	0.453
*	931.53597	931.53614	$c^{\ddagger}_{15}{}^{\ 2+}$	0.188
	952.06743	952.06737	$c_{16}^{\ 2+}$	-0.063
	955.55978	955.56012	$a^{\ddagger}_{8}$ - H_2O	0.361
	958.04229	958.04224	$z_{17}^{\bullet\ 2+}$	-0.047
	958.55436	958.55437	$[M+4H]^{3+\bullet}$	-0.177
	959.57849	959.57874	c_8	0.261
	962.55454	962.55453	$[M^{\ddagger}\text{-}H_2O\text{-}CO+4H]^{3+\bullet}$	-0.010
	965.88247	965.88266	$[M^{\ddagger}\text{-}2H_2O+4H]^{3+\bullet}$	0.197
	970.51983	970.52061	$z^{\bullet}_{9}-H^{\bullet}$	0.809
	971.52820	971.52840	$z_9^{\bullet}$	0.206
	971.88599	971.88599	$[M^{\ddagger}\text{-}H_2O+4H]^{3+\bullet}$	0.000
	981.07017	981.07029	$c^{\ddagger}_{16}{}^{\ 2+}$	0.122
	987.54692	987.54687	y_9	-0.051
	995.58345	995.58333	$c_{17}^{\ 2+}$	-0.116
	1002.57937	1002.57915	$a^{\ddagger}_{17}{}^{\ 2+}$	-0.217

THEORETICAL (m/z)	EXPERIMENTAL (m/z)	ASSIGNMENTS	ERROR (ppm)
* 1015.58090	1015.58118	$(c^{\ddagger}_{17}- H_2O)^{2+}$	0.273
1017.58397	1017.58411	$c^{\ddagger}_{8}$	0.138
1024.58619	1024.58633	$c^{\ddagger}_{17}{}^{2+}$	0.142
1027.08756	1027.08733	$(z_{18}{}^{\bullet}-H_2O)^{2+}$	-0.222
1036.09284	1036.09290	$z_{18}{}^{\bullet 2+}$	0.058
1065.09558	1065.09555	$z^{\ddagger}_{18}{}^{\bullet 2+}$	-0.028
1069.58824	1069.58875	$z_{10}{}^{\bullet}+H^{\bullet}$	-0.037
1070.59661	1070.59671	$z_{10}{}^{\bullet}$	0.093
1078.62819	1078.62865	a_9	0.426
1085.62705	1085.62712	$z_{14}{}^{\bullet 2+}$	0.064
1086.13096	1086.13050	$z_{14}{}^{2+}$	-0.424
1086.61533	1086.61525	y_{10}	-0.074
1094.63367	1094.63342	$c_{19}{}^{2+}$	-0.228
1105.62450	1105.62472	$(z^{\ddagger}_{19}{}^{\bullet}- H_2O)^{2+}$	0.199
1114.62979	1114.63031	$z^{\ddagger}_{19}{}^{\bullet 2+}$	0.467
* 1114.63112	1114.63031	$(c^{\ddagger}_{19}- H_2O)^{2+}$	0.199
1121.63400	1121.63408	$c_9{}^{\bullet}$	0.071
1122.64182	1122.64199	c_9	0.151
1124.65052	1124.65016	$(z_{20}{}^{\bullet}- H_2O - NH_3)^{2+}$	-0.320
1136.63367	1136.63363	$a^{\ddagger}_{9}$	-0.035
1140.62591	1140.62522	w_{11}	-0.605
1142.16908	1142.16915	$z_{20}{}^{\bullet 2+}$	0.061
1142.67299	1142.67248	$z_{20}{}^{2+}$	-0.446
1150.17844	1150.17943	$y_{20}{}^{2+}$	0.861
1151.17570	1151.17554	$c_{20}{}^{2+}$	-0.139
1162.16653	1162.16653	$(z^{\ddagger}_{20}{}^{\bullet}- H_2O)^{2+}$	0.000
1162.63674	1162.63603	$c^{\ddagger}_{9}- H_2O$	-0.611
1171.17182	1171.17214	$z^{\ddagger}_{20}{}^{\bullet 2+}$	0.273
1171.17315	1171.17214	$(c^{\ddagger}_{20}- H_2O)^{2+}$	-0.862
1178.63166	1178.63180	$b_{20}-C_2H_4$	0.119
1178.70309	1178.70425	$a_{21}{}^{2+}$	0.984
1181.68456	1181.68340	$(z_{21}{}^{\bullet}-2NH_3)^{2+}$	-0.982
1189.70582	1189.70531	$(z_{21}{}^{\bullet}- H_2O)^{2+}$	-0.429
1190.20974	1190.20947	$(z_{21}- H_2O)^{2+}$	-0.227
1197.64737	1197.64721	$z_{11}{}^{\bullet}-H_2{}^{\bullet}$	-0.134
1198.20719	1198.20683	$(z_{21}{}^{\bullet}-H^{\bullet})^{2+}$	-0.300
1198.65519	1198.65529	$z_{11}{}^{\bullet}$	0.083
1198.71111	1198.71088	$z_{21}{}^{\bullet 2+}$	-0.192
* 1199.21502	1199.21420	$z_{21}{}^{2+}$	-0.684
1206.72047	1206.72042	$y_{21}{}^{2+}$	-0.041
1209.70328	1209.70294	$(z^{\ddagger}_{21}{}^{\bullet}-2H_2O)^{2+}$	-0.281
1210.20719	210.20673	$(z^{\ddagger}_{21}-2H_2O)^{2+}$	-0.380
1214.67391	1214.67446	y_{11}	0.453
1218.70856	1218.70844	$(z^{\ddagger}_{21}{}^{\bullet}-H_2O)^{2+}$	-0.098

	THEORETICAL (m/z)	EXPERIMENTAL (m/z)	ASSIGNMENTS	ERROR (ppm)
	1220.70736	1220.70627	$(c^{\ddagger}_{21}\text{-}H_2O)^{2+}$	-0.893
	1222.68168	1222.68108	$c_{10}^{\bullet}$	-0.491
	1223.68950	1223.68961	c_{10}	0.090
	1227.71385	1227.71374	$z^{\ddagger}_{21}{}^{\bullet\,2+}$	-0.090
	1234.22966	1234.22921	z_{22}^{2+}	-0.365
	1234.73357	1234.73243	z_{22}^{2+}	-0.923
	1237.68135	1237.68158	$a^{\ddagger}_{10}$	0.186
	1242.23902	1242.23876	y_{22}^{2+}	-0.209
	1245.72575	1245.72465	$(z^{\ddagger}_{22}\text{-}2H_2O)^{2+}$	-0.883
	1254.22712	1254.22677	$(z^{\ddagger\bullet}_{22}\text{-}H_2O)^{2+}$	-0.279
	1263.23240	1263.23253	$z^{\ddagger\bullet\,2+}_{22}$	0.103
	1263.68442	1263.68429	$c^{\ddagger}_{10}\text{ -}H_2O$	-0.103
	1263.73631	1263.73513	$z^{\ddagger\,2+}_{22}$	-0.934
	1265.23120	1265.23028	c_{22}^{2+}	-0.727
*	1285.22865	1285.22745	$(c^{\ddagger}_{22}\text{ -}H_2O)^{2+}$	-0.934
	1291.25113	1291.25104	$z_{23}^{\bullet\,2+}$	-0.070
	1291.75504	1291.75454	z_{23}^{2+}	-0.387
	1307.77083	1307.77147	a_{11}	0.489
	1311.24858	1311.24839	$(z_{23}^{\bullet}\text{-}H_2O)^{2+}$	-0.145
	1311.72667	1311.72634	y_{12}	-0.252
	1314.76540	1314.76531	c_{23}^{2+}	-0.068
	1320.25387	1320.25379	$z^{\ddagger}_{23}{}^{\bullet 2+}$	-0.061
	1327.26432	1327.26560	$(a_{24}\text{- }H_2O)^{2+}$	0.964
	1334.76286	1334.76234	$(c^{\ddagger}_{23}\text{- }H_2O)^{2+}$	-0.390
	1336.27460	1336.27447	a_{24}^{2+}	-0.097
	1346.77905	1346.77961	$(z_{24}\text{- }H_2O)^{2+}$	0.416
	1350.77664	1350.77681	$c_{11}^{\bullet}$	0.126
	1351.78446	1351.78445	c_{11}	-0.007
	1355.28042	1355.28015	$z_{24}^{\bullet\,2+}$	-0.199
	1355.78433	1355.78405	z_{24}^{2+}	-0.207
	1358.28142	1358.28113	c_{24}^{2+}	-0.214
	1365.27734	1365.27714	$a^{\ddagger}_{24}{}^{2+}$	0.344
	1369.27359	1369.27355	$(c^{\ddagger}_{24}\text{- }2H_2O)^{2+}$	-0.029
	1375.78179	1375.78166	$z^{\ddagger}_{24}{}^{2+}$	-0.094
	1378.27887	1378.27841	$(c^{\ddagger}_{24}\text{- }H_2O)^{2+}$	-0.334
	1391.77938	1391.77859	$c^{\ddagger}_{11}\text{- }H_2O$	-0.568
	1393.76854	1393.76790	$z_{13}^{\bullet}\text{- }H^{\bullet}$	-0.459
	1394.77636	1394.77644	$z_{13}^{\bullet}$	0.057
	1410.79508	1410.79467	y_{13}	-0.291
	1429.81884	1429.81984	$c_{12}\text{- }H_2O\text{ - }NH_3$	0.699
	1448.82398	1448.82389	$[M^{\ddagger}\text{- }2H_2O\text{ }+4H]^{2+\bullet\bullet}$	-0.442
	1456.82144	1456.82104	$[M^{\ddagger}\text{- }H_2O\text{ }+2H]^{2+}$	-0.275
*	1465.82672	1465.82691	$[M^{\ddagger}+2H]^{2+}$	0.130
	1478.87160	1478.87069	$c_{12}^{\bullet}$	-0.615
	1479.87942	1479.87974	c_{12}	0.216

	THEORETICAL (m/z)	EXPERIMENTAL (m/z)	ASSIGNMENTS	ERROR (ppm)
	1504.83695	1504.83747	y_{14}-2NH_3	0.346
	1505.86858	1505.86813	$z_{14}^{\bullet}$- H_2O	-0.299
	1521.86404	1521.86380	z_{14}-$H^{\bullet}$	-0.158
*	1522.87132	1522.87086	$z_{14}^{\bullet}$	-0.302
	1538.89004	1538.88971	y_{14}	-0.214
	1632.93191	1632.93127	y_{15}-2NH_3	-0.392
	1649.95900	1649.95860	$z_{15}^{\bullet}$- $H^{\bullet}$	0.085
*	1650.96628	1650.96555	$z_{15}^{\bullet}$	-0.442
	1651.97411	1651.97447	z_{15}	0.218
	1666.98500	1666.98531	y_{15}	0.186
	1674.99277	1674.99304	$c_{14}^{\bullet}$	0.161
*	1676.00059	1676.00088	c_{14}	0.173
	1715.99551	1715.99523	$c^{\ddagger}_{14}$- H_2O	-0.163
	1732.99557	1732.99533	y_{16}- H_2O - NH_3	-0.138
	1734.00340	1734.00258	$z_{16}^{\bullet}$- H_2O	-0.473
	1735.01122	1735.01090	$z_{16}^{\bullet}$- H_2O	-0.184
	1751.00668	1751.00592	$z_{16}^{\bullet}$- $H^{\bullet}$	-0434
	1753.02179	1753.02222	z_{16}	0.245
	1803.05135	1803.05103	$c_{15}^{\bullet}$	-0.177
	1804.05917	1804.05965	c_{15}	0.266
*	1898.07455	1898.07415	$z_{17}^{\bullet}$- H_2O	-0.211
	1902.11976	1902.12108	$c_{16}^{\bullet}$	0.694
	1903.12758	1903.12834	c_{16}	0.399
	1916.08512	1916.08454	z_{17}	-0.303
*	1990.15961	1990.15989	c_{17}	0.141
	2054.17566	2054.17545	$z_{18}^{\bullet}$- H_2O	-0.102
	2070.17112	2070.17238	z_{18}-$H^{\bullet}$	0.609
*	2072.18623	2072.18717	z_{18}	0.454
	2094.17058	2094.17017	$z^{\ddagger}_{18}{}^{\bullet}$- 2$H_2O$	-0.196
	2111.17332	2111.17270	$z^{\ddagger}_{18}{}^{\bullet}$- H_2O	-0.294
	2112.18114	2112.18085	$z^{\ddagger}_{18}$- H_2O	-0.137
	2171.25464	2171.25526	z_{19}	0.286
	2188.26005	2188.26019	c_{19}	0.064
	2211.24955	2211.24892	$z^{\ddagger}_{19}{}^{\bullet}$- H_2O	-0.285
	2284.33870	2284.33923	z_{20}	0.232
	2301.34411	2301.34553	c_{20}	0.617
	2342.34418	2342.34369	$z^{\ddagger}_{20}$	-0.209
	2397.42276	2397.42389	z_{21}	0.471
	2468.45987	2468.45995	z_{22}	0.032
	2508.45478	2508.45626	z_{22}- H_2O	0.590
	2528.44729	2528.44709	$c_{22}^{\bullet}$	-0.079
	2529.45511	2529.45503	c_{22}	-0.032
*	2582.50280	2582.50513	z_{23}	0.902
			mean	-0.051

St. Dv.	0.462

C

Mass Error tables with assignments used to interpret the data of Chapter 5

TABLE OF CONTENTS.

Table C-14 CAD mass error analysis for the parent ion $[M+C_2 - H_2+3H]^{3+}$ of the glyoxal-derived glycation product formed at EK-15 with addition of sodium chloride. C-22

Table C-1. Mass error of the internal calibration of the direct infusion spectra of the reacted EK-15 peptide in MeOH/H_2O solution. Every chosen ion did not contain the added mass of the modification.

THEORETICAL (m/z)	EXPERIMENTAL (m/z)	INTERNAL CALIBRANT CHOSEN ION	ERROR (ppm)
446.77629	446.77621	$[M+4H]^{4+}$	-0.186
446.52545	446.52542	$[M+^{13}C+4H]^{4+}$	-0.078
456.52418	456.52428	$[M+C_2O+4H]^{4+}$	0.209
461.02682	461.02688	$[M+C_2H_2O_2+4H]^{4+}$	0.128
595.03151	595.03148	$[M+3H]^{3+}$	-0.042
595.36596	595.36564	$[M+^{13}C+3H]^{3+}$	-0.544
608.36315	608.36332	$[M+C_2O+3H]^{3+}$	0.287
614.36667	614.36680	$[M+C_2H_2O_2+3H]^{3+}$	0.213
892.54530	892.54527	$[M+2H]^{2+}$	-0.032
892.04362	892.04388	$[M+^{13}C+2H]^{2+}$	-0.294
912.04108	912.04101	$[M+^{13}C_2+2H]^{2+}$	-0.082
921.04636	921.04621	$[M+C_2H_2O_2+2H]^{2+}$	-0.167
		Standard deviation:	0.275

Table C-2. Mass error of the internal calibration of the direct infusion spectra of the reacted FR-25 peptide in MeOH/H_2O solution. Every chosen ion did not contain the added mass of the modification.

THEORETICAL (m/z)	EXPERIMENTAL (m/z)	INTERNAL CALIBRANT CHOSEN ION	ERROR (ppm)
958.21843	958.21847	$[M + 3H]^{3+}$	0.049
958.55288	958.55307	$[M + ^{13}C + 3H]^{3+}$	0.205
958.88733	958.88754	$[M + ^{13}C_2 + 3H]^{3+}$	0.223
977.55358	977.55405	$[M + C_2H_2O_2 + 3H]^{3+}$	0.490
971.55005	971.54913	$[M + C_2O + 3H]^{3+}$	-0.955
718.91564	718.91560	$[M+4H]^{4+}$	-0.052
719.16648	719.16656	$[M+^{13}C+4H]^{4+}$	0.113
719.41732	719.41732	$[M+^{13}C_2+4H]^{4+}$	0.004
719.66815	719.66816	$[M+^{13}C_3+4H]^{4+}$	0.003

THEORETICAL (m/z)	EXPERIMENTAL (m/z)	INTERNAL CALIBRANT CHOSEN ION	ERROR (ppm)
728.91436	728.91426	$[M + C_2O + 4H]^{4+}$	-0.142
733.41700	733.41704	$[M + C_2H_2O_2 + 4H]^{4+}$	0.060
575.33397	575.33399	$[M+5H]^{5+}$	0.038
575.53464	575.53472	$[M+^{13}C+5H]^{5+}$	0.153
575.73531	575.73586	$[M+^{13}C_2+5H]^{5+}$	-0.205
575.93598	575.93586	$[M+^{13}C_3+5H]^{5+}$	-0.205
		Standard deviation	0.342

Table C-3 Mass error of the internal calibration of the direct infusion spectra of the sodiated EK-15 peptide. Every chosen ion did not contain the added mass of the sodiation.

THEORETICAL (m/z)	EXPERIMENTAL (m/z)	INTERNAL CALIBRANT CHOSEN ION	ERROR (ppm)
446.52545	446.52550	$[M + 4H]^{4+}$	0.106
446.77629	446.77624	$[M + {}^{13}C + 4H]^{4+}$	-0.107
595.03151	595.03154	$[M + 3H]^{3+}$	0.055
595.36596	595.36593	$[M + {}^{13}C+ 3H]^{3+}$	-0.054
892.04362	892.04362	$[M + 2H]^{2+}$	-0.000
		Standard deviation	0.127

Table C-4 Mass error of the internal calibration of the direct infusion spectra of the sodiated FR-25 peptide. Every chosen ion did not contain the added mass of the sodiation.

THEORETICAL (m/z)	EXPERIMENTAL (m/z)	INTERNAL CALIBRANT CHOSEN ION	ERROR (ppm)
575.33397	575.33398	$[M + 5H]^{5+}$	0.030
575.53464	575.53480	$[M + {}^{13}C + 5H]^{5+}$	0.278
718.91564	718.91548	$[M + 4H]^{4+}$	-0.226
719.16648	719.16630	$[M + {}^{13}C + 4H]^{4+}$	-0.241
958.21843	958.21917	$[M + 3H]^{3+}$	0.781
958.88733	958.88732	$[M + {}^{13}C+ 3H]^{3+}$	-0.014
		Standard deviation	0.399

Table C-5. DR(595.03)-ECD(602.36) mass error analysis for the parent ion $[M+C_2 - H_2+3H]^{3+}$ of the glyoxal-derived glycation product formed at EK-15 peptide in MeOH/H_2O solution. * indicates the masses used for calibration.

THEORETICAL (m/z)	EXPERIMENTAL (m/z)	ASSIGNMENTS	ERROR (ppm)
* 230.16249	230.16250	$z_2^{\bullet}$	0.043
246.18121	246.18123	y_2	0.081
285.16695	285.16696	$c_2 - H_2O$	0.018
302.16969	302.16973	$c_2^{\bullet}$	0.116
303.17752	303.17750	c_2	-0.066
* 325.16187	325.16184	c^*_2	-0.092
343.24655	343.24652	$z_3^{\bullet}$	-0.087
344.25438	344.25435	z_3	-0.087
359.26527	359.26529	y_3	0.056
387.22247	387.22245	a_3	-0.052
400.75868	400.75868	c_6^{2+}	0.000
411.75086	411.75093	$c^*_6{}^{2+}$	0.170
413.22553	413.22554	c_3-H_20	0.012
413.27584	413.27582	w_4	-0.048
431.23610	431.23612	c_3	0.046
436.77620	436.77627	y_8^{2+}	0.160
* 453.22045	453.22046	c^*_3	0.022
464.78797	464.78801	c_7^{2+}	0.086
472.28914	472.28914	$z_4^{\bullet}$	0.000
473.29697	473.29699	z_4	0.042
475.78015	475.78022	$c^*_7{}^{2+}$	0.147
488.30786	488.30794	y_4	0.164
500.30653	500.30678	a_4	0.500
515.31181	515.31190	c_8^{2+}	0.175
517.30499	517.30500	$(a^*_9 - {}^{\bullet}CONH_2)^{2+}$	0.019
522.29088	522.29083	a_9	-0.096
526.30399	526.30383	$c^*_8{}^{2+}$	-0.304
526.30959	526.30956	$c_4 - H_2O$	-0.067
544.32016	544.32022	c_4	0.110
550.83037	550.83087	c_9^{2+}	0.908
556.84361	556.84351	$z_{10}{}^{\bullet 2+}$	-0.180
561.82254	561.82281	$c^*_9{}^{2+}$	0.481
564.85297	564.85352	y_{10}^{2+}	0.974
* 566.30451	566.30444	c^*_4	-0.124
570.35027	570.35039	z_5-$H^{\bullet}$	0.210
571.35755	571.35763	$z_5^{\bullet}$	0.140
587.37627	587.37629	y_5	0.034
596.35610	596.35589	$[M+C_2-H_2- H_2O +3H]^{3+}$	-0.352
602.35963	602.35946	$[M+C_2-H_2+3H]^{3+}$	-0.282
620.89109	620.89103	$z_{11}{}^{\bullet 2+}$	-0.097
621.39500	621.39503	z_{11}^{2+}	0.048
	641.38689	?	

THEORETICAL (m/z)	EXPERIMENTAL (m/z)	ASSIGNMENTS	ERROR (ppm)
654.40455	654.40448	$c_5 - H_2O$	-0.115
656.90660	656.90657	c_{11}^{2+}	-0.046
672.41512	672.41505	c_5	-0.104
677.37293	677.37340	b_5	0.694
677.43312	677.43348	$z_{12}^{\bullet 2+}$	0.219
684.44161	684.44176	$z_6^{\bullet}$	0.219
* 694.39947	694.39962	c^*_5	0.216
700.46033	700.46032	y_6	-0.014
	712.42387	?	
721.42790	721.42827	c_{12}^{2+}	-0.500
741.46241	741.46221	$z_{13}^{\bullet 2+}$	-0.270
741.96632	741.96642	z_{13}^{2+}	0.135
749.47177	749.47240	y_{13}^{2+}	0.841
* 755.47872	755.47875	$z_7^{\bullet}$	0.040
771.49744	771.49711	y_7	-0.428
777.96993	777.96940	c_{13}^{2+}	-0.681
782.49951	782.49995	$c_6 - H_2O$	0.556
	813.47179	?	
819.51297	819.51305	$z_{14}^{\bullet 2+}$	0.098
* 822.49443	822.49417	c^*_6	-0.316
827.50413	827.50453	c_{14}^{2+}	0.483
838.49631	838.49577	$c^*_{14}{}^{2+}$	-0.644
855.51912	855.51904	$z_8^{\bullet} - H^{\bullet}$	-0.094
872.54512	872.54523	y_8	0.126
903.03580	903.03661	$[M+C_2-H_2+2H]^{2+}$	0.897
903.53971	903.53932	$[M+3H]^{2+\bullet}$	-0.432
910.55809	910.55750	$c_7 - H_2O$	-0.653
926.55570	926.55619	w_9	0.529
928.56866	928.56904	c_7	0.409
* 950.55301	950.55319	c^*_7	0.189
984.58498	984.58480	$z_9^{\bullet}$	-0.183
* 1000.60370	1000.60455	y_9	0.849
1011.60577	1011.60588	$c_8 - H_2O$	0.104
1029.61634	1029.61645	c_8	0.107
1051.60069	1051.60072	c^*_8	0.029
1082.64288	1082.64334	$c_9 - H_2O$	0.420
1112.67994	1112.68058	$z_{10}^{\bullet}$	0.575
* 1122.63780	1122.63750	c^*_9	-0.267
1128.69866	1128.69869	y_{10}	0.027
* 1235.72186	1235.72167	c^*_{10}	-0.154
1240.77490	1240.77500	$z_{11}^{\bullet}$	0.081
1294.79535	1294.79484	$c_{11} - H_2O$	-0.398
* 1334.79027	1334.79007	c^*_{11}	-0.150
1353.85896	1353.85873	$z_{12}^{\bullet}$	-0.170
* 1463.83286	1463.83254	c^*_{12}	-0.157

THEORETICAL (m/z)	EXPERIMENTAL (m/z)	ASSIGNMENTS	ERROR (ppm)
1481.91754	1481.91766	z_{14}	0.081
1789.06941	1789.06759	$[M+(C_2-H_2)- H_2O +3H]^{1+\bullet\bullet}$	-1.017
* 1807.07997	1807.07946	$[M+(C_2-H_2)+3H]^{1+\bullet\bullet}$	-0.282
		mean	-0.059
		St. Dv.	0.463

Table C-6. Mass error of the internal calibration of the DR(595.03)-ECD(602.36) spectra for the parent ion m/z 602.36 of the reacted EK-15 peptide in MeOH/H_2O solution. Every chosen ion did not contain the added mass of the modification.

THEORETICAL (m/z)	EXPERIMENTAL (m/z)	INTERNAL CALIBRANT CHOSEN ION	ERROR (ppm)
230.16249	230.16250	$z^{\bullet}_2$	0.024
343.24655	343.24652	$z^{\bullet}_3$	-0.101
431.23610	431.23610	c_3	0.011
544.32020	544.32018	c_4	-0.031
672.41510	672.41499	c_5	-0.170
755.47872	755.47866	$z^{\bullet}_7$	-0.083
856.52640	856.52716	$z^{\bullet}_8$	0.886
928.56870	928.56888	c_7	0.195
1029.61640	1029.61624	c_8	0.159
1112.67994	1112.68033	$z^{\bullet}_{10}$	0.346
1240.77490	1240.77466	$z^{\bullet}_{11}$	-0.194
1353.85896	1353.85832	$z^{\bullet}_{12}$	-0.474
1441.84851	1441.84823	c_{12}	-0.192
1481.91754	1481.91714	$z^{\bullet}_{13}$	-0.267
		Standard deviation	0.362

Table C-7. Mass error of the internal calibration of the CAD spectra for the parent ion $[M+C_2 - H_2+4H]^{4+}$ of the reacted EK-15 peptide in PBS buffer. Every chosen ion did not contain the added mass of the modification.

THEORETICAL (m/z)	EXPERIMENTAL (m/z)	INTERNAL CALIBRANT CHOSEN ION	ERROR (ppm)
359.26527	359.26534	y_3	0.195
396.19899	396.19872	$b_3- H_2O$	-0.681
414.20956	414.20962	b_3	0.144
527.29362	527.29354	b_4	-0.146

THEORETICAL (m/z)	EXPERIMENTAL (m/z)	INTERNAL CALIBRANT CHOSEN ION	ERROR (ppm)
655.38858	655.38857	b_5	-0.015
765.47297	765.47335	b_6- H_2O	0.496
872.54120	872.54155	y_8	0.401
1000.60370	1000.60304	y_9	0.009
1128.69866	1128.69945	y_{10}	-0.699
		Standard deviation	0.428

Table C-8. Mass error of the internal calibration of the DR(718.91)-ECD(724.41) spectrum of the parent ion $[M+C_2-H_2+4H]^{4+}$ with ejection of $[M+4H]^{4+}$ of the FR-25 peptide in MeOH/H_2O solution. Every chosen ion did not contain the added mass of the modification.

THEORETICAL (m/z)	EXPERIMENTAL (m/z)	INTERNAL CALIBRANT CHOSEN ION	ERROR (ppm)
246.13226	246.13226	$z^{\bullet}_2$	0.020
345.20067	345.20066	$z^{\bullet}_3$	-0.035
474.24326	474.24322	$z^{\bullet}_4$	-0.079
573.31167	573.31164	$z^{\bullet}_5$	-0.057
686.39573	686.39572	$z^{\bullet}_6$	-0.015
704.40843	704.40886	c_6	-0.150
761.93930	761.93939	$z^{\bullet}_{14}{}^{2+}$	0.116
803.47684	803.47742	c_7	0.044
825.98678	825.98678	$z^{\bullet}_{17}{}^{2+}$	0.003
876.51062	876.51064	$z^{\bullet}_{17}{}^{2+}$	0.019
958.04229	958.04232	$z^{\bullet}_{17}{}^{2+}$	0.032
971.52820	971.52846	$z^{\bullet}_9$	0.271
1070.59661	1070.59680	$z^{\bullet}_{10}$	0.176
1122.64182	1122.64227	c_9	0.398
1223.68950	1223.68996	c_{10}	0.380
1394.77636	1394.77641	$z^{\bullet}_{13}$	0.035
1522.87132	1522.87046	$z^{\bullet}_{14}$	-0.562
1650.96628	1650.96582	$z^{\bullet}_{15}$	-0.281
1752.01396	1752.01292	$z^{\bullet}_{16}$	-0.596
		Standard deviation	0.475

Table C-9. Mass error of the internal calibration of the CAD spectrum of the parent ion $[M+C_2-H_2+4H]^{4+}$ of the FR-25 peptide in PBS buffer. Every chosen ion did not contain the added mass of the modification.

THEORETICAL (m/z)	EXPERIMENTAL (m/z)	INTERNAL CALIBRANT CHOSEN ION	ERROR (ppm)
262.15098	262.15094	y_2	-0.163
361.21939	361.21958	y_3	0.538
461.21431	461.21429	b_4	-0.023
574.29836	574.29819	b_5	-0.311
603.83512	603.83498	b_{10}^{2+}	-0.238
702.41445	702.41478	y_6	0.467
799.46721	799.46671	y_7	-0.622
900.51489	900.51425	y_8	-0.706
1086.61533	1086.61471	y_{10}	-0.571
1214.67391	1214.67491	y_{11}	0.824
1311.72667	1311.72795	y_{12}	0.975
		Standard deviation	0.594

Table C-10. CAD mass error analysis for the parent ion $[M+C_2 - H_2+3H]^{3+}$ of the glyoxal-derived glycation product formed at EK-15 peptide in $MeOH/H_2O$ solution. * indicates the masses used for calibration.

THEORETICAL (m/z)	EXPERIMENTAL (m/z)	ASSIGNMENTS	ERROR (ppm)
* 308.13533	308.13531	b^*_2	-0.049
350.73381	350.73369	y_6^{2+}	-0.342
359.26527	359.26534	y_3	0.195
394.23230	394.23205	$(b^*_6 - H_2O)^{2+}$	-0.634
396.19899	396.19872	$b_3 - H_2O$	-0.681
403.23758	403.23740	b^{*2+}_6	-0.446
413.27584	413.27579	w_4	-0.121
* 436.19390	436.19386	b^*_3	-0.103
456.27470	456.27446	b_7^{2+}	-0.526
458.26159	458.26144	$(b^*_7 - H_2O)^{2+}$	-0.327
458.75360	458.75355	$(b^*_7 - NH_3)^{2+}$	-0.109
467.26687	467.26649	b^{*2+}_7	-0.813
470.29730	470.29736	$y_4 - H_2O$	0.128
488.30786	488.30781	y_4	-0.102
491.80021	491.80004	$(y_9 - H_2O)^{2+}$	-0.346
498.28527	498.28562	$(b_8 - NH_3)^{2+}$	0.702
506.79854	506.79833	b_8^{2+}	-0.414
509.28305	509.28281	$b_4 - H_2O$	-0.471
517.79071	517.79067	b^{*2+}_8	0.384

	THEORETICAL (m/z)	EXPERIMENTAL (m/z)	ASSIGNMENTS	ERROR (ppm)
	521.28305	521.28259	a^*_4	-0.882
	524.79854	524.79834	$(b_9 - H_2O - NH_3)^{2+}$	-0.381
	527.29362	527.29322	b_4	-0.749
	533.31181	533.31142	$(b_9 - H_2O)^{2+}$	-0.731
	542.31709	542.31698	b_9^{2+}	-0.203
	544.30399	544.30376	$(b^*_9 - H_2O)^{2+}$	-0.423
*	549.27796	549.27768	b^*_4	-0.519
	559.34500	559.34514	y_{14}^{3+}	-0.518
	564.85297	564.85279	y_{10}^{2+}	-0.319
	569.36571	569.36618	$y_5 - H_2O$	0.825
	581.34057	581.34047	$(b_{10} - H_2O - NH_3)^{2+}$	0.172
	587.37627	587.37653	y_5	0.443
	589.85384	589.85337	$(b_{10} - H_2O)^{2+}$	-0.797
	590.68059	590.68064	$[M+C_2-H_2 - H_2O - NH_3+3H]^{3+}$	0.085
	590.68059	590.68064	$[M+C_2-H_2 - H_2O - NH_3+3H]^{3+}$	0.688
	595.35610	595.35651	$[M+C_2-H_2 - H_2O +3H]^{3+}$	-0.585
	596.68411	596.68374	$[M+C_2-H_2 - NH_3+3H]^{3+}$	-0.620
	598.85912	598.85944	b_{10}^{2+}	-0.969
	602.35963	602.35948	$[M+C_2-H_2 +3H]^{3+}$	-0.249
*	609.85130	609.85127	$b^*_{10}^{2+}$	-0.667
	628.90045	628.89986	y_{11}^{2+}	-0.938
	637.37801	637.37741	$b_5 - H_2O$	-0.941
	655.38857	655.38803	b_5	-0.832
	677.37293	677.37273	b^*_5	-0.288
	682.44977	682.44936	$y_6 - H_2O$	-0.601
	700.46033	700.46093	y_6	0.857
	703.90934	703.90977	$(b_{12} - H_2O)^{2+}$	0.611
	712.91462	712.91427	b_{12}^{2+}	-0.491
	714.90152	714.90180	$(b^*_{12} - H_2O)^{2+}$	0.392
	765.47297	765.47335	$b_6 - H_2O$	0.496
	712.91462	712.91427	b_{13}^{2+}	0.611
*	769.45665	769.45618	$(b^*_{13} - H_2O)^{2+}$	0.881
	771.49744	771.49741	y_7	-0.039
	780.44883	780.44820	$(b^*_{13} - H_2O)^{2+}$	-0.807
	787.45732	787.45720	$b^*_6 - H_2O$	-0.152
*	829.98306	829.98357	$b^*_{14}^{2+}$	0.614
	872.54120	872.54140	y_8	-0.321
	915.51590	915.51532	$b^*_7 - H_2O$	-0.634
*	933.52647	933.52574	b^*_7	-0.777
	982.59314	982.59384	$y_9 - H_2O$	0.717
*	1000.60370	1000.60304	y_9	-0.660
			Mean	-0.019
			St. Dv.	0.524

Table C-11. DR(718.91)-ECD(724.41) mass error analysis for the parent ion $[M+C_2 – H_2+4H]^{4+}$ of the glyoxal-derived glycation product formed at FR-25 peptide in MeOH/H_2O solution. * indicates the masses used for calibration.

	THEORETICAL (m/z)	EXPERIMENTAL (m/z)	ASSIGNMENTS	ERROR (ppm)
*	246.13226	246.13212	$z_2^{\bullet}$	-0.569
	293.16081	293.16065	c_2	-0.546
*	345.20067	345.20045	$z_3^{\bullet}$	-0.637
		351.08983	?	
	361.21939	361.21934	y_3	-0.138
	407.20374	407.20343	c_3	-0.761
	415.22996	415.22971	w_4	-0.590
*	474.24326	474.24296	$z_4^{\bullet}$	-0.633
	475.25109	475.25081	z_4	-0.579
	478.24085	478.24060	c_4	-0.523
	490.26198	490.26167	y_4	-0.632
	572.30385	572.30336	$y_5 – NH_3$	-0.847
	572.30330	572.30336	$z^{\bullet}_5–H^{\bullet}$	0.114
*	573.31167	573.31134	$z_5^{\bullet}$	-0.576
	589.33039	589.32980	y_5	-1.001
	591.32491	591.32446	c_5	-0.761
	643.34041	643.34035	$z_6^{\bullet}$-C_3H_7	-0.085
	685.38791	685.38774	$y_6 – NH_3$	-0.241
	685.38736	685.38774	$z^{\bullet}_6–H^{\bullet}$	0.562
*	686.39573	686.39540	$z_6^{\bullet}$	-0.481
	702.41445	702.41418	y_6	-0.384
	704.40897	704.40855	c_6	-0.596
	724.41172	724.41172	$[M-H_2+(C_2-H_2)+4H]^{4+}$	0.000
	751.43553	751.43518	c^{*2+}_{12}	-0.459
	761.93930	761.93955	$z_{14}^{\bullet 2+}$	0.328
*	769.94866	769.94817	y_{14}^{2+}	-0.636
	799.46721	799.46689	y_7	-0.400
	803.47738	803.47710	c_7	-0.348
	825.48259	825.48243	$(z^{\bullet}_{15}–H^{\bullet})^{2+}$	-0.197
	833.99614	833.99609	y_{15}^{2+}	-0.060
	849.49611	849.49579	c^{*2+}_{14}	-0.377
	865.47778	865.47771	$y_8 –H_2O-NH_3$	-0.081
	867.49343	867.49306	$z_8^{\bullet}- H_2O$	-0.427
*	876.51062	876.51069	$z_{16}^{\bullet 2+}$	0.080
	882.47997	882.48028	$z^{\bullet}_8–H_2^{\bullet}$	0.351
	883.48780	883.48822	$z^{\bullet}_8–H^{\bullet}$	0.481
	884.49617	884.49644	$z_8^{\bullet}$	0.305
	900.51489	900.51470	y_8	-0.211
	903.85604	903.85632	$z_{24}^{\bullet 3+}$	0.313

THEORETICAL (m/z)	EXPERIMENTAL (m/z)	ASSIGNMENTS	ERROR (ppm)
912.51490	912.51468	w_{a9}	-0.236
913.52540	913.52507	$c^{*}_{15}{}^{2+}$	-0.361
958.04229	958.04202	$z_{17}{}^{\bullet 2+}$	-0.277
* 959.57849	959.57839	c_8	-0.104
960.20696	960.20633	$[M+(C_2\text{-}H_2)\text{-}NH_3+4H]^{3+\bullet}$	-0.656
965.54653	965.54565	$[M+(C_2\text{-}H_2)+3H]^{3+}$	-0.913
969.51200	969.51283	$z^{\bullet}_9 – H_2{}^{\bullet}$	0.856
970.51983	970.52038	$z^{\bullet}_9 – H^{\bullet}$	0.572
971.52820	971.52816	$z_9{}^{\bullet}$	-0.041
980.55502	980.55535	$c^{*}_8{}^{\bullet}$	0.342
981.56284	981.56268	c^{*}_8	-0.163
987.54692	987.54693	y_9	0.010
1006.57562	1006.57537	$c^{*}_{17}{}^{2+}$	-0.248
1027.08756	1027.08835	$(z_{18}{}^{\bullet}\text{-}H_2O)^{2+}$	0.772
	1031.59953	?	
1035.58865	1035.58814	$(z_{18} – H^{\bullet})^{2+}$	-0.495
* 1036.09284	1036.09228	$z_{18}{}^{\bullet 2+}$	-0.540
1036.59675	1036.59667	$z_{18}{}^{2+}$	-0.077
1044.10220	1044.10256	$y_{18}{}^{2+}$	0.345
1052.58605	1052.58665	$z_{10}{}^{\bullet}\text{- } H_2O$	0.570
1069.58934	1069.58852	$z_{10}{}^{\bullet}\text{- } H^{\bullet}$	-0.762
1070.59661	1070.59653	$z_{10}{}^{\bullet}$	-0.075
1086.13096	1086.13127	$z_{19}{}^{2+}$	0.285
1086.61533	1086.61511	y_{10}	-0.202
1105.62584	1105.62572	$c^{*}_{19}{}^{2+}$	-0.109
1122.64182	1122.64201	c_9	0.169
1142.67299	1142.67317	$z_{20}{}^{2+}$	0.158
1143.61835	1143.61862	$c^{*}_9{}^{\bullet}$	0.236
1144.62617	1144.62610	c^{*}_9	-0.061
1162.16787	1162.16776	$c^{*}_{20}{}^{2+}$	-0.095
1181.65245	1181.65171	$z_{11}{}^{\bullet}\text{-}H_20$	-0.626
1189.70592	1189.70550	$(z_{21}{}^{\bullet}\text{-}H_2O)^{2+}$	-0.269
1197.64737	1197.64741	$z_{11}{}^{\bullet}\text{- } H^{\bullet}$	0.422
1198.65519	1198.65509	$z_{11}{}^{\bullet}$	-0.083
1199.21502	1199.21517	$z_{21}{}^{2+}$	0.125
1211.70208	1211.70212	$c^{*}_{21}{}^{2+}$	0.033
1214.67391	1214.67380	y_{11}	-0.091
* 1223.68950	1223.68976	c_{10}	0.212
1234.73357	1234.73411	$z_{22}{}^{2+}$	0.437
1245.67385	1245.67381	c^{*}_{10}	-0.032
1276.22337	1276.22364	$c^{*}_{22}{}^{2+}$	0.212
1284.24531	1284.24488	$(b_{23}\text{-}{}^{\bullet}CONH_2)^{2+}$	-0.335

	THEORETICAL (m/z)	EXPERIMENTAL (m/z)	ASSIGNMENTS	ERROR (ppm)
	1284.72475	1284.72481	$(z^{*}_{23}{}^{\bullet}\text{-}H_2O\text{-}\ NH_3)^{2+}$	0.047
	1291.75504	1291.75522	$z_{23}{}^{2+}$	0.139
	1299.26049	1299.26030	$y_{23}{}^{2+}$	-0.146
	1301.73966	1301.73977	$(z^{*}_{23}\text{-}H^{\bullet})^{2+}$	0.085
	1311.72667	1311.72646	y_{12}	-0.160
	1325.75758	1325.75796	$c^{*}_{23}{}^{2+}$	0.287
	1347.26677	1347.26742	$a^{*}_{24}{}^{2+}$	0.482
	1349.27613	1349.27556	$(c_{24}\text{-}\ H_2O)^{2+}$	-0.422
	1351.78446	1351.78545	c_{11}	0.732
	1355.28042	1355.28098	$z_{24}{}^{\bullet 2+}$	0.413
	1355.78433	1355.78472	$z_{24}{}^{2+}$	0.288
	1369.27359	1369.27420	$c^{*}_{24}{}^{2+}$	0.445
	1372.76099	1372.76053	$c^{*}_{11}{}^{\bullet}$	-0.335
	1393.76909	1393.76797	$z_{13}{}^{\bullet}\text{-}H^{\bullet}$	-0.795
	1394.77636	1394.77631	$z_{13}{}^{\bullet}$	-0.036
*	1410.79508	1410.79487	y_{13}	-0.149
	1448.32007	1448.32128	$[M+C_2\text{-}H_2+3H]^{2+\bullet}$	0.835
	1448.82398	1448.82455	$[M+C_2\text{-}H_2+4H]^{2+\bullet\bullet}$	0.393
	1501.86377	1501.86403	c^{*}_{12}	0.173
	1504.83695	1504.83723	$y_{14}\text{-}2\ NH_3$	0.186
	1521.86350	1521.86373	$z_{14}{}^{\bullet}\text{-}H^{\bullet}$	0.151
	1522.87132	1522.87047	$z_{14}{}^{\bullet}$	-0.558
	1523.87915	1523.87960	z_{14}	0.295
	1538.89004	1538.88973	y_{14}	-0.201
	1632.93191	1632.93214	$y_{15}\text{-}2NH_3$	0.141
	1633.96354	1633.96383	$z_{15}{}^{\bullet}\text{-}\ H_2O$	0.177
	1651.97411	1651.97467	z_{15}	0.339
	1666.98500	1666.98641	y_{15}	0.846
*	1697.98494	1697.98473	c^{*}_{14}	-0.124
	1732.99557	1732.99588	$y_{16}\text{-}\ H_2O\ \text{-}\ NH_3$	0.179
	1735.01122	1735.00983	$z_{16}\text{-}\ H_2O$	-0.801
	1751.00614	1751.00621	$z_{16}{}^{\bullet}\text{-}H^{\bullet}$	0.040
	1752.01396	1752.01315	$z_{16}{}^{\bullet}$	-0.462
	1753.02179	1753.02263	z_{16}	0.479
	1826.04352	1826.04435	c^{*}_{15}	0.455
	1914.07001	1914.07089	$z_{17}{}^{\bullet}\text{-}H^{\bullet}$	0.460
	1916.08512	1916.08533	z_{17}	0.110
	1925.11193	1925.11257	c^{*}_{16}	0.332
	1931.09601	1931.09604	y_{17}	0.016
	2012.14396	12012.14579	c^{*}_{17}	0.909
*	2072.18890	2072.18810	$c_{19}{}^{\bullet}\text{-}\ H_2O$	-0.386
			Mean	-0.072
			St. Dv.	0.503

Table C-12. DR(595.03)-ECD(602.36) mass error analysis for the parent ion $[M+C_2 - H_2+3H]^{3+}$ of the glyoxal-derived glycation product formed at EK-15 peptide in PBS buffer.

THEORETICAL (m/z)	EXPERIMENTAL (m/z)	ASSIGNMENTS	ERROR (ppm)
* 325.16187	325.16188	c^*_2	0.031
343.24655	343.24654	$z_3^\bullet$	-0.029
359.26527	359.26528	y_3	0.028
* 453.22045	453.22031	c^*_3	-0.309
472.28914	472.28904	$z_4^\bullet$	-0.212
488.30786	488.30773	y_4	-0.266
* 566.30451	566.30444	c^*_4	-0.124
571.35755	571.35751	$z_5^\bullet$	-0.070
587.37627	587.37613	y_5	-0.238
650.38584	650.38583	a^*_5	-0.015
684.44161	684.44150	$z_6^\bullet$	-0.161
* 694.39947	694.39934	c^*_5	-0.187
700.46033	700.46015	y_6	-0.257
* 755.47872	755.47863	$z_7^\bullet$	-0.119
771.49744	771.49743	y_7	-0.013
788.96210	788.96181	c^{*2+}_{13}	-0.368
816.48949	816.48921	a^{*2+}_{14}	-0.343
822.49443	822.49432	c^*_6	-0.134
830.50514	830.50437	$z^{*\bullet 2+}_{14}$	1.019
* 838.49631	838.49619	c^{*2+}_{14}	-0.137
838.51450	838.51425	y^*_{14}	-0.298
856.52640	856.52639	$z_8^\bullet$	-0.012
872.54512	872.54598	y_8	0.986
885.51724	885.51698	$[M-H_2O-NH_3+2H]^{2+}$	-0.294
895.02644	895.02604	$[M-NH_3+3H]^{2+\bullet}$	-0.445
903.53971	903.53960	$[M+3H]^{2+\bullet}$	-0.122
* 950.55301	950.55285	c^*_7	-0.168
984.58498	984.58478	$z_9^\bullet$	-0.203
1000.60370	1000.60336	y_9	-0.340
1007.58706	1007.58787	a^*_8	0.804
* 1051.60069	1051.60075	c^*_8	0.057
1112.67994	1112.68007	$z_{10}^\bullet$	0.117
* 1122.63780	1122.63772	c^*_9	-0.071
1128.69866	1128.69936	y_{10}	0.620
* 1235.72186	1235.72195	c^*_{10}	0.073
1240.77490	1240.77497	$z_{11}^\bullet$	0.056
1256.79362	1256.79437	y_{11}	0.597
* 1334.79027	1334.79013	c^*_{11}	-0.105
1353.85896	1353.85786	$z_{12}^\bullet$	-0.812
1369.87768	1369.87772	y_{12}	0.029
* 1463.83286	1463.83267	c^*_{12}	-0.129
1481.91754	1481.91668	$z_{13}^\bullet$	-0.580
1807.07966	1807.07890	$[M+3H]^{1+\bullet\bullet}$	-0.421
* 1789.06940	1789.06859	$[M-H_2O+3H]^{1+\bullet\bullet}$	-0.453
		Mean	-0.083
		St. Dv.	0.385

Table C-13. CAD mass error analysis for the parent ion $[M+C_2 - H_2+3H]^{3+}$ of the glyoxal-derived glycation product formed at EK-15 peptide in PBS buffer.

	THEORETICAL (m/z)	EXPERIMENTAL (m/z)	ASSIGNMENTS	ERROR (ppm)
*	246.18121	246.18128	y_2	0.284
	268.14041	268.14052	b_2-H2O	0.410
	273.09821	273.09826	b^*_2-H_2O-NH_3	0.165
	286.15098	286.15096	b_2	-0.070
	290.12476	290.12483	b^*_2-H_2O	0.241
	291.10878	291.10885	b^*_2-NH_3	0.240
*	308.13533	308.13534	b^*_2	0.049
	324.22816	324.22828	y_3-H_2O-NH_3	0.370
	341.25471	341.25480	y_3- H_2O	0.264
	359.26527	359.26537	y_3	0.278
	366.21358	366.21388	b_6-H_2O-$2NH_3$	0.819
	369.24267	369.24232	$(a_6$- $H_2O)^{2+}$	-0.948
	371.72157	371.72171	$(a^*_6$-H_2O-$NH_3)^{2+}$	0.377
	374.14590	374.14606	a^*_3-$2NH_3$	0.428
	379.17245	379.17248	b_3- H_2O-NH_3	0.079
	380.23484	380.23496	$(a^*_6$- $H_2O)^{2+}$	0.309
	380.72713	380.72692	$(a^*_6$-$NH_3)^{2+}$	-0.538
	381.24722	381.24736	y_3+Na-H	0.367
	383.24013	383.24017	$(b_6$- $H_2O)^{2+}$	0.104
	384.13025	384.13037	b^*_3-H_2O-$2NH_3$	0.312
	385.71903	385.71912	$(b^*_6$- H_2O - $NH_3)^{2+}$	0.240
	389.24013	389.24019	$a^{*\ 2+}_6$	0.161
	390.18842	390.18853	a^*_3- H_2O	0.269
	394.23230	394.23239	$(b^*_6$- $H_2O)^{2+}$	0.228
	394.72431	394.72445	$(b^*_6$- $NH_3)^{2+}$	0.355
	396.19899	396.19901	$(b_3$- $H_2O)^{2+}$	0.050
	401.15679	401.15685	b^*_3- H_2O - NH_3	0.137
	402.14081	402.14090	b^*_3-$2NH_3$	0.211
	403.23758	403.23764	$b^{*\ 2+}_6$	0.143
	408.19899	408.19903	a^*_3	0.098
	413.27583	413.27589	w_4	0.133
	414.20956	414.20961	b_3	0.121
	418.18334	418.18337	b^*_3- H_2O	0.072
	419.16736	419.16739	b^*_3- NH_3	0.072
	427.23759	427.23752	$(a^*_7$- H_2O - $2NH_3)^{2+}$	-0.158
	427.77092	427.77082	$(y_8$- $H_2O)^{2+}$	-0.228
	430.24287	430.24259	$(b_7$-H_2O - $2NH_3)^{2+}$	-0.651
	435.75086	435.75091	$(a^*_7$- H_2O - $NH_3)^{2+}$	0.115
*	436.19390	436.19388	b^*_3	-0.046
	444.26413	444.26405	$(a^*_7$- $H_2O)^{2+}$	-0.186
	444.75642	444.75609	$(a^*_7$ - $NH_3)^{2+}$	-0.731
	447.26942	447.26947	$(b_7$- $H_2O)^{2+}$	0.112
	447.76143	447.76151	$(b_7$ - $NH_3)^{2+}$	0.179
	449.74832	449.74829	$(b^*_7$- H_2O - $NH_3)^{2+}$	-0.061
	452.28673	452.28669	y_4- $2H_2O$	-0.088

THEORETICAL (m/z)	EXPERIMENTAL (m/z)	ASSIGNMENTS	ERROR (ppm)
453.26941	453.26919	$a^{*}_{7}{}^{2+}$	-0.496
453.27075	453.27091	y_4- H_2O - NH_3	0.353
458.26159	458.26154	$(b^{*}_{7}$- $H_2O)^{2+}$	-0.109
458.75360	458.75352	$(b^{*}_{7}$ - $NH_3)^{2+}$	-0.174
467.26687	467.26682	$b^{*}_{7}{}^{2+}$	-0.112
470.29730	470.29725	y_4- H_2O	-0.096
471.76143	471.76127	$(b_8$-2H_2O -2$NH_3)^{2+}$	-0.339
477.76143	477.76098	$(a^{*}_{8}$- H_2O -2$NH_3)^{2+}$	-0.937
480.27470	480.27451	$(b_8$-2H_2O - $NH_3)^{2+}$	-0.396
481.28814	481.28807	a_4 - H_2O	-0.145
482.79492	482.79485	$(y_9$-2$H_2O)^{2+}$	-0.155
482.94029	482.94032	$b^{*}_{12}{}^{3+}$	0.059
485.78269	485.78284	$(a^{*}_{8}$-2$H_2O)^{2+}$	0.309
486.27470	486.27465	$(a^{*}_{8}$- H_2O - NH_3 $)^{2+}$	-0.103
487.22996	487.22990	a^{*}_{4}- 2NH_3	-0.123
488.30786	488.30780	y_4	-0.123
488.78797	488.78782	$(b_8$-2$H_2O)^{2+}$	-0.307
491.26688	491.26679	$(b^{*}_{8}$-2H_2O - $NH_3)^{2+}$	-0.173
491.75889	491.75900	$(b^{*}_{8}$- H_2O -2$NH_3)^{2+}$	0.234
491.80021	491.80014	$(y_9$- $H_2O)^{2+}$	-0.138
492.25651	492.25661	b_4- H_2O - NH_3	0.203
494.78797	494.78795	$(a^{*}_{8}$- $H_2O)^{2+}$	-0.045
495.28026	495.28004	$(a^{*}_{8}$-NH3$)^{2+}$	-0.434
497.21431	497.21439	b^{*}_{4}- H_2O -2NH_3	0.161
497.79326	497.79331	$(b_8$- $H_2O)^{2+}$	0.100
499.29870	499.29863	a_4	-0.140
499.78015	499.78002	$(b^{*}_{8}$-2$H_2O)^{2+}$	-0.255
500.27216	500.27206	$(b^{*}_{8}$- H_2O - $NH_3)^{2+}$	-0.195
503.27249	503.27237	a^{*}_{4}- H_2O	-0.229
503.79325	503.79321	$a^{*}_{8}{}^{2+}$	-0.089
508.78543	508.78535	$(b^{*}_{8}$- $H_2O)^{2+}$	-0.157
509.27744	509.27744	$(b^{*}_{8}$- $NH_3)^{2+}$	0.000
509.28305	509.28295	b_4- H_2O	-0.196
513.27998	513.27979	$(a^{*}_{9}$- H_2O -2$NH_3)^{2+}$	-0.375
514.24086	514.24080	b^{*}_{4}- H_2O - NH_3	-0.107
514.63146	514.63120	$(b^{*}_{13}$- $H_2O)^{3+}$	-0.499
515.22487	515.22484	b^{*}_{4}-2NH_3	-0.068
517.79071	517.79062	$b^{*}_{8}{}^{2+}$	-0.179
518.27216	518.27241	$(b^{*}_{9}$-2H_2O -2$NH_3)^{2+}$	0.486
520.63498	520.63488	$b^{*}_{13}{}^{3+}$	-0.189
521.28305	521.28297	a^{*}_{4}	-0.153
521.79326	521.79318	$(a^{*}_{9}$- H_2O - $NH_3)^{2+}$	-0.144
526.78543	526.78541	$(b^{*}_{9}$-2H_2O - $NH_3)^{2+}$	-0.038
527.29362	527.29354	b_4	-0.152
530.30653	530.30652	$(a^{*}_{9}$- $H_2O)^{2+}$	-0.014
530.79881	530.79848	$(a^{*}_{9}$- $NH_3)^{2+}$	-0.622
531.26740	531.26733	b^{*}_{4}- H_2O	-0.132
532.25142	532.25135	b^{*}_{4}- NH_3	-0.132
533.31181	533.31173	$(b_9$- $H_2O)^{2+}$	-0.150

THEORETICAL (m/z)	EXPERIMENTAL (m/z)	ASSIGNMENTS	ERROR (ppm)
535.29870	535.29859	$(b^*_9\text{-}2H_2O)^{2+}$	-0.210
535.79071	535.79062	$(b^*_9\text{- }H_2O\text{ - }NH_3)^{2+}$	-0.173
539.31181	539.31166	$a^*_9{}^{2+}$	-0.278
544.30399	544.30388	$(b^*_9\text{- }H_2O)^{2+}$	-0.193
544.79599	544.79596	$(b^*_9\text{- }NH_3)^{2+}$	-0.064
* 549.27796	549.27790	b^*_4	-0.118
551.35514	551.35515	$y_5\text{-}2H_2O$	0.018
552.01731	552.01729	$y_{14}{}^{3+}$	-0.036
552.33916	552.33918	$y_5\text{- }H_2O\text{ - }NH_3$	0.036
553.30927	553.30919	$b^*_9{}^{2+}$	-0.140
555.84769	555.84765	$(y_{10}\text{- }H_2O)^{2+}$	-0.067
556.33970	556.33966	$(y_{10}\text{- }NH_3)^{2+}$	-0.067
559.34543	559.34500	$y^*_{14}{}^{3+}$	-0.763
564.85297	564.85287	$y_{10}{}^{2+}$	-0.177
569.36571	569.36569	$y_5\text{- }H_2O$	-0.026
569.82201	569.82203	$(a^*_{10}\text{- }H_2O\text{ -}2NH_3)^{2+}$	0.031
572.33529	572.33504	$(b_{10}\text{-}2H_2O\text{ - }NH_3)^{2+}$	-0.437
572.82730	572.82710	$(b_{10}\text{- }H_2O\text{ -}2NH_3)^{2+}$	-0.349
574.34599	574.34608	$a_5\text{-}2H_2O\text{ - }NH_3$	0.157
577.84327	577.84301	$(a^*_{10}\text{-}2H_2O)^{2+}$	-0.459
578.33528	578.33519	$(a^*_{10}\text{- }H_2O\text{ - }NH_3)^{2+}$	0.164
580.84856	580.84808	$(b_{10}\text{-}2H_2O)^{2+}$	-0.826
581.34057	581.34044	$(b_{10}\text{- }H_2O\text{ - }NH_3{}^{2+})$	-0.224
583.32746	583.32741	$(b^*_{10}\text{- }H_2O\text{ - }NH_3)^{2+}$	-0.086
583.81947	583.81955	$(b^*_{10}\text{- }H_2O\text{ -}2NH_3)^{2+}$	0.137
584.67707	584.67683	$[M\text{-}2H_2O\text{ -NH3+3H}]^{3+}$	-0.410
586.29838	586.29809	$b_5\text{-}2H_2O\text{ -}2NH_3$	-0.495
586.84856	586.84845	$(a^*_{10}\text{- }H_2O)^{2+}$	-0.183
587.34084	587.34053	$(a^*_{10}\text{- }NH_3)^{2+}$	-0.528
587.37627	587.37624	y_5	-0.051
589.85384	589.85397	$(b_{10}\text{- }H_2O)^{2+}$	0.220
590.35258	590.35250	$[M\text{-}2H_2O\text{ +3H}]^{3+}$	-0.136
590.68059	590.68048	$[M\text{- }H_2O\text{- }NH_3\text{+3H}]^{3+}$	-0.186
591.84073	591.84065	$(b^*_{10}\text{-}2H_2O)^{2+}$	-0.139
592.33274	592.33253	$(b^*_{10}\text{- }H_2O\text{ - }NH_3)^{2+}$	-0.359
593.02799	593.02756	[M-CO+3H]3+	-0.725
595.85384	595.85377	$a^*_{10}{}^{2+}$	-0.117
596.35610	596.35602	$[M\text{- }H_2O\text{ +3H}]^{3+}$	-0.134
596.68411	596.68409	$[M\text{- }NH_3\text{+3H}]^{3+}$	-0.034
600.84601	600.84596	$(b^*_{10}\text{- }H_2O)^{2+}$	-0.092
601.33803	601.33807	$(b^*_{10}\text{- }NH_3)^{2+}$	0.075
603.32492	603.32502	$b_5\text{- }H_2O\text{ -}2NH_3$	0.166
609.85130	609.85122	$b^*_{10}{}^{2+}$	-0.127
614.36471	614.36451	$a^*_5\text{-}2H_2O$	-0.326
615.32492	615.32491	$a^*_5\text{-}2NH_3$	-0.016
619.35622	619.35596	$(a^*_{11}\text{- }H_2O\text{ -}2NH_3)^{2+}$	0.416
619.89517	619.89508	$(y_{11}\text{- }H_2O)^{2+}$	-0.141
620.35147	620.35146	$b_5\text{- }H_2O\text{ - }NH_3$	-0.016
621.33549	621.33550	$b_5\text{-}2NH_3$	0.016

	THEORETICAL (m/z)	EXPERIMENTAL (m/z)	ASSIGNMENTS	ERROR (ppm)
	621.86949	621.86943	$(b_{11}\text{-}2H_2O - NH_3)^{2+}$	-0.096
	627.86949	627.86937	$(a^*_{11} - H_2O - NH_3)^{2+}$	0.191
*	628.90045	628.90035	y_{11}^{2+}	-0.159
	630.87477	630.87434	$(b_{11} - H_2O - NH_3)^{2+}$	-0.682
	631.36744	631.36745	$a^*_5 - H_2O$	0.008
	632.86167	632.86154	$(b^*_{11}\text{-}2H_2O - NH_3)^{2+}$	-0.198
	636.38276	636.38277	$(a^*_{11} - H_2O)^{2+}$	0.012
	636.87505	636.87471	$(a^*_{11} - NH_3)^{2+}$	-0.526
	637.37801	637.37816	$b_5 - H_2O$	0.235
	639.38805	639.38772	$(b_{11} - H_2O)^{2+}$	-0.516
	639.88006	639.87967	$(b_{11} - NH_3)^{2+}$	-0.609
	641.37494	641.37505	$(b^*_{11}\text{-}2H_2O)^{2+}$	0.175
	641.86695	641.86687	$(b^*_{11} - H_2O - NH_3)^{2+}$	-0.121
	642.33582	642.33573	$b^*_5 - H_2O - NH_3$	-0.132
	643.31984	643.31981	$b^*_5\text{-}2NH_3$	-0.039
	645.38805	645.38801	$a^{*\,2+}_{11}$	-0.054
	648.39333	648.39367	b_{11}^{2+}	0.524
	649.37801	649.37801	a^*_5	0.000
	650.38022	650.38027	$(b^*_{11} - H_2O)^{2+}$	0.077
	650.87223	650.87216	$(b^*_{11} - NH_3)^{2+}$	-0.108
	655.38858	655.38856	b_5	-0.031
	659.36236	659.36233	$b^*_5 - H_2O$	-0.045
	659.38550	659.38546	$b^{*\,2+}_{11}$	-0.064
	660.34638	660.34638	$b^*_5 - NH_3$	0.000
	664.43920	664.43924	$y_6\text{-}2H_2O$	0.060
	665.42322	665.42347	$y_6 - H_2O - NH_3$	0.376
	677.37293	677.37293	b^*_5	0.007
	682.44976	682.44974	$y_6 - H_2O$	-0.037
	683.87751	683.87744	$(a^*_{12} - H_2O\text{-}2NH_3)^{2+}$	-0.106
	685.44248	685.44257	y_{12}^{2+}	0.131
	686.39079	686.39048	$(b_{12}\text{-}2H_2O - NH_3)^{2+}$	-0.444
	691.89878	691.89872	$(a^*_{12}\text{-}2H_2O)^{2+}$	-0.079
	692.39079	692.39081	$(a^*_{12} - H_2O - NH_3)^{2+}$	0.036
	696.89095	696.89089	$(b^*_{12}\text{-}3H_2O)^{2+}$	-0.086
	697.38296	697.38294	$(b^*_{12}\text{-}2H_2O - NH_3)^{2+}$	-0.029
	697.87497	697.87478	$(b^*_{12} - H_2O\text{-}2NH_3)^{2+}$	-0.272
*	700.46033	700.46031	y_6	-0.029
	700.90406	700.90406	$(a^*_{12} - H_2O)^{2+}$	0.004
	701.39634	701.39588	$(a^*_{12} - NH_3)^{2+}$	-0.656
	703.90934	703.90929	$(b_{12} - H_2O)^{2+}$	-0.071
	705.89623	705.89619	$(b^*_{12}\text{-}2\ H_2O)^{2+}$	-0.060
	706.38824	706.38820	$(b^*_{12} - H_2O - NH_3)^{2+}$	-0.060
	709.43686	709.43672	$x_6 - H_2O$	-0.190
	709.90934	709.90940	$a^{*\,2+}_{12}$	0.081
	714.90152	714.90148	$(b^*_{12} - H_2O)^{2+}$	-0.049
	715.39352	715.39358	$(b^*_{12} - NH_3)^{2+}$	0.077
	722.44227	722.44220	y_6+Na-H	-0.104
*	723.90680	723.90676	$b^{*\,2+}_{12}$	-0.052
	727.44742	727.44750	x_6	0.110

	THEORETICAL (m/z)	EXPERIMENTAL (m/z)	ASSIGNMENTS	ERROR (ppm)
	731.41988	731.42034	b_6- H_2O -2NH_3	0.629
	731.46120	731.46106	$(y_{13}$-2$H_2O)^{2+}$	-0.198
	734.41954	734.41947	$(b_{13}$-2H_2O -2$NH_3)^{2+}$	-0.099
	736.46033	736.46011	y_7- H_2O - NH_3	-0.299
	740.41954	740.41961	$(a^*_{13}$- H_2O -2$NH_3)^{2+}$	0.091
	740.46649	740.46649	$(y_{13}$- $H_2O)^{2+}$	0.003
	740.95850	740.95855	$(y_{13}$- $NH_3)^{2+}$	0.071
	743.41988	743.41976	a^*_6 -2NH_3	-0.161
	747.46241	747.46305	b_6-2H_2O	0.856
	748.44643	748.44655	b_6- H_2O - NH_3	0.160
	748.93282	748.93278	$(a^*_{13}$- H_2O - $NH_3)^{2+}$	-0.047
	749.47177	749.47136	y_{13}^{2+}	-0.547
	751.44609	751.44608	$(b_{13}$-2$H_2O)^{2+}$	-0.010
	753.40423	753.40452	b^*_6 -H2O-2 NH_3	0.385
	753.43298	753.43331	$(b^*_{13}$-3$H_2O)^{2+}$	0.438
	753.48688	753.48679	y_7- H_2O	-0.113
	753.92499	753.92495	$(b^*_{13}$-2H_2O- $NH_3)^{2+}$	-0.053
	754.41700	754.41717	$(b$-$^*_{13}$- H_2O -2$NH_3)^{2+}$	0.225
	757.44609	757.44612	$(a^*_{13}$- $H_2O)^{2+}$	0.043
	757.93837	757.93807	$(a^*_{13}$- $NH_3)^{2+}$	-0.396
	759.46240	759.46244	a^*_6 - H_2O	0.046
	762.43826	762.43829	$(b^*_{13}$-2$H_2O)^{2+}$	0.036
	762.93027	762.93030	$(b^*_{13}$- H_2O - $NH_3)^{2+}$	0.036
	765.47297	765.47306	b_6- H_2O	0.118
	766.45137	766.45130	$a^*_{13}^{2+}$	-0.091
	769.44676	769.44707	b^*_6 -2H_2O	0.409
	769.45665	769.45656	b_{13}^{2+}	-0.120
	770.43078	770.43071	b^*_6 - H_2O - NH_3	-0.084
	771.41480	771.41552	b^*_6 -2NH_3	0.940
	771.44354	771.44360	$(b^*_{13}$- $H_2O)^{2+}$	0.071
	771.49744	771.49743	y_7	-0.013
	771.93556	771.93543	$(b^*_{13}$- $NH_3)^{2+}$	-0.162
	777.47297	777.47280	a^*_6	-0.219
	780.44883	780.44884	$b^*_{13}^{2+}$	0.016
	781.45799	781.45724	x_7- NH_3	-0.953
	783.48354	783.48363	b_6	0.115
	787.45732	787.45729	b^*_6 - H_2O	-0.038
	788.44134	788.44129	b^*_6 - NH_3	-0.063
	789.95375	789.95449	$(a^*_{14}$ - H_2O -2$NH_3)^{2+}$	0.940
	793.47938	793.47937	y_7+Na-H	-0.019
	797.97501	797.97501	$(a^*_{14}$ 2$H_2O)^{2+}$	0.000
	798.46702	798.46696	$(a^*_{14}$ -H2O- $NH_3)^{2+}$	-0.075
	802.96718	802.96775	$(b^*_{14}$ -3$H_2O)^{2+}$	0.704
*	805.46789	805.46789	b^*_6	0.006
	806.98029	806.98012	$(a^*_{14}$ - $H_2O)^{2+}$	-0.214
	809.98558	809.98569	$(b_{14}$- $H_2O)^{2+}$	0.142
	811.97247	811.97253	$(b^*_{14}$ -2$H_2O)^{2+}$	0.077
	812.46448	812.46430	$(b^*_{14}$ - H_2O - $NH_3)^{2+}$	-0.218
	815.98558	815.98539	$a^*_{14}^{2+}$	-0.227

	THEORETICAL (m/z)	EXPERIMENTAL (m/z)	ASSIGNMENTS	ERROR (ppm)
	820.97775	820.97772	$(b^{*}_{14} - H_2O)^{2+}$	-0.037
	821.46976	821.47051	$(b^{*}_{14} - NH_3)^{2+}$	0.913
	829.98303	829.98299	b^{*2+}_{14}	-0.051
	836.52399	836.52363	y_8-2H_2O	-0.430
	842.45192	842.45107	b_7-2H_2O -2NH_3	-1.009
	854.53455	854.53458	y_8- H_2O	0.029
	859.47846	859.47840	b_7- H_2O -2NH_3	-0.070
	860.53451	860.53396	$[M- H_2O+2H]^{2+}$	-0.642
	862.51450	862.51467	$[M- H_2O - NH_3 +2H]^{2+}$	0.197
	871.47846	871.47854	a^{*}_7-2NH_3	0.092
	872.54512	872.54509	y_8	-0.034
	876.50501	876.50497	b_7- H_2O - NH_3	-0.046
	877.48903	877.48957	b_7-2NH_3	0.615
	881.46281	881.46325	b^{*}_7 - H_2O -2NH_3	0.499
	887.52098	887.52032	a^{*}_7 - H_2O	-0.749
	893.53155	893.53141	b_7- H_2O	-0.157
	894.52706	894.52738	y_8+Na-H	0.352
	897.50533	897.50448	b^{*}_7-2H_2O	-0.953
	898.48936	898.48961	b^{*}_7 - H_2O - NH_3	0.284
	899.47338	899.47358	b^{*}_7-2NH_3	0.228
	915.51590	915.51585	b^{*}_7 - H_2O	-0.055
	916.49992	916.49987	b^{*}_7 - NH_3	-0.055
*	933.52647	933.52645	b^{*}_7	-0.016
	956.50743	956.50650	a^{*}_8-3NH_3	-0.967
	961.51016	961.51014	b_8-3NH_3	-0.021
	964.58257	964.58266	y_9-2H_2O	0.093
	965.56659	965.56659	y_9- H_2O - NH_3	0.000
	972.52614	972.52584	a^{*}_8-2NH_3	-0.308
	977.55269	977.55244	b_8- H_2O - NH_3	-0.256
	982.59313	982.59312	y_9- H_2O	-0.015
	986.56560	986.56516	a_9-2NH_3-2H_2O	-0.446
	998.55301	998.55291	b^{*}_8-2H_2O	-0.105
	999.53703	999.53706	b^{*}_8- H_2O - NH_3	0.025
	1000.60370	1000.60366	y_9	-0.040
	1004.57617	1004.57520	a_9-2NH_3- H_2O	-0.966
	1005.56019	1005.55931	a_9-3NH_3	-0.875
	1006.57923	1006.57997	a^{*}_8	0.735
	1016.56358	1016.56361	b^{*}_8- H_2O	0.030
	1017.54760	1017.54772	b^{*}_8- NH_3	0.118
	1022.58564	1022.58591	y_9+Na-H	0.259
	1022.58673	1022.58591	a_9-2NH_3	-0.802
	1031.56325	1031.56351	b_9- H_2O -2NH_3	0.252
*	1034.57415	1034.57415	b^{*}_8	0.005
	1043.56325	1043.56321	a^{*}_9-2NH_3	-0.038
	1053.54760	1053.54713	b^{*}_9- H_2O -2NH_3	-0.446
	1059.60577	1059.60644	a^{*}_9- H_2O	0.628
	1065.61634	1065.61545	b_9- H_2O	-0.835
	1069.59012	1069.58944	b^{*}_9-2H_2O	-0.640
	1070.57415	1070.57345	b^{*}_9- H_2O - NH_3	-0.649

THEORETICAL (m/z)	EXPERIMENTAL (m/z)	ASSIGNMENTS	ERROR (ppm)
1077.61634	1077.61625	a^*_9	-0.084
1087.60069	1087.60060	b^*_9- H_2O	-0.083
1088.58471	1088.58477	b^*_9- NH_3	0.055
1092.67753	1092.67762	y_{10}-2H_2O	0.082
1093.66155	1093.66157	y_{10}- H_2O - NH_3	0.018
1105.61126	1105.61120	b^*_9	-0.050
1110.68809	1110.68814	y_{10}- H_2O	0.041
1127.62077	1127.62085	b_{10}-2H_2O -2NH_3	0.071
* 1128.69866	1128.69881	y_{10}	0.133
1145.63133	1145.63193	b_{10}-3NH_3	0.524
1157.65514	1157.65511	a^*_{10} -2NH_3	-0.026
1172.68983	1172.68953	a^*_{10} - H_2O	-0.260
1178.70040	1178.70076	b_{10}- H_2O	0.305
1183.65820	1183.65821	b^*_{10} - H_2O - NH_3	0.004
1190.70040	1190.70010	a^*_{10}	-0.252
1200.68475	1200.68452	b^*_{10} - H_2O	-0.192
1201.66877	1201.66899	b^*_{10} - NH_3	0.183
* 1218.69531	1218.69542	b^*_{10}	0.086
1220.70242	1220.70236	a^*_{11} -2NH_3-2 H_2O	-0.049
1256.79362	1256.79398	y_{11}	0.286
1271.75824	1271.75827	a^*_{11}- H_2O	0.020
1277.76881	1277.76808	b_{11}- H_2O	-0.571
* 1289.76881	1289.76868	a^*_{11}	-0.101
		Mean	-0.031
		St. Dv.	0.401

Table C-13. CAD mass error analysis for the parent ion $[M+C_2 - H_2+3H]^{3+}$ of the glyoxal-derived glycation product formed at FR-25 peptide in PBS buffer.

THEORETICAL (m/z)	EXPERIMENTAL (m/z)	ASSIGNMENTS	ERROR (ppm)
* 262.15098	262.15094	y_2	-0.167
361.21939	361.21958	y_3	0.526
390.17719	390.17726	b_3	0.175
400.23724	400.23735	y_7^{+2}	0.262
433.21939	433.21926	a_4	-0.300
441.75580	441.75582	$(y_8$-$H_2O)^{2+}$	0.040
444.18776	444.18770	b_4-NH_3	-0.135
450.76108	450.76111	y_8^{2+}	0.055
461.21431	461.21430	b_4	-0.011
472.25142	472.25154	y_4- H_2O	0.265
476.26653	476.26657	$(y_9$- 2$H_2O)^{2+}$	0.073
482.77179	482.77143	b_8^{2+}	-0.741
485.27182	485.27170	$(y_9$- $H_2O)^{2+}$	-0.242
* 490.26198	490.26194	y_4	-0.082
494.27710	494.27689	y_9^{2+}	-0.425
525.80074	525.80073	$(y_{10}$- 2$H_2O)^{2+}$	-0.019
539.81774	539.81821	a_9^{2+}	0.871

	THEORETICAL (m/z)	EXPERIMENTAL (m/z)	ASSIGNMENTS	ERROR (ppm)
	540.24527	540.24516	b_5-2NH_3	-0.213
	546.30345	546.30331	a_5	-0.256
	557.27182	557.27164	b_5-NH_3	-0.323
*	574.29836	574.29821	b^*_5	-0.270
	589.33039	589.33028	y_5	-0.187
	590.01575	590.01581	y_{16}^{3+}	0.107
	596.34906	596.34934	b_{15}^{3+}	0.467
	598.83531	598.83526	$(y_{11}$- $H_2O)^{2+}$	-0.088
	603.67718	603.67696	$b^*_{15}{}^{3+}$	-0.362
	603.83512	603.83501	b_{10}^{2+}	-0.182
	607.84060	607.83997	y_{11}^{2+}	-1.028
	629.37186	629.37184	b_{16}^{3+}	-0.040
	636.36659	636.36721	$(a_{11}$-H_2O-$NH_3)^{2+}$	0.974
*	636.69998	636.69969	$b^*_{16}{}^{3+}$	-0.458
	638.35641	638.35626	$(y_{12}$- 2$H_2O)^{2+}$	-0.235
	644.37019	644.36949	y_{17}^{3+}	-1.086
	645.37877	645.37916	$(a_{11}$- $H_2O)^{2+}$	0.604
	656.36698	656.36691	y_{12}^{2+}	-0.099
	665.71066	665.71083	$b^*_{17}{}^{3+}$	0.258
	670.35588	670.35564	b_6-NH_3	-0.358
	680.05806	680.05791	$(b_{18}$- 2$H_2O)^{3+}$	-0.218
	687.38617	687.38612	$(b^*_{18}$- 2$H_2O)^{3+}$	-0.080
	689.38953	689.38974	a_7-2NH_3-2H_2O	0.305
	692.06510	692.06480	b_{18}^{3+}	-0.436
	697.38791	697.38782	$(y_{13}$- $NH_3)^{2+}$	-0.125
	702.41445	702.41484	y_6	0.555
	705.89825	705.89787	$(b_{12}$-H_2O-2$NH_3)^{2+}$	-0.538
	711.40624	711.40623	$(a^*_{12}$- H_2O-2$NH_3)^{2+}$	-0.014
	714.41152	714.41134	$(b_{12}$-H_2O-$NH_3)^{2+}$	-0.255
	715.40644	715.40645	$[M$-2H_2O+4$H]^{4+}$	0.014
	718.41250	718.41237	$(b_{19}$-$H_2O)^{3+}$	-0.181
	720.15508	720.15525	$[M$-HN_3+4$H]^{4+}$	0.236
	762.11071	762.11068	b_{20}^{3+}	-0.037
	767.12138	767.12092	y_{20}^{3+}	-0.604
	769.94600	769.94654	$(a^*_{13}$-$NH_3)^{2+}$	0.701
	781.46428	781.46382	b_{13}^{2+}	-0.592
	783.45118	783.45099	$(b^*_{13}$-$H_2O)^{2+}$	-0.236
*	792.45646	792.45578	$b^*_{13}{}^{2+}$	-0.855
	795.13351	795.13377	b_{21}^{3+}	0.325
	799.46721	799.46680	y_7	-0.513
	804.81607	804.81617	y_{21}^{3+}	0.124
	828.49511	828.49521	y_{22}^{3+}	0.125
	838.14771	838.14847	b_{22}^{3+}	0.909
	845.47582	845.47574	$b^*_{22}{}^{3+}$	-0.101
	866.50942	866.50982	y_{23}^{3+}	0.465
	876.00671	876.00657	$(y_{16}$-$NH_3)^{2+}$	-0.157
	882.50167	882.50241	$(a_{15}$-$NH_3)^{2+}$	0.839
*	884.51998	884.51979	y_{16}^{2+}	-0.215
	894.01995	894.01974	b_{15}^{2+}	-0.238

	THEORETICAL (m/z)	EXPERIMENTAL (m/z)	ASSIGNMENTS	ERROR (ppm)
	898.01352	898.01280	x_{16}^{2+}	-0.807
	900.51489	900.51439	y_8	-0.555
*	905.01213	905.01149	$b^*_{15}{}^{2+}$	-0.704
	909.19561	909.19580	y_{24}^{3+}	0.209
	943.55416	943.55447	b_{16}^{2+}	0.331
	950.56199	950.56108	$(a_{17}\text{-}C_2H_3)^{2+}$	-0.952
	951.52579	951.52593	$y_9\text{-}2H_2O$	0.147
	953.53949	953.53996	$[M\text{-}2H_2O+3H]^{3+}$	0.493
	954.54633	954.54646	$b^*_{16}{}^{2+}$	0.134
	964.53629	964.53623	b^*_8	-0.067
	964.55971	964.56017	$(a_{17}\text{-}NH_3)^{3+}$	0.472
	966.05165	966.05121	y_{17}^{2+}	-0.450
	969.53635	969.53597	$y_9\text{-}H_2O$	-0.397
	970.54018	970.54022	$(x_{17}\text{-}H_2O)^{2+}$	0.041
	987.07017	987.07059	b_{17}^{2+}	0.423
	987.54692	987.54694	y_9	0.020
*	998.06235	998.06280	$b^*_{17}{}^{2+}$	0.453
	1034.58873	1034.58803	$a^*_{18}{}^{2+}$	-0.677
	1037.59401	1037.59479	b_{18}^{2+}	0.749
	1048.54888	1048.54851	$a^*_9\text{-}2NH_3\text{-}H_2O$	-0.358
*	1048.58619	1048.58683	$b^*_{18}{}^{2+}$	0.613
	1086.61533	1086.61495	y_{10}	-0.350
*	1127.59963	1127.60059	b^*_9	0.856
	1214.67391	1214.6749	y_{11}	0.824
	1228.64731	1228.66632	b^*_{10}	-0.804
*	1311.72667	1311.72795	y_{12}	0.975
			Mean	-0.029
			St. Dv.	0.471

Table C-14. CAD mass error analysis for the parent ion $[M+C_2 - H_2+3H]^{3+}$ of the glyoxal-derived glycation product formed at EK-15 with addition of sodium chloride.

THEORETICAL (m/z)	EXPERIMENTAL (m/z)	ASSIGNMENTS	ERROR (ppm)
246.18121	246.18120	y_2	-0.041
291.10878	291.10874	$b^*_2\text{- } NH_3$	-0.137
308.13533	308.13532	b^*_2	-0.016
324.22816	324.22825	$y_3\text{- } H_2O\text{ - } NH_3$	0.278
359.26527	359.26522	y_3	-0.139
379.17245	379.17267	$b_3\text{- } H_2O\text{ - } NH_3$	0.580
381.24721	381.24699	y_3+Na-H	-0.590
385.71903	385.71890	$(b^*_6\text{- } H_2O\text{ - } NH_3)^{2+}$	-0.331
394.23230	394.23225	$(b^*_6\text{- } H_2O)^{2+}$	-0.127
394.72431	394.72438	$(b^*_6\text{- } NH_3)^{2+}$	0.177
396.19899	396.19898	$b_3\text{- } H_2O$	-0.025
401.15679	401.15670	$b^*_3\text{- } H_2O\text{ - } NH_3$	-0.237
403.23758	403.23761	$b^*_6{}^{2+}$	0.068
408.19899	408.19910	a^*_3	0.269

THEORETICAL (m/z)	EXPERIMENTAL (m/z)	ASSIGNMENTS	ERROR (ppm)
413.27583	413.27592	w_4	0.206
418.18334	418.18332	$b^*_3 - H_2O$	-0.048
419.16736	419.16740	$b^*_3 - NH_3$	0.095
436.19390	436.19392	b^*_3	0.034
438.75614	438.75617	$(b_7 - H_2O - NH_3)^{2+}$	0.068
449.74832	449.74830	$(b^*_7 - H_2O - NH_3)^{2+}$	-0.039
458.26159	458.26159	$(b^*_7 - H_2O)^{2+}$	0.000
458.75360	458.75350	$(b^*_7 - NH_3)^{2+}$	-0.218
467.26687	467.26689	$b^*_7{}^{2+}$	0.037
470.29730	470.29729	$y_4 - H_2O$	-0.011
481.28814	481.28809	$a_4 - H_2O$	-0.104
482.79492	482.79511	$(y_9 - 2H_2O)^{2+}$	0.383
487.22996	487.23021	$a^*_4 - 2NH_3$	0.513
488.30786	488.30788	y_4	0.041
491.80021	491.80022	$(y_9 - H_2O)^{2+}$	0.025
497.79326	497.79356	$(b_8 - H_2O)^{2+}$	0.603
499.78015	499.78010	$(b^*_8 - 2H_2O)^{2+}$	-0.095
500.27216	500.27217	$(b^*_8 - H_2O - NH_3)^{2+}$	0.025
503.27249	503.27238	$a^*_4 - H_2O$	-0.209
508.78543	508.78529	$(b^*_8 - H_2O)^{2+}$	-0.275
509.28305	509.28304	$b_4 - H_2O$	-0.020
517.79071	517.79072	$b^*_8{}^{2+}$	0.014
521.28305	521.28302	a^*_4	-0.058
526.78543	526.78511	$(b^*_9 - 2H_2O - NH_3)^{2+}$	-0.607
527.29362	527.29345	b_4	-0.322
531.26740	531.26740	$b^*_4 - H_2O$	0.000
532.25142	532.25141	$b^*_4 - NH_3$	-0.019
535.29870	535.29879	$(b^*_9 - 2H_2O)^{2+}$	0.163
535.79071	535.79081	$(b^*_9 - H_2O - NH_3)^{2+}$	0.182
539.31181	539.31160	$a^*_9{}^{2+}$	-0.389
544.30399	544.30394	$(b^*_9 - H_2O)^{2+}$	-0.083
544.79599	544.79619	$(b^*_9 - NH_3)^{2+}$	0.358
549.27796	549.27795	b^*_4	-0.027
551.35514	551.35509	$y_5 - 2H_2O$	-0.091
552.01731	552.01700	$y_{14}{}^{3+}$	-0.562
553.30927	553.30921	$b^*_9{}^{2+}$	-0.104
555.84769	555.84743	$(y_{10} - H_2O)^{2+}$	-0.463
564.85297	564.85298	$y_{10}{}^{2+}$	0.018
569.36571	569.36558	$y_5 - H_2O$	-0.220
587.37627	587.37627	y_5	0.000
590.68059	590.68024	$[M - H_2O - NH_3 + 3H]^{3+}$	-0.593
595.85384	595.85361	$a^*_{10}{}^{2+}$	-0.386
596.35610	596.35600	$[M - H_2O + 3H]^{3+}$	-0.168
600.84601	600.84568	$(b^*_{10} - H_2O)^{2+}$	-0.558
609.85130	609.85130	$b^*_{10}{}^{2+}$	0.004
615.32492	615.32445	$a^*_5 - 2NH_3$	-0.764
620.35147	620.35101	$b_5 - H_2O - NH_3$	-0.742
627.86949	627.86952	$(a^*_{11} - H_2O - NH_3)^{2+}$	0.048
628.90045	628.90021	$y_{11}{}^{2+}$	-0.382

THEORETICAL (m/z)	EXPERIMENTAL (m/z)	ASSIGNMENTS	ERROR (ppm)
631.36744	631.36799	a^*_5 - H_2O	0.863
632.86167	632.86197	$(b^*_{11}$-2 H_2O - $NH_3)^{2+}$	0.482
636.38276	636.38227	$(a^*_{11}$- $H_2O)^{2+}$	-0.774
636.87505	636.87485	$(a^*_{11}$- $NH_3)^{2+}$	-0.306
637.37801	637.37798	b_5- H_2O	-0.047
639.38805	639.38820	$(b_{11}$- $H_2O)^{2+}$	0.235
641.86695	641.86635	$(b^*_{11}$- H_2O - $NH_3)^{2+}$	-0.931
645.38805	645.38815	$a^*_{11}{}^{2+}$	0.159
649.37801	649.37810	a^*_5	0.139
650.38022	650.38037	$(b^*_{11}$ - $H_2O)^{2+}$	0.231
650.87223	650.87239	$(b^*_{11}$ - $NH_3)^{2+}$	0.246
655.38858	655.38856	b_5	-0.031
659.36236	659.36245	b^*_5- H_2O	0.136
659.38550	659.38539	$b^*_{11}{}^{2+}$	-0.171
660.34638	660.34644	b^*_5- NH_3	0.091
677.37293	677.37292	b^*_5	-0.007
682.44976	682.44983	y_6- H_2O	0.095
692.39079	692.39115	$(a^*_{12}$ - H_2O - $NH_3)^{2+}$	0.527
697.38296	697.38320	$(b^*_{12}$-2H_2O - $NH_3)^{2+}$	0.344
700.46033	700.46031	y_6	-0.029
700.90406	700.90410	$(a^*_{12}$- $H_2O)^{2+}$	0.061
701.39634	701.39597	$(a^*_{12}$- $NH_3)^{2+}$	-0.528
703.90934	703.90906	$(b$- $H_2O)^{2+}$	-0.398
705.89623	705.89632	b^*_{12}-2 $H_2O)^{2+}$	0.124
706.38824	706.38807	$(b^*_{12}$- H_2O - $NH_3)^{2+}$	-0.244
709.90934	709.90941	a^{2+}	0.095
714.90152	714.90147	$(b^*_{12}$- $H_2O)^{2+}$	-0.063
715.39352	715.39337	b^*_{12}- $NH_3{}^{2+}$	-0.217
723.90680	723.90662	$b^*_{12}{}^{2+}$	-0.245
731.46120	731.46084	y_{13}-2H_2O^{2+}	-0.499
734.41954	734.41982	b_{13}-2H_2O -2$NH_3{}^{2+}$	0.377
740.46649	740.46644	y_{13}- H_2O^{2+}	-0.064
740.95850	740.95819	y_{13}- $NH_3{}^{2+}$	-0.415
748.44643	748.44707	b_6- H_2O - NH_3	0.855
748.93282	748.93270	a^*_{13}-H2O- $NH_3{}^{2+}$	-0.154
757.44609	757.44575	a^*_{13}- H_2O^{2+}	-0.446
757.93837	757.93809	a^*_{13}- $NH_3{}^{2+}$	-0.369
759.46240	759.46294	a^*_6 - H_2O	0.704
762.43826	762.43825	b^*_{13}-2H_2O^{2+}	-0.016
763.44742	763.44668	x_7- H_2O - NH_3	-0.969
765.47297	765.47302	b_6- H_2O	0.065
766.45137	766.45086	$a^*_{13}{}^{2+}$	-0.665
771.44354	771.44366	b^*_{13}- H_2O^{2+}	0.149
771.49744	771.49747	y_7	0.039
780.44883	780.44873	$b^*_{13}{}^{2+}$	-0.125
783.48354	783.48423	b_6	0.881
787.45732	787.45722	b^*_6- H_2O	-0.127
788.44134	788.44137	b^*_6- NH_3	0.038
793.47938	793.47907	y_7+Na-H	-0.397

THEORETICAL (m/z)	EXPERIMENTAL (m/z)	ASSIGNMENTS	ERROR (ppm)
805.46789	805.46791	b^*_6	0.031
809.98558	809.98602	b_{14}- H_2O^{2+}	0.549
811.97247	811.97192	b^*_{14}-$2H_2O^{2+}$	-0.674
812.46448	812.46383	b^*_{14}- H_2O - $NH_3{}^{2+}$	-0.797
815.98558	815.98493	$a^*_{14}{}^{2+}$	-0.790
820.97775	820.97758	b^*_{14}- H_2O^{2+}	-0.207
829.98303	829.98288	$b^*_{14}{}^{2+}$	-0.184
854.53455	854.53452	y_8- H_2O	-0.041
872.54512	872.54515	y_8	0.034
876.50501	876.50477	b_7- H_2O - NH_3	-0.274
894.52706	894.52680	y_8+Na-H	-0.296
898.48936	898.48962	b^*_7- H_2O - NH_3	0.295
915.51590	915.51609	b^*_7- H_2O	0.208
916.49992	916.50003	b^*_7- NH_3	0.120
933.52647	933.52652	b^*_7	0.059
964.58257	964.58261	y_9-$2H_2O$	0.041
965.56659	965.56671	y_9- H_2O - NH_3	0.124
982.59313	982.59330	y_9- H_2O	0.168
1000.60370	1000.60368	y_9	-0.020
1016.56358	1016.56347	b^*_8- H_2O	-0.108
1022.58564	1022.58542	y_9+Na-H	-0.220
1031.56325	1031.56371	b_9- H_2O -$2NH_3$	0.446
1034.57415	1034.57396	b^*_8	-0.179
1087.60069	1087.60069	b^*_9- H_2O	0.000
1088.58471	1088.58361	b^*_9- NH_3	-1.010
1092.67753	1092.67757	y_{10}-$2H_2O$	0.037
1093.66155	1093.66112	y_{10}- H_2O - NH_3	-0.393
1105.61126	1105.61118	b^*_9	-0.068
1110.68809	1110.68805	y_{10}- H_2O	-0.041
1128.69866	1128.69852	y_{10}	-0.124
1183.65820	1183.65776	b-$^*_{10}$ H_2O - NH_3	-0.376
1190.69800	1190.69800	a_{10}+Na-H	0.000
1200.68475	1200.68416	b^*_{10}- H_2O	-0.491
1201.66877	1201.66925	b^*_{10}- NH_3	0.399
1218.69531	1218.69546	b^*_{10}	0.119
1289.76881	1289.76965	a^*_{11}	0.651
		Mean	-0.064
		St. Dv.	0.416

D

Mass Error tables with assignments used to interpret the data of Chapter 6

TABLE OF CONTENTS.

Table D-1. Mass error of the direct infusion spectra of the reacted KM-11 peptide reacted in MeOH/H_2O at 11 days of reaction. * indicates the ions used for calibration.

THEORICAL (m/z)	**EXPERIMENTAL (m/z)**	**ASSINGMENT**	**ERROR (ppm)**
* 449.91665	449.91667	$[M+3H]^{3+}$	0.022
* 469.25182	469.25172	$[M+C_2H_2O_2+3H]^{3+}$	-0.208
488.58698	488.58690	$[M+2(C_2H_2O_2)+3H]^{3+}$	-0.158
494.59050	494.59052	$[M+2(C_2H_2O_2)+H_2O+3H]^{3+}$	0.055
513.92566	513.92571	$[M+3(C_2H_2O_2)+H_2O+3H]^{3+}$	0.055

* 674.37134	674.37115	$[M+2H]^{2+}$	-0.292
* 703.37408	703.37391	$[M+C_2H_2O_2+2H]^{2+}$	-0.251
723.37154	723.37178	$[M+C_2H_2O_2+2H]^{2+}$	0.326
732.37682	732.37680	$[M+2(C_2H_2O_2)+2H]^{2+}$	-0.027
741.38211	741.38222	$[M+2(C_2H_2O_2)+H_2O+2H]^{2+}$	0.152
770.38485	770.38514	$[M+3(C_2H_2O_2)+H_2O+2H]^{2+}$	0.378
* 779.39013	779.39066	$[M+3(C_2H_2O_2)+2H_2O+2H]^{2+}$	0.680
808.39287	808.39356	$[M+4(C_2H_2O_2)+2H_2O+2H]^{2+}$	0.853
* 1347.73542	1347.73529	$[M+H]^{1+}$	-0.099
		Mean	0.074
		St. Dv.	0.388

Table D-2. Mass error of the direct infusion spectra of the reacted KM-11 peptide reacted in PBS. * indicates the ions used for calibration.

THEORICAL (m/z)	**EXPERIMENTAL (m/z)**	**ASSINGMENT**	**ERROR (ppm)**
* 449.91665	449.91682	$[M+3H]^{3+}$	0.368
463.24829	463.24813	$[M+C_2O+3H]^{3+}$	-0.348
* 469.25182	469.25193	$[M+C_2H_2O_2+3H]^{3+}$	0.232
474.58345	474.58321	$[M+C_2H_2O_3+3H]^{3+}$	-0.512
488.58698	488.58678	$[M+2(C_2H_2O_2)+3H]^{3+}$	-0.407
674.37134	674.37202	$[M+2H]^{2+}$	0.997
685.36352	685.36304	$[M+(C_2-H_2)+2H]^{2+}$	-0.697
* 694.87048	694.87077	$[M+C_2O+2H]^{2+}$	0.420
* 703.37408	703.37375	$[M+C_2H_2O_2+2H]^{2+}$	-0.464
723.37154	723.37172	$[M+C_4H_2O_3+C_2O+2H]^{2+}$	0.252
* 732.37682	732.37654	$[M+2(C_2H_2O_2)++2H]^{2+}$	-0.384
		Mean	-0.085
		St. Dv.	0.519

Table D-3. Mass error of the direct infusion spectra of the reacted AcKM-11 peptide reacted in MeOH/H_2O at 11 hours of reaction. * indicates the ions used for calibration.

THEORICAL (m/z)	EXPERIMENTAL (m/z)	ASSINGMENT	ERROR (ppm)
* 463.92018	463.92027	$[M+3H]^{3+}$	-0.194
483.25534	483.25540	$[M+C_2H_2O_2+3H]^{3+}$	0.115
502.59050	502.59057	$[M+2(C_2H_2O_2)+3H]^{3+}$	0.138
* 508.59402	508.59371	$[M+2(C_2H_2O_2)+H_2O+3H]^{3+}$	-0.600
527.92918	527.92937	$[M+3(C_2H_2O_2)+H_2O+3H]^{3+}$	0.367
695.37663	695.37677	$[M+2H]^{2+}$	0.204
* 724.37937	724.37935	$[M+C_2H_2O_2+2H]^{2+}$	-0.021
753.38211	753.38222	$[M+2(C_2H_2O_2)+2H]^{2+}$	0.149
762.38739	762.38752	$[M+2(C_2H_2O_2)+H_2O+2H]^{2+}$	0.166
791.39013	791.39024	$[M+3(C_2H_2O_2)+H_2O+2H]^{2}$	0.143
* 800.39541	800.39578	$[M+3(C_2H_2O_2)+2H_2O+2H]^{2+}$	0.463
820.39287	820.39328	$[M+4(C_2H_2O_2)+H_2O+2H]^{2+}$	0.003
* 829.39815	829.39865	$[M+4(C_2H_2O_2)+2H_2O+2H]^{2+}$	0.603
		mean	0.075
		St. Dv.	0.315

Table D-4. Mass error of the direct infusion spectra of the reacted AcKM-11 peptide reacted in PBS. * indicates the ions used for calibration.

THEORICAL (m/z)	EXPERIMENTAL (m/z)	ASSINGMENT	ERROR (ppm)
* 463.92018	463.92030	$[M+3H]^{3+}$	0.254
483.25534	483.25545	$[M+C_2H_2O_2+3H]^{3+}$	0.234
* 695.37663	695.37683	$[M+2H]^{2+}$	0.291
706.36880	706.36866	$[M+(C_2-H_2)+2H]^{2+}$	-0.198
* 715.37408	715.37370	$[M+C_2O+2H]^{2+}$	-0.536
724.88104	724.88119	$[M+C_2H_2O_2+C_2O+2H]^{2+}$	0.203
753.38211	753.38140	$[M+2(C_2H_2O_2)+2H]^{2+}$	-0.942
* 1389.74597	1389.74599	$[M+H]^{1+}$	0.017
		Mean	-0.084

	St. Dv.	0.448

Table D-5. DR(703)ECD(732) error analysis of the glycated KM-11 peptide in MeOH/H_2O (50:50) for the precursor ion $[M+2(C_2H_2O_2)+2H]^{2+}$. * indicates the ions used for calibration.

THEORETICAL (m/z)	EXPERIMENTAL (m/z)	ASSIGNMENTS	ERROR (ppm)
* 243.18154	243.18154	c_2	0.000
301.18702	301.18701	$c^{\ddagger}_2$	-0.033
319.17983	319.17979	y_3	-0.125
376.21050	376.21056	$z_4^{\bullet}$-C_3H_6S	0.162
450.22952	450.22952	$z_4^{\bullet}$	0.000
451.23735	451.23736	z_4	0.033
466.24824	466.24820	y_4	-0.086
478.76296	478.76303	$c^{\ddagger}_7{}^{\bullet\ 2+}$	0.151
479.26687	479.26673	$c^{\ddagger}_7{}^{\ 2+}$	-0.292
495.32758	495.32761	$c_4^{\bullet}$	0.050
* 496.33541	496.33543	c_4	0.040
499.26433	499.26435	$(c^{\ddagger}_7\text{-}H_2O)^{\ 2+}$	0.045
523.27891	523.27894	$z_5^{\bullet}$-C_3H_6S	0.059
530.79426	530.79449	$a^{\ddagger}_{10}{}^{\ 2+}$	0.433
535.32250	535.32256	$c^{\ddagger}_4\text{-}H_2O$	0.112
536.33033	536.33037	$c^{\ddagger}_4\text{-}H_2O$	0.084
543.29188	543.29177	$(c^{\ddagger}_8\text{-}H_2O)^{\ 2+}$	-0.202
552.29716	552.29725	$c^{\ddagger}_8{}^{\bullet\ 2+}$	0.158
552.80107	552.80116	$c^{\ddagger}_8{}^{\ 2+}$	0.154
553.33307	553.33309	$c^{\ddagger}_4{}^{\bullet}$	0.045
* 554.34089	554.34097	$c^{\ddagger}_4$	0.144
572.29462	572.29442	$(c^{\#}_8{}^{\bullet}\text{-}H_2O)^{\ 2+}$	-0.349
572.30652	572.30670	$c^{\ddagger}_9{}^{\ 2+}$	0.310
572.79853	572.79884	$b^{\ddagger}_9{}^{\ 2+}$	0.537
580.80789	580.80779	$c^{\ddagger}_9{}^{\bullet\ 2+}$	-0.176
581.29990	581.30027	$c^{\#}_8{}^{\bullet\ 2+}$	0.632
581.31181	581.31184	$c^{\ddagger}_9{}^{\ 2+}$	0.060
581.80381	581.80419	$c^{\#}_8{}^{\ 2+}$	0.645
590.80022	590.80009	$y^{\ddagger}_9{}^{\ 2+}$	-0.220
592.30398	592.30397	$(c^{\#}_8\text{-}2H_2O)^{\ 2+}$	-0.017
592.79599	592.79641	$(b^{\#}_8\text{-}H_2O)^{\ 2+}$	0.709
593.32798	593.32798	$c^{\#}_4{}^{\bullet}\text{-}H_2O$	0.000
594.33581	594.33612	$c^{\#}_4\text{-}H_2O$	0.530
597.29793	597.29802	$z_5^{\bullet}$	0.151
598.30575	598.30586	z_5	0.175
600.80535	600.80534	$(c^{\#}_9{}^{\bullet}\text{-}H_2O)^{\ 2+}$	-0.017
601.30926	601.30937	$(c^{\#}_9\text{-}H_2O)^{\ 2+}$	0.179
609.81063	609.81059	$c^{\#}_9{}^{\bullet\ 2+}$	-0.070
610.31454	610.31463	$c^{\#}_9{}^{\ 2+}$	0.139
611.33854	611.33861	$c^{\#}_4{}^{\bullet}$	0.106
* 612.34637	612.34649	$c^{\#}_4$	0.196
613.31665	613.31684	y_5	0.310

THEORETICAL (m/z)	EXPERIMENTAL (m/z)	ASSIGNMENTS	ERROR (ppm)
619.80296	619.80315	$y^{\#}_{9}{}^{2+}$	0.307
620.37472	620.37489	$c^{\ddagger}_{5}$-H_2O -$^{\bullet}CONH_2$.	0.274
623.38617	623.38625	$c_5^{\bullet}$	0.136
624.39399	624.39400	c_5	0.016
628.84855	628.84904	$(c^{\ddagger}_{10}$ -$H_2O)^{2+}$	0.775
630.81360	630.81359	$(y_{10} – NH_3)^{2+}$	-0.016
637.85384	637.85389	$c^{\ddagger}_{10}{}^{2+}$	0.086
638.38528	638.38526	$c^{\ddagger}_{7}$-$^{\bullet}CONH_2$.	-0.039
639.33423	639.33402	$[M\text{-}2H_2O\text{-}2NH_3+H]^{2+}$	-0.328
646.37834	646.37809	$c^{\ddagger}_{7}$-$2H_2O$	-0.387
651.33749	651.33763	$z_6^{\bullet}$- C_3H_6S	0.216
657.85129	657.85129	$(c^{\#}_{10}$-$H_2O)^{2+}$	-0.004
662.33823	662.33763	$a^{\#}_{5}$-$2NH_3$	-0.906
663.38108	663.38111	$c^{\ddagger}_{5}{}^{\bullet}$-$H_2O$	0.045
664.38891	664.38900	$c^{\ddagger}_{5}$-H_2O	0.143
666.85658	666.85613	$c^{\#}_{10}{}^{2+}$	-0.667
674.37134	674.37117	$[M+H]^{2+}$	-0.252
678.38076	678.38081	$a^{\#}_{5}$ -H_2O	0.081
681.36726	681.36760	$[M^{\ddagger}\text{-}^{\bullet}CONH_2+2H]^{2+}$	0.492
681.39165	681.39176	$c^{\ddagger}_{5}{}^{\bullet}$	0.169
682.39947	682.39957	$c^{\ddagger}_{5}$	0.147
685.36352	685.36377	$[M^{\ddagger}\text{-}2H_2O+2H]^{2+}$	0.372
694.36880	694.36903	$[M^{\ddagger}\text{-}H_2O+2H]^{2+}$	0.335
694.86081	694.86094	$[M^{\ddagger-}NH_3+2H]^{2+}$	0.191
696.37020	696.37023	$a^{\ddagger}_{8}$-$2NH_3$-$2H_2O$	0.043
696.39132	696.39138	$a^{\#}_{5}$	0.086
703.37408	703.37415	$[M^{\ddagger}+2H]^{2+}$	0.100
705.36784	705.36777	$b^{\#}_{5}$-H_2O	-0.099
707.32214	707.32199	y_6-$2NH_3$	-0.212
* 714.36626	714.36566	$[M\text{-}2H_2O+H]^{2+}$	-0.833
714.85827	714.85805	$[M\text{-}H_2O\text{-}NH_3+2H]^{2+}$	-0.308
721.38656	721.38666	$c^{\#}_{5}{}^{\bullet}$-H_2O	0.139
722.39439	722.39455	$c^{\#}_{5}$-H_20	0.228
723.37154	723.37150	$[M^{\#}\text{-}H_2O+2H]^{2+}$	-0.055
723.86355	723.86307	$[M^{\#}\text{-}NH_3+2H]^{2+}$	-0.663
724.34131	724.34064	$b^{\ddagger}_{6}$-$3NH_3$	-0.918
725.35651	725.35645	$z_6^{\bullet}$	-0.083
726.36433	726.36445	z_6	0.158
732.37682	732.37662	$[M^{\#}+2H]^{2+}$	-0.273
735.42602	735.42604	b_6	0.020
739.39712	739.39720	$c^{\#}_{5}{}^{\bullet}$	0.101
740.40495	740.40518	$c^{\#}_{5}$	0.311
748.43385	748.43384	$c^{\ddagger}_{6}$-$^{\bullet}CONH_2$-H_2O	-0.013
751.44475	751.44476	$c_6^{\bullet}$	0.020
752.45257	752.45263	c_6	0.080
757.41038	757.41009	$b^{\ddagger}_{6}$-H_2O	-0.376
766.44442	766.44490	$a^{\ddagger}_{6}$	0.626
774.43692	774.43709	$c^{\ddagger}_{6}$-$2H_2O$	0.220

THEORETICAL (m/z)	EXPERIMENTAL (m/z)	ASSIGNMENTS	ERROR (ppm)
788.42877	788.42929	$a^{\#}_{6}$-2H_2O	0.660
791.43966	791.43979	$c^{\ddagger}_{6}{}^{\bullet}$-$H_2O$	0.164
792.44749	792.44763	$c^{\ddagger}_{6}$-H_2O	0.183
793.43151	793.43192	$b^{\ddagger}_{6}$	0.523
806.43934	806.43945	$a^{\#}_{5}$-H_2O	0.143
809.45023	809.45034	$c^{\ddagger}_{6}{}^{\bullet}$	0.142
810.45805	810.45821	$c^{\ddagger}_{6}$	0.197
824.44990	824.44994	$a^{\#}_{6}$	0.049
833.42642	833.42644	$b^{\#}_{6}$-H_2O	0.024
834.41044	834.41063	$b^{\#}_{6}$-NH_3	0.228
849.44514	849.44519	$c^{\#}_{6}{}^{\bullet}$-H_2O	0.059
850.45296	850.45309	$c^{\#}_{6}$-H_2O	0.147
851.43699	851.43708	$b^{\#}_{6}$	0.112
867.45570	867.45585	$c^{\#}_{6}{}^{\bullet}$	0.167
* 868.46353	868.46377	$c^{\#}_{6}$	0.276
882.49443	882.49517	b_7	0.833
895.50226	895.50248	$a^{\ddagger}_{7}$-H_2O	0.240
898.51315	898.51327	$c_7{}^{\bullet}$	0.128
899.52098	899.52100	c_7	0.022
* 913.51283	913.51298	$a^{\ddagger}_{7}$	0.164
921.50533	921.50552	$c^{\ddagger}_{7}$-2H_2O	0.206
938.50807	938.50838	$c^{\ddagger}_{7}{}^{\bullet}$-$H_2O$	0.330
939.51590	939.51612	$c^{\ddagger}_{7}$-H_2O	0.239
953.50774	953.50748	$c^{\#}_{7}$-$^{\bullet}CONH_2$-H_2O	-0.273
956.51864	956.51875	$c^{\ddagger}_{7}{}^{\bullet}$	0.120
957.52646	957.52668	$c^{\ddagger}_{7}$	0.230
966.48657	966.48666	y_8	0.093
971.51831	971.51857	$a^{\#}_{7}$	0.268
980.49483	980.49493	$b^{\#}_{7}$-H_2O	0.102
981.47885	981.47885	$b^{\#}_{7}$-NH_3	0.000
996.51355	996.51378	$c^{\#}_{7}{}^{\bullet}$-H_2O	0.231
997.52138	997.52152	$c^{\#}_{7}$-H_2O	0.145
998.50540	998.50537	$b^{\#}_{7}$	-0.025
1002.57576	1002.57597	a_8	0.209
1014.52412	1014.52441	$c^{\#}_{7}{}^{\bullet}$	0.291
*1015.53194	1015.53213	$c^{\#}_{7}$	0.187
1042.57067	1042.57051	$c^{\ddagger}_{8}$-$^{\bullet}CONH_2$-H_2O	-0.153
1045.58156	1045.58210	$c_8{}^{\bullet}$	0.512
1046.58939	1046.58954	c_8	0.143
1060.58124	1060.58149	$a^{\ddagger}_{8}$	0.236
1072.54485	1072.54486	$z^{\ddagger}_{9}{}^{\bullet}$-$C_3H_6D$- H_2O	0.006
1082.56559	1082.56515	$a^{\#}_{8}$-2H_2O	-0.406
1085.57648	1085.57719	$c^{\ddagger}_{8}{}^{\bullet}$-$H_2O$	0.654
1086.56655	1086.56604	y_9-2H_2O	-0.469
1086.58431	1086.58442	b_9	0.106
1088.53459	1088.53418	y_9-2NH_3	-0.377
1090.55542	1090.55517	$z^{\ddagger}_{9}{}^{\bullet}$-$C_3H_6S$	-0.228
1099.59213	1099.59206	$c^{\ddagger}_{8}$-$^{\bullet}CONH_2$.-H_2O	-0.064

THEORETICAL (m/z)	EXPERIMENTAL (m/z)	ASSIGNMENTS	ERROR (ppm)
1100.57615	1100.57661	$a^{\#}_{8}$-H_2O	0.413
1102.60302	1102.60307	$c_9^{\bullet}$	0.041
1103.61085	1103.61103	c_9	0.163
1104.59487	1104.59510	$c^{\ddagger}_{7}$	0.208
1112.53976	1112.54031	$c^{\#}_{8}$-H_2O-NH_3	0.490
1117.60270	1117.60314	$a^{\ddagger}_{8}$	0.394
1118.58672	1118.58658	$a^{\#}_{8}$	-0.125
1125.59520	1125.59428	$c^{\ddagger}_{9}$-$2H_2O$	-0.817
1126.57922	1126.57950	$b^{\ddagger}_{9}$-H_2O	0.249
1127.56324	1127.56360	$b^{\#}_{8}$-H_2O	0.319
1128.54726	1128.54620	$b^{\#}_{8}$-NH_3	-0.939
1129.53733	1129.53824	$z^{\ddagger}_{9}{}^{\bullet}$-$H_2O$-$NH_3$	0.806
1130.55033	1130.55014	$z^{\#}_{9}{}^{\bullet}$-C_3H_6D-H_2O	-0.172
1142.59794	1142.59870	$c^{\ddagger}_{9}{}^{\bullet}$-$H_2O$	0.665
1143.60577	1143.60595	$c^{\ddagger}_{9}$-H_2O	0.162
*1144.58978	1144.58986	$c^{\#}_{8}$-H_2O	0.066
1145.57380	1145.57353	$b^{\#}_{8}$	-0.240
1146.56388	1146.56396	$z^{\ddagger}_{9}{}^{\bullet}$-$H_2O$	0.074
1147.60471	1147.60411	b_{10}-H_2O-$2NH_3$	-0.523
1148.56090	1148.55971	$z^{\#}_{9}{}^{\bullet}$-C_3H_6S	-1.035
1157.59761	1157.59815	$a^{\#}_{9}$-H_2O	0.462
1160.60850	1160.60840	$c^{\ddagger}_{9}{}^{\bullet}$	-0.090
1161.59656	1161.59531	$a^{\ddagger}_{10}$-$3NH_3$-H_2O	-1.076
1161.61633	1161.61643	$c^{\ddagger}_{9}$	0.086
1162.60035	1162.60021	$c^{\#}_{8}$	-0.120
1164.57444	1164.57465	$z^{\ddagger}_{9}{}^{\bullet}$	0.180
1175.60818	1175.60801	$a^{\#}_{9}$	-0.145
1180.59316	1180.59327	$y^{\ddagger}_{9}$	0.093
1184.58470	1184.58469	$b^{\#}_{9}$-H_2O	-0.008
1186.55879	1186.55984	$z^{\#}_{9}{}^{\bullet}$-$2H_2O$	0.885
1187.54281	1187.54191	$z^{\#}_{9}{}^{\bullet}$-H_2O-NH_3	-0.758
1200.60342	1200.60405	$c^{\#}_{9}{}^{\bullet}$-H_2O	0.525
1201.61125	1201.61123	$c^{\#}_{9}$-H_2O	-0.012
1202.59526	1202.59499	$b^{\#}_{9}$	-0.229
1204.56936	1204.56968	$z^{\#}_{9}{}^{\bullet}$-H_2O	0.270
1212.67564	1212.67590	$c^{\ddagger}_{10}$-$^{\bullet}CONH_2$-H_2O	0.214
1215.68709	1215.68697	$c_{10}^{\bullet}$	-0.095
1216.69491	1216.69532	c_{10}	0.337
*1219.62181	1219.62175	$c^{\#}_{9}$	-0.049
1222.57992	1222.58001	$z^{\#}_{9}{}^{\bullet}$	0.074
1230.68676	1230.68712	$a^{\ddagger}_{10}$	0.293
1238.67926	1238.67933	$c^{\ddagger}_{10}$-$2H_2O$	0.057
1252.67111	1252.67060	$a^{\#}_{10}$-$2H_2O$	-0.407
1255.68200	1255.68196	$c^{\ddagger}_{10}{}^{\bullet}$-$H_2O$	-0.032
1256.68982	1256.69008	$c^{\ddagger}_{10}$-H_2O	0.203
1274.70039	1274.70054	$c^{\ddagger}_{10}$	0.118
1288.69224	1288.69230	$a^{\#}_{10}$	0.047
1297.66876	1297.66849	$c^{\#}_{10}$-H_2O-NH_3	-0.208

THEORETICAL (m/z)	EXPERIMENTAL (m/z)	ASSIGNMENTS	ERROR (ppm)
1303.72177	1303.72217	$[M^{\ddagger}\text{-}HCONH_2+2H]^{1+\bullet}$	0.307
*1314.69530	1314.69572	$c^{\#}_{10}\text{-}H_2O$	0.316
1315.67933	1315.67923	$b^{\#}_{10}$	-0.072
1330.70886	1330.70974	$[M\text{-}NH_3+H]^{1+}$	0.665
1331.71668	1331.71641	$[M\text{-}NH_3+2H]^{1+\bullet}$	-0.203
1332.70587	1332.70508	$c^{\#}_{10}$	-0.593
1343.71668	1343.71657	$[M^{\ddagger}\text{-}^{\bullet}CONH_2\text{-}H_2O+H]^{1+}$	-0.082
1347.73540	1347.73538	$[M+H]^{1+}$	-0.015
1352.69321	1352.69317	$[M^{\ddagger}\text{-}2H_2O\text{-}NH_3+H]^{1+}$	-0.026
1353.70103	1353.70142	$[M^{\ddagger}\text{-}2H_2O\text{-}NH_3+2H]^{1+\bullet}$	0.288
1354.68505	1354.68508	$[M^{\ddagger}\text{-}H_2O\text{-}2NH_3+2H]^{1+\bullet}$	0.022
1361.72725	1361.72715	$[M^{\ddagger}\text{-}^{\bullet}CONH_2+H]^{1+}$	-0.073
1371.71159	1371.71146	$[M^{\ddagger}\text{-}H_2O\text{-}NH_3+2H]^{1+\bullet}$	-0.098
1383.71160	1383.71235	$[M^{\ddagger}\text{-}^{\bullet}CONH_2\text{-}2H_2O+H]^{1+}$	0.542
1387.73032	1387.73052	$[M^{\ddagger}\text{-}H_2O+1H]^{1+}$	0.144
1388.73815	1388.73809	$[M^{\ddagger}\text{-}H_2O+2H]^{1+\bullet}$	-0.439
1401.72162	1401.72292	$[M^{\ddagger}\text{-}H_2O\text{-}^{\bullet}CONH_2+1H]^{1+}$	0.927
1402.70727	1402.70613	$[M^{\#}\text{-}NH3\text{-}^{\bullet}CONH_2+1H]^{1+}$	-0.813
*1405.74089	1405.74127	$[M^{\ddagger}+1H]^{1+}$	0.270
1411.70651	1411.70590	$[M^{\#}\text{-}NH3\text{-}2H_2O+2H]^{1+\bullet}$	-0.432
1412.69053	1412.68972	$[M^{\#}\text{-}H_2O\text{-}2NH_3+2H]^{1+\bullet}$	-0.573
1419.73218	1419.73312	$[M^{\#}\text{-}^{\bullet}CONH_2+1H]^{1+}$	0.662
1428.70926	1428.70903	$[M^{\#}\text{-}H_2O\text{-}NH_3+1H]^{1+}$	-0.157
1428.73306	1428.73350	$[M^{\#}\text{-}2H_2O+2H]^{1+\bullet}$	0.308
1429.71708	1429.71703	$[M^{\#}\text{-}H_2O\text{-}NH_3+2H]^{1+\bullet}$	-0.035
1445.73580	1445.73626	$[M^{\#}\text{-}H_2O+H]^{1+}$	0.318
1446.74363	1446.74433	$[M^{\#}\text{-}H_2O+2H]^{1+\bullet}$	0.487
*1463.74637	1463.74554	$[M^{\#}+H]^{1+}$	-0.564
		mean	0.066
		St. Dv.	0.448

Table D-6. ECD(732) error analysis of the KM-11 peptide in MeOH/H_2O (50:50) for the precursor ion $[M+2(C_2H_2O_2)+2H]^{2+}$. * indicates the ions used for calibration.

THEORETICAL (m/z)	EXPERIMENTAL (m/z)	ASSIGNMENTS	ERROR (ppm)
* 243.18154	243.18154	c_2	0.000
301.18702	301.18690	$c^{\ddagger}_2$	-0.398
319.17983	319.17973	y_3	-0.313
376.21050	376.21044	$z_4^{\bullet}\text{-}\ C_3H_6S$	-0.157
450.22952	450.22944	$z_4^{\bullet}$	-0.178
451.23735	451.23726	z_4	-0.188
466.24824	466.24852	y_4	0.601
478.76296	478.76293	$c^{\ddagger}_7{}^{\bullet 2+}$	-0.057
479.26687	479.26703	$c^{\ddagger}_7{}^{2+}$	0.334
495.32758	495.32762	$c_4^{\bullet}$	0.071

THEORETICAL (m/z)	EXPERIMENTAL (m/z)	ASSIGNMENTS	ERROR (ppm)
496.33541	496.33535	c_4	-0.121
499.26433	499.26453	$(c^{\#}_7\text{-}H_2O)^{2+}$	0.406
523.27891	523.27891	$z_5^{\bullet}\text{-}C_3H_6S$	0.002
530.79426	530.79464	$a^{\ddagger}_8{}^{2+}$	0.716
535.32250	535.32246	$c^{\ddagger}_4{}^{\bullet}\text{-}H_2O$	-0.075
536.33033	536.33033	$c^{\ddagger}_4\text{-}H_2O$	0.009
552.29716	552.29703	$c^{\ddagger}_8{}^{\bullet 2+}$	-0.240
552.80107	552.80116	$c^{\ddagger}_8{}^{2+}$	0.154
553.33307	553.33308	$c^{\ddagger}_4{}^{\bullet}$	0.027
554.34089	554.34082	$c^{\ddagger}_4$	-0.126
571.80261	571.80264	$(c^{\ddagger}_9\text{-}H_2O)^{2+}$	0.052
572.29462	572.29446	$(c^{\#}_8{}^{\bullet}\text{-}H_2O)^{2+}$	-0.280
572.79853	572.79849	$b^{\ddagger}_9{}^{2+}$	-0.074
577.30926	577.30948	$c^{\#}_4\text{-}H_2O\text{-}NH_3$	0.381
580.80789	580.80822	$c^{\ddagger}_9{}^{\bullet 2+}$	0.564
581.31181	581.31172	$c^{\ddagger}_9{}^{2+}$	-0.146
589.35688	589.35695	$b_5\text{-}H_2O$	0.119
590.80022	590.80020	$y^{\ddagger}_9{}^{2+}$	-0.034
592.30398	592.30395	$(c^{\#}_9\text{-}2H_2O)^{2+}$	-0.051
593.32798	593.32798	$c^{\#}_4{}^{\bullet}\text{-}H_2O$	0.000
594.33581	594.33618	$c^{\#}_4\text{-}H_2O$	0.631
597.29793	597.29790	$z_5^{\bullet}$	-0.050
598.30575	598.30575	z_5	-0.008
600.80535	600.80533	$(c^{\#}_9{}^{\bullet}\text{-}H_2O)^{2+}$	-0.033
601.30926	601.30921	$(c^{\#}_9\text{-}H_2O)^{2+}$	-0.087
609.81063	609.81032	$c^{\#}_9{}^{\bullet 2+}$	-0.512
611.33854	611.33852	$c^{\#}_4{}^{\bullet}$	-0.041
612.34637	612.34640	$c^{\#}_4$	0.049
613.31665	613.31697	y_5	0.522
619.80296	619.80242	$y^{\#}_9{}^{2+}$	-0.871
623.38617	623.38612	$c_5^{\bullet}$	-0.072
624.39399	624.39391	c_5	-0.128
628.84855	628.84833	$(c^{\ddagger}_{10}\text{-}H_2O)^{2+}$	-0.354
637.85384	637.85375	$c^{\ddagger}_{10}{}^{2+}$	-0.133
651.33749	651.33740	$z_6^{\bullet}\text{-}C_3H_6S$	-0.137
657.85129	657.85125	$(c^{\#}_{10}\text{-}H_2O)^{2+}$	-0.065
657.86061	657.86025	$[M\text{-}H_2O\text{+}H]^{2+}$	-0.547
658.35262	658.35274	$[M\text{-}2NH_3\text{+}H]^{2+}$	0.182
662.33823	662.33783	$a^{\#}_5\text{-}2NH_3$	-0.604
663.38108	663.38104	$c^{\ddagger}_5{}^{\bullet}\text{-}H_2O$	-0.060
664.38891	664.38897	$c^{\ddagger}_5\text{-}H_2O$	0.098
665.37293	665.37317	$b^{\ddagger}_5$	0.368
666.85658	666.85645	$c^{\#}_{10}{}^{2+}$+	-0.187
672.36198	672.36171	$[M^{\ddagger}\text{-}^{\bullet}CONH_2\text{+}2H]^{2+}$	-0.405
674.37134	674.37164	$[M\text{+}H]^{2+}$	0.445
678.38076	678.38118	$a^{\#}_5\text{-}H_2O$	0.626
681.36726	681.36780	$[M^{\ddagger}\text{-}^{\bullet}CONH_2\text{+}H]^{2+}$	0.785

THEORETICAL (m/z)	EXPERIMENTAL (m/z)	ASSIGNMENTS	ERROR (ppm)
681.39165	681.39164	$c^{\ddagger}_{5}{}^{\bullet}$	-0.007
682.39947	682.39947	$c^{\ddagger}_{5}$	0.000
685.85552	685.85511	$[M-{}^{\ddagger}\text{-}H_2O\ NH_3+2H]^{2+}$	-0.605
	686.35972	?	
694.36880	694.36869	$[M^{\ddagger}\text{-}H_2O+H]^{2+}$	-0.155
696.39132	696.39154	$a^{\#}_{5}$	0.316
703.37408	703.37392	$[M^{\ddagger}+H]^{2+}$	-0.227
705.36784	705.36784	$b^{\#}_{5}\text{-}H_2O$	0.000
714.85827	714.85756	$[M^{\#}\text{-}H_2O\text{-}NH_3+2H]^{2+}$	-0.993
721.38656	721.38658	$c^{\#}_{5}{}^{\bullet}\text{-}H_2O$	0.028
722.39439	722.39441	$c^{\#}_{5}\text{-}H_2O$	0.035
723.37154	723.37147	$[M^{\#}\text{-}H_2O+2H]^{2+}$	-0.097
723.37841	723.37911	$b^{\#}_{5}$	0.975
723.86355	723.86322	$[M^{\#}\text{-}NH_3+2H]^{2+}$	-0.456
725.35651	725.35621	$z_6^{\bullet}$	-0.414
726.36433	726.36454	z_6	0.282
732.37682	732.37667	$[M^{\#}+2H]^{2+}$	-0.205
735.42602	735.42595	b_6	-0.102
739.39712	739.39712	$c^{\#}_{5}{}^{\bullet}$	-0.007
740.40495	740.40511	$c^{\#}_{5}$	0.216
751.44475	751.44481	$c_6^{\bullet}$	0.087
752.45257	752.45246	c_6	-0.146
774.43692	774.43659	$c^{\ddagger}_{6}\text{-}2H_2O$	-0.426
791.43966	791.43950	$c^{\ddagger}_{6}{}^{\bullet}\text{-}H_2O$	-0.202
792.44749	792.44746	$c^{\ddagger}_{6}\text{-}H_2O$	-0.032
806.43934	806.43969	$a^{\#}_{6}\text{-}H_2O$	0.440
809.45023	809.45032	$c^{\ddagger}_{6}{}^{\bullet}$	0.117
810.45805	810.45814	$c^{\ddagger}_{6}$	0.111
824.44990	824.44981	$a^{\#}_{6}$	-0.109
833.42642	833.42642	$b^{\#}_{6}\text{-}H_2O$	0.000
834.41044	834.41085	$b^{\#}_{6}\text{-}NH_3$	0.491
849.44514	849.44517	$c^{\#}_{6}{}^{\bullet}\text{-}H_2O$	0.035
850.45296	850.45301	$c^{\#}_{6}\text{-}H_2O$	0.053
851.43699	851.43705	$b^{\#}_{6}$	0.076
867.45570	867.45576	$c^{\#}_{6}{}^{\bullet}$	0.063
868.46353	868.46363	$c^{\#}_{6}$	0.115
898.51315	898.51339	$c_7^{\bullet}$	0.262
899.52098	899.52088	c_7	-0.111
921.50533	921.50488	$c^{\ddagger}_{7}\text{-}2H_2O$	-0.488
938.50807	938.50818	$c^{\ddagger}_{7}{}^{\bullet}\text{-}H_2O$	0.117
939.51590	939.51597	$c^{\ddagger}_{7}\text{-}H_2O$	0.080
956.51864	956.51874	$c^{\ddagger}_{7}{}^{\bullet}$	0.110
957.52646	957.52658	$c^{\ddagger}_{7}$	0.125
971.51831	971.51827	$a^{\#}_{7}{}^{\bullet}$	-0.041
980.49483	980.49506	$b^{\#}_{7}\text{-}H_2O$	0.235
981.47885	981.47920	$b^{\#}_{7}\text{-}NH_3$	0.357
996.51355	996.51340	$c^{\#}_{7}{}^{\bullet}\text{-}H_2O$	-0.151

THEORETICAL (m/z)	EXPERIMENTAL (m/z)	ASSIGNMENTS	ERROR (ppm)
997.52138	997.52143	$c^{\#}_{7}$-H_2O	0.055
998.50540	998.50524	$b^{\#}_{7}$	-0.155
1014.52412	1014.52437	$c^{\#}_{7}{}^{\bullet}$	0.251
1015.53194	1015.53205	$c^{\#}_{7}$	0.108
1042.57012	1042.56990	$c^{\ddagger}_{8}$-H_2O -$^{\bullet}CONH_2$.	-0.211
1045.58156	1045.58182	$c_8{}^{\bullet}$	0.244
1046.58939	1046.58950	c_8	0.105
1060.58068	1060.58085	$c^{\ddagger}_{8}$-$^{\bullet}CONH_2$.	0.156
1072.54485	1072.54484	$z^{\ddagger}_{9}{}^{\bullet}$-$H_2O$ -C_3H_6S	-0.013
1085.57648	1085.57573	$c^{\ddagger}_{8}{}^{\bullet}$-$H_2O$	-0.691
1086.58431	1086.58433	b_9	0.023
1088.53459	1088.53474	y_9-2NH3	0.138
1090.55542	1090.55545	$z^{\ddagger}_{9}{}^{\bullet}$-$C_3H_6S$	0.028
1100.57615	1100.57637	$a^{\#}_{8}$-H_2O	0.195
1102.60302	1102.60288	$c_9{}^{\bullet}$	-0.132
1103.61085	1103.61093	c_9	0.072
1104.59487	1104.59500	$c^{\ddagger}_{8}$	0.118
1118.58672	1118.58671	$a^{\#}_{8}$	-0.009
1125.59520	1125.59487	$c^{\ddagger}_{9}$-H_2O -H_2O	-0.293
1126.57922	1126.57934	$b^{\ddagger}_{9}$-H_2O	0.107
1127.56324	1127.56337	$b^{\#}_{8}$-H_2O	0.115
1129.53733	1129.53778	$z^{\ddagger}_{9}{}^{\bullet}$-$H_2O$-$NH_3$	0.398
1130.55033	1130.55043	$z^{\#}_{9}{}^{\bullet}$-C_3H_6S -H_2O	0.085
1142.59794	1142.59840	$c^{\ddagger}_{9}{}^{\bullet}$-$H_2O$	0.403
1143.60577	1143.60581	$c^{\ddagger}_{9}$-H_2O	0.039
1144.58978	1144.58972	$b^{\ddagger}_{9}$	-0.057
1145.57380	1145.57330	$b^{\#}_{8}$	-0.441
1146.56388	1146.56382	$z^{\ddagger}_{9}{}^{\bullet}$-$H_2O$	-0.048
1160.60850	1160.60772	$c^{\ddagger}_{9}{}^{\bullet}$	-0.676
1161.61633	1161.61629	$c^{\ddagger}_{9}$	-0.034
1162.60035	1162.60031	$c^{\#}_{8}$	-0.034
1164.57444	1164.57437	$z^{\ddagger}_{9}{}^{\bullet}$	-0.060
1175.60818	1175.60880	$a^{\#}_{9}$	0.527
1180.59316	1180.59331	$y^{\ddagger}_{9}$	0.127
1184.58470	1184.58443	$b^{\#}_{9}$-H_2O	-0.228
1185.56872	1185.56860	$b^{\#}_{9}$-NH_3	-0.101
1185.58735	1185.58827	y_{10}-2NH_3	0.776
1186.55879	1186.55905	$z^{\#}_{9}{}^{\bullet}$-2H_2O	0.219
1201.61125	1201.61119	$c^{\#}_{9}$-H_2O	-0.046
1202.59526	1202.59479	$b^{\#}_{9}$	-0.395
1204.56936	1204.56955	$z^{\#}_{9}{}^{\bullet}$-H_2O	0.162
1215.68709	1215.68737	$c_{10}{}^{\bullet}$	0.234
1216.69491	1216.69509	c_{10}	0.148
1219.62181	1219.62179	$c^{\#}_{9}$	-0.016
1222.57992	1222.58013	$z^{\#}_{9}{}^{\bullet}$	0.172
1230.68676	1230.68652	$a^{\ddagger}_{10}$	-0.195

THEORETICAL (m/z)	EXPERIMENTAL (m/z)	ASSIGNMENTS	ERROR (ppm)
1256.68982	1256.69011	$c^{\ddagger}_{10}$-H_2O	0.227
1274.70039	1274.70054	$c^{\ddagger}_{10}$	0.118
1288.69224	1288.69227	$a^{\#}_{10}$	0.023
1297.66876	1297.66818	$b^{\#}_{10}$-H_2O	-0.447
1303.72177	1303.72194	$[M\text{-}HCONH_2+2H]^{1+\bullet}$	0.130
1313.68231	1313.68204	$[M\text{-}2NH_3+H]^{1+}$	-0.206
1314.69530	1314.69569	$c^{\#}_{10}$-H_2O	0.293
1315.67933	1315.67861	$b^{\#}_{10}$	-0.543
1330.70886	1330.70824	$[M\text{-}NH_3+H]^{1+}$	-0.462
1331.71668	1331.71650	$[M\text{-}NH_3+2H]^{1+\bullet}$	-0.135
1332.70587	1332.70541	$c^{\#}_{10}$	-0.345
1343.71613	1343.71635	$[M^{\ddagger}\text{-}^{\bullet}CONH_2\text{-}H_2O+H]^{1+}$	0.164
1347.73540	1347.73533	$[M+H]^{1+}$	-0.052
1352.69321	1352.69251	$[M^{\ddagger}\text{-}NH_3\text{-}2H_2O+H]^{1+}$	-0.514
1353.70103	1353.70128	$[M^{\ddagger}\text{-}NH_3\text{-}2H_2O+2H]^{1+\bullet}$	0.185
1354.68505	1354.68457	$[M^{\ddagger}\text{-}2NH_3\text{-}H_2O+2H]^{1+\bullet}$	-0.354
1361.72725	1361.72711	$[M^{\ddagger}\text{-}^{\bullet}CONH_2+H]^{1+}$	-0.103
1370.70377	1370.70238	$[M^{\ddagger}\text{-}NH_3\text{-}H_2O+H]^{1+}$	-1.014
1371.71159	1371.71139	$[M^{\ddagger}\text{-}NH_3\text{-}H_2O+2H]^{1+\bullet}$	-0.149
1383.71160	1383.71174	$[M^{\ddagger}\text{-}^{\bullet}CONH_2\text{-}2H_2O+H]^{1+}$	0.101
1387.73032	1387.73054	$[M^{\ddagger}\text{-}H_2O+H]^{1+}$	0.159
1388.73815	1388.73830	$[M^{\ddagger}\text{-}H_2O+2H]^{1+\bullet}$	-0.288
1401.72162	1401.72281	$[M^{\#}\text{-}H_2O\text{-}^{\bullet}CONH_2+H]^{1+}$	0.849
1402.70727	1402.70607	$[M^{\#}\text{-}NH_3\text{-}^{\bullet}CONH_2+H]^{1+}$	-0.855
1405.74089	1405.74137	$[M^{\ddagger}+1H]^{1+}$	0.341
1406.74871	1406.74837	$[M^{\ddagger}+2H]^{1+\bullet}$	-0.533
1411.70651	1411.70596	$[M^{\#}\text{-}NH_3\text{-}2H_2O+2H]^{1+\bullet}$	-0.390
1419.73218	1419.73312	$[M^{\#}\text{-}^{\bullet}CONH_2+H]^{1+}$	0.662
1428.70926	1428.70903	$[M^{\#}\text{-}NH_3\text{-}H_2O+H]^{1+}$	-0.157
1428.73306	1428.73359	$[M^{\#}\text{-}2H_2O+2H]^{1+\bullet}$	0.371
1429.71708	1429.71703	$[M^{\#}\text{-}NH_3\text{-}H_2O+2H]^{1+\bullet}$	-0.035
1445.73580	1445.73626	$[M^{\#}\text{-}H_2O+H]^{1+}$	0.318
1446.74363	1446.74433	$[M^{\#}\text{-}H_2O+2H]^{1+\bullet}$	0.487
1447.72765	1447.72829	$[M^{\#}\text{-}NH_3+2H]^{1+\bullet}$	0.446
1463.74637	1463.74554	$[M^{\#}+H]^{1+}$	-0.564
		mean	-0.015
		St. Dv.	0.446

Table D-7. CAD(732) error analysis of the glycated KM-11 peptide in MeOH/H_2O (50:50) for the precursor ion $[M+2(C_2H_2O_2)+2H]^{2+}$. * indicates the ions used for calibration.

THEORETICAL (m/z)	EXPERIMENTAL (m/z)	ASSIGNMENTS	ERROR (ppm)
* 284.16048	284.16053	$b^{\ddagger}_2$	0.194
382.25610	382.25609	b_3	-0.039

THEORETICAL (m/z)	EXPERIMENTAL (m/z)	ASSIGNMENTS	ERROR (ppm)
* 387.21391	387.21398	$b^{\ddagger}_{3}$-H_2O -H_2O-NH_3	0.181
404.24045	404.24046	$b^{\ddagger}_{3}$-H_2O -H_2O	0.012
405.22447	405.22446	$b^{\ddagger}_{3}$-H_2O -NH_3	-0.037
422.25102	422.25105	$b^{\ddagger}_{3}$-H_2O	0.071
423.23504	423.23505	$b^{\ddagger}_{3}$-NH_3	0.024
434.25102	434.25122	$a^{\#}_{3}$-$2H_2O$	0.461
439.23759	439.23758	$(a^{\ddagger}_{7}$-H_2O-$NH_3)^{2+}$	-0.011
* 440.26159	440.26157	$b^{\ddagger}_{3}$	-0.034
441.75086	441.75092	b_7^{2+}	0.141
444.23537	444.23551	$b^{\#}_{3}$-$3H_2O$	0.315
449.22170	449.22170	y_4-NH_3	0.011
452.74303	452.74272	$(b^{\ddagger}_{7}$-H_2O -H2O)$^{2+}$	-0.690
461.74831	461.74834	$(b^{\ddagger}_{7}$-H_2O +H]2+	0.054
462.24032	462.24042	$(b^{\ddagger}_{7}$-NH_3+H]2+	0.206
462.24593	462.24603	$b^{\#}_{3}$-$2H_2O$	0.206
462.28232	462.28220	b_4-NH_3	-0.260
463.22996	463.22990	$b^{\#}_{3}$-H_2O-NH_3	-0.119
466.24824	466.24826	y_4	0.043
470.75360	470.75356	$b^{\ddagger}_{7}{}^{2+}$	-0.080
473.23250	473.23252	$(b^{\#}_{7}$-$2H_2O$-$NH_3)^{2+}$	0.042
480.25650	480.25656	$b^{\#}_{3}$-H_2O	0.125
481.24052	481.24052	$b^{\#}_{3}$-NH_3	0.000
481.74577	481.74580	$(b^{\#}_{7}$-$2H_2O)^{2+}$+	0.057
482.23778	482.23775	$(b^{\#}_{7}$-H_2O-$NH_3)^{2+}$	-0.067
490.75106	490.75103	$(b^{\#}_{7}$-$H_2O)^{2+}$+	-0.051
506.77179	506.77195	$(b_8$-$NH_3)^{2+}$	0.316
512.77179	512.77195	$(a^{\ddagger}_{8}$-H_2O-$NH_3)^{2+}$	0.312
515.28506	515.28506	b_8^{2+}	-0.005
* 519.30378	519.30361	$b^{\ddagger}_{4}$-H_2O	-0.327
521.28506	521.28501	$(a^{\ddagger}_{8}$-H_2O $)^{2+}$	-0.101
526.27724	526.27720	$(b^{\ddagger}_{8}$-$2H_2O)^{2+}$	-0.071
526.76925	526.76931	$(b^{\ddagger}_{8}$-H_2O -$NH_3)^{2+}$	0.119
532.27724	532.27708	$(a^{\ddagger}_{9}$-$2H_2O$-$NH_3)^{2+}$	-0.296
532.76925	532.76935	$(a^{\ddagger}_{9}$-H_2O-$2NH_3)^{2+}$	0.192
535.28252	535.28260	$(b^{\ddagger}_{8}$-$H_2O)^{2+}$	0.149
535.77453	535.77469	$(b^{\ddagger}_{8}$-$NH_3)^{2+}$	0.299
537.31435	537.31472	$b^{\ddagger}_{4}$	0.698
541.28252	541.28262	$(a^{\#}_{8}$-$2H_2O)^{2+}$	0.185
541.77453	541.77451	$(a^{\#}_{8}$-H_2O-$NH_3)^{2+}$	-0.037
543.79579	543.79585	b_9^{2+}	0.106
544.28780	544.28782	$b^{\ddagger}_{8}{}^{2+}$	0.032
546.27469	546.27472	$(b^{\ddagger}_{9}$-$2H_2O$-$NH_3)^{2+}$	0.046
546.76671	546.76667	$(b^{\#}_{8}$-$2H_2O$-$NH_3)^{2+}$	-0.064
549.79579	549.79578	$(a^{\ddagger}_{9}$-$H_2O)^{2+}$+	-0.023
550.28780	550.28776	$(a^{\#}_{8}$-$H_2O)^{2+}$	-0.077
554.78797	554.78807	$(b^{\ddagger}_{9}$-$2H_2O)^{2+}$	0.185
555.27998	555.28008	$(b^{\ddagger}_{9}$-H_2O -$NH_3)^{2+}$+	0.185

THEORETICAL (m/z)	EXPERIMENTAL (m/z)	ASSIGNMENTS	ERROR (ppm)
555.77199	555.77200	$(b^{\#}_{8}\text{-}H_2O\text{-}NH_3)^{2+}$	0.022
556.28781	556.28789	$b_5\text{-}3NH_3$	0.144
561.77199	561.77215	$(a^{\#}_{9}\text{-}H_2O\text{-}2NH_3)^{2+}$	0.289
563.79325	563.79332	$(b^{‡}_{9}\text{-}H_2O)^{2+}$	0.124
564.28526	564.28528	$(b^{\#}_{8}\text{-}H_2O)^{2+}$	0.035
564.77727	564.77746	$(b^{\#}_{8}\text{-}NH_3)^{2+}$	0.336
569.79325	569.79319	$(a^{\#}_{9}\text{-}2H_2O)^{2+}$	-0.105
570.28526	570.28535	$(a^{\#}_{9}\text{-}H_2O\text{-}NH_3)^{2+}$	0.158
572.79853	572.79855	$b^{‡}_{9}{}^{2+}$	0.031
573.29054	573.29053	$b^{\#}_{8}{}^{2+}$	-0.022
574.78543	574.78541	$(b^{\#}_{9}\text{-}3H_2O)^{2+}$	-0.026
575.27743	575.27747	$(b^{\#}_{9}\text{-}2H_2O\text{-}NH_3)^{2+}$	0.061
575.76945	575.76938	$(b^{\#}_{9}\text{-}H_2O\text{-}2NH_3)^{2+}$	-0.113
577.30926	577.30945	$b^{\#}_{4}\text{-}H_2O$	0.329
578.79853	578.79849	$(a^{\#}_{9}\text{-}H_2O)^{2+}$	-0.073
582.81927	582.81952	$(b_{10}\text{-}H_2O\text{-}NH_3)^{2+}$	0.433
583.79071	583.79079	$(b^{\#}_{9}\text{-}2H_2O)^{2+}$	0.141
584.28272	584.28276	$(b^{\#}_{9}\text{-}H_2O\text{-}NH_3)^{2+}$	0.073
586.32218	586.32254	$a^{‡}_{5}\text{-}H_2O\ \text{-}2NH_3$	0.605
586.34037	586.34040	$a_{10}{}^{2+}+$	0.055
588.81927	588.81934	$(b^{‡}_{10}\text{-}2H_2O\text{-}CO\text{-}NH_3)^{2+}$	0.122
589.31128	589.31110	$(a^{‡}_{10}\text{-}H_2O\text{-}2NH_3)^{2+}$	-0.301
591.82455	591.82455	$(b_{10}\text{-}NH_3)^{2+}$	0.000
592.79599	592.79590	$(b^{\#}_{9}\text{-}H_2O)^{2+}+$	-0.152
593.28800	593.28832	$(b^{\#}_{9}\text{-}NH_3)^{2+}$	0.539
* 596.29011	596.29015	$y_5\text{-}NH_3$	0.075
597.33254	597.33255	$(a^{‡}_{10}\text{-}2H_2O)^{2+}$	0.017
597.82455	597.82460	$(a^{‡}_{10}\text{-}H_2O\text{-}NH_3)^{2+}$	0.084
600.33782	600.33768	$b_{10}{}^{2+}$	-0.237
601.80127	601.80126	$b^{\#}_{9}{}^{2+}$	-0.021
601.81059	601.81068	$(y_{10}\text{-}NH_3)^{2+}+$	0.154
602.81673	602.81679	$(b^{‡}_{10}\text{-}2H_2O\text{-}NH_3)^{2+}$	0.108
603.30873	603.30884	$(b^{‡}_{10}\text{-}H_2O\text{-}2NH_3)^{2+}$	0.174
606.33782	606.33781	$(a^{‡}_{10}\text{-}H_2O)^{2+}$	-0.021
607.36744	607.36745	b_5	0.008
610.32386	610.32392	$y_{10}{}^{2+}$	0.098
611.33000	611.32999	$(b^{‡}_{10}\text{-}2H_2O)^{2+}$	-0.012
611.82201	611.82209	$(b^{‡}_{10}\text{-}H_2O\ \text{-}NH_3)^{2+}+$	0.135
613.31665	613.31685	y_5	0.326
615.34311	615.34318	$a^{‡}_{10}{}^{2+}$	0.118
618.31402	618.31440	$(a^{\#}_{10}\text{-}H_2O\text{-}2NH_3)^{2+}$	0.619
620.33528	620.33481	$(b^{‡}_{10}\text{-}H_2O\ )^{2+}$	-0.758
620.82729	620.82764	$(^{‡}_{10}\text{-}NH_3)^{2+}$	0.564
621.80304	621.80276	$(y^{‡}_{10}\text{-}NH_3\text{-}H_2O)^{2+}$	-0.458
621.80804	621.80815	$(y^{‡}_{10}\text{-}\ H_2O\text{-}NH_3)^{2+}$	0.169
623.30619	623.30640	$(b^{\#}_{10}\text{-}2H_2O\text{-}2NH_3)^{2+}$	0.332
623.81741	623.81766	$x_{10}{}^{2+}$	0.409
626.33528	626.33529	$(a^{\#}_{10}\text{-}2H_2O)^{2+}$	0.016

THEORETICAL (m/z)	EXPERIMENTAL (m/z)	ASSIGNMENTS	ERROR (ppm)
* 629.34056	629.34002	$b^{\ddagger}_{10}{}^{2+}$+	-0.862
630.32132	630.32160	$(y^{\ddagger}_{10}$- $H_2O)^{2+}$	0.448
631.32745	631.32754	$(b^{\#}_{10}$-3$H_2O)^{2+}$	0.135
631.81947	631.81956	$(b^{\#}_{10}$-2H_2O-$NH_3)^{2+}$	0.150
635.34056	635.34058	$(a^{\#}_{10}$-$H_2O)^{2+}$+	0.028
639.32660	639.32684	$y^{\ddagger}_{10}{}^{2+}$	0.375
640.33274	640.33262	$(b^{\#}_{10}$-2$H_2O)^{2+}$	-0.183
640.82475	640.82487	$(b^{\#}_{10}$-H_2O-$NH_3)^{2+}$	0.191
643.34761	643.34770	$[M$-NH3+H$]^{2+}$	0.140
644.34585	644.34634	$a^{\#}_{10}{}^{2+}$	0.764
645.82624	645.82667	$[M^{\ddagger}$-2H_2O-2NH_3+H$]^{2+}$	0.666
647.36236	647.36241	$b^{\ddagger}_{5}$- H_2O	0.077
648.34638	648.34604	$b^{\ddagger}_{5}$-NH3	-0.524
649.33802	649.33758	$[b^{\#}_{10}$-H_2O+H$]^{2+}$	-0.678
649.83003	649.83056	$[b^{\#}_{10}$-NH_3+H$]^{2+}$	0.816
651.86061	651.86063	$[M$+H$]^{2+}$	0.027
657.34479	657.34493	$[M$-NH_3+H$]^{2+}$	0.205
658.34330	658.34332	$b^{\#}_{10}{}^{2+}$	0.027
661.33040	661.32985	$a^{\#}_{5}$-2NH_3	-0.832
665.37293	665.37307	$b^{\ddagger}_{5}$	0.218
665.85807	665.85791	$[M$+2H$]^{2+}$	-0.237
668.33697	668.33701	$[M^{\ddagger}$-2H_2O-2NH_3+2H$]^{2+}$	0.060
668.82898	668.82922	$[M^{\ddagger}$-H_2O-3NH_3+2H$]^{2+}$	0.359
671.85807	671.85812	$[M^{\ddagger}$-CO-NH_3+2H$]^{2+}$	0.074
674.37134	674.37078	$[M$+2H$]^{2+}$	-0.830
676.85024	676.85033	$[M^{\ddagger}$-2H_2O-NH_3+2H$]^{2+}$	0.129
677.34225	677.34235	$[M^{\ddagger}$-H_2O -2NH_3+2H$]^{2+}$	0.144
680.86335	680.86352	$[M^{\ddagger}$-CO NH_3+2H$]^{2+}$	0.246
683.83426	683.83465	$[M^{\#}$-H_2O-3NH_3+2H$]^{2+}$	0.567
685.36352	685.36354	$[M^{\ddagger}$-2H_2O-NH_3+2H$]^{2+}$	0.036
685.85552	685.85533	$[M^{\ddagger}$-NH_3-H_2O +2H$]^{2+}$	-0.284
687.35727	687.35714	$b^{\#}_{5}$-2H_2O	-0.196
688.34129	688.34102	$b^{\#}_{5}$-H_2O-NH_3	-0.400
688.82644	688.82671	$[M^{\#}$-2H_2O-3NH_3+2H$]^{2+}$	0.395
691.85552	691.85558	$[M^{\#}$-2H_2O-NH_3+2H$]^{2+}$	0.079
692.34753	692.34781	$[M^{\#}$-H_2O-2NH_3+2H$]^{2+}$	0.397
* 694.36880	694.36873	$[M^{\ddagger}$-H_2O +2H$]^{2+}$	-0.097
694.86081	694.86050	$[M^{\ddagger}$-NH_3+2H$]^{2+}$	-0.443
696.37020	696.37077	$a^{\ddagger}_{6}$-2NH_3-2H_2O	0.819
696.84770	696.84772	$[M^{\#}$-3H_2O-NH_3+2H$]^{2+}$	0.029
697.33971	697.33982	$[M^{\#}$-2H_2O-2NH_3+2H]2	0.158
700.36880	700.36911	$[M^{\#}$-2H_2O-CO+2H]2	0.443
700.86081	700.86083	$[M^{\#}$-H_2O- NH_3-CO +2H$]^{2+}$	0.032
703.37408	703.37361	$[M^{\ddagger}$+2H$]^{2+}$	-0.668
705.36784	705.36796	$b^{\#}_{5}$-H_2O	0.170
705.85299	705.85297	$[M^{\#}$-2H_2O-NH_3+2H$]^{2+}$	-0.028
706.34499	706.34520	$[M^{\#}$-H_2O-2NH_3+H$]^{2+}$	0.294

THEORETICAL (m/z)	EXPERIMENTAL (m/z)	ASSIGNMENTS	ERROR (ppm)
707.32214	707.32239	y_6-2NH_3	0.353
707.43111	707.43120	a_6	0.127
714.85827	714.85798	$[M^{\#}$-H_2O-NH_3+2H$]^{2+}$	-0.406
718.39948	718.39941	b_6-NH_3	-0.097
* 723.37154	723.37136	$[M^{\#}$-H_2O+2H$]^{2+}$	-0.249
723.86355	723.86390	$[M^{\#}$-NH_3+2H$]^{2+}$	0.484
724.34131	724.34158	$b^{\ddagger}_6$-H_2O -3NH_3	0.380
732.37682	732.37692	$[M^{\#}$+2H$]^{2+}$	0.137
735.42602	735.42602	b_6	-0.007
740.38383	740.38382	$b^{\ddagger}_6$ -2H_2O-NH_3	-0.014
741.37523	741.37540	y_6	0.229
757.41038	757.41043	$b^{\ddagger}_6$-2H_2O	0.073
758.39440	758.39448	$b^{\ddagger}_6$-H_2O -NH_3	0.112
759.39841	759.39795	$b^{\ddagger}_6$-2NH_3	-0.612
765.43659	765.43584	$a^{\ddagger}_6$	-0.980
769.41038	769.41025	$a^{\#}_6$-3H_2O	-0.162
770.39440	770.39452	$a^{\#}_6$-2H_2O-NH_3	0.162
775.42094	775.42114	$b^{\ddagger}_6$-H_2O	0.258
776.40496	776.40482	$b^{\ddagger}_6$-NH_3	-0.180
787.42094	787.42111	$a^{\#}_6$-2H_2O	0.216
793.43151	793.43174	$b^{\ddagger}_6$	0.296
797.40529	797.40543	$b^{\#}_6$-3H_2O	0.176
799.37333	799.37377	$b^{\#}_6$-H_2O-2NH_3	0.550
805.43151	805.43169	$a^{\#}_6$-H_2O	0.230
815.41585	815.41599	$b^{\#}_6$-2H_2O	0.166
816.39987	816.39988	$b^{\#}_6$-H_2O-NH_3	0.006
817.40390	817.40341	$b^{\#}_6$-2NH_3	-0.593
833.42642	833.42654	$b^{\#}_6$-H_2O	0.144
834.41044	834.41046	$b^{\#}_6$-NH_3	0.024
835.38072	835.38138	y_7-2NH3	0.790
852.40727	852.40745	y_7-NH_3	0.217
* 869.43381	869.43423	y_7	0.483
882.49443	882.49463	b_7	0.221
887.45224	887.45225	$b^{\ddagger}_7$-2H_2O-NH_3	0.011
894.49443	894.49474	$a^{\ddagger}_7$-H_2O	0.341
904.47879	904.47920	$b^{\ddagger}_7$-2H_2O	0.459
905.46281	905.46273	$b^{\ddagger}_7$-H_2O -NH_3	0.083
906.46682	906.46668	$b^{\ddagger}_7$-2NH_3	-0.160
912.50500	912.50555	$a^{\ddagger}_7$	0.603
916.47879	916.47941	$a^{\#}_7$-3H_2O	0.682
917.46281	917.46283	$a^{\#}_7$-2H_2O-NH_3	0.027
922.48935	922.48958	$b^{\ddagger}_7$-H_2O	0.249
923.47337	923.47340	$b^{\ddagger}_7$-NH_3	0.032
932.43348	932.43365	y_8-2NH_3	0.182
934.48935	934.48974	$a^{\#}_7$-2H_2O	0.417
940.49991	940.50006	$b^{\ddagger}_7$	0.154
944.47370	944.47400	$b^{\#}_7$-3H_2O	0.318

THEORETICAL (m/z)	EXPERIMENTAL (m/z)	ASSIGNMENTS	ERROR (ppm)
946.44174	946.44140	$b^{\#}_{7}$-H2O-2NH_3	-0.359
952.49991	952.50005	$a^{\#}_{7}$-H_2O	0.142
962.48427	962.48418	$b^{\#}_{7}$-2H_2O	-0.088
963.46829	963.46857	$b^{\#}_{7}$-H_2O-NH_3	0.296
964.47231	964.47215	$b^{\#}_{7}$-2NH_3	-0.161
* 966.48657	966.48654	y_8	-0.031
980.49483	980.49512	$b^{\#}_{7}$-H_2O	0.296
981.47885	981.47902	$b^{\#}_{7}$-NH_3	0.173
1012.53630	1012.53615	b-NH_3	-0.148
1024.53630	1024.53637	a_9-2NH_3	0.068
1029.56284	1029.56275	b_8	-0.092
1035.50467	1035.50402	$b^{\ddagger}_{8}$-H_2O-2NH_3	-0.628
1041.56284	1041.56342	$a^{\ddagger}_{8}$-H_2O	0.552
1051.54720	1051.54778	$b^{\ddagger}_{8}$-2H_2O	0.556
1052.53121	1052.53117	$b^{\ddagger}_{8}$-H_2O -NH_3	-0.043
1053.53524	1053.53494	b-2NH_3	-0.280
1059.57341	1059.57330	$a^{\ddagger}_{8}$	-0.104
1064.53121	1064.53088	$a^{\ddagger}_{9}$-H_2O -2NH_3	-0.315
*1069.55776	1069.55759	$b^{\ddagger}_{8}$-H_2O	-0.159
1070.54178	1070.54202	$b^{\ddagger}_{8}$-NH_3	0.224
1074.51556	1074.51575	$b^{\ddagger}_{9}$-H_2O -H_2O-2NH_3	0.172
1075.49959	1075.49950	$b^{\ddagger}_{9}$-H_2O -3NH_3	-0.079
1081.55776	1081.55790	$a^{\#}_{8}$-2H_2O	0.129
1082.54178	1082.54078	$a^{\ddagger}_{9}$-2NH_3	-0.924
1086.58431	1086.58408	b_9	-0.207
1087.56832	1087.56831	$b^{\ddagger}_{8}$	-0.014
1091.54211	1091.54247	$b^{\#}_{8}$-3H_2O	0.330
1092.52613	1092.52665	$b^{\ddagger}_{9}$-H_2O-2NH_3	0.476
1092.54613	1092.54618	$b^{\ddagger}_{9}$-H_2O -2NH_3	0.046
1099.56832	1099.56890	$a^{\#}_{8}$-H_2O	0.523
*1105.56113	1105.56097	y_9-NH_3	-0.149
1108.56866	1108.56900	$b^{\ddagger}_{9}$-H_2O -H_2O	0.311
1109.55267	1109.55251	$b^{\ddagger}_{9}$-H_2O -NH_3	-0.149
1110.53670	1110.53659	$b^{\#}_{8}$-H_2O-NH_3	-0.095
1110.55669	1110.55595	$b^{\ddagger}_{9}$ -2NH_3	-0.671
1121.55267	1121.55312	$a^{\#}_{9}$-2H_2O-NH_3	0.397
1122.58768	1122.58734	y_9	-0.303
1126.57922	1126.57900	$b^{\ddagger}_{9}$-H_2O	-0.195
1127.56324	1127.56304	$b^{\#}_{8}$-H2O	-0.177
1128.54726	1128.54762	$b^{\#}_{8}$-NH_3	0.319
1144.58978	1144.58982	$b^{\ddagger}_{9}$-H_2O	0.031
1145.55605	1145.55582	$y^{\ddagger}_{9}$-H_2O -NH_3	-0.201
1145.57381	1145.57481	$b^{\#}_{8}$	0.873
1148.56357	1148.56421	$b^{\#}_{9}$-3H_2O	0.557
1150.53161	1150.53102	$b^{\#}_{9}$-H_2O-2NH_3	-0.513
1156.58978	1156.59046	$a^{\#}_{9}$-H_2O	0.584
1162.58260	1162.58314	$y^{\ddagger}_{9}$-H_2O	0.469

THEORETICAL (m/z)	EXPERIMENTAL (m/z)	ASSIGNMENTS	ERROR (ppm)
1163.56661	1163.56678	$y^{\ddagger}_{9}$-NH_3	0.142
1166.57414	1166.57403	$b^{\#}_{9}$-$2H_2O$	-0.090
1167.55815	1167.55854	$b^{\#}_{9}$-H_2O-NH_3	0.330
1168.56218	1168.56222	$b^{\#}_{9}$-$2NH_3$	0.039
1171.67345	1171.67402	a_{10}	0.486
1178.62310	1178.62249	$a^{\ddagger}_{10}$-H_2O -$2NH_3$	-0.522
*1180.59316	1180.59284	$y^{\ddagger}_{9}$	-0.271
1184.58470	1184.58509	$b^{\#}_{9}$-H_2O	0.329
1185.56872	1185.56904	$b^{\#}_{9}$-NH_3	0.270
1199.66836	1199.66826	b_{10}	-0.088
1202.59526	1202.59624	$b^{\#}_{9}$	0.811
1202.61389	1202.61414	y_{10}-NH_3	0.204
1203.56153	1203.56258	$y^{\ddagger}_{10}$-$2H_2O$ -NH_3	0.872
1205.61019	1205.61045	$b^{\ddagger}_{10}$-H_2O-$2NH_3$	0.216
1211.66836	1211.66921	$a^{\ddagger}_{10}$-H_2O	0.697
1219.64044	1219.64020	y_{10}	-0.197
1221.65271	1221.65333	$b^{\ddagger}_{10}$-$2H_2O$	0.503
1222.63674	1222.63704	$b^{\ddagger}_{10}$-H_2O -NH_3	0.249
1223.64075	1223.64100	$b^{\ddagger}_{10}$-$2NH_3$	0.200
1225.58227	1225.58283	y-$2NH_3$	0.461
1229.67893	1229.67893	$a^{\ddagger}_{10}$	0.000
1233.65271	1233.65335	$a^{\#}_{10}$-$3H_2O$	0.515
1234.63674	1234.63615	$a^{\#}_{10}$-$2H_2O$-NH_3	-0.474
*1239.66328	1239.66403	$b^{\ddagger}_{10}$-H_2O	0.605
1240.64730	1240.64747	$b^{\ddagger}_{10}$-NH_3	0.137
1242.60881	1242.60821	$y^{\ddagger}_{10}$-H_2O -NH_3	-0.483
1246.58912	1246.58835	$b^{\#}_{10}$-$2H_2O$-$2NH_3$	-0.622
1251.66328	1251.66334	$a^{\#}_{10}$-$2H_2O$	0.048
1254.63915	1254.63911	$a^{\#}_{10}$-$2NH_3$	-0.032
1257.67385	1257.67371	$b^{\ddagger}_{10}$	-0.107
1259.63535	1259.63472	$y^{\ddagger}_{10}$-H_2O	-0.504
1261.64763	1261.64874	$b^{\#}_{10}$-$3H_2O$	0.880
1263.61567	1263.61500	$b^{\#}_{10}$-H_2O-$2NH_3$	-0.475
1279.65819	1279.65828	$b^{\#}_{10}$-H_2O	0.070
1280.64222	1280.64258	$b^{\#}_{10}$-H_2O- NH_3	0.281
1297.66876	1297.66771	$b^{\#}_{10}$-H_2O	-0.809
*1298.65278	1298.65182	$b^{\#}_{10}$-NH_3	-0.739
		mean	0.073
		St. Dv.	0.444

Table D-8. DR(703)ECD(732) error analysis of the KM-11 peptide in PBS for the precursor ion $[M+2(C_2H_2O_2)+2H]^{2+}$. * indicates the ions used for calibration.

THEORETICAL (m/z)	EXPERIMENTAL (m/z)	ASSIGNMENTS	ERROR (ppm)
* 301.18702	301.18704	$c^{\ddagger}_{2}$	0.066

THEORETICAL (m/z)	EXPERIMENTAL (m/z)	ASSIGNMENTS	ERROR (ppm)
495.32758	495.32763	$c_4^{\bullet}$	0.091
* 496.33541	496.33515	c_4	-0.524
501.79152	501.79192	a_8^{2+}	0.797
517.31193	517.31194	$c^{\ddagger}_4{}^{\bullet}-2H_2O$	0.010
535.32250	535.32258	$c^{\ddagger}_4{}^{\bullet}$-$H_2O$	0.149
536.33033	536.33030	$c^{\ddagger}_4$-H_2O	-0.047
550.78672	550.78714	$(a^{\#}_8$-$H_2O)^{2+}$	0.767
552.80107	552.80141	$c^{\ddagger}_4{}^{2+}$	0.606
553.33307	553.33315	$c^{\ddagger}_4{}^{\bullet}$	0.154
* 554.34089	554.34059	$c^{\ddagger}_4$	-0.541
593.32798	593.32816	$c^{\#}_4{}^{\bullet}$-H_2O	0.303
594.27504	594.27559	$(z^{\#}_9{}^{\bullet}$-H_2O-$NH_3)^{2+}$	0.917
594.33581	594.33585	$c^{\#}_4$-H_2O	0.076
606.83674	606.83631	$(a^{\ddagger}_{10}$-$H_2O)^{2+}$	-0.704
611.33854	611.33868	$c^{\#}_4{}^{\bullet}$	0.221
* 612.34637	612.34652	$c^{\#}_4$	0.245
623.38617	623.38640	$c_5^{\bullet}$	0.377
624.39399	624.39416	c_5	0.272
628.34464	628.34412	$(c^{\ddagger}_{10}{}^{\bullet}$ -$H_2O)^{2+}$	-0.828
663.38108	663.38130	$c^{\ddagger}_5{}^{\bullet}$-$H_2O$	0.332
664.38891	664.38905	$c^{\ddagger}_5$-H_2O	0.218
674.37134	674.37068	$[M+2H]^{2+}$	-0.979
681.39165	681.39187	$c^{\ddagger}_5{}^{\bullet}$	0.330
682.39947	682.39971	$c^{\ddagger}_5$	0.352
685.36352	685.36323	$[M^{\ddagger}$-2H_2O+2H$]^{2+}$	-0.416
694.36880	694.36883	$[M^{\ddagger}$- H_2O +H$]^{2+}$	0.047
* 703.37408	703.37387	[M+H]2+	-0.299
705.36097	705.36042	$b^{\#}_5$-H_2O	-0.783
715.36478	715.36493	$[M^{\#}$-2H_2O+2H$]^{2+}$	0.203
721.38656	721.38678	$c^{\#}_5{}^{\bullet}$-H_2O	0.305
722.39439	722.39463	$c^{\#}_5$-H_2O	0.339
723.37154	723.37169	$[M^{\#}$-H_2O+2H$]^{2+}$	0.207
723.86355	723.86341	$[M^{\#}$-NH_3+2H$]^{2+}$	-0.193
732.37682	732.37669	[$M^{\#}$+2H]2+	-0.178
739.39712	739.39734	$c^{\#}_5{}^{\bullet}$	0.291
740.40495	740.40521	$c^{\#}_5$	0.351
751.44475	751.44481	$c_6^{\bullet}$	0.087
752.45257	752.45282	c_6	0.332
791.43966	791.44000	$c^{\ddagger}_6{}^{\bullet}$-$H_2O$	0.430
792.44749	792.44775	$c^{\ddagger}_6$-H_2O	0.334
809.45023	809.45058	$c^{\ddagger}_6{}^{\bullet}$	0.439
810.45805	810.45832	$c^{\ddagger}_6$	0.333
849.44514	849.44537	$c^{\#}_6{}^{\bullet}$-H_2O	0.271
850.45296	850.45324	$c^{\#}_6$-H_2O	0.323
867.45570	867.45598	$c^{\#}_6{}^{\bullet}$	0.317
* 868.46353	868.46380	$c^{\#}_6$	0.311
899.52098	899.52099	c_7	0.011

THEORETICAL (m/z)	EXPERIMENTAL (m/z)	ASSIGNMENTS	ERROR (ppm)
938.50807	938.50816	$c^{\ddagger}_{7}{}^{\bullet}$-$H_2O$	0.096
* 939.51590	939.51608	$c^{\ddagger}_{7}$-H_2O	0.197
957.52646	957.52659	$c^{\ddagger}_{7}$	0.136
971.51831	971.51837	$a^{\#}_{7}$	0.062
996.51355	996.51380	$c^{\#}_{7}{}^{\bullet}$-H_2O	0.251
997.52138	997.52150	$c^{\#}_{7}$-H_2O	0.125
1014.52412	1014.52423	$c^{\#}_{7}{}^{\bullet}$	0.113
*1015.53194	1015.53202	$c^{\#}_{7}$	0.079
1046.58939	1046.58977	c_8	0.363
1072.54485	1072.54471	$z^{\ddagger}_{9}{}^{\bullet}$-$C_3H_6D$-$H_2O$	-0.134
1085.57648	1085.57645	$c^{\ddagger}_{8}{}^{\bullet}$-$H_2O$	-0.028
1086.58431	1086.58423	b_9	-0.069
1088.53459	1088.53485	y_9-$2NH_3$	0.239
1090.55542	1090.55533	$z^{\ddagger}_{9}{}^{\bullet}$-$C_3H_6S$	-0.082
1100.57615	1100.57654	$a^{\#}_{8}$-H_2O	0.350
1103.61085	1103.61080	c_9	-0.045
1104.59487	1104.59491	$c^{\ddagger}_{8}$	0.036
1118.58672	1118.58661	$a^{\#}_{8}$	-0.098
*1143.60577	1143.60569	$c^{\ddagger}_{9}$-H_2O	-0.066
1144.58978	1144.58962	$b^{\ddagger}_{9}$	-0.144
1146.56388	1146.56376	$z^{\ddagger}_{9}{}^{\bullet}$-$H_2O$	-0.100
1148.56090	1148.56001	$z^{\#}_{9}{}^{\bullet}$-C_3H_6S	-0.774
1161.59253	1161.59226	$c^{\#}_{8}{}^{\bullet}$	-0.228
1161.61633	1161.61614	$c^{\ddagger}_{9}$	-0.164
1162.60035	1162.60024	$c^{\#}_{8}$	-0.095
1164.57444	1164.57442	$z^{\ddagger}_{9}{}^{\bullet}$	-0.017
1175.60818	1175.60817	$a^{\#}_{9}$	-0.009
1186.55879	1186.55808	$z^{\#}_{9}{}^{\bullet}$-$2H_2O$	-0.598
*1201.61125	1201.61103	$c^{\#}_{9}$-H_2O	-0.179
1204.56936	1204.56895	$z^{\#}_{9}{}^{\bullet}$-H_2O	-0.336
1215.68709	1215.68681	$c_{10}{}^{\bullet}$	-0.226
1219.62181	1219.62142	$c^{\#}_{9}$	-0.320
1222.57992	1222.57942	$z^{\#}_{9}{}^{\bullet}$	-0.409
1256.68982	1256.68947	$c^{\ddagger}_{10}$ -H_2O	-0.282
1274.70039	1274.70010	$c^{\ddagger}_{10}$	-0.228
1288.69224	1288.69208	$a^{\#}_{10}$	-0.124
*1314.69530	1314.69487	$c^{\#}_{10}$-H_2O	-0.331
1330.70886	1330.70790	$[M\text{-}NH_3+H]^{1+}$	-0.718
1331.71668	1331.71581	$[M\text{-}\ NH_3+2H]^{1+\bullet}$	-0.653
1332.70587	1332.70509	$c^{\#}_{10}$	-0.585
1343.71613	1343.71550	$[M^{\ddagger}\text{-}{}^{\bullet}CONH_2\text{-}H_2O+H]^{1+}$	-0.469
1347.73540	1347.73445	$[M+H]^{1+}$	-0.705
1361.72670	1361.72674	$[M^{\ddagger}\text{-}{}^{\bullet}CONH_2+H]^{1+}$	0.033
1383.71160	1383.71012	$[M\text{-}2H_2O\text{-}{}^{\bullet}CONH_2+H]^{1+}$	-1.070
1387.73032	1387.73023	$[M^{\ddagger}\text{-}H_2O+H]^{1+\bullet}$	-0.061
1388.73815	1388.73787	$[M^{\ddagger}\text{-}H_2O+2H]^{1+\bullet}$	-0.598
1401.72162	1401.72179	$[M^{\#}\text{-}H_2O\text{-}{}^{\bullet}CONH_2+1H]^{1+}$	0.121

THEORETICAL (m/z)	EXPERIMENTAL (m/z)	ASSIGNMENTS	ERROR (ppm)
*1405.74089	1405.74033	$[M^{\ddagger} +2H]^{1+\bullet}$	-0.391
1411.70651	1411.70516	$[M^{\#}$-NH3- $2H_2O$ $+1H]^{1+}$	-0.956
1419.73218	1419.73311	$[M^{\#}$-$^{\bullet}CONH_2$+1H$]^{1+}$	0.655
1428.73306	1428.73294	$[M^{\#}$-$2H_2O$ $+2H]^{1+\bullet}$	-0.084
1445.73580	1445.73632	$[M^{\#}$-H_2O $+H]^{1+}$	0.360
1446.74363	1446.74380	$[M^{\#}$-H_2O $+2H]^{1+\bullet}$	0.118
1447.72765	1447.72669	$[M^{\#}$-H_2O $+2H]^{1+\bullet}$	-0.656
*1463.74637	1463.74528	$[M^{\#}+H]^{1+}$	-0.745
		mean	-0.077
		St. Dv.	0.497

Table D-9. DR(724)ECD(753) error analysis of the glycated AcKM-11 peptide MeOH/H_2O (50:50) for the precursor ion $[M+2(C_2H_2O_2)+2H]^{2+}$. * indicates the ions used for calibration.

THEORETICAL (m/z)	EXPERIMENTAL (m/z)	ASSIGNMENTS	ERROR (ppm)
538.34597	538.34595	c_4	-0.046
577.33307	577.33325	$c^{\ddagger}_4{}^{\bullet}$-$H_2O$	0.320
578.34089	578.34102	$c^{\ddagger}_4$-H_2O	0.225
595.34363	595.34378	$c^{\ddagger}_4{}^{\bullet}$	0.252
596.35145	596.35156	$c^{\ddagger}_4$	0.176
635.33854	635.33847	$c^{\#}_4{}^{\bullet}$-H_2O	-0.118
653.34911	653.34921	$c^{\#}_4{}^{\bullet}$	0.153
654.35694	654.35695	$c^{\#}_4$	0.023
665.39673	665.39662	$c_5{}^{\bullet}$	-0.165
666.40455	666.40454	c_5	-0.023
705.39165	705.39154	$c^{\ddagger}_5{}^{\bullet}$-$H_2O$	-0.149
706.39947	706.39940	$c^{\ddagger}_5$-H_2O	-0.099
723.40221	723.40229	$c^{\ddagger}_5{}^{\bullet}$	0.111
724.41003	724.41009	$c^{\ddagger}_5$	0.076
735.86355	735.86339	$[M^{\#}$-H_2O-NH_3+2H$]^{2+}$	-0.217
736.35556	736.35606	$[M^{\#}$-$2NH_3$+2H$]^{2+}$	0.679
744.86883	744.86870	$[M^{\#}$-NH_3+2H$]^{2+}$	-0.178
747.37841	747.37840	$b^{\#}_5$-H_2O	-0.007
753.38211	753.38192	$[M^{\#}+2H]^{2+}$	-0.246
763.39712	763.39742	$c^{\#}_5{}^{\bullet}$-H_2O	0.386
764.40495	764.40469	$c^{\#}_5$-H_2O	-0.340
781.40769	781.40769	$c^{\#}_5{}^{\bullet}$	0.000
782.41552	782.41554	$c^{\#}_5$	0.032
793.45531	793.45565	$c_6{}^{\bullet}$	0.429
794.46313	794.46286	c_6	-0.346
833.45023	833.44988	$c^{\ddagger}_6{}^{\bullet}$-$H_2O$	-0.414
834.45805	834.45853	$c^{\ddagger}_6$-H_2O	0.575
851.46079	851.46077	$c^{\ddagger}_6{}^{\bullet}$	-0.023
852.46861	852.46860	$c^{\ddagger}_6$	-0.018
891.45570	891.45583	$c^{\#}_6{}^{\bullet}$-H_2O	0.140

THEORETICAL (m/z)	EXPERIMENTAL (m/z)	ASSIGNMENTS	ERROR (ppm)
892.46353	892.46348	$c^{\#}_{6}$-H_2O	-0.056
893.44755	893.44744	$b^{\#}_{6}$	-0.123
909.46627	909.46627	$c^{\#}_{6}{}^{\bullet}$	0.000
910.47410	910.47426	$c^{\#}_{6}$	0.181
941.53155	941.53170	c_7	0.165
980.51864	980.51871	$c^{\ddagger}_{7}{}^{\bullet}$-$H_2O$	0.076
981.52646	981.52703	$c^{\ddagger}_{7}$-H_2O	0.581
998.52920	998.52958	$c^{\ddagger}_{7}{}^{\bullet}$	0.381
999.53702	999.53715	$c^{\ddagger}_{7}$	0.125
1039.53194	1039.53206	$c^{\#}_{7}$-H_2O	0.115
1040.51596	1040.51553	$b^{\#}_{7}$	-0.413
1056.53468	1056.53537	$c^{\#}_{7}{}^{\bullet}$	0.653
1057.54250	1057.54285	$c^{\#}_{7}$	0.326
1102.59125	1102.59116	$a^{\ddagger}_{8}$	-0.082
1145.59761	1145.59756	$c^{\ddagger}_{8}{}^{\bullet}$	-0.044
1145.62142	1145.62127	c_9	-0.127
1146.56388	1146.56378	$z^{\ddagger}_{9}{}^{\bullet}$-$H_2O$	-0.083
1146.60543	1146.60554	$c^{\ddagger}_{8}$	0.092
1148.56090	1148.56026	$z^{\#}_{9}{}^{\bullet}$-C_3H_6S	-0.556
1160.59673	1160.59644	$c^{\#}_{8}$-$^{\bullet}CONH_2$	-0.250
1164.57444	1164.57398	$z^{\ddagger}_{9}{}^{\bullet}$	-0.395
1185.61633	1185.61626	$c^{\ddagger}_{9}$-H_2O	-0.059
1186.55879	1186.55902	$z^{\#}_{9}{}^{\bullet}$-$2H_2O$	0.194
1186.60035	1186.60058	$b^{\ddagger}_{9}$	0.194
1203.62690	1203.62717	$c^{\ddagger}_{9}$	0.228
1204.56936	1204.56956	$z^{\#}_{9}{}^{\bullet}$-H_2O	0.170
1204.61091	1204.61126	$c^{\#}_{8}$	0.286
1222.57992	1222.58011	$z^{\#}_{9}{}^{\bullet}$	0.155
1226.59526	1226.59499	$b^{\#}_{9}$-H_2O	-0.224
1242.61398	1242.61319	$c^{\#}_{9}{}^{\bullet}$-H_2O	-0.640
1243.62181	1243.62159	$c^{\#}_{9}$-H_2O	-0.177
1258.70547	1258.70603	c_{10}	0.441
1261.63237	1261.63252	$c^{\#}_{9}$	0.115
1297.69257	1297.69367	$c^{\ddagger}_{10}{}^{\bullet}$-$H_2O$	0.852
1298.70039	1298.69906	$c^{\ddagger}_{10}$-H_2O	-1.024
1315.70313	1315.70305	$c^{\ddagger}_{10}{}^{\bullet}$	-0.061
1316.71096	1316.71132	$c^{\ddagger}_{10}$	0.277
1331.71662	1331.71671	$[M\text{-}CH_3CONH_2+2H]^{1+\bullet}$	0.204
1339.67933	1339.67923	$b^{\#}_{10}$-H_2O	-0.071
1345.73227	1345.73242	$[M\text{-}HCONH_2+2H]^{1+\bullet}$	0.113
1355.69805	1355.69830	$c^{\#}_{10}{}^{\bullet}$-H_2O	0.188
1356.70587	1356.70627	$c^{\#}_{10}$-H_2O	0.295
1371.71153	1371.71171	$[M^{\ddagger}\text{-}CH_3CONH_2\text{-}H_2O+2H]^{1+\bullet}$	0.129
1374.71644	1374.71603	$c^{\#}_{10}$	-0.295
1385.72718	1385.72814	$[M^{\ddagger}\text{-}^{\bullet}CONH_2\text{-}H_2O+H]^{1+}$	0.690
1388.71433	1388.71409	$[M^{\ddagger}\text{-}CH_3CONH_2+H]^{1+}$	-0.176
1389.72210	1389.72194	$[M^{\ddagger}\text{-}CH_3CONH_2+2H]^{1+\bullet}$	-0.114

THEORETICAL (m/z)	EXPERIMENTAL (m/z)	ASSIGNMENTS	ERROR (ppm)
1389.74597	1389.74615	$[M^{\ddagger}+H]^{1+}$	0.133
1403.73726	1403.73867	$[M^{\ddagger}-{}^{\bullet}CONH_2+H]^{1+}$	0.133
	1411.70639	?	
1412.73815	1412.73784	$[M^{\ddagger}- 2H_2O +2H]^{1+\bullet}$	-0.216
1414.73517	1414.73485	$[M^{\#}-H_2O-C_3H_6S+2H]1+^{\bullet}$	-0.225
	1429.71719	?	
1429.74088	1429.74149	$[M^{\ddagger}- H_2O +H]^{1+}$	0.427
1430.74871	1430.74910	$[M^{\ddagger}- H_2O +2H]^{1+\bullet}$	0.273
1443.73218	1443.73368	$[M^{\#}-{}^{\bullet}CONH_2- H_2O +H]^{1+}$	1.042
1447.75145	1447.75256	$[M^{\ddagger}+H]^{1+}$	0.770
1452.73306	1452.73363	$[M^{\#}-3H_2O+2H]^{1+\bullet}$	-0.392
1461.74275	1461.74352	$[M^{\#}-{}^{\bullet}CONH_2+H]^{1+}$	0.530
1470.74363	1470.74342	$[M^{\#}-2H_2O+2H]^{1+\bullet}$	0.139
	1487.74826	?	
1505.75693	1505.75566	$[M^{\#}+H]^{1+}$	-0.845
		mean	0.086
		St. Dv.	0.493

Table D-10. CAD (753) error analysis of the glycated Ac-KM-11 peptide in MeOH/H_2O (50:50) for the precursor ion $[M+2(C_2H_2O_2)+2H]^{2+}$. * indicates the ions used for calibration.

THEORETICAL (m/z)	EXPERIMENTAL (m/z)	ASSIGNMENTS	ERROR (ppm)
* 302.15329	302.15338	y_3-NH_3	0.313
319.17983	319.17993	y_3	0.313
424.26667	424.26667	b_3	0.000
446.25102	446.25074	$b^{\ddagger}_3$-$2H_2O$	-0.627
447.23504	447.23518	$b^{\ddagger}_3$-H_2O -NH_3	0.313
449.22170	449.22172	y_4-NH_3	0.045
462.75614	462.75625	b_7^{2+}	0.238
464.26159	464.26160	$b^{\ddagger}_3$-H_2O	0.032
* 466.24824	466.24827	y_4	0.064
474.24032	474.24041	$(b^{\ddagger}_7$-H_2O -$NH_3)^{2+}$	0.179
482.27215	482.27214	$b^{\ddagger}_3$	-0.021
482.75360	482.75352	$(b^{\ddagger}_7$-$H_2O)^{2+}$	-0.161
483.24561	483.24570	$(b^{\ddagger}_7$-$NH_3)^{2+}$	0.191
491.75888	491.75884	$b^{\ddagger}_7{}^{2+}$	-0.081
499.25634	499.25584	$a^{\ddagger}_4$-$2NH_3$-H_2O	-1.001
504.25650	504.25648	$b^{\#}_3$-$2H_2O$	-0.040
511.75634	511.75611	$(b^{\#}_7$-H_2O+H]2+	-0.445
522.26707	522.26708	$b^{\#}_3$-H_2O	0.029
523.25108	523.25121	$b^{\#}_3$-NH_3	0.239
527.77707	527.77689	(b_8-NH_3+H]2+	-0.346
533.77707	533.77707	$(a^{\ddagger}_8$-H_2O-NH_3+H]2	-0.005
536.29035	536.29034	b_8^{2+}	-0.009
540.27763	540.27736	$b^{\#}_3$	-0.500

THEORETICAL (m/z)	EXPERIMENTAL (m/z)	ASSIGNMENTS	ERROR (ppm)
542.29035	542.29035	$(a^{\ddagger}_{8}\text{-}H_2O)^{2+}$	0.005
547.28252	547.28261	$(b^{\ddagger}_{8}\text{-}H_2O)^{2+}$	0.164
547.77453	547.77452	$(b^{\ddagger}_{8}\text{-}H_2O\text{ -}NH_3)^{2+}$	-0.018
551.29563	551.29554	$a^{\ddagger}_{8}{}^{2+}$	-0.159
556.28780	556.28778	$b_9\text{-}NH_3$	-0.036
556.77981	556.77978	$(b^{\ddagger}_{8}\text{-}NH_3)^{2+}$	-0.058
561.31435	561.31429	$b^{\ddagger}_{4}\text{-}H_2O$	-0.098
562.28780	562.28764	$(a^{\#}_{8}\text{-}2H_2O)^{2+}$	-0.289
* 564.80107	564.80101	$b_9{}^{2+}$	-0.115
565.29309	565.29306	$b^{\ddagger}_{8}{}^{2+}$	-0.044
570.80107	570.80105	$(a^{\ddagger}_{9}\text{-}H_2O)^{2+}$	-0.044
571.29309	571.29317	$(a^{\#}_{8}\text{-}H_2O)^{2+}$	0.149
575.29103	575.29133	$x_9{}^{2+}$	0.521
575.79325	575.79323	$(b^{\ddagger}_{9}\text{-}2H_2O)^{2+}$	-0.035
576.28526	576.28524	$(b^{\ddagger}_{9}\text{-}H_2O\text{ -}NH_3)^{2+}$	-0.035
576.77727	576.77718	$(b^{\#}_{8}\text{-}H_2O\text{-}NH_3)^{2+}$	-0.156
584.79853	584.79852	$(b^{\ddagger}_{9}\text{-}H_2O)^{2+}$	-0.021
585.29054	585.29055	$(b^{\#}_{8}\text{-}H_2O)^{2+}$	0.013
585.78255	585.78260	$(b^{\#}_{8}\text{-}NH_3)^{2+}$	0.081
593.80381	593.80384	$b^{\ddagger}_{9}{}^{2+}$+	0.042
594.29583	594.29577	$b^{\#}_{8}{}^{2+}$+	-0.093
595.79071	595.79061	$(b^{\#}_{9}\text{-}3H_2O)^{2+}$	-0.164
596.28272	596.28274	$(b^{\#}_{9}\text{-}2H_2O\text{-}NH_3)^{2+}$	0.038
596.29011	596.29008	$y_5\text{-}NH_3$	-0.050
601.81059	601.81055	$(y_{10}\text{-}NH_3)^{2+}$	-0.066
604.79599	604.79594	$(b^{\#}_{9}\text{-}2H_2O)^{2+}$	-0.083
605.28800	605.28800	$(b^{\#}_{9}\text{-}H_2O\text{-}NH_3)^{2+}$	0.000
607.34565	607.34572	$a_{10}{}^{2+}$	0.115
610.32386	610.32384	$y_{10}{}^{2+}$	-0.033
612.82983	612.82980	$(b_{10}\text{-}NH_3)^{2+}$	-0.053
* 613.31665	613.31666	y_5	0.016
613.80127	613.80127	$(b^{\#}_{9}\text{-}H_2O)^{2+}$	-0.004
614.29328	614.29326	$(b^{\#}_{9}\text{-}NH_3)^{2+}$	-0.037
618.33782	618.33756	$(a^{\ddagger}_{10}\text{-}2H_2O)^{2+}$	-0.425
618.82983	618.82975	$(a^{\ddagger}_{10}\text{-}H_2O\text{-}NH_3)^{2+}$	-0.133
621.31604	621.31601	$(y^{\ddagger}_{10}\text{-}2H_2O)^{2+}$	-0.040
621.34311	621.34309	$b_{10}{}^{2+}$	-0.024
621.80804	621.80804	$(y^{\ddagger}_{10}\text{- }H_2O\text{-}NH_3)^{2+}$	-0.008
622.80656	622.80626	$b^{\#}_{9}{}^{2+}$+	-0.474
623.33000	623.33004	$(b^{\ddagger}_{10}\text{- }H_2O\text{ -}2H_2O)^{2+}$	0.068
623.82201	623.82197	$(b^{\ddagger}_{10}\text{-}2H_2O\text{-}NH_3)^{2+}$	-0.060
624.31402	624.31388	$(b^{\ddagger}_{10}\text{-}H_2O\text{-}2NH_3)^{2+}$	-0.220
627.34311	627.34309	$(a^{\ddagger}_{10}\text{-}H_2O)^{2+}$	-0.024
630.32132	630.32130	$(y^{\ddagger}_{10}\text{-}H_2O)^{2+}$	-0.028
630.81333	630.81333	$(y^{\ddagger}_{10}\text{-}NH_3)^{2+}$	0.004
632.33528	632.33527	$(b^{\ddagger}_{10}\text{-}H_2O\text{ -}H_2O)^{2+}$	-0.016
632.82729	632.82727	$(b^{\ddagger}_{10}\text{-}H_2O\text{ -}NH_3)^{2+}$	-0.032

THEORETICAL (m/z)	EXPERIMENTAL (m/z)	ASSIGNMENTS	ERROR (ppm)
636.34839	636.34838	$a^{\ddagger}_{10}{}^{2+}$	-0.012
639.32660	639.32658	$y^{\ddagger}_{10}{}^{2+}$	-0.031
641.34056	641.34055	$(b^{\ddagger}_{10}\text{-}H_2O)^{2+}$	-0.019
641.83257	641.83257	$(b^{\ddagger}_{10}\text{-}NH_3)^{2+}$	-0.004
647.34056	647.34052	$(a^{\#}_{10}\text{-}2H_2O)^{2+}$	-0.066
647.83257	647.83238	$(a^{\#}_{10}\text{-}H_2O\text{-}NH_3)^{2+}$	-0.297
649.37801	649.37799	b_5	-0.031
650.31877	650.31873	$(y^{\#}_{10}\text{-}2H_2O)^{2+}$	-0.069
650.34585	650.34581	$b^{\ddagger}_{10}{}^{2+}$	-0.054
652.33274	652.33271	$(b^{\#}_{10}\text{-}3H_2O)^{2+}$	-0.042
652.82475	652.82468	$(b^{\#}_{10}\text{-}2H_2O\text{-}NH_3)^{2+}$	-0.103
656.34585	656.34581	$(a^{\#}_{10}\text{-}H_2O)^{2+}$	-0.053
656.84779	656.84744	$[M\text{-}NH_3\text{-}H_2O)^{2+}$	-0.533
659.32406	659.32413	$(y^{\#}_{10}\text{-}H_2O)^{2+}$	0.110
659.81607	659.81598	$(y^{\#}_{10}\text{-}NH_3)^{2+}$	-0.133
661.33802	661.33800	$(b^{\#}_{10}\text{-}2H_2O)^{2+}$	-0.030
661.83003	661.83001	$(b^{\#}_{10}\text{-}H_2O\text{-}NH_3)^{2+}$	-0.030
664.35262	664.35256	$[M\text{-}HCONH_2\text{-}NH_3\text{+}2H]^{2+}$	-0.500
665.35113	665.35114	$a^{\#}_{10}{}^{2+}$	0.015
* 668.32934	668.32911	$y^{\#}_{10}{}^{2+}$	-0.344
670.34330	670.34329	$(b^{\#}_{10}\text{-}H_2O)^{2+}$	-0.019
670.83531	670.83531	$(b^{\#}_{10}\text{-}NH_3)^{2+}$	-0.004
672.86589	672.86579	$[M\text{-}HCONH_2\text{+}2H]^{2+}$	-0.152
677.85807	677.85814	$[M\text{-}H_2O\text{-}NH_3\text{+}2H]^{2+}$	0.107
678.35008	678.35002	$[M^{\ddagger}\text{-}H_2O\ 2NH_3\text{+}2H]^{2+}$	-0.085
679.34858	679.34851	$[b^{\#}_{10}\text{+}H]^{2+}$	-0.110
683.85807	683.85799	$[M^{\ddagger}\text{-}HCONH_2\text{-}2H_2O\text{+}2H]^{2+}$	-0.113
684.35008	684.34997	$[M^{\ddagger}\text{-}H_2O\text{-}HCONH_2\text{-}NH_3\text{+}2H]^{2+}$	-0.157
685.85552	685.85536	$[M^{\ddagger}\text{-}CH_2CO\text{-}H_2O\text{-}NH_3\text{+}2H]^{2+}$	-0.241
686.86335	686.86332	$[M\text{-}HCONH_2\text{-}H_2O\ \text{+}2H]^{2+}$	-0.044
689.34225	689.34219	$[M^{\ddagger}\text{-}2H_2O\text{-}2NH_3\text{+}2H]^{2+}$	-0.091
689.37293	689.37297	$b^{\ddagger}_5\text{-}H_2O$	0.065
690.35694	690.35704	$b^{\ddagger}_5\text{-}NH_3$	0.138
692.86335	692.86333	$[M^{\ddagger}\text{-}HCONH_2\text{-}H_2O\ \text{+}2H]^{2+}$	-0.029
694.36880	694.36879	$[M^{\ddagger}\text{-}H_2O\text{-}CH_2CO\text{+}2H]^{2+}$	-0.011
695.37663	695.37671	$[M\text{+}2H]^{2+}$	-0.115
697.85552	697.85552	$[M^{\ddagger}\text{-}2H_2O\text{-}NH_3\text{+}2H]^{2+}$	-0.007
698.34753	698.34749	$[M^{\ddagger}\text{-}H_2O\ \text{-}2NH_3\text{+}2H]^{2+}$	-0.064
701.86863	701.86856	$[M^{\ddagger}\text{-}HCONH_2\text{+}2H]^{2+}$	-0.103
703.37408	703.37419	$[M^{\ddagger}\text{-}CH_2CO\ \text{+}2H]^{2+}$	0.156
706.36880	706.36887	$[M^{\ddagger}\text{-}2H_2O\text{+}2H]^{2+}$	-0.099
706.86081	706.86078	$[M^{\ddagger}\text{-}H_2O\text{-}NH_3\text{+}2H]^{2+}$	-0.039
707.32214	707.32230	$y_6\text{-}2NH_3$	0.226
707.35282	707.35277	$[M^{\ddagger}\text{-}2NH_3\text{+}2H]^{2+}$	-0.067
712.86081	712.86092	$[M^{\#}\text{-}HCONH_2\text{-}2H_2O\text{+}2H]^{2+}$	0.158
713.35282	713.35277	$[M^{\#}\text{-}HCONH_2\text{-}H_2O\text{-}NH_3\text{+}2H]^{2+}$	-0.067
715.37408	715.37417	$[M^{\ddagger}\text{-}H_2O\text{+}2H]^{2+}$	-0.126

THEORETICAL (m/z)	EXPERIMENTAL (m/z)	ASSIGNMENTS	ERROR (ppm)
715.86609	715.86606	$[M^{\ddagger}-NH_3+2H]^{2+}$	-0.042
717.85298	717.85289	$[M^{\#}-3H_2O-NH_3+2H]^{2+}$	-0.129
718.34499	718.34523	$[M^{\#}-2H_2O-2NH_3+2H]^{2+}$	0.331
721.37408	721.37419	$[M^{\#}-2H_2O-CO+2H]^{2+}$	0.149
721.86609	721.86595	$[M^{\#}-HCONH_2-H_2O+2H]^{2+}$	-0.194
724.34869	724.34891	y_6-NH3	0.304
724.37991	724.37994	$[M^{\ddagger}+2H]^{2+}$	-0.041
725.37293	725.37305	$b_6-H_2O-2NH_3$	0.159
726.36626	726.36641	$[M^{\#}-3H_2O+2H]^{2+}$	-0.206
726.85827	726.85826	$[M^{\#}-2H_2O-NH_3+2H]^{2+}$	-0.010
727.35028	727.35027	$[M^{\#}-H_2O-2NH_3+2H]^{2+}$	-0.007
729.36784	729.36797	$b^{\#}_5-2H_2O$	0.178
730.87137	730.87151	$[M^{\#}$-HCONH2+2H$]^{2+}$	0.185
735.86355	735.86349	$[M^{\#}-H_2O-NH_3+2H]^{2+}$	-0.082
736.35556	736.35551	$[M^{\#}-2NH_3+2H]^{2+}$	-0.068
741.37523	741.37522	y_6	0.013
744.37682	744.37678	$[M^{\#}-H_2O+2H]^{2+}$	-0.057
744.86883	744.86878	$[M^{\#}-NH_3+2H]^{2+}$	-0.070
747.37841	747.37834	$b^{\#}_5-H_2O$	-0.087
748.36243	748.36299	$b^{\#}_5-NH_3$	0.755
754.39948	754.39950	$a^{\ddagger}_6-2H_2O-NH_3$	0.027
755.38350	755.38357	$a^{\ddagger}_6-H_2O-NH_3$	0.093
771.42602	771.42595	$a^{\ddagger}_6-2H_2O$	-0.097
* 777.43659	777.43664	b_6	0.064
799.42094	799.42093	$b^{\ddagger}_6-2H_2O$	-0.013
801.40898	801.40850	$b^{\ddagger}_6-2NH_3$	-0.599
811.42094	811.42101	$a^{\#}_6$-3H2O	0.086
812.40496	812.40496	$a^{\#}_6-2H_2O-NH_3$	0.000
817.43151	817.43150	$b^{\ddagger}_6-H_2O$	-0.006
829.43151	829.43208	$a^{\#}_6-2H_2O$	0.693
* 835.44207	835.44209	$b^{\ddagger}_6-$	0.024
839.41585	839.41535	$b^{\#}_6-3H_2O$	-0.602
857.42642	857.42625	$b^{\#}_6-2H_2O$	-0.198
858.41044	858.41025	$b^{\#}_6-H_2O-NH_3$	-0.221
875.43699	875.43682	$b^{\#}_6-H_2O$	-0.188
876.42101	876.42084	$b^{\#}_6-NH_3$	-0.188
901.46789	901.46788	$a^{\ddagger}_7-2H_2O-NH_3$	-0.011
902.45191	902.45215	$a^{\ddagger}_7-H_2O-2NH_3$	0.266
924.50500	924.50495	b_7	-0.054
932.43348	932.43353	y_8-2NH_3	0.054
946.48935	946.48969	$b^{\ddagger}_7-2H_2O$	0.359
947.47337	947.47336	$b^{\ddagger}_7-H_2O-NH_3$	-0.011
948.47739	948.47768	$b^{\ddagger}_7--2NH_3$	0.306
949.46003	949.46004	y_8-NH_3	0.011
958.48935	958.48942	$a^{\#}_7-3H_2O$	0.073
959.47337	959.47328	$a^{\#}_7-2H_2O-NH_3$	-0.094
964.49991	964.49993	$b^{\ddagger}_7-H_2O$	0.016
965.48393	965.48364	$b^{\ddagger}_7--NH_3$	-0.306

THEORETICAL (m/z)	EXPERIMENTAL (m/z)	ASSIGNMENTS	ERROR (ppm)
966.48657	966.48666	y_8	0.093
976.49991	976.49907	$a^{\#}_7$-2H_2O	-0.865
* 982.51048	982.51050	$b^{\ddagger}_7$-	0.020
986.48427	986.48438	$b^{\#}_7$-3H_2O	0.117
1004.49483	1004.49478	$b^{\#}_7$-2H_2O	-0.050
1005.47885	1005.47836	$b^{\#}_7$-H_2O-NH_3	-0.487
1022.50540	1022.50534	$b^{\#}_7$-H_2O	-0.054
1023.48942	1023.48989	$b^{\#}_7$-NH_3	0.464
*1043.57849	1043.57839	a_8	-0.101
1054.54687	1054.54648	b_8-NH_3	-0.365
1066.54687	1066.54738	a_9-2NH_3	0.483
1083.57341	1083.57369	$a^{\ddagger}_8$-H_2O	0.258
1093.55776	1093.55775	$b^{\ddagger}_8$-2H_2O	-0.009
1094.54178	1094.54191	$b^{\ddagger}_8$-H_2O -NH_3	0.119
1095.54580	1095.54579	$b^{\ddagger}_8$-2NH_3	-0.009
1101.58398	1101.58432	$a^{\ddagger}_8$	0.313
1112.55235	1112.55247	$b^{\ddagger}_8$-NH_3	0.112
1124.55235	1124.55252	$a^{\ddagger}_9$-2NH_3	0.156
*1128.59487	1128.59487	b_9	0.000
1129.57889	1129.57884	$b^{\ddagger}_8$	-0.044
1133.55267	1133.55255	$b^{\#}_8$-3H_2O	-0.110
1134.53670	1134.53597	$b^{\ddagger}_9$-H_2O-2NH_3	-0.639
1150.57922	1150.57937	$b^{\ddagger}_9$-H_2O -H2O	0.130
1151.56324	1151.56331	$b^{\ddagger}_9$-H_2O -NH_3	0.061
1152.54726	1152.54718	$b^{\#}_8$-H_2O-NH_3	-0.069
1152.56726	1152.56667	$b^{\ddagger}_9$-2NH_3	-0.512
1153.55128	1153.55084	$b^{\#}_8$-2NH_3	-0.381
1159.58946	1159.59005	$a^{\#}_8$	0.513
1162.57922	1162.57883	$a^{\#}_9$-3H_2O	-0.335
1168.58978	1168.58988	$b^{\ddagger}_9$-H_2O	0.081
1169.57380	1169.57390	$b^{\#}_8$-H_2O	0.081
1170.55783	1170.55794	$b^{\#}_8$-NH_3	0.098
1186.60035	1186.60104	$b^{\ddagger}_9$	0.581
1190.57414	1190.57445	$b^{\#}_9$-3H_2O	0.265
1192.54218	1192.54317	$b^{\#}_9$-H_2O-2NH_3	0.834
1208.58470	1208.58501	$b^{\#}_9$-2H_2O	0.256
1209.56872	1209.56880	$b^{\#}_9$-H_2O-NH_3	0.066
1210.57274	1210.57215	$b^{\#}_9$-2NH_3	-0.487
*1219.64044	1219.64059	y_{10}	0.123
1224.59824	1224.59950	$y^{\ddagger}_{10}$-H_2O-NH_3	1.025
1225.58227	1225.58236	$y^{\ddagger}_{10}$-H_2O -2NH_3	0.078
1226.59526	1226.59535	$b^{\#}_9$-H_2O	0.069
1227.57929	1227.57919	$b^{\#}_9$-NH_3	-0.077
1241.62479	1241.62469	$y^{\ddagger}_{10}$-H_2O	-0.081
1241.67893	1241.67893	b_{10}	0.000
1242.60881	1242.60870	$y^{\ddagger}_{10}$-H_2O -NH_3	-0.089
1243.59283	1243.59273	$y^{\ddagger}_{10}$-2NH_3	-0.080

THEORETICAL (m/z)	EXPERIMENTAL (m/z)	ASSIGNMENTS	ERROR (ppm)
1259.63535	1259.63549	$y^{\ddagger}_{10}$-H_2O	0.107
1260.61937	1260.61948	$y^{\ddagger}_{10}$-NH_3	0.083
1263.66328	1263.66317	$b^{\ddagger}_{10}$-$2H_2O$	-0.087
1264.64730	1264.64739	$b^{\ddagger}_{10}$-NH_3-H_2O	0.071
1265.65132	1265.65173	$b^{\ddagger}_{10}$-$2NH_3$	0.324
1277.64592	1277.64572	$y^{\ddagger}_{10}$	-0.157
1281.67385	1281.67376	$b^{\ddagger}_{10}$-H_2O	-0.066
1282.65786	1282.65788	b-NH_3	0.012
1293.67385	1293.67355	$a^{\#}_{10}$-$2H_2O$	-0.228
1299.63027	1299.63034	$y^{\#}_{10}$-$2H_2O$	0.054
1299.68441	1299.68416	$b^{\ddagger}_{10}$	-0.192
*1300.61429	1300.61432	$y^{\#}_{10}$-H_2O-NH_3	0.023
		mean	0.023
		St. Dv.	0.396

Table D-11. CAD(753) error analysis of the AcKM-11 peptide PBS for the precursor ion $[M+2(C_2H_2O_2)+2H]^{2+}$. * indicates the ions used for calibration.

THEORETICAL (m/z)	EXPERIMENTAL (m/z)	ASSIGNMENTS	ERROR (ppm)
* 302.15329	302.15304	y_3-NH_3	-0.827
424.26667	424.26659	b_3	-0.189
446.25102	446.25102	$b^{\ddagger}_3$-$2H_2O$	0.000
449.22170	449.22170	y_4-NH_3	0.000
464.26159	464.26159	$b^{\ddagger}_3$-H_2O	0.011
* 466.24824	466.24828	y_4	0.086
473.74831	473.74837	$(b^{\ddagger}_7$-$2H_2O)^{2+}$	0.116
482.27215	482.27225	$b^{\ddagger}_3$	0.207
504.25650	504.25644	$b^{\#}_3$-$2H_2O$	-0.119
511.75634	511.75634	$(b^{\#}_7$-$H_2O)^{2+}$	0.005
521.31943	521.31949	b_4	0.115
522.26707	522.26712	$b^{\#}_3$-H_2O	0.105
522.29289	522.29302	a_8^{2+}	0.249
536.29035	536.29032	b_8^{2+}	-0.047
542.29035	542.29033	$(a^{\ddagger}_8$-$H_2O)^{2+}$	-0.028
547.28252	547.28253	$(b^{\ddagger}_8$-$2H_2O)^{2+}$	0.018
556.28780	556.28773	b_9-NH_3	-0.126
564.80107	564.80113	b_9^{2+}	0.097
565.29309	565.29312	$b^{\ddagger}_8{}^{2+}$	0.062
567.27998	567.28032	$(b^{\ddagger}_9$-$2H_2O$-$NH_3)^{2+}$	0.604
571.29309	571.29315	$(a^{\#}_8$-$H_2O)^{2+}$	0.114
575.79325	575.79307	$(b^{\ddagger}_9$-$H_2O)^{2+}$	-0.313
576.28526	576.28543	$(b^{\ddagger}_9$-H_2O -$NH_3)^{2+}$	0.295
584.79853	584.79858	$(b^{\ddagger}_9$-$H_2O)^{2+}$	0.081
585.29054	585.29048	$(b^{\#}_8$-$H_2O)^{2+}$	-0.107

THEORETICAL (m/z)	EXPERIMENTAL (m/z)	ASSIGNMENTS	ERROR (ppm)
593.80381	593.80392	$b^{\ddagger}_{9}{}^{2+}$	0.177
594.29583	594.29582	$b^{\#}_{8}{}^{2+}$	-0.008
* 596.29011	596.29025	y_5-NH_3	0.235
599.80381	599.80393	$(a^{\#}_{9}$-$H_2O)^{2+}$	0.192
601.81059	601.81053	$(y_{10}$-$NH_3)^{2+}$	-0.100
603.82455	603.82467	$(b_{10}$-H_2O-$NH_3)^{2+}$	0.199
604.79599	604.79617	$(b^{\#}_{9}$-$2H_2O)^{2+}$	0.298
605.28800	605.28808	$(b^{\#}_{9}$-H_2O-$NH_3)^{2+}$	0.132
607.34565	607.34572	$a_{10}{}^{2+}$	0.115
610.32386	610.32397	$y_{10}{}^{2+}$	0.180
612.33782	612.33775	$(b_{10}$-$H_2O)^{2+}$	-0.118
612.82983	612.82974	$(b_{10}$-$NH_3)^{2+}$	-0.151
613.31665	613.31701	y_5	0.587
613.80127	613.80118	$(b^{\#}_{9}$-$H_2O)^{2+}$	-0.151
621.34311	621.34310	$b_{10}{}^{2+}$	-0.008
622.80656	622.80665	$b^{\#}_{9}{}^{2+}$	0.153
627.34311	627.34320	$(a^{\ddagger}_{10}$-$H_2O)^{2+}$	0.147
* 630.32132	630.32139	$(y^{\ddagger}_{10}$-$H_2O)^{2+}$	0.115
632.33528	632.33520	$(b^{\ddagger}_{10}$-$2H_2O)^{2+}$	-0.127
632.82729	632.82753	$(b^{\ddagger}_{10}$-H_2O -$NH_3)^{2+}$	0.379
636.34839	636.34851	$a^{\ddagger}_{10}{}^{2+}$	0.189
639.32660	639.32681	$y^{\ddagger}_{10}{}^{2+}$	0.328
641.34056	641.34041	$(b^{\ddagger}_{10}$-$H_2O)^{2+}$	-0.238
649.37801	649.37793	b_5	-0.123
650.31877	650.31882	$(y^{\#}_{10}$-$2H_2O)^{2+}$	0.069
650.34585	650.34600	$b^{\ddagger}_{10}{}^{2+}$	0.238
656.34585	656.34597	$(a^{\#}_{10}$-$H_2O)^{2+}$	0.190
656.84779	656.84759	$[M$-$2NH_3$-H2O+H$]^{2+}$	-0.304
659.32406	659.32422	$(y^{\#}_{10}$-$H_2O)^{2+}$	0.246
659.81607	659.81619	$(y^{\#}_{10}$-$NH_3)^{2+}$	0.186
661.33802	661.33796	$(b^{\#}_{10}$-$2H_2O)^{2+}$	-0.091
661.83003	661.83037	$(b^{\#}_{10}$-H_2O-$NH_3)^{2+}$	0.514
664.35289	664.35280	$[M$-$HCONH_2$-NH_3+2H$]^{2+}$	-0.139
665.35113	665.35152	$a^{\#}_{10}{}^{2+}$	0.586
668.32934	668.32971	$y^{\#}_{10}{}^{2+}$	0.554
670.34330	670.34353	$(b^{\#}_{10}$-$H_2O)^{2+}$	0.339
671.36236	671.36291	$b^{\ddagger}_{5}$-$2H_2O$	0.819
677.85807	677.85839	$[M$-H_2O-NH_3+2H$]^{2+}$	0.476
678.35008	678.35045	$[M$-$2NH_3$+2H$]^{2+}$	0.549
679.34858	679.34880	$b^{\#}_{10}{}^{2+}$	0.316
686.86335	686.86334	$[M$-NH_3-$HCONH_2$+2H$]^{2+}$	-0.015
689.37293	689.37335	$b^{\ddagger}_{5}$-H_2O	0.617
695.37663	695.37683	$[M$+2H$]^{2+}$	0.288
694.86081	694.86089	$[M^{\ddagger}$-CH_2CO -NH_3+2H$]^{2+}$	0.119
706.36880	706.36830	$[M^{\ddagger}$-$2H_2O$ +2H$]^{2+}$	0.707
707.32214	707.32246	y_6-$2NH_3$	0.452
707.35282	707.35336	$[M^{\ddagger}$-$2NH_3$+2H$]^{2+}$	0.767
* 707.38349	707.38396	$b^{\ddagger}_{5}$	0.664

THEORETICAL (m/z)	EXPERIMENTAL (m/z)	ASSIGNMENTS	ERROR (ppm)
707.86234	707.86220	$[M\text{-}H_2O + 2H]2+$	-0.201
717.85298	717.85226	$[M^{\#}\text{-}3H_2O+2H]2+$	-1.006
718.34499	718.34428	$[M^{\#}\text{-}2H_2O\text{-}2NH_3+2H]2$	-0.992
724.37936	724.37956	$[M^{\ddagger}+2H]2+$	0.273
726.35695	726.35722	$b_6\text{-}3NH_3$	0.365
735.86355	735.86342	$[M^{\#}\text{-}H_2O\text{-}NH_3+2H]2$	-0.177
737.36293	737.36334	$a^{\ddagger}_6\text{-}2NH_3\text{-}H2O$	0.549
744.37682	744.37695	$[M^{\#}\text{-}H_2O+2H]2+$	0.171
744.86883	744.86929	$[M^{\#}\text{-}NH_3+2H]2+$	0.614
754.39948	754.39894	$a^{\ddagger}_6\text{-}2H_2O\text{-}NH_3$	-0.716
771.42602	771.42626	$a^{\ddagger}_6\text{-}2H_2O$	0.305
777.43659	777.43654	b_6	-0.064
799.42094	799.42059	$b^{\ddagger}_6\text{-}2H_2O$	-0.438
811.42094	811.42099	$a^{\#}_6\text{-}3H_2O$	0.062
812.40496	812.40518	$a^{\#}_6\text{-}2H_2O\text{-}NH_3$	0.271
817.43151	817.43206	$b^{\ddagger}_6\text{-}H_2O$	0.679
* 835.44207	835.44261	$b^{\ddagger}_6$	0.646
857.42642	857.42675	$b^{\#}_6\text{-}2H_2O$	0.385
875.43699	875.43644	$b^{\#}_6\text{-}H_2O$	-0.623
901.46789	901.46826	$a^{\ddagger}_7\text{-}2H_2O\text{-}NH3$	0.410
924.50500	924.50515	b_7	0.162
932.43348	932.43410	$y_8\text{-}2NH_3$	0.665
946.48935	946.48855	$b^{\ddagger}_7\text{-}2H_2O$	-0.845
949.46003	949.46028	$y_8\text{-}NH3$	0.263
958.48935	958.48963	$a^{\#}_7\ \text{-}3H_2O$	0.292
964.49991	964.50011	$b^{\ddagger}_7\text{-}H_2O$	0.202
966.48657	966.48650	y_8	-0.072
982.51048	982.51053	$b^{\ddagger}_7$	0.051
988.45231	988.45177	$b^{\#}_7\text{-}H_2O\text{-}2NH_3$	-0.541
1022.50540	1022.50604	$b^{\#}_7\text{-}H_2O$	0.631
1043.57849	1043.57822	a_8	-0.264
1071.57341	1071.57289	b_8	-0.485
1093.55776	1093.55885	$b^{\ddagger}_8\text{-}2H_2O$	0.997
1111.56832	1111.56780	$b^{\ddagger}_8\text{-}H_2O$	-0.472
1128.59487	1128.59383	b_9	-0.921
1133.55267	1133.55236	$b^{\#}_8\text{-}3H_2O$	-0.278
1150.57922	1150.57802	$b^{\ddagger}_9\text{-}2H_2O$	-1.043
1169.57380	1169.57447	$b^{\#}_8\text{-}H_2O$	0.569
1186.60035	1186.60037	$b^{\ddagger}_9$	0.017
1213.68402	1213.68414	a_{10}	0.103
*1219.64044	1219.63975	y_{10}	0.556
1226.59526	1226.59616	$b^{\#}_9\text{-}H_2O$	0.734
1241.67893	1241.67882	b_{10}	-0.089
1259.63535	1259.63649	$y^{\ddagger}_{10}\text{-}H_2O$	0.905
1281.67385	1281.67348	$b^{\ddagger}_{10}\text{-}H_2O$	-0.288
1299.63027	1299.63099	$y^{\#}_{10}\text{-}2H_2O$	0.554
1299.68441	1299.68450	$b^{\ddagger}_{10}$	0.069

*1300.61429	1300.61449	$y^{\#}_{10}$-H_2O-NH_3	0.154

mean	0.101
St. Dv.	0.471

E

Original paper. Determination of types and binding sites of advanced glycation end products for Substance P. Anal. Chem. 2012 (84), 10568-10575.

analytical chemistry

Article

pubs.acs.org/ac

Determination of Types and Binding Sites of Advanced Glycation End Products for Substance P

Andrea F. Lopez-Clavijo,[†] Mark P. Barrow,[†] Naila Rabbani,[‡] Paul J. Thornalley,[‡] and Peter B. O'Connor*,[†]

[†]Warwick Centre for Analytical Science, Department of Chemistry, University of Warwick, Coventry, CV4 7AL, United Kingdom

[‡]Clinical Sciences Research Laboratories, Warwick Medical School, University of Warwick, University Hospital, Coventry, CV2 2DX, United Kingdom

Supporting Information

ABSTRACT: Glycation by endogenous dicarbonyl metabolites such as glyoxal is an important spontaneous post-translational (PTM) modification of peptides and proteins associated with structural and functional impairment. The aim of this study was to investigate types and site of PTM of glyoxal-derived advanced glycation end-products—in the neuropeptide substance P by ultrahigh-resolution Fourier transform ion cyclotron resonance (FTICR), mass spectrometry, and tandem mass spectrometry (MS/MS) experiments. The main site of PTM by glyoxal was the side chain guanidine moiety of the arginine residue. Binding site identification has been achieved by electron capture dissociation, double-resonance electron capture dissociation, and collision-activated dissociation, with assignment of the modified amino acid residue with mass error <1 ppm.

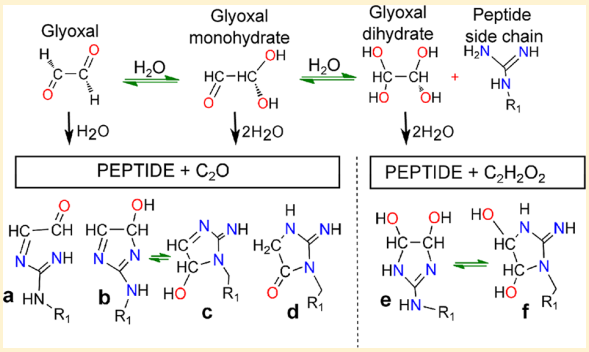

Glyoxal (ethanedial), an α-dicarbonyl compound (also known as α-oxoaldehyde), is a physiological metabolite. It is formed by the degradation of glucose,[1] glucose-modified proteins (degradation of Schiff's base adduct and Amadori product),[2] the autoxidation of glycolaldehyde from the oxidation of serine residues by hypochlorite in the phagocyte respiratory burst,[3] lipid peroxidation, and degradation of nucleotides.[4,5] Glyoxal and related dicarbonyl metabolites (such as methylglyoxal or 3-deoxyglucosone) react mainly, but not exclusively, with guanidine groups of arginine residues of peptides and proteins. These reactions are spontaneous and part of complex parallel and sequential reactions, in which monosaccharides and related metabolites modify proteins, known as the Maillard reaction,[6] or glycation.[2] Dicarbonyl-derived glycation products are called advanced glycation end-products (AGEs). Important AGEs quantitatively formed from methylglyoxal are the arginine residue-derived hydroimidazolone, N_{δ}-(5-hydro-5-methyl-4-imidazolon-2-yl)ornithine (MG-H1), and N_{ω}-carboxymethylarginine (CMA), and lysine residue-derived N_{ε}-carboxymethyl-lysine (CML), and the glyoxal-derived bis(lysyl)imidazolium cross-links (GOLD, glyoxal–lysine dimer[7]). CML is also formed by the oxidative degradation of *N*-fructosyl-lysine residues in proteins glycated by glucose.[8]

Glycation of proteins is commonly measured via the HbA_{1c} test, and the values are used in diabetes treatment. Glycation by glyoxal and related dicarbonyls occurs also in physiological systems. Arginine-directed glycation is insidious because arginine residue-derived AGEs have increased molecular volume and change in electrostatic charge, producing structural distortion and loss of electrostatic interactions. Arginine residues have high probability of location at functional sites of proteins, and functionally important arginine residues are often hot spots for dicarbonyl glycation leading to protein and enzyme inactivation or dysfunction.[8] Increased dicarbonyl glycation occurs in aging and chronic disease (particularly diabetes and its complications[9,10]—nephropathy,[11,12] retinopathy, neuropathy,[13] and heart disease[11]), where increased formation of dicarbonyls and decreased in situ activity of their metabolism leads to increased dicarbonyl-derived AGEs and pathogenesis.[14,15]

A method for detection of dicarbonyl-derived AGEs is stable isotope dilution analysis with tandem mass spectrometry after exhaustive enzymatic hydrolysis of peptide and protein substrates.[16] Identification of dicarbonyl glycation within proteins has been achieved by mass spectrometric peptide mapping and proteomics[17−20] with collision-activated dissociation (CAD),[21−23] electron capture dissociation (ECD),[24,25] and electron-transfer dissociation[26] capabilities, fragmentation techniques widely applied to determine the site of the post-translational modifications (PTMs).[27−37] In this study, the dicarbonyl glycation reaction is studied through glyoxal binding

Received: June 8, 2012
Accepted: November 18, 2012
Published: November 19, 2012

to the neuropeptide substance P using Fourier transform ion cyclotron resonance mass spectrometry (FTICR-MS). Substance P has the amino acid sequence RPKPQQFFGLM and normally contains an amidated C-terminus. Thus, the guanidino group of arginine, the amino group of lysine, the N-terminus, and the amidated C-terminus are the potential glyoxal glycation sites for substance P. The glyoxal-derived AGEs were fragmented by ECD, double resonance electron capture dissociation (DR-ECD), and CAD, and glyoxal binding site was assigned within 1 ppm error (accurate mass assignments are available in the Supporting Information).

MATERIALS AND METHODS

Materials. Substance P and substance P acetate salt, ammonium acetate (~99.6%), triethylamine, ammonium phosphate monobasic, and acetic acid (≥99% pure) were purchased from Sigma-Aldrich (St. Louis, MO, U.S.A.). Methanol (LC–MS grade), ethanol (HPLC grade), and isopropyl alcohol (IPA, GLC pesticide grade) were purchased from Fisher Scientific (Loughborough, Leicestershire, U.K.) and were used without further purification. All aqueous solutions were prepared using water from a Milli-Q water system (Millipore Inc., Durham, U.K.). Microdialysis cassettes (GeBa flex-tube, 1 kDa cutoff), were obtained from Chembio Diagnostic Systems, Inc. (Hertfordshire, U.K.). Glyoxal solution (~39% in water) was purchased from TCI Europe (Zwijndrecht, Belgium). High-purity glyoxal solution was difficult to obtain because higher concentration favors the formation of glyoxal dimers and trimers through dioxolane rings.[38] Nuclear magnetic resonance analysis of glyoxal solution showed hydrolysis and dimer species, as previously reported by Whipple.[39]

Substance P Glycation. In vitro glycation with glyoxal was performed with substance P (1 mg/mL) or amidated substance P (1 mg/mL). The concentration of anhydrous glyoxal reacted with substance P was estimated of around 800 μmol/L, based in the presence of hydrated, dimer, hemiacetals, hemiketal, and bicyclic structures. The reaction was carried out at 37 °C in MeOH/H_2O (50:50), 100% water, and phosphate buffer [30 mM ammonium phosphate monobasic ($NH_4H_2PO_4$) and 30 μL triethylamine ($N(CH_2CH_3)_3$) pH 7.5], for 21, 21, and 12 h, respectively. The samples reacted in phosphate buffer were dialyzed against water and 10 mM CH_3COONH_4 over a period of 24 h, dried, and redissolved in MeOH/H_2O (50:50). Prior to injection in the FTICR-MS, samples were prepared to a concentration of ~1 to 5 pmol/μL using electrospray solution (composed either of MeOH or EtOH/IPA/acetic acid/H_2O; 50:10:1:39). Methanol was used as a glyoxal polymerization inhibitor instead of acetonitrile, which promotes glyoxal dimerization.[40]

Mass Spectrometry. The experiments were performed in a 12 T solariX FTICR-MS (Bruker Daltonics, Coventry, United Kingdom). The sample was ionized in positive mode with a capillary voltage of 4.5 kV. To perform ECD, the parent ion was isolated in the quadrupole (Q1) and accumulated in the collision cell (1–15 s). After being transferred and trapped in the infinity cell,[41] low-energy electrons (<1 eV) were generated with an indirectly heated dispenser cathode[42] (1.3 V and 1.7 V) for 150 and 250 ms. Double-resonance ECD (DR–ECD)[43,44] was performed in the cell varying the ejection pulse between 120 and 220 ms. The laser pulse for the infrared multiphoton dissociation (IRMPD)[45,46] experiment was kept at 90 ms followed by electron injection. CAD experiments were performed in the collision cell prior to selection of the precursor ion in the quadrupole with potentials around 5–15 V. The data was processed with DataAnalysis software 4.0 SP 3 (Bruker Daltonics) and internally calibrated.

RESULTS AND DISCUSSION

Experiments were carried out in phosphate buffer, because of its biological relevance, and in MeOH/H_2O (50:50), in order to develop the method aiming to determine the types of AGEs and its binding site for amidated substance P. Figure 1a shows

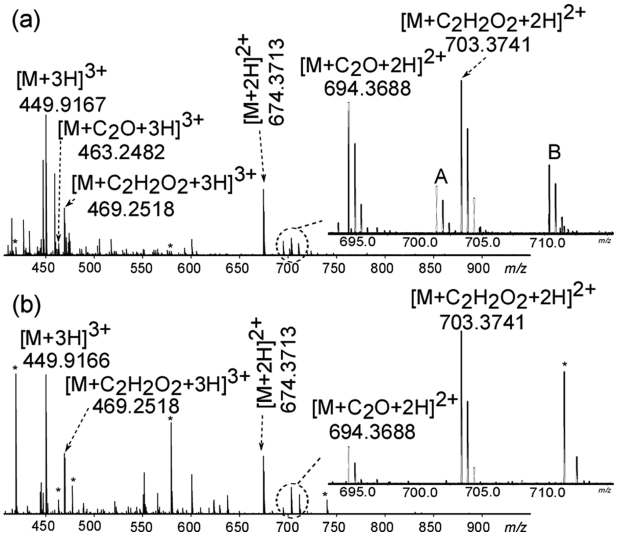

Figure 1. (a) Spectrum of glyoxal-derived AGEs in MeOH/H_2O (50:50), electrosprayed with a solution containing MeOH, IPA, H_2O, and acetic acid. (b) Spectrum of glyoxal-derived glycation products (AGEs) in 100% H_2O, electrosprayed with a solution containing EtOH, MeOH, IPA, H_2O, and acetic acid.

doubly $[M + 2H]^{2+}$ and triply charged $[M + 3H]^{3+}$ ions from unmodified amidated substance P. The spectrum also shows four more doubly charged ions, $[M + C_2O + 2H]^{2+}$, with a net increase of 39.9949 Da, $[M + C_2H_2O_2 + 2H]^{2+}$, with the net addition of 58.0055 Da, and A and B. A and B showed a mass difference of 14.0156 Da (CH_2), with respect to both modified ions, and were identified as ion/molecule reaction ions with methanol and were eliminated when the reaction was carried out in 100% water and ethanol was used in the electrospray solution, Figure 1b. The reaction in phosphate buffer, sprayed in methanol-containing solution, showed the same ions discussed above for Figure 1a. The glyoxal-derived AGE observed ions $[M + C_2O + 2H]^{2+}$ (m/z 694.3688) and $[M + C_2H_2O_2 + 2H]^{2+}$ (m/z 703.3741) are formed following the pathway reaction showed in Scheme 1, for both reaction solutions (MeOH/H_2O and phosphate buffer). Scheme 1 shows the possible structures that may be formed by glyoxal and dihydrated glyoxal; in particular structures **e** and **f** were identified, by De Haan et. al.,[47] to coexist in a 3:1 ratio. Thus, the glyoxal-derived AGEs formed by the net addition of C_2O and $C_2H_2O_2$ were fragmented by ECD and CAD in order to identify the glyoxal binding site.

Substance P Modified by C_2O. Figure 2a shows the ECD spectra of the parent ion $[M + C_2O + 2H]^{2+}$ in MeOH/H_2O (50:50), with two kind of c fragment ions: unmodified c_4–c_{10} and modified $c^{\dagger}_4$–$c^{\dagger}_{10}$. A dagger symbol was added to the

dx.doi.org/10.1021/ac301583d | Anal. Chem. 2012, 84, 10568–10575

Scheme 1. Glyoxal-Derived AGEs Based in the Presence of Monohydrate and Dihydrate Species in Glyoxal Reagent (~39%) in Water[a]

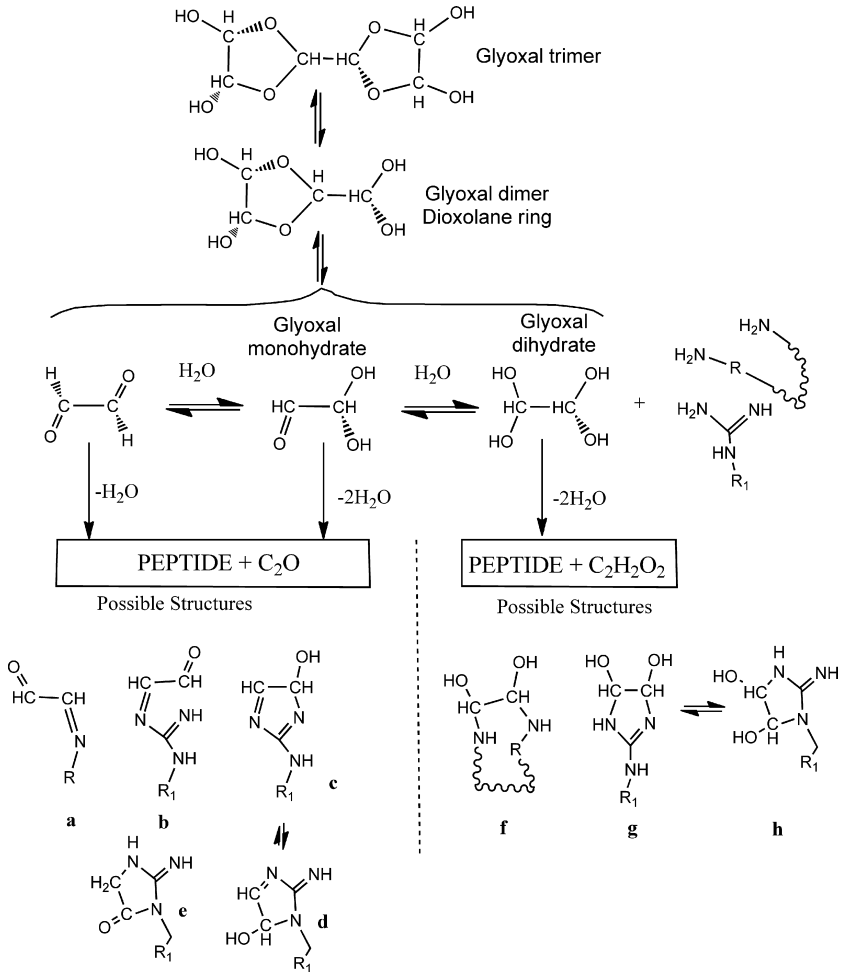

[a]Structures: **a**, Schiff base at the N-terminus or amine group of lysine; **b**, Schiff base at the guanidine group of arginine; **c**, 3-hydroxyimidazole; **d**, 2-imino-5-hydroxyimidazoline; **e**, 2-imino-imidazolidinone (also known as a creatinine side chain); **f**, cross-linking between amino group of lysine with the N-terminus; **g**, 3,4-dihydroxyimidazoline; **h**, 2-imino-imidazolidine.

standard Roepstorff nomenclature[48] (c/z), to differentiate the ions with the glyoxal modification. The radical $z_9^{\bullet}$ fragment ion, water loss, y_9, and side chain losses were also observed, but the pair $c_1/z_{10}^{\bullet}$, $c_3/z_8^{\bullet}$, $c^{\dagger}_1/z_{10}^{\bullet}$, and $c^{\dagger}_3/z_8^{\bullet}$, together c_2 and $c^{\dagger}_2$ were absent in the spectrum. Figure 2a additionally shows the unmodified doubly charged $[M + 2H]^{2+}$ ion, which is not usual during ECD experiments, because the capture of low-energy electrons by the molecule generates the charge reduce radical species ($[M + C_2O + 2H]^{2+} + e^-$ becomes $[M + C_2O + 2H]^{+\bullet}$) and not the loss of the modification. Thus, an isolation spectrum of the parent ion $[M + C_2O + 2H]^{2+}$ was acquired in order to determine if the $[M + 2H]^{2+}$ ion originated during quadrupole isolation. The isolation spectra of the parent ion $[M + C_2O + 2H]^{2+}$ shows a low abundance of the molecular ion $[M + 2H]^{2+}$ indicating that loss of C_2O is a low-energy, facile process. The presence of the $[M + 2H]^{2+}$ ion indicates that during isolation some small, unknown, amount of energy was given to the parent ion $[M + C_2O + 2H]^{2+}$, which activates it causing loss of the modification and generating the $[M + 2H]^{2+}$ ion. The $[M + 2H]^{2+}$ ion may therefore be responsible for the secondary fragmentation (c_4–c_{10}) observed during the ECD experiment.

Additionally, because the $[M + 2H]^{2+}$ ion and the c_4–c_{10} ions were formed *during* ECD, preisolation yielded no new information about their provenance. So, in order to test if they were secondary fragments formed from the $[M + 2H]^{2+}$ ion, double-resonance ECD[49] was used to eject the ion $[M + 2H]^{2+}$ during the ECD experiment of the parent ion $[M + C_2O + 2H]^{2+}$. The notation adopted for the double-resonance experiments is represented as DR(X)–ECD(Y), where X is the m/z value of the ejected fragment and Y corresponds to the m/z value of the parent ion. The DR(674.37)–ECD(694.36) spectrum of glycated, amidated substance P for the parent ion $[M + C_2O + 2H]^{2+}$ (Figure 2b) exhibited similar features as those described above for the ECD spectrum, but the difference lies in the absence of c_8, c_9, c_{10}, $z_7^{\bullet}$, and $z_5^{\bullet}$. The observed relative intensities of the c_n and $c^{\dagger}_n$ fragment ions (n = 2–10) were normalized to check that the observed c fragment ions were secondary fragments from the unmodified doubly charged ion $[M + 2H]^{2+}$. The normalized relative intensity (I_i) was calculated by application of eq S-1 (Supporting Information)

dx.doi.org/10.1021/ac301583d | *Anal. Chem.* 2012, 84, 10568–10575

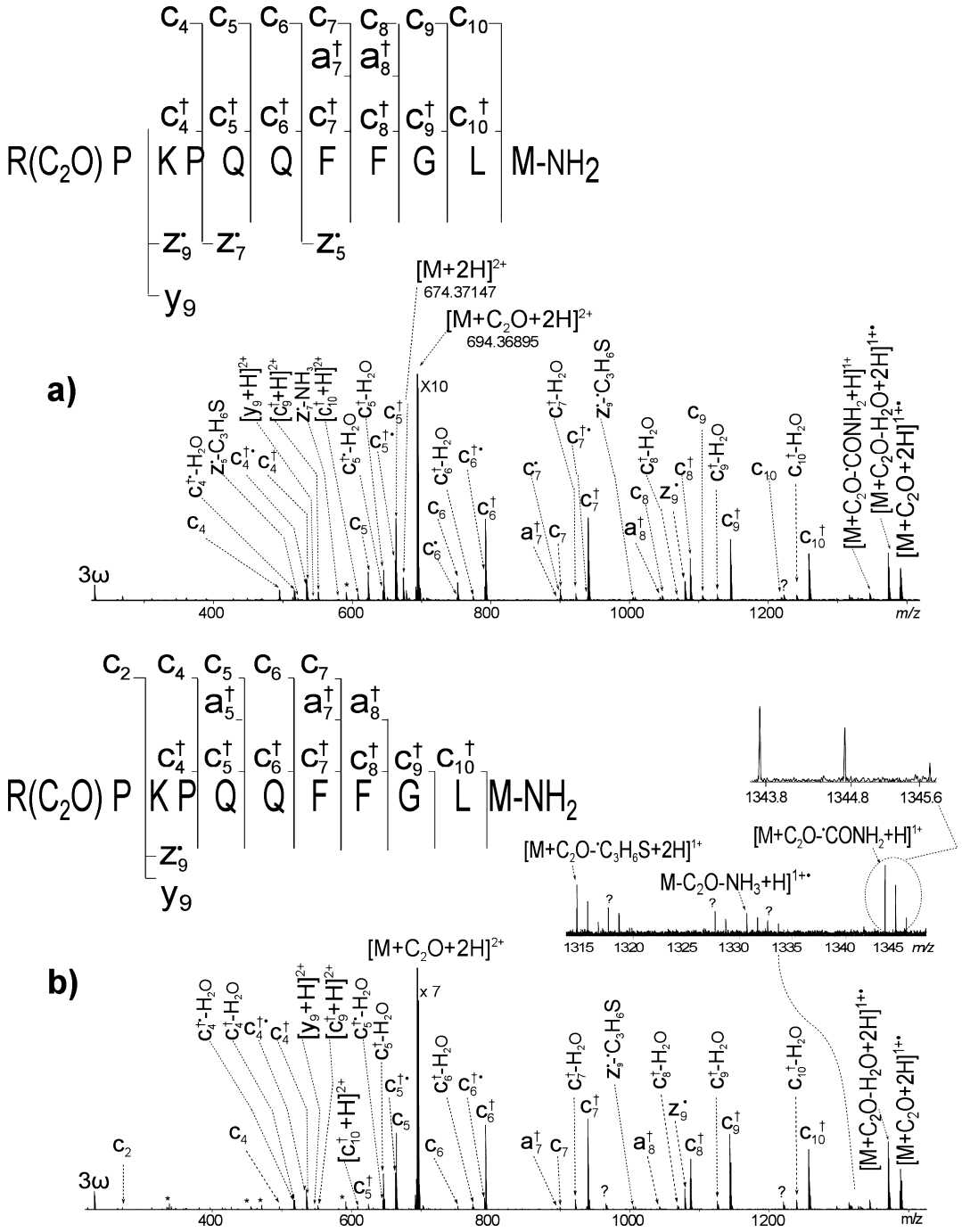

Figure 2. Glyoxal-derived AGEs of substance P for the parent ion $[M + C_2O + 2H]^{2+}$ in $MeOH/H_2O$ (50:50): (a) ECD spectrum; (b) DR(674.37)−ECD(694.37) spectrum with ejection of $[M + 2H]^{2+}$. The symbol ? indicates unassigned peaks by the current understanding of the fragmentation mechanism, and ∗ indicates background peaks where not isotopologues were observed.

and plotted in Figure 3. I_i of the c fragment ions decreased and I_i of $c^{\dagger}$ and $z_9^{\bullet}$ fragment ions increased during the DR−ECD experiment. Thus, based on those results, it is inferred that all c fragment ions observed in the DR−ECD and ECD spectrum are secondary fragments of the unmodified $[M + 2H]^{2+}$ ion and are derived from a long-lived radical intermediate species (millisecond to microsecond time frame).[49] Additionally, from Figure 3, the radical fragment $z_9^{\bullet}$ is considered a long-lived species[49] and is a fragment from the doubly charged modified species.

The $c^{\dagger}_n$ fragment ions locate the C_2O modification within four residues of the N-terminus, and the presence of $z_9^{\bullet}$ and y_9 in Figure 2b, indicate an unmodified lysine. Thus, this glyoxal-derived AGEs for substance P is located at the arginine residue and more specifically at the guanidine group.[49] The guanidine group reacts with glyoxal causing the loss of water and resulting in the net addition of C_2O (39.9949 Da), which can form

dx.doi.org/10.1021/ac301583d | Anal. Chem. 2012, 84, 10568−10575

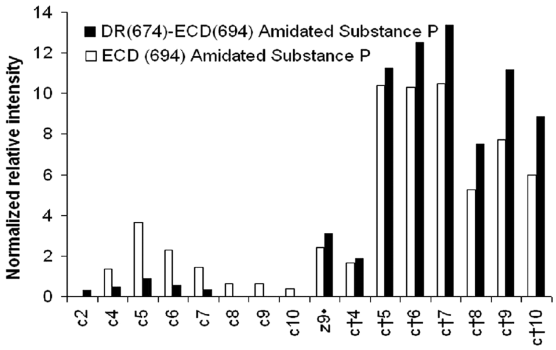

Figure 3. Comparison of the relative intensity of the c_n and $c^{\dagger}_n$ (n = 2–10) fragment ions of the parent ion $[M + C_2O + 2H]^{2+}$ for the ECD and DR(674.37)–ECD(694.36) spectra of glyoxal-derived AGEs of the normal form of substance P (amidated at the C-terminus). The relative intensity of each c_n and $c^{\dagger}_n$ fragment ion was calculated by application of eq S-1 (Supporting Information) where I_i is the relative intensity of the ion.

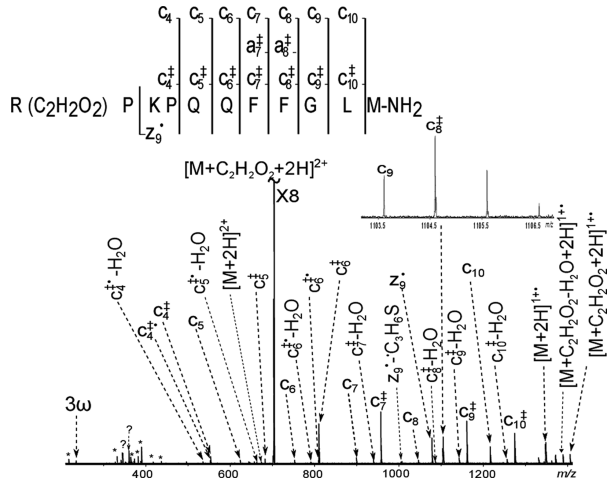

Figure 4. DR(674.37)–ECD(703.37) spectrum with ejection of $[M + 2H]^{2+}$ of the parent ion $[M + C_2O_2H_2 + 2H]^{2+}$. The symbol ? indicates unassigned peaks by the current understanding of the fragmentation mechanism, and ∗ indicates background peaks where not isotopologues were observed.

structure **b** and/or structure **c** (hydroxyimidazole) shown in Scheme 1.

Substance P Modified by $C_2H_2O_2$. Figure 4 shows the DR(674.37)–ECD(703.37) spectrum of the parent ion $[M + C_2H_2O_2 + 2H]^{2+}$ with unmodified c_n and modified $c^{\ddagger}_n$ (n = 4–10) fragment ion. The double-dagger (‡) symbol is added to the standard Roepstorff nomenclature to identify the modified fragments. $z_9^{\bullet}$ radical fragment ion, side chain losses, and up to two losses of water from the $c^{\ddagger}$ fragment ions are observed in Figure 4, with absence of c_2, $c^{\ddagger}_2$, $c^{\dagger}_1/z_{10}^{\bullet}$, and $c^{\dagger}_3/z_8^{\bullet}$ fragment ions. Thus, according with those results the modified $c^{\ddagger}_n$ (n = 4–10) fragment ions locate the modification $C_2H_2O_2$ toward the N-terminus and the presence of $z_9^{\bullet}$ indicate that the lysine is unmodified. This modification is located also at the arginine residue (Scheme 1, structures **e** and **f**), where glyoxal dihydrate (94.0266 Da, $C_2H_6O_4$) binds to the guanidine group forming the dihydroxyimidazoline group by the loss of two molecules of water.

All the results of the ECD and DR–ECD spectra for the parent ions $[M + C_2O + 2H]^{2+}$ (Figure 2), and $[M + C_2H_2O_2 + 2H]^{2+}$ (Figure 4), shared three features. First, the absence of the complementary pair $c^{\dagger}_1/z_{10}^{\bullet}$, $c^{\dagger}_3/z_8^{\bullet}$, $c^{\ddagger}_1/z_{10}^{\bullet}$, and $c^{\ddagger}_3/z_8^{\bullet}$ that is due to proline; which requires cleavage of two bonds in order to observe the fragments.[51] Second, c_2 was absent in the ECD spectrum (Figure 2a), but appeared in the DR–ECD spectrum (Figure 2b), whereas $c^{\dagger}_2$ and $c^{\ddagger}_2$ were completely absent, which is attributed to the low abundance of the c_2 fragment ion from unmodified substance P, rarely observed in the ECD spectrum.[52,51] Third, the loss of water from every $c^{\dagger}$ and $c^{\ddagger}$ fragment ion, is attributed to the glyoxal modification. So, it was hypothesized that hydrogen bond interactions may be involved for both glyoxal modifications, which may be broken during the ECD event causing the loss of water. Thus, IRMPD was applied to amidated substance P, prior to the ECD experiment, in order to facilitate disruption of the noncovalent interactions (Supporting Information, Figure S-1). The obtained relative intensity of the $c^{\dagger}_n$ and $c^{\dagger}_n - H_2O$ (n = 4–10) fragment ions was normalized using eq S-1 (Supporting Information) and plotted in Figure 5. It is observed that I_i of $c^{\dagger}_n$

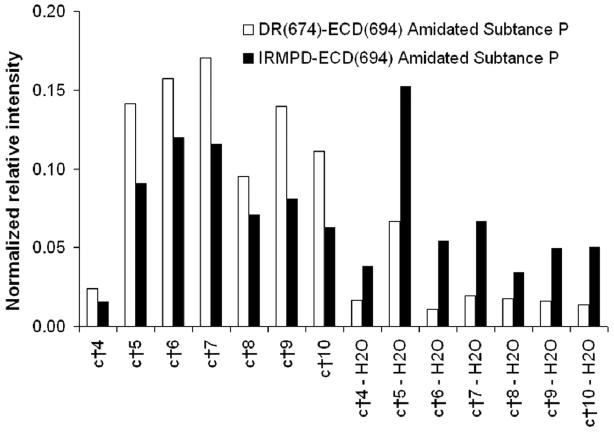

Figure 5. Comparison of relative intensity of the $c^{\dagger}_n$ and $c^{\dagger}_n - H_2O$ fragment ions for the DR(674.37)–ECD(694.37) and IRMPD–ECD spectra of glycated amidated substance P. The relative intensity was calculated using eq S-1 (Supporting Information), only considering the relative intensity of the $c^{\dagger}_n$ and $c^{\dagger}_n - H_2O$ fragment ions.

$- H_2O$ (n = 4–10) during the IRMPD–ECD experiment increased in all observed fragments. Thus, use of infrared heating to disrupt the hydrogen bonding network induced water loss from the glyoxal-derived AGEs.

On the basis of the previous results it is possible to propose an ECD mechanism for the loss of water of the glyoxal-derived AGEs for substance P. Therefore, after the electron is captured in the peptide, it is suggested that the modified guanidine group at the arginine residue loses water forming the imidazole radical moiety, as shown in Scheme 2a. Moreover, for the dihydroxyimidazoline group, it is proposed that the capture of the electron initially generates the loss of one molecule of water forming an intermediate structure. The imidazole ring (structure II in Scheme 2b) is formed by an extra loss of water that is not driven by the radical, although the energy deposited during electron capture, as well as the additional stabilization energy from conjugation of the π system with the radical, would promote this additional loss.

dx.doi.org/10.1021/ac301583d | Anal. Chem. 2012, 84, 10568–10575

Scheme 2. Proposed Reaction Mechanism of the Loss of Water after Electron Capture Dissociation from the Glyoxal-Derived Glycation Products (AGE) Formed at the Guanidine Group[a]

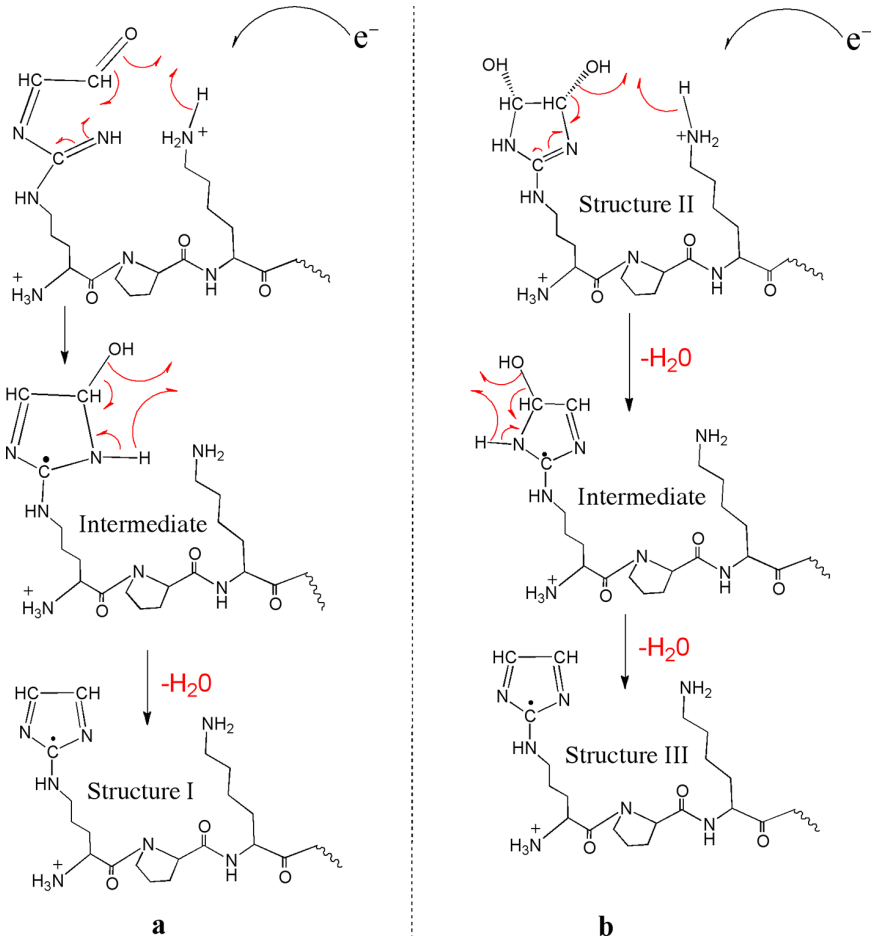

[a](a) The AGE product formed at the guanidine group (open ring) loses one molecule of water after electron capture generating the radical imidazole moiety structure I. (b) The 3,4-dihydroxyimidazole (structure II) loses one molecule of water after electron capture generating the intermediate structure, but the extra loss of water that originates the radical imidazole moiety structure III is not driven by the capture of another electron.

Fragmentation with CAD, for both glyoxal-derived AGEs (modifications with net addition of C_2O and $C_2H_2O_2$), for amidated substance P agrees with the ECD and DR–ECD results, and the spectra are shown in the Supporting Information (Figure S-2, Tables S-5 and S-6). Moreover, similar results were obtained about the types (net addition of C_2O and $C_2H_2O_2$) and binding sites of glyoxal-derived AGEs formed for the free acid form of substance P. DR(674.86)–ECD(694.86), DR(674.86)–ECD(703.86), and CAD results for both types of glyoxal-derived AGEs for the free acid form of substance P are available in the Supporting Information (Figure S-3, Tables S-7–S-10).

Additionally, as was mentioned before, similar glyoxal-derived AGEs formed for amidated substance P were observed under biological conditions (modifications with net addition of C_2O and $C_2H_2O_2$). Thus, further analysis of the DR–ECD and CAD spectrum of both parent ions $[M + C_2O + 2H]^{2+}$ and $[M + C_2H_2O_2 + 2H]^{2+}$ showed that glyoxal-derived AGES and dihydrated glyoxal-derived AGEs are modified at the guanidine group in the arginine moiety (refer to Figure S-4 and Tables S-11–S-14 in the Supporting Information). This preferred glycation site, that does not change at physiological conditions (pH 7.5), can be explained from the high pK_a of arginine compared with lysine or the N-terminus amino group (pK_a 12.48, 10.53, and 9.0, respectively).[50] Moreover, studies of glyoxal with only arginine found that protonation of one of the three nitrogen atoms at the side chain did not limit the reactivity of the guanidine group, and products at the N-terminus (α-amino group) rarely happen.[49] Glycation at the amide group of glutamine residues was not observed that can be attributed to the lowest nucleophilicity (low basicity) of the lone pair of the nitrogen atom. Thus, it can be concluded that different conformers may be present as a result of glycation by glyoxal, particularly the creatinine conformer generated at the guanidine group of arginine, which is used as a biomarker in renal failure. Although in this work no evidence was found for intramolecular or intermolecular cross-linking, the formation of imidazolone (a common product found in methylglyoxal-derived glycation products)[53] or diglycation[54] longer reaction times may show otherwise.

dx.doi.org/10.1021/ac301583d | Anal. Chem. 2012, 84, 10568–10575

CONCLUSIONS

In studying the types of glyoxal-derived AGEs, at physiological conditions (pH 7.5), of amidated and free acid form of substance P by FTICR-MS, use of CAD, ECD, and double-resonance ECD experiments allowed confident assignment of the binding site to the side chain guanidine group of arginine. The intermediates hydroxyimidazoline and dihydroxyimidazoline products, at the arginine residue, were also detected by DR−ECD and CAD fragmentation. In the ECD, DR−ECD, and IRMPD−ECD experiments carried out a characteristic loss of water from every modified $c^{\dagger}_{n}$ and $c^{\ddagger}_{n}$ fragment was observed. Thus, it is proposed that the electron is captured at the modification site and subsequent water occurs in addition to the typical fragmentation pattern of the peptide at the backbone N−Cα bond.

This work represents a first approach to understand glycation by α-dicarbonyl compounds and the types of glyoxal-derived AGEs formed, including the potential artifacts given by the use of methanol during sample preparation. However, further research needs to be carried out in order to determine whether same types of glyoxal-derived AGEs are formed in other peptides under similar solution conditions and temperature. In order to extend this research into analysis of clinical samples, additional understanding of competitive binding between the residues and between peptides in complex biological samples will be needed. However, the current research has defined some of the fundamental chemistry involved in glyoxal binding to arginine-containing peptides.

ASSOCIATED CONTENT

Supporting Information

Additional information as noted in text. This material is available free of charge via the Internet at http://pubs.acs.org.

AUTHOR INFORMATION

Corresponding Author

*Phone: +44 024 7615 1008. Fax: +44 024 7615 1009. E-mail: p.oconnor@warwick.ac.uk.

Notes

The authors declare no competing financial interest.

ACKNOWLEDGMENTS

Financial support from the Warwick Centre for Analytical Science (EPSRC-funded Grant EP/F034210/1) is gratefully acknowledged. The authors also thank Isolda Romero for the NMR results and Dr. Carlos Duque, Dr. David Kilgour, Pilar Perez-Hurtado, Rebecca Wills, Huilin Li, and Tzu-Yung Lin, for their helpful discussions.

REFERENCES

(1) Thornalley, P. J. *Environ. Health Perspect.* **1985**, *64*, 297−307.
(2) Abordo, E. A.; Minhas, H. S.; Thornalley, P. J. *Biochem. Pharmacol.* **1999**, *58*, 641−648.
(3) Anderson, M. M.; Haxen, S. L.; Hsu, F. F.; Heinecke, J. W. *J. Clin. Invest.* **1997**, *99*, 424−432.
(4) Awada, M.; Dedon, P. C. *Biochemistry* **2001**, *40*, 8649−8650.
(5) Loidl-Stahlhofen, A.; Spiteller, G. *Biochim. Biophys. Acta* **1994**, *1211*, 156−160.
(6) Namiki, O. *Adv. Food Res.* **1988**, *32*, 115−184.
(7) Odani, H.; Shinzato, T.; Usami, J.; Matsumoto, Y.; Frye, E. B.; Baynes, J. W.; Maeda, K. *FEBS Lett.* **1998**, *427*, 381−385.
(8) Rabbani, N.; Thornalley, P. J. *Amino Acids* **2011**, *42*, 1133−1142.
(9) Beisswenger, P. J.; Howell, S. K.; Nelson, R. G.; Mauer, M.; Szwergold, B. S. *Biochem. Soc. Trans.* **2003**, *31*, 1358−1363.
(10) Rabbani, N.; Sebekova, K.; Heidland, A.; Thornalley, P. J. *Kidney Int.* **2007**, *72*, 1113−1121.
(11) Makita, Z.; Yanagisawa, K.; Kuwajima, S.; Yoshioka, N.; Atsumi, T.; Hasunuma, Y.; Koike, T. *J. Diabetes Complications* **1995**, *9*, 265−268.
(12) Deguchi, T.; Kusuhara, H.; Takadate, A.; Endou, H.; Otagiri, M.; Sugiyama, Y. *Kidney Int.* **2004**, *65*, 162−174.
(13) Thornalley, P. J. *Int. Rev. Neurobiol.* **2002**, *50*, 37−57.
(14) Karachalias, N.; Babaei-Jadidi, R.; Rabbani, N.; Thornalley, P. J. *Diabetologia* **2010**, *53*, 1506−1516.
(15) Degenhardt, T. P.; Thorpe, S. R.; Baynes, J. W. *Cell. Mol. Biol.* **1998**, *44*, 1139−1145.
(16) Thornalley, P. J.; Battah, S.; Ahmed, N.; Karachalias, N.; Agalou, S.; Babaei-Jadidi, R.; Dawnay, A. *Biochem. J.* **2003**, *375*, 581−592.
(17) Zhang, Y.; Cocklin, R. R.; Bidasee, K. R.; Wang, M. *J. Biomol. Tech.* **2003**, *14*, 224−230.
(18) Montgomery, H.; Tanaka, K.; Belgacem, O. *Rapid Commun. Mass Spectrom.* **2010**, *24*, 841−848.
(19) Brancia, F. L.; Bereszczak, J. A.; Lapola, A.; Fedele, D.; Baccarin, L.; Seraglia, R.; Traldi, P. *J. Mass Spectrom.* **2006**, *41*, 1179−1185.
(20) Ahmed, N.; Dobler, D.; Dean, M.; Thornalley, P. J. *J. Biol. Chem.* **2005**, *280*, 5724−5732.
(21) Lapolla, A.; Fedele, D.; Reitano, R.; Aricò, N. C.; Seraglia, R.; Traldi, P.; Marotta, E.; Tonani, R. *J. Am. Soc. Mass Spectrom.* **2004**, *15*, 496−509.
(22) Cotham, W. E.; Metz, T. O.; Ferguson, P. L.; Brock, J. W. C.; Hinton, D. J. S.; Thorpe, S. R.; Baynes, J. W. *Mol. Cell. Proteomics* **2004**, *3*, 1145−1153.
(23) Wynne, C.; Edwards, N. J.; Fenselau, C. *Proteomics* **2010**, *10*, 3631−3643.
(24) Zubarev, R. A.; Kelleher, N. L.; McLafferty, F. W. *J. Am. Chem. Soc.* **1998**, *120*, 3265−3266.
(25) Stefanowicz, P.; Kijewska, M.; Szewczuk, Z. *J. Mass Spectrom.* **2009**, *44*, 1047−1052.
(26) Syka, J. E. P. *Proc. Natl. Acad. Sci. U.S.A.* **2004**, *101*, 9528−9533.
(27) Harrison, R.; Hitchen, P. G.; Panico, M.; Morris, H. R.; Mekhaiel, D.; Pleass, R. J.; Dell, A.; Hewitt, J. E.; Hasla, S. M. *Glycobiology* **2012**, *22*, 662−675.
(28) Leymarie, N.; McCobb, M.; Naymy, H.; Staples, G. O.; Zaia, J. *Int. J. Mass Spectrom.* **2012**, *312*, 144−154.
(29) Benshnbg, L.; Held, J. M.; Schilling, B.; Danielson, S. R.; Gibson, B. W. *J. Proteomics* **2011**, *74*, 2510−2521.
(30) Zhang, Q.; Schepmoes, A. A.; Brock, J. W. C.; Wu, S.; Moore, R. J.; Purvine, S. O.; Baynes, J. W.; Smith, R. D.; Metz, T. O. *Anal. Chem.* **2008**, *80*, 9822−9829.
(31) Zhao, C.; Sethuraman, M.; Clavreul, N.; Kaur, P.; Cohen, R. A.; O'Connor, P. B. *Anal. Chem.* **2006**, *78*, 5134−5142.
(32) Kelleher, N. L.; Zubarev, R. A.; Bush, K.; Furie, B. C.; McLafferty, F. W.; Walsh, C. T. *Anal. Chem.* **1999**, *71*, 4250−4253.
(33) Hakansson, K.; Cooper, H. J.; Emmett, M. R.; Costello, C. E.; Marshall, A. G.; Nilson, C. L. *Anal. Chem.* **2001**, *73*, 4530−4536.
(34) Mirgorodskaya, E.; Hassan, H.; Clausen, H.; Roepstorff, P. *Anal. Chem.* **2001**, *73*, 1263−1269.
(35) Wang, Z.; Udeshi, N. D.; ÓMalley; Shabanowitz, J.; Hunt, D. F.; Hart, G. W.; Gobert, J. *Mol. Cell. Proteomics* **2010**, *9*, 153−160.
(36) Cournoyer, J. J.; Lin, C.; O'Connor, P. B. *Anal. Chem.* **2006**, *78*, 1264−1271.
(37) Sargaeva, N. P.; Lin, C.; O'Connor, P. B. *Anal. Chem.* **2011**, *83*, 6675−6682.
(38) Kua, J.; Hanley, S. W.; Haan, D. O. D. *J. Phys. Chem. A* **2008**, *112*, 66−72.
(39) Whipple, E. B. *J. Am. Chem. Soc.* **1970**, *92*, 7183−7186.
(40) Nakajima, K.; Ohta, K.; Mostefaoui, T. A.; Chai, W.; Utsukihara, T.; Horiuchi, C. A.; Murakami, M. *J. Chromatogr., A* **2007**, *1161*, 338−341.
(41) Caravatti, P.; Alleman, M. *Org. Mass Spectrom.* **1991**, *26*, 514−518.

(42) Tsybin, Y. O.; Håkansson, P.; Budnik, B. A.; Haselmann, K. F.; Kjeldsen, F.; Gorshkov, M.; Zubarev, R. A. *Rapid Commun. Mass Spectrom.* **2001**, *15*, 1849−1854.
(43) Comisarow, M. B.; Grassi, V.; Parisor, G. *Chem. Phys. Lett.* **1978**, *57*, 413−416.
(44) Beauchamp, J. L. *Rev. Sci. Instrum.* **1969**, *40*, 123.
(45) He, H.; Emmett, M.; Nilsson, C. L.; Conrad, A. C.; Marshall, A. G. *Int. J. Mass Spectrom.* **2011**, *305*, 116−119.
(46) Tsybin, Y. O.; Witt, M.; Baykut, G.; Kjeldsen, F.; Håkansson, P. *Rapid Commun. Mass Spectrom.* **2003**, *17*, 1759−1768.
(47) De Haan, D. O.; Corrigan, A. L.; Smith, K. W.; Stroiik, D. R.; Turley, J. J.; Lee, F. E.; Tolbert, M. A.; Cordova, K. E.; Ferrell, G. R. *Environ. Sci. Technol.* **2009**, *43*, 2818−2824.
(48) Roepstorff, P.; Fohlman, J. *Biomed. Mass Spectom.* **1984**, *11*, 601.
(49) Lin, C.; Cournoyer, J. J.; O'Connor, P. B. *J. Am. Soc. Mass Spectrom.* **2006**, *17*, 1605−1615.
(50) Bunn, H. F.; Shapiro, R.; McManus, M.; Garrick, L.; McDonald, M. J.; Gallop, P. M.; Gabbay, K. *J. Biol. Chem.* **1979**, *254*, 3892−3898.
(51) Axelsson, J.; Palmblad, M.; Håkansson, K.; Håkansson, P. *Rapid Commun. Mass Spectrom.* **1999**, *13*, 474−477.
(52) Tsybin, Y. O.; Haselmann, K. F.; Emmett, M. R.; Hendrickson, C. L.; Marshall, A. G. *J. Am. Soc. Mass Spectrom.* **2006**, *17*, 1704−1711.
(53) Ahmed, N.; Thornalley, P. J.; Dawczynski, J.; Franke, S.; Strobel, J.; Stein, G.; Haik, G. M. *Invest. Ophthalmol. Visual Sci.* **2003**, *44*, 5287−5292.
(54) Mittelmainer, S.; Pischetsrieder, M. *Anal. Chem.* **2011**, *83*, 9660−9668.

References

[1] Shutskaya, Z. V. and Shakhmatova, E. I. and Kuznetsova, A. A. and Natochin, Yu. V. The role of the kidneys in the regulation of osmolality and concentrations of cations in the blood serum in hyperglycemia. *Human Physiology*, 34(5):601–607, 2008.

[2] Adler, A. I. and Stevens, R. J. and Manley, S. E. and Bilous, R. W. and Cull, C. A. and Holman, R.R. Development and progression of neprhopathy in type 2 diabetes: The united Kingdom prospective diabetes study (UKPDS 64). *Kidney Int.*, 63:225–232, 2003.

[3] Knezevic, M. Estimating the long-term costs of diabetic kidney disease: an economic approach. *Appl. Econ. Lett.*, 16:1059–1064, 2009.

[4] Lapolla, A and Traldi, P and Fedele, D. Importance of measuring products of non-enzymatic glycation of proteins. *Clin. Biochem.*, 38(2):103–15, 2005.

[5] Thornalley, P J. Monosaccharide autoxidation in health and disease. *Environ. Health Perspect.*, 64:297–307, 1985.

[6] Ahmed, N. Advanced glycation endproducts–role in pathology of diabetic complications. *Diabetes Res. Clin. Pr.*, 67(1):3–21, 2005.

[7] Cooper, H. J. and Hakansson, K. and Marshall, A. G. The role of electron capture dissociation in biomolecular analysis. *Mass Spectrom. Rev.*, 24:201–222, 2005.

[8] Zubarev, R. A. and Kelleher, N L. and McLafferty, F W. Electron Capture Dissociation of Multiply Charged Protein Cations. A Nonergodic Process. *J. Am. Chem. Soc.*, 120(13):3265–3266, 1998.

[9] Jennings, K R. The changing impact of the collision-induced decomposition of ions on mass spectrometry. *Int. J. Mass Spectrom.*, 200(1-3):479–493, 2000.

[10] Mirgorodskaya, E. and Roepstorff, P. and Zubarev, R. A. Localization of O-Glycosylation Sites in Peptides by Electron Capture Dissociation in a Fourier Transform Mass Spectrometer. *Anal. Chem.*, 71(20):4431–4436, 1999.

[11] El-Aneed, A and Cohen, A and Banoub, J. *Mass Spectrometry, Review of the Basics: Electrospray, MALDI, and Commonly Used Mass Analyzers*, volume 44. 2009.

[12] McLafferty, F W and Turecek, F. *Interpretation of Mass Spectra 4th Edition*. Univeristy Science Books, Sausalito, Califronia, U.S.A, 1993.

[13] De Hoffman, E. and Stroobant, V. *Mass Spectrometry principles and applications.* John Wiley & Sons, London, 2007.

[14] Davis, R and Fearson, M. *Mass Spectrometry: Analytical Chemistry by Open Learning*. 1987.

[15] Fenn, J B. Mass spectrometric implications of high-pressure ion sources. *Int. J. Mass Spectrom.*, 200:459–478, 2000.

[16] Houk, R. S. and Fassel, V. A. and Flesch, G. D. and Svec, H. J. and Gray, A. L. and Taylor, C. H. Inductively coulpled argon plasma as an ions source for mass spectrometric determination of trace elements. *Anal. Chem.*, 52:2283–2289, 1980.

[17] Karas, M. and Bachmann, D. and Bahr, U. and Hillenkamp, F. Matrix-assisted ultraviolet laser desorption of non-volatile compounds. *Int. J. Mass Spectrom.*, 78 (24):53–68, 1987.

[18] Tanaka, K and Waki, H and Ido, Y and Akita, Sa and Yoshida, Y and Yoshida, T and Matsuo, T. Protein and polymer analyses up to m/z 100,000 by laser ionization time-of-flight mass spectrometry. *Rapid Commun. Mass Spectrom.*, 2 (8):151–153, 1988.

[19] Zenobi, R. and Knochenmuss, R. Ion formation in MALDI mass spectrometry. *Mass Spectrom. Rev.*, 17:337–366, 1998.

[20] Wilm, M S and Mann, M. Electrospray and Taylor-Cone theory , Dole's beam of macromolecules at last ? *Int. J. Mass Spectrom.*, 136:167–180, 1994.

[21] Wu, X. and Oleschuk, R. D. and Cann, N. M. Characterization of microstructured fibre emitters: in pursuit of improved nano electrospray ionization performance. *Analyst*, 137:4150, 2012.

[22] Fenn, J B and Mann, Ma and Meng, C K and Wong, S F and Whitehouse, C M. Electrospray Ionization of Large for Mass Spectrometry Biomolecules. *Science*, 246(4926):64–71, 1989.

[23] Konermann, L and Ahadi, E and Rodriguez, A D and Vahidi, S. Unraveling The Mechanism of Electrospray Ionization. *Anal. Chem.*, 85:2–9, 2013.

[24] Dole, M. and Mack, L. L. and Hines, R. L. and Mobley, R. C. and Ferguson, L. D. and Alice, M. B. *J. Chem. Phys.*, 49:5, 1968.

[25] Thomson, B.A. and Iribarne, J. V. Field induced ion evaporation from liquid surfaces at atmospheric pressure. *J. Chem. Phys.*, 71:4451, 1979.

[26] Grimm, R. L. and Beauchamp, J. L. Field-induced droplet ionization mass spectrometry. *J. Phys. Chem. B.*, 107:14161–14163, 2003.

[27] Wilm, M and Mann, M. Analytical properties of the nanoelectrospray ion source. *Anal.Chem.*, 68:1–8, 1996.

[28] March, R.E. and Hughes, R.J. *Quadrupole Storage Mass Spectrometry*. John Wiley & Sons, Inc., New York, 1989.

[29] Hu, Q. and Noll, R. J. and Li, H. and Makarov, A. and Hardman, M. and Cooks, G. R. The Orbitrap: a new mass spectrometer. *J. Mass Spectrom.*, 40:430–443, 2005.

[30] Shvartsburg, A. A., and Smith, R. D. Fundamentals of traveling wave ion mobility spectrometry. *Anal. Chem.*, 80:9689–9699, 2008.

[31] Marshall, A. G. and Hendrickson, C. L. and Jackson, G. S. Fourier transform ion cyclotron resonance mass spectrometry: a primer. *Mass Spectrom. Rev.*, 17(1): 1–35, 1998.

[32] Barrow, M. P. and Burkitt, W. I. and Derrick, P. J. Principles of Fourier transform ion cyclotron resonance mass spectrometry and its application in structural biology. *Analyst*, 130(1):18–28, 2005.

[33] Ledford, E. B. and Rempel, D. L. and Gross, M. Space-charge effects in Fourier-transform mass-spectrometry - mass calibration. *Anal. Chem.*, 56:2744–2748, 1984.

[34] Guan, S. and Marshall. A. G. Stored waveform inverse Fourier transform (SWIFT) ion excitation in trapped-ion mass spectrometry: Theory and applications. *Int. J. Mass Spectrom.*, 157-158:5–37, 1996.

[35] Aizikov, K. and Mathur, R. and O'Connor P. B. The spontaneous loss of coherence catastrophe in Fourier Transform Ion Cyclotron Resonance Mass Spectrometry. *J. Am. Soc. Mass Spectrom.*, 20:247–256, 2009.

[36] Horn, D. M. and Ge, Y. and McLafferty, F. W. Activated ion electron capture dissociation for mass spectral sequencing of larger (42 kDa) proteins. *Anal. Chem.*, 72(20):4778–84, 2000.

[37] Hakansson, K. and Chalmers, M. J and Quinn, J. P and Mcfarland, M. A. and Hendrickson, C. L. and Marshall, A. G. Combined Electron Capture and Infrared Multiphoton Dissociation for Multistage MS / MS in Fourier Transform Ion Cyclotron Resonance Mass Spectrometer. *Anal. Chem.*, 75(13):3256–3262, 2003.

[38] Mikhailov, V. A. and Cooper, H. J. Activated Ion Electron Capture Dissociation (AI ECD) of proteins: synchronization of infrared and electron irradiation with ion magnetron motion. *J. Am. Soc. Mass. Spectrom.*, 20:763–771, 2009.

[39] Tsybin, Y. O. and Witt, M. and Baykut, G. and Kjeldsen, F. and Hakansson, P. Combined infrared multiphoton dissociation and electron capture dissociation with a hollow electron beam in Fourier transform ion cyclotron resonance mass spectrometry. *Rapid Commun. Mass Spectrom.*, 17(15):1759–1768, 2003.

[40] Shi, S. D. and Hemling, M. E. and Carr, S. A. and Horn, D. M. and Lindh, I. and McLafferty, F. W. Phosphopeptide/phosphoprotein mapping by electron capture dissociation mass spectrometry. *Anal. Chem.*, 73(1):19–22, 2001.

[41] Mirgorodskaya, E. and Hassan, H. and Clausen, H. and Roepstorff, P. Mass spectrometric determination of O-glycosylation sites using beta-elimination and partial acid hydrolysis. *Anal. Chem.*, 73(6):1263–1269, 2001.

[42] Kelleher, N. L. and Zubarev, R. A. and Bush, K. and Furie, B. C. and McLafferty, F. W. and Walsh, C T. Localization of labile posttranslational modifications by electron capture dissociation: the case of gamma-carboxyglutamic acid. *Anal. Chem.*, 71(19):4250–4253, 1999.

[43] Zubarev, R. A. and Horn, D. M. and Fridriksson, E. K. and Kelleher, N. L. and Kruger, N. A. and Lewis, M. A. and Carpenter, B. K. and McLafferty, F. W. Electron capture dissociation for structural characterization of multiply charged protein cations. *Anal. Chem.*, 72(3):563–573, 2000.

[44] Whitelegge, J. P. and Zabrouskov, V. and Halgand, F. and Souda, P. and Bassilian, S. and Yan, W. and Wolinsky, L. and Loo, J. A and Wong, D. T. W. and Faull, K. F. Protein-Sequence Polymorphisms and Post-translational Modifications in Proteins from Human Saliva using Top-Down Fourier-transform Ion Cyclotron Resonance Mass Spectrometry. *Int. J. Mass Spectrom.*, 268(2-3):190–197, 2007.

[45] Bergquist, J and Palmblad, M. and Wetterhall, M. and Hakansson, P. and Markides, K. E. Peptide mapping of proteins in human body fluids using electrospray ionization Fourier transform ion cyclotron resonance mass spectrometry. *Mass Spectrom. Rev.*, 21(1):2–15, 2002.

[46] Bogdanov, B. and Smith, R. D. Proteomics by FTICR mass spectrometry: top down and bottom up. *Mass Spectrom. Rev.*, 24(2):168–200, 2005.

[47] Roepstorff, P. and Fohlman, J. Proposal for a common nomenclature for sequence ions in mass spectra of peptides. *Biomed. Mass Spectrom.*, 11(11):601, 1984.

[48] Biemann, K. Nomenclature for peptide fragment ions (positive ions). *Methods Enzymol.*, 193:886–887, 1990.

[49] Todd, J. and McLafferty, F. W. Collisionally Actived decompositions of gaseous ions: the effect of multiple collision. *Int. J. Mass Spectrom.*, 38:371–378, 1981.

[50] Haddon, W. F. and McLafferty, F. W. Metastable Ion characteristics. VII. Collision-Induced Metastables. *J. Am. Chem. Soc.*, 90:4745–4746, 1968.

[51] Jennings, K. R. colllision-induced decompositions of aromatic ions. *Int. J . Mass Spectrom.*, 1:227–235, 1968.

[52] Laskin, J. and Futrell, J. H. Collisional activation of peptide ions in FT-ICR mass spectrometry. *Mass Spectrom. Rev.*, 22(3):158–81, 2003.

[53] Mcluckey, S. A. and Goeringer, D. E. Slow Heating Methods in Tandem Mass Spectrometry. *J. Mass Spectrom.*, 32:461–474, 1997.

[54] Wysocki, V. H. and Resing, K. A. and Zhang, Q. and Cheng, G. Mass spectrometry of peptides and proteins. *Methods*, 35(3):211–222, 2005.

[55] Zhao, C. and Sethuraman, M. and Clavreul, N. and Kaur, P. and Cohen, R. A. and O'Connor, P. B. Detailed map of oxidative post-translational modifications of human p21ras using Fourier transform mass spectrometry. *Anal. Chem.*, 78(14): 5134–5142, 2006.

[56] Zhao, C. and Xie, B. and Chan, S. and Costello, C. E. and O'Connor, P. B. Collisionally activated dissociation and electron capture dissociation provide complementary structural information for branched permethylated oligosaccharides. *J. Am. Soc. Mass Spectrom.*, 19(1):138–50, 2008.

[57] J. Zhao, T. Shoeib, K.W. M. Siu, and A. C. Hopkinson. The fragmentation of protonated tyrosine and iodotyrosines: The effect of substituents on the losses of NH_3 and of H_2O and CO. *Int. J. Mass Spectrom.*, 255-256:265–278, 2006.

[58] Lioe, H. and O'Hair, R. J. Comparison of collision-induced dissociation and electron-induced dissociation of singly protonated aromatic amino acids, cystine and related simple peptides using a hybrid linear ion trap-FT-ICR mass spectrometer. *Anal. Bioanal. Chem.*, 389(5):1429–37, 2007.

[59] Bush, K.L. and Glish, G. L. and McLuckey, S. A. *Mass spectrometry/mass spectrometry: techniques and applications of tandem mass spectrometry*. VCH, New York.

[60] Laskin, J. and Futrell, J. H. Activation of large ions in FT-ICR mass spectrometry. *Mass Spectrom. Rev.*, 24(2):135–67, 2005.

[61] Burlet, O. and Yang, C. and Gaskell, S. Influence of Cysteine to Cysteic Acid Oxidation on the Collision-Activated Decomposition of Protonated Peptides: Evidence for Intraionic Interactions. *J. Am. Soc. Mass Spectrom.*, 130:337–344, 2008.

[62] Wysocki, V. H. and Tsaprailis, G. and Smith, L. L. and Breci, L. A. Mobile and localized protons: a framework for understanding peptide dissociation. *J. Mass Spectrom.*, 35(12):1399–406, 2000.

[63] Bythell, B. J and Somogyi, A. and Paizs, B. What is the structure of b_2 ions generated from doubly protonated tryptic peptides? *J. Am. Soc. Mass Spectrom.*, 20(4):618–24, 2009.

[64] Gucinski, A. C. and Chamot-Rooke, J. and Nicol, E. and Somogyi, A. and Wysocki, V. H. Structural influences on preferential oxazolone versus diketopiperazine b_2^+ ion formation for histidine analogue-containing peptides. *J. Phys. Chem. A*, 116 (17):4296–304, 2012.

[65] Bleiholder, C. and Osburn, S. and Williams, T. D. Suhai, S. and Van Stipdonk, M.

and Harrison, A. G. and Paizs, B. Sequence-Scrambling Fragmentation Pathways of Protonated Peptides. *J. Am. Chem. Soc.*, 3:1775–1789, 2008.

[66] Paizs, B. and Suhai, S. Fragmentation pathways of protonated peptides. *Mass Spectrom. Rev.*, 24(4):508–48, 2005.

[67] Chalmers, M. J. and Hakansson, K. and Johnson, R. and Smith, R. and Shen, J. and Emmett, M. R. and Marshall, A. G. Protein kinase A phosphorylation characterized by tandem Fourier transform ion cyclotron resonance mass spectrometry. *Proteomics*, 4(4):970–981, 2004.

[68] Crowe, M. C. and Brodbelt, J. S. Infrared multiphoton dissociation (IRMPD) and collisionally activated dissociation of peptides in a quadrupole ion trap with selective IRMPD of phosphopeptides. *J. Am. Soc. Mass Spectrom.*, 15:1581–1592, 2004.

[69] Wilson, J. J. and Brodbelt, J. S. Infrared multiphoton dissociation (IRMPD) for enhanced $de\ novo$ sequence interpretation of $N-$terminal sulfonated peptides in a quadrupole ion trap. *Anal. Chem.*, 78:6855–6862, 2006.

[70] Lancaster, K. S. and An, H. J. and Li, B. S. and Lebrilla, C. B. Interrogation of N-linked oligosaccharides using infrared multiphoton dissociation in FT-ICR mass spectrometry. *Anal. Chem.*, 78:4990–4997, 2006.

[71] Zhang, J. H. and Schubothe, K. and Li, B. S. and Russell, S. and Lebrilla, C. B. Infrared multiphoton dissociation of O-linked mucin-type oligosaccharides. *Anal. Chem.*, 77:208–214, 2005.

[72] Pikulski, M. and Hargrove, A. and Shabbir, S. H. and Anslyn, E. and Brodbelt, J. S. Sequence and characterization of oligosaccharides using infrared multiphoton

dissociation and boronic acid derivatization in a quadrupole ion trap. *J. Am. Soc. Mass Spectrom.*, 18:2094–2106, 2007.

[73] Lopez-Clavijo, A. F. and Barrow, M. P. and Rabbani, N. and Thornalley, P. J. and O'Connor, P. B. Determination of types and binding sites of advanced glycation end products for substance P. *Anal. Chem.*, 84(24):10568–10575, 2012.

[74] Tsybin, Y. O. and He, H. and Emmett, M. R. and Hendrickson, C. L. and Marshall, A. G. Ion activation in electron capture dissociation to distinguish between N-terminal and C-terminal product ions. *Anal. Chem.*, 79(20):7596–7602, 2007.

[75] Cournoyer, J. J. and Lin, C. and O'Connor, P. B. Detecting deamidation products in proteins by electron capture dissociation. *Anal. Chem.*, 78(4):1264–1271, 2006.

[76] Perez-Hurtado, P. and O'Connor, P. B. Deamidation of collagen. *Anal. Chem.*, 84 (6):3017–25, 2012.

[77] Leach, F. E. and Wolff, J. J. and Laremore, T. N. and Linhardt, R. J. and Amster, I. J. International Journal of Mass Spectrometry Evaluation of the experimental parameters which control electron detachment dissociation , and their effect on the fragmentation efficiency of glycosaminoglycan carbohydrates. *Int. J. Mass Spectrom.*, 276:110–115, 2008.

[78] Creese, A. J and Cooper, H. J. Liquid Chromatography electron capture dissociation tandem mass spectrometry (LC-MS/MS) versus liquid chromatography collision-induced dissociation tandem mass spectrometry (LC-CID-MS/MS) for the Identification of Proteins. *J. Am. Soc. Mass Spectrom.*, 18:891–897, 2007.

[79] Sweet, S. M. and Cooper, H. J. Electron capture dissociation in the analysis of protein phosphorylation. *Expert Rev. Proteomics*, 4(2):149–159, 2007.

[80] Hakansson, K. and Cooper, H. J. and Emmett, M. R. and Costello, C. E. and Marshall, A. G. and Nilsson, C. L. Electron capture dissociation and infrared multiphoton dissociation MS/MS of an N-glycosylated tryptic peptide to yield complementary sequence information. *Anal. Chem.*, 73(18):4530–4536, 2001.

[81] Liu, H. and Yoo, H. J. and Hakansson, K. Characterization of phosphate-containing metabolites by calcium adduction and electron capture dissociation. *J. Am. Soc. Mass Spectrom.*, 19(6):799–808, 2008.

[82] Horn, D. M. and Zubarev, R. A. and McLafferty, F. W. Automated de novo sequencing of proteins by tandem high-resolution mass spectrometry. *Proc. Natl. Acad. Sci. USA*, 97(19):10313–7, 2000.

[83] McLafferty, F. W. and Horn, D. M. and Breuker, K. and Ge, Y. and Lewis, M. a. and Cerda, B. and Zubarev, R. A. and Carpenter, B. K. Electron capture dissociation of gaseous multiply charged ions by Fourier-transform ion cyclotron resonance. *J. Am. Soc. Mass Spectrom.*, 12(3):245–9, 2001.

[84] Wills, R H and Tosin, M and O'Connor, P B. Structural Characterization of Polyketides Using High Mass Accuracy Tandem Mass Spectrometry. *Anal. Chem.*, 84:8863–8870, 2012.

[85] Mosely, J. A. and Smith, M. J. P. and Prakash, A. S. and Sims, M. and Bristow, A. W. T. Electron-Induced Dissociation of Singly Charged Organic Cations Molecules. *Anal. Chem.*, 83:4068–4075, 2011.

[86] Hakansson, K. and Hudgins, R. R. and Marshall, A. G. and O'Hair, R. A J. Electron capture dissociation and infrared multiphoton dissociation of Oligodeoxynucleotide Dications. *J. Am. Soc. Mass Spectrom.*, 14:23–41, 2003.

[87] Cooper, H. J. Electron capture dissociation Fourier transform ion cyclotron

resonance mass spectrometry of cyclodepsipeptides, branched peptides, and epsilon-peptides. *Int. J. Mass Spectrom.*, 234(1-3):23–35, 2004.

[88] Nousiainen, M. and Vainiotalo, P. and Derrick, P. and Cooper, H. J. and Hoxha, A. and Fati, D. and Trayer, H. and Ward, D. and Trayer, I. Calcium and peptide binding to folded and unfolded conformations of cardiac Troponin C. Electrospray ionization and Fourier transform ion cyclotron resonance mass spectrometry. *Eur. J. Mass Spectrom.*, 8(1):471, 2002.

[89] Namiki, M. Chemistry of Maillard reactions: recent studies on the browning reaction mechanism and the development of antioxidants and mutagens. *Adv. Food Res.*, 32:115–184, 1988.

[90] Degen, J. and Hellwig, M. and Henle, T. 1,2-Dicarbonyl Compounds in Commonly Consumed Foods. *J. Agr. Food Chem.*, 60(28):7071–9, 2012.

[91] Abordo, E. A. and Minhas, H. S. and Thornalley, P. J. Accumulation of alpha-oxoaldehydes during oxidative stress: a role in cytotoxicity. *Biochem. Pharmacol.*, 58(4):641–8, 1999.

[92] Rabbani, N. and Thornalley, P. J. Methylglyoxal, glyoxalase 1 and the dicarbonyl proteome. *Amino Acids*, 42:1133–1142, 2012.

[93] Miyata, T. and Kurokawa, K. and Van Ypersele De Strihou, C. Advanced glycation and lipoxidation end products: role of reactive carbonyl compounds generated during carbohydrate and lipid metabolism. *J. Am. Soc. Nephrol.*, 11(9):1744–1752, 2000.

[94] Anderson, M. M. and Hazen, S. L. and Hsu, F. F. and Heinecke, J. W. Human Neutrophils Employ the Myeloperoxidase – Hydrogen Peroxide – Chloride System to Convert Hydroxy-amino Acids into Glycolaldehyde, 2-Hydroxypropanal, and

Acrolein. A mechanism for the generation of highly reactive alpha-hydroxy and alpha, beta-unsaturated aldehydes by phagocytes at sites of inflammation. *J. Clin. Invest.*, 99(3):424–432, 1997.

[95] Awada, M. and Dedon, P. C. Oxidation of deoxyribose in DNA produces 3'-phosphoglycolaldehyde residues that give rise to glyoxal by a novel phosphonate rearrangement. *Biochemistry*, 40:8649–8650, 2001.

[96] Loidl-Stahlhofen, A. and Spiteller, G. Alpha-hydroxyaldehydes, products of lipid peroxidation. *Biochim. Biophys. Acta*, 1211:156–160, 1994.

[97] Henle, T. Protein-bound advanced glycation endproducts (AGEs) as bioactive amino acid derivatives in foods. *Amino acids*, 29(4):313–22, 2005.

[98] Schwarzenbolz, U. and Mende, S. and Henle, T. Model studies on protein glycation: influence of cysteine on the reactivity of arginine and lysine residues toward glyoxal. *Ann. NY Acad. Sci.*, 1126:248–52, 2008.

[99] Thornalley, P. J. Glycation in diabetic neuropathy. *Int. Rev. Neurobiol.*, 50:37–57, 2002.

[100] Zeng, J. and Dunlop, R. A. and Rodgers, K. J. and Davies, M. J. Evidence for inactivation of cysteine proteases by reactive carbonyls via glycation of active site thiols. *Biochem. J.*, 398:197–206, 2006.

[101] Beisswenger, P. J. and Howell, S. K. and Nelson, R. G. and Mauer, M. and Szwergold, B. S. α -Oxoaldehyde metabolism and diabetic complications. *Biochem. Soc. Trans.*, 31:1358–1363, 2003.

[102] Rabbani, N. and Sebekova, K. and Heidland, A. and Thornalley, P. J. Accumulation of free adduct glycation, oxidation, and nitration products follows acute loss of renal function. *Kidney Int.*, 72(9):1113–1121, 2007.

[103] Makita, Z. and Yanagisawa, K. and Kuwajima, S. and Yoshioka, N. and Atsumi, T. and Hasunuma, Y. and Koike, T. Advanced glycation endproducts and diabetic nephropathy. *J. Diabetes Complications*, 9(4):265–268, 1995.

[104] Deguchi, T. and Kusuhara, H. and Takadate, A. and Endou, H. and Otagiri, M. and Sugiyama, Y. Characterization of uremic toxin transport by organic anion transporters in the kidney. *Kidney Int.*, 65(1):164–174, 2004.

[105] Popova, E. A. and Mironova, R. S. and Odjakova, M. K. Non-enzymatic glycosylation and deglycating enzymes. *Biotechnol. Biotec. Eq.*, 24(3):1928–1935, 2010.

[106] Vanholder, R. and Glorieux, G. and De Smet, R. and Lameire, N. New insights in uremic toxins. *Kidney Int. Supplement*, 63(84):S6–10, 2003.

[107] Miyata, T. and Sugiyama, S. and Saito, A. and Kurokawa, K. Reactive carbonyl compounds related uremic toxicity ("carbonyl stress"). *Kidney Int.*, 59(Suppl. 78): S–25–S–31, 2001.

[108] Ahmed, N. and Dobler, D. and Dean, M. and Thornalley, P. J. Peptide mapping identifies hotspot site of modification in human serum albumin by methylglyoxal involved in ligand binding and esterase activity. *J. Biol. Chem.*, 280:5724–5732, 2005.

[109] Westwood, M. E. and Thornalley, P. J. Molecular characteristics of methylglyoxal-modified bovine and human serum albumins. Comparison with glucose-derived advanced glycation endproduct-modified serum albumins. *Journal Protein Chem.*, 14(5):359–72, 1995.

[110] Klöpfer, A. and Spanneberg, R. and Glomb, M. A. Formation of arginine modifica-

tions in a model system of Nα-tert-butoxycarbonyl (Boc)-arginine with methylglyoxal. *J. Agr. Food Chem.*, 59(1):394–401, 2011.

[111] Cotham, W. E. and Metz, T. O. and Ferguson, P. L. and Brock, J. W. C. and Hinton, D. J. S. and Thorpe, S. R. and Baynes, J. W. and Ames, J. M. Proteomic analysis of arginine adducts on glyoxal-modified ribonuclease. *Mol.Cell. Proteomics*, 3 (12):1145–53, 2004.

[112] Ames, J. M. Mass spectrometry to detect the site specificity of advanced glycation/lipoxidation end-product formation on protein: some challenges and solutions. *Biochem. Soc. Trans.*, 36(Pt 5):1051–4, 2008.

[113] Thornalley, P. J. and Battah, N. and Ahmed, N. and Karachalias, S. and Agalou, R. Babaei-Jadidi, A. and Dawnay, A. Quantitative screening of advanced glycation endproducts in cellular and extracellular proteins by tandem mass spectrometry. *Biochem. J.*, 375:581–592, 2003.

[114] Glomb, M. A. and Lang, G. Isolation and characterization of glyoxal-arginine modifications. *J. Agr. Food Chem.*, 49(3):1493–501, 2001.

[115] Brock, J. W. C. and Hinton, D. J. S. and Cotham, W. E. and Metz, T. O. and Thorpe, S. R. and Baynes, J. W. and Ames, J. M. Proteomic Analysis of the Site Specificity of Glycation and Carboxymethylation of Ribonuclease. *J. Proteome Res.*, 2:506–513, 2003.

[116] Ahmed, M. U. and Thorpe, S. R. and Baynes, J. W. Identification of N-epsilon-carboxymethyllysine as a degradation product of fructoselysine in glycated protein. *J. Biol. Chem.*, 261(11):4889–4894, 1986.

[117] Al-Abed, Y. M. and Bucala, R. N^{ϵ}-carboxymethyllysine formation by direct addition

of glyoxal to lysine during the maillard reaction. *Bioorg. Med. Chem. Lett.*, 5(18): 2161–2162, 1995.

[118] Hayashi, C. M. and Nagai, R. and Miyazaki, K. and Hayase, F. and Tomohiro, A. and Tomomichi, O. and Horiuchi, S. Conversion of Amadori Products of the Maillard Reaction to N^{ϵ}- (carboxymethyl)lysine by Short-Term Heating : Possible Detection of Artifacts by Immunohistochemistry. *Lab. Invest.*, 82(6):795–807, 2002.

[119] Shangari, N. and O'Brien, P. J. The cytotoxic mechanism of glyoxal involves oxidative stress. *Biochem. Pharmacol.*, 68(7):1433–42, 2004.

[120] Mera, K. and Takeo, K. and Izumi, M. and Maruyama, T. and Nagai, R. and Otagiri, M. and Masaki, O. Effect of reactive-aldehydes on the modification and dysfunction of human serum albumin. *J. Pharm. Sci.*, 99(3):1614–1625, 2010.

[121] Mittelmainer, S. and Pischetsrieder, M. Multistep ultrahigh performance liquid chromatography/tandem mass spectrometry analysis for untargeted quantification of glycating activity and identification of most relevant glycation products. *Anal. Chem.*, 83:9660–9668, 2011.

[122] Van Lancker, F. and Adams, A. and De Kimpe, N. Formation of pyrazines in Maillard model systems of lysine-containing dipeptides. *J. Agr. Food Chem.*, 58 (4):2470–8, 2010.

[123] Krause, R. and Kühn, J. and Penndorf, I. and Knoll, K. and Henle, T. N-Terminal pyrazinones: a new class of peptide-bound advanced glycation end-products. *Amino Acids*, 27(1):9–18, 2004.

[124] Chellan, P. and Nagaraj, R. H. Protein crosslinking by the Maillard reaction:

dicarbonyl-derived imidazolium crosslinks in aging and diabetes. *Arch. Biochem. Biophys.*, 368(1):98–104, 1999.

[125] H. Odani, T. Shinzato, J. Usami, Y. Matsumoto, E. B. Frye, J. W. Baynes, and K. Maeda. Imidazolium crosslinks derived from reaction of lysine with glyoxal and methylglyoxal are increased in serum proteins of uremic patients:Evidence for increased oxidative stress in uremia. *FEBS Lett.*, 427(3):381–385, 1998.

[126] Eble, A. S. and Thorpe, S. R. and Baynes, J. W. Nonenzymatic glucosylation and glucose-dependent cross-linking of protein. *J. Biol. Chem.*, 258(15):9406–12, 1983.

[127] Makita, Z. and Yanagisawa, K. and Kuwajima, S. and Yoshioka, N. and Atsumi, T. and Hasunuma, Y. and Koike, T. Amides are novel protein modifications formed by physiological sugars. *J. Biol. Chem.*, 276(45):41638–41647, 2001.

[128] Biemel, K. M and Friedl, D. A. and Lederer, M. O. Identification and quantification of major maillard cross-links in human serum albumin and lens protein. Evidence for glucosepane as the dominant compound. *J. Biol. Chem.*, 277(28):24907–15, 2002.

[129] Sell, D. R. and Monnier, V. M. Structure Elucidation of a Senescence Cross-link from Human Extracellular Matrix. *J. Biol. Chem.*, 264:21597–21602, 1989.

[130] Biemel, K. M. and Conrad, J. and Lederer, M. O. Unexpected carbonyl mobility in aminoketoses: the key to major Maillard crosslinks. *Angew. Chem. Int. Ed.*, 41(5): 801–4, 2002.

[131] Sell, D. R. and Biemel, K. M. and Reihl, O. and Lederer, M. O. and Strauch, C. M. and Monnier, V. M. Glucosepane is a major protein cross-link of the senescent

human extracellular matrix. Relationship with diabetes. *J. Biol. Chem.*, 280(13): 12310–5, 2005.

[132] Alt, N. and Carson, J. A. and Alderson, N. L and Wang, Y. and Nagai, R.i and Henle, T. and Thorpe, S. R. and Baynes, J. W. Chemical modification of muscle protein in diabetes. *Arch. Biochem. Biophys.*, 425(2):200–6, 2004.

[133] Zimmermang, M. B. and Blaine, E. H. Nonenzymatic Browning in vivo : Possible Process for Ageing of Long-Lived Proteins. *Science*, 211(30):491–493, 1981.

[134] Zhang, Y. and Coclking, R. R. and Bidasee, K. R. and Wang, M. Rapid determination of advanced glycation end products of proteins using MALDI-TOF-MS and PERLS script peptide searching algorithm. *J. Biomol. Tech*, 14(3):224–230, 2003.

[135] Montgomery, H. and Tanaka, K. and Belgacem, O. Glycation pattern of peptides condensed with maltose, lactose and glucose determined by ultraviolet matrix-assisted laser desorption/ionization tandem mass spectrometry. *Rapid Commun. Mass Spectrom.*, 24(6):841–848, 2010.

[136] Brancia, F. L. and Bereszczak, J. A. and Lapola, A. and Fedele, D. and Baccarin, L. and Seraglia, R. and Traldi, P. Comprehensive analysis of glycated human serum albumin tryptic peptides by off-line liquid chromatography followed by MALDI analysis on a time-of-flight/curved field reflectron tandem mass spectrometer. *J. Mass Spectrom.*, 41(9):1179–1185, 2006.

[137] Zhang, Q. and Frolov, A. and Tang, N. and Hoffmann, R. and Metz, T. O. and Smith, R. D. Application of electron transfer dissociation mass spectrometry in analyses of non-enzymatically glycated peptides. *Rapid Commun. Mass Spectrom.*, pages 661–666, 2007.

[138] Lapolla, A. and Fedele, D. and Reitano, R. and Aricò, N. C. and Seraglia, R.

and Traldi, P. and Marotta, E. and Tonani, R. Enzymatic digestion and mass spectrometry in the study of advanced glycation end products/peptides. *J. Am. Soc. Mass Spectrom.*, 15(4):496–509, 2004.

[139] Wynne, C. and Edwards, N. J. and Fenselau, C. Phyloproteomic classification of unsequenced organisms by top-down identification of bacterial proteins using capLC-MS-MS on an Orbitrap. *Proteomics*, 10(20):3631–3643, 2010.

[140] Stefanowicz, P. and Kijewska, M. and Szewczuk, Z. Sequencing of peptide-derived Amadori products by the electron capture dissociation method. *J. Mass Spectrom.*, 44(7):1047–1052, 2009.

[141] Heck, A. J.R. and Jorgensen, T. J. D. Vancomycin in vacuo. *Int. J. Mass Spectrom.*, 236(1-3):11–23, 2004.

[142] O'Connor, P. B. and Lin, C. and Cournoyer, J. J. and Pittman, J. L. and Belyayev, M. and Budnik, B. A. Long-lived electron capture dissociation product ions experience radical migration via hydrogen abstraction. *J. Am. Soc. Mass Spectrom.*, 17(4): 576–585, 2006.

[143] Skurski, P. and Sobczyk, M. and Jakowski, J. and Simons, J. Possible mechanisms for protecting N$-$Cα bonds in helical peptides from electron-capture (or transfer) dissociation. *Int. J. Mass Spectrom.*, 265(2-3):197–212, 2007.

[144] Turecek, F. and Syrstad, E. A. and Seymour, J. L. and Chen, X. and Yao, C. Peptide cation-radicals. A computational study of the competition between peptide N-Calpha bond cleavage and loss of the side chain in the [GlyPhe $-\mathrm{NH_2} + 2\,\mathrm{H}]^{+\bullet}$ cation-radical. *J. Mass Spectrom.*, 38(10):1093–1104, 2003.

[145] Carpenter, F. H. and Polce, M. J. and Wesdemiotis, C. Glycyl Radical Is a Stable Species in the Gas Phase. *J. Am. Chem. Soc.*, 121(21):7955–7956, 1999.

[146] Headlam, H. A. and Mortimer, A. and Easton, C. J. and Davies, M. J. $\beta-$Scission of C-3 ($\beta-$carbon) alkoxyl radicals on peptides and proteins: a novel pathway which results in the formation of alpha-carbon radicals and the loss of amino acid side chains. *Chem. Res. Toxicol.*, 13(11):1087–1095, 2000.

[147] O'Hair, R. A. J. and Blanksby, S. and Styles, M.e and Bowie, J. H. Characterization of [M$-$H] cations, radicals and anions of glycine in the gas phase: a combined experimental and *ab initio* study. *Int. J. Mass Spectrom.*, 182-183:203–211, 1999.

[148] Zubarev, R. A. Reactions of polypeptide ions with electrons in the gas phase. *Mass Spectrom. Rev.*, 22(1):57–77, 2003.

[149] Bythell, B. J. To Jump or Not To Jump? *J. Phys. Chem. A*, 117:1189–1196, 2013.

[150] Cooper, H. J. and Hudgins, R. R and Hakansson, K. and Marshall, A. G. Secondary fragmentation of linear peptides in electron capture dissociation. *Int. J. Mass Spectrom.*, 228:723–728, 2003.

[151] Cooper, H. J. Investigation of the presence of b ions in electron capture dissociation mass spectra. *J. Am. Soc. Mass Spectrom.*, 16(12):1932–1940, 2005.

[152] Lee, S. and Chung, G. and Kim, J. and Oh, H. B. Electron capture dissociation mass spectrometry of peptide cations containing a lysine homologue: a mobile proton model for explaining the observation of $b-$type product ions. *Rapid Commun. Mass Spectrom.*, 20:3167–3175, 2006.

[153] Liu, H. and Hakansson, K. Abundant b-type ions produced in electron capture dissociation of peptides without basic amino acid residues. *J. Am. Soc. Mass Spectrom.*, 18(11):2007–2013, 2007.

[154] Haselmann, K. F. and Schmidt, M. Do $b-$ions occur from vibrational excitation

upon H-desorption in electron capture dissociation? *Rapid Commun. Mass Spectrom.*, 21:1003–1008, 2007.

[155] Zubarev, R. A. and Savitski, M. M. Electron capture/transfer versus collisionally activated/induced dissociations: solo or duet? *J. Am. Soc. Mass Spectrom.*, 19: 753–761, 2008.

[156] Gorshkov, M. V. and Masselon, C. D. and Nikolaev, E. N. and Udseth, H. R. and Smith, R. D. Considerations for electron capture dissociation efficiency in FTICR mass spectrometry. *Int. J. Mass Spectrom.*, 234(1-3):131–136, 2004.

[157] Zubarev, R. A. and Witt, M. and Baykut, G. Two-fold efficiency increase by selective excitation of ions for consecutive activation by ion-electron reactions and vibrational excitation in tandem fourier transform ion cyclotron resonance mass spectrometry. *Anal. Chem.*, 77(9):2992–2996, 2005.

[158] Iavarone, A. T. and Paech, K. and Williams, E. R. Effects of charge state and cationizing agent on the electron capture dissociation of a peptide. *Anal. Chem.*, 76(8):2231–2238, 2004.

[159] McFarland, M. A. and Chalmers, M. J and Quinn, J. P. and Hendrickson, C. L. and Marshall, A. G. Evaluation and optimization of electron capture dissociation efficiency in fourier transform ion cyclotron resonance mass spectrometry. *J. Am. Soc. Mass Spectrom.*, 16(7):1060–1066, 2005.

[160] Hakansson, K. and Emmett, M. R. and Hendrickson, C. L. and Marshall, A.G. High-sensitivity electron capture dissociation tandem FTICR mass spectrometry of microelectrosprayed peptides. *Anal. Chem.*, 73(15):3605–3610, 2001.

[161] Kruger, N. A. and Zubarev, R. A. and Horn, D. M. and McLafferty, Fred W. Electron

capture dissociation of multiply charged peptide cations. *Int. J. Mass Spectrom.*, 185-187:787–793, 1999.

[162] Polfer, N. C. and Haselmann, K. F. and Zubarev, R. A. and Langridge-Smith, P. R. R. Electron capture dissociation of polypeptides using a 3 Tesla Fourier transform ion cyclotron resonance mass spectrometer. *Rapid Commun. Mass Spectrom.*, 16 (10):936–943, 2002.

[163] Tsybin, Y. O. and Hakansson, P. and Budnik, B. A. and Haselmann, K. F. and Kjeldsen, F. and Gorshkov, M. and Zubarev, R. A. Improved low-energy electron injection systems for high rate electron capture dissociation in Fourier transform ion cyclotron resonance mass spectrometry. *Rapid Commun. Mass Spectrom.*, 15 (19):1849–1854, 2001.

[164] Tsybin, Y. O. and Quinn, J. P. and Hendrickson, C. L. and Marshall, A. G. Electron capture dissociation implementation progress in Fourier transform ion cyclotron resonance mass spectrometry. *J. Am. Soc. Mass Spectrom.*, 19(6):762–771, 2008.

[165] Chan, W.Y.K. and Chan, T.W.D. Natural structural motifs that suppress peptide ion fragmentation after electron capture. *J. Am. Soc. Mass Spectrom.*, 21(7): 1235–1244, 2010.

[166] Mormann, M. and Peter-Katalinić, J. Improvement of electron capture efficiency by resonant excitation. *Rapid Commun. Mass Spectrom.*, 17(19):2208–2214, 2003.

[167] Freiser, B. S. and Beauchamp, J. L. Electron impact dissociation of cyanobenzene radical cations by ion cyclotron resonance spectroscopy. *Chem. Phys. Lett.*, 42(2): 380–382, 1976.

[168] Cody, R. B. and Freiser, B. S. Electron impact excitation of ions from organics: an alternative to collision induced dissociation. *Anal. Chem.*, 51(4):547–551, 1979.

[169] Wang, B. and McLafferty, F. W. Electron impact excitation of ions from larger organic molecules. *Org. Mass Spectrom.*, 25:554–556, 1990.

[170] Guan, Z. and Kelleher, N. L. and O'Connor, P. B. and Aaserud, D. J. and Little, D. P. and McLafferty, F. W. 193 nm Photodissociation of Larger Multiply-Charged Biomolecules. *Int. J. Mass Spectrom.*, 157-158(96):357–364, 1996.

[171] Axelsson, J. and Palmblad, M. and Hakansson, K. and Hakansson, P. Electron capture dissociation of substance P using a commercially available Fourier transform ion cyclotron resonance mass spectrometer. *Rapid Commun. Mass Spectrom.*, 13 (6):474–477, 1999.

[172] Kruger, N. A and Zubarev, R. A. and Carpenter, B. K. and Kelleher, N. L. and Horn, D. M. and Mclafferty, F. W. Electron capture versus energetic dissociation of protein ions. *Int. J. Mass Spectrom.*, 182-183:1–5, 1999.

[173] Fung, Y. M. E. and Chan, T-W. D. Experimental and theoretical investigations of the loss of amino acid side chains in electron capture dissociation of model peptides. *J. Am. Soc. Mass Spectrom.*, 16:1523–1535, 2005.

[174] Zubarev, R. A. and Kruger, N. A. and Fridriksson, E. K. and Lewis, M. A. and Horn, D. M. and Carpenter, B. K. and McLafferty, F. W. Electron Capture Dissociation of Gaseous Multiply-Charged Proteins Is Favored at Disulfide Bonds and Other Sites of High Hydrogen Atom Affinity. *J. Am. Chem. Soc.*, 121(12):2857–2862, 1999.

[175] Kalli, A. and Hakansson, K. Preferential cleavage of S−S and C−S bonds in electron detachment dissociation and infrared multiphoton dissociation of disulfide-linked peptide anions. *Int. J. Mass Spectrom.*, 263(1):71–81, 2007.

[176] Li, H. and O'Connor, P. B. Electron capture dissociation of disulfide, sulfur-selenium, and diselenide bound peptides. *J. Am. Soc. Mass Spectrom.*, 23(11): 2001–2010, 2012.

[177] Sawicka, A. and Skurski, P. and Hudgins, R. R. and Simons, J. Model Calculations Relevant to Disulfide Bond Cleavage via Electron Capture Influenced by Positively Charged Groups. *J. Phys. Chem.*, 107(48):13505–13511, 2003.

[178] Simons, J. Mechanisms for S-S and N-Cα bond cleavage in peptide ECD and ETD mass spectrometry. *Chem. Phys. Lett.*, 484(4-6):81–95, 2010.

[179] Uggerud, E. Electron capture dissociation of the disulfide bond? A quantum chemical model study. *Int. J. Mass Spectrom.*, 234(1-3):45–50, 2004.

[180] Tsutakawa, S. E. and Medzihradszky, K. F. and Flint, A. J. and Burlingame, A. L. and Koshland, D.l E. Determination of in vivo phosphorylation sites in protein kinase c. *J. Biol. Chem.*, 270:26807–26812, 1995.

[181] Stensballe, A. and Jensen, O. N. and Olsen, J. V. and Haselmann, K. F. and Zubarev, R. A. Electron capture dissociation of singly and multiply phosphorylated peptides. *Rapid Commun. Mass Spectrom.*, 14:1793–1800, 2000.

[182] Appella, E. and Anderson, C. W. New prospects for proteomics–electron-capture (ECD) and electron-transfer dissociation (ETD) fragmentation techniques and combined fractional diagonal chromatography (COFRADIC). *FEBS journal*, 274 (24):6255, 2007.

[183] Bakhtiar, R. and Guan, Z. Electron capture dissociation mass spectrometry in characterization of post-translational modifications. *Biochem. Bioph. Res. Co.*, 334:1–8, 2005.

[184] Lill, J. Proteomic tools for quantitation by mass spectrometry. *Mass Spectrom. Rev.*, 22(3):182–194, 2003.

[185] Cooper, H. and Hakansson, K. and Marshall, A. and Hudgins, R. and Haselmann, K. and Kjeldsen, F. and Budnik, B. and Polfer, N. C. and Zubarev, R. A. The diagnostic value of amino acid side-chain losses in electron capture dissociation of polypeptides. Comment on: "Can the $[M^{\bullet} - X]$ region in electron capture dissociation provide reliable information on amino acid composition of polypeptides?". *Eur. J. Mass Spectrom.*, 9:221–222, 2003.

[186] Cooper, H. J. and Hudgins, R. R. and Hakansson, K. and Marshall, A. G. Characterization of amino acid side chain losses in electron capture dissociation. *J. Am.n Soc. Mass Spectrom.*, 13(3):241–9, 2002.

[187] Turecek, F. and Chung, T. W. and Moss, C. L. and Wyer, J. A. and Ehlerding, A. and Holm, A. I. S. and Zettergren, H. and Nielsen, S. B. and Hvelplund, P. and Chamot-Rooke, J. and Bythell, B. and Paizs, B. The histidine effect. Electron transfer and capture cause different dissociations and rearrangements of histidine peptide cation-radicals. *J. Am. Chem. Soc.*, 132(31):10728–10740, 2010.

[188] Chen, X. and Turecek, F. The arginine anomaly: arginine radicals are poor hydrogen atom donors in electron transfer induced dissociations. *J. Am. Chem. Soc.*, 128(38):12520–12530, 2006.

[189] Siegbahn, P. E. M. and Blomberg, M. R. A. and Crabtree, R. H. Hydrogen transfer in the presence of amino acid radicals. *Theor. Chem. Acc.*, 97:289–300, 1997.

[190] Haselmann, K. F. and Budnik, B. A. and Zubarev, R. A. Electron capture dissociation of b^{2+} peptide fragments reveals the presence of the acylium ion structure. *Rapid Commun. Mass Spectrom.*, 14(23):2242–2246, 2000.

[191] Savitski, M. M and Nielsen, M. L. and Zubarev, R. A. Side-chain losses in electron capture dissociation to improve peptide identification. *Anal. Chem.*, 79(6):2296–2302, 2007.

[192] Leymarie, N. and Costello, C. E. and O'Connor, P. B. Electron capture dissociation initiates a free radical reaction cascade. *J. Am. Chem. Soc.*, 125(29):8949–8958, 2003.

[193] Turecek, F. N-C(α) bond dissociation energies and kinetics in amide and peptide radicals. Is the dissociation a non-ergodic process? *J. Am. Chem. Soc.*, 125: 5954–5963, 2003.

[194] Ding, L. and Brancia, F. L. Electron capture dissociation in a digital ion trap mass spectrometer. *Anal. Chem.*, 78(6):1995–2000, 2006.

[195] Baba, T. and Hashimoto, Y. and Hasegawa, H. and Hirabayashi, A. and Waki, I. Electron capture dissociation in a radio frequency ion trap. *Anal Chem.*, 76: 4263–4266, 2004.

[196] Lawson, J. D. Laser and accelerators. *IEEE T. Nucl. Sci.*, NS-26:4217–4219, 1979.

[197] Syka, J. E. P. and Coon, J. J. and Schroeder, M. J. and Shabanowitz, J. and Hunt, D. F. Peptide and protein sequence analysis by electron transfer dissociation mass spectrometry. *Proc. Natl. Acad. Sci. U.S.A.*, 101(26):9528–9533, 2004.

[198] Kjeldsen, F. and Haselmann, K. F. and Budnik, B. A. and Jense, F. and Zubarev, R. A. Dissociative capture of hot (3-13 eV) electrons by polypeptide polycations: an efficient process accompanied by secondary fragmentation. *Chem. Phys. Lett.*, 355(1-2):201–206, 2002.

[199] Nguyen, V. H.and Afonso, C. and Tabet, J-C. Comparison of collision-induced

dissociation and electron-induced dissociation of singly charged mononucleotides. *Int. J. Mass Spectrom.*, 316-318:140–146, 2012.

[200] Williams, J P. and Creese, A J. and Roper, D R. and Green, B N. and Cooper, H J. . Hot electron capture dissociation distinguishes leucine from isoleucine in a novel hemoglobin variant, hb askew, β54(d5)Val$-$ $>$Ile. *J. Am. Soc. Mass Spectrom.*, 20 (9):1707–1713, 2009.

[201] Budnik, B. A. and Zubarev, R. A. $MH^{2+\bullet}$ ion production from protonated polypeptides by electron impact: observation and determination of ionization energies and a cross-section. *Chem. Phys. Lett.*, 316(1-2):19–23, 2000.

[202] Fung, Y. M. E. and Adams, C. M and Zubarev, R. A. Electron ionization dissociation of singly and multiply charged peptides. *J. Am. Chem. Soc.*, 131(29):9977–9985, 2009.

[203] Nielsen, M. L. and Budnik, B. A. and Haselmann, Kim F. and Olsen, Jesper V. and Zubarev, R. A. Intramolecular hydrogen atom transfer in hydrogen-deficient polypeptide radical cations. *Chem. Phys. Lett.*, 330(5-6):558–562, 2000.

[204] Nielsen, M. L. and Budnik, B. A and Haselmann, K. F. and Zubarev, R. A. Tandem MALDI/EI ionization for tandem Fourier transform ion cyclotron resonance mass spectrometry of polypeptides. *Int. J. Mass Spectrom.*, 226:181–187, 2003.

[205] Yoo, E. J. and Feketeova, L. and Khairallah, G. N. and O'Hair, R. A. J. Unimolecular chemistry of doubly protonated zwitterionic clusters. *J. Phys. Chem. A*, 115(17): 4179–4185, 2011.

[206] Yoo, H. J. and Liu, H. and Hakansson, K. Infrared Multiphoton Dissociation and Electron-Induced Dissociation as Alternative MS / MS Strategies for Metabolite Identification. *Anal. Chem.*, 79(20):7858–7866, 2007.

[207] Wolff, J. J. and Laremore, T. N. and Aslam, H. and Linhardt, R. J. and Amster, I. J. Electron-Induced Dissociation of Glycosaminoglycan Tetrasaccharides. *J. Am. Soc. Mass Spectrom.*, 19:1449–1458, 2008.

[208] Kaczorowska, M. A. and Cooper, H. J. Electron induced dissociation: a mass spectrometry technique for the structural analysis of trinuclear oxo-centred carboxylate-bridged iron complexes. *J. Am. Soc. Mass Spectrom.*, 21(8):1398–403, 2010.

[209] Budnik, B. A. and Haselmann, K. F. and Zubarev, R. A. Electron detachment dissociation of peptide di-anions: an electron hole recombination phenomenon. *Chem. Phys. Lett.*, 342(3-4):299–302, 2001.

[210] Kjeldsen, F. and Silivra, O. A. and Ivonin, I. A. and Haselmann, K. F. and Gorshkov, M. and Zubarev, R. A. Cα-C backbone fragmentation dominates in electron detachment dissociation of gas-phase polypeptide polyanions. *Chem. Eur. J.*, 11 (6):1803–1812, 2005.

[211] McFarland, M. A. and Marshall, A. G. and Hendrickson, C. L. and Nilsson, C. L and Fredman, P. and Mansson, J-E. Structural characterization of the GM1 ganglioside by infrared multiphoton dissociation, electron capture dissociation, and electron detachment dissociation electrospray ionization FT-ICR MS/MS. *J. Am. Soc. Mass Spectrom.*, 16(5):752–762, 2005.

[212] Wolff, J. J. and Amster, I. J. and Chi, L. and Linhardt, R. J. Electron detachment dissociation of Glycosaminoglycan Tetrasaccharides. *J. Am. Soc. Mass Spectrom.*, 18:234–244, 2007.

[213] Adamson, J. T. and Hakansson, K. Electron detachment dissociation of neutral and sialylated oligosaccharides. *J. Am. Soc. Mass Spectrom.*, 18(12):2162–2172, 2007.

[214] Nguyen, V. H. and Afonso, C. and Tabet, J-C. Concomitant EDD and EID of DNA evidenced by MSn and double resonance experiments. *Int. J. Mass Spectrom.*, 301 (1-3):224–233, 2011.

[215] Yang, J. and Mo, J. and Adamson, J. T. and Hakansson, K. Characterization of Oligodeoxynucleotides by Electron Detachment Dissociation Fourier Spectrometry. 77(6):1876–1882, 2005.

[216] Yoo, H. Y. and Wang, N. and Zhuang, S. and Song, H. and Hakansson, K. Negative-ion electron capture dissociation: radical-driven fragmentation of charge-increased gaseous peptide anions. *J. Am. Chem. Soc*, 133(42):16790–16793, 2011.

[217] Gauthier, J. W. and Trautman, T. R. and Jacobson, D. B. Sustained off-resonance irradiation for collision-activated dissociation involving Fourier transform mass spectrometry . Collision-activated dissociation technique that emulates infrared multiphoton dissociation. *Anal. Chim. Acta*, 246:211–225, 1991.

[218] Mirgorodskaya, E. and O'Connor, P. B. and Costello, C. E. A General Method for Precalculation of Irradiation / Collision-Induced Dissociation. *J. Am. Soc. Mass Spectrom.*, 13:318–324, 2002.

[219] Li, H. and Lin, T-Y. and Orden, S. L. V. and Zhao, Y. and Barrow, M. P. and Pizarro, A. M. and Qi, Y. and Sadler, P. J and O'Connor, P. B. Use of Top-Down and bottom-up Fourier transform ion cyclotorn resonance mass spectrometry for Mapping Calmodulin Sites modified by platinum anticancer drugs. *Anal. Chem.*, 83:9507–9515, 2011.

[220] Horn, D. M. and Breuker, K. and Frank, A. J. and McLafferty, F. W. Kinetic intermediates in the folding of gaseous protein ions characterized by electron

capture dissociation mass spectrometry. *J. Am. Chem. Soc.*, 123(40):9792–9799, 2001.

[221] Sze, S. K. and Ge, Y. and Oh, H. B. and McLafferty, F. W. Plasma electron capture dissociation for the characterization of large proteins by top down mass spectrometry. *Anal. Chem.*, 75(7):1599–1603, 2003.

[222] Tsybin, Y. O. and Ramstrom, M. and Witt, M. and Baykut, G. and Hakansson, P. Peptide and protein characterization by high-rate electron capture dissociation Fourier transform ion cyclotron resonance mass spectrometry. *J. Mass Spectrom.*, 39(7):719–729, 2004.

[223] Oh, H. and McLafferty, F. W. A varieet of activation methods employed in 'Activated-ion' electron capture. *Bull. Korean. Chem. Soc.*, 27(3):389–394, 2006.

[224] Hamidane, H. B. and He, H. and Tsybin, O. Y. and Emmett, M. R. and Hendrickson, C. L. and Marshall, A. G. and Tsybin, Y. O. Periodic sequence distribution of product ion abundances in electron capture dissociation of amphipathic peptides and proteins. *J. Am. Soc. Mass Spectrom.*, 20:1182–1192, 2009.

[225] Ge, Y. and Horn, D. M. and McLafferty, F. W. Blackbody infrared radiative dissociation of larger (42 kDa) multiply charged proteins. *Int. J . Mass Spectrom.*, 210-211:203–214, 2001.

[226] Breuker, K. and Oh, H. B. and Horn, D. M. and Cerda, B. A. and McLafferty, F. W. Detailed unfolding and folding of gaseous ubiquitin ions characterized by electron capture dissociation. *J. Am. Chem. Soc.*, 124(22):6407–20, 2002.

[227] Beauchamp, J. L. and Armstrong, J. T. An Ion Ejection Technique for the Study of Ion-Molecule Reactions with Ion Cyclotron Resonance Spectroscopy. *Rev. Sci. Instrum.*, 40:123–128, 1969.

[228] Comisarov, M. B. and Grassi, V. and Parisor, G. Fourier transform ion cyclotron double resonance. *J. Chem. Phys.*, 57:413–416, 1978.

[229] Lin, C. and Cournoyer, J. J. and O'Connor, P. B. Use of a double resonance electron capture dissociation experiment to probe fragment intermediate lifetimes. *J. Am. Soc. Mass Spectrom.*, 17(11):1605–15, 2006.

[230] Lin, C. and Cournoyer, J. J. and O'Connor, P. B. Probing the gas-phase folding kinetics of peptide ions by IR activated DR-ECD. *J. Am. Soc. Mass Spectrom.*, 19 (6):780–789, 2008.

[231] Boltalina, O. and Hvelplund, P. and Jorgensen, T. and Larsen, M. and Larsson, M. and Sharoitchenko, D. Electron capture by fluorinated fullerene anions in collisions with Xe atoms. *Phys. Rev. A*, 62(2):023202, 2000.

[232] Hvelplund, P. and Liu, B. and Nielsen, S. B. and Panja, S. and Poully, J.-C. and Stochkel, K. Electron capture induced dissociation of peptide ions: Identification of neutral fragments from secondary collisions with cesium vapor. *Int. J. Mass Spectrom.*, 263(1):66–70, 2007.

[233] Chakraborty, T. and Holm, A. I. S. and Hvelplund, P. and Nielsen, S. B. and Poully, J.-C. and Worm, E. S. and Williams, E. R. On the survival of peptide cations after electron capture: role of internal hydrogen bonding and microsolvation. *J. Am. Soc. Mass Spectrom.*, 17(12):1675–1680, 2006.

[234] P. Hvelplund, B. Liu, S.B. Nielsen, S. Tomita, H. Cederquist, J. Jensen, H.T. Schmidt, and H. Zettergren. Electron capture and loss by protonated peptides and proteins in collisions with C60 and Na. *Eur. Phys. J. D*, 22(1):75–79, 2003.

[235] Holm, A. I. S. and Hvelplund, P. and Kadhane, U. and Larsen, M. K. and Liu, B. and Nielsen, S. B. and Panja, S. and Pedersen, J. M. and Skrydstrup, T. and Stochkel,

K.n and Williams, E. R. and Worm, E. S. On the mechanism of electron-capture-induced dissociation of peptide dications from $15N-$labeling and crown-ether complexation. *J. Phys. Chem. A*, 111(39):9641–9643, 2007.

[236] S. Bari, R. Hoekstra, and T. Schlatholter. Fast side-chain losses in keV ion-induced dissociation of protonated peptides. *Int. J. Mass Spectrom.*, 299(1):64–70, 2011.

[237] Vasil'ev, Y. V. and Figard, B. J. and Morré, J. and Deinzer, M. L. Fragmentation of peptide negative molecular ions induced by resonance electron capture. *J. Chem. Phys.*, 131(4):044317–1 – 044317–11, 2009.

[238] Thorne, L. R. and Beauchamp, J. L. and in M.T. Bowers (Ed.). *Gas Phase Ion Chemistry, Vol. 3, Academic Press, New York*. 1984.

[239] Zubarev, R. and Haselmann, K. and Budnik, B. and Kjeldsen, F. and Jensen, F. Towards an understanding of the mechanism of electron- capture dissociation: a historical perspective and modern ideas. *Eur. J. Mass Spectrom.*, 8:337–349, 2002.

[240] Syrstad, E. A. and Turecek, F. Toward a general mechanism of electron capture dissociation. *J. Am. Soc. Mass Spectrom.*, 16:208–224, 2005.

[241] Turecek, F. and Syrstad, E. A. Mechanism and Energetics of Intramolecular Hydrogen Transfer in Amide and Peptide Radicals and Cation-Radicals as a result of radiation or oxidative damage and mainly involves. *J. Am. Chem. Soc.*, 125 (11):3353–3369, 2003.

[242] Neff, D. and Sobczyk, M. and Simons, J. Theoretical study of through-space and through-bond electron transfer within positively charged peptides in the gas phase. *Int. J. Mass Spectrom.*, 269:149–164, 2008.

[243] Simons, J. and Ledvina, A. R. Spatial extent of fragment-ion abundances in electron transfer dissociation and electron capture dissociation mass spectrometry of peptides. *Int. J . Mass Spectrom.*, 330-332:85–94, 2012.

[244] Price, S. D. Interactions of molecular doubly charged ions with atoms, molecules and photons. *J. Chem. Soc Faraday T.*, 93(15):2451–2460, 1997.

[245] Anusiewicz, I. and Berdys-Kochanska, J. and Simons, J. Electron attachment step in electron capture dissociation (ECD) and electron transfer dissociation (ETD). *J. Phys. Chem. A*, 109(26):5801–5813, 2005.

[246] Neff, D. and Smuczynska, S. and Simons, J. Electron shuttling in electron transfer dissociation. *Int. J. Mass Spectrom.*, 283(1-3):122–134, 2009.

[247] Sobczyk, M. and Simons, J. The role of excited Rydberg States in electron transfer dissociation. *J. Phys. Chem. B*, 110(14):7519–27, 2006.

[248] Gunawardena, H. P. and Gorenstein, L. and Erickson, D. E. and Xia, Y. and McLuckey, S. A. Electron transfer dissociation of multiply protonated and fixed charge disulfide linked polypeptides. *Int. J. Mass Spectrom.*, 265(2-3):130–138, 2007.

[249] Sobczyk, M. and Neff, D. and Simons, J. Theoretical study of through-space and through-bond electron transfer within positively charged peptides in the gas phase. *Int. J . Mass Spectrom.*, 269(3):149–164, 2008.

[250] Frison, G. and Van der Rest, G. and Turecek, F. and Besson, T. and Lemaire, J. and Maitre, P. and Chamot-Rooke, J. Structure of electron-capture dissociation fragments from charge-tagged peptides probed by tunable infrared multiple photon dissociation. *J. Am. Chem. Soc.*, 130(45):14916–14917, 2008.

[251] Sun, Q. and Nelson, H. and Ly, T. and Stoltz, B. M. and Julian, R. R. Side chain chemistry mediates backbone fragmentation in hydrogen deficient peptide radicals. *J. Proteome Res.*, 8(2):958–966, 2009.

[252] Li, X. and Cournoyer, J. J and Lin, C. and O'Connor, P. B. The effect of fixed charge modifications on electron capture dissociation. *J. Am. Soc. Mass Spectrom.*, 19(10):1514–26, 2008.

[253] Turecek, F. and McLafferty, F. W. Non-ergodic behavior in acetone-enol ion dissociations. *J. Am. Chem. Soc.*, 106:2525–2531, 1984.

[254] Simons, J. Analytical model for rates of electron attachment and intramolecular electron transfer in electron transfer dissociation mass spectrometry. *J. Am. Chem. Soc.*, 132(20):7074–85, 2010.

[255] Lifshitz, C. Intramolecular vibrational redistribution and ergodicity of biomolecular dissociation. In *Principles of mas spectrometry applied to biomolecules*. 2006.

[256] Robertson, S. H. and Pilling, M. J. and Robinson, P. J. *Unimolecular reactions.* 1996.

[257] M. A. Belyayev, C. Cournoyer, J. J .and Lin, and P. B. O'Connor. The effect of radical trap moieties on electron capture dissociation spectra of substance P. *J. Am. Soc. Mass Spectrom.*, 17(10):1428–36, 2006.

[258] Sohn, C. H. and Chung, C. K. and Yin, S. and Ramachandran, P. and Loo, J. A. and Beauchamp, J. L. Probing the Mechanism of Electron Capture and Electron Transfer Dissociation Using Tags with Variable Electron Affinity. *J. Am. Chem. Soc.*, 131(15):5444–5459, 2009.

[259] Hodyss, R. and Cox, H. A. and Beauchamp, J. L. Bioconjugates for tunable peptide

fragmentation: free radical initiated peptide sequencing (FRIPS). *J. Am. Chem. Soc.*, 127(36):12436–12437, 2005.

[260] Syrstad, E. A. and Stephens, D. D. and Turecek, F. Hydrogen Atom Adducts to the Amide Bond. Generation and Energetics of Amide Radicals in the Gas Phase. *J. Phys. Chem. A*, 107(1):115–126, 2003.

[261] Kua, J. and Hanley, S. W. and De Haan, D. O. Thermodynamics and kinetics of glyoxal dimer formation: a computational study. *J. Phys. Chem. A*, 112:66–72, 2008.

[262] Whipple, E. B. Structure of glyoxal in water. *J. Am. Chem. Soc.*, 92(24):7183–7186, 1970.

[263] Nakajima, K.i and Ohta, K. and Mostefaoui, T. a and Chai, W. and Utsukihara, T. and Horiuchi, C. A. and Murakami, M. Glyoxal sample preparation for high-performance liquid chromatographic detection of 2,4-dinitro-phenylhydrazone derivative: Suppression of polymerization and mono-derivative formation by using methanol medium. *J. Chromatogr., A*, 1161(1-2):338–341, 2007.

[264] Caravatti, P. and Alleman, M. The infinity cell - a new reapped-ion cell with radiofrequency covered trapping electrodes for Fourier transform ion cyclotron mass spectrometry. *Org. Mass Spectrom.*, 26(5):514–518, 1991.

[265] He, H. and Emmett, M. and Nilsson, C. L. and Conrad, A. C. and Marshall, A. G. High mass accuracy and resolution facilitate identification of glycosphingolipids and phospholipids. *Int. J. Mass Spectrom.*, 305:116–119, 2011.

[266] De Haan, D. O. and Corrigan, A. L. and Smith, K. W. and Stroiik, D. R., D. R. and Turley, J. J. and Lee, F. E. and Tolbert, M. A. and and Cordova, K. E. and Ferrell,

G. R. Secondary organic aerosol-forming reactions of glyoxal with amino acids. *Environ. Sci. Technol.*, 43(8):2818–2824, 2009.

[267] Bunn, H. F and Shapiro, R. and McManus, M. and Garrick, L. and McDonald, M. J. and Gallop, P. M. and J., Gabbay K. Structural heterogeneity of human hemoglobin-A due to non-enzmatic glycosylation. *J. Biol. Chem.*, 254(10):3892–3898, 1979.

[268] Ahmed, N. and Thornalley, P. J. and Dawczynski, J. and Franke, S. and Strobel, J. and Stein, G. and Haik, G. M. Methylglyoxal-derived hydroimidazolone advanced glycation end-products of human lens proteins. *Invest. Ophthalmol. Visual Sci.*, 44(12):5287–5292, 2003.

[269] Carter, D. C. and Ho, J. X. Structure of serum albumin. In *Adv. Protein Chem.*, pages 158–159. 1994.

[270] Morgan, D. G. and Bursey, M. M. Linear free energy correlation in the low-energy tandem mass spectra of sodiated tripeptides Gly-Gly-X. *J. Mass Spectrom.*, 30(3): 473–477, 1995.

[271] Bensadek, D. and Monigatti, F. and a.J. Steen, J. and Steen, H. Why b, y's? Sodiation-induced tryptic peptide-like fragmentation of non-tryptic peptides. *Int. J. Mass Spectrom.*, 268(2-3):181–189, 2007.

[272] Chan, T. W. D. and Herman-Ip, W. H. . Optimization of experimental parameters for electron capture dissociation of peptides in a Fourier transform mass spectrometer. *J. Am. Soc. Mass Spectrom.*, 13(12):1396–406, 2002.